



MONASH University

Epigenetic Drug Discovery: Bromodomain Inhibitors

Joseph Phillip Hilton-Proctor

Bachelor of Pharmaceutical Science – Monash University

Bachelor of Pharmaceutical Science (Honours) – Monash University

A thesis submitted for the degree of Doctor of Philosophy at
Monash University in 2018
Medicinal Chemistry, Monash Institute of Pharmaceutical Sciences

Table of Contents

Table of Contents	i
Table of Figures.....	iv
Table of Tables	vi
Copyright Notice	vii
Declaration.....	viii
Acknowledgements	ix
Abstract.....	x
Chapter 1 – History of Epigenetics, Bromodomains and Their Inhibitors	1
Abbreviations.....	1
1.1 Defining Epigenetics.....	5
1.1.1 Dutch Hunger Winter	8
1.2 Epigenetic Regulation	9
1.2.1 DNA Modification.....	9
1.2.2 RNA Interference.....	12
1.2.3 Histone Modification	13
1.2.4 The Histone Code.....	15
1.3 Bromodomain Structure.....	18
1.4 (+)-JQ1 and I-BET762 – The First BET Bromodomain Ligands.....	23
1.5 Post-(+)-JQ1 and I-BET762	26
1.5.1 About BRD4	26
1.5.2 Association with Disease States.....	28
1.5.2.1 Cardiovascular Disease.....	29
1.5.2.2 NUT Midline Carcinoma	32
1.5.2.3 Myc-Related Cancer	35
1.5.2.4 Human Immunodeficiency Virus Type 1	36
1.5.3 Fragment-Based Drug Design.....	38
1.5.3.1 Fragment Screening Techniques.....	39
1.5.3.2 Fragment Discovery	41
1.5.3.3 Fragment-to-Lead Development.....	45
1.6 Project Aims.....	50
1.6.1 N-Methylpyrrolidone.....	50
1.6.2 5-Methyl-3-aryl-1H-pyrazole	53

References	54
Chapter 2 – Synthesis and Elaboration of <i>N</i>-Methylpyrrolidone as an Acetamide Fragment Substitute in Bromodomain Inhibition	78
Keywords.....	78
Abbreviations.....	78
Abstract	78
2.1 Introduction	79
2.2 Results and Discussion	82
2.2.1 Synthesis.....	82
2.2.2 BRD4 BD1 FRET Assay Results	85
2.2.3 X-ray Crystallography.....	87
2.3 Conclusion and Future Directions	90
Experimental.....	91
References	101
Chapter 3 – Substituted 1-methyl-4-phenylpyrrolidin-2-ones – Fragment-Based Design of <i>N</i>-Methylpyrrolidone-Derived Bromodomain Inhibitors.....	105
Keywords.....	105
Abbreviations.....	105
Abstract	105
3.1 Introduction	106
3.2 Results and Discussion	108
3.2.1 Synthesis.....	108
3.2.2 BRD4 BD1 FRET Assay Results	114
3.2.3 X-ray Crystallography.....	119
3.3 Conclusion and Future Directions	128
Experimental.....	129
References	153
Chapter 4 – 5-methyl-3-aryl-1<i>H</i>-pyrazoles as Poised, Ligand Efficient Fragments for the Development of Novel Bromodomain Inhibitors	157
Keywords.....	157
Abbreviations.....	157
Abstract	157
4.1 Introduction	158
4.2 Results and Discussion	160
4.2.1 Synthesis.....	161

4.2.2	BRD4 BD1 FRET Assay Results	163
4.2.3	X-ray Crystallography.....	166
4.3	Conclusion and Future Directions	168
	Experimental.....	169
	References	185
Chapter 5 –	Conclusion and Future Directions	189
Appendices.....		192
Appendix A –	Video of Bromodomain Structure.....	192
Appendix B –	Video of NMP Bound to Various Bromodomains.....	193
Appendix C –	Dose Response Curves of Olinone Analogues	194
Appendix D –	Video of Olinone-based Derivatives	195
Appendix E –	Electron Density Map of NMP Derivatives	196
Appendix F –	Chapter 2 NMR Data.....	197
Appendix G –	Chapter 2 X-ray Crystallographic Data Collection and Refinement Statistics.....	213
Appendix H –	Chapter 3 Lipophilic Ligand Efficiency Plot Graphs	216
Appendix I –	Dose Response Curves of Phenyl NMP Derivatives.....	217
Appendix J –	Video of Phenyl NMP Derivatives.....	218
Appendix K –	Electron Density Map of NMP Derivatives.....	219
Appendix L –	Chapter 3 NMR Data.....	221
Appendix M –	Chapter 3 X-ray Crystallographic Data Collection and Refinement Statistics.....	283
Appendix N –	Dose Response Curve of 5-methyl-3-aryl-1 <i>H</i> -pyrazoles	287
Appendix O –	Video of Pyrazole 3h.....	288
Appendix P –	Electron Density Map of 3h.....	289
Appendix Q –	Chapter 4 NMR Data	290
Appendix R –	Chapter 4 X-ray Crystallographic Data Collection and Refinement Statistics.....	331

Table of Figures

Figure 1. Simplified pathways of cytosine and adenine modification.^{48, 49} [A] DNMT enzymes methylate cytosine to give 5-methylcytosine. From here, 5-methylcytosine is demethylated through different mechanisms that involve three unique enzymes: ten eleven translocation (Tet) enzymes, which add a hydroxyl group to the 5-methyl moiety and then oxidise it to a formyl and carboxyl group; activation-induced cytosine deaminase (AID) or apolipoprotein B mRNA editing enzyme, catalytic polypeptide-like (APOBEC) enzymes, which deaminate the amine; and TDG enzymes, which replace the modified base with a cytosine. [B] DNA adenine methyltransferase (DAMT) enzymes methylate adenine to give N⁶-methyladenine. The methyl group is then removed by either N⁶-methyl adenine demethylase (NMAD) enzymes or alpha-ketoglutarate-dependent dioxygenase (AlkB). The latter gives a hydroxyl and formyl intermediate before returning adenine to its original state..... 10

Figure 2. Detailed mechanism of the transfer of a methyl group from SAM to cytosine to give 5mC..... 12

Figure 3. The RNAi pathway, showing the generation of siRNA molecules from dsRNA to be taken up by the RISC, which is then used to cleave mRNA and silence gene expression. dsRNA, double-stranded RNA; siRNA, small interfering RNA; Ago-2, argonaute-2; TRBP, TAR RNA binding protein; RISC, RNA-induced silencing complex; mRNA, messenger RNA. 15

Figure 4. Composition and condensation of DNA and histones into a chromosome.⁸⁰ Double-stranded DNA is coiled around eight histone proteins to create nucleosomes. An extra H1 histone gives a chromatosome. These undergo several levels of compression, folding and coiling to produce a chromosome. © 2013 Nature Education. Adapted from Pierce, Benjamin. Genetics: A Conceptual Approach, 2nd ed. All rights reserved. 16

Figure 5. General schematic of the attachment of a functional group by writer enzymes, the recognition of the modified tail by reader proteins, and the removal of a functional group by eraser enzymes on histones..... 17

Figure 6. X-ray crystal structure of BRD4 BD1 (PDB: 3UVW). [A]. α -helices and loops shown. [B] Cutaway view to show the cavity. [C] Close-up of the binding pocket with the interactions between K-ac (purple blue) and the conserved Asn140 and Tyr97 (white) shown. Water molecules shown as red spheres. Pro86, Val87 and Asp88 were hidden for better visualisation. Distances in Å, highlighted by red dashes. Images generated by Joseph Hilton-Proctor..... 19

Figure 7. Bromodomain phylogenetic tree highlighting each group and including KIAA2026. N.B. This tree shows 62 bromodomains. Reprinted with permission from Smith SG, Zhou MM. The Bromodomain: A New Target in Emerging Epigenetic Medicine. ACS Chem Biol. 2016;11(3):598-608. Copyright 2016 American Chemical Society.¹²⁷20

Figure 8. Schematics of identical BCPs. [A] CBP and EP300. These two BCPs share a high percentage of homology,¹²⁸ but are still considered separate. [B] The three isoforms of BRD4.¹²⁹ Only one isoform is counted due to the identical sequence of each isoform. TAZ, transcription adaptor putative zinc finger; KIX; kinase-inducible domain interacting domain; BD, bromodomain; PHD, plant homeodomain; HAT, histone acetyltransferase; ZZ, ZZ-type zinc finger; ET, extra-terminal domain; CTD, C-terminal domain.21

Figure 9. Comparison of bromodomains with ZA channel (green), shelf (orange) and gatekeeper (purple) residues highlighted. [A] BRD4 BD1 (PDB: 3UVW). The ‘reference’ bromodomain. The shelf has commonly been referred to as the ‘WPF shelf’ because of three amino acids that form it (Trp81, Pro82 and Phe83). [B] CBP (PDB: 3P1D). CBP possesses a good degree of similarity to BRD4 in all three segments, despite being in a different family. The change from a tyrosine to a leucine (Tyr81 to Leu1109) in the shelf opens the site for bulkier compounds.¹³⁶ [C] ATAD2 (PDB: 4QSS). The ZA channel of ATAD2 possesses a shorter sequence and multiple negatively charged residues (Asp1014, Asp1016 and Glu1017), while the shelf contains an arginine (Arg1007). The increased polarity and flexibility, and decreased depth of the binding pocket make ATAD2 more difficult to interact with.¹³³ [D] BRD9 (PDB: 5IGN). BRD9 also has a shorter ZA channel sequence, but it is less polar than ATAD2. The bulky gatekeeper residue (Tyr106) allows for π - π interactions, but restricts access to the shelf.¹³⁵ Images generated by Joseph Hilton-Proctor.22

Figure 10. Comparison of (+)-JQ1 (yellow, PDB: 3MXF) and I-BET762 (purple, PDB: 3P5O). [A, B] Chemical structures. [C, D] X-ray crystal structures of each compound bound to BRD4 BD1. Water molecules shown as red spheres. Pro86, Val87 and Asp88 were hidden for better visualisation. Distances in Å, highlighted by red dashes.24

Figure 11. Reported inhibitors that have been used in the association between bromodomain inhibition and disease.....31

Figure 12. Structure of the fusion oncoprotein BRD4-NUT.^{226, 227}32

Figure 13. Schematic of the perpetual acetylation of chromatin by EP300 and the recruitment of BRD4-NUT to hyper-acetylated chromatin.²³⁹34

Figure 14. Bromodomain fragments grouped by author with values reported.43

Figure 15. Compounds elaborated from known fragments with binding or inhibition values reported. [A] Starting fragment. [B] Reported inhibitors.50

Figure 16. Known X-ray crystal structures of NMP bound to bromodomains. Water molecules shown as red spheres. Distances in Å, highlighted by red dashes.52

Table of Tables

Table 1. Reported definitions of epigenetics before 1994.6

Table 2. List of histone PTMs and their respective functions.^{98,99}17

Table 3. Types of cardiovascular diseases.29

Copyright Notice

© Joseph Phillip Hilton-Proctor (2018).

I certify that I have made all reasonable efforts to secure copyright permissions for third-party content included in this thesis and have not knowingly added copyright content to my work without the owner's permission.

Declaration

This thesis contains no material which has been accepted for the award of any other degree or diploma at any university or equivalent institution and that, to the best of my knowledge and belief, this thesis contains no material previously published or written by another person, except where due reference is made in the text of the thesis.

Signature:



Print Name: Joseph Phillip Hilton-Proctor

Date: 30/11/18

Acknowledgements

I would first like to extend my gratitude to my supervisors Prof. Philip Thompson and Prof. Martin Scanlon for allowing me the opportunity to undertake this project, as well as the Milestone panel members, Dr. David Manallack and Dr. Shane Devine, for allowing me to continue with this project.

I especially wish to thank Prof. Philip Thompson, who has dedicated an enormous amount of time and effort into providing assistance and feedback over the duration of this project.

I would like to thank the members of Lab 4.133, in particular, Dr. Simon Mountford, Dr. Jo-Anne Pinson, Dr. Nicholas Barlow and many other PhD and Honours students of past and present for their collective contribution and synthesis advice in this project.

I would like to thank Dr. Olga Ilyichova and Dr. Ian Jennings for creating the X-ray crystal structures and electron density maps that have become an integral piece, not just for this project, but also for future work. I would also like to thank Dr. Ian Jennings, Dr. Zhaohua Zheng and Ali Noor for their collaborative work on the BRD4 BD1 bioassays.

Finally, I wish to thank my family for their everlasting support during such a tumultuous time. I especially wish to thank my mother, Sallie-Ann Proctor, who took the time to support me during my journey around the world to present this work.

This page and these words alone cannot truly express how grateful I am for all your help. Thank you.

This work was supported by a Research Training Program scholarship from the Monash Institute of Pharmaceutical Sciences and a Cancer Council Victoria Venture Grant. This research was undertaken in part using the MX2 beamline at the Australian Synchrotron, part of ANSTO, and made use of the Australian Cancer Research Foundation (ACRF) detector.

Abstract

Epigenetics has emerged as a prominent field for drug discovery. Bromodomains have been exemplary targets, with the development of compounds that have affirmed their link to certain diseases. The development of bromodomain inhibitors has also been the subject of varied strategic techniques in drug discovery and development, with fragment-based drug design being employed widely. Strategic and technical approaches to fragment-based drug design in bromodomain inhibitor discovery are also the subject of this thesis.

N-Methylpyrrolidone is a well-known solvent that has been shown to mimic acetyl-lysine. This knowledge has been used to develop other high-affinity warheads, including dimethylisoxazoles and dihydroquinoxalinones, but the original chemotype has yet to be directly elaborated in the same manner.

Firstly, *N*-Methylpyrrolidone was modified to allow the preparation of a versatile set of analogues that could be utilised in fragment-based drug design. Two mesylate derivatives were then coupled to a tetrahydropyridoinolone scaffold as potential mimics of the reported bromodomain inhibitor, Olinone. These products showed comparable affinity to Olinone itself in the first bromodomain of bromodomain-containing protein 4 and X-ray crystallography showed the preservation of key interactions between Olinone and the bromodomain. These results support the utilisation of the elaborated fragments in other settings.

Secondly, a phenyl group was initially attached to *N*-methylpyrrolidone, which afforded a “new” racemic fragment that retained the ligand efficiency of *N*-methylpyrrolidone. This fragment was derivatised using electrophilic aromatic substitution, bromination/cross-coupling and enantiomeric separation to yield a derivative with an IC₅₀ of 14.1 μM. Interestingly, X-ray crystallography revealed an unusual binding pose with the catechol ether acting as the mimetic in place of *N*-methylpyrrolidone. This shows the importance of X-ray crystallography in the

fragment-based drug design process, but the new compound presents as a lead that may be further pursued.

Thirdly, the 5-methyl-3-aryl-1*H*-pyrazole fragment was examined as a potential isostere to other bromodomain-binding heterocycles, which include dimethylisoxazoles and methyltriazoles. To examine its potential as a bromodomain ligand, a series of substituted pyrazoles were synthesised as part of a “poised” fragment library, employing a simple set of reactions from readily available reagents. Using a simple two-step scheme, 15 pyrazoles with diverse aryl substitutions were synthesised. Given the synthetic instability of certain phenol-containing compounds, a modified – but still efficient – four-step scheme was also employed, which yielded six additional pyrazoles. Subsequent assays with the first bromodomain of bromodomain-containing protein 4 identified compounds with improved affinity and good ligand efficiency. One compound in particular – a dimethylphenol derivative – displayed an unexpected, but not entirely unprecedented, binding mode in X-ray crystallographic studies. Similar to the above, these products represent interesting starting points for further elaboration. Collectively, these studies have shown that fragment elaboration from simple, low-affinity fragments to moderately potent, ligand efficient lead compounds can be achieved and that synthetic approaches can and should be utilised as a basis for compound novelty and library design. Bromodomain-containing protein 4 is a validated therapeutic target, but these approaches could equally be applied to other bromodomain targets, especially those where *N*-methylpyrrolidone has been co-crystallised, but others for which fragment-based drug design has not yet been attempted.

Chapter 1 – History of Epigenetics, Bromodomains and Their Inhibitors

Abbreviations

5mC	5-methylcytosine
Ago-2	Argonaute-2
AID	Activation-induced Cytosine Deaminase
AIDS	Acquired Immune Deficiency Syndrome
AlkB	Alpha-ketoglutarate-dependent Dioxygenase
AlphaScreen	Amplified Luminescence Proximity Homogeneous Assay Screen
AML	Acute Myeloid Leukemia
ApoA1	Apolipoprotein A1
APOBEC	Apolipoprotein B mRNA Editing Enzyme, Catalytic Polypeptide-like
ART	Antiretroviral Therapy
ATAD2	ATPase Family, AAA Domain-containing Protein 2
AUC	Area Under the Curve
BAZ2	Bromodomain Adjacent To Zinc Finger Domain 2
Bcl-2	B-cell Lymphoma 2
BCP	Bromodomain-containing Protein
BD#	Bromodomain #
BET	Bromodomain and Extra-terminal Domain
BPV	Bovine Papillomavirus
BRD#	Bromodomain-containing Protein #
BRPF1	Bromodomain and PHD Finger-containing Protein 1
CBP	Cyclic AMP Response Element Binding Protein Binding Protein
CDK9	Cyclin-dependent Kinase 9
CD#	Cluster of Differentiation #
CECR2	Cat Eye Syndrome Chromosome Region, Candidate 2
C _{max}	Maximum Serum Concentration
CTD	C-terminal Domain

CYP	Cytochrome P450
DMF	Dimethylformamide
DMSO	Dimethyl Sulfoxide
DNA	Deoxyribonucleic Acid
DNMT#	DNA Methyltransferase #
dsRNA	Double-stranded RNA
EP300	E1A Binding Protein P300
ET	Extra-terminal
FA	Fluorescence Anisotropy
FBDD	Fragment-based Drug Design
GCN5	General Control of Amino Acid Synthesis 5
H#K#	Histone # Lysine #
HAT	Histone Acetyltransferase
HDL	High-density Lipoprotein
HepG2	Hepatoma G2
HIV	Human Immunodeficiency Virus
HSQC	Heteronuclear Single Quantum Correlation
HTS	High-throughput Screening
IC ₅₀	Half Maximal Inhibitory Concentration
IgH	Immunoglobulin Heavy Chain
IL-6	Interleukin-6
IMiD	Immunomodulator
ITC	Isothermal Titration Calorimetry
JMJD6	Jumonji Domain-containing Protein 6
K-ac	Acetyl-lysine
K-bu	Butyryl-lysine
K-cr	Crotonyl-lysine
K-pr	Propionyl-lysine
kcal	Kilocalories
K _d	Dissociation Constant

K _i	Inhibitory Constant
LE	Ligand Efficiency
LRA	Latency Reversing Agent
MCAP	Mitotic Chromosome-Associated Protein
miR-204	MicroRNA 204
miRNA	MicroRNA
mRNA	Messenger RNA
ncRNA	Non-coding RNA
NFATc2	Nuclear Factor of Activated T Cells 2
NF-κB	Nuclear Factor Kappa-light-chain-enhancer of Activated B Cells
NMAD	N ⁶ -methyl Adenine Demethylase
NMC	NUT Midline Carcinoma
NMP	<i>N</i> -Methylpyrrolidone
NMR	Nuclear Magnetic Resonance
NSD3	Nuclear Receptor Binding SET Domain Protein 3
NUT	Nuclear Protein in Testis
OS	Overall Survival
p-TEFb	Positive Transcription Elongation Factor b
PCAF	p300/CBP-association Factor
PAH	Pulmonary Arterial Hypertension
PDB	Protein Data Bank
PFS	Progress-free Survival
PID	p-TEFb Interaction Domain
PTM	Post-translational Modification
RISC	RNA-induced Silencing Complex
RLC	RISC Loading Complex
RNA	Ribonucleic Acid
RNAi	RNA Interference
RNA Pol II	RNA Polymerase II
RNase #	Ribonuclease #

SAM	S-adenosyl Methionine
SAR	Structure-activity Relationship
SPR	Surface Plasmon Resonance
siRNA	Small Interfering RNA
STD	Saturation Transfer Difference
TAF1	Transcription Initiation Factor TFIID Subunit 1
Tat	Transactivator of Transcription
TAZ	Transcription Adaptor Putative Zinc Finger
Tet	Ten Eleven Translocation
TIP60	Tat Interactive Protein 60 kDa
TRIM24	Tripartite Motif-Containing Protein 24
TRBP	TAR RNA Binding Protein
WaterLOGSY	Water-Ligand Observed via Gradient Spectroscopy
WHO	World Health Organization

1.1 Defining Epigenetics

Over the past 70 years, interest in epigenetics has grown exponentially, not just in the usage of the word, but also what it entails, even to the point where it has been constantly re-defined to reflect all of this.

The term ‘epigenetics’ was first derived by Conrad Waddington in 1942 from the theory of ‘epigenesis’ when he used it to describe “the processes involved in the mechanism by which the genes of the genotype bring about phenotypic effects”, as well as the term ‘epigenotype’ to describe the development processes that linked the genotype and phenotype.¹

For over half a century after Waddington introduced the term, many researchers used ‘epigenetics’ to cover various topics. However, there was no consensus as to what ‘epigenetics’ truly portrayed during this period, particularly due to a second origin of epigenetics which, according to Haig, was what made epigenetics difficult to define.²

According to Boris Ephrussi, David Nanney also used this term in 1958 to describe “all mechanisms that regulate the expression of genetic potentialities, in contradistinction to the truly genetic mechanisms that regulate the maintenance of the structural information”,³ which was expanded upon in a separate report as “auxiliary mechanisms with different principles of operation are involved in determining which specificities are to be expressed in any particular cell” in relation to control systems in cells.⁴ However, Nanney originally coined the term ‘paragenetics’ to describe this, later changing it to ‘epigenetics’.

From this point until the early 1990s, the term ‘epigenetics’ was used in a broad sense to cover topics such as carcinogenic effects,⁵⁻⁸ cellular differentiation⁹⁻¹¹ and control systems,¹² while at the same time, taking on multiple wide-ranging meanings (Table 1). Susan Herring perhaps gave the most accurate summary of epigenetics during this time period when she stated that

epigenetics meant “whatever we want at the moment”, given the lack of agreement with the definition.¹³

Definition	Author	Year
“...the science of developmental process in general...”	Huxley ¹⁴	1957
“...the branch of biological science which deals with the causal analysis of development.”	Sherbet ¹⁵	1966
“...an expression of the genes affecting development.”	Berry et al. ¹⁶	1967
“Directed heritable alterations in phenotypic expression”	Meins et al. ¹⁰	1977
“Epigenetic carcinogens are defined as those that do not damage DNA but rather, act by indirect mechanisms.”	Williams ¹⁷	1983
“The changes in gene activity during development...”	Holliday ¹⁸	1987
“...heritable causal interactions between genes and their products during development that arise externally to a particular cell or group of cells and condition the expression of the cell's intrinsic genetic factors in an extrinsic manner.”	Cowley ¹⁹	1992
“...the dynamic interaction between the genome and its environment, and its study is the study of the mechanisms which effect ontogeny.”	Herring ¹³	1993

Table 1. Reported definitions of epigenetics before 1994.

In 1994, Holliday put forward two definitions to epigenetics to break this impasse. The first definition covered all types of deoxyribonucleic acid (DNA)-protein interactions, as well as changes on the DNA level: “the study of the changes in gene expression, which occur in organisms with differentiated cells, and the mitotic inheritance of given patterns of gene expression”. The second definition covered the transmission of information from one generation to another: “nuclear inheritance which is not based on differences in DNA sequence”. Both of these definitions were created in an attempt to cover all epigenetic processes known at the time. While they accomplished this, it was admitted that they only do so when both meanings were put together. As separate meanings, they were incomplete.²⁰

In 1996, the meaning of epigenetics was condensed further. Riggs et al. defined epigenetics as “the study of mitotically and/or meiotically heritable changes in gene function that cannot be explained by changes in DNA sequence”.²¹ Wu and Morris in 2001 also gave a similar meaning: “the study of changes in gene function that are heritable and that do not entail a

change in DNA sequence”,²² but made no reference to Riggs et al. Regardless, these definitions became the most commonly used in relation to epigenetics today.²³⁻²⁹ While there is some degree of consensus, a few people still had issues with the scope of epigenetics, particularly in relation to heritability.

Adrian Bird acknowledged the problem with having multiple known definitions of epigenetics in 2007, drawing attention to the rift between the definitions provided by Waddington and Riggs et al. and offered an alternative definition: “the structural adaptation of chromosomal regions so as to register, signal or perpetuate altered activity states”.³⁰ According to Bird, this definition includes a focus on chromosomes and genes, as well as the idea that epigenetic systems respond to changes created by certain events, such as a development switch in gene regulation, instead of establishing such a change.³⁰

In 2008, a meeting was hosted by the Banbury Conference Center and Cold Spring Harbor Laboratory to discuss the definition of ‘epigenetics’ and reach a consensus. As outlined by Berger et al., the proposed definition, “a stably heritable phenotype resulting from changes in a chromosome without alterations in the DNA sequence”, focused on the inheritance of a phenotype while discussing different signal types that covered a stable epigenetic state.³¹

Bonasio et al. also recognized the above meanings in 2010 and provided their own perspective. They labelled epigenetics more literally as “the inheritance of variation (“-genetic”) above and beyond (“epi-”) changes in the DNA sequence” while looking at epigenetic signals that altered a cell’s transcriptional state and heritability.³²

Lastly, in 2014, Jeffrey Mann also drew upon some of these recent definitions, pointing out that the previously-used term ‘epigenetic inheritance’ had the same meaning as ‘epigenetics’ in relation to inherited epigenetic states, thus rendering the ‘inheritance’ part redundant. A proposal was put forward to refer to these states as part of ‘memigenetics’, with the prefix

‘memi-’ being “a contraction of ‘memoepi-’, and therefore is intended to mean a ‘remembering’ of what is ‘over’”.³³

While many groups nowadays use the definition – exact or varied – provided by Riggs et al. and Wu et al., the debate still continues as to what fields epigenetics encompasses and what it excludes.

1.1.1 Dutch Hunger Winter

One of the key components that formed the definition of epigenetics is inheritance. The Dutch Hunger Winter is a commonly referenced example in history that demonstrates phenotypic inheritance across generations.

Between November 1944 and May 1945, near the end of World War II, a Nazi-occupied region of the Netherlands was blockaded, resulting in an extreme shortage of food supplies to the Dutch population. Adding to these woes was a winter period that arrived earlier and harsher than usual. Around 3.5 million people were affected by this famine to the point of surviving on less than 500 kilocalories (kcal) per day. In an active lifestyle, the average daily intake for a woman is 2,300 kcal, while a man requires 2,900 kcal. By the time food supplies were restored, more than 22,000 people had died.³⁴

While tragic, this famine created a unique study population where epidemiologists monitored the long-term effects of those who suffered from malnutrition. The main focus was the birth weight of children who were subjected to this period of time. If a mother was well-fed during conception, but malnourished for the last few months, the baby was born smaller than usual.³⁵ Conversely, if a mother was malnourished during conception but well-fed for the last few months, the baby was normal-sized.³⁶ After studying these babies for decades, their development was surprising. The babies who were born small had remained small and the rate of obesity was lower than the general population.³⁷ Even more strikingly, the normal-sized

babies not only had higher obesity rates,³⁸ but an increase in other health problems, including mental health.^{39, 40}

The Dutch Hunger Winter serves as a prime example of the inheritance aspect of epigenetics, as changes to our environment can shape us – and future generations – biologically, even when our genetic code remains the same.

1.2 Epigenetic Regulation

Epigenetic regulation is important for various biological processes. Using the definitions provided by Riggs et al. and Wu et al., there are three known ways the epigenome is regulated: DNA modification, RNA interference and histone post-translational modification.

1.2.1 DNA Modification

DNA modification is the alteration of DNA bases to regulate gene expression in animals and plants. So far, the only modified bases to have been reported are cytosine⁴¹ and adenine.⁴² Figure 1 shows the pathways of these modifications and their respective products.

The most studied modification to date is the methylation of cytosine to create 5-methylcytosine (5mC). The existence of 5mC can be traced back to as early as 1925 when Treat Johnson and Robert Coghill reported to have discovered it in tubercle bacillus as a hydrolysis product from tuberculinic acid.⁴³ However, Vischer et al. were unable to replicate this experiment.⁴⁴ Rollin Hotchkiss was able to confirm the presence of 5mC from a sample of calf thymus DNA in 1948 when he noted that a modified cytosine (“epicytosine”) had the absorption characteristics of cytosine and shared a similar absorption and mobility relationship to thymine and uracil.⁴⁵ It wasn’t until 1975 when, using different DNA methylation models, it became associated with gene regulation and differentiation in bacteria and other organisms.^{46, 47}

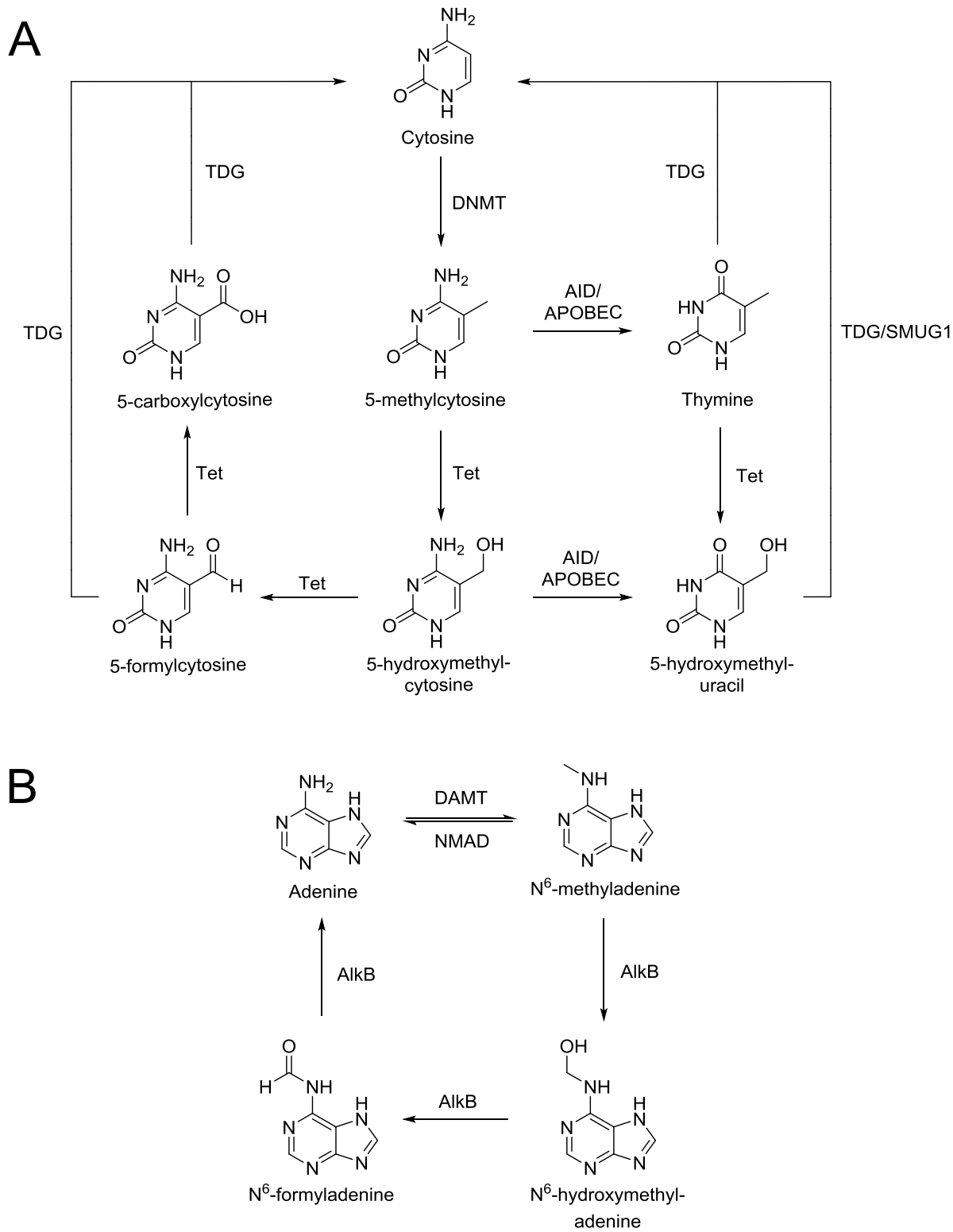


Figure 1. Simplified pathways of cytosine and adenine modification.^{48, 49} [A] DNMT enzymes methylate cytosine to give 5-methylcytosine. From here, 5-methylcytosine is demethylated through different mechanisms that involve three unique enzymes: ten eleven translocation (Tet)

enzymes, which add a hydroxyl group to the 5-methyl moiety and then oxidise it to a formyl and carboxyl group; activation-induced cytosine deaminase (AID) or apolipoprotein B mRNA editing enzyme, catalytic polypeptide-like (APOBEC) enzymes, which deaminate the amine; and TDG enzymes, which replace the modified base with a cytosine. [B] DNA adenine methyltransferase (DAMT) enzymes methylate adenine to give N⁶-methyladenine. The methyl group is then removed by either N⁶-methyl adenine demethylase (NMAD) enzymes or alpha-ketoglutarate-dependent dioxygenase (AlkB). The latter gives a hydroxyl and formyl intermediate before returning adenine to its original state.

DNA methylation is carried out by methyltransferase enzymes DNA methyltransferase 1 (DNMT1), 3A and 3B using *S*-adenosyl methionine (SAM) as the donor (Figure 2). DNMT1 is responsible for maintaining DNA methylating patterns during cell division,⁵⁰ while DNMT3A and 3B are *de novo* methyltransferases which determine the pattern and extent of DNA methylation during foetal development.⁵¹ This modification is important for functions which include X chromosome inactivation⁴⁶ and genomic imprinting.⁵²

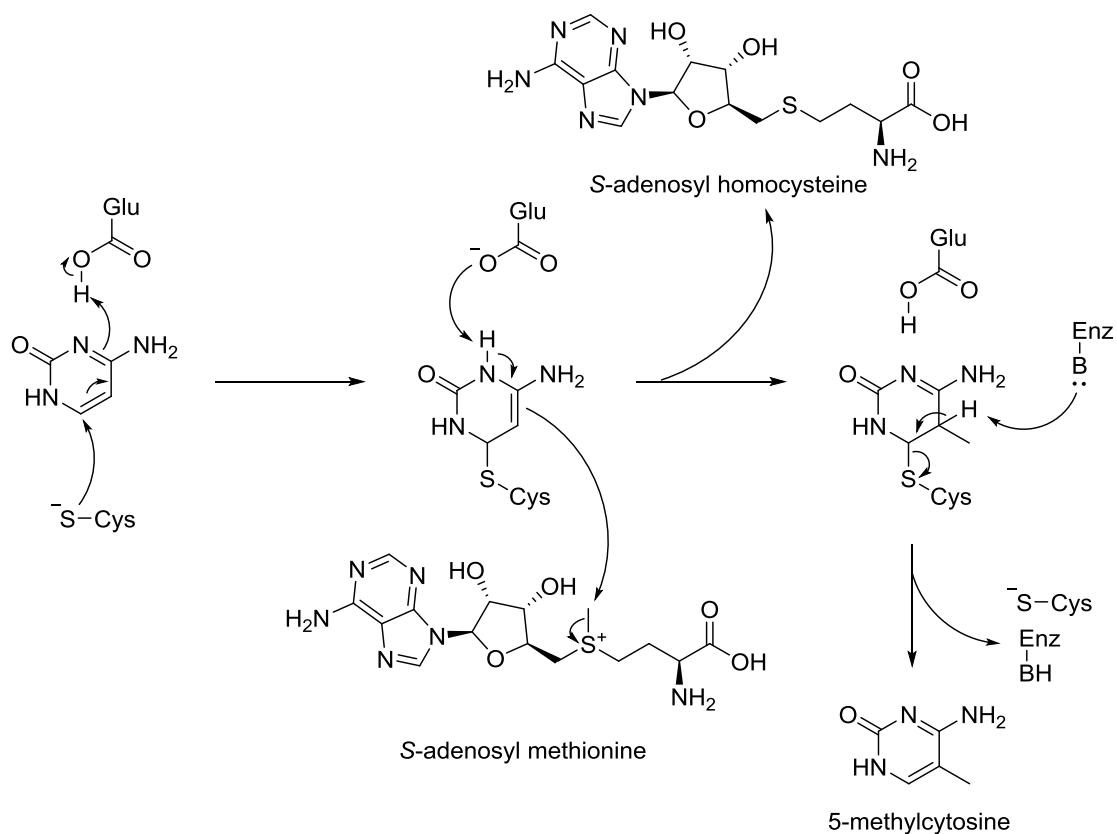


Figure 2. Detailed mechanism of the transfer of a methyl group from SAM to cytosine to give 5mC.

1.2.2 RNA Interference

RNA interference (RNAi) is the process of converting non-coding RNA (ncRNA) molecules to inhibit gene expression and translation through the degradation of specific messenger RNA (mRNA). The first instances of RNAi were discovered in the early 1990s in plants⁵³ and fungi⁵⁴ where it was originally referred to as “co-suppression” and “quelling”, respectively. The first successful application of RNAi was reported in 1998 by Fire *et al.*⁵⁵ through injecting double-stranded RNA (dsRNA) in *C. elegans* to interfere with RNA transcripts.

RNAi is triggered by dsRNA that is cleaved via the ribonuclease (RNase) III endonuclease Dicer⁵⁶ to create small interfering RNA (siRNA) molecules of approximately 25 nucleotides in length. These molecules are then taken up into the RNA-induced silencing complex

(RISC) by the RISC Loading Complex (RLC), which consists of Dicer complexed with TAR RNA binding protein (TRBP) and the Argonaute cleavage protein Argonaute-2 (Ago-2).⁵⁷ Once loaded, Ago-2 cleaves off one of the siRNA strands (the passenger strand) which is then degraded. The other strand (the guide strand) is retained, activates the RISC and seeks out mRNA with sequences that match the guide strand. Once a complementary strand is found, the mRNA is cleaved by Ago-2⁵⁸ and the expression of the gene related to the mRNA is silenced (Figure 3). The biological role of RNAi is that of a defence mechanism for preventing viral infections,^{59, 60} but over time, RNAi became an integral tool for determining gene function^{61, 62} and is being explored as a therapeutic option.^{63, 64}

1.2.3 Histone Modification

Histones are alkaline proteins that are a key component of chromatin. These proteins are found inside eukaryotic cells and act as ‘spools’ to compact long strands of DNA. There are five known types of histones. Four of these (H2A, H2B, H3, H4) exist as dimers. Together with 145-147 base pairs of DNA, they make up one nucleosome.⁶⁵ The fifth histone unit (H1) acts as a linker histone which resides outside of the nucleosome.⁶⁶ Together with 10-80 base pairs of DNA, it connects two nucleosomes via the DNA entry and exit sites of the nucleosome to produce a higher-order chromatin structure called the chromatosome (Figure 4).⁶⁷ The four histone dimers possess exposed residue tails that undergo a variety of post-translational modifications (PTMs) that include mitosis,⁶⁸ transcriptional regulation,⁶⁹⁻⁷¹ and DNA repair.⁷² DNA and histones exist in a negatively – and positively – charged state, respectively. Certain modifications, such as acetylation and citrullination, have the capacity to neutralise the positive charge on histones. The loss of this charge weakens the association between histones and DNA, relaxing the chromatin structure and increasing accessibility for transcriptional machinery.⁷³

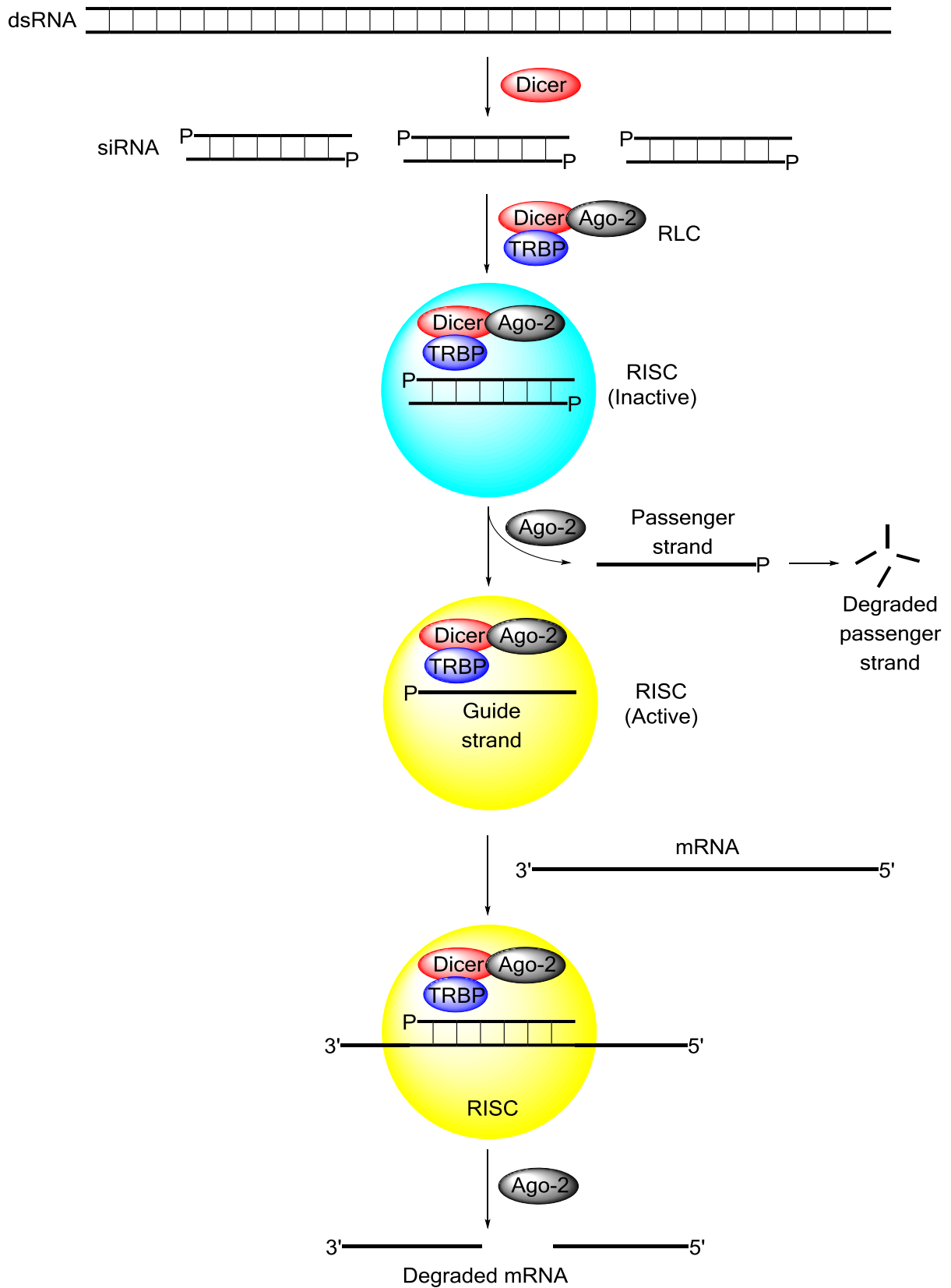


Figure 3. The RNAi pathway, showing the generation of siRNA molecules from dsRNA to be taken up by the RISC, which is then used to cleave mRNA and silence gene expression. dsRNA, double-stranded RNA; siRNA, small interfering RNA; Ago-2, argonaute-2; TRBP, TAR RNA binding protein; RISC, RNA-induced silencing complex; mRNA, messenger RNA.

1.2.4 The Histone Code

The observation of complex combinations of modifications on histone residues has led to the hypothesis that these modifications are responsible for modulating the state of chromatin and the downstream effects associated with it. This hypothesis has been called the “histone code”⁷⁴ and it has led to the idea that three protein families are responsible for its governance. The first family of proteins catalyse the transfer of a functional group from a donor substrate and attach it to an exposed residue tail. The second family recognizes the modified residue and mediates the aforementioned downstream effects. The third family catalyses the removal of the moiety from the residue and returns it to its original state (Figure 5). Lysine acetylation and methylation were among the first PTMs to be discovered in 1964.⁷⁵ Since then, many more PTMs have been uncovered.⁷⁶⁻⁷⁹ Even to this day, the list of known PTMs is gradually expanding. Table 2 lists a majority of these modifications including their general functions. In this work, the main focus will be on the ‘readers’ of acetyl-lysine (K-ac): the bromodomain.

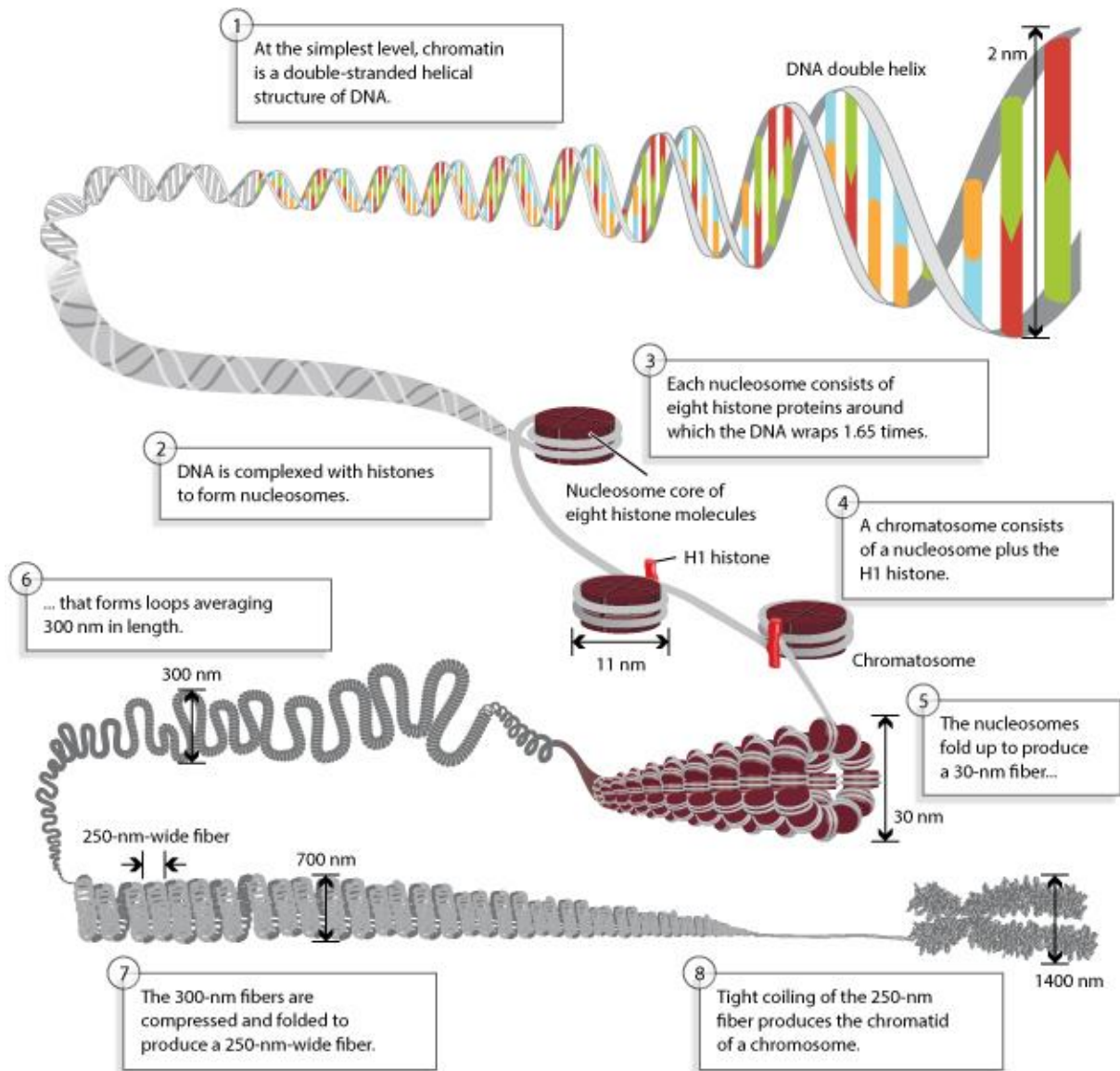


Figure 4. Composition and condensation of DNA and histones into a chromosome.⁸⁰ Double-stranded DNA is coiled around eight histone proteins to create nucleosomes. An extra H1 histone gives a chromatosome. These undergo several levels of compression, folding and coiling to produce a chromosome. © 2013 Nature Education. Adapted from Pierce, Benjamin. Genetics: A Conceptual Approach, 2nd ed. All rights reserved.

Modification	Residue(s) Affected	Function(s)
Acetylation	Lysine Serine Threonine	Chromatin remodelling ⁸¹ DNA repair ⁸² DNA replication ⁸³
Propionylation	Lysine	Transcriptional activation ⁸⁴
Butyrylation	Lysine	Transcriptional activation ⁸⁴
Crotonylation	Lysine	Transcriptional activation ⁸⁵
2-Hydroxyisobutyrylation	Lysine	Associated with transcription and translation processes ⁸⁶
Malonylation	Lysine	Cellular metabolism ⁸⁷
Succinylation	Lysine	Cellular metabolism ⁸⁷
Glutarylation	Lysine	Cellular metabolism ⁸⁷
Methylation	Lysine Arginine	Transcriptional activation ⁸⁸ Transcriptional repression ⁸⁹
Formylation	Lysine	Loss of protein function ⁹⁰
Phosphorylation	Serine Threonine Tyrosine Histidine	Transcriptional activation ⁹¹ DNA repair ⁹² Apoptosis ⁹³
Ubiquitination	Lysine	Transcriptional activation ⁹⁴
SUMOylation	Lysine	Transcriptional repression ⁹⁵
ADP ribosylation	Glutamate Lysine	DNA repair ⁹⁶ Cell cycle regulation ⁹⁶
Citrullination/Deimination	Arginine	Transcriptional repression ⁹⁷

Table 2. List of histone PTMs and their respective functions.^{98, 99}

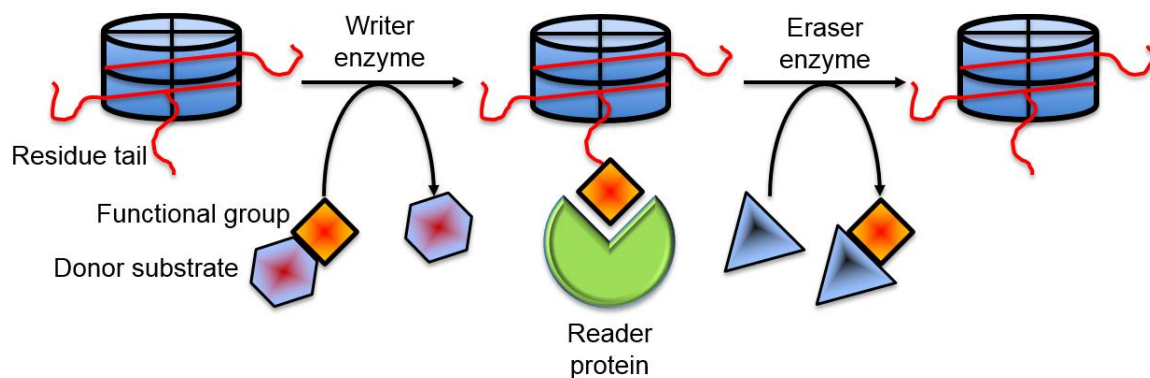


Figure 5. General schematic of the attachment of a functional group by writer enzymes, the recognition of the modified tail by reader proteins, and the removal of a functional group by eraser enzymes on histones.

1.3 Bromodomain Structure

The bromodomain was first identified in 1992 by Tamkun et al.¹⁰⁰ and named after the *Drosophila* gene *brahma*. Since then, it has been recognized in a wide variety of proteins including methyltransferases,¹⁰¹ acetyltransferases,¹⁰²⁻¹⁰⁴ chromatin remodelling complexes,¹⁰⁵⁻¹⁰⁷ and transcriptional regulators¹⁰⁸⁻¹¹¹ in multiple organisms including humans, yeast¹¹² and parasites.^{113, 114}

The three-dimensional structure of the bromodomain was first revealed by Dhalluin et al.¹¹⁵ in the histone acetyltransferase (HAT) protein p300/CBP-association factor (PCAF) through nuclear magnetic resonance (NMR) experiments. The bromodomain consists of a set of four α -helices (αZ , αA , αB , αC) arranged in a left-hand twist, which are connected by two interhelical loops (ZA, BC) with a cavity formed by the loops. This cavity is the binding pocket where modified lysine residues bind (Figure 6 and Appendix A). Originally, bromodomains were observed to bind K-ac, but a select few were also found to bind propionyl-lysine (K-pr),¹¹⁶ butyryl-lysine (K-bu)^{116, 117} and crotonyl-lysine (K-cr)¹¹⁷ residues. There are four or five water molecules that form the base of the pocket with the added support of a “backstop” residue.¹¹⁸ The primary interactions between K-ac and the bromodomain are a direct hydrogen bond with the side chain of a highly conserved asparagine residue, and a water-mediated hydrogen bond with a conserved tyrosine residue.^{119, 120} The bromodomain-containing proteins (BCPs) that have been discovered are grouped into eight families based on their structural and sequential similarities.¹²¹ While bromodomains can span between 90-120 amino acids, their three-dimensional structure remains comparatively consistent.

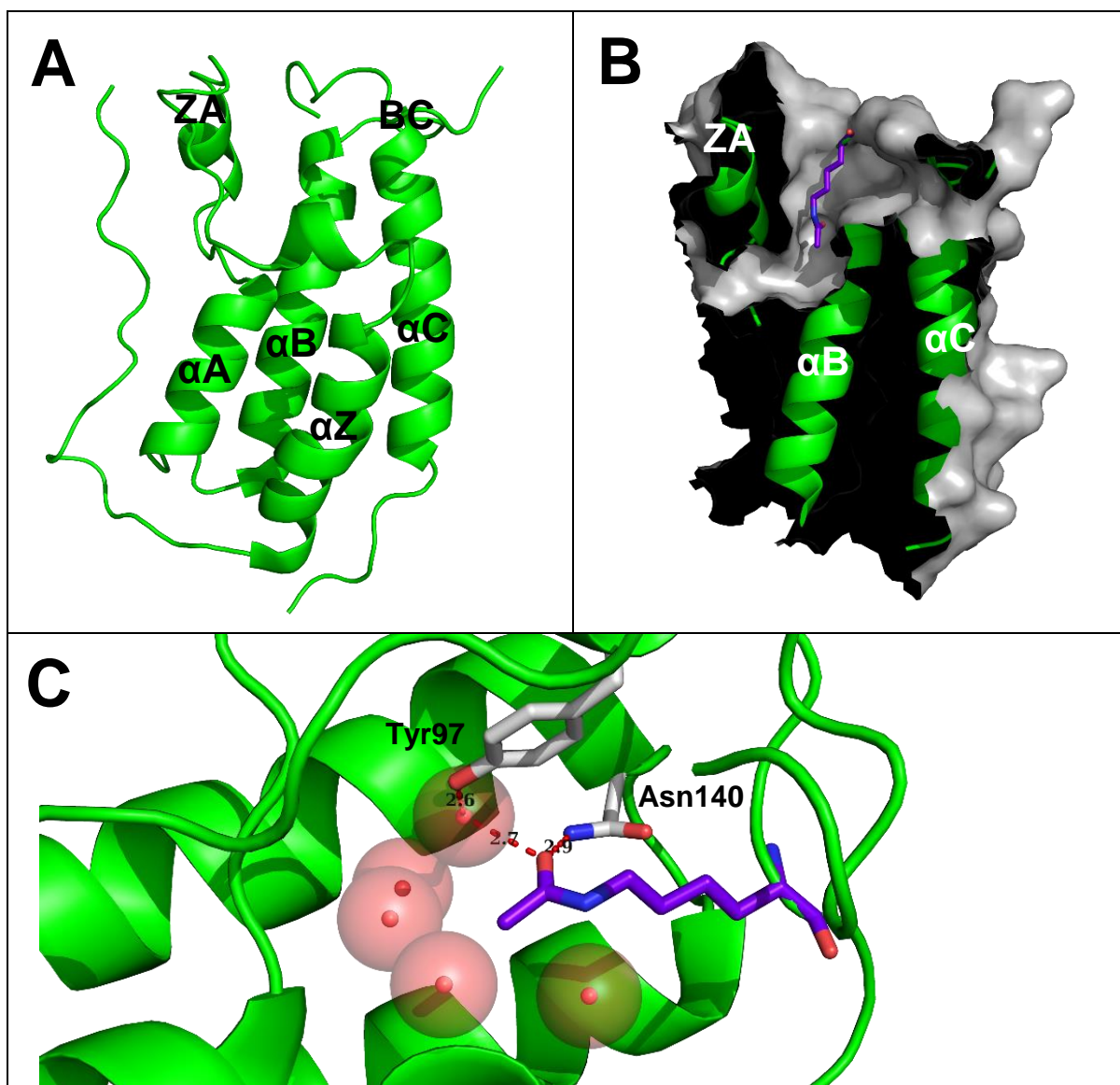


Figure 6. X-ray crystal structure of BRD4 BD1 (PDB: 3UVW). [A]. α -helices and loops shown. [B] Cutaway view to show the cavity. [C] Close-up of the binding pocket with the interactions between K-ac (purple blue) and the conserved Asn140 and Tyr97 (white) shown. Water molecules shown as red spheres. Pro86, Val87 and Asp88 were hidden for better visualisation. Distances in Å, highlighted by red dashes. Images generated by Joseph Hilton-Proctor.

The reported number of bromodomains in humans is 61 bromodomains in 46 different proteins (Figure 7).¹²¹⁻¹²³ However, this excludes the relatively-unknown protein KIAA2026,¹²⁴ which only exists as an entry in the human gene database, as well as certain protein isoforms. For example, there are two known isoforms of bromodomain-containing protein 3 (BRD3)¹²⁵ and

three known isoforms of BRD4,¹²⁶ but only one of each is counted, possibly due to each group of isoforms sharing the same sequence from the first amino acid to after the second tandem bromodomain (Figure 8).

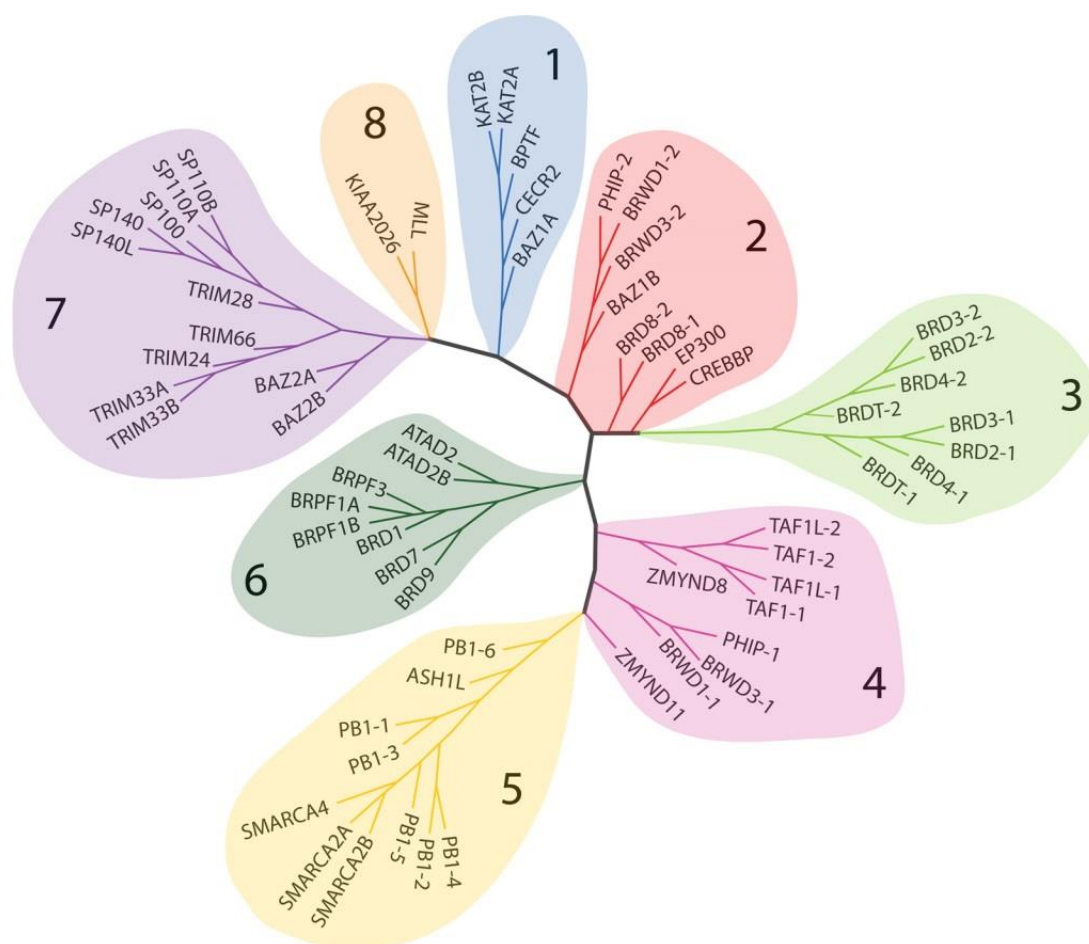


Figure 7. Bromodomain phylogenetic tree highlighting each group and including KIAA2026. N.B. This tree shows 62 bromodomains. Reprinted with permission from Smith SG, Zhou MM. The Bromodomain: A New Target in Emerging Epigenetic Medicine. ACS Chem Biol. 2016;11(3):598-608. Copyright 2016 American Chemical Society.¹²⁷

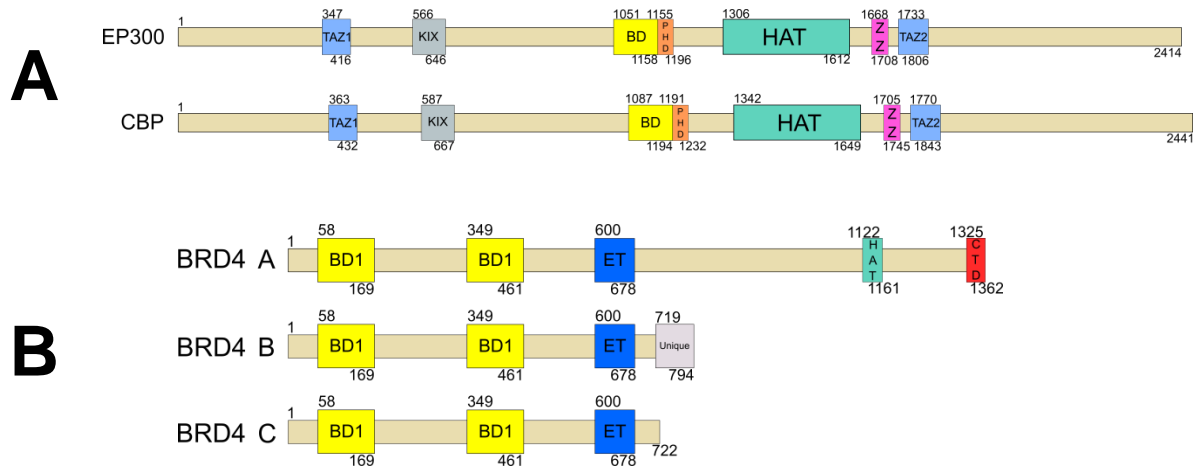


Figure 8. Schematics of identical BCPs. [A] CBP and EP300. These two BCPs share a high percentage of homology,¹²⁸ but are still considered separate. [B] The three isoforms of BRD4.¹²⁹ Only one isoform is counted due to the identical sequence of each isoform. TAZ, transcription adaptor putative zinc finger; KIX; kinase-inducible domain interacting domain; BD, bromodomain; PHD, plant homeodomain; HAT, histone acetyltransferase; ZZ, ZZ-type zinc finger; ET, extra-terminal domain; CTD, C-terminal domain.

There are three features that contribute to the binding selectivity between each bromodomain. The first feature is the ZA channel, which is formed by the ZA loop just outside the binding pocket.^{130, 131} This area can contain its own network of structural water molecules. The second aspect is a shelf that lies adjacent to the ZA channel. This is often referred to as the WPF shelf, given its name from the three amino acids that form it in human bromodomain and extra-terminal domain (BET) bromodomains, although the residues are not conserved among other bromodomains.¹³² The differences in these residues affect the polarity and flexibility of the binding site. For example, the shelf of the first bromodomain of BRD (BRD4 BD1) consists of Trp81, Pro82 and Phe83, making it rigid and non-polar. In comparison, the shelf of ATPase family, AAA domain-containing protein 2 (ATAD2) is more flexible and polar because of the arginine and valine residues that are in place of the tryptophan and proline residues.¹³³ The third feature is a single non-conserved residue called the ‘gatekeeper’ which is positioned at

the start of the α C-helix. This residue defines the shape of the binding site and can affect the conformation of certain ligands.¹³⁴ Bromodomains such as cyclic AMP response element binding protein binding protein (CBP) and BRD4 have a small residue such as an isoleucine or valine that serves as a gatekeeper. Bromodomains such as BRD9 possess a bulkier residue such as a tyrosine, which prevents access to the shelf (Figure 9).¹³⁵

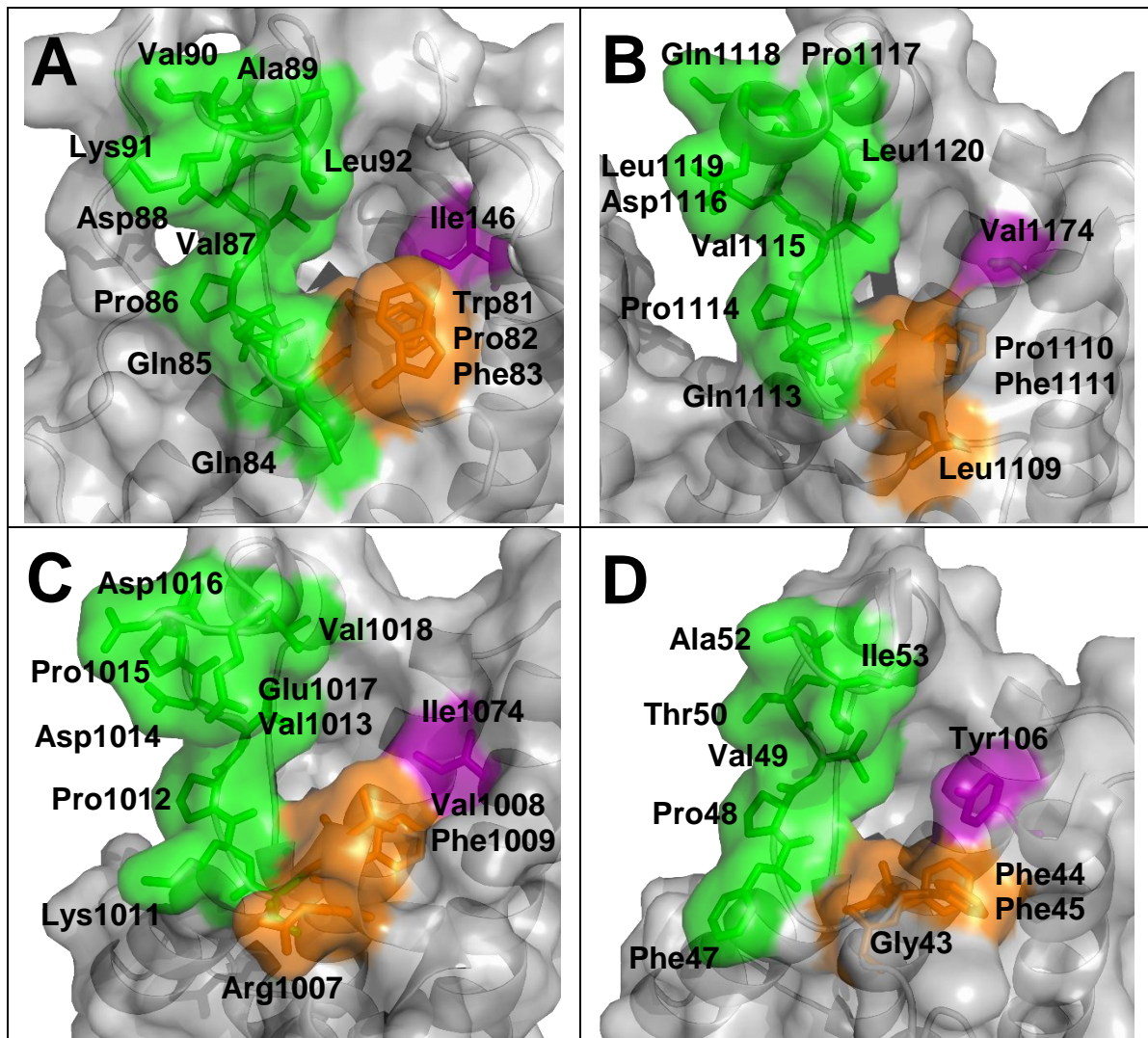


Figure 9. Comparison of bromodomains with ZA channel (green), shelf (orange) and gatekeeper (purple) residues highlighted. [A] BRD4 BD1 (PDB: 3UVW). The ‘reference’ bromodomain. The shelf has commonly been referred to as the ‘WPF shelf’ because of three amino acids that form it (Trp81, Pro82 and Phe83). [B] CBP (PDB: 3P1D). CBP possesses a good degree of similarity to BRD4 in all three segments, despite being in a different family.

The change from a tyrosine to a leucine (Tyr81 to Leu1109) in the shelf opens the site for bulkier compounds.¹³⁶ [C] ATAD2 (PDB: 4QSS). The ZA channel of ATAD2 possesses a shorter sequence and multiple negatively charged residues (Asp1014, Asp1016 and Glu1017), while the shelf contains an arginine (Arg1007). The increased polarity and flexibility, and decreased depth of the binding pocket make ATAD2 more difficult to interact with.¹³³ [D] BRD9 (PDB: 5IGN). BRD9 also has a shorter ZA channel sequence, but it is less polar than ATAD2. The bulky gatekeeper residue (Tyr106) allows for π - π interactions, but restricts access to the shelf.¹³⁵ Images generated by Joseph Hilton-Proctor.

While the binding pocket itself is seen as a desirable target for small molecule inhibitors, the above features can impact the druggability of the bromodomain.¹³⁷ However, paying particular attention to these details can assist in obtaining the desired selectivity between bromodomains.

1.4 (+)-JQ1 and I-BET762 – The First BET Bromodomain Ligands

The main goal for targeting a bromodomain is to block K-ac from binding to it. The first compounds to be described that achieve this in a potent and selective manner were (+)-**JQ1**¹³⁸ and **I-BET762**.¹³⁹ Despite being developed by separate groups using different methods, both compounds were published in the same issue of Nature^{138, 139} and possess similar features: a methyltriazolodiazepine scaffold with a stereogenic centre. Both of these compounds bind to BRD4 in the same manner: the methyltriazole portion of each molecule acts as the K-ac mimetic to prevent K-ac from binding to the bromodomain (Figure 10).

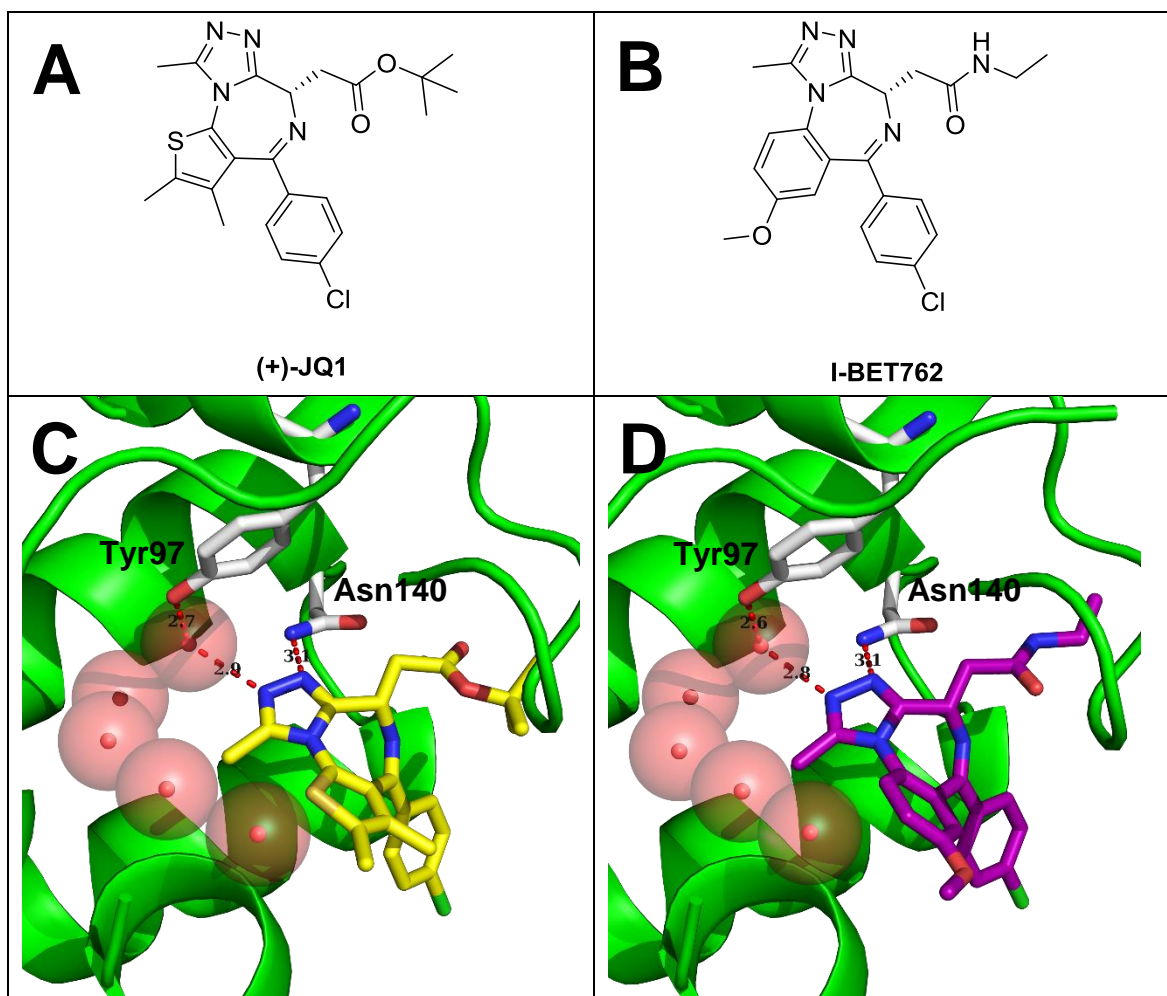


Figure 10. Comparison of (+)-**JQ1** (yellow) (PDB: 3MXF) and **I-BET762** (purple) (PDB: 3P5O). [A, B] Chemical structures. [C, D] X-ray crystal structures of each compound bound to BRD4 BD1. Water molecules shown as red spheres. Pro86, Val87 and Asp88 were hidden for better visualisation. Distances in Å, highlighted by red dashes.

Filippakopoulos et al. designed (+)-**JQ1** as a “prototype ligand” based on molecular modelling efforts with BRD4 BD1, with the methyltriazolodiazepine scaffold being selected from a patent filed by Mitsubishi Tanabe Pharma.¹⁴⁰ The *t*-butyl ester group was selected for two purposes: to allow pendant group diversity and to mitigate binding to the central benzodiazepine receptor. Isothermal titration calorimetry (ITC) experiments revealed that (+)-**JQ1** had bound to the majority of bromodomains in the BET family with dissociation constant (K_d) values in the nanomolar range ($K_d = 49 - 190$ nM), while in amplified luminescence proximity

homogeneous assay screens (AlphaScreens) with a tetra-acetylated histone H4 peptide, (+)-**JQ1** recorded IC₅₀ values of 77 nM and 33 nM for BRD4 BD1 and BD2, respectively.¹³⁸

Despite its affinity, (+)-**JQ1** has not been submitted for clinical trials. While (+)-**JQ1** did possess some favourable pharmacokinetic aspects in cluster of differentiation 1 (CD1) mouse models such as oral bioavailability (F = 49%), peak plasma concentration (C_{max} = 1180 ng/mL) and drug exposure (AUC = 2090 hr*ng/mL), its main drawback was the relatively low half-life (0.9 hr intravenous, 1.4 hr oral). In spite of this, it has been extensively tested as a probe and remains the most studied bromodomain inhibitor to date. (+)-**JQ1** has been tested to showcase bromodomains as a potential target for human immunodeficiency virus (HIV),¹⁴¹⁻¹⁴⁵ cardiovascular diseases,¹⁴⁶⁻¹⁴⁸ inflammatory diseases,¹⁴⁹⁻¹⁵³ male contraception¹⁵⁴ and multiple types of cancer¹⁵⁵⁻¹⁶² (Mechanisms explained in Section 1.5.1).

Nicodeme et al.¹³⁹ used a phenotypic screening approach to develop **I-BET762** (alternate names: GSK525762A, molibresib). As reported by Mirguet et al.,¹⁶³ their approach started with an Apolipoprotein A1 (ApoA1) luciferase reporter in a human hepatoma G2 (HepG2) hepatocyte cell-line to screen for upregulators of reporter activity. This led to the identification of a benzodiazepine, which was used as a starting point for a medicinal chemistry-driven program to optimize the efficacy in the ApoA1 assay, while admitting to the lack of any knowledge of the target at the time. Pull-down experiments revealed that benzodiazepines were general binders of bromodomains.¹⁶⁴ Structure-activity relationship (SAR) optimizations focused around the benzodiazepine phenyl rings to improve inhibition and the carbamate to prevent hydrolysis at acidic pH. This work culminated in the development of **I-BET762**.

The pharmacokinetic properties of **I-BET762** were tested in four different species, compared to one in (+)-**JQ1**. Its oral bioavailability was seen as “moderate” in rats (F = 27%) but was higher in mice, primates and dogs (F = 61%, 52%, 44%, respectively). The half-life showed

the same spread, with rats showing the lowest half-life (0.5 hr), but was higher in the other animal models (1.5 hr in mice and primates, 5.9 hr in dogs). Additionally, it was seen to have low potential in inhibiting human Cytochrome P450 (CYP) isoforms.¹⁶³ Unlike (+)-**JQ1**, **I-BET762**, has been submitted for clinical trials. As this moment, it has been identified in seven clinical trials,¹⁶⁵⁻¹⁷¹ but only the Phase I trial for ‘Drug Interactions’ has been completed. Phase I/II trials for cancer, solid tumours and NUT midline carcinoma are still underway.

1.5 Post-(+)-JQ1 and I-BET762

After the publication of (+)-**JQ1** and **I-BET762**, there has been very significant interest in targeting bromodomains, not just for dealing with diseases, but also pinpointing their specific function where they are less well understood. A majority of the focus has been on the BET family of bromodomains, but this has gradually branched out into many other BCPs outside the BET family, including CBP and E1A Binding Protein P300 (EP300),^{128, 136, 172-175} ATAD2,^{176, 177} Bromodomain Adjacent To Zinc Finger Domain 2A/B (BAZ2A/B),^{178, 179} cat eye syndrome chromosome region, candidate 2 (CECR2),¹⁸⁰ BRD9,^{135, 181, 182} the bromodomain and PHD finger-containing protein (BRPF) family,¹⁸³ transcription initiation factor TFIID Subunit 1 (TAF1)¹⁸⁴ and tripartite motif-containing protein 24 (TRIM24).¹⁸⁵

1.5.1 About BRD4

BRD4 is a ubiquitously expressed transcriptional regulator, which was originally given the name mitotic chromosome-associated protein (MCAP) for its association with mitotic chromosomes and regulation of the cell cycle.¹⁰⁹ It belongs to a family of four similarly structured BCPs which are collectively known as the BET family, given that each protein contains two tandem bromodomains and an extra-terminal (ET) domain. Despite being the last human BCP in the BET family to be discovered chronologically, BRD4 has quickly become

one of the most studied BCPs today with over 350 PubMed entries; more than the other three BET proteins combined, and more than the majority of other BCPs.

There are three different isoforms of BRD4, all of which possess both bromodomains and the ET domain. The sequences between these isoforms from the first amino acid to after the ET domain seem to be completely identical. The HAT motif and C-terminal domain (CTD) are exclusive to the long isoform of BRD4, as the two shorter isoforms lack these regions (Figure 8).¹²⁶

The bromodomains of BRD4 recognize K-ac in both histone and non-histone proteins. In early immunoblotting assays, the most notable histone marks that bound to BRD4 were H3K14ac, H3K9K14(ac)₂ and H4K5K12(ac)₂.¹⁸⁶ However, there was no description as to whether either or both bromodomains recognized these histones. SPOT assays completed later by Filippakopoulos et al.¹²¹ revealed the interactions between individual bromodomains and different histone marks. Both bromodomains of BRD4 are known to recognize K310ac of RelA, a subunit of the inflammatory and immune response regulator nuclear factor kappa-light-chain-enhancer of activated B cells (NF-κB). This binding, in co-operation with the HAT protein EP300, co-activates the transcriptional activation of NF-κB.¹⁸⁷ BRD4 BD2 also participates in the binding of the positive transcription elongation factor b (p-TEFb) subunit Cyclin T1 through the recognition of three K-ac residues: K380ac, K386ac and K390ac.¹⁸⁸ This binding works in tandem with the CTD of BRD4, which will be explained later.

The ET domain mediates its own activation of transcription through binding to different effectors including nuclear receptor binding SET domain protein 3 (NSD3)^{189, 190} and jumonji domain-containing protein 6 (JMJD6).¹⁹¹ These effectors have been shown to contribute to the full activation of bovine papillomavirus 1 (BPV1) by BRD4 and the transcriptional regulation of BRD4-related target genes.¹⁸⁹

BRD4 was also found to have its own intrinsic HAT activity,¹⁹² but it has its own selectivity towards H3 and H4 histones compared to other HATs. BRD4 was found to acetylate K8, K5, K12 and K16 on histone H4 in decreasing order of preference, but not K14 or K56 of histone H3. The most striking revelation was that BRD4 acetylated H3K122, a modification known for causing histone eviction and nucleosome instability.¹⁹³ Through this modification, BRD4 was able to clear nucleosomes from chromatin.

The last domain of BRD4 is the CTD, which is sometimes called the p-TEFb interaction domain (PID), given that its main interaction is with p-TEFb.^{188, 194, 195} The interaction between the CTD of BRD4 and the p-TEFb subunit cyclin-dependent kinase 9 (CDK9) stimulates the kinase activity of p-TEFb which causes the phosphorylation of the RNA polymerase II (RNA Pol II) CTD,^{196, 197} which is needed for the recruitment of splicing factors.¹⁹⁸ Together with the binding between Cyclin T1 and BRD4 BD2, p-TEFb transcription becomes fully active. However, this binding is often in competition with the transactivator of transcription (Tat).¹⁹⁹

Before high-affinity ligands were reported and BRD4 became an appealing target, it was primarily associated with papillomaviruses,²⁰⁰⁻²⁰² small DNA viruses that are associated with warts and cervical cancer; and NUT midline carcinoma (NMC),^{203, 204} a rare but highly aggressive form of squamous cell carcinoma. Since then, BRD4 inhibition has been increasingly connected to other diseases, such as cardiovascular diseases, HIV, inflammatory diseases and various types of cancers.

1.5.2 Association with Disease States

Bromodomains and their respective proteins have been linked to many different diseases. The first ligands, (+)-**JQ1** and **I-BET762**, were used as probes to assess the therapeutic potential of inhibiting bromodomains. Since then, many more inhibitors have contributed to that knowledge. This section discusses how each disease is connected to bromodomain inhibition.

1.5.2.1 Cardiovascular Disease

Cardiovascular disease is a term used to describe various diseases that relate to the heart and blood vessels. Examples of these conditions are outlined in Table 3.

Cardiovascular disease is currently the leading cause of healthcare expenditure, hospitalization and mortality in the modern world with nearly 18 million deaths attributed to cardiovascular diseases in 2016, accounting for 31% of global deaths.²⁰⁵ Cardiovascular disease is also costly in Australia. During 2008-09, 10.4% (AU\$7.7 billion) of healthcare expenditure was attributed to cardiovascular diseases, the most out of all disease groups.²⁰⁶ This trend is expected to continue with costs rising to AU\$16.8 billion by 2022-23 and AU\$22.6 billion by 2032-33 based on 2008 projections.²⁰⁷ Cardiovascular disease also remains one of the major causes of death in Australia with 27-34% of all deaths related to cardiovascular diseases during 2008-17.²⁰⁸

Cardiovascular Disease Type	Definition
Coronary Artery Disease	Disease of the blood vessels supplying the heart
Heart Failure	Weakened blood flow to the body
Cardiomyopathy	Thickening, enlarging, or stiffening of the heart muscle which reduces the effectiveness of the heart
Congenital Heart Defect	Defects of the heart or blood vessels present at birth, which include
Peripheral Heart Disease	Disease of large arteries that supply blood to the peripheries
Cerebrovascular Disease	Disease of the blood vessels supplying the brain
Rheumatic Heart Disease	Disease that damages the heart valves caused by rhematic fever, which is caused by streptococcal bacteria

Table 3. Types of cardiovascular diseases.

There are many options available for the treatment of cardiovascular diseases, which include lifestyle changes, medication and surgery. A comprehensive list of available medication – including ACE inhibitors, β -blockers and statins – is covered by the Heart Foundation²⁰⁹ and American Heart Association.²¹⁰ Despite this level of intervention, the costs to finances and mortality still remain unreasonably high.

Bromodomain inhibition has been examined as another potential mechanism for treating cardiovascular diseases. However, only BET bromodomains – with the exception of BRDT – have been assessed so far. BET proteins were found to be expressed in cardiomyocytes, but only BRD4 expression was increased in response to phenylephrine-mediated hypertrophy.¹⁴⁶¹⁴⁷ This created a hyperactive state of p-TEFb which has been linked to previous hypertrophic conditions.^{211, 212} The effects stemming from this cardiac remodelling were remedied through inhibition with BET inhibitors (+)-**JQ1**, **I-BET762**, **I-BET151**, **PFI-1** and **RVX-208** (Figure 11). This could possibly be due to the disruption of binding between BRD4 BD2 and Cyclin T1, rendering p-TEFb transcription inactive.

Overexpression of BRD4 caused by the downregulation of microRNA 204 (miR-204), a microRNA (miRNA) biomarker in pulmonary arterial hypertension (PAH),²¹³ also led to a decrease in p21 and an increase in nuclear factor of activated T cells 2 (NFATc2), Survivin and B-cell Lymphoma 2 (Bcl-2),²¹⁴ which are known to be overexpressed in PAH.^{215, 216} Additionally, the proinflammatory cytokine interleukin-6 (IL-6) was overexpressed in a BRD4-dependent manner, triggering DNA damage in smooth muscle cells. Together, these events caused an imbalance of proliferative and apoptotic activities, which caused subsequent remodelling of the heart.²¹⁷ Upon treatment with (+)-**JQ1**, this balance was restored and the effects of PAH in those cells were resolved.

Some of these inhibitors have also been associated with the upregulation of ApoA1,^{163, 218, 219} an essential component of high-density lipoprotein (HDL) cholesterol, which has been linked to a decreased risk of atherosclerosis.²²⁰ While it is known that BRD4 inhibition – out of all four BET proteins – is solely responsible for the increase in ApoA1,^{164, 221} the exact mechanism that causes this increase is still yet to be determined.²²²

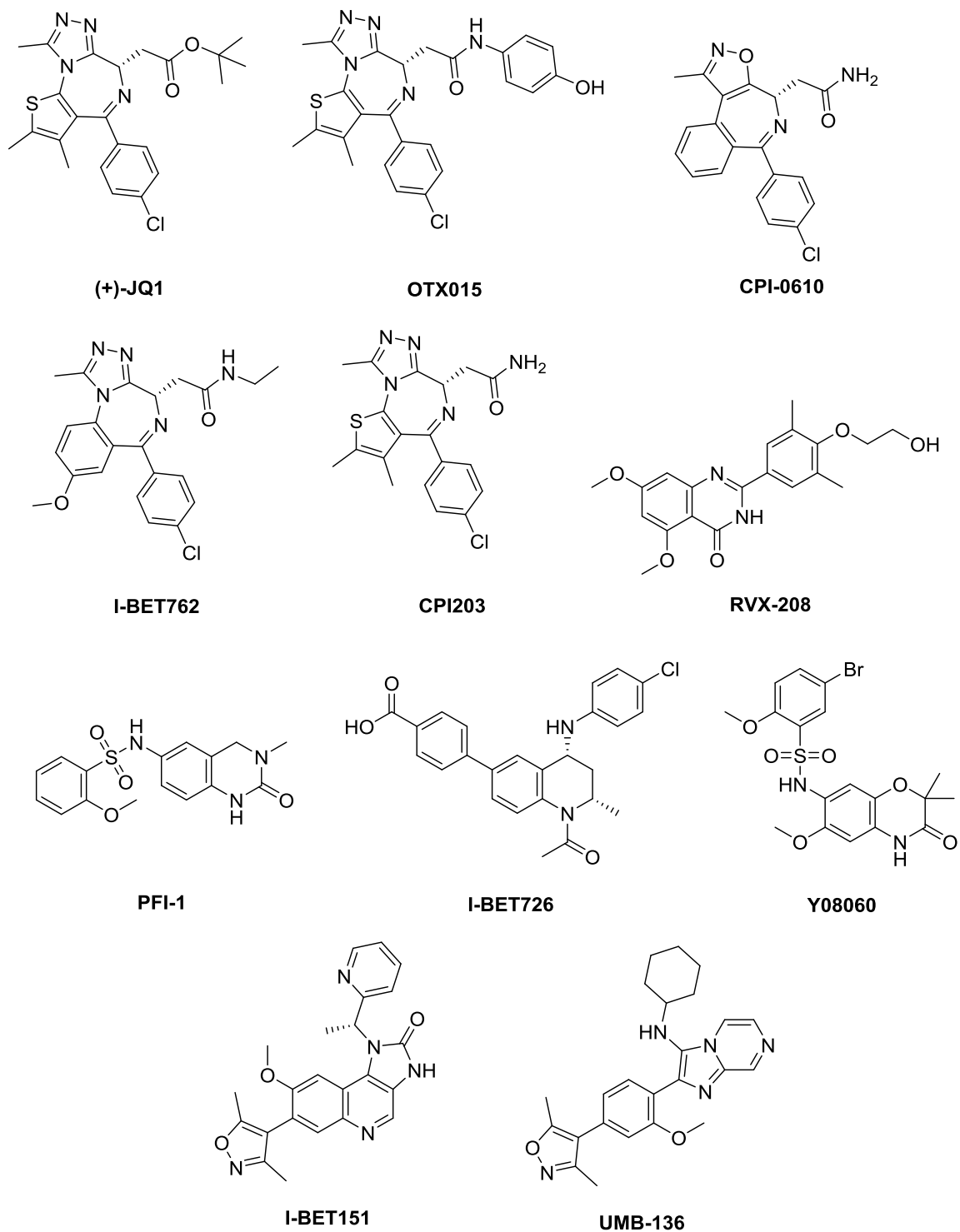


Figure 11. Reported inhibitors that have been used in the association between bromodomain inhibition and disease.

1.5.2.2 NUT Midline Carcinoma

NMC is a rare form of squamous cell carcinoma generated from a chromosome translocation. This translocation causes the fusion of nearly the whole length of nuclear protein in testis (NUT) (amino acids 6-1132) on chromosome 15 with another protein. Nearly 70% of the time, NUT fuses with BRD4 (amino acids 1-719) due to the t(15;19) chromosome translocation (Figure 12).²⁰³ Other proteins have been reported to fuse to NUT, including BRD3 on chromosome 9²²³ and NSD3 on chromosome 8,²²⁴ but there are more fusion proteins that have yet to be characterized.²²⁵

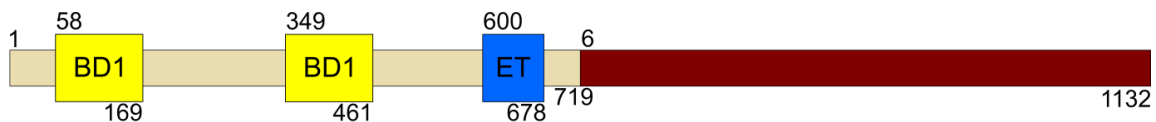


Figure 12. Structure of the fusion oncoprotein BRD4-NUT.^{226, 227}

Originally, NMC was known to originate from the midline region (head, neck and mediastinum) and occur predominantly in young adults. However, recent cases suggested that the occurrence of NMC was not restricted by age, gender, organ or tissue. The age of known diagnosis can range from newborns²²⁸ to the elderly, with the oldest case being a 78-year old patient.²²⁹ Additionally, there are cases where NMC has arisen outside the midline region, such as the bladder²³⁰ and salivary gland.²³¹

Despite its rarity, NMC is widely considered to be the most clinically aggressive form of squamous cell carcinoma with more than 80% of patient deaths occurring within 1 year of diagnosis despite intensive treatment, a median progress-free survival (PFS) rate of 6.6 months and a median overall survival (OS) rate of 9.7 months.²³² Out of every known case of NMC, only one patient has ever been cured.²³³ NMC is also known for its poor differentiation, even to the point where it is mistaken for other carcinomas,^{234, 235} meaning that it is under-diagnosed and these cases sometimes go unrecognized. Recently, NMC has gained more recognition with

it being added to the 2015 World Health Organization (WHO) Classification of Lung Tumours as “NUT Carcinoma”.²³⁶

When the BRD4-NUT fusion oncoprotein is formed, the NUT section recruits multiple HAT proteins such as CBP, EP300,²³⁷ Tat interactive protein 60 kDa (TIP60) and general control of amino acid synthesis 5 (GCN5).²³⁸ So far, only the interaction between EP300 and BRD4-NUT has been explained with the second transcription adaptor putative zinc finger (TAZ) domain of EP300 binding directly to the NUT portion of the oncoprotein, stimulating HAT activity and resulting in the formation of hyper-acetylated chromatin.²³⁷ This creates a self-perpetuating system where chromatin acetylation and subsequent BRD4-NUT recruitment become uncontrollable, creating “megadomains” (Figure 13) which provide the main driving force of the aggressively active gene transcription seen in NMC, as well as its increased affinity to chromatin.²³⁹

When (+)-**JQ1** was reported, its first use was against NMC.¹³⁸ (+)-**JQ1** competes with the hyper-acetylated chromatin for binding to BRD4-NUT, and ultimately displaces the oncoprotein from chromatin. As a result, it stops the perpetual cycle of chromatin acetylation and BRD4-NUT recruitment, and induces growth arrest and apoptosis in NMC cells. Despite the development of over a dozen different BET inhibitors, the only other bromodomain inhibitor to be used in treating NMC is **OTX-015**, which has been used in a clinical setting.²⁴⁰ Administration of **OTX-015** to patients with NMC did afford improvement to survival that surpassed both median PFS and OS rates. While limited, it does nonetheless provide evidence for further clinical treatment of NMC using BET inhibitors.²⁴⁰

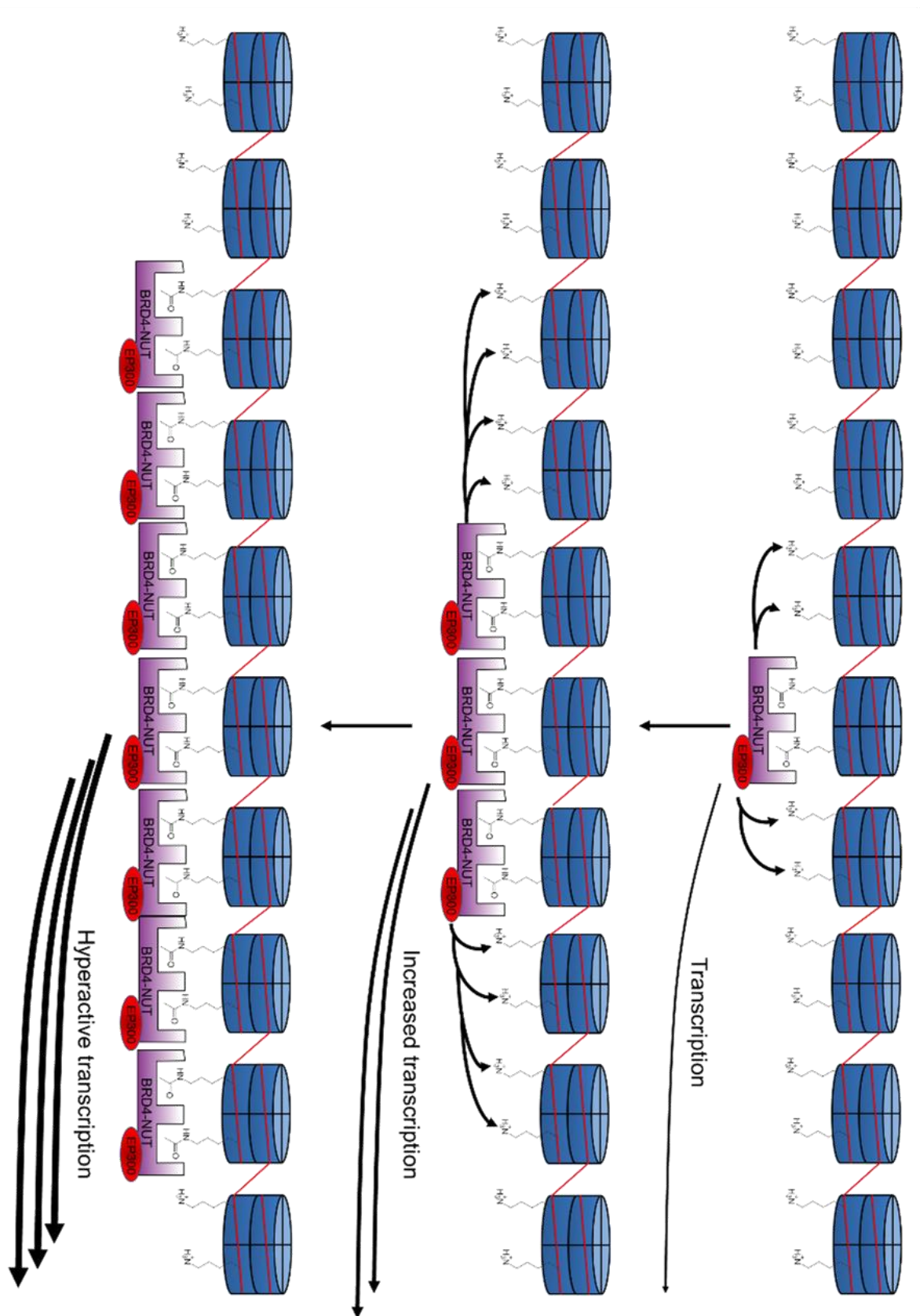


Figure 13. Schematic of the perpetual acetylation of chromatin by EP300 and the recruitment of BRD4-NUT to hyper-acetylated chromatin.²³⁹

1.5.2.3 Myc-Related Cancer

Myc is a family of proto-oncogenes that contains three members: *c-Myc*, *N-Myc* and *L-Myc*. In its physiological state, *Myc* serves as a master regulatory factor that responsible for regulating up to 15% of all genes in humans,²⁴¹ whose functions include transcription, DNA repair and proliferation and differentiation in the cell cycle.²⁴² However, *Myc* is susceptible to mutations from chromosome translocations and gene amplification,²⁴³ which convert *Myc* into an oncogene. In this state, *Myc* possesses the ability to cause overexpression and growth acceleration in cell proliferation, metabolism and differentiation.²⁴⁴

Given that *Myc* has been reported to lose regulation in at least 50% of all known human cancers,^{245, 246} it has been long sought after as an anti-cancer target. However, the lack of a distinct binding site for small molecules, a predominant expression in the nucleus, and the ability to exert its expression across multiple mechanisms, make *Myc* a challenging target. Despite there still being a lack of a method to directly target *Myc*, there are many known strategies to indirectly affect it.²⁴⁵

One example is to target *Myc* transcription through BRD4 inhibition. There have been a few mechanisms detailing the connection between BRD4 and *Myc*. The first mechanism was reported in 2008 where *c-Myc* expression and the association of CDK9 to *c-Myc* was dependent on BRD4.²⁴⁷ The second mechanism, reported in 2011, mentioned that BRD4 itself regulates *Myc* expression through binding to immunoglobulin heavy chain (IgH) enhancers.^{248, 249} Most recently, a third mechanism suggested that BRD4 binds to the *c-Myc* promoter region through H3K27ac and induces its expression.^{250, 251} Regardless of the specific mechanism with how BRD4 activates *c-Myc* expression, the inhibition or knockdown of BRD4 consistently resulted in its downregulation.

The downregulation of *Myc* through bromodomain inhibition in a therapeutic setting was first tested in a multiple myeloma model because of its previously known dysregulation. Only BRD4 was found to be correlated with disease progression. The inhibition of *Myc* expression using (+)-**JQ1** was an unexpected observation, which was confirmed to be bromodomain-specific when **I-BET762** also inhibited *Myc*.²⁵² Other BET inhibitors (**I-BET151**, **I-BET762**,²⁵³ **CPI203**,²⁵⁴ **CPI-0610**,²⁵⁵ **I-BET726**,²⁵⁶ **OTX015**²⁵⁷ and **Y08060**, Figure 11)²⁵⁸ have further added to their use potential use to target *Myc* in multiple myeloma,²⁵³⁻²⁵⁵ but they have also been tested in other *Myc*-related cancers for their potential connection to bromodomain inhibition, including lymphoma,²⁵⁹ neuroblastoma,²⁵⁶ medulloblastoma,^{260, 261} leukemia,^{257, 262} prostate,²⁵⁸ lung,^{156, 263} ovarian²⁶⁴ and endometrial²⁶⁵ cancers.

1.5.2.4 Human Immunodeficiency Virus Type 1

HIV is a retrovirus that weakens the immune system, allowing the body to become more susceptible to infection, and overtime, develop into Acquired Immune Deficiency Syndrome (AIDS). There are two known types: HIV-1, which is the more commonly observed form, and HIV-2, which has been rarely observed outside of Africa. It is transmitted either through unprotected sexual intercourse, or sharing injecting equipment such as needles. According to the WHO, at the end of 2017, 36.9 million people were living with HIV globally, with 21.7 million people receiving antiretroviral therapy (ART) and nearly 1 million people dying from HIV-related causes.²⁶⁶

There are five different classes of ARTs. A list of the available medication for each class is detailed by the United States Food and Drug Administration.²⁶⁷ While such treatments have been effective in reducing viral infection, preventing its growth and allowing people to still live healthy, normal lives, this treatment is permanent as it does not completely eliminate the virus. Perhaps the greatest challenge in curing HIV-1 is dealing with the viral reservoirs that

remain in infected patients. Additionally, consistent treatment sometimes leads to resistance due to the development of viral mutations.^{268, 269}

One strategy that has been employed is the development of another class of agents called latency reversing agents (LRAs). Instead of targeting the viral life cycle, LRAs bring these viral reservoirs out of latency. In combination with ARTs and cytolysis or immune-mediated clearance, they prevent the spread of the re-activated HIV and eliminate the infected cells, giving rise to the phrase “shock and kill”.²⁷⁰ Given that LRAs do not target the viral protein itself, there is less risk of resistant strains forming from these treatments.

Bromodomains are one of many targets found to be useful for the ‘shock’ phase of this strategy. As established previously, the CTD of BRD4 interacts with p-TEFb and mediates phosphorylation of RNA Pol II.^{196, 197} However, p-TEFb is also recruited by Tat, a transcriptional transactivator protein encoded by HIV-1 which enhances viral transcription and replication. Once p-TEFb is bound to the activation domain of Tat, it mediates transcriptional elongation of viral proteins.²⁷¹ While BRD4 itself is not required for Tat-activated HIV-1 transcription, it does compete with Tat for binding to p-TEFb, in which BRD4 overexpression is correlated to reduced Tat transactivation.¹⁹⁹ **(+)-JQ1** was the first bromodomain inhibitor to be tested as an LRA. When BRD4 was inhibited, its association with p-TEFb decreased, while association between p-TEFb and Tat increased and brought viral reservoirs out of latency in CD4⁺ T cells.²⁷² While initial efforts with **(+)-JQ1** resulted in weak reactivation, it did lay the groundwork for the further study of bromodomain inhibitors such as **UMB-136**,²⁷³ **OTX015**,²⁷⁴ **RVX-208** and **PFI-1**²⁷⁵ (Figure 11) to serve as LRAs. This includes the potential use of a combination of LRAs to effectively reactivate HIV reservoirs.^{141, 276} The inhibitors have also shown promise as While recent reviews have called for more work to be done in optimizing

the ‘kill’ phase of this strategy,^{277, 278} bromodomain inhibitors are part of a promising approach to a full-fledged cure for HIV-1.

1.5.3 Fragment-Based Drug Design

Fragment-based drug design (FBDD) was first introduced as a concept by William Jencks in 1981 who described the free energy change for a molecule binding to a protein and its component parts as “intrinsic binding energies” as well as the energy change from translational and rotational entropy as “connection Gibbs energy”.²⁷⁹ The first demonstration of FBDD came 15 years later from Abbott Laboratories who linked a small series of micromolar fragments discovered from NMR to create five molecules with nanomolar binding.²⁸⁰ Since then, FBDD has gradually become a viable alternative to more traditional screening approaches.

As opposed to high-throughput screening (HTS), where millions upon millions out of $\sim 10^{60}$ drug-sized compounds are screened,²⁸¹ FBDD takes a much smaller sample size that spans in the thousands out of $\sim 10^7$ potential compounds²⁸² and finds smaller “fragment” compounds that, despite having lower affinity, bind more efficiently to a protein target. These fragments are then either linked or grown into drug-like compounds with affinities that match HTS compounds. FBDD holds many advantages over HTS, including being able to search chemical space more efficiently, being more cost-effective, and theoretically having a higher hit-rate.²⁸³⁻²⁸⁵ This method has already generated several clinical-stage compounds, and at least one approved drug.²⁸⁶

Bromodomains have become a key target for FBDD efforts because their binding pocket is seen as a suitable size and shape to occupy molecules of low weight²⁸⁷ and the use of sensitive fragment screening methods such as NMR and surface plasmon resonance (SPR) overcome the challenge of developing other screening methods for weak binding partners.¹³¹ While most FBDD effects have focused on the BET family of bromodomains, it has been helpful with

identifying novel fragments outside of this family, particularly those that were originally predicted to be difficult to drug.^{287, 288} This section will focus on what techniques have been used to discover new bromodomain fragments, the groups that have used these techniques in BET proteins with the resulting fragments and any efforts undertaken to evolve the fragments into more potent hits, leads or inhibitors, regardless of whether these target the BET family.

1.5.3.1 Fragment Screening Techniques

There have been many techniques developed that have helped in the discovery and validation of novel fragments and inhibitors. The following methods have been applied recently to identifying new fragments for bromodomains.

The AlphaScreen is a proximity-based chemiluminescent tool that utilises coated donor and acceptor beads that are linked via biological interactions to generate a signal.²⁸⁹ When the donor bead becomes excited from exposure to lasers, oxygen is converted to a singlet state. This then travels to the acceptor bead and reacts with molecules contained within it. Upon activating fluorophores within this bead, light is then emitted. When the beads are unlinked, the distance between donor and acceptor becomes too great for the oxygen singlet to travel, therefore preventing this reaction from occurring.^{290, 291} The versatility of the AlphaScreen comes from its ability to measure either an increase or a decrease in signal strength,^{130, 292} depending on the needs of the user, as well as detecting interactions across a wide range of affinities, from sub-nanomolar to mid-micromolar.

Surface plasmon resonance detects the binding response of molecules in real time. The most common setup in SPR is the Kretschmann configuration where polarized light is sent through a prism that is attached to a gold-glass sensor chip and picked up by a detector. The protein of choice is immobilised onto the gold surface and a buffer solution is flown over it. The gold layer is then exposed to the analyte containing the molecule. The change in refractive index

caused by the association and dissociation of the analyte is then measured.^{293, 294} Given that the difference in refractive index is measured in this assay, labelling molecules with fluorescent or radioactive tags are not required. This method is useful for determining the binding kinetics and affinity of both fragment-like and drug-like compounds due to its suitability over picomolar and millimolar affinities.^{295, 296}

Fluorescence anisotropy is used to measure a fluorophore's rotational mobility. When a ligand tagged with a fluorophore is exposed to polarized light, it enters an excited state and tumbles in solution. In a free state, the ligand moves around freely, but the emitted light becomes quickly depolarized. However, when the ligand is bound to a receptor, its movement becomes more restrained and the polarization of light is more retained.^{297, 298} Fluorescence anisotropy can be used to measure the displacement of a labelled substrate²⁹⁹ and it is typically suited for compounds with micromolar affinity. Compounds with nanomolar affinity require very low fluorophore concentrations, which can result in a weak fluorescent signal.³⁰⁰

Nuclear magnetic resonance is a spectroscopic method that detects and measures the binding of a molecule to a target protein. Each NMR-based technique is able to screen for these interactions, but accomplishes this through different means. A few examples include heteronuclear single quantum correlation (HSQC), which uses 2D spectra (e.g. ^1H - ^{15}N) to detect for any protein perturbations in the absence and presence of a molecule;³⁰¹ water-ligand observed via gradient spectroscopy (WaterLOGSY), which compares the phases of 1D spectra between binding and non-binding compounds;^{302, 303} and saturation transfer difference (STD), which compares the intensities in 1D spectra between a free and bound ligand.^{304, 305} These techniques are more suitable for identifying new fragment-like hits (micromolar to millimolar)^{302, 306-308} for a protein of interest as drug-like compounds tend to suffer from slow exchange rates between the protein and ligand.

X-ray crystallography is a structural technique that is used to determine the three-dimensional structure of a crystallised macromolecule, such as a protein or DNA. The crystal is exposed to an X-ray beam that causes it to diffract in different directions to create a pattern on an imaging plate. This is then repeated while rotating the crystal at different angles. The collective patterns are used to generate an electron density map of the atoms and amino acids in the protein. After refinement, the three-dimensional structure is resolved.³⁰⁹ This method can be used to determine how a fragment binds to the desired target protein.³¹⁰

Virtual screening is a computational tool that identifies potential ligands based on certain parameters. This method makes more efficient use of chemical space because, as mentioned previously, the number of fragment-like compounds spans in the millions as opposed to the near-infinite number of drug-like compounds. The fragments are often filtered based on desired structural properties such as rotatable bonds or hydrogen bond donors and acceptors,³¹¹ as well as biological properties such as affinity³¹² and selectivity between targets.³¹⁰ The fragment hits are then validated using any of the methods mentioned above.³¹³

1.5.3.2 Fragment Discovery

The techniques described above have been applied – either individually or in combination – to identify novel mimetic fragments for bromodomains. Each fragment has been grouped by author and can be found in Figure 14.

Dimethyl sulfoxide (DMSO) is normally the solvent of choice when carrying out the AlphaScreen. However, in a bromodomain-based AlphaScreen done by Philpott et al.,³¹⁴ DMSO was found to act as an inhibitor itself and interfered with these assays. As a result, water-miscible solvents such as *N*-methylpyrrolidone (NMP), DMSO and dimethylformamide (DMF) (**A**, **B** and **C**, respectively) were tested as standalone compounds in AlphaScreens

across five different bromodomains. In these assays, NMP was found to be a fragment with high ligand efficiency, which has laid the groundwork for the discovery of other fragments.

The 3,5-dimethylisoxazole was one such fragment that was inspired by NMP. Hewings et al.³¹⁵ identified this as a potential – albeit, serendipitous – bioisostere for K-ac in studies of methyl-bearing heterocycles. Their work started with a dimethylisoxazole coupled to a dihydroquinazolinone (**D**); a compound with unexpectedly high affinity for BRD4 BD1 and CBP which potentially had two binding modes. X-ray crystallography confirmed that the dimethylisoxazole acts as the K-ac mimetic.

Navratilova et al.³¹⁶ screened a total of 656 fragments against three different BCPs: BRD4, CBP and PCAF. Using SPR with varying concentrations of DMSO, they identified three fragments that bound to BRD4 and CBP (**E-G**) and two fragments to PCAF (**H, I**). The X-ray crystal structures for **E**, **H** and **I** were solved, each interacting with the conserved asparagine residue in the bromodomain binding pocket via the carbonyl. Just like with the AlphaScreen, it was noted that the main challenge associated with using SPR fragment screening for bromodomains is overcoming the interference caused by the commonly-used solvent DMSO in detecting low-binding fragments.

Chung et al.³¹⁷ carried out a fragment screening program against every BET protein except BRDT. They used a fluorescence anisotropy (FA) assay on 1,376 compounds, in which 132 compounds showed displacement of K-ac from at least one BET protein. From their work, five fragments (**A, J-M**) were taken forward to determine their respective binding modes with X-ray crystallography. Each fragment possesses a carbonyl that forms the canonical bonds to asparagine and tyrosine, while an adjacent methyl fills the water pocket. Their work also confirmed the dihydroquinazolinone (**M**) and NMP (**A**) as bromodomain fragments.

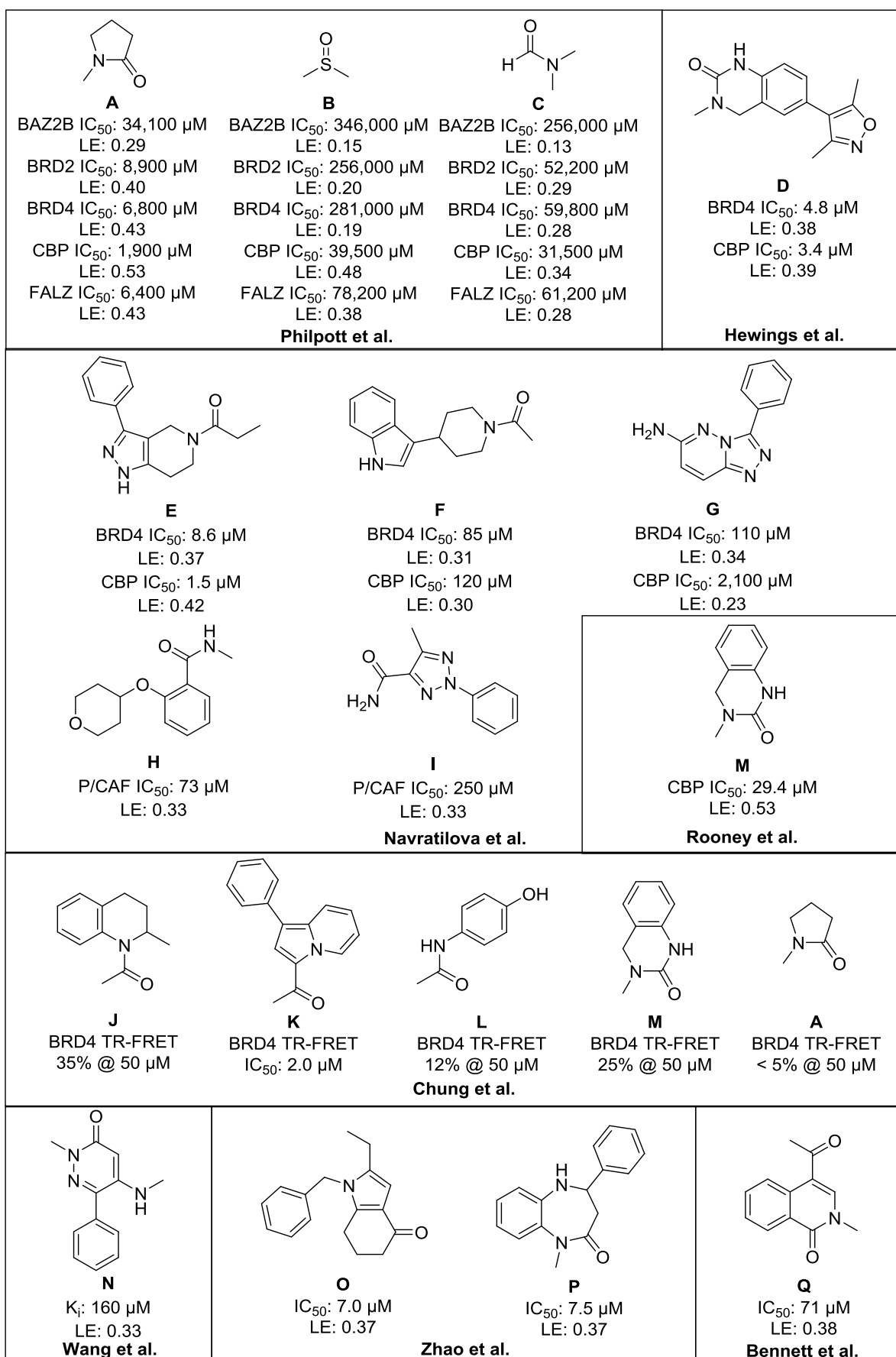


Figure 14. Bromodomain fragments grouped by author with values reported.

In addition to being a BET bromodomain fragment, the dihydroquinazolinone **M** was also found to bind to the bromodomain of CBP. In work carried out by Rooney et al., **M** was discovered from an AlphaScreen of analogues based on NMP, which retained NMP's high ligand efficiency.

Wang et al.³¹⁸ carried out a protein-based NMR fragment screen on BRD4 BD2. While the exact method in which they carried out the filtering and testing of fragments was not disclosed, their most potent hit was a pyridazinone compound (**N**) which shares a similar binding scaffold as the dihydroquinazolinone and NMP.

Zhao et al.³¹⁹ screened a total of 9 million compounds from the ZINC library. This was condensed down to 17,179 fragments based on restrictions with molecular weight, hydrogen-bond acceptors, rotatable bonds and docking parameters with BRD4 BD1. Over 665,000 compounds were found to possess at least one of these fragments. The efforts involving binding predictions, molecular dynamics simulations and in vitro validation through thermal shift assays resulted in four compounds, which were selected for further testing in AlphaScreens. The two compounds with the highest affinity from these assays (**O**, **P**) are shown in Figure 14. The tetrahydroindolone fragment **O** is an intriguing mimetic because unlike the other inhibitors depicted, it does not have an explicit methyl group that fills the water pocket, but nonetheless binds to the bromodomain via the carbonyl.

Bennett et al.³²⁰ briefly mentioned a screening effort on a focused library of 2,600 compounds based around a pharmacophore model and a rational fragment design using an AlphaScreen against BRD4 BD1. From this, an isoquinolinone hit emerged (**Q**). Much like with other inhibitors and fragments before it, the K-ac mimicry comes from the carbonyl forming the essential bonds to asparagine and tyrosine, with the *N*-methyl group filling out the water pocket. The additional aromatic group further fills the binding pocket.

1.5.3.3 Fragment-to-Lead Development

Several of these fragments have been involved in the design of potent bromodomain inhibitors. While the majority of these fragments started off targeting the BET family, their activity has been explored outside the BET family. The inhibitors have been grouped by mimetic scaffold and can be found in Figure 15.

Since the report of the dimethylisoxazole fragment **D** by Hewings et al., it has become one of the most exploited mimetic scaffolds in bromodomain inhibition to date. The dimethylisoxazole alone has accounted for numerous attempts at optimization, which has seen the development of over a dozen ligands. The majority of these serve as probes or preclinical inhibitors for the BET family of bromodomains (**I-BET151**,³²¹ **RX-37**,³²² **CD161**,³²³ **UMB-32**,³²⁴ **Y02234**,³²⁵ **OXFBD02**,³²⁶ **OXFBD04**,³²⁷ and compounds **R**,³²⁸ **S**³²⁹ and **T**)³³⁰ and the bromodomain of CBP (**SGC-CBP30**,¹²⁸ and compounds **U** and **V**).³³¹ The dimethylisoxazole has also been used in the Phase Ib clinical inhibitor **PLX51107**.³³²

Exploration around the tetrahydroquinaldine scaffold has remained focused on targeting the BET family of bromodomains. Fragment **J** has been useful in ratifying the binding mode of the BET inhibitor **I-BET726**,³³³ a nanomolar inhibitor which has shown promise in the silencing of Myc-related tumour models.²⁵⁶ However, it has not been submitted for clinical trials, possibly due to its poor preclinical profile. **J** has also been modified into a tetrahydroquinoxaline by two other groups. Millan et al.³³⁴ explored the potential of this scaffold, which led to the discovery of **FT001**. Despite its nanomolar affinity, antiproliferative effects and Myc suppression, the group is still seeking to optimize it further. Law et al.³³⁵ also used this scaffold to develop selectivity between BD1 and BD2 of each BET protein. Their lead compound, **GSK340**, is 50-fold selective for BRD4 BD2 over BD1, and serves as a tool to help investigate the role of BD2 in BET proteins.

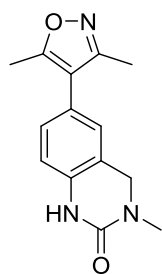
While the indolizine fragment **K** was originally discovered as a BET fragment by Chung et al.,³¹⁷ there has been no known progress of its elaboration towards BET bromodomains. However, in a BAZ2A bromodomain AlphaScreen conducted by Chen et al.,¹⁷⁸ its activity was matched in BAZ2A and BRD4. The BAZ2A and BAZ2B bromodomains then became the focus of selectivity, with medicinal chemistry-driven SARs resulting in the probe **GSK2801**.

The dihydroquinazolinone **M** inspired the development of probes in three separate bromodomain families. Fish et al.³³⁶ used a similar fragment (**W**) to develop the BET probe **PFI-1**, which has assisted in highlighting the role of BET bromodomain inhibitors in leukemia and HIV. GlaxoSmithKline discovered ATAD2 inhibitors using another fragment based off of **M (X)**.³³⁷ Despite **X** starting with inhibitory activity that was preferable to BRD4 over ATAD2, it was successfully optimized³³⁸ to yield the first-ever nanomolar, selective and cell permeable probe for ATAD2: **GSK8814**.¹⁷⁶ Lastly, Rooney et al.³³⁹ used **M** for the development of CBP probes. Due to **M**'s susceptibility to oxidation, the core scaffold was redesigned into two alternate mimetics: a benoxazinone (**Y**) and a dihydroquinoxalinone (**Z**). While the affinity of **Y** for CBP was lower than **M**, **Z** showed a 91-fold improvement compared to **M**.

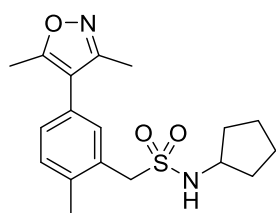
Despite the pyridazinone fragment **N** being discovered much more recently than other fragments, AbbVie have already reported a few low nanomolar inhibitors. The most notable ligand in this series is the clinical inhibitor **ABBV-075**³⁴⁰ (alternate name: mivebresib), which is in a Phase I clinical trial for the treatment of several different cancers and carcinomas. It has also served as a template for constrained tetracyclic derivatives. Among these derivatives, the *N*-methylpyridone mimetic was preserved (e.g. **AB**), but was also swapped for an *N*-methylpyrrole (e.g. **AC**).³⁴¹ Separately, Wang et al.³¹⁸ explored the potential of **N** in a series of macrocycles (example: **AA**). All of these derivatives showed similar affinity for BRD4 compared to **ABBV-075**.

A

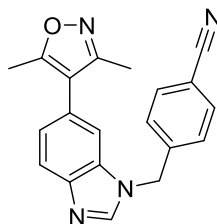
Dimethylisoxazole

**D**

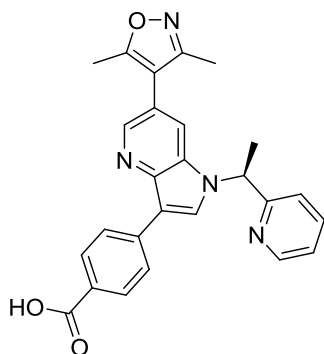
BRD4 IC₅₀: 4.8 μM
 LE: 0.38
 CBP IC₅₀: 3.4 μM
 LE: 0.39

**R**

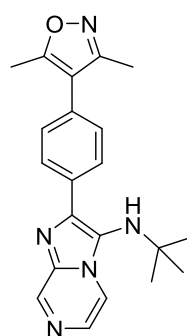
BRD4 IC₅₀: 0.50 μM
 LE: 0.36

**S**

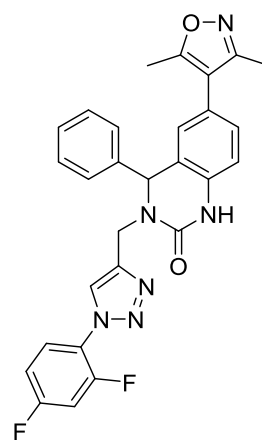
BRD4 pIC₅₀: 6.7
 LE: 0.37
 CBP pIC₅₀: < 4.0
 LE: < 0.22

**PLX51107**

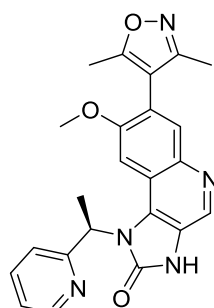
BRD4 K_d: 0.017 μM
 LE: 0.37

**UMB-32**

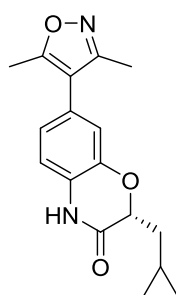
BRD4 K_d: 0.55 μM
 LE: 0.31

**T**

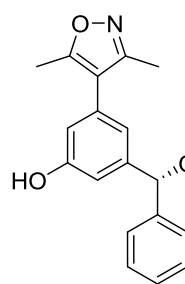
BRD4 IC₅₀: 0.27 μM
 LE: 0.27

**I-BET151**

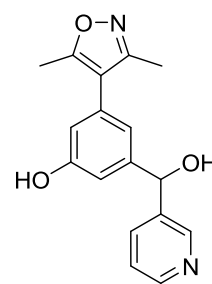
BRD4 pIC₅₀: 6.1
 LE: 0.27

**Y02234**

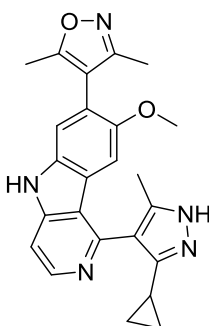
BRD4 IC₅₀: 0.10 μM
 LE: 0.42

**OXFBD02**

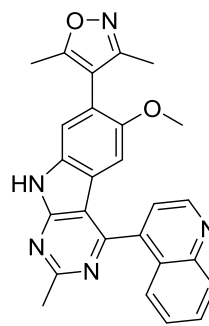
BRD4 IC₅₀: 0.38 μM
 LE: 0.40

**OXFBD04**

BRD4 IC₅₀: 0.17 μM
 LE: 0.43

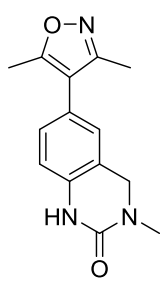
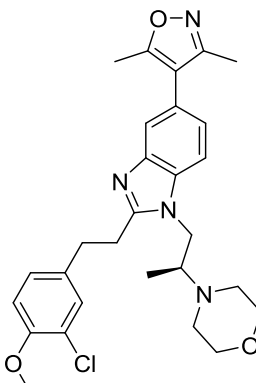
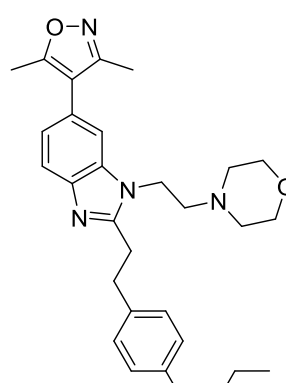
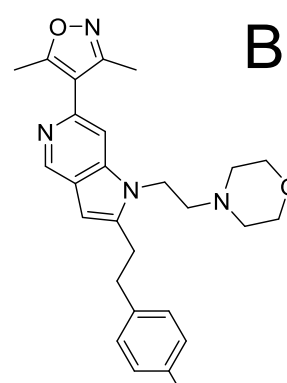
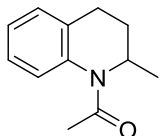
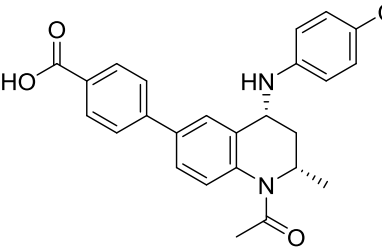
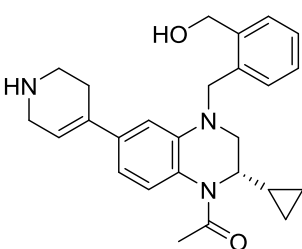
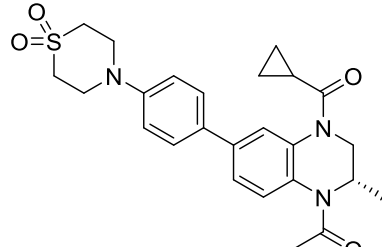
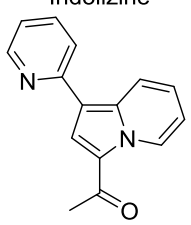
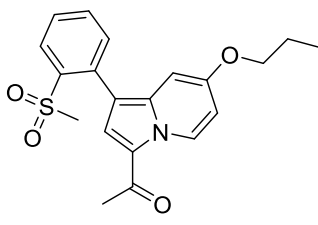
**RX-37**

BRD4 IC₅₀: 0.075 μM
 LE: 0.31

**CD161**

BRD4 IC₅₀: 0.028 μM
 LE: 0.36

B

<p>A</p> <p>Dimethylisoxazole</p>  <p>D</p> <p>BRD4 IC₅₀: 4.8 μM LE: 0.38 CBP IC₅₀: 3.4 μM LE: 0.39</p>	 <p>SGC-CBP30</p> <p>BRD4 K_d: 0.89 μM LE: 0.23 CBP K_d: 0.026 μM LE: 0.29</p>  <p>U</p> <p>BRD4 IC₅₀: 18 μM LE: 0.18 CBP IC₅₀: 0.13 μM LE: 0.26</p>  <p>V</p> <p>BRD4 IC₅₀: 18 μM LE: 0.19 CBP IC₅₀: 0.17 μM LE: 0.27</p>
<p>Tetrahydroquinaldine</p>  <p>J</p> <p>BRD4 IC₅₀: 100 μM LE: 0.39</p>	 <p>I-BET726</p> <p>BRD4 IC₅₀: 0.10 μM LE: 0.31</p>  <p>GSK340</p> <p>BRD4 BD1 IC₅₀: 3.2 μM LE: 0.24 BRD4 BD2 IC₅₀: 0.06 μM LE: 0.32</p>  <p>FT001</p> <p>BRD4 IC₅₀: 0.10 μM LE: 0.29</p>
<p>Indolizine</p>  <p>K</p> <p>BRD4 IC₅₀: 2.0 μM LE: 0.43 BAZ2A IC₅₀: 1.5 μM LE: 0.43 BAZ2B IC₅₀: 7.0 μM LE: 0.43</p>	 <p>GSK2801</p> <p>BRD4 IC₅₀: > 50 μM LE: < 0.23 BAZ2A IC₅₀: 0.40 μM LE: 0.34 BAZ2B IC₅₀: 0.43 μM LE: 0.34</p>

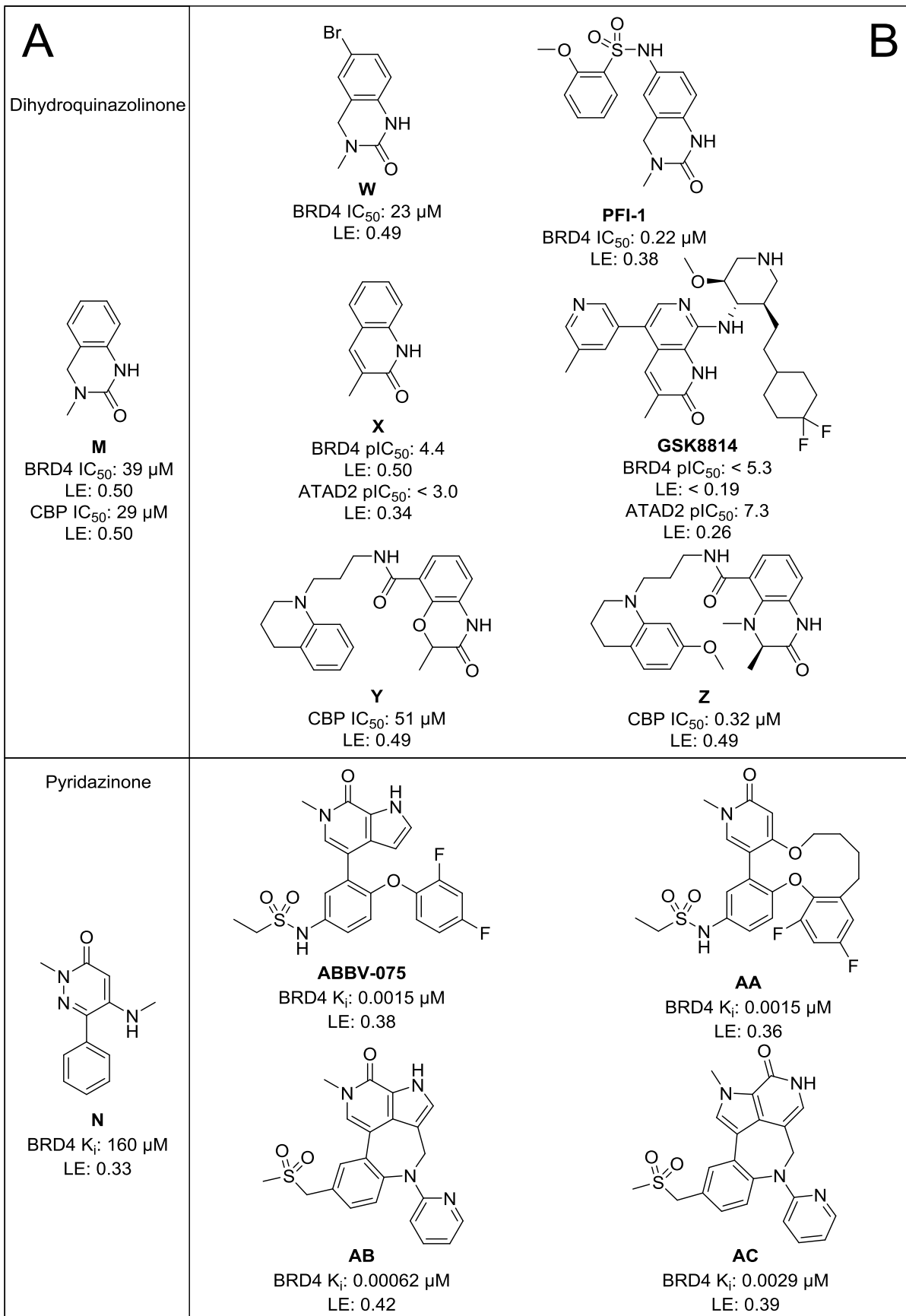


Figure 15. Compounds elaborated from known fragments with binding or inhibition values reported. [A] Starting fragment. [B] Reported inhibitors.

Over the past decade, the bromodomain has become a target for inhibitor design, with a variety of mimetics and scaffolds being developed. Multiple techniques have been applied to explore the binding site of the bromodomain and not only achieve the desired selectivity, but to also establish the role it plays in the whole protein. Even though this chapter provides an in-depth coverage of the work done on the bromodomains of BRD4 and scratches the surface on non-BET inhibitors, in truth, this still only covers a fraction of the overall work carried out to determine the physiological and pathological function of the bromodomain in each BCP.

1.6 Project Aims

We believe that there are certain mimetic scaffolds that remain undiscovered or untouched in the search for novel inhibitors. The primary aim of this PhD project is to employ different strategies to synthesise a variety of potential bromodomain inhibitors using these untouched mimetic fragments and to evaluate their effectiveness in preventing K-ac from binding to bromodomains. The two fragments that will be explored in this project are *N*-methylpyrrolidone and 5-methyl-3-aryl-1*H*-pyrazole. These fragments will be used as part of three different design strategies: acetamide substitution, fragment growing and the “poised fragment” library.

1.6.1 *N*-Methylpyrrolidone

NMP is an organic solvent widely used in industrial applications such as paint stripping and graffiti removal, as well as pharmaceutical applications like solubilising hydrophobic drugs³⁴² and depot injections, remarked for its low volatility, high boiling point and low toxicity in humans.

The first records of NMP's mimetic activity came from Philpott et al.,³¹⁴ who as previously mentioned, compared NMP to K-ac in five different bromodomains, with NMP's inhibitory activity rivalling K-ac in most cases. Chung et al.³¹⁷ also compared the mimetic properties of NMP to other fragments in three BET bromodomains, but its activity was near undetectable at the given concentrations.

At the moment, there are seven crystal structures available where NMP is bound to a bromodomain (Figure 16). Six of them share the same interactions and orientation; the carbonyl of NMP imitates the interactions to asparagine and tyrosine, while the *N*-methyl group replicates the K-ac methyl in the water pocket. The outlier to this group is PHIP BD2, where the conformation is flipped around the carbonyl and the *N*-methyl group points away from the water-lined pocket. On top of that, it is one of the few bromodomains where the asparagine is not conserved, and instead replaced with a threonine.¹²¹

Compared to other fragments, the therapeutic applications of NMP have been explored to a much greater degree. Well before it was known to mimic K-ac in bromodomains, NMP demonstrated properties of bone regeneration and osteoclast differentiation inhibition.³⁴³⁻³⁴⁶ Even today, the evidence towards NMP being used as a treatment for osteoporosis and other bone-erosive diseases is accumulating.³⁴⁷⁻³⁵⁰ Additionally, Shortt et al. made the serendipitous discovery that NMP possessed anti-myeloma and immunomodulatory activity.³⁵¹ Surprisingly, it is being used in a Phase I clinical trial as a first-in-class dual immunomodulator (IMiD) and bromodomain inhibitor for treating relapsed refractory multiple myeloma.³⁵²

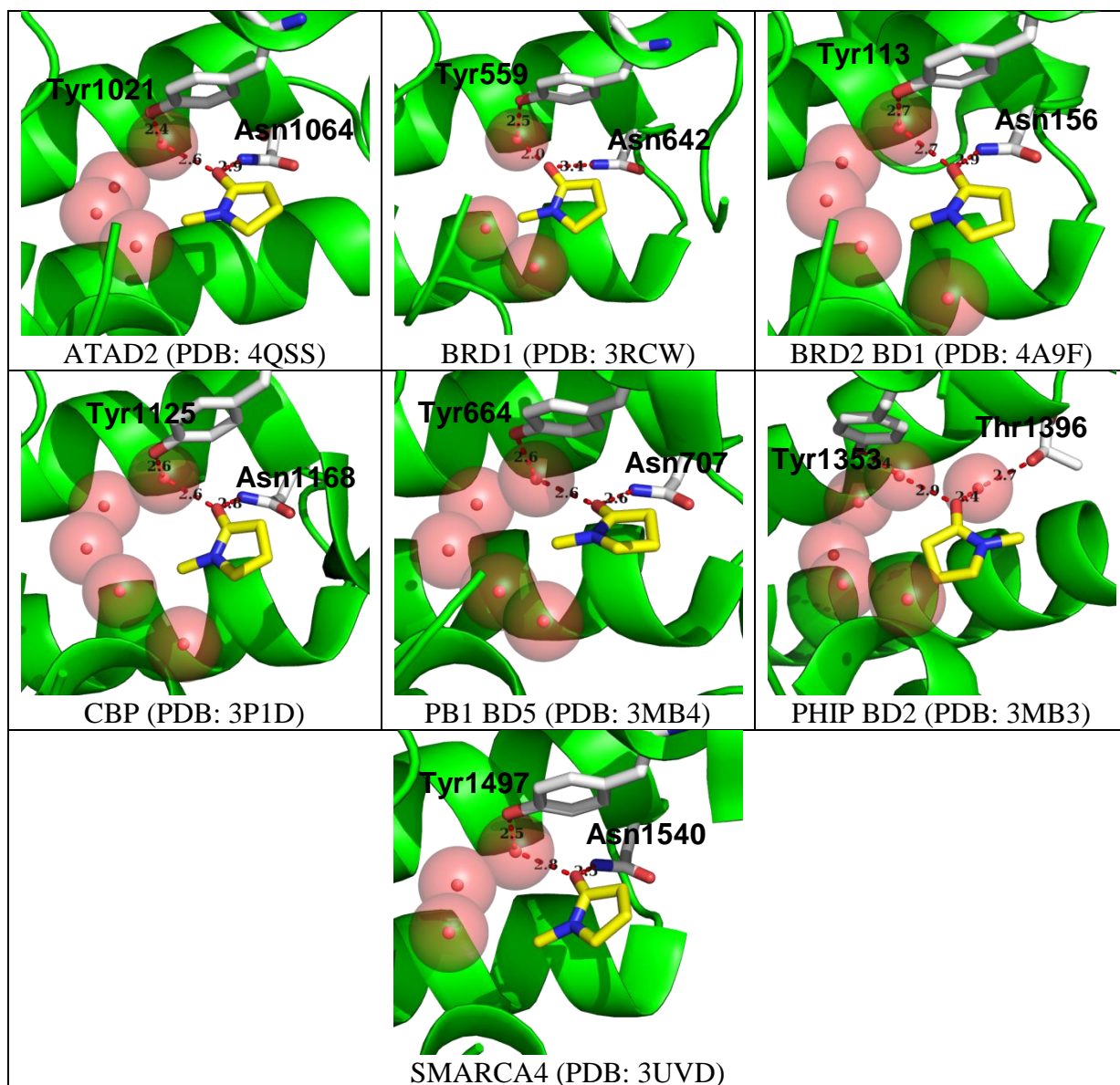


Figure 16. Known X-ray crystal structures of NMP bound to bromodomains. Water molecules shown as red spheres. Distances in Å, highlighted by red dashes.

NMP has inspired the development of other mimetic warheads such as the dimethylisoxazole **D**, benzoxazinone **Y** and dihydroquinoxalinone **Z** described above. While these three fragments have yielded ligands for both inside and outside the BET family, we noticed that these efforts have not been applied to the NMP scaffold in the same manner, in spite of its own therapeutic potential and bromodomain inhibition. In order to prove NMP's capacity as a mimetic for bromodomains, the aim is to functionalise NMP in such a way that the derivatives

can be used to appropriately substitute the K-ac mimetic of a known inhibitor while retaining its inhibitory activity, as well as grown with improved affinity into potential lead candidates.

1.6.2 5-Methyl-3-aryl-1*H*-pyrazole

As covered in Sections 1.4 and 1.5, there have been a large amount of non-acetylated heterocyclic scaffolds created that serve as K-ac mimetics, which include triazoles, isoxazoles and quiazolinones (Figures 11, 14 and 15). While these scaffolds have proved to be successful with many of these moving into clinical trials or serving as probes, the need to create ligand-efficient fragments from novel mimetics still remains.

We hypothesised that another scaffold – the pyrazole – could be a potential isostere to these heterocyclic inhibitors as it bears a strong resemblance to most of them. However, much like with NMP, there are no reports of it being used as a mimetic fragment in bromodomain inhibition. In order to prove that the pyrazole has the potential to be an K-ac mimetic, the aim is to develop a “poised fragment” library of substituted pyrazoles by devising a synthetic scheme that can allow for quick and efficient elaboration with a focus on 5-methyl-3-aryl derivatives.

References

1. Waddington CH. The epigenotype. 1942. *Int J Epidemiol.* 2012;41(1):10-3.
2. Haig D. The (dual) origin of epigenetics. *Cold Spring Harb Symp Quant Biol.* 2004;69:67-70.
3. Ephrussi B. The cytoplasm and somatic cell variation. *J Cell Physiol Suppl.* 1958;52(Supp 1):35-49; discussion -53.
4. Nanney DL. Epigenetic Control Systems. *Proc Natl Acad Sci U S A.* 1958;44(7):712-7.
5. Holliday R. DNA methylation and epigenetic defects in carcinogenesis. *Mutat Res.* 1987;181(2):215-7.
6. Lutz WK, Maier P. Genotoxic and epigenetic chemical carcinogenesis: one process, different mechanisms. *Trends Pharmacol Sci.* 1988;9(9):322-6.
7. Berry DL, Helmes CT. Role of epigenetic factors in dietary carcinogenesis. *Adv Exp Med Biol.* 1984;177:91-113.
8. Weisburger JH, Horn C. Nutrition and cancer: mechanisms of genotoxic and epigenetic carcinogens in nutritional carcinogenesis. *Bull N Y Acad Med.* 1982;58(3):296-312.
9. Lovtrup S. Epigenetic mechanisms in the early amphibian embryo: cell differentiation and morphogenetic elements. *Biol Rev Camb Philos Soc.* 1983;58(1):91-130.
10. Meins F, Jr., Binns A. Epigenetic variation of cultured somatic cells: evidence for gradual changes in the requirement for factors promoting cell division. *Proc Natl Acad Sci U S A.* 1977;74(7):2928-32.
11. Abercrombie M. General Review of the Nature of Differentiation. *Ciba Foundation Symposium - Cell Differentiation: John Wiley & Sons, Ltd.; 2008.* p. 3-17.
12. Allen SL. Genetic and epigenetic control of several isozymic systems in *Tetrahymena*. *Ann N Y Acad Sci.* 1968;151(1):190-207.
13. Herring SW. Formation of the Vertebrate Face - Epigenetic and Functional Influences. *American Zoologist.* 1993;33(4):472-83.
14. Huxley J. Cancer Biology - Viral and Epigenetic. *Biological Reviews of the Cambridge Philosophical Society.* 1957;32(1):1-37.
15. Sherbet GV. Cybernetic interactions in epigenetics. *Prog Biophys Mol Biol.* 1966;16:89-106.
16. Carolineberry A, Berry RJ. Epigenetic variation in the human cranium. *J Anat.* 1967;101(Pt 2):361-79.
17. Williams GM. Epigenetic effects of liver tumor promoters and implications for health effects. *Environ Health Perspect.* 1983;50:177-83.
18. Holliday R. The inheritance of epigenetic defects. *Science.* 1987;238(4824):163-70.

19. Cowley DE, Atchley WR. Quantitative Genetic Models for Development, Epigenetic Selection, and Phenotypic Evolution. *Evolution*. 1992;46(2):495-518.
20. Holliday R. Epigenetics: an overview. *Dev Genet*. 1994;15(6):453-7.
21. Riggs AD, Martienssen RA, Russo VEA. *Epigenetic Mechanisms of Gene Regulation*: Cold Spring Harbor Laboratory Press; 1996.
22. Wu C, Morris JR. Genes, genetics, and epigenetics: a correspondence. *Science*. 2001;293(5532):1103-5.
23. Sawalha AH. Epigenetics and T-cell immunity. *Autoimmunity*. 2008;41(4):245-52.
24. Biel M, Wascholowski V, Giannis A. Epigenetics--an epicenter of gene regulation: histones and histone-modifying enzymes. *Angew Chem Int Ed Engl*. 2005;44(21):3186-216.
25. Tchurikov NA. Molecular mechanisms of epigenetics. *Biochemistry (Mosc)*. 2005;70(4):406-23.
26. Feinberg AP. Cancer epigenetics takes center stage. *Proc Natl Acad Sci U S A*. 2001;98(2):392-4.
27. Momparler RL. Cancer epigenetics. *Oncogene*. 2003;22(42):6479-83.
28. Egger G, Liang G, Aparicio A, Jones PA. Epigenetics in human disease and prospects for epigenetic therapy. *Nature*. 2004;429(6990):457-63.
29. Kelly TL, Trasler JM. Reproductive epigenetics. *Clin Genet*. 2004;65(4):247-60.
30. Bird A. Perceptions of epigenetics. *Nature*. 2007;447(7143):396-8.
31. Berger SL, Kouzarides T, Shiekhatar R, Shilatifard A. An operational definition of epigenetics. *Genes Dev*. 2009;23(7):781-3.
32. Bonasio R, Tu S, Reinberg D. Molecular signals of epigenetic states. *Science*. 2010;330(6004):612-6.
33. Mann JR. Epigenetics and memigenetics. *Cell Mol Life Sci*. 2014;71(7):1117-22.
34. Franzek EJ, Sprangers N, Janssens AC, Van Duijn CM, Van De Wetering BJ. Prenatal exposure to the 1944-45 Dutch 'hunger winter' and addiction later in life. *Addiction*. 2008;103(3):433-8.
35. Lumey LH, Ravelli AC, Wiessing LG, Koppe JG, Treffers PE, Stein ZA. The Dutch famine birth cohort study: design, validation of exposure, and selected characteristics of subjects after 43 years follow-up. *Paediatr Perinat Epidemiol*. 1993;7(4):354-67.
36. Stein AD, Zybert PA, van de Bor M, Lumey LH. Intrauterine famine exposure and body proportions at birth: the Dutch Hunger Winter. *Int J Epidemiol*. 2004;33(4):831-6.
37. Ravelli GP, Stein ZA, Susser MW. Obesity in young men after famine exposure in utero and early infancy. *N Engl J Med*. 1976;295(7):349-53.

38. Kyle UG, Pichard C. The Dutch Famine of 1944-1945: a pathophysiological model of long-term consequences of wasting disease. *Curr Opin Clin Nutr Metab Care*. 2006;9(4):388-94.
39. Brown AS, Susser ES. Prenatal nutritional deficiency and risk of adult schizophrenia. *Schizophr Bull*. 2008;34(6):1054-63.
40. Hoek HW, Brown AS, Susser E. The Dutch famine and schizophrenia spectrum disorders. *Soc Psychiatry Psychiatr Epidemiol*. 1998;33(8):373-9.
41. Yin Y, Morgunova E, Jolma A, Kaasinen E, Sahu B, Khund-Sayeed S, et al. Impact of cytosine methylation on DNA binding specificities of human transcription factors. *Science*. 2017;356(6337).
42. Luo GZ, Blanco MA, Greer EL, He C, Shi Y. DNA N(6)-methyladenine: a new epigenetic mark in eukaryotes? *Nat Rev Mol Cell Biol*. 2015;16(12):705-10.
43. Johnson TB, Coghill RD. Researches on Pyrimidines. C111. The Discovery of 5-Methyl-Cytosine in Tuberculinic Acid, the Nucleic Acid of the Tubercle Bacillus1. *Journal of the American Chemical Society*. 1925;47(11):2838-44.
44. Vischer E, Zamenhof S, Chargaff E. Microbial nucleic acids; the desoxyribose nucleic acids of avian tubercle bacilli and yeast. *J Biol Chem*. 1949;177(1):429-38.
45. Hotchkiss RD. The quantitative separation of purines, pyrimidines, and nucleosides by paper chromatography. *J Biol Chem*. 1948;175(1):315-32.
46. Riggs AD. X inactivation, differentiation, and DNA methylation. *Cytogenet Cell Genet*. 1975;14(1):9-25.
47. Holliday R, Pugh JE. DNA modification mechanisms and gene activity during development. *Science*. 1975;187(4173):226-32.
48. Kumar S, Chinnusamy V, Mohapatra T. Epigenetics of Modified DNA Bases: 5-Methylcytosine and Beyond. *Front Genet*. 2018;9:640.
49. Moore LD, Le T, Fan G. DNA methylation and its basic function. *Neuropsychopharmacology*. 2013;38(1):23-38.
50. Goyal R, Reinhardt R, Jeltsch A. Accuracy of DNA methylation pattern preservation by the Dnmt1 methyltransferase. *Nucleic Acids Res*. 2006;34(4):1182-8.
51. Okano M, Bell DW, Haber DA, Li E. DNA methyltransferases Dnmt3a and Dnmt3b are essential for de novo methylation and mammalian development. *Cell*. 1999;99(3):247-57.
52. Li E, Beard C, Jaenisch R. Role for DNA methylation in genomic imprinting. *Nature*. 1993;366(6453):362-5.
53. Napoli C, Lemieux C, Jorgensen R. Introduction of a Chimeric Chalcone Synthase Gene into *Petunia* Results in Reversible Co-Suppression of Homologous Genes in trans. *Plant Cell*. 1990;2(4):279-89.

54. Romano N, Macino G. Quelling: transient inactivation of gene expression in *Neurospora crassa* by transformation with homologous sequences. *Mol Microbiol.* 1992;6(22):3343-53.
55. Fire A, Xu S, Montgomery MK, Kostas SA, Driver SE, Mello CC. Potent and specific genetic interference by double-stranded RNA in *Caenorhabditis elegans*. *Nature.* 1998;391(6669):806-11.
56. Carmell MA, Hannon GJ. RNase III enzymes and the initiation of gene silencing. *Nat Struct Mol Biol.* 2004;11(3):214-8.
57. Chendrimada TP, Gregory RI, Kumaraswamy E, Norman J, Cooch N, Nishikura K, et al. TRBP recruits the Dicer complex to Ago2 for microRNA processing and gene silencing. *Nature.* 2005;436(7051):740-4.
58. Hammond SM. Dicing and slicing: the core machinery of the RNA interference pathway. *FEBS Lett.* 2005;579(26):5822-9.
59. van Rij RP, Andino R. The silent treatment: RNAi as a defense against virus infection in mammals. *Trends Biotechnol.* 2006;24(4):186-93.
60. Buchon N, Vaury C. RNAi: a defensive RNA-silencing against viruses and transposable elements. *Heredity (Edinb).* 2006;96(2):195-202.
61. Curtis CD, Nardulli AM. Using RNA interference to study protein function. *Methods Mol Biol.* 2009;505:187-204.
62. Zhai Z, Sooksa-nguan T, Vatamaniuk OK. Establishing RNA interference as a reverse-genetic approach for gene functional analysis in protoplasts. *Plant Physiol.* 2009;149(2):642-52.
63. Xin Y, Huang M, Guo WW, Huang Q, Zhang LZ, Jiang G. Nano-based delivery of RNAi in cancer therapy. *Mol Cancer.* 2017;16(1):134.
64. Bobbin ML, Rossi JJ. RNA Interference (RNAi)-Based Therapeutics: Delivering on the Promise? *Annu Rev Pharmacol Toxicol.* 2016;56:103-22.
65. Luger K, Mader AW, Richmond RK, Sargent DF, Richmond TJ. Crystal structure of the nucleosome core particle at 2.8 Å resolution. *Nature.* 1997;389(6648):251-60.
66. Kalashnikova AA, Rogge RA, Hansen JC. Linker histone H1 and protein-protein interactions. *Biochim Biophys Acta.* 2016;1859(3):455-61.
67. Bharath MM, Chandra NR, Rao MR. Molecular modeling of the chromatosome particle. *Nucleic Acids Res.* 2003;31(14):4264-74.
68. Dai J, Sultan S, Taylor SS, Higgins JM. The kinase haspin is required for mitotic histone H3 Thr 3 phosphorylation and normal metaphase chromosome alignment. *Genes Dev.* 2005;19(4):472-88.
69. Zhang Y, Griffin K, Mondal N, Parvin JD. Phosphorylation of histone H2A inhibits transcription on chromatin templates. *J Biol Chem.* 2004;279(21):21866-72.

70. Cao R, Wang L, Wang H, Xia L, Erdjument-Bromage H, Tempst P, et al. Role of histone H3 lysine 27 methylation in Polycomb-group silencing. *Science*. 2002;298(5595):1039-43.
71. Kuo MH, Brownell JE, Sobel RE, Ranalli TA, Cook RG, Edmondson DG, et al. Transcription-linked acetylation by Gcn5p of histones H3 and H4 at specific lysines. *Nature*. 1996;383(6597):269-72.
72. Masumoto H, Hawke D, Kobayashi R, Verreault A. A role for cell-cycle-regulated histone H3 lysine 56 acetylation in the DNA damage response. *Nature*. 2005;436(7048):294-8.
73. Verdone L, Agricola E, Caserta M, Di Mauro E. Histone acetylation in gene regulation. *Brief Funct Genomic Proteomic*. 2006;5(3):209-21.
74. Strahl BD, Allis CD. The language of covalent histone modifications. *Nature*. 2000;403(6765):41-5.
75. Allfrey VG, Faulkner R, Mirsky AE. Acetylation and Methylation of Histones and Their Possible Role in the Regulation of Rna Synthesis. *Proc Natl Acad Sci U S A*. 1964;51:786-94.
76. Chen Y, Sprung R, Tang Y, Ball H, Sangras B, Kim SC, et al. Lysine propionylation and butyrylation are novel post-translational modifications in histones. *Mol Cell Proteomics*. 2007;6(5):812-9.
77. Xu Y, Ding YX, Ding J, Wu LY, Xue Y. Mal-Lys: prediction of lysine malonylation sites in proteins integrated sequence-based features with mRMR feature selection. *Sci Rep*. 2016;6:38318.
78. Weinert BT, Scholz C, Wagner SA, Iesmantavicius V, Su D, Daniel JA, et al. Lysine succinylation is a frequently occurring modification in prokaryotes and eukaryotes and extensively overlaps with acetylation. *Cell Rep*. 2013;4(4):842-51.
79. Thompson PR, Fast W. Histone citrullination by protein arginine deiminase: is arginine methylation a green light or a roadblock? *ACS Chem Biol*. 2006;1(7):433-41.
80. Annunziato AT. DNA Packaging: Nucleosomes and Chromatin. *Nature Education*. 2008;1(1):26.
81. Williams SK, Truong D, Tyler JK. Acetylation in the globular core of histone H3 on lysine-56 promotes chromatin disassembly during transcriptional activation. *Proc Natl Acad Sci U S A*. 2008;105(26):9000-5.
82. Bird AW, Yu DY, Pray-Grant MG, Qiu Q, Harmon KE, Megee PC, et al. Acetylation of histone H4 by Esa1 is required for DNA double-strand break repair. *Nature*. 2002;419(6905):411-5.
83. Unnikrishnan A, Gafken PR, Tsukiyama T. Dynamic changes in histone acetylation regulate origins of DNA replication. *Nat Struct Mol Biol*. 2010;17(4):430-7.
84. Kebede AF, Nieborak A, Shahidian LZ, Le Gras S, Richter F, Gomez DA, et al. Histone propionylation is a mark of active chromatin. *Nat Struct Mol Biol*. 2017;24(12):1048-56.

85. Sabari BR, Tang Z, Huang H, Yong-Gonzalez V, Molina H, Kong HE, et al. Intracellular crotonyl-CoA stimulates transcription through p300-catalyzed histone crotonylation. *Mol Cell*. 2015;58(2):203-15.
86. Dai L, Peng C, Montellier E, Lu Z, Chen Y, Ishii H, et al. Lysine 2-hydroxyisobutyrylation is a widely distributed active histone mark. *Nat Chem Biol*. 2014;10(5):365-70.
87. Hirschev MD, Zhao Y. Metabolic Regulation by Lysine Malonylation, Succinylation, and Glutarylation. *Mol Cell Proteomics*. 2015;14(9):2308-15.
88. Krogan NJ, Kim M, Tong A, Golshani A, Cagney G, Canadien V, et al. Methylation of histone H3 by Set2 in *Saccharomyces cerevisiae* is linked to transcriptional elongation by RNA polymerase II. *Mol Cell Biol*. 2003;23(12):4207-18.
89. Waldmann T, Izzo A, Kamieniarz K, Richter F, Vogler C, Sarg B, et al. Methylation of H2AR29 is a novel repressive PRMT6 target. *Epigenetics Chromatin*. 2011;4:11.
90. Wisniewski JR, Zougman A, Mann M. Nepsilon-formylation of lysine is a widespread post-translational modification of nuclear proteins occurring at residues involved in regulation of chromatin function. *Nucleic Acids Res*. 2008;36(2):570-7.
91. Bungard D, Fuerth BJ, Zeng PY, Faubert B, Maas NL, Viollet B, et al. Signaling kinase AMPK activates stress-promoted transcription via histone H2B phosphorylation. *Science*. 2010;329(5996):1201-5.
92. Mavuluri J, Beesetti S, Surabhi R, Kremerskothen J, Venkatraman G, Rayala SK. Phosphorylation-Dependent Regulation of the DNA Damage Response of Adaptor Protein KIBRA in Cancer Cells. *Mol Cell Biol*. 2016;36(9):1354-65.
93. Niemi NM, MacKeigan JP. Mitochondrial phosphorylation in apoptosis: flipping the death switch. *Antioxid Redox Signal*. 2013;19(6):572-82.
94. Chattopadhyay S, Kuzmanovic T, Zhang Y, Wetzel JL, Sen GC. Ubiquitination of the Transcription Factor IRF-3 Activates RIPA, the Apoptotic Pathway that Protects Mice from Viral Pathogenesis. *Immunity*. 2016;44(5):1151-61.
95. Nathan D, Ingvarsdottir K, Sterner DE, Bylebyl GR, Dokmanovic M, Dorsey JA, et al. Histone sumoylation is a negative regulator in *Saccharomyces cerevisiae* and shows dynamic interplay with positive-acting histone modifications. *Genes Dev*. 2006;20(8):966-76.
96. Messner S, Hottiger MO. Histone ADP-ribosylation in DNA repair, replication and transcription. *Trends Cell Biol*. 2011;21(9):534-42.
97. Cuthbert GL, Daujat S, Snowden AW, Erdjument-Bromage H, Hagiwara T, Yamada M, et al. Histone deimination antagonizes arginine methylation. *Cell*. 2004;118(5):545-53.
98. Huang H, Sabari BR, Garcia BA, Allis CD, Zhao Y. SnapShot: histone modifications. *Cell*. 2014;159(2):458- e1.
99. Kouzarides T. Chromatin modifications and their function. *Cell*. 2007;128(4):693-705.

100. Tamkun JW, Deuring R, Scott MP, Kissinger M, Pattatucci AM, Kaufman TC, et al. *brahma*: a regulator of *Drosophila* homeotic genes structurally related to the yeast transcriptional activator SNF2/SWI2. *Cell*. 1992;68(3):561-72.
101. Gregory GD, Vakoc CR, Rozovskaia T, Zheng X, Patel S, Nakamura T, et al. Mammalian ASH1L is a histone methyltransferase that occupies the transcribed region of active genes. *Mol Cell Biol*. 2007;27(24):8466-79.
102. Manning ET, Ikehara T, Ito T, Kadonaga JT, Kraus WL. p300 forms a stable, template-committed complex with chromatin: role for the bromodomain. *Mol Cell Biol*. 2001;21(12):3876-87.
103. Mujtaba S, He Y, Zeng L, Yan S, Plotnikova O, Sachchidanand, et al. Structural mechanism of the bromodomain of the coactivator CBP in p53 transcriptional activation. *Mol Cell*. 2004;13(2):251-63.
104. Hudson BP, Martinez-Yamout MA, Dyson HJ, Wright PE. Solution structure and acetyl-lysine binding activity of the GCN5 bromodomain. *J Mol Biol*. 2000;304(3):355-70.
105. Banting GS, Barak O, Ames TM, Burnham AC, Kardel MD, Cooch NS, et al. CECR2, a protein involved in neurulation, forms a novel chromatin remodeling complex with SNF2L. *Hum Mol Genet*. 2005;14(4):513-24.
106. Chandrasekaran R, Thompson M. Polybromo-1-bromodomains bind histone H3 at specific acetyl-lysine positions. *Biochem Biophys Res Commun*. 2007;355(3):661-6.
107. Shen W, Xu C, Huang W, Zhang J, Carlson JE, Tu X, et al. Solution structure of human Brg1 bromodomain and its specific binding to acetylated histone tails. *Biochemistry*. 2007;46(8):2100-10.
108. Zou JX, Revenko AS, Li LB, Gemo AT, Chen HW. ANCCA, an estrogen-regulated AAA+ ATPase coactivator for ERalpha, is required for coregulator occupancy and chromatin modification. *Proc Natl Acad Sci U S A*. 2007;104(46):18067-72.
109. Dey A, Ellenberg J, Farina A, Coleman AE, Maruyama T, Sciortino S, et al. A bromodomain protein, MCAP, associates with mitotic chromosomes and affects G(2)-to-M transition. *Mol Cell Biol*. 2000;20(17):6537-49.
110. Zhou Y, Grummt I. The PHD finger/bromodomain of NoRC interacts with acetylated histone H4K16 and is sufficient for rDNA silencing. *Curr Biol*. 2005;15(15):1434-8.
111. Mantovani F, Drost J, Voorhoeve PM, Del Sal G, Agami R. Gene regulation and tumor suppression by the bromodomain-containing protein BRD7. *Cell Cycle*. 2010;9(14):2777-81.
112. Cattaneo M, Morozumi Y, Perazza D, Boussouar F, Jamshidikia M, Rousseaux S, et al. Lessons from yeast on emerging roles of the ATAD2 protein family in gene regulation and genome organization. *Mol Cells*. 2014;37(12):851-6.
113. Josling GA, Petter M, Oehring SC, Gupta AP, Dietz O, Wilson DW, et al. A *Plasmodium Falciparum* Bromodomain Protein Regulates Invasion Gene Expression. *Cell Host Microbe*. 2015;17(6):741-51.

114. Alonso VL, Ritagliati C, Cribb P, Cricco JA, Serra EC. Overexpression of bromodomain factor 3 in *Trypanosoma cruzi* (TcBDF3) affects differentiation of the parasite and protects it against bromodomain inhibitors. *FEBS J.* 2016;283(11):2051-66.
115. Dhalluin C, Carlson JE, Zeng L, He C, Aggarwal AK, Zhou MM. Structure and ligand of a histone acetyltransferase bromodomain. *Nature.* 1999;399(6735):491-6.
116. Vollmuth F, Geyer M. Interaction of propionylated and butyrylated histone H3 lysine marks with Brd4 bromodomains. *Angew Chem Int Ed Engl.* 2010;49(38):6768-72.
117. Flynn EM, Huang OW, Poy F, Oppikofer M, Bellon SF, Tang Y, et al. A Subset of Human Bromodomains Recognizes Butyryllysine and Crotonyllysine Histone Peptide Modifications. *Structure.* 2015;23(10):1801-14.
118. Crawford TD, Tsui V, Flynn EM, Wang S, Taylor AM, Cote A, et al. Diving into the Water: Inducible Binding Conformations for BRD4, TAF1(2), BRD9, and CECR2 Bromodomains. *J Med Chem.* 2016;59(11):5391-402.
119. Owen DJ, Ornaghi P, Yang JC, Lowe N, Evans PR, Ballario P, et al. The structural basis for the recognition of acetylated histone H4 by the bromodomain of histone acetyltransferase gcn5p. *EMBO J.* 2000;19(22):6141-9.
120. Umehara T, Nakamura Y, Jang MK, Nakano K, Tanaka A, Ozato K, et al. Structural basis for acetylated histone H4 recognition by the human BRD2 bromodomain. *J Biol Chem.* 2010;285(10):7610-8.
121. Filippakopoulos P, Picaud S, Mangos M, Keates T, Lambert JP, Barsyte-Lovejoy D, et al. Histone recognition and large-scale structural analysis of the human bromodomain family. *Cell.* 2012;149(1):214-31.
122. Liu Z, Wang P, Chen H, Wold EA, Tian B, Brasier AR, et al. Drug Discovery Targeting Bromodomain-Containing Protein 4. *J Med Chem.* 2017;60(11):4533-58.
123. Perez-Salvia M, Esteller M. Bromodomain inhibitors and cancer therapy: From structures to applications. *Epigenetics.* 2017;12(5):323-39.
124. Hofvander J, Tayebwa J, Nilsson J, Magnusson L, Brosjo O, Larsson O, et al. RNA sequencing of sarcomas with simple karyotypes: identification and enrichment of fusion transcripts. *Lab Invest.* 2015;95(6):603-9.
125. Shao Z, Zhang R, Khodadadi-Jamayran A, Chen B, Crowley MR, Festok MA, et al. The acetyllysine reader BRD3R promotes human nuclear reprogramming and regulates mitosis. *Nat Commun.* 2016;7:10869.
126. Floyd SR, Pacold ME, Huang Q, Clarke SM, Lam FC, Cannell IG, et al. The bromodomain protein Brd4 insulates chromatin from DNA damage signalling. *Nature.* 2013;498(7453):246-50.
127. Smith SG, Zhou MM. The Bromodomain: A New Target in Emerging Epigenetic Medicine. *ACS Chem Biol.* 2016;11(3):598-608.

128. Hay DA, Fedorov O, Martin S, Singleton DC, Tallant C, Wells C, et al. Discovery and optimization of small-molecule ligands for the CBP/p300 bromodomains. *J Am Chem Soc.* 2014;136(26):9308-19.
129. Shi J, Vakoc CR. The mechanisms behind the therapeutic activity of BET bromodomain inhibition. *Mol Cell.* 2014;54(5):728-36.
130. Jennings LE, Measures AR, Wilson BG, Conway SJ. Phenotypic screening and fragment-based approaches to the discovery of small-molecule bromodomain ligands. *Future Med Chem.* 2014;6(2):179-204.
131. Bamborough P, Chung CW. Fragments in bromodomain drug discovery. *Medchemcomm.* 2015;6(9):1587-604.
132. Romero FA, Taylor AM, Crawford TD, Tsui V, Cote A, Magnuson S. Disrupting Acetyl-Lysine Recognition: Progress in the Development of Bromodomain Inhibitors. *J Med Chem.* 2016;59(4):1271-98.
133. Chaikuad A, Petros AM, Fedorov O, Xu J, Knapp S. Structure-based approaches towards identification of fragments for the low-druggability ATAD2 bromodomain. *MedChemComm.* 2014;5(12):1843-8.
134. Unzue A, Zhao H, Lolli G, Dong J, Zhu J, Zechner M, et al. The "Gatekeeper" Residue Influences the Mode of Binding of Acetyl Indoles to Bromodomains. *J Med Chem.* 2016;59(7):3087-97.
135. Theodoulou NH, Bamborough P, Bannister AJ, Becher I, Bit RA, Che KH, et al. Discovery of I-BRD9, a Selective Cell Active Chemical Probe for Bromodomain Containing Protein 9 Inhibition. *J Med Chem.* 2016;59(4):1425-39.
136. Taylor AM, Cote A, Hewitt MC, Pastor R, Leblanc Y, Nasveschuk CG, et al. Fragment-Based Discovery of a Selective and Cell-Active Benzodiazepinone CBP/EP300 Bromodomain Inhibitor (CPI-637). *ACS Med Chem Lett.* 2016;7(5):531-6.
137. Vidler LR, Brown N, Knapp S, Hoelder S. Druggability analysis and structural classification of bromodomain acetyl-lysine binding sites. *J Med Chem.* 2012;55(17):7346-59.
138. Filippakopoulos P, Qi J, Picaud S, Shen Y, Smith WB, Fedorov O, et al. Selective inhibition of BET bromodomains. *Nature.* 2010;468(7327):1067-73.
139. Nicodeme E, Jeffrey KL, Schaefer U, Beinke S, Dewell S, Chung CW, et al. Suppression of inflammation by a synthetic histone mimic. *Nature.* 2010;468(7327):1119-23.
140. Miyoshi S, Ooike S, Iwata K, Hikawa H, Sugahara K, inventors; Mitsubishi Tanabe Pharma Corporation, Japan . assignee. Antitumor agent patent WO2009084693A1. 2009.
141. Darcis G, Kula A, Bouchat S, Fujinaga K, Corazza F, Ait-Ammar A, et al. An In-Depth Comparison of Latency-Reversing Agent Combinations in Various In Vitro and Ex Vivo HIV-1 Latency Models Identified Bryostatins-1+JQ1 and Ingenol-B+JQ1 to Potently Reactivate Viral Gene Expression. *PLoS Pathog.* 2015;11(7):e1005063.

142. Jiang G, Mendes EA, Kaiser P, Wong DP, Tang Y, Cai I, et al. Synergistic Reactivation of Latent HIV Expression by Ingenol-3-Angelate, PEP005, Targeted NF- κ B Signaling in Combination with JQ1 Induced p-TEFb Activation. *PLoS Pathog.* 2015;11(7):e1005066.
143. Li Z, Guo J, Wu Y, Zhou Q. The BET bromodomain inhibitor JQ1 activates HIV latency through antagonizing Brd4 inhibition of Tat-transactivation. *Nucleic Acids Res.* 2013;41(1):277-87.
144. Zhu J, Gaiha GD, John SP, Pertel T, Chin CR, Gao G, et al. Reactivation of latent HIV-1 by inhibition of BRD4. *Cell Rep.* 2012;2(4):807-16.
145. Zinchenko MK, Siliciano RF. Editorial: JQ1: giving HIV-1 expression a boost by blocking bromodomains? *J Leukoc Biol.* 2012;92(6):1127-9.
146. Anand P, Brown JD, Lin CY, Qi J, Zhang R, Artero PC, et al. BET bromodomains mediate transcriptional pause release in heart failure. *Cell.* 2013;154(3):569-82.
147. Spiltoir JI, Stratton MS, Cavašin MA, Demos-Davies K, Reid BG, Qi J, et al. BET acetyl-lysine binding proteins control pathological cardiac hypertrophy. *J Mol Cell Cardiol.* 2013;63:175-9.
148. Mumby S, Gambaryan N, Meng C, Perros F, Humbert M, Wort SJ, et al. Bromodomain and extra-terminal protein mimic JQ1 decreases inflammation in human vascular endothelial cells: Implications for pulmonary arterial hypertension. *Respirology.* 2017;22(1):157-64.
149. Suarez-Alvarez B, Morgado-Pascual JL, Rayego-Mateos S, Rodriguez RM, Rodriguez-Diez R, Cannata-Ortiz P, et al. Inhibition of Bromodomain and Extraterminal Domain Family Proteins Ameliorates Experimental Renal Damage. *J Am Soc Nephrol.* 2017;28(2):504-19.
150. Belkina AC, Nikolajczyk BS, Denis GV. BET protein function is required for inflammation: Brd2 genetic disruption and BET inhibitor JQ1 impair mouse macrophage inflammatory responses. *J Immunol.* 2013;190(7):3670-8.
151. Das A, Chai JC, Yang CS, Lee YS, Das ND, Jung KH, et al. Dual transcriptome sequencing reveals resistance of TLR4 ligand-activated bone marrow-derived macrophages to inflammation mediated by the BET inhibitor JQ1. *Sci Rep.* 2015;5:16932.
152. Jung KH, Das A, Chai JC, Kim SH, Morya N, Park KS, et al. RNA sequencing reveals distinct mechanisms underlying BET inhibitor JQ1-mediated modulation of the LPS-induced activation of BV-2 microglial cells. *J Neuroinflammation.* 2015;12:36.
153. Toniolo PA, Liu S, Yeh JE, Moraes-Vieira PM, Walker SR, Vafaizadeh V, et al. Inhibiting STAT5 by the BET bromodomain inhibitor JQ1 disrupts human dendritic cell maturation. *J Immunol.* 2015;194(7):3180-90.
154. Matzuk MM, McKeown MR, Filippakopoulos P, Li Q, Ma L, Agno JE, et al. Small-molecule inhibition of BRDT for male contraception. *Cell.* 2012;150(4):673-84.
155. Choi SK, Hong SH, Kim HS, Shin CY, Nam SW, Choi WS, et al. JQ1, an inhibitor of the epigenetic reader BRD4, suppresses the bidirectional MYC-AP4 axis via multiple mechanisms. *Oncol Rep.* 2016;35(2):1186-94.

156. Kato F, Fiorentino FP, Alibes A, Perucho M, Sanchez-Cespedes M, Kohno T, et al. MYCL is a target of a BET bromodomain inhibitor, JQ1, on growth suppression efficacy in small cell lung cancer cells. *Oncotarget*. 2016;7(47):77378-88.
157. Shahbazi J, Liu PY, Atmadibrata B, Bradner JE, Marshall GM, Lock RB, et al. The Bromodomain Inhibitor JQ1 and the Histone Deacetylase Inhibitor Panobinostat Synergistically Reduce N-Myc Expression and Induce Anticancer Effects. *Clin Cancer Res*. 2016;22(10):2534-44.
158. Shao Q, Kannan A, Lin Z, Stack BC, Jr., Suen JY, Gao L. BET protein inhibitor JQ1 attenuates Myc-amplified MCC tumor growth in vivo. *Cancer Res*. 2014;74(23):7090-102.
159. Wu Z, Hu Z, Han X, Li Z, Zhu Q, Wang Y, et al. The BET-Bromodomain Inhibitor JQ1 synergized ABT-263 against colorectal cancer cells through suppressing c-Myc-induced miR-1271-5p expression. *Biomed Pharmacother*. 2017;95:1574-9.
160. Yao W, Yue P, Khuri FR, Sun SY. The BET bromodomain inhibitor, JQ1, facilitates c-FLIP degradation and enhances TRAIL-induced apoptosis independent of BRD4 and c-Myc inhibition. *Oncotarget*. 2015;6(33):34669-79.
161. Zhang HT, Gui T, Sang Y, Yang J, Li YH, Liang GH, et al. The BET Bromodomain Inhibitor JQ1 Suppresses Chondrosarcoma Cell Growth via Regulation of YAP/p21/c-Myc Signaling. *J Cell Biochem*. 2017;118(8):2182-92.
162. Fahey JM, Stancill JS, Smith BC, Girotti AW. Nitric oxide antagonism to glioblastoma photodynamic therapy and mitigation thereof by BET bromodomain inhibitor JQ1. *J Biol Chem*. 2018;293(14):5345-59.
163. Mirguet O, Gosmini R, Toum J, Clement CA, Barnathan M, Brusq JM, et al. Discovery of epigenetic regulator I-BET762: lead optimization to afford a clinical candidate inhibitor of the BET bromodomains. *J Med Chem*. 2013;56(19):7501-15.
164. Chung CW, Coste H, White JH, Mirguet O, Wilde J, Gosmini RL, et al. Discovery and characterization of small molecule inhibitors of the BET family bromodomains. *J Med Chem*. 2011;54(11):3827-38.
165. A Dose Escalation Study to Investigate the Safety, Pharmacokinetics (PK), Pharmacodynamics (PD) and Clinical Activity of GSK525762 in Subjects With Relapsed, Refractory Hematologic Malignancies. <https://ClinicalTrials.gov/show/NCT01943851>.
166. Dose Escalation and Expansion Study of GSK525762 in Combination With Fulvestrant in Subjects With Estrogen Receptor Positive (ER+) Breast Cancer. <https://ClinicalTrials.gov/show/NCT02964507>.
167. A Study to Investigate the Safety, Pharmacokinetics, Pharmacodynamics, and Clinical Activity of GSK525762 in Subjects With NUT Midline Carcinoma (NMC) and Other Cancers. <https://ClinicalTrials.gov/show/NCT01587703>.
168. A Dose Escalation Study to Investigate the Safety, Pharmacokinetics (PK), Pharmacodynamics (PD), and Clinical Activity of GSK525762 Plus Trametinib in Subjects With Solid Tumors. <https://ClinicalTrials.gov/show/NCT03266159>.

169. Dose Escalation and Dose Expansion Study of GSK525762 in Combination With Androgen Deprivation Therapy and Other Agents in Subjects With Castrate-resistant Prostate Cancer. <https://ClinicalTrials.gov/show/NCT03150056>.
170. A Cross-over Study to Evaluate the Effect of Itraconazole and Rifampicin on the Pharmacokinetics (PK) of GSK525762 in Healthy Female Subjects of Non Child Bearing Potential. <https://ClinicalTrials.gov/show/NCT02706535>.
171. Compassionate Use Individual Request Program for GSK525762 in NUT Midline Carcinoma. <https://ClinicalTrials.gov/show/NCT03702036>.
172. Romero FA, Murray J, Lai KW, Tsui V, Albrecht BK, An L, et al. GNE-781, A Highly Advanced Potent and Selective Bromodomain Inhibitor of Cyclic Adenosine Monophosphate Response Element Binding Protein, Binding Protein (CBP). *J Med Chem.* 2017;60(22):9162-83.
173. Crawford TD, Romero FA, Lai KW, Tsui V, Taylor AM, de Leon Boenig G, et al. Discovery of a Potent and Selective in Vivo Probe (GNE-272) for the Bromodomains of CBP/EP300. *J Med Chem.* 2016;59(23):10549-63.
174. Lai KW, Romero FA, Tsui V, Beresini MH, de Leon Boenig G, Bronner SM, et al. Design and synthesis of a biaryl series as inhibitors for the bromodomains of CBP/P300. *Bioorg Med Chem Lett.* 2018;28(1):15-23.
175. Picaud S, Fedorov O, Thanasopoulou A, Leonards K, Jones K, Meier J, et al. Generation of a Selective Small Molecule Inhibitor of the CBP/p300 Bromodomain for Leukemia Therapy. *Cancer Res.* 2015;75(23):5106-19.
176. Bamborough P, Chung CW, Demont EH, Furze RC, Bannister AJ, Che KH, et al. A Chemical Probe for the ATAD2 Bromodomain. *Angew Chem Int Ed Engl.* 2016;55(38):11382-6.
177. Fernandez-Montalvan AE, Berger M, Kuroпка B, Koo SJ, Badock V, Weiske J, et al. Isoform-Selective ATAD2 Chemical Probe with Novel Chemical Structure and Unusual Mode of Action. *ACS Chem Biol.* 2017;12(11):2730-6.
178. Chen P, Chaikuad A, Bamborough P, Bantscheff M, Bountra C, Chung CW, et al. Discovery and Characterization of GSK2801, a Selective Chemical Probe for the Bromodomains BAZ2A and BAZ2B. *J Med Chem.* 2016;59(4):1410-24.
179. Drouin L, McGrath S, Vidler LR, Chaikuad A, Monteiro O, Tallant C, et al. Structure enabled design of BAZ2-ICR, a chemical probe targeting the bromodomains of BAZ2A and BAZ2B. *J Med Chem.* 2015;58(5):2553-9.
180. Crawford TD, Audia JE, Bellon S, Burdick DJ, Bommi-Reddy A, Cote A, et al. GNE-886: A Potent and Selective Inhibitor of the Cat Eye Syndrome Chromosome Region Candidate 2 Bromodomain (CECR2). *ACS Med Chem Lett.* 2017;8(7):737-41.
181. Crawford TD, Vartanian S, Cote A, Bellon S, Duplessis M, Flynn EM, et al. Inhibition of bromodomain-containing protein 9 for the prevention of epigenetically-defined drug resistance. *Bioorg Med Chem Lett.* 2017;27(15):3534-41.

182. Clark PG, Vieira LC, Tallant C, Fedorov O, Singleton DC, Rogers CM, et al. LP99: Discovery and Synthesis of the First Selective BRD7/9 Bromodomain Inhibitor. *Angew Chem Int Ed Engl.* 2015;54(21):6217-21.
183. Igoe N, Bayle ED, Fedorov O, Tallant C, Savitsky P, Rogers C, et al. Design of a Biased Potent Small Molecule Inhibitor of the Bromodomain and PHD Finger-Containing (BRPF) Proteins Suitable for Cellular and in Vivo Studies. *J Med Chem.* 2017;60(2):668-80.
184. Wang S, Tsui V, Crawford TD, Audia JE, Burdick DJ, Beresini MH, et al. GNE-371, a Potent and Selective Chemical Probe for the Second Bromodomains of Human Transcription-Initiation-Factor TFIID Subunit 1 and Transcription-Initiation-Factor TFIID Subunit 1-like. *J Med Chem.* 2018;61(20):9301-15.
185. Palmer WS, Poncet-Montange G, Liu G, Petrocchi A, Reyna N, Subramanian G, et al. Structure-Guided Design of IACS-9571, a Selective High-Affinity Dual TRIM24-BRPF1 Bromodomain Inhibitor. *J Med Chem.* 2016;59(4):1440-54.
186. Dey A, Chitsaz F, Abbasi A, Misteli T, Ozato K. The double bromodomain protein Brd4 binds to acetylated chromatin during interphase and mitosis. *Proc Natl Acad Sci U S A.* 2003;100(15):8758-63.
187. Huang B, Yang XD, Zhou MM, Ozato K, Chen LF. Brd4 coactivates transcriptional activation of NF-kappaB via specific binding to acetylated RelA. *Mol Cell Biol.* 2009;29(5):1375-87.
188. Schroder S, Cho S, Zeng L, Zhang Q, Kaehlcke K, Mak L, et al. Two-pronged binding with bromodomain-containing protein 4 liberates positive transcription elongation factor b from inactive ribonucleoprotein complexes. *J Biol Chem.* 2012;287(2):1090-9.
189. Rahman S, Sowa ME, Ottinger M, Smith JA, Shi Y, Harper JW, et al. The Brd4 extraterminal domain confers transcription activation independent of pTEFb by recruiting multiple proteins, including NSD3. *Mol Cell Biol.* 2011;31(13):2641-52.
190. Zhang Q, Zeng L, Shen C, Ju Y, Konuma T, Zhao C, et al. Structural Mechanism of Transcriptional Regulator NSD3 Recognition by the ET Domain of BRD4. *Structure.* 2016;24(7):1201-8.
191. Konuma T, Yu D, Zhao C, Ju Y, Sharma R, Ren C, et al. Structural Mechanism of the Oxygenase JMJD6 Recognition by the Extraterminal (ET) Domain of BRD4. *Sci Rep.* 2017;7(1):16272.
192. Devaiah BN, Case-Borden C, Gegonne A, Hsu CH, Chen Q, Meerzaman D, et al. BRD4 is a histone acetyltransferase that evicts nucleosomes from chromatin. *Nat Struct Mol Biol.* 2016;23(6):540-8.
193. Tropberger P, Pott S, Keller C, Kamieniarz-Gdula K, Caron M, Richter F, et al. Regulation of transcription through acetylation of H3K122 on the lateral surface of the histone octamer. *Cell.* 2013;152(4):859-72.
194. Bisgrove DA, Mahmoudi T, Henklein P, Verdin E. Conserved P-TEFb-interacting domain of BRD4 inhibits HIV transcription. *Proc Natl Acad Sci U S A.* 2007;104(34):13690-5.

195. Itzen F, Greifenberg AK, Bosken CA, Geyer M. Brd4 activates P-TEFb for RNA polymerase II CTD phosphorylation. *Nucleic Acids Res.* 2014;42(12):7577-90.
196. Devaiah BN, Lewis BA, Cherman N, Hewitt MC, Albrecht BK, Robey PG, et al. BRD4 is an atypical kinase that phosphorylates serine2 of the RNA polymerase II carboxy-terminal domain. *Proc Natl Acad Sci U S A.* 2012;109(18):6927-32.
197. Jang MK, Mochizuki K, Zhou M, Jeong HS, Brady JN, Ozato K. The bromodomain protein Brd4 is a positive regulatory component of P-TEFb and stimulates RNA polymerase II-dependent transcription. *Mol Cell.* 2005;19(4):523-34.
198. Buratowski S. Progression through the RNA polymerase II CTD cycle. *Mol Cell.* 2009;36(4):541-6.
199. Yang Z, Yik JH, Chen R, He N, Jang MK, Ozato K, et al. Recruitment of P-TEFb for stimulation of transcriptional elongation by the bromodomain protein Brd4. *Mol Cell.* 2005;19(4):535-45.
200. Schweiger MR, You J, Howley PM. Bromodomain protein 4 mediates the papillomavirus E2 transcriptional activation function. *J Virol.* 2006;80(9):4276-85.
201. McPhillips MG, Oliveira JG, Spindler JE, Mitra R, McBride AA. Brd4 is required for e2-mediated transcriptional activation but not genome partitioning of all papillomaviruses. *J Virol.* 2006;80(19):9530-43.
202. Baxter MK, McPhillips MG, Ozato K, McBride AA. The mitotic chromosome binding activity of the papillomavirus E2 protein correlates with interaction with the cellular chromosomal protein, Brd4. *J Virol.* 2005;79(8):4806-18.
203. French CA, Miyoshi I, Kubonishi I, Grier HE, Perez-Atayde AR, Fletcher JA. BRD4-NUT fusion oncogene: a novel mechanism in aggressive carcinoma. *Cancer Res.* 2003;63(2):304-7.
204. French CA, Miyoshi I, Aster JC, Kubonishi I, Kroll TG, Dal Cin P, et al. BRD4 bromodomain gene rearrangement in aggressive carcinoma with translocation t(15;19). *Am J Pathol.* 2001;159(6):1987-92.
205. World Health Organization. Cardiovascular diseases (CVDs) 2017 [cited 2018 7 Nov]. Available from: [http://www.who.int/en/news-room/fact-sheets/detail/cardiovascular-diseases-\(cvds\)](http://www.who.int/en/news-room/fact-sheets/detail/cardiovascular-diseases-(cvds)).
206. Australian Institute of Health and Welfare. Health-care expenditure on cardiovascular diseases 2008–09. 2014.
207. Goss J. Projection of Australian health care expenditure by disease, 2003 to 2033. Canberra: Australian Institute of Health and Welfare; 2008.
208. Australian Bureau of Statistics. Causes of Death, Australia, 2017. 2018.
209. Heart Foundation. Medicines [cited 2018 28 Nov]. Available from: <https://www.heartfoundation.org.au/your-heart/living-with-heart-disease/medicines>.

210. American Heart Association. Cardiac Medications 2015 [updated 31 Jul 2015; cited 2018 7 Nov]. Available from: <https://www.heart.org/en/health-topics/heart-attack/treatment-of-a-heart-attack/cardiac-medications#.Wu-R3qSFO70>.
211. Espinoza-Derout J, Wagner M, Saliccioli L, Lazar JM, Bhaduri S, Mascareno E, et al. Positive transcription elongation factor b activity in compensatory myocardial hypertrophy is regulated by cardiac lineage protein-1. *Circ Res*. 2009;104(12):1347-54.
212. Yoshikawa N, Shimizu N, Maruyama T, Sano M, Matsuhashi T, Fukuda K, et al. Cardiomyocyte-specific overexpression of HEXIM1 prevents right ventricular hypertrophy in hypoxia-induced pulmonary hypertension in mice. *PLoS One*. 2012;7(12):e52522.
213. Courboulin A, Paulin R, Giguere NJ, Saksouk N, Perreault T, Meloche J, et al. Role for miR-204 in human pulmonary arterial hypertension. *J Exp Med*. 2011;208(3):535-48.
214. Meloche J, Potus F, Vaillancourt M, Bourgeois A, Johnson I, Deschamps L, et al. Bromodomain-Containing Protein 4: The Epigenetic Origin of Pulmonary Arterial Hypertension. *Circ Res*. 2015;117(6):525-35.
215. Bonnet S, Rochefort G, Sutendra G, Archer SL, Haromy A, Webster L, et al. The nuclear factor of activated T cells in pulmonary arterial hypertension can be therapeutically targeted. *Proc Natl Acad Sci U S A*. 2007;104(27):11418-23.
216. Chen R, Yan J, Liu P, Wang Z, Wang C, Zhong W, et al. The role of nuclear factor of activated T cells in pulmonary arterial hypertension. *Cell Cycle*. 2017;16(6):508-14.
217. Meloche J, Lampron MC, Nadeau V, Maltais M, Potus F, Lambert C, et al. Implication of Inflammation and Epigenetic Readers in Coronary Artery Remodeling in Patients With Pulmonary Arterial Hypertension. *Arterioscler Thromb Vasc Biol*. 2017;37(8):1513-23.
218. Mirguet O, Lamotte Y, Donche F, Toum J, Gellibert F, Bouillot A, et al. From ApoA1 upregulation to BET family bromodomain inhibition: discovery of I-BET151. *Bioorg Med Chem Lett*. 2012;22(8):2963-7.
219. Bailey D, Jahagirdar R, Gordon A, Hafiane A, Campbell S, Chatur S, et al. RVX-208: a small molecule that increases apolipoprotein A-I and high-density lipoprotein cholesterol in vitro and in vivo. *J Am Coll Cardiol*. 2010;55(23):2580-9.
220. Toth PP. Cardiology patient page. The "good cholesterol": high-density lipoprotein. *Circulation*. 2005;111(5):e89-91.
221. McLure KG, Gesner EM, Tsujikawa L, Kharenko OA, Attwell S, Campeau E, et al. RVX-208, an inducer of ApoA-I in humans, is a BET bromodomain antagonist. *PLoS One*. 2013;8(12):e83190.
222. van der Krieken SE, Popeijus HE, Mensink RP, Plat J. Link Between ER-Stress, PPAR-Alpha Activation, and BET Inhibition in Relation to Apolipoprotein A-I Transcription in HepG2 Cells. *J Cell Biochem*. 2017;118(8):2161-7.
223. French CA, Ramirez CL, Kolmakova J, Hickman TT, Cameron MJ, Thyne ME, et al. BRD-NUT oncoproteins: a family of closely related nuclear proteins that block epithelial differentiation and maintain the growth of carcinoma cells. *Oncogene*. 2008;27(15):2237-42.

224. French CA, Rahman S, Walsh EM, Kuhnle S, Grayson AR, Lemieux ME, et al. NSD3-NUT fusion oncoprotein in NUT midline carcinoma: implications for a novel oncogenic mechanism. *Cancer Discov.* 2014;4(8):928-41.
225. French CA. Pathogenesis of NUT midline carcinoma. *Annu Rev Pathol.* 2012;7:247-65.
226. Wang R, You J. Mechanistic analysis of the role of bromodomain-containing protein 4 (BRD4) in BRD4-NUT oncoprotein-induced transcriptional activation. *J Biol Chem.* 2015;290(5):2744-58.
227. French CA. The importance of diagnosing NUT midline carcinoma. *Head Neck Pathol.* 2013;7(1):11-6.
228. Shehata BM, Steelman CK, Abramowsky CR, Olson TA, French CA, Saxe DF, et al. NUT midline carcinoma in a newborn with multiorgan disseminated tumor and a 2-year-old with a pancreatic/hepatic primary. *Pediatr Dev Pathol.* 2010;13(6):481-5.
229. Bellizzi AM, Bruzzi C, French CA, Stelow EB. The cytologic features of NUT midline carcinoma. *Cancer.* 2009;117(6):508-15.
230. French CA, Kutok JL, Faquin WC, Toretzky JA, Antonescu CR, Griffin CA, et al. Midline carcinoma of children and young adults with NUT rearrangement. *J Clin Oncol.* 2004;22(20):4135-9.
231. den Bakker MA, Beverloo BH, van den Heuvel-Eibrink MM, Meeuwis CA, Tan LM, Johnson LA, et al. NUT midline carcinoma of the parotid gland with mesenchymal differentiation. *Am J Surg Pathol.* 2009;33(8):1253-8.
232. Chau NG, Hurwitz S, Mitchell CM, Aserlind A, Grunfeld N, Kaplan L, et al. Intensive treatment and survival outcomes in NUT midline carcinoma of the head and neck. *Cancer.* 2016;122(23):3632-40.
233. Mertens F, Wiebe T, Adlercreutz C, Mandahl N, French CA. Successful treatment of a child with t(15;19)-positive tumor. *Pediatr Blood Cancer.* 2007;49(7):1015-7.
234. Rutt AL, Poulik J, Siddiqui AH, Konski A, Kalaf M, Madgy DN, et al. NUT midline carcinoma mimicking tonsillitis in an eight-year-old girl. *Ann Otol Rhinol Laryngol.* 2011;120(8):546-9.
235. Gokmen-Polar Y, Kesler K, Loehrer PJ, Sr., Badve S. NUT Midline Carcinoma Masquerading As a Thymic Carcinoma. *J Clin Oncol.* 2016;34(14):e126-9.
236. Travis WD, Brambilla E, Nicholson AG, Yatabe Y, Austin JHM, Beasley MB, et al. The 2015 World Health Organization Classification of Lung Tumors: Impact of Genetic, Clinical and Radiologic Advances Since the 2004 Classification. *J Thorac Oncol.* 2015;10(9):1243-60.
237. Reynoird N, Schwartz BE, Delvecchio M, Sadoul K, Meyers D, Mukherjee C, et al. Oncogenesis by sequestration of CBP/p300 in transcriptionally inactive hyperacetylated chromatin domains. *EMBO J.* 2010;29(17):2943-52.

238. Yan J, Diaz J, Jiao J, Wang R, You J. Perturbation of BRD4 protein function by BRD4-NUT protein abrogates cellular differentiation in NUT midline carcinoma. *J Biol Chem.* 2011;286(31):27663-75.
239. Alekseyenko AA, Walsh EM, Wang X, Grayson AR, Hsi PT, Kharchenko PV, et al. The oncogenic BRD4-NUT chromatin regulator drives aberrant transcription within large topological domains. *Genes Dev.* 2015;29(14):1507-23.
240. Stathis A, Zucca E, Bekradda M, Gomez-Roca C, Delord JP, de La Motte Rouge T, et al. Clinical Response of Carcinomas Harboring the BRD4-NUT Oncoprotein to the Targeted Bromodomain Inhibitor OTX015/MK-8628. *Cancer Discov.* 2016;6(5):492-500.
241. Dang CV, O'Donnell KA, Zeller KI, Nguyen T, Osthus RC, Li F. The c-Myc target gene network. *Semin Cancer Biol.* 2006;16(4):253-64.
242. Seth A, Gupta S, Davis RJ. Cell cycle regulation of the c-Myc transcriptional activation domain. *Mol Cell Biol.* 1993;13(7):4125-36.
243. Conacci-Sorrell M, McFerrin L, Eisenman RN. An overview of MYC and its interactome. *Cold Spring Harb Perspect Med.* 2014;4(1):a014357.
244. Meyer N, Penn LZ. Reflecting on 25 years with MYC. *Nat Rev Cancer.* 2008;8(12):976-90.
245. Chen H, Liu H, Qing G. Targeting oncogenic Myc as a strategy for cancer treatment. *Signal Transduct Target Ther.* 2018;3:5.
246. Gabay M, Li Y, Felsher DW. MYC activation is a hallmark of cancer initiation and maintenance. *Cold Spring Harb Perspect Med.* 2014;4(6).
247. Yang Z, He N, Zhou Q. Brd4 recruits P-TEFb to chromosomes at late mitosis to promote G1 gene expression and cell cycle progression. *Mol Cell Biol.* 2008;28(3):967-76.
248. Delmore JE, Issa GC, Lemieux ME, Rahl PB, Shi J, Jacobs HM, et al. BET bromodomain inhibition as a therapeutic strategy to target c-Myc. *Cell.* 2011;146(6):904-17.
249. Loven J, Hoke HA, Lin CY, Lau A, Orlando DA, Vakoc CR, et al. Selective inhibition of tumor oncogenes by disruption of super-enhancers. *Cell.* 2013;153(2):320-34.
250. Sengupta D, Kannan A, Kern M, Moreno MA, Vural E, Stack B, Jr., et al. Disruption of BRD4 at H3K27Ac-enriched enhancer region correlates with decreased c-Myc expression in Merkel cell carcinoma. *Epigenetics.* 2015;10(6):460-6.
251. Ba M, Long H, Yan Z, Wang S, Wu Y, Tu Y, et al. BRD4 promotes gastric cancer progression through the transcriptional and epigenetic regulation of c-MYC. *J Cell Biochem.* 2018;119(1):973-82.
252. Dean M, Kent RB, Sonenshein GE. Transcriptional activation of immunoglobulin alpha heavy-chain genes by translocation of the c-myc oncogene. *Nature.* 1983;305(5933):443-6.
253. Chaidos A, Caputo V, Gouvedenou K, Liu B, Marigo I, Chaudhry MS, et al. Potent antimyeloma activity of the novel bromodomain inhibitors I-BET151 and I-BET762. *Blood.* 2014;123(5):697-705.

254. Diaz T, Rodriguez V, Lozano E, Mena MP, Calderon M, Rosinol L, et al. The BET bromodomain inhibitor CPI203 improves lenalidomide and dexamethasone activity in in vitro and in vivo models of multiple myeloma by blockade of Ikaros and MYC signaling. *Haematologica*. 2017;102(10):1776-84.
255. Siu KT, Ramachandran J, Yee AJ, Eda H, Santo L, Panaroni C, et al. Preclinical activity of CPI-0610, a novel small-molecule bromodomain and extra-terminal protein inhibitor in the therapy of multiple myeloma. *Leukemia*. 2017;31(8):1760-9.
256. Wyce A, Ganji G, Smitheman KN, Chung CW, Korenchuk S, Bai Y, et al. BET inhibition silences expression of MYCN and BCL2 and induces cytotoxicity in neuroblastoma tumor models. *PLoS One*. 2013;8(8):e72967.
257. Coude MM, Braun T, Berrou J, Dupont M, Bertrand S, Masse A, et al. BET inhibitor OTX015 targets BRD2 and BRD4 and decreases c-MYC in acute leukemia cells. *Oncotarget*. 2015;6(19):17698-712.
258. Xiang Q, Zhang Y, Li J, Xue X, Wang C, Song M, et al. Y08060: A Selective BET Inhibitor for Treatment of Prostate Cancer. *ACS Med Chem Lett*. 2018;9(3):262-7.
259. Trabucco SE, Gerstein RM, Evens AM, Bradner JE, Shultz LD, Greiner DL, et al. Inhibition of bromodomain proteins for the treatment of human diffuse large B-cell lymphoma. *Clin Cancer Res*. 2015;21(1):113-22.
260. Venkataraman S, Alimova I, Balakrishnan I, Harris P, Birks DK, Griesinger A, et al. Inhibition of BRD4 attenuates tumor cell self-renewal and suppresses stem cell signaling in MYC driven medulloblastoma. *Oncotarget*. 2014;5(9):2355-71.
261. Bolin S, Borgenvik A, Persson CU, Sundstrom A, Qi J, Bradner JE, et al. Combined BET bromodomain and CDK2 inhibition in MYC-driven medulloblastoma. *Oncogene*. 2018;37(21):2850-62.
262. Ott CJ, Kopp N, Bird L, Paranal RM, Qi J, Bowman T, et al. BET bromodomain inhibition targets both c-Myc and IL7R in high-risk acute lymphoblastic leukemia. *Blood*. 2012;120(14):2843-52.
263. Riveiro ME, Astorgues-Xerri L, Vazquez R, Frapolli R, Kwee I, Rinaldi A, et al. OTX015 (MK-8628), a novel BET inhibitor, exhibits antitumor activity in non-small cell and small cell lung cancer models harboring different oncogenic mutations. *Oncotarget*. 2016;7(51):84675-87.
264. Qiu H, Jackson AL, Kilgore JE, Zhong Y, Chan LL, Gehrig PA, et al. JQ1 suppresses tumor growth through downregulating LDHA in ovarian cancer. *Oncotarget*. 2015;6(9):6915-30.
265. Qiu H, Li J, Clark LH, Jackson AL, Zhang L, Guo H, et al. JQ1 suppresses tumor growth via PTEN/PI3K/AKT pathway in endometrial cancer. *Oncotarget*. 2016;7(41):66809-21.
266. World Health Organization. HIV/AIDS 2018 [updated 19 Jul 2018; cited 2018 12 Nov]. Available from: <http://www.who.int/en/news-room/fact-sheets/detail/hiv-aids>.

267. United States Food and Drug Administration. Antiretroviral drugs used in the treatment of HIV infection [updated 14 May 2018; cited 2018 9 Nov]. Available from: <https://www.fda.gov/forpatients/illness/hivaids/treatment/ucm118915.htm>.
268. Rhee SY, Taylor J, Fessel WJ, Kaufman D, Towner W, Troia P, et al. HIV-1 protease mutations and protease inhibitor cross-resistance. *Antimicrob Agents Chemother.* 2010;54(10):4253-61.
269. Paintsil E. Resistance, resistance, go away: persistence of nevirapine-resistant HIV mutations in HIV-infected infants. *AIDS.* 2011;25(7):997-9.
270. Hamer D. Can HIV be Cured? Mechanisms of HIV Persistence and Strategies to Combat It. *Current HIV Research.* 2004;2(2):99-111.
271. Price DH. P-TEFb, a cyclin-dependent kinase controlling elongation by RNA polymerase II. *Mol Cell Biol.* 2000;20(8):2629-34.
272. Banerjee C, Archin N, Michaels D, Belkina AC, Denis GV, Bradner J, et al. BET bromodomain inhibition as a novel strategy for reactivation of HIV-1. *J Leukoc Biol.* 2012;92(6):1147-54.
273. Huang H, Liu S, Jean M, Simpson S, Huang H, Merkley M, et al. A Novel Bromodomain Inhibitor Reverses HIV-1 Latency through Specific Binding with BRD4 to Promote Tat and P-TEFb Association. *Front Microbiol.* 2017;8:1035.
274. Lu P, Qu X, Shen Y, Jiang Z, Wang P, Zeng H, et al. The BET inhibitor OTX015 reactivates latent HIV-1 through P-TEFb. *Sci Rep.* 2016;6:24100.
275. Lu P, Shen Y, Yang H, Wang Y, Jiang Z, Yang X, et al. BET inhibitors RVX-208 and PFI-1 reactivate HIV-1 from latency. *Sci Rep.* 2017;7(1):16646.
276. Abner E, Stoszko M, Zeng L, Chen HC, Izquierdo-Bouldstridge A, Konuma T, et al. A New Quinoline BRD4 Inhibitor Targets a Distinct Latent HIV-1 Reservoir for Reactivation from Other "Shock" Drugs. *J Virol.* 2018;92(10).
277. Kim Y, Anderson JL, Lewin SR. Getting the "Kill" into "Shock and Kill": Strategies to Eliminate Latent HIV. *Cell Host Microbe.* 2018;23(1):14-26.
278. Gallo RC. Shock and kill with caution. *Science.* 2016;354(6309):177-8.
279. Jencks WP. On the attribution and additivity of binding energies. *Proc Natl Acad Sci U S A.* 1981;78(7):4046-50.
280. Shuker SB, Hajduk PJ, Meadows RP, Fesik SW. Discovering high-affinity ligands for proteins: SAR by NMR. *Science.* 1996;274(5292):1531-4.
281. Bohacek RS, McMartin C, Guida WC. The art and practice of structure-based drug design: a molecular modeling perspective. *Med Res Rev.* 1996;16(1):3-50.
282. Fink T, Bruggesser H, Reymond JL. Virtual exploration of the small-molecule chemical universe below 160 Daltons. *Angew Chem Int Ed Engl.* 2005;44(10):1504-8.
283. Congreve M, Chessari G, Tisi D, Woodhead AJ. Recent developments in fragment-based drug discovery. *J Med Chem.* 2008;51(13):3661-80.

284. Murray CW, Rees DC. The rise of fragment-based drug discovery. *Nat Chem.* 2009;1(3):187-92.
285. Erlanson DA. Introduction to fragment-based drug discovery. *Top Curr Chem.* 2012;317:1-32.
286. Baker M. Fragment-based lead discovery grows up. *Nat Rev Drug Discov.* 2013;12(1):5-7.
287. Ferguson FM, Fedorov O, Chaikuad A, Philpott M, Muniz JR, Felletar I, et al. Targeting low-druggability bromodomains: fragment based screening and inhibitor design against the BAZ2B bromodomain. *J Med Chem.* 2013;56(24):10183-7.
288. Harner MJ, Chauder BA, Phan J, Fesik SW. Fragment-based screening of the bromodomain of ATAD2. *J Med Chem.* 2014;57(22):9687-92.
289. Sekirnik Nee Measures AR, Hewings DS, Theodoulou NH, Jursins L, Lewendon KR, Jennings LE, et al. Isoxazole-Derived Amino Acids are Bromodomain-Binding Acetyl-Lysine Mimics: Incorporation into Histone H4 Peptides and Histone H3. *Angew Chem Int Ed Engl.* 2016;55(29):8353-7.
290. Eglen RM, Reisine T, Roby P, Rouleau N, Illy C, Bosse R, et al. The use of AlphaScreen technology in HTS: current status. *Curr Chem Genomics.* 2008;1:2-10.
291. Yasgar A, Jadhav A, Simeonov A, Coussens NP. AlphaScreen-Based Assays: Ultra-High-Throughput Screening for Small-Molecule Inhibitors of Challenging Enzymes and Protein-Protein Interactions. *Methods Mol Biol.* 2016;1439:77-98.
292. Silva-Santisteban MC, Westwood IM, Boxall K, Brown N, Peacock S, McAndrew C, et al. Fragment-based screening maps inhibitor interactions in the ATP-binding site of checkpoint kinase 2. *PLoS One.* 2013;8(6):e65689.
293. Cooper MA. Label-free screening of bio-molecular interactions. *Anal Bioanal Chem.* 2003;377(5):834-42.
294. Englebienne P, Van Hoonacker A, Verhas M. Surface plasmon resonance: principles, methods and applications in biomedical sciences. *Spectroscopy-an International Journal.* 2003;17(2-3):255-73.
295. Shepherd CA, Hopkins AL, Navratilova I. Fragment screening by SPR and advanced application to GPCRs. *Prog Biophys Mol Biol.* 2014;116(2-3):113-23.
296. Neumann T, Junker HD, Schmidt K, Sekul R. SPR-based fragment screening: advantages and applications. *Curr Top Med Chem.* 2007;7(16):1630-42.
297. Jameson DM, Ross JA. Fluorescence polarization/anisotropy in diagnostics and imaging. *Chem Rev.* 2010;110(5):2685-708.
298. Moerke NJ. Fluorescence Polarization (FP) Assays for Monitoring Peptide-Protein or Nucleic Acid-Protein Binding. *Curr Protoc Chem Biol.* 2009;1(1):1-15.
299. Arslan Yildiz A, Kang C, Sinner EK. Biomimetic membrane platform containing hERG potassium channel and its application to drug screening. *Analyst.* 2013;138(7):2007-12.

300. Zhang H, Wu Q, Berezin MY. Fluorescence anisotropy (polarization): from drug screening to precision medicine. *Expert Opin Drug Discov.* 2015;10(11):1145-61.
301. Rajagopal P, Waygood EB, Reizer J, Saier MH, Jr., Klevit RE. Demonstration of protein-protein interaction specificity by NMR chemical shift mapping. *Protein Sci.* 1997;6(12):2624-7.
302. Dalvit C, Fogliatto G, Stewart A, Veronesi M, Stockman B. WaterLOGSY as a method for primary NMR screening: practical aspects and range of applicability. *J Biomol NMR.* 2001;21(4):349-59.
303. Dalvit C, Pevarello P, Tato M, Veronesi M, Vulpetti A, Sundstrom M. Identification of compounds with binding affinity to proteins via magnetization transfer from bulk water. *J Biomol NMR.* 2000;18(1):65-8.
304. Mayer M, Meyer B. Characterization of Ligand Binding by Saturation Transfer Difference NMR Spectroscopy. *Angew Chem Int Ed Engl.* 1999;38(12):1784-8.
305. Viegas A, Manso J, Nobrega FL, Cabrita EJ. Saturation-Transfer Difference (STD) NMR: A Simple and Fast Method for Ligand Screening and Characterization of Protein Binding. *Journal of Chemical Education.* 2011;88(7):990-4.
306. Williamson MP. Using chemical shift perturbation to characterise ligand binding. *Prog Nucl Magn Reson Spectrosc.* 2013;73:1-16.
307. Wang YS, Liu D, Wyss DF. Competition STD NMR for the detection of high-affinity ligands and NMR-based screening. *Magn Reson Chem.* 2004;42(6):485-9.
308. Sugiki T, Furuita K, Fujiwara T, Kojima C. Current NMR Techniques for Structure-Based Drug Discovery. *Molecules.* 2018;23(1).
309. Smyth MS, Martin JH. x ray crystallography. *Mol Pathol.* 2000;53(1):8-14.
310. Smith CR, Dougan DR, Komandla M, Kanouni T, Knight B, Lawson JD, et al. Fragment-Based Discovery of a Small Molecule Inhibitor of Bruton's Tyrosine Kinase. *J Med Chem.* 2015;58(14):5437-44.
311. Congreve M, Carr R, Murray C, Jhoti H. A 'rule of three' for fragment-based lead discovery? *Drug Discov Today.* 2003;8(19):876-7.
312. Han X, Jiang M, Zhou C, Zhou Z, Xu Z, Wang L, et al. Discovery of potent and selective CDK8 inhibitors through FBDD approach. *Bioorg Med Chem Lett.* 2017;27(18):4488-92.
313. Mochalkin I, Miller JR, Narasimhan L, Thanabal V, Erdman P, Cox PB, et al. Discovery of antibacterial biotin carboxylase inhibitors by virtual screening and fragment-based approaches. *ACS Chem Biol.* 2009;4(6):473-83.
314. Philpott M, Yang J, Tumber T, Fedorov O, Uttarkar S, Filippakopoulos P, et al. Bromodomain-peptide displacement assays for interactome mapping and inhibitor discovery. *Mol Biosyst.* 2011;7(10):2899-908.

315. Hewings DS, Wang M, Philpott M, Fedorov O, Uttarkar S, Filippakopoulos P, et al. 3,5-dimethylisoxazoles act as acetyl-lysine-mimetic bromodomain ligands. *J Med Chem.* 2011;54(19):6761-70.
316. Navratilova I, Aristotelous T, Picaud S, Chaikuad A, Knapp S, Filippakopoulos P, et al. Discovery of New Bromodomain Scaffolds by Biosensor Fragment Screening. *ACS Med Chem Lett.* 2016;7(12):1213-8.
317. Chung CW, Dean AW, Woolven JM, Bamborough P. Fragment-based discovery of bromodomain inhibitors part 1: inhibitor binding modes and implications for lead discovery. *J Med Chem.* 2012;55(2):576-86.
318. Wang L, Pratt JK, Soltwedel T, Sheppard GS, Fidanze SD, Liu D, et al. Fragment-Based, Structure-Enabled Discovery of Novel Pyridones and Pyridone Macrocycles as Potent Bromodomain and Extra-Terminal Domain (BET) Family Bromodomain Inhibitors. *J Med Chem.* 2017;60(9):3828-50.
319. Zhao H, Gartenmann L, Dong J, Spiliotopoulos D, Caflisch A. Discovery of BRD4 bromodomain inhibitors by fragment-based high-throughput docking. *Bioorg Med Chem Lett.* 2014;24(11):2493-6.
320. Bennett MJ, Wu Y, Bloor A, Matuszkiewicz J, O'Connell SM, Shi L, et al. Design, synthesis and biological evaluation of novel 4-phenylisoquinolinone BET bromodomain inhibitors. *Bioorg Med Chem Lett.* 2018;28(10):1811-6.
321. Seal J, Lamotte Y, Donche F, Bouillot A, Mirguet O, Gellibert F, et al. Identification of a novel series of BET family bromodomain inhibitors: binding mode and profile of I-BET151 (GSK1210151A). *Bioorg Med Chem Lett.* 2012;22(8):2968-72.
322. Ran X, Zhao Y, Liu L, Bai L, Yang C-Y, Zhou B, et al. Structure-Based Design of γ -Carboline Analogues as Potent and Specific BET Bromodomain Inhibitors. *Journal of Medicinal Chemistry.* 2015;58(12):4927-39.
323. Zhao Y, Bai L, Liu L, McEachern D, Stuckey JA, Meagher JL, et al. Structure-Based Discovery of 4-(6-Methoxy-2-methyl-4-(quinolin-4-yl)-9H-pyrimido[4,5-b]indol-7-yl)-3,5-dimethylisoxazole (CD161) as a Potent and Orally Bioavailable BET Bromodomain Inhibitor. *J Med Chem.* 2017;60(9):3887-901.
324. McKeown MR, Shaw DL, Fu H, Liu S, Xu X, Marineau JJ, et al. Biased multicomponent reactions to develop novel bromodomain inhibitors. *J Med Chem.* 2014;57(21):9019-27.
325. Xue X, Zhang Y, Wang C, Zhang M, Xiang Q, Wang J, et al. Benzoxazinone-containing 3,5-dimethylisoxazole derivatives as BET bromodomain inhibitors for treatment of castration-resistant prostate cancer. *Eur J Med Chem.* 2018;152:542-59.
326. Hewings DS, Fedorov O, Filippakopoulos P, Martin S, Picaud S, Tumber A, et al. Optimization of 3,5-dimethylisoxazole derivatives as potent bromodomain ligands. *J Med Chem.* 2013;56(8):3217-27.

327. Jennings LE, Schiedel M, Hewings DS, Picaud S, Laurin CMC, Bruno PA, et al. BET bromodomain ligands: Probing the WPF shelf to improve BRD4 bromodomain affinity and metabolic stability. *Bioorg Med Chem*. 2018;26(11):2937-57.
328. Bamborough P, Diallo H, Goodacre JD, Gordon L, Lewis A, Seal JT, et al. Fragment-based discovery of bromodomain inhibitors part 2: optimization of phenylisoxazole sulfonamides. *J Med Chem*. 2012;55(2):587-96.
329. Hay D, Fedorov O, Filippakopoulos P, Martin S, Philpott M, Picaud S, et al. The design and synthesis of 5- and 6-isoxazolylbenzimidazoles as selective inhibitors of the BET bromodomains. *Medchemcomm*. 2013;4(1):140-4.
330. Li X, Zhang J, Zhao L, Yang Y, Zhang H, Zhou J. Design, Synthesis, and in vitro Biological Evaluation of 3,5-Dimethylisoxazole Derivatives as BRD4 Inhibitors. *ChemMedChem*. 2018;13(13):1363-8.
331. Denny RA, Flick AC, Coe J, Langille J, Basak A, Liu S, et al. Structure-Based Design of Highly Selective Inhibitors of the CREB Binding Protein Bromodomain. *J Med Chem*. 2017;60(13):5349-63.
332. Ozer HG, El-Gamal D, Powell B, Hing ZA, Blachly JS, Harrington B, et al. BRD4 Profiling Identifies Critical Chronic Lymphocytic Leukemia Oncogenic Circuits and Reveals Sensitivity to PLX51107, a Novel Structurally Distinct BET Inhibitor. *Cancer Discov*. 2018;8(4):458-77.
333. Gosmini R, Nguyen VL, Toum J, Simon C, Brusq JM, Krysa G, et al. The discovery of I-BET726 (GSK1324726A), a potent tetrahydroquinoline ApoA1 up-regulator and selective BET bromodomain inhibitor. *J Med Chem*. 2014;57(19):8111-31.
334. Millan DS, Kayser-Bricker KJ, Martin MW, Talbot AC, Schiller SER, Herbertz T, et al. Design and Optimization of Benzopiperazines as Potent Inhibitors of BET Bromodomains. *ACS Med Chem Lett*. 2017;8(8):847-52.
335. Law RP, Atkinson SJ, Bamborough P, Chung CW, Demont EH, Gordon LJ, et al. Discovery of Tetrahydroquinoxalines as Bromodomain and Extra-Terminal Domain (BET) Inhibitors with Selectivity for the Second Bromodomain. *J Med Chem*. 2018;61(10):4317-34.
336. Fish PV, Filippakopoulos P, Bish G, Brennan PE, Bunnage ME, Cook AS, et al. Identification of a chemical probe for bromo and extra C-terminal bromodomain inhibition through optimization of a fragment-derived hit. *J Med Chem*. 2012;55(22):9831-7.
337. Demont EH, Chung CW, Furze RC, Grandi P, Michon AM, Wellaway C, et al. Fragment-Based Discovery of Low-Micromolar ATAD2 Bromodomain Inhibitors. *J Med Chem*. 2015;58(14):5649-73.
338. Bamborough P, Chung CW, Furze RC, Grandi P, Michon AM, Sheppard RJ, et al. Structure-Based Optimization of Naphthyridones into Potent ATAD2 Bromodomain Inhibitors. *J Med Chem*. 2015;58(15):6151-78.
339. Rooney TP, Filippakopoulos P, Fedorov O, Picaud S, Cortopassi WA, Hay DA, et al. A series of potent CREBBP bromodomain ligands reveals an induced-fit pocket stabilized by a cation- π interaction. *Angew Chem Int Ed Engl*. 2014;53(24):6126-30.

340. McDaniel KF, Wang L, Soltwedel T, Fidanze SD, Hasvold LA, Liu D, et al. Discovery of N-(4-(2,4-Difluorophenoxy)-3-(6-methyl-7-oxo-6,7-dihydro-1H-pyrrolo[2,3-c]pyridin-4-yl)phenyl)ethanesulfonamide (ABBV-075/Mivebresib), a Potent and Orally Available Bromodomain and Extraterminal Domain (BET) Family Bromodomain Inhibitor. *J Med Chem*. 2017;60(20):8369-84.
341. Fidanze SD, Liu D, Mantei RA, Hasvold LA, Pratt JK, Sheppard GS, et al. Discovery and optimization of novel constrained pyrrolopyridone BET family inhibitors. *Bioorg Med Chem Lett*. 2018;28(10):1804-10.
342. Sanghvi R, Narazaki R, Machatha SG, Yalkowsky SH. Solubility improvement of drugs using N-methyl pyrrolidone. *AAPS PharmSciTech*. 2008;9(2):366-76.
343. Weber FE, San Miguel B, Ehrbar M, Ghayor C, Jung R, Zwahlen R. The small molecule nmp is an enhancer of bone regeneration. *Bone*. 2006;38(3):S20-S1.
344. Miguel BS, Ghayor C, Ehrbar M, Jung RE, Zwahlen RA, Hortschansky P, et al. N-methyl pyrrolidone as a potent bone morphogenetic protein enhancer for bone tissue regeneration. *Tissue Eng Part A*. 2009;15(10):2955-63.
345. McKenzie G, Hardwick B, SanMiguel B, Chopra B, Creasey G, Gewert D, et al. The small molecule N-Methyl pyrrolidone tunes the natriuretic peptide hormone system into a pro osteogenic state. *Bone*. 2008;42:S80-S.
346. Ghayor C, Corroero RM, Lange K, Karfeld-Sulzer LS, Gratz KW, Weber FE. Inhibition of osteoclast differentiation and bone resorption by N-methylpyrrolidone. *J Biol Chem*. 2011;286(27):24458-66.
347. Ghayor C, Gjoksi B, Siegenthaler B, Weber FE. N-methyl pyrrolidone (NMP) inhibits lipopolysaccharide-induced inflammation by suppressing NF-kappaB signaling. *Inflamm Res*. 2015;64(7):527-36.
348. Gjoksi B, Ghayor C, Siegenthaler B, Ruangsawasdi N, Zenobi-Wong M, Weber FE. The epigenetically active small chemical N-methyl pyrrolidone (NMP) prevents estrogen depletion induced osteoporosis. *Bone*. 2015;78:114-21.
349. Gjoksi B, Ghayor C, Bhattacharya I, Zenobi-Wong M, Weber FE. The bromodomain inhibitor N-methyl pyrrolidone reduced fat accumulation in an ovariectomized rat model. *Clin Epigenetics*. 2016;8:42.
350. Gjoksi B, Ruangsawasdi N, Ghayor C, Siegenthaler B, Zenobi-Wong M, Weber FE. Influence of N-methyl pyrrolidone on the activity of the pulp-dentine complex and bone integrity during osteoporosis. *Int Endod J*. 2017;50(3):271-80.
351. Shortt J, Hsu AK, Martin BP, Doggett K, Matthews GM, Doyle MA, et al. The drug vehicle and solvent N-methylpyrrolidone is an immunomodulator and antimyeloma compound. *Cell Rep*. 2014;7(4):1009-19.
352. NMP in Relapsed Refractory Myeloma. <https://ClinicalTrials.gov/show/NCT02468687>.

Chapter 2 – Synthesis and Elaboration of *N*-Methylpyrrolidone as an Acetamide Fragment Substitute in Bromodomain Inhibition

Keywords

BRD4, Bromodomain, K-ac, NMP, Olinone

Abbreviations

ATAD2, ATPase Family AAA Domain-containing Protein 2; BCP, Bromodomain-containing Protein; BET, Bromodomain and Extra-terminal; BRD#, Bromodomain-containing Protein #; BRD4 BD1, First Bromodomain of BRD4; CBP, Cyclic Adenosine Monophosphate Response Element Binding Protein; FBDD, Fragment-based Drug Design; K-ac, Acetyl-lysine; IRF-4, Interferon Regulatory Factor 4; LE, Ligand Efficiency; LPS, Lipopolysaccharide; NHA, Non-hydrogen Atom; NMP, *N*-Methylpyrrolidone; NMR, Nuclear Magnetic Resonance; PHIP, Pleckstrin Homology Domain Interacting Protein; RMS, Root Mean Square; SAR, Structure-Activity Relationship; SD, Standard Deviation; SEM, Standard Error of Mean; SMARCA4, SWI/SNF Related Matrix Associated Actin Dependent Regulator of Chromatin Subfamily A Member 4; vdW, van der Waals; WPF, Tryptophan-proline-phenylalanine.

Abstract

N-Methylpyrrolidone is a solvent molecule which has been shown to compete with acetyl-lysine-containing peptides for binding to bromodomains. From crystallographic studies, it has also been shown to closely mimic the acetamide binding motif in several bromodomains, but has not yet been pursued as a fragment in bromodomain inhibition. In this paper, we report the elaboration of *N*-methylpyrrolidone as a potential lead in fragment-based drug design. Firstly, *N*-methylpyrrolidone was functionalised to provide points for fragment elaboration. Two of these derivatives were then utilised as part of analogues of the reported bromodomain inhibitor,

Olinone. X-ray crystallography revealed that the modified analogues showed comparable binding affinity and structural mimicry to Olinone in the bromodomain binding site.

2.1 Introduction

Bromodomains are recognition elements for K-ac residues, and act as “readers” to regulate the cellular functions of BCPs. In total, 46 BCPs have been reported in humans that comprise 61 different bromodomains divided into 8 subfamilies. With established roles in transcriptional activation,¹ BCPs have been associated with a number of disease states relating to cancer,²⁻⁴ viral diseases⁵⁻⁹, inflammation^{10, 11} and cardiovascular diseases.^{12, 13} Bromodomain inhibitors have therefore been identified as potential therapeutic agents¹⁴⁻¹⁶ and numerous compounds are currently under clinical investigation.¹⁷⁻²⁰

Bromodomains have a characteristic three-dimensional structure comprised of a series of four α -helices (α Z, α A, α B, α C) linked by two interhelical loops (ZA, BC)²¹ where the space between these loops creates the cavity where K-ac is recognized. This binding site has been effectively targeted by various bromodomain inhibitors, with the BET family of BCPs serving as the prototype for inhibitor design. Initially, the methyltriazolodiazepines (+)-JQ1²² and I-BET762¹¹ were identified as K-ac mimetics among a host of other chemotypes. Since then, it has become a fruitful subject for FBDD approaches. Chung²³ and Bamborough²⁴ both described a FBDD approach that identified an array of low molecular weight compounds, including the 3,5-dimethylisoxazoles, which were also described by Hewings et al.²⁵ Additionally, the alkylacetamide function of K-ac has been mimicked directly in the inhibitor Olinone,²⁶ which selectively targets the first bromodomain of BET proteins (Figure 1).

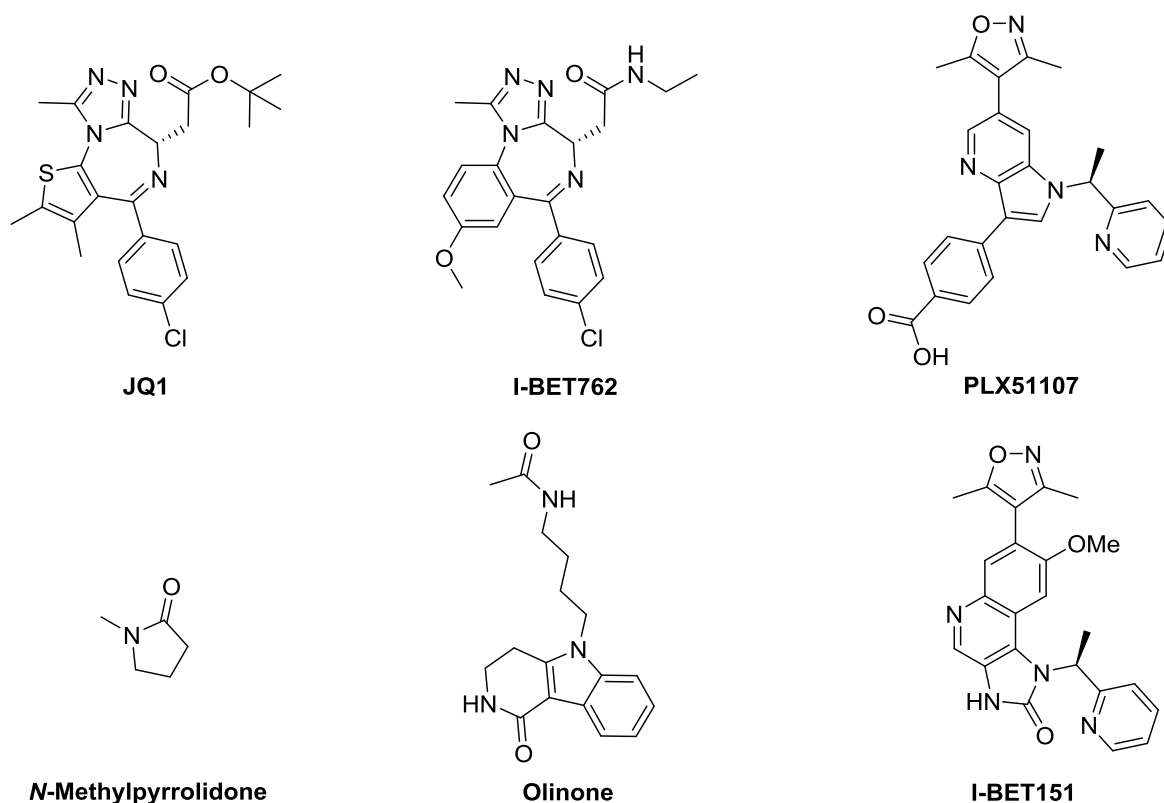


Figure 1. Reported bromodomain inhibitors and probes.^{11, 22, 26-29}

The 3,5-dimethylisoxazoles were described as being inspired by the solvent molecule NMP, which interacts with the binding pocket of a range of bromodomains.²⁹ NMP was also shown to be a mimetic of K-ac in crystallographic studies where it binds to the conserved areas of the bromodomain binding pocket in BRD1 (PDB: 3RCW), BRD2 (PDB: 4A9F), ATAD2 (PDB: 4QSS), CBP (PDB: 3P1D), SMARCA4 (PDB: 3UVD), PB1 (PDB: 3MB4) and PHIP (PDB: 3MB3). NMP was able to inhibit a range of BCPs at millimolar concentrations³⁰ while its affinity was comparable to that of K-ac, giving it good LE due to its low molecular weight.²⁹

We have hypothesised that this pleiotropic bromodomain inhibition may result in the anti-myeloma and immunomodulatory activity with hallmark reduction in transcription factors *c-Myc* and IRF-4 in multiple myeloma models.³⁰ This activity has seen it submitted into a phase I clinical trial for multiple myeloma (NCT02468687).³¹ Moreover, the history of NMP with bone diseases such as osteoporosis is acknowledged as it has been shown to prevent osteoclast

differentiation,³² inhibit LPS-induced inflammatory mediators³³ and reduce the effects of adipocyte accumulation.³⁴

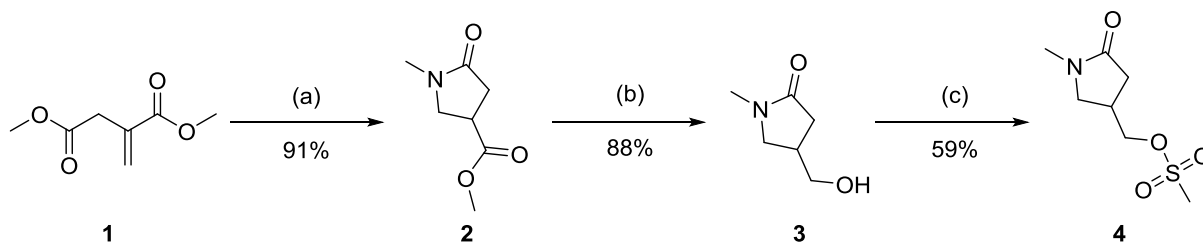
Despite the structural, functional and inspirational evidence of NMP's bromodomain mimicry,^{25, 35} there has not been any attempt made to explore its potential as a direct mimetic in FBDD. We considered that NMP holds potential advantages over other reported fragments, including its low molecular weight and high LE. However, additional functionalisation would be necessary to explore its potential in fragment elaboration. Here, we report our expansion of NMP with a range of functional groups and the subsequent elaboration by mimicry of Olinone as an exemplar of the broader approach to bromodomain inhibition. X-ray crystal structures of the NMP derivatives show the successful mimicry of the native acetamide binding pose.

2.2 Results and Discussion

There are seven entries in the Protein Data Bank where NMP is bound to a bromodomain and acting as an K-ac mimetic. The carbonyl moiety of NMP replicates the interactions with the highly conserved asparagine residue and a water-mediated hydrogen bond to a conserved tyrosine, while the *N*-methyl substituent sits adjacent to the water-lined pocket. We determined that the 4-position of NMP would be a suitable point to elaborate the NMP structure (Appendix B), while noting that such derivatives would also exist as pairs of enantiomers.

2.2.1 Synthesis

We generated a variety of functional groups from which to elaborate NMP, which were synthesised using two synthetic routes.

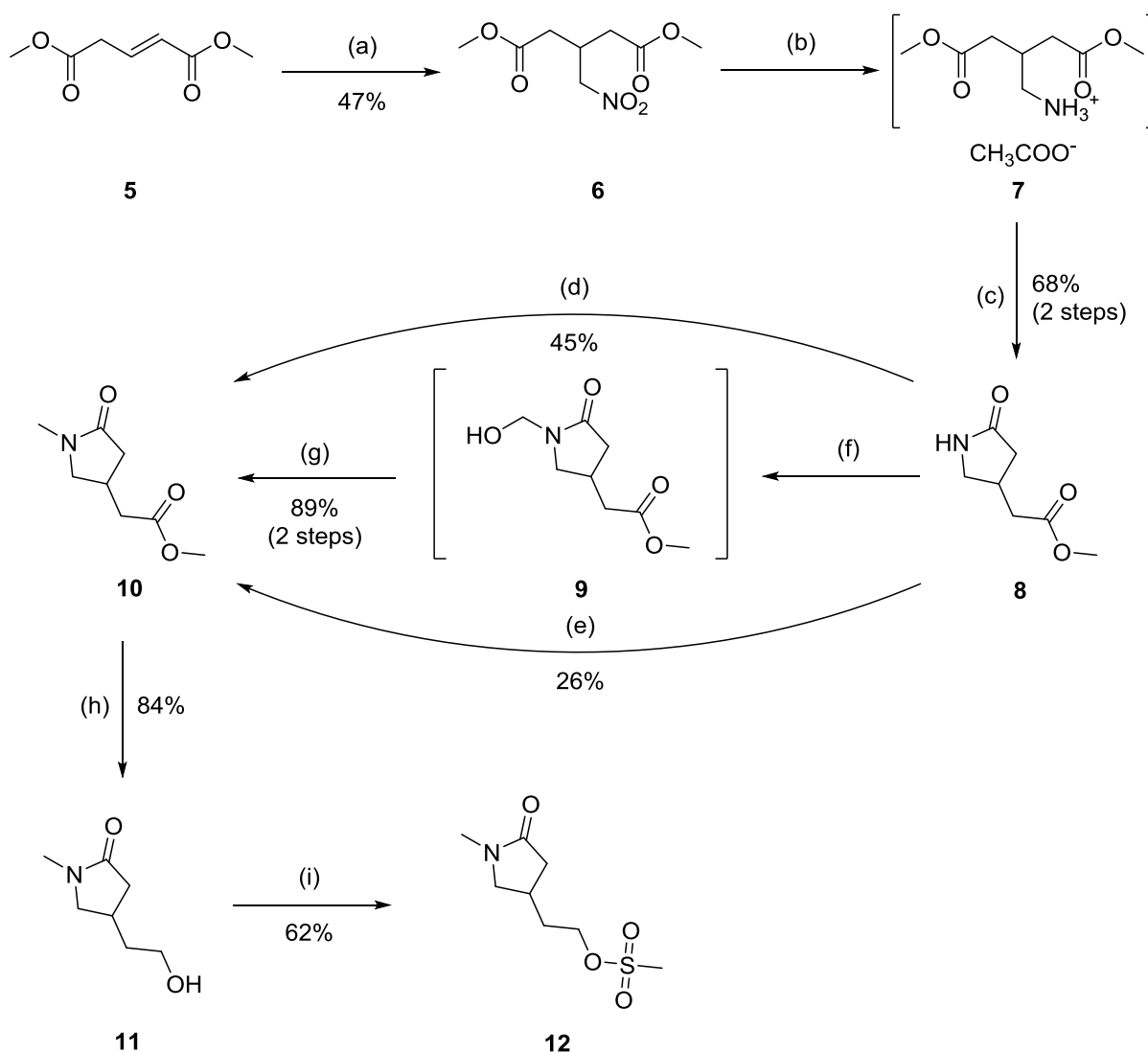


Scheme 1. Formation of **4**, a mesylate NMP derivative. (a): CH₃NH₂, MeOH, 0 °C → rt, o/n; (b): NaBH₄, EtOH; rt, o/n (c): N₂, MsCl, DIPEA, CH₂Cl₂, 0 °C, 4 h.

The first series of compounds were derived from methyl 1-methyl-5-oxopyrrolidine-3-carboxylate **2** (Scheme 1). Dimethyl itaconate **1** was treated with methylamine and then cyclised *in situ* to give **2** in 91% yield as previously reported.^{36, 37} The ester **2** was then reduced to the alcohol **3** with excess sodium borohydride in excellent yield.³⁶ The final step was the conversion of the alcohol to a mesylate through the use of methanesulfonyl chloride and DIPEA under an inert atmosphere to give **4** in 59% yield.^{38, 39}

In the second series, NMP homologues **10**, **11** and **12** were prepared as shown in Scheme 2. Dimethyl glutaconate **5** was treated with nitromethane and 1,1,3,3-tetramethylguanidine⁴⁰ to

afford the nitroester **6** in moderate yield. The nitroester **6** was then reduced to the amine **7** and then cyclised to the lactam **8**, starting with the use of palladium on carbon under a hydrogen atmosphere with acetic acid as the solvent, which gave the amine **7** as an acetate salt. The amine **7** was then refluxed in a mixture of methanol and triethylamine to neutralise the acetate salt and catalyse the cyclisation to form the lactam **8** in 68% yield over two steps.



Scheme 2. Formation of **12**, a dimethylene NMP mesylate. (a): CH_3NO_2 , 1,1,3,3-tetramethylguanidine, 42 h, rt; (b): H_2 , Pd/C, CH_3COOH , 5 d, rt; (c): Et_3N , MeOH, o/n, rf; (d): N_2 , *t*-BuOK, MeI, THF, 6 h, 0 °C; (e): K_2CO_3 , MeI, CH_3CN , 6 d, rf; (f): Paraformaldehyde,

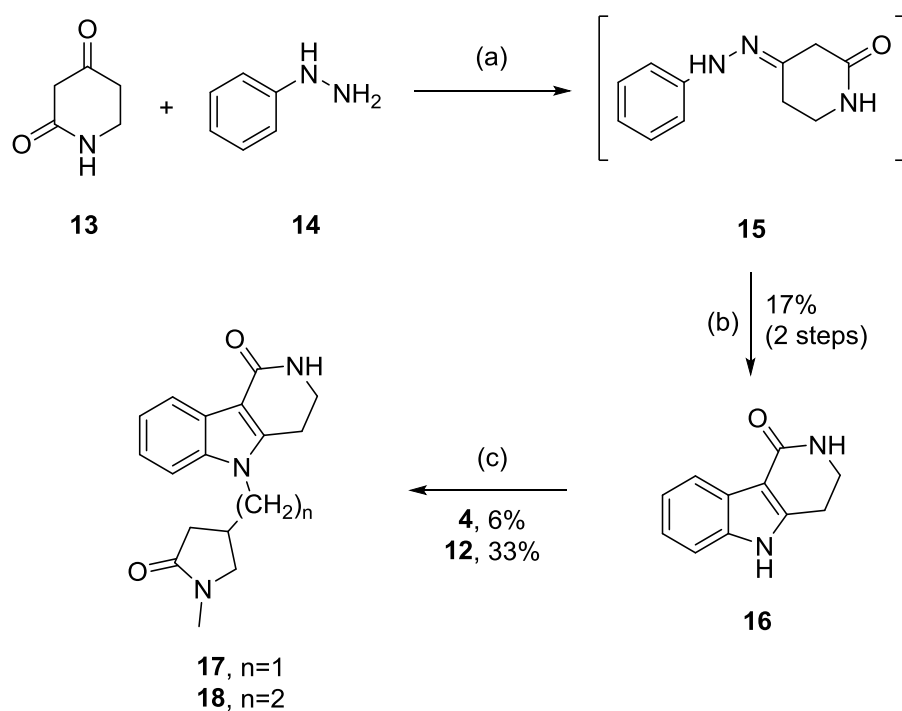
K₂CO₃, acetone, H₂O, 4 h, rt; (g): Et₃SiH, CF₃COOH, CHCl₃, o/n, rt; (h): NaBH₄, EtOH; rt, o/n (i): N₂, MsCl, DIPEA, CH₂Cl₂, 0 °C, 4 h.

The lactam derivative **8** was methylated by conversion to the hemiaminal intermediate **9** through the treatment of paraformaldehyde and potassium carbonate, which was then reduced with triethylsilane and trifluoroacetic acid to give **10** in 89% yield across the two steps.⁴¹ In contrast, yields for direct methylation with methyl iodide in the presence of base were modest at best.⁴²⁻⁴⁴ Finally, the reduction of the ester **10** to the alcohol **11** and subsequent conversion to the mesylate **12** were carried out using the same methods described for **3** and **4** in similar yields. Collectively, we have built a set of six 4-substituted analogues of NMP. Each of these compounds – **2-4**, **10-12** – are ready for further elaboration in FBDD.

Olinone was originally reported by Gacias et al.²⁶ as a molecule that showed selectivity for the first bromodomain of BET proteins. It possesses an alkylacetamide chain similar to K-ac, linked to a 2,3,4,5-tetrahydro-1*H*-pyrido[4,3-*b*]indol-1-one scaffold which interacts with residues that are unique to BRD4 BD1. With a K_d of 3.4 μM, Olinone was a suitable starting point for trying to recapitulate the acetamide binding motif in an NMP-containing analogue and we considered that either **4** or its homologue **12** would be suitable in creating this mimetic.

Following the reported procedure (Scheme 3),²⁶ 2,4-piperidinedione **13** was treated with phenylhydrazine **14** in ethanol to give the hydrazone intermediate **15**, which was then subjected to Fischer indole synthesis conditions, using 70% sulfuric acid to give the desired tricyclic scaffold **16**, albeit in modest yield. Alkylation of **16** with mesylates **4** and **12** were attempted using sodium bis(trimethylsilyl)amide as the base. While the yield of **17** was poor and **18** was moderate, both compounds were isolated. The difference in yields points to some hindrance due to the proximity of the NMP moiety in **4** towards **16**. ¹H NMR showed the disappearance

of the indole NH proton, confirming that alkylation occurred selectively at the indole nitrogen of the tricyclic and not the lactam.



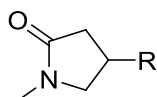
Scheme 3. Preparation of 2,3,4,5-tetrahydro-1*H*-pyrido[4,3-*b*]indol-1-one **16** and coupling to NMP derivatives **4** and **12**. (a): EtOH, rf, o/n; (b): 70% H₂SO₄, 0 °C, 4 h; (c): N₂, NaHMDS, DMF, -78 °C → 90 °C, o/n.

2.2.2 BRD4 BD1 FRET Assay Results

With this series of compounds in hand, the esters **2** and **10**, alcohols **3** and **11**, and Olinone analogues **17** and **18** were all evaluated as inhibitors of BRD4 BD1 in comparison to NMP using a FRET-based assay developed by Cisbio Assays. This method is a competitive binding assay that relies on the proximity of a Eu³⁺ cryptate donor attached to a GST-tagged bromodomain (BRD4 BD1), and a Streptavidin D2 acceptor attached to a biotinylated tetra-acetylated histone peptide (H4K5K8K12K16(ac₄)) to generate fluorescence. When an inhibitor is present, it competes for binding to the bromodomain with the histone peptide. Once bound,

the distance between donor and acceptor becomes too great and fluorescence is lost. The results of the assays are shown in Table 1.

Table 1. Preliminary SAR data on NMP derivatives.



Compound Number	R=	IC ₅₀ (μM ± SEM) ^a	LE (kcal/mol NHA) ^c
	H	2660 ± 480	0.50
2		6880 ± 300	0.27
3		4110 ± 380	0.36
10		2120 ± 270	0.30
11		4810 ± 60	0.32
17		24 ± 2 ^b	0.29
18		79 ± 3 ^b	0.24

Assays carried out by Dr. Ian Jennings, Zhaohua Zheng and Ali Noor. ^aUnless stated otherwise, all results of means are $n \geq 2$. ^bSD reported. ^cLigand efficiency = $1.37(-\log(\text{IC}_{50})) / \text{NHA}$. Control compound used: **I-BET726** (IC₅₀: 0.01 μM). NHA, non-hydrogen atom.

The simple functionalisation of NMP had no major effect on inhibition with compounds **2**, **3**, **10** and **11** showing comparable activity to NMP itself. The ester **2** showed the lowest affinity, indicating that the adjacent ester group may hinder access of the NMP portion to the binding site.

The Olinone analogues **17** and **18** showed much improved affinity, which was consistent with the anticipated mimicry of the K-ac motif by the NMP functional group. Compound **17** was the higher affinity ligand with an IC₅₀ of 24 μM, while compound **18** had an IC₅₀ of 79 μM, marking an improvement of NMP's activity by 110-fold and 33-fold, respectively (dose response curves of **17** and **18** are available in Appendix C).

2.2.3 X-ray Crystallography

To verify the retention of the mimicry of K-ac in these compounds, we obtained crystal structures of compounds **10**, **17** and **18** in complex with BRD4 BD1 (for videos, refer to Appendix D. For electron density maps, refer to Appendix E).

As shown in Figure 2, the NMP segment of **10** indeed retains its mimicry of K-ac, interacting with Asn140 and Tyr97, while the ester interacts with the WPF shelf of BRD4 BD1, a recognized feature of selective inhibitors given its lack of conservation between bromodomains.⁴⁵ Here, the ester moiety interacts with residues Trp81 and Pro82 through weak vdW interactions.

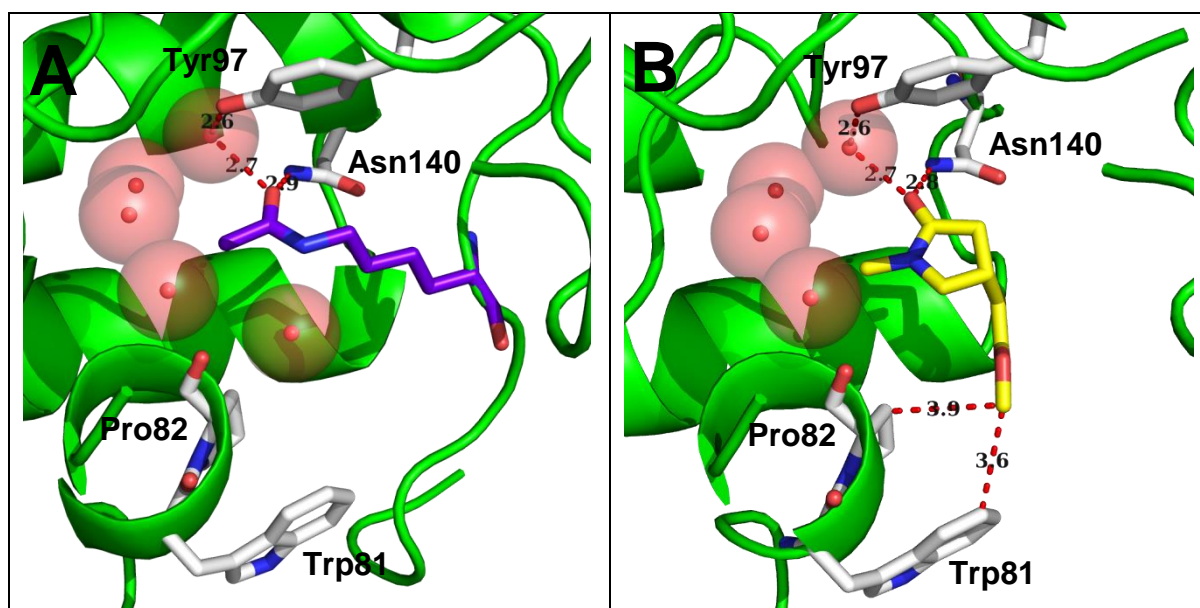


Figure 2. Comparison of binding substrates in the bromodomain binding site of BRD4 BD1.

A. K-ac (purple blue, PDB: 3UVW). B. (*R*)-**10** (yellow, resolution: 1.3 Å). Water molecules

shown as red spheres. Pro86, Val87 and Asp88 were hidden for better visualisation. Distances in Å, highlighted by red dashes. X-ray crystal structure of **10** developed by Dr. Ian Jennings and Dr. Olga Ilyichova.

The X-ray crystal structures of **17** and **18** show that, in both cases, the tricyclic scaffolds align with that of Olinone with a RMS for the heavy atoms of 0.56 Å and 0.24 Å, respectively. As anticipated, the NMP moiety of **17** and **18** mimics the acetamide group of Olinone and closely overlays with the reported structures of NMP.

While the pharmacophore elements of **17** and **18** are identical, the linkers differ in the conformation and stereochemical configuration at the NMP stereocentre. Despite each NMP derivative being submitted as a racemic mixture, single enantiomers were observed in the crystal form. Interestingly, compound **17** adopts the same *R*-configuration as the fragment **10** and their backbones overlay closely (RMS = 0.36 Å). On the other hand, compound **18** shows the opposite sense of stereochemistry while accommodating an extended chain conformation (Figure 3). It is still designated the *R*-absolute configuration under the Cahn-Ingold-Prelog nomenclature.

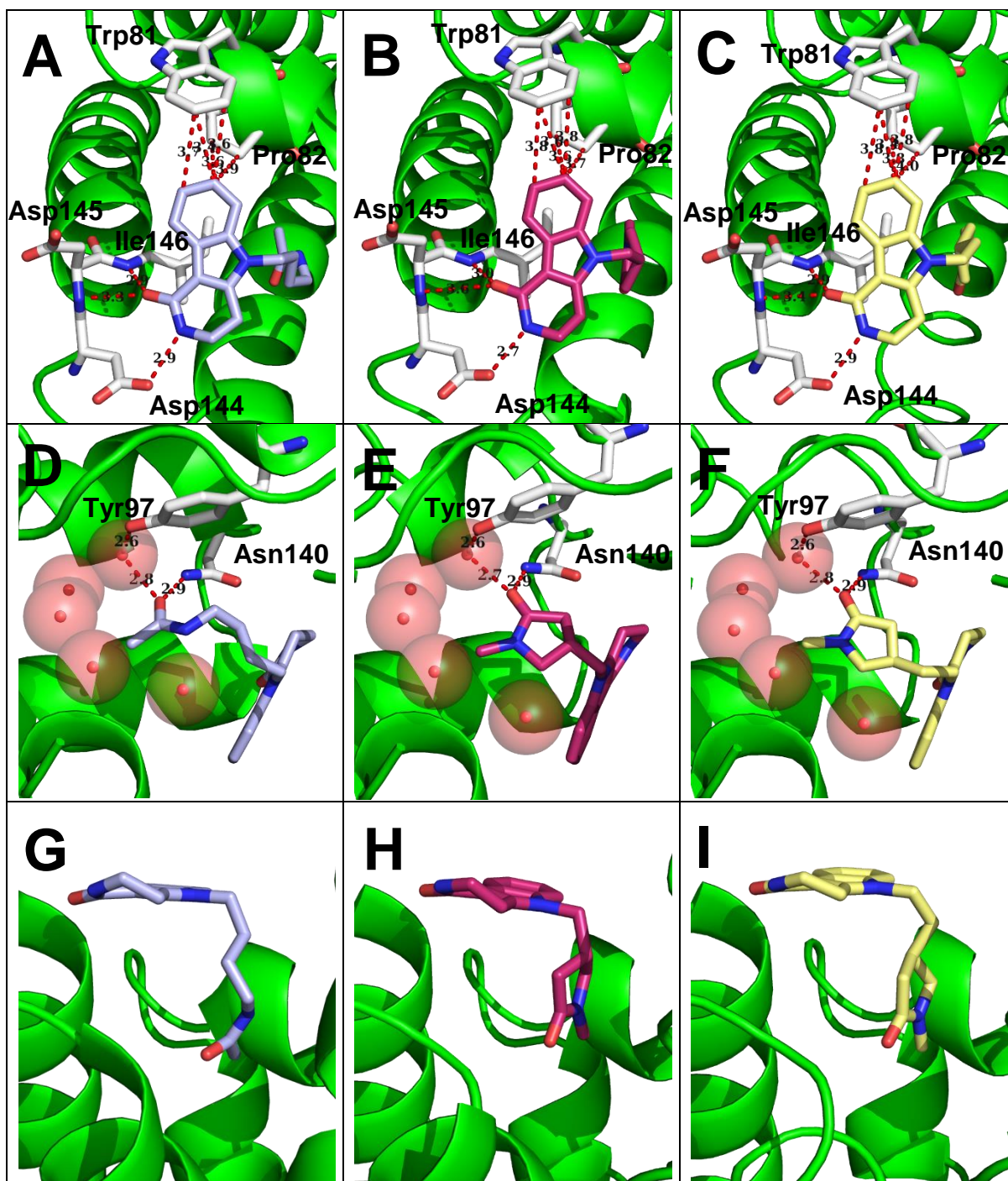


Figure 3. Comparison of Olinone and its respective analogues in BRD4 BD1. [A, B, C] 2,3,4,5-tetrahydro-1*H*-pyrido[4,3-*b*]indol-1-one scaffold. [D, E, F] K-ac binding site. Water molecules shown as red spheres. Pro86, Val87 and Asp88 were hidden for better visualisation. Distances in Å, highlighted by red dashes. [G, H, I] Linker group visualisation. [A, D, G] Olinone (light blue, PDB: 4QB3). [B, E, H] (*R*)-**17** (warm pink, resolution: 1.59 Å). [C, F, I] (*R*)-**18** (pale

yellow, resolution: 1.21 Å). X-ray crystal structures of **17** and **18** developed by Dr. Ian Jennings and Dr. Olga Ilyichova.

2.3 Conclusion and Future Directions

In summary, we have demonstrated the use of NMP derivatives as fragments that can be used in the design of bromodomain ligands. We have successfully developed two synthetic schemes for six functionalised derivatives of NMP which can be produced on multigram scales. An X-ray crystal structure of one of these derivatives (**10**) in complex with BRD4 BD1 shows the retained presentation of the NMP pharmacophore by these derivatives.

The precursors **4** and **12** have been employed in the synthesis of two compounds – **17** and **18** – based on the inhibitor Olinone. The bromodomain inhibition is comparable to the parent compound and both compounds precisely mimic the parent compound in the BRD4 BD1 binding site.

These results should encourage the further exploration of NMP as a fragment in bromodomain inhibition for three reasons. Firstly, the pre-existing literature suggests that NMP is a general mimic of the acetamide function of acetyl-lysine. This suggests that the strategy applied here for BRD4 BD1 could be applied equally against one or more of the other 60 bromodomains in the epigenome. Secondly, the structures of **17** and **18** show that either of the stereochemical configurations of the NMP derivatives can be applied with success. Therefore, these are actually pairs of fragments which may be expected to have their own selectivity profiles. Further work to resolve or synthesise the individual stereoisomers is on-going. Finally, the variety of functionalities in the six fragments described here opens the door for alternate reactions to make products such as amines, ethers, amides and esters. Taken together, these results have further proved the usefulness of NMP as a mimetic fragment and the potential of its incorporation into other known inhibitors.

Experimental

^1H and ^{13}C Nuclear Magnetic Resonance spectra were conducted on a Bruker Advance III Nanobay 400 MHz spectrometer coupled to the BACS 60 automatic sample changer and obtained at 400.1 MHz and 100.6 MHz, respectively. All spectra were processed using MestReNova 6.0 software. The chemical shifts of all ^1H were measured relative to the expected solvent peaks of the respective NMR solvents; CDCl_3 , 7.26; MeOD, 3.31. The chemical shifts of all ^{13}C were measured relative to the expected solvent peaks of the respective NMR solvents; CDCl_3 , 77.2; MeOD, 49.0. The data for all spectra are reported in the following format: chemical shift (integration, multiplicity, coupling constant, assignment). Multiplicity is defined as; s = singlet, d = doublet, t = triplet, q = quartet, quint. = quintet, dd = doublet of doublets, td = triplet of doublets, qd = quartet of doublets, ddd = doublet of doublet of doublets, m = multiplet. Coupling constants are applied as J in Hertz (Hz). For ^1H and ^{13}C spectra, refer to Appendix F.

All HRMS analyses were done on an Agilent 6224 TOF LC/MS Mass Spectrometer coupled to an Agilent 1290 Infinity (Agilent, Palo Alto, CA). All data were acquired and reference mass corrected via a dual-spray electrospray ionisation (ESI) source. Each scan or data point on the Total Ion Chromatogram (TIC) is an average of 13,700 transients, producing a spectrum every second. Mass spectra were created by averaging the scans across each peak and background subtracted against the first 10 seconds of the TIC. Acquisition was performed using the Agilent Mass Hunter Data Acquisition software version B.05.00 Build 5.0.5042.2 and analysis was performed using Mass Hunter Qualitative Analysis version B.05.00 Build 5.0.519.13.

All LCMS analyses were carried out on an Agilent 6100 Series Single Quad LC/MS coupled with an Agilent 1200 Series HPLC, 1260 Infinity G1312B Binary pump, 1260 Infinity G1367E 1260 HiP ALS autosampler and 1290 Infinity G4212A 1290 DAD detector. The liquid

chromatography conditions were: reverse phase HPLC analysis fitted with a Luna C8(2) 5 μ L 50 X 4.6mm 100Å at a temperature of 30 °C. The sample injection volume was 5 μ L, which was run in 0.1% formic acid in acetonitrile at a gradient of 5-100% over 10 minutes. Detection methods were either 254 nm or 214 nm. The mass spectrum conditions were: Quadrupole ion source with Multimode-ES. The drying gas temperature was 300 °C and the vaporizer temperature was 200 °C. The capillary voltage in positive mode was 2000V, while in negative mode, the capillary voltage was 4000V. The scan range was 100-1000 m/z with a step size of 0.1 second over 10 minutes.

TLCs were carried on Merck TLC Silica gel 60 F₂₅₄ plates using the appropriate mobile phase. Purification by column chromatography was conducted with Davisil Chromatographic Silica LC60A (40-63 micron) using the specified mobile phases.

Compound purity was determined using an Agilent 1260 Infinity Analytical HPLC (1260 Infinity G1322A Degasser, 1260 Infinity G1312B Binary pump, G1367E HiP ALS autosampler, 1260 Infinity G1316A Thermostatted Column Compartment, and 1260 Infinity G4212B DAD detector). The liquid chromatography conditions were: reverse phase HPLC analysis fitted with a Zorbax Eclipse Plus C18 Rapid Resolution 4.6 X 100 mm 3.5-Micron. The sample injection volume was 1 μ L, which was run in Solvent A (0.1% TFA in H₂O) and Solvent B (0.1% TFA in CH₃CN), with a gradient of 5-100% Solvent B over a 10-minute period. All compounds submitted for assays and X-ray crystallography studies were assessed for purity of 95% or greater on 214 nm and 254 nm.

The IC₅₀s were measured using a Fluorescence Resonance Energy Transfer (FRET) assay, which was carried out based on the protocol developed by CisBio Assay, France. The assay consists of a europium (Eu³⁺) cryptate-conjugated antibody attached to glutathione S-transferase (GST) fused to BRD4 BD1 (49-170) and Streptavidin-D2 bound to biotin which is

attached to a Histone H4 peptide, SGRG-K(Ac)-GG-K(Ac)-GLG-K(Ac)-GGAK(Ac)-RHRKVGG-K (Biotin). Both Streptavidin-D2 and the Eu³⁺ cryptate-conjugated antibody were purchased from CisBio Assays. In the absence of inhibitors, the Histone H4 peptide is bound to BRD4 BD1. When both are in close proximity, a 337 nm laser light activates the Eu³⁺ donor and emits at 620 nm, which causes D2 to fluoresce at 665 nm. In the presence of a ligand, this reaction is interrupted. The assays were performed in 384-well small volume microtiter plates. The serially diluted small molecule inhibitors were added to a buffer mixture with a final concentration of 1% DMSO. The final buffer concentrations were 10 nM of GST-BRD4 BD1, 40 nM of Histone H4 peptide, 5 nM of Eu³⁺ cryptate-conjugated GST-antibody, 6.25 nM Streptavidin-D2, 50 mM Hepes, 50 mM NaCl, 0.5 mM CHAPS, 400 mM KF, 0.01% BSA, pH 7.5. After mixing and incubation at room temperature for at least 1.5 hours, the plates were measured in a PheraStar plate reader (BMG Labtech) (excitation: 337 nm with 10 flashes; emission: 620 and 665 nm).

X-ray crystal structures were obtained using a 6-His tagged bromodomain, BRD4 BD1, which was expressed in E.coli and purified using Ni-agarose chromatography. The 6-His tag was then removed by TEV protease digestion. The bromodomain was purified using gel filtration chromatography using a Superdex-75, 16/60 column (GE Healthcare) in a buffer containing 50 mM Hepes pH 7.5, 0.3 M NaCl and 5% glycerol. The concentrated BRD4 BD1 protein (17 mg/ml) was then incubated with 50 mM of the ligand at 40 °C for 16h. The final ligand concentration used in the hanging drop was 5 mM. Crystals were obtained using the hanging drop method in 24-well plates using 1 µl drops of protein and the reservoir solution containing 0.2 M NaNO₃, PEG-3350 (35%) and ethylene glycol (6% v/v) concentrations. This was then flash frozen in liquid nitrogen. All datasets were collected at the Australian Synchrotron on MX1 and MX2 beamlines.⁴⁶ Datasets were merged and scaled using *MOSFLM*⁴⁷ and *AIMLESS*⁴⁸ from the CCP4 suite.⁴⁹ 5% of reflections in each dataset were flagged for

calculation of R_{free} . A summary of statistics is provided in Appendix G. Molecular replacement was performed with *Phaser*⁵⁰ using a previously solved structure of BRD4 as a search model (PDB: 5DW2). The final structures were obtained after several rounds of manual refinement using *Coot*⁵¹ and refinement with *phenix.refine*.⁵²

Methyl 1-methyl-5-oxo-3-pyrrolidine carboxylate (2) – 40% Methylamine solution in H₂O (10 mL) was dissolved in methanol (125 mL) in an ice-bath and stirred. Dimethyl itaconate **1** (15.1 g, 94.8 mmol) dissolved in methanol (275 mL) was added dropwise to the stirring mixture. After an hour, the ice-bath was removed and the reaction continued to stir for further 24 hours. The mixture was concentrated under reduced pressure and the residue purified by vacuum distillation to afford **2** as an oil (13.7 g, 91%). **¹H NMR** (400 MHz, CDCl₃) δ 3.71 (s, 3H), 3.58 (ddd, $J = 22.8, 14.4, 8.2$ Hz, 2H), 3.27 – 3.16 (m, 1H), 2.82 (s, 3H), 2.73 – 2.57 (m, 2H) ppm. **¹³C NMR** (101 MHz, CDCl₃) δ 173.4, 172.5, 52.6, 51.2, 35.9, 34.0, 29.6 ppm. **ESI-MS**, m/z 158.2 [M+H]⁺; **HR-MS**: m/z calcd. for C₇H₁₁NO₃ [M+H]⁺: 158.0812; found 158.0813; **HPLC** (PP gradient, MeOH): 3.27 min.

4-(hydroxymethyl)-1-methylpyrrolidin-2-one (3) – Methyl 1-methyl-5-oxo-3-pyrrolidine carboxylate **2** (10.5 g, 67.1 mmol) was dissolved in ethanol (400 mL) and stirred at room temperature. Sodium borohydride (25.3 g, 0.671 mol) was added slowly in small portions over a 7-hour period. After this period, water (20 mL) was added to form a cloudy mixture. The quenched mixture was then filtered through Celite 545 and carefully concentrated to a white solid by rotary evaporation. The solid was taken up in CHCl₃ (500 mL) and left to stir overnight. The mixture was dried with Na₂SO₄, filtered through filter paper and concentrated under reduced pressure to afford a crude oil. Purification by column chromatography (Mobile phase: 5% MeOH in CHCl₃) afforded **3** as a clear oil (6.82 g, 79%). **¹H NMR** (400 MHz, MeOD) δ 3.58 – 3.47 (m, 3H), 3.26 (dd, $J = 10.1, 5.2$ Hz, 1H), 2.61 – 2.44 (m, 2H), 2.19 (dd, $J = 16.5,$

5.4 Hz, 1H) ppm. ^{13}C NMR (101 MHz, MeOD) δ 176.7, 64.9, 53.4, 34.77, 34.37, 29.8 ppm. **ESI-MS**, m/z 130.1 $[\text{M}+\text{H}]^+$. **HR-MS**: m/z calcd. for $\text{C}_6\text{H}_{10}\text{NO}_2$ $[\text{M}+\text{H}]^+$: 130.0863; found 130.0863; **HPLC** (PP gradient, MeOH): 1.75 min.

(1-methyl-5-oxopyrrolidin-3-yl)methyl methanesulfonate (4) – In a 50 ml round-bottom flask, 4-(hydroxymethyl)-1-methylpyrrolidin-2-one **3** (209 mg, 1.62 mmol) was weighed out, then dissolved in CH_2Cl_2 (5 mL). The flask was placed on an ice bath, sealed with a rubber septum and purged with N_2 . DIPEA (565 μL , 3.24 mmol) and MsCl (150 μL , 1.95 mmol) were added via syringe and the mixture was left to stir for 4 hours. After this time, the mixture was quenched with water (20 mL) and the CH_2Cl_2 layer separated. The aqueous layer was washed with additional CH_2Cl_2 (3 x 20mL). The organic layers were combined, dried with MgSO_4 , filtered and concentrated via rotary evaporation to give the crude mesylate as a yellow oil. This oil was then purified using a silica column (Mobile phase: 2% MeOH in CH_2Cl_2) to give **4** as a clear oil (190 mg, 59%). ^1H NMR (400 MHz, CDCl_3) δ 4.16 (qd, $J = 10.0, 6.8$ Hz, 2H), 3.51 (dd, $J = 10.2, 8.2$ Hz, 1H), 3.21 (dd, $J = 10.2, 5.2$ Hz, 1H), 3.01 (s, 3H), 2.85 – 2.73 (m, 4H), 2.53 (dd, $J = 17.1, 9.4$ Hz, 1H), 2.16 (dd, $J = 17.1, 6.2$ Hz, 1H) ppm. ^{13}C NMR (101 MHz, CDCl_3) δ 172.8, 70.4, 51.4, 37.5, 33.3, 30.7, 29.6 ppm. **ESI-MS**, m/z 208.0 $[\text{M}+\text{H}]^+$; **HR-MS**: m/z calcd. for $\text{C}_7\text{H}_{13}\text{NO}_4\text{S}$ $[\text{M}+\text{H}]^+$: 207.0565; found 207.0567; **HPLC** (PP gradient, MeOH): 2.36 min.

Dimethyl 3-(nitromethyl)glutarate (6) – In a 250 mL round-bottom flask, nitromethane (14.9 mL, 0.352 mol) was added to dimethyl glutaconate **5** (5.56 g, 35.2 mmol). 1,1,3,3-tetramethylguanidine (882 μL , 7.03 mmol) was added dropwise to the mixture. After complete addition, the mixture was left to stir overnight. The mixture was quenched with 5% HCl (75 mL), then washed with diethyl ether (3 x 75 mL). The organic layers were collected, combined and dried with MgSO_4 . The solvent was filtered and evaporated under reduced pressure to give

a brown-coloured oil. The resin was purified using silica gel chromatography (Mobile phase: 10% EtOAc in petroleum benzene, TLCs checked at 25% EtOAc in petroleum benzene) to afford **7** as a clear oil (3.32 g, 47%). ¹H NMR (400 MHz, CDCl₃) δ 4.62 (d, *J* = 6.1 Hz, 2H), 3.71 (s, 6H), 3.13 – 3.00 (m, 1H), 2.56 (dd, *J* = 6.6, 1.1 Hz, 4H) ppm. ¹³C NMR (101 MHz, CDCl₃) δ 171.6, 77.5, 52.1, 35.1, 30.7 ppm.

Methyl 2-(5-oxopyrrolidin-3-yl)acetate (8) – In a 250 mL three-neck round-bottom flask purged with N₂, 10% Pd/C (332 mg) was added and submerged in CH₂Cl₂. Dimethyl 3-(nitromethyl)glutarate **6** (3.32 g, 15.2 mmol) was dissolved in acetic acid (150 mL) and added to the flask, then stirring began. The flask was then flushed with N₂ three times, followed by H₂ three times. Progress was monitored using NMR and LCMS. Once the starting material and hydroxylamine intermediate were consumed, the flask was purged with N₂ and the Pd/C was filtered through glass microfiber filter paper. The solvent was then evaporated off to give the amine **7** as a caramel-coloured oil. The amine was then dissolved in MeOH (75mL), basified with Et₃N (1 mL) and heated under reflux. The solvent and base were evaporated off under reduced pressure to give the crude lactam **8** as a yellow resin. The resin was purified with column chromatography (Mobile phase: 2% MeOH in CH₂Cl₂) to afford **8** as a white solid (1.61 g, 68%). ¹H NMR (400 MHz, CDCl₃) δ 7.07 (br s, 1H), 3.62 (s, 3H), 3.54 (dd, *J* = 9.9, 7.8 Hz, 1H), 3.02 (dd, *J* = 9.9, 6.2 Hz, 1H), 2.86 – 2.75 (m, 1H), 2.52 – 2.40 (m, 3H), 1.99 (dd, *J* = 16.9, 7.3 Hz, 1H) ppm. ¹³C NMR (101 MHz, CDCl₃) δ 177.7, 171.8, 51.3, 47.4, 38.0, 36.2, 30.6 ppm. **ESI-MS**: *m/z* 158.1 [M+H]⁺

Methyl 2-(1-methyl-5-oxopyrrolidin-3-yl)acetate (10) – To a solution of lactam **8** (1.12 g, 7.09 mmol) in acetone (120 mL) was added paraformaldehyde (1.07 g, 35.5 mmol) and K₂CO₃ (132 mg), followed by the addition of water (13 mL). The mixture was then sonicated for 4 hours at 20-minute intervals with 10-minute rests. The mixture was then filtered and the filtrate was

concentrated under reduced pressure to give the crude hemiaminal **9** as an opaque oil. The oil was purified by a silica column chromatography (Mobile phase: 5% MeOH in CH₂Cl₂) to give **9** as a clear oil. The hemiaminal **9** was then dissolved in CHCl₃ (125 mL), to which CF₃COOH (25 mL) and Et₃SiH (25 mL) were added, and the mixture was stirred at room temperature overnight. The mixture was then quenched with water (75 mL) and the organic layer was separated. The aqueous layer was washed with additional CHCl₃ (2 x 75 mL). The organic layers were combined, dried with MgSO₄, filtered and concentrated under reduced pressure to afford a biphasic oil. This was purified by column chromatography (neat EtOAc), giving **10** as a clear oil (1.08 g, 89%). **¹H NMR** (400 MHz, CDCl₃) δ 3.67 (s, 3H), 3.57 (dd, *J* = 10.0, 7.9 Hz, 1H), 3.06 (dd, *J* = 10.0, 6.0 Hz, 1H), 2.85 – 2.68 (m, 4H), 2.58 (dd, *J* = 16.8, 9.0 Hz, 1H), 2.53 – 2.38 (m, 2H), 2.08 (dd, *J* = 16.8, 7.0 Hz, 1H) ppm. **¹³C NMR** (101 MHz, CDCl₃) δ 173.7, 172.2, 54.8, 51.9, 38.8, 37.1, 29.6, 27.9 ppm. **ESI-MS**: *m/z* 172.1 [M+H]⁺ **HR-MS**: *m/z* calc. for C₈H₁₃NO₃ [M+H]⁺: 171.0895; found 171.0899. **HPLC** (PP gradient, MeOH): 3.31 min.

4-(2-hydroxyethyl)-1-methylpyrrolidin-2-one (11) – In a 100 mL round-bottom flask, methyl 2-(1-methyl-5-oxopyrrolidin-3-yl)acetate **10** (446 mg, 2.61 mmol) was dissolved in EtOH (25 mL). NaBH₄ (0.99 g, 26.1 mmol) was then added over a period of 4 hours, and the mixture was left to stir overnight. After completion, the mixture was quenched with water and the solvent was evaporated off under reduced pressure to give a white solid. The solid was then purified with column chromatography (Mobile phase: 5% MeOH in CH₂Cl₂) to obtain **11** as a clear oil (313 mg, 84%). **¹H NMR** (400 MHz, CDCl₃) δ 3.72 – 3.58 (m, 2H), 3.49 (dd, *J* = 9.7, 8.1 Hz, 1H), 3.07 (dd, *J* = 9.7, 6.7 Hz, 1H), 2.80 (s, 3H), 2.58 – 2.25 (m, 3H), 2.13 – 2.01 (m, 1H), 1.76 – 1.61 (m, 2H) ppm. **¹³C NMR** (101 MHz, CDCl₃) δ 174.7, 60.7, 55.5, 37.51, 37.49, 29.68, 28.79 ppm. **ESI-MS**: *m/z* 222.0 [M+H]⁺. **HR-MS**: *m/z* calc. for C₇H₁₃NO₂ [M+H]⁺: 143.0946; found 143.0951. **HPLC** (PP gradient, MeOH): 2.09 min.

2-(1-methyl-5-oxopyrrolidin-3-yl)ethyl methanesulfonate (12) – In a 50 ml round-bottom flask, 4-(2-hydroxyethyl)-1-methylpyrrolidin-2-one **11** (128 mg, 0.893 mmol) was weighed out, then dissolved in CH₂Cl₂ (10 mL). The flask was placed on an ice bath, sealed with a rubber septum and purged with N₂. DIPEA (233 μL, 1.34 mmol) and MsCl (103 μL, 1.34 mmol) were added via syringe and the mixture was left to stir for 4 hours. After this time, the mixture was quenched with water (20 mL) and the CH₂Cl₂ layer separated. The aqueous layer was washed with additional CH₂Cl₂ (3 x 20 mL). The organic layers were combined, dried with MgSO₄, filtered and concentrated via rotary evaporation to give the crude mesylate **12** as a yellow oil. This oil was then purified using silica gel chromatography (Mobile phase: 2% MeOH in CH₂Cl₂) to give **12** as a clear oil (122 mg, 62%). ¹H NMR (400 MHz, CDCl₃) δ 4.31 – 4.18 (m, 2H), 3.53 (dd, *J* = 9.7, 8.0 Hz, 1H), 3.07 (dd, *J* = 9.7, 6.6 Hz, 1H), 3.01 (s, 3H), 2.82 (s, 3H), 2.61 – 2.47 (m, 2H), 2.14 – 2.03 (m, 1H), 1.94 – 1.86 (m, 2H) ppm. ¹³C NMR (101 MHz, CDCl₃) δ 173.7, 67.7, 54.8, 37.60, 37.13, 34.1, 29.67, 28.60 ppm. **ESI-MS**: *m/z* 222.0 [M+H]⁺. **HR-MS**: *m/z* calc. for C₈H₁₅NO₄S [M+H]⁺: 221.0726; found 221.0726. **HPLC** (PP gradient, MeOH): 3.28 min.

2,3,4,5-tetrahydro-1H-pyrido[4,3-b]indol-1-one (16) – 2,4-piperidinedione **13** (500 mg, 4.42 mmol) was weighed into a 100 mL round-bottom flask, and phenylhydrazine **14** (434 μL, 4.42 mmol) was added. The mixture was dissolved in EtOH (50 mL) and refluxed overnight. The solvent was evaporated off to give the hydrazone **15** as a crimson oil. This was cooled to 0 °C, dissolved in 70% sulfuric acid (20 mL) and stirred for 4 hours. The acid was neutralised with 2 M NaOH and the aqueous layer was washed with EtOAc (3 x 50 mL). The organic layers were combined, dried with dried with MgSO₄, filtered and concentrated under reduced pressure to afford a yellow/brown resin. This was purified with silica gel chromatography (Mobile phase: Gradient of 3-5% MeOH in CH₂Cl₂) to acquire **16** as a yellow resin (137 mg, 17%). ¹H NMR (400 MHz, CDCl₃) δ 8.91 (br s, 1H), 8.17 – 8.09 (m, 1H), 7.38 – 7.31 (m, 1H), 7.25 –

7.17 (m, 2H), 5.53 (br s, 1H), 3.63 (t, $J = 6.9$ Hz, 2H), 3.02 (t, $J = 6.9$ Hz, 2H) ppm. **ESI-MS**: m/z 187.1 $[M+H]^+$. **HPLC** (PP gradient, MeOH): 4.36 min.

5-((1-methyl-5-oxopyrrolidin-3-yl)methyl)-2,3,4,5-tetrahydro-1H-pyrido[4,3-b]indol-1-one (**17**) – In a 25 mL round-bottom flask, 2,3,4,5-tetrahydro-1H-pyrido[4,3-b]indol-1-one **16** (36.5 mg, 0.196 mmol) was weighed out and dissolved in DMF (3 mL). The flask was sealed, purged with N₂ and then chilled to –78 °C. NaHMDS (94 μL, 0.294 mmol, 1 M in THF) was added via syringe and the mixture was stirred for 30 minutes. After this time, 2-(1-methyl-5-oxopyrrolidin-3-yl)ethyl methanesulfonate **12** (60.9 mg, 0.294 mmol) was weighed, dissolved in DMF (1 mL) and added via syringe. The mixture was warmed to room temperature, then heated to 90 °C and left stirring overnight. After this time, the mixture was quenched with a saturated aqueous solution of NaHCO₃ (40 mL) and washed with EtOAc (3 x 40 mL). The combined organic layers were dried with MgSO₄, filtered and concentrated under reduced pressure to obtain a yellow oil. The oil was purified using a silica column (Mobile phase: 5% MeOH in CH₂Cl₂) to obtain **17** as a yellow oil (3.80 mg, 6%). **¹H NMR** (400 MHz, CDCl₃) δ 8.23 – 8.18 (m, 1H), 7.33 – 7.26 (m, 3H), 5.53 (br s, 1H), 4.14 (d, $J = 8.0$ Hz, 2H), 3.70 (t, $J = 6.9$ Hz, 2H), 3.38 (dd, $J = 10.2, 7.2$ Hz, 1H), 3.12 – 2.92 (m, 4H), 2.85 (s, 3H), 2.57 (dd, $J = 17.1, 8.3$ Hz, 1H), 2.18 (dd, $J = 16.9, 4.8$ Hz, 1H) ppm. **¹³C NMR** (101 MHz, CDCl₃) δ 123.13, 122.58, 121.62, 109.4, 52.2, 46.7, 40.8, 35.2, 32.2, 29.9, 22.5 ppm. **ESI-MS**: m/z 297.9 $[M+H]^+$. **HR-MS**: m/z calc. for C₁₇H₁₉N₃O₂ $[M+H]^+$: 297.1477; found 297.1475. **HPLC** (PP gradient, MeOH): 4.32 min.

5-(2-(1-methyl-5-oxopyrrolidin-3-yl)ethyl)-2,3,4,5-tetrahydro-1H-pyrido[4,3-b]indol-1-one (**18**) – In a 50 mL round-bottom flask, 2,3,4,5-tetrahydro-1H-pyrido[4,3-b]indol-1-one **16** (45 mg, 0.241 mmol) was weighed out and dissolved in DMF (3 mL). The flask was sealed, purged with N₂ and then chilled to –78 °C. NaHMDS (362 μL, 0.362 mmol, 1 M in THF) was added

via syringe and the mixture was stirred for 30 minutes. After this time, 2-(1-methyl-5-oxopyrrolidin-3-yl)ethyl methanesulfonate **12** (80 mg, 0.362 mmol) was weighed, dissolved in DMF (1 mL) and added via syringe. The mixture was warmed to room temperature, then heated to 90 °C and left stirring overnight. After this time, the mixture was quenched with a saturated aqueous solution of NaHCO₃ (40 mL) and washed with EtOAc (3 x 40 mL). The combined organic layers were dried with MgSO₄, filtered and concentrated under reduced pressure to obtain a yellow oil. The oil was purified with a silica column (Mobile phase: Gradient of 2-7% MeOH in CH₂Cl₂) to obtain **18** as a yellow oil (24.7 mg, 33%). **¹H NMR** (400 MHz, CDCl₃) δ 8.24 – 8.18 (m, 1H), 7.33 – 7.24 (m, 3H), 5.68 (br s, 1H), 4.21 – 4.05 (m, 2H), 3.69 (td, *J* = 6.8, 1.9 Hz, 2H), 3.46 (dd, *J* = 9.7, 8.1 Hz, 1H), 3.05 – 2.97 (m, 3H), 2.82 (s, 3H), 2.59 (dd, *J* = 16.5, 8.9 Hz, 1H), 2.42 – 2.28 (m, 1H), 2.14 (dd, *J* = 16.5, 7.2 Hz, 1H), 2.07 – 1.86 (m, 2H) ppm. **¹³C NMR** (101 MHz, CDCl₃) δ 173.5, 166.9, 143.8, 136.5, 125.7, 122.72, 122.17, 121.44, 109.2, 106.2, 55.1, 42.0, 40.7, 37.2, 35.1, 29.7, 29.2, 22.2 ppm. **ESI-MS**: *m/z* 312.0 [M+H]⁺. **HR-MS**: *m/z* calc. for C₁₈H₂₁N₃O₂ [M+H]⁺: 311.1634; found 311.1641. **HPLC** (PP gradient, MeOH): 4.644 min.

References

1. Huang B, Yang XD, Zhou MM, Ozato K, Chen LF. Brd4 coactivates transcriptional activation of NF-kappaB via specific binding to acetylated RelA. *Mol Cell Biol.* 2009;29(5):1375-87.
2. Ciro M, Prosperini E, Quarto M, Grazini U, Walfridsson J, McBlane F, et al. ATAD2 is a novel cofactor for MYC, overexpressed and amplified in aggressive tumors. *Cancer Res.* 2009;69(21):8491-8.
3. French CA, Miyoshi I, Kubonishi I, Grier HE, Perez-Atayde AR, Fletcher JA. BRD4-NUT fusion oncogene: a novel mechanism in aggressive carcinoma. *Cancer Res.* 2003;63(2):304-7.
4. Zou JX, Guo L, Revenko AS, Tepper CG, Gemo AT, Kung HJ, et al. Androgen-induced coactivator ANCCA mediates specific androgen receptor signaling in prostate cancer. *Cancer Res.* 2009;69(8):3339-46.
5. Mujtaba S, He Y, Zeng L, Farooq A, Carlson JE, Ott M, et al. Structural basis of lysine-acetylated HIV-1 Tat recognition by PCAF bromodomain. *Mol Cell.* 2002;9(3):575-86.
6. Cardenas-Mora J, Spindler JE, Jang MK, McBride AA. Dimerization of the papillomavirus E2 protein is required for efficient mitotic chromosome association and Brd4 binding. *J Virol.* 2008;82(15):7298-305.
7. Lin A, Wang S, Nguyen T, Shire K, Frappier L. The EBNA1 protein of Epstein-Barr virus functionally interacts with Brd4. *J Virol.* 2008;82(24):12009-19.
8. Lu P, Shen Y, Yang H, Wang Y, Jiang Z, Yang X, et al. BET inhibitors RVX-208 and PFI-1 reactivate HIV-1 from latency. *Sci Rep.* 2017;7(1):16646.
9. Darcis G, Kula A, Bouchat S, Fujinaga K, Corazza F, Ait-Ammar A, et al. An In-Depth Comparison of Latency-Reversing Agent Combinations in Various In Vitro and Ex Vivo HIV-1 Latency Models Identified Bryostatins-1+JQ1 and Ingenol-B+JQ1 to Potently Reactivate Viral Gene Expression. *PLoS Pathog.* 2015;11(7):e1005063.
10. Das A, Chai JC, Yang CS, Lee YS, Das ND, Jung KH, et al. Dual transcriptome sequencing reveals resistance of TLR4 ligand-activated bone marrow-derived macrophages to inflammation mediated by the BET inhibitor JQ1. *Sci Rep.* 2015;5:16932.
11. Nicodeme E, Jeffrey KL, Schaefer U, Beinke S, Dewell S, Chung CW, et al. Suppression of inflammation by a synthetic histone mimic. *Nature.* 2010;468(7327):1119-23.
12. Anand P, Brown JD, Lin CY, Qi J, Zhang R, Artero PC, et al. BET bromodomains mediate transcriptional pause release in heart failure. *Cell.* 2013;154(3):569-82.
13. Gilham D, Wasiak S, Tsujikawa LM, Halliday C, Norek K, Patel RG, et al. RVX-208, a BET-inhibitor for treating atherosclerotic cardiovascular disease, raises ApoA-I/HDL and represses pathways that contribute to cardiovascular disease. *Atherosclerosis.* 2016;247:48-57.

14. Crawford TD, Audia JE, Bellon S, Burdick DJ, Bommi-Reddy A, Cote A, et al. GNE-886: A Potent and Selective Inhibitor of the Cat Eye Syndrome Chromosome Region Candidate 2 Bromodomain (CECR2). *ACS Med Chem Lett.* 2017;8(7):737-41.
15. Igoe N, Bayle ED, Fedorov O, Tallant C, Savitsky P, Rogers C, et al. Design of a Biased Potent Small Molecule Inhibitor of the Bromodomain and PHD Finger-Containing (BRPF) Proteins Suitable for Cellular and in Vivo Studies. *J Med Chem.* 2017;60(2):668-80.
16. Picaud S, Fedorov O, Thanasopoulou A, Leonards K, Jones K, Meier J, et al. Generation of a Selective Small Molecule Inhibitor of the CBP/p300 Bromodomain for Leukemia Therapy. *Cancer Res.* 2015;75(23):5106-19.
17. Siebel AL, Trinh SK, Formosa MF, Mundra PA, Natoli AK, Reddy-Luthmoodoo M, et al. Effects of the BET-inhibitor, RVX-208 on the HDL lipidome and glucose metabolism in individuals with prediabetes: A randomized controlled trial. *Metabolism.* 2016;65(6):904-14.
18. Stathis A, Zucca E, Bekradda M, Gomez-Roca C, Delord JP, de La Motte Rouge T, et al. Clinical Response of Carcinomas Harboring the BRD4-NUT Oncoprotein to the Targeted Bromodomain Inhibitor OTX015/MK-8628. *Cancer Discov.* 2016;6(5):492-500.
19. Siu KT, Ramachandran J, Yee AJ, Eda H, Santo L, Panaroni C, et al. Preclinical activity of CPI-0610, a novel small-molecule bromodomain and extra-terminal protein inhibitor in the therapy of multiple myeloma. *Leukemia.* 2017;31(8):1760-9.
20. Mirguet O, Gosmini R, Toum J, Clement CA, Barnathan M, Brusq JM, et al. Discovery of epigenetic regulator I-BET762: lead optimization to afford a clinical candidate inhibitor of the BET bromodomains. *J Med Chem.* 2013;56(19):7501-15.
21. Dhalluin C, Carlson JE, Zeng L, He C, Aggarwal AK, Zhou MM. Structure and ligand of a histone acetyltransferase bromodomain. *Nature.* 1999;399(6735):491-6.
22. Filippakopoulos P, Qi J, Picaud S, Shen Y, Smith WB, Fedorov O, et al. Selective inhibition of BET bromodomains. *Nature.* 2010;468(7327):1067-73.
23. Chung CW, Dean AW, Woolven JM, Bamborough P. Fragment-based discovery of bromodomain inhibitors part 1: inhibitor binding modes and implications for lead discovery. *J Med Chem.* 2012;55(2):576-86.
24. Bamborough P, Diallo H, Goodacre JD, Gordon L, Lewis A, Seal JT, et al. Fragment-based discovery of bromodomain inhibitors part 2: optimization of phenylisoxazole sulfonamides. *J Med Chem.* 2012;55(2):587-96.
25. Hewings DS, Wang M, Philpott M, Fedorov O, Uttarkar S, Filippakopoulos P, et al. 3,5-dimethylisoxazoles act as acetyl-lysine-mimetic bromodomain ligands. *J Med Chem.* 2011;54(19):6761-70.
26. Gacias M, Gerona-Navarro G, Plotnikov AN, Zhang G, Zeng L, Kaur J, et al. Selective chemical modulation of gene transcription favors oligodendrocyte lineage progression. *Chem Biol.* 2014;21(7):841-54.
27. Ozer HG, El-Gamal D, Powell B, Hing ZA, Blachly JS, Harrington B, et al. BRD4 Profiling Identifies Critical Chronic Lymphocytic Leukemia Oncogenic Circuits and Reveals

Sensitivity to PLX51107, a Novel Structurally Distinct BET Inhibitor. *Cancer Discov.* 2018;8(4):458-77.

28. Dawson MA, Prinjha RK, Dittmann A, Giotopoulos G, Bantscheff M, Chan WI, et al. Inhibition of BET recruitment to chromatin as an effective treatment for MLL-fusion leukaemia. *Nature.* 2011;478(7370):529-33.

29. Philpott M, Yang J, Tumber T, Fedorov O, Uttarkar S, Filippakopoulos P, et al. Bromodomain-peptide displacement assays for interactome mapping and inhibitor discovery. *Mol Biosyst.* 2011;7(10):2899-908.

30. Shortt J, Hsu AK, Martin BP, Doggett K, Matthews GM, Doyle MA, et al. The drug vehicle and solvent N-methylpyrrolidone is an immunomodulator and antimyeloma compound. *Cell Rep.* 2014;7(4):1009-19.

31. NMP in Relapsed Refractory Myeloma. <https://ClinicalTrials.gov/show/NCT02468687>.

32. Ghayor C, Corroero RM, Lange K, Karfeld-Sulzer LS, Gratz KW, Weber FE. Inhibition of osteoclast differentiation and bone resorption by N-methylpyrrolidone. *J Biol Chem.* 2011;286(27):24458-66.

33. Ghayor C, Gjoksi B, Siegenthaler B, Weber FE. N-methyl pyrrolidone (NMP) inhibits lipopolysaccharide-induced inflammation by suppressing NF-kappaB signaling. *Inflamm Res.* 2015;64(7):527-36.

34. Gjoksi B, Ghayor C, Bhattacharya I, Zenobi-Wong M, Weber FE. The bromodomain inhibitor N-methyl pyrrolidone reduced fat accumulation in an ovariectomized rat model. *Clin Epigenetics.* 2016;8:42.

35. Rooney TP, Filippakopoulos P, Fedorov O, Picaud S, Cortopassi WA, Hay DA, et al. A series of potent CREBBP bromodomain ligands reveals an induced-fit pocket stabilized by a cation-pi interaction. *Angew Chem Int Ed Engl.* 2014;53(24):6126-30.

36. Zoretic PA, Barcelos F, Jardin J, Bhakta C. Synthetic Approaches to 10-Azaprostaglandins. *Journal of Organic Chemistry.* 1980;45(5):810-4.

37. Stanetty P, Turner M, Mihovilovic MD. Synthesis of pyrrolo[2,3-d][1,2,3]thiadiazole-6-carboxylates via the Hurd-Mori reaction. Investigating the effect of the N-protecting group on the cyclization. *Molecules.* 2005;10(2):367-75.

38. Hanessian S, Buckle R, Bayrakdarian M. Design and synthesis of a novel class of constrained tricyclic pyrrolizidinone carboxylic acids as carbapenem mimics. *Journal of Organic Chemistry.* 2002;67(10):3387-97.

39. Kobayashi S, Kobayashi K, Hirai K. Trials for the synthesis of (R)-4-mercapto-pyrrolidin-2-one ((R)-MPD). *Synlett.* 1999;1999(Sup. 1):909-12.

40. Felluga F, Gombac V, Pitacco G, Valentin E. A convenient chemoenzymatic synthesis of (R)-(-) and (S)-(+)-homo-β-proline. *Tetrahedron: Asymmetry.* 2004;15(20):3323-7.

41. Wang L, Dong M, Lowary TL. Synthesis of unusual N-acylated aminosugar fragments of *Mycobacterium marinum* lipooligosaccharide IV. *J Org Chem.* 2015;80(5):2767-80.

42. Kwak H-S, Koo KD, Lim D, Min K, Park H, Choi D-Y, et al., inventors; LG Life Sciences, Ltd., S. Korea . assignee. Preparation of 5-oxopyrrolidine-2-carboxamide and 2-oxoimidazolidine-4-carboxamide derivatives as beta-secretase inhibitors patent WO2009038412A2. 2009.
43. Ma S, Han X, Krishnan S, Virgil SC, Stoltz BM. Catalytic enantioselective stereoablative alkylation of 3-halooxindoles: facile access to oxindoles with C3 all-carbon quaternary stereocenters. *Angew Chem Int Ed Engl.* 2009;48(43):8037-41.
44. Bennett SNL, Goldberg FW, Leach A, Whittamore PRO, Soerme P, inventors; AstraZeneca AB, Swed. . assignee. Preparation of adamantyl iminocarbonyl-substituted pyrimidines as inhibitors of 11 β HSD1 patent US20110092526A1. 2011.
45. Romero FA, Taylor AM, Crawford TD, Tsui V, Cote A, Magnuson S. Disrupting Acetyl-Lysine Recognition: Progress in the Development of Bromodomain Inhibitors. *J Med Chem.* 2016;59(4):1271-98.
46. McPhillips TM, McPhillips SE, Chiu H-J, Cohen AE, Deacon AM, Ellis PJ, et al. Blu-Ice and the Distributed Control System: software for data acquisition and instrument control at macromolecular crystallography beamlines. *Journal of synchrotron radiation.* 2002;9(6):401-6.
47. Battye TGG, Kontogiannis L, Johnson O, Powell HR, Leslie AGW. iMOSFLM: a new graphical interface for diffraction-image processing with MOSFLM. *Acta crystallographica Section D, Biological crystallography.* 2011;67(Pt 4):271-81.
48. Evans PR, Murshudov GN. How good are my data and what is the resolution? *Acta crystallographica Section D, Biological crystallography.* 2013;69(Pt 7):1204-14.
49. Winn MD, Ballard CC, Cowtan KD, Dodson EJ, Emsley P, Evans PR, et al. Overview of the CCP4 suite and current developments. *Acta Crystallogr D Biol Crystallogr.* 2011;67(Pt 4):235-42.
50. McCoy AJ, Grosse-Kunstleve RW, Adams PD, Winn MD, Storoni LC, Read RJ. Phaser crystallographic software. *J Appl Crystallogr.* 2007;40(Pt 4):658-74.
51. Emsley P, Lohkamp B, Scott WG, Cowtan K. Features and development of Coot. *Acta Crystallogr D Biol Crystallogr.* 2010;66(Pt 4):486-501.
52. Afonine PV, Grosse-Kunstleve RW, Echols N, Headd JJ, Moriarty NW, Mustyakimov M, et al. Towards automated crystallographic structure refinement with phenix.refine. *Acta Crystallogr D Biol Crystallogr.* 2012;68(Pt 4):352-67.

Chapter 3 – Substituted 1-methyl-4-phenylpyrrolidin-2-ones – Fragment-Based Design of N-Methylpyrrolidone-Derived Bromodomain Inhibitors

Keywords

BRD4, Bromodomain, Epigenetics, K-ac, NMP

Abbreviations

BET, Bromodomain and Extra Terminal; BRD4, Bromodomain-containing Protein 4; BRD4 BD1, First Bromodomain of BRD4; FBDD, Fragment-based Drug Design; HPLC, High Performance Liquid Chromatography; K-ac, Acetyl-lysine; LE, Ligand Efficiency; LLE, Lipophilic Ligand Efficiency; NHA, Non-hydrogen Atom; NMP, *N*-Methylpyrrolidone; RMS, Root Mean Square; SAR, Structure-Activity Relationship; SD, Standard Deviation; SEM, Standard Error of Mean; vdW, van der Waals; WPF, tryptophan-proline-phenylalanine.

Abstract

N-Methylpyrrolidone is one of several chemotypes that have been described as a mimetic of acetyl-lysine in the development of bromodomain inhibitors. In this paper, we describe the synthesis of a 4-phenyl substituted analogue – 1-methyl-4-phenylpyrrolidin-2-one – and the use of aryl substitution reactions as a divergent route for derivatives. Ultimately, this has led to structurally complex, chiral compounds with progressively improved affinity as inhibitors of bromodomain-containing protein 4.

3.1 Introduction

Fragment-based drug discovery is a molecular design strategy that has gained significant traction as a means to develop new drug candidates.^{1, 2} It fundamentally enacts a process of “growing” a small molecule with weak, but ligand efficient interactions with a target macromolecule into a high-affinity drug-like molecule. That growth is typically achieved by identifying a set of vectors and using functional group manipulations to extend away from the fragment to gain new interactions and thus improve binding affinity.³⁻⁵

In practice, the nature of the FBDD process has shown a tendency towards extended structures as the functional group transformations are based around building block chemistry.^{6, 7} Obtaining more compact structures demands accessing multiple functional groups for elaboration on the same core fragment. There has also been a tendency to avoid chirality in fragment sets as it can lead to more complex syntheses.⁸

In our work, we wanted to consider both of these features as they might contribute towards compounds with increased novelty and characteristics such as structural rigidity that might provide for improved target selectivity. Here, we report on the elaboration by successive aryl substitution of 1-methyl-4-phenylpyrrolidin-2-one, a chiral, phenyl-substituted version of the solvent NMP as a BET bromodomain inhibitor.

Despite the vast amount of effort that has gone into elaborating the many fragments that are known to fit inside the K-ac binding site,⁹⁻¹⁵ NMP has been neglected in these efforts. NMP's historic use has been in industrial applications such as paint removal and coatings, along with pharmaceutical purposes including drug solubilisation¹⁶ and depot injections, remarked for its low reactivity and toxicity. NMP has affinity for several bromodomains¹⁷ and crystallographic work has established that NMP fits into the conserved areas of the K-ac binding pocket. NMP shows antimyeloma and immunomodulatory activity in multiple myeloma models, which is

attributed to pleiotropic bromodomain inhibition.¹⁸ At the moment, it is in a phase I clinical trial for the treatment of multiple myeloma.¹⁹ NMP also has a well-documented history with bone diseases like rheumatoid arthritis and osteoporosis²⁰ by preventing bone resorption²¹ and fat accumulation in bone marrow.²²

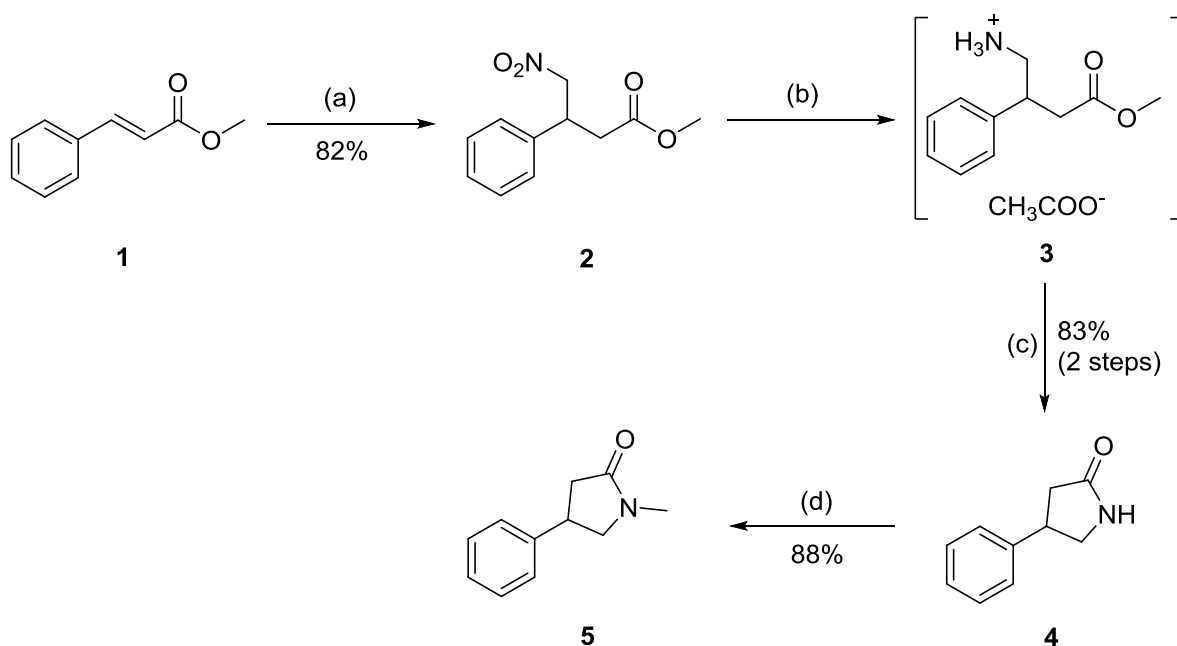
NMP has also served as the inspiration to the development of other novel mimetic warheads, including the dimethylisoxazole⁹ and dihydroquinazolinone.²³ Both of these mimetics have been greatly utilised in the development of clinical inhibitors²⁴ and probes.^{14, 25, 26} However, the same level of elaboration has not been applied to NMP. We believe that with suitable functionalisation, NMP, with its ligand efficient interactions, could have excellent utility in bromodomain inhibitor design. In this manuscript, we describe the efforts undertaken to develop aryl-functionalised derivatives of NMP as inhibitors of BRD4 BD1.

3.2 Results and Discussion

In the Protein Data Bank, six entries show NMP binding to a bromodomain in close mimicry of K-ac; the carbonyl group imitates the interactions of K-ac to a conserved tyrosine and asparagine residue, while the *N*-methyl substituent rests within the water-lined pocket. In order to build upon the mimicry of NMP, we decided that the 4-position would be the most appropriate place to develop functionalised derivatives (Appendix B). As a starting point, we reasoned that, based on the existing literature, a phenyl moiety would be a suitable group to functionalise to explore and interact with sections of the bromodomain binding pocket – including the ZA channel and WPF shelf – in a similar manner to other inhibitors reported previously.

3.2.1 Synthesis

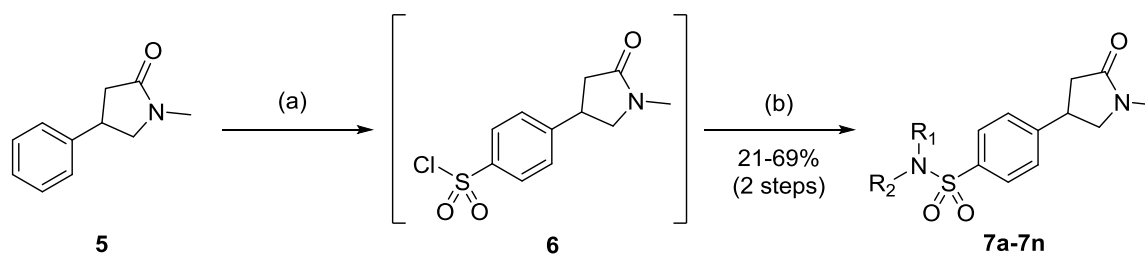
The strategy for preparing the desired aryl NMP fragment is outlined in Scheme 1. Commercially-available methyl *trans*-cinnamate **1** was reacted with nitromethane and 1,1,3,3-tetramethylguanidine via Michael addition as previously reported²⁷ to afford the nitroester **2** in 82% yield. The reduction of **2** to the amine **3** and then cyclisation to the lactam **4** was achieved by hydrogenation with acetic acid as the solvent. Reduction under these conditions gave the amine **3** as an acetate salt. Refluxing **3** in a mixture of ethanol and triethylamine drove cyclisation of **3** to the lactam **4** in good yields across the 2 steps. The lactam was then methylated by methyl iodide and sodium hydride to give the desired phenyl NMP derivative **5**.²⁸ On multigram scales, this procedure was reliably reproduced in 50% overall yield.



Scheme 1. Formation of **5**, a phenyl NMP derivative. (a): CH_3NO_2 , 1,1,3,3-tetramethylguanidine, 42 h, rt; (b): H_2 , Pd/C, CH_3COOH , 4 d, rt; (c): Et_3N , EtOH, o/n, rf; (d): N_2 , NaH, MeI, THF, o/n, $0\text{ }^\circ\text{C} \rightarrow \text{rt}$.

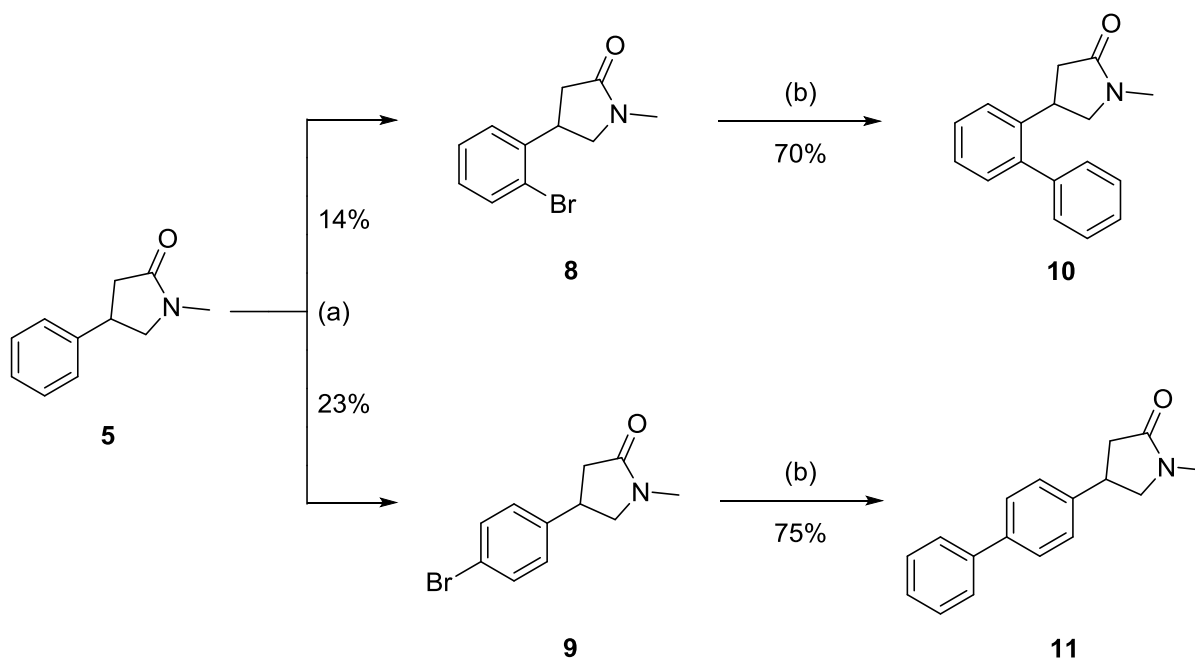
With the core scaffold in hand, the next step was to functionalise the phenyl group using electrophilic aromatic substitution. We envisioned that an appropriate functional group was one that would allow for quick and efficient derivatisation. For this, we selected two functional groups: a sulfonyl chloride and a bromide.

We first used chlorosulfonylation using an excess of chlorosulfonic acid to give the intermediate **6**. The *para*-substituted sulfonyl chloride **6** was treated with a range of primary and secondary amines based on their availability, with minor adjustments to the amine based on assay results (discussed later). These were used to generate sulfonamides **7a-7n** in yields ranging from 21-69% (Scheme 2).



Scheme 2. General formation of sulfonamides **7**. (a): ClSO_3H , CH_2Cl_2 , o/n, rt; (b): NR_1R_2 , Et_3N , CH_2Cl_2 , o/n, rt.

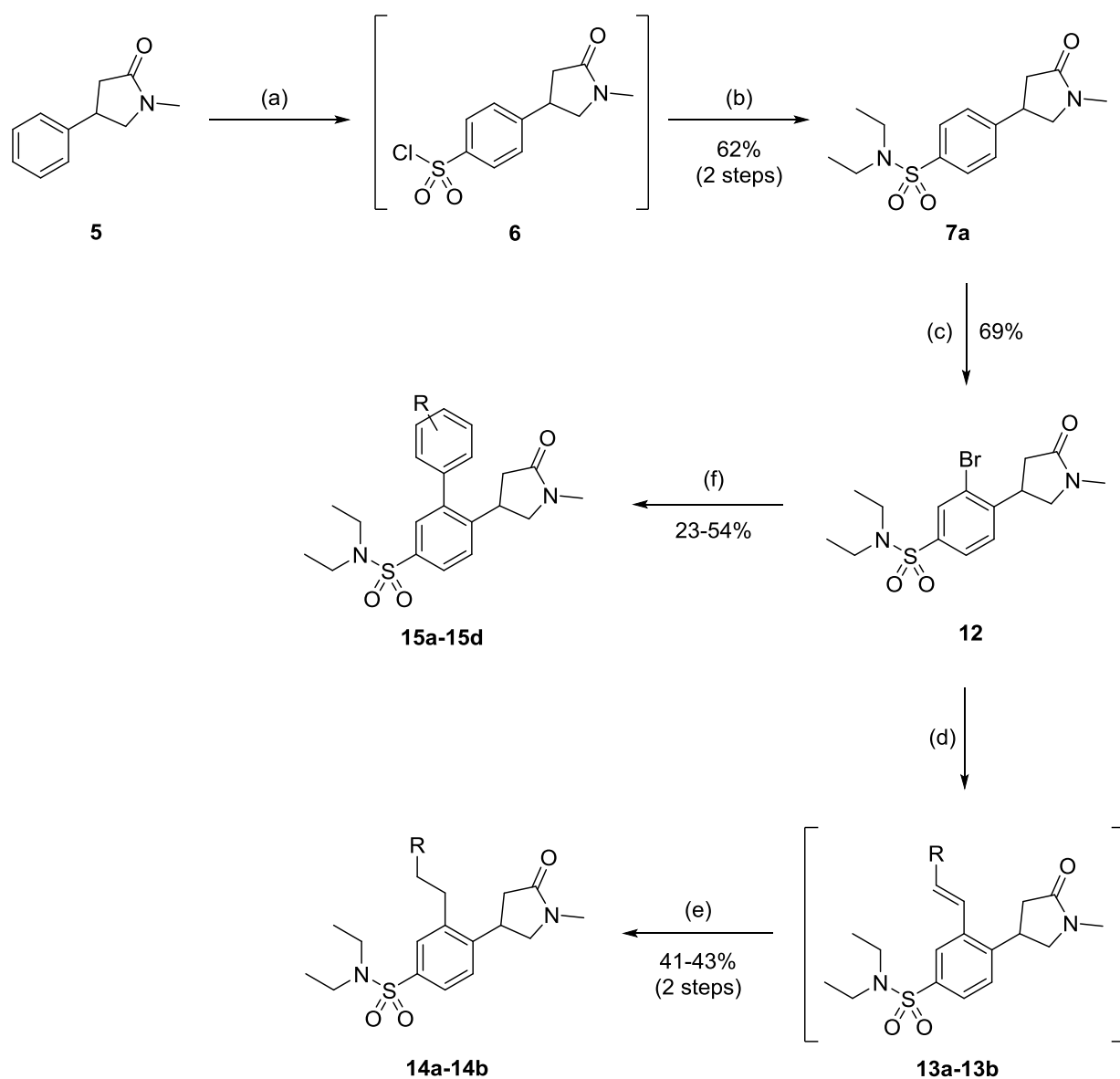
Alternatively, bromination using sodium bromide and sulfuric acid from a reported method²⁹ gave a mixture of both *ortho*- (**8**) and *para*-substituted (**9**) products (Scheme 3) which were separated by column chromatography. Given the limited availability of **8** and **9**, each of the aryl bromides were used for Suzuki coupling with phenylboronic acid, giving the biphenyl NMP derivatives **10** and **11** in respectable yields.³⁰



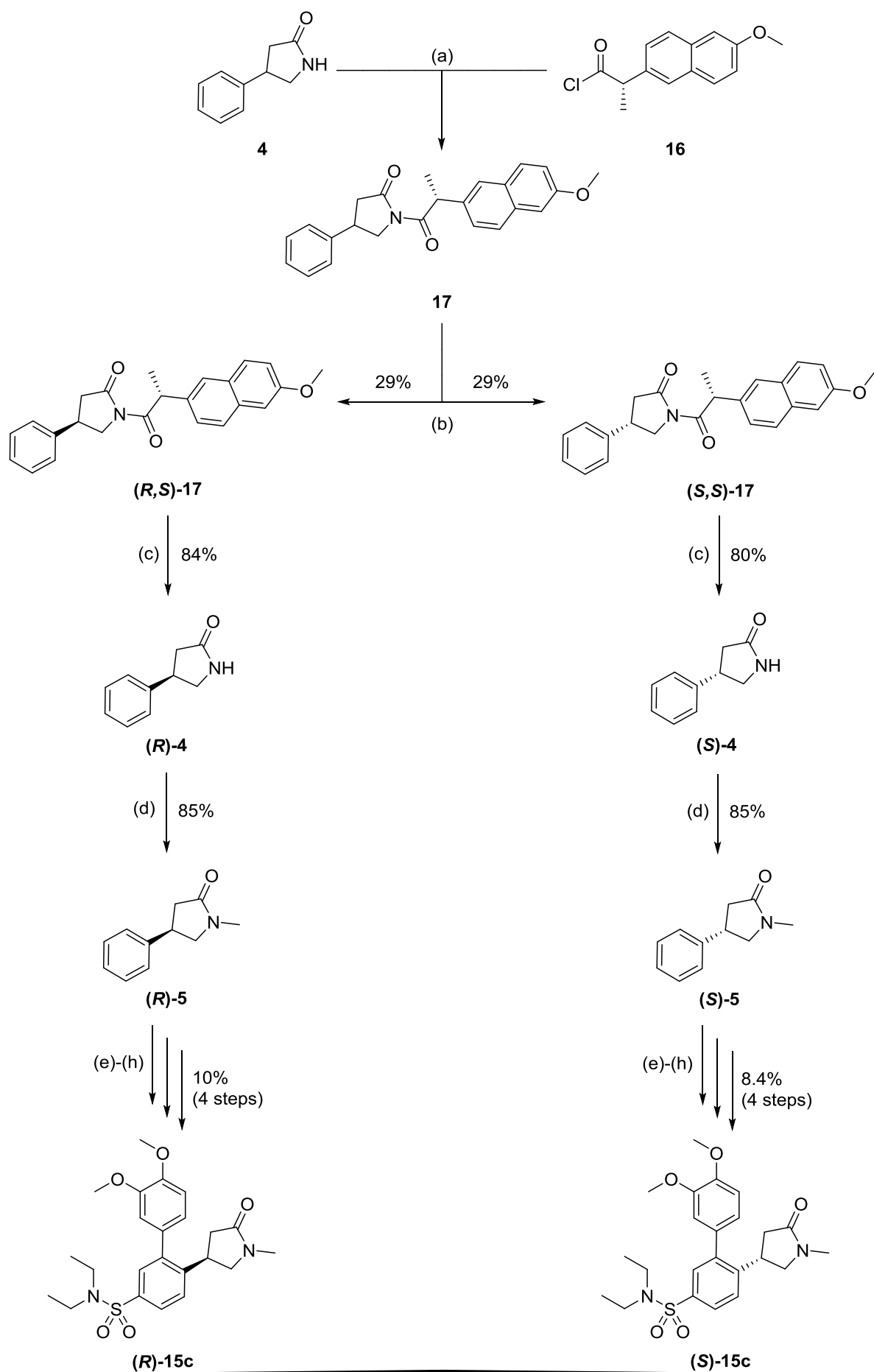
Scheme 3. Formation of bromides **8** and **9** with subsequent Suzuki coupling. (a): NaBr , H_2SO_4 , 2 h, 80°C . (b): N_2 , $\text{PhB}(\text{OH})_2$, $\text{Pd}(\text{PPh}_3)_4$, 1,2-dimethoxyethane, 2 M Na_2CO_3 , 4 h, rf.

The alkyl sulfonamides showed promising affinity (discussed later), so the diethyl sulfonamide **7a** was used to further functionalise the aryl group. As outlined in Scheme 4, **7a** was treated with a mixture of *N*-bromosuccinimide and sulfuric acid to give **12** in good yield.³¹ Bromide **12** was then used in a series of cross-coupling reactions, using reagents that were readily available to conduct these couplings, with a small amount of variety in the limited set. Heck coupling gave a series of alkenes (**13**) which were reduced to the corresponding alkanes (**14**). Suzuki coupling using the method described above gave a series of biaryl compounds (**15**).³² The coupling of a thianaphthene group (**15d**) resulted in atropisomerism due to the hindered rotation between the thianaphthene and NMP moieties. This was shown by the broadening of the NMP signals in the ¹H NMR, while the signals for the other compounds in this series were well-defined.

The co-crystal structures generated during this work, coupled with the inhibitory activity of the biaryl derivative **15c** (discussed later) inspired the application of diastereomeric resolution to separate the NMP isomers. As shown in Scheme 5, lactam **4** was treated with lithium diisopropylamide and (*S*)-Naproxen chloride **16**³³ to give diastereomers **17**, which were separated carefully by column chromatography to acquire the enantiopure imides (*R,S*)-**17** and (*S,S*)-**17**. In agreement with the literature, the ¹H NMR signals of the first eluted product corresponded with the (*R,S*)-diastereomer, and the proton signals of the second product matched the (*S,S*)-diastereomer. The imides were hydrolysed with aqueous potassium hydroxide to give (*R*)-**4** and (*S*)-**4**. The specific rotation of each enantiomer was consistent with literature values. They were then methylated using as above to give the respective isomers (*R*)-**5** and (*S*)-**5**, which were carried forward to (*R*)-**15c** and (*S*)-**15c** using the same conditions described previously.



Scheme 4. Formation of sulfonamide **7a** with bromination and cross-coupling of **12**. (a): ClSO_3H , CH_2Cl_2 , o/n, rt; (b): Et_2NH , Et_3N , CH_2Cl_2 , o/n, rt. (c): NBS , H_2SO_4 , o/n, rt. (d): N_2 , R-alkene , P(o-tol)_3 , Pd(OAc)_2 , DIPEA , DMF , o/n, $90\text{ }^\circ\text{C}$; (e): H_2 , Pd/C , EtOAc , o/n, rt; (f): N_2 , R-B(OH)_2 , $\text{Pd(PPh}_3)_4$, 1,2-dimethoxyethane, 2 M Na_2CO_3 , 4 h, rf.



Scheme 5. Stereoisomer resolution of **4** with corresponding synthesis of phenyl NMP isomers. (a): LDA, THF, 3 h, $-78\text{ }^{\circ}\text{C}$. (b): Column chromatography, 10% EtOAc in petroleum benzine. (c): 1 M KOH, THF, o/n, rt. (d): NaH, MeI, THF, N_2 , o/n, $0\text{ }^{\circ}\text{C} \rightarrow \text{rt}$. (e): ClSO_3H , CH_2Cl_2 , o/n, rt; (f): Et_2NH , Et_3N , CH_2Cl_2 , o/n, rt. (g): NBS, H_2SO_4 , o/n, rt. (h): N_2 , $(\text{CH}_3\text{O})_2\text{-C}_6\text{H}_3\text{-B(OH)}_2$, $\text{Pd(PPh}_3)_4$, 1,2-dimethoxyethane, 2 M Na_2CO_3 , 4 h, rf.

3.2.2 BRD4 BD1 FRET Assay Results

The phenyl-substituted NMP compounds were all assessed for binding inhibition against BRD4 BD1 in a FRET-based assay. This method, developed by Cisbio Assays, is a competitive binding assay that measures the fluorescence created between a Eu^{3+} cryptate donor attached to a GST-tagged bromodomain (BRD4 BD1), and a Streptavidin D2 acceptor attached to a biotinylated tetra-acetylated histone peptide (H4K5K8K12K16(ac₄)). When an inhibitor is added, it competes for binding with the histone peptide to the bromodomain, ultimately disrupting the donor-acceptor transfer and preventing fluorescence from occurring.

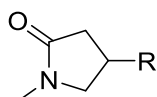
The results of the first series of assays are shown in Table 1. Firstly, the addition of a phenyl group to NMP (**5**) increased the binding affinity for BRD4 BD1 by approximately 2-fold. This confirmed the suitability of the aryl substituent for functionalisation of NMP.

Introduction of the sulfonamide group gave some significant improvements with alkyl sulfonamides **7a**, **7b**, **7h** and **7i** having IC_{50} values between 120 – 150 μM , nearly a 10-fold increase from **5**. However, other alterations to the sulfonamide – arylpiperidines, tetrahydroquinolines, benzylamines and nipecotic acids – resulted in a loss of activity. An interesting observation was that the activity of **7n** was similar to compounds **7a**, **7b**, **7h** and **7i**, despite possessing a bulky adamantyl group. These observations, paired with our generated X-ray crystal structures to be discussed later, suggest that certain aliphatic substituents are best tolerated.

Intriguingly, while both bromides had improved on this affinity compared to **5**, the *ortho*-bromide **8** (321 μM) had higher affinity than the *para*-bromide **9** (417 μM). The substitution to a phenyl group was also tolerated, but was preferable in the *para* position **11** (434 μM) compared to the *ortho* position **10** (575 μM).

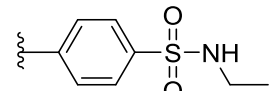
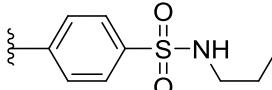
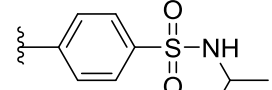
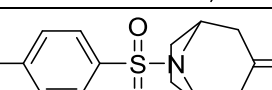
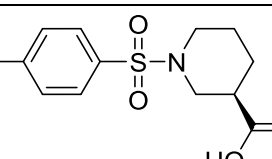
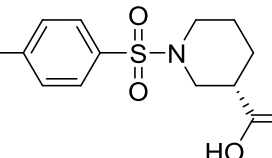
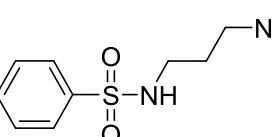
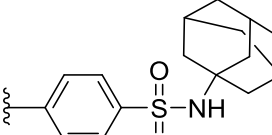
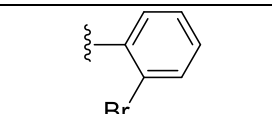
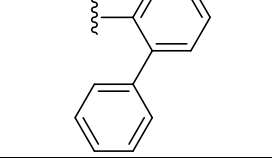
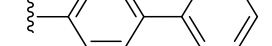
These compounds were also assessed for any correlation between lipophilicity and affinity. Given that the r^2 value of this series was 0.00006, there was no apparent correlation (Appendix H, Figure S1).

Table 1. SAR data on initial phenyl NMP derivatives.



Compound Number	R=	IC ₅₀ (μM \pm SEM) ^a	LE (kcal/mol NHA) ^d	cLogP ^e	LLE ^f
	H	2659 \pm 478	0.50	-0.40	2.97
5		1143 \pm 6	0.31	1.16	1.78
7a		123 \pm 29	0.26	1.08	2.83
7b		144 \pm 18	0.24	1.55	2.29
7c		276 \pm 12	0.22	0.30	3.26
7d		473 \pm 13	0.16	2.96	0.37
7e		450 \pm 33	0.18	2.48	0.87
7f		443 ^c	0.19	1.71	1.65

Table 1 (continued).

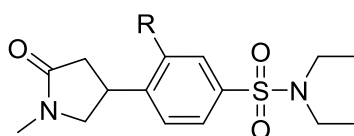
7g		250 ± 3^b	0.26	0.14	3.46
7h		147 ± 5^b	0.26	0.67	3.16
7i		134 ± 7^b	0.27	0.45	3.42
7j		223 ± 23^b	0.20	0.55	3.10
7k		1682 ± 242	0.15	0.76	2.01
7l		1963 ± 90	0.15	0.76	1.95
7m		1389 ± 15	0.16	0.19	2.67
7n		151 ± 43	0.19	2.60	1.22
8		321 ± 48	0.34	2.02	1.47
9		417 ± 25	0.33	2.02	1.36
10		575 ± 177	0.23	2.75	0.49
11		434 ± 116	0.24	3.05	0.31

Assays carried out by Dr. Ian Jennings, Zhaohua Zheng and Ali Noor. ^aUnless stated otherwise, all results of means are $n \geq 2$. ^bSD reported. ^c $n = 1$. ^dLigand efficiency = $1.37(-\log(\text{IC}_{50})) / \text{NHA}$. ^ecLogP values were calculated using ChemDraw 17.0. ^fLipophilic ligand efficiency = $-\log(\text{IC}_{50}) - \text{clogP}$. Control compound used: **I-BET726** (IC_{50} : 0.01 μM). NHA, non-hydrogen atom.

The synthetic elaboration of **7a** yielded di-substituted aryl NMP analogues that produced a range of activities, which are shown in Table 2. The preliminary addition of the bromide to the selected sulfonamide (**12**) caused a 5-fold drop in inhibition compared to **7a**. The products from the Heck/hydrogenation steps (**14a** – **14b**) were found to be inactive. The change to a phenyl group (**15a**) was detrimental to activity, but compound **15c** showed much improved inhibition with an IC_{50} of 51.6 μM .

Despite the limited number of compounds, we were interesting in learning whether lipophilicity and affinity were connected in this set. The r^2 value of 0.56 suggests that a correlation exists, in that the affinity is negatively affected by an increase in lipophilicity (Appendix H, Figure S2).

Table 2. SAR data on halide-coupled NMP derivatives from **7a**.



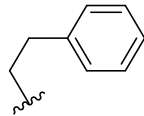
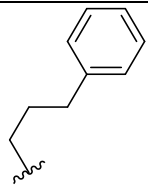
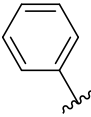
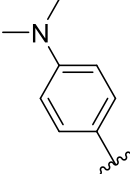
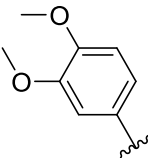
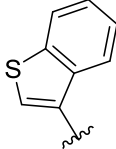
Compound Number	R=	IC_{50} ($\mu\text{M} \pm \text{SEM}$) ^a	LE (kcal/mol NHA) ^b	cLogP ^c	LLE ^d
7a	H	123 ± 29	0.26	1.08	2.83
12	Br	652 ± 116	0.20	1.95	1.24
14a		4495 ± 39	0.11	3.48	-1.13

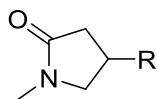
Table 2 (continued).

14b		>5000	0.11	4.01	-1.70
15a		3193 ± 76	0.13	2.67	-0.18
15b		217 ± 19	0.17	2.90	0.77
15c		51.6 ± 2.5	0.19	2.35	1.75
15d		2665 ± 217	0.12	3.72	-1.14

Assays carried out by Dr. Ian Jennings. ^aUnless stated otherwise, all results of means are $n \geq 2$. ^bLigand efficiency = $1.37(-\log(\text{IC}_{50})) / \text{NHA}$. ^ccLogP values were calculated using ChemDraw 17.0. ^dLipophilic ligand efficiency = $-\log(\text{IC}_{50}) - \text{clogP}$. Control compound used: **I-BET726** (IC_{50} : 0.01 μM). NHA, non-hydrogen atom.

We were interested to learn if this series of compounds showed stereoselective interactions and so we resolved the enantiomers by both chiral auxiliary and chromatography. Both enantiomers of **5** were shown to inhibit binding with the (*R*)-enantiomer having approximately twice as high affinity compared to the (*S*)-enantiomer (Table 3). The isomers of **15c** maintained this difference in activity with (*R*)-**15c** being the higher affinity isomer compared to (*S*)-**15c**. At 14.1 μM , it is 190-fold more potent than NMP itself (dose response curves of **15c**, (*R*)-**15c** and (*S*)-**15c** are available in Appendix I).

Table 3. Assay data on resolved isomers.



Compound Number	R=	IC ₅₀ (μM ± SEM) ^a	LE (kcal/mol NHA) ^c
5		1143 ± 6	0.31
(<i>R</i>)- 5		629 ± 26 ^b	0.34
(<i>S</i>)- 5		1425 ± 169	0.30
15c		51.6 ± 2.5	0.19
(<i>R</i>)- 15c		14.1 ± 0.3	0.21
(<i>S</i>)- 15c		35.2 ± 1.3	0.20

Assays carried out by Dr. Ian Jennings. ^aUnless stated otherwise, all results of means are n ≥ 2. ^bSD reported. ^cLigand efficiency = 1.37(-log(IC₅₀)) / NHA. Control compound used: **I-BET726** (IC₅₀: 0.01 μM). NHA, non-hydrogen atom.

3.2.3 X-ray Crystallography

We were able to gather a number of X-ray structures of our compound series to support the SAR studies of these compounds (For videos, refer to Appendix J. For electron density maps, refer to Appendix K).

Firstly, a crystal structure of **5** bound to BRD4 BD1 was solved (Figure 1). The NMP segment of **5** retains the K-ac mimetic function, replicating the interactions between Asn140 and Tyr97. The phenyl group moiety of **5** emerges from the pocket and rests on the WPF shelf and appears to form weak interactions of its own with the WPF shelf residues Trp81 and Pro82 and the gatekeeper residue Ile146. While **5** was submitted as a racemic mixture, only the (*R*)-enantiomer was observed in the X-ray crystal structure of BRD4 BD1. This observation is consistent with the binding activity acquired from both (*R*)-**5** and (*S*)-**5**. The (*S*)-isomer in this pose would have more than likely produced a steric clash with the wall created by the ZA loop.

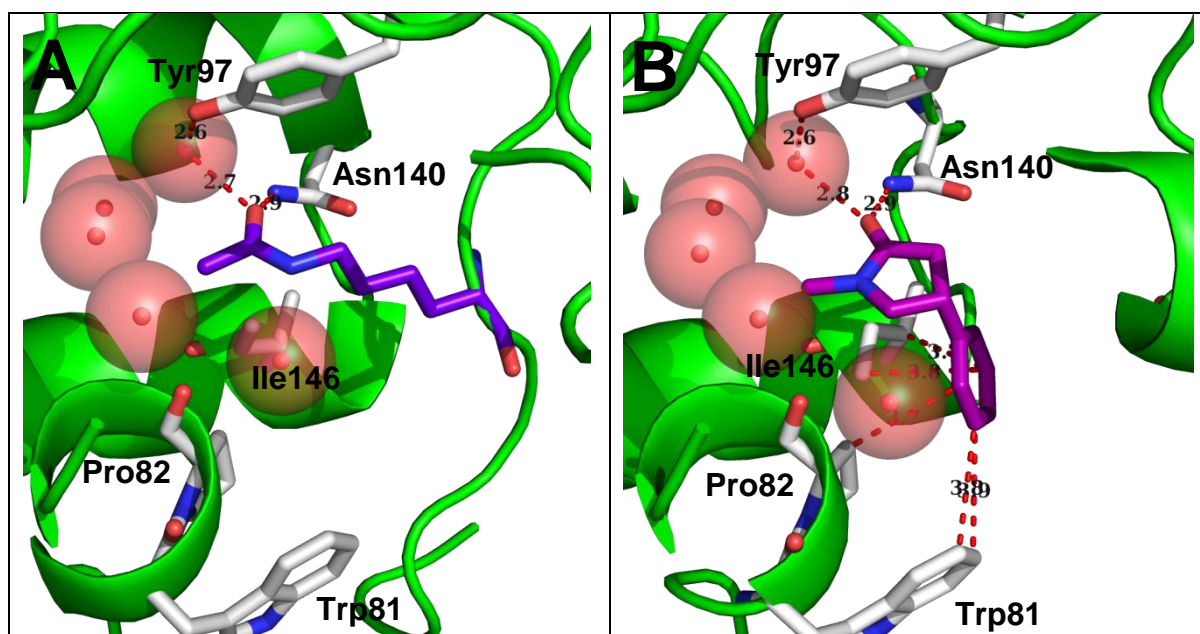
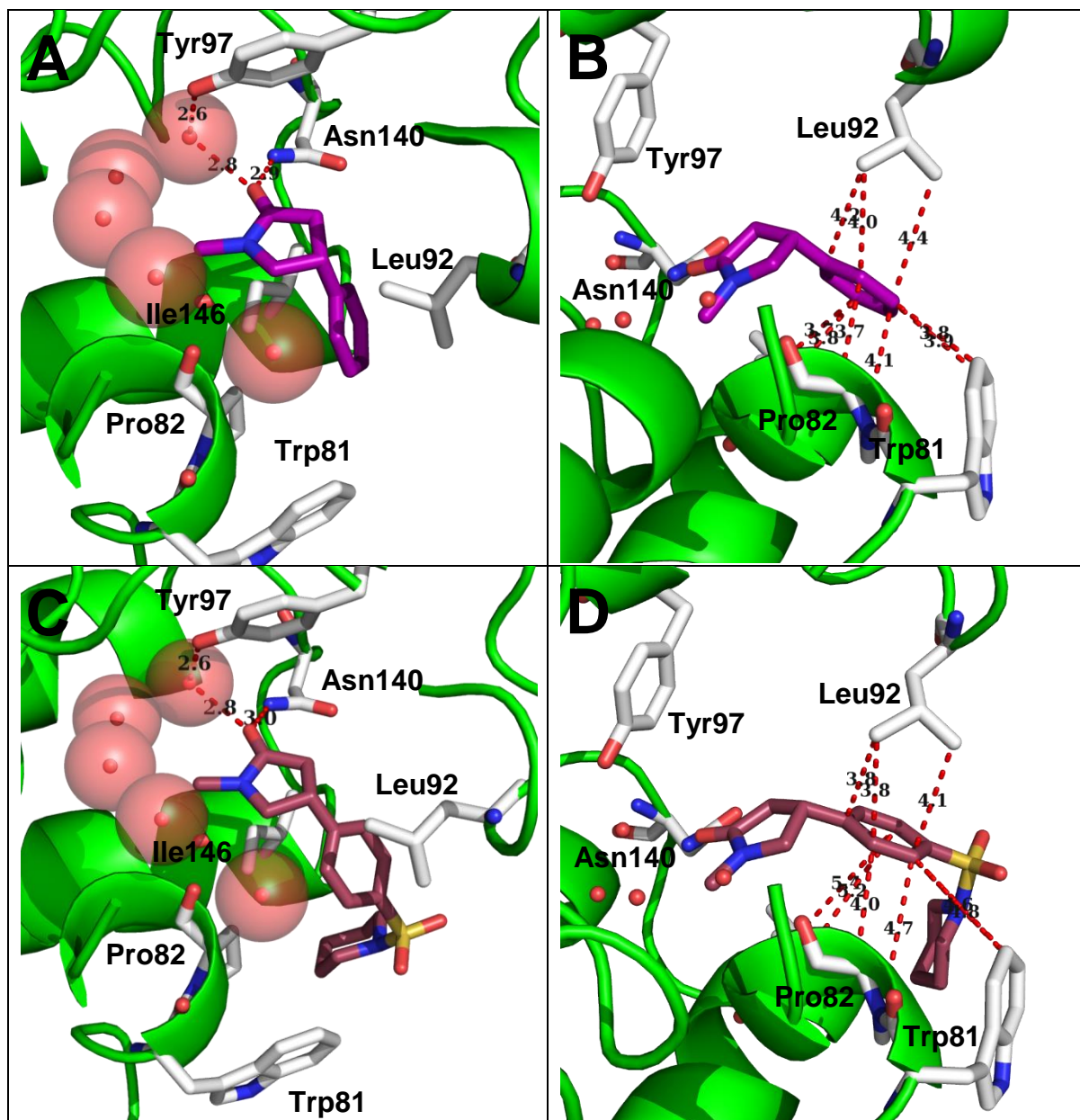


Figure 1. Comparison of binding substrates in BRD4 BD1. [A] K-ac (purple blue) (PDB: 3UVW). [B] (*R*)-**5** (purple, resolution: 1.5 Å). Water molecules shown as red spheres. Pro86, Val87 and Asp88 were hidden for better visualisation. Distances in Å, highlighted by red dashes. X-ray crystal structure of **5** developed by Dr. Ian Jennings and Dr. Olga Ilyichova.

Crystal structures of the sulfonamides **7b** and **7h** were also solved. As shown in Figure 2, only the (*R*)-isomer was evident in these co-crystal structures and the orientation of the NMP ring in the binding pocket matches closely with compound **5**. Despite the NMP backbone atoms overlaying closely (RMS = 0.20 and 0.37, respectively), the phenyl group appears to have

shifted slightly (RMS = 1.25 and 1.63, respectively). This change has positioned the phenyl group closer towards the side chain of Leu92, but further away from Trp81, Pro82 and Ile146. Both the piperidyl group of **7b** and *n*-propyl moiety of **7h** rest in a pocket adjacent to the WPF shelf and form weak vdW interactions with Trp81, Asp145 and Met149 (Figure 3).



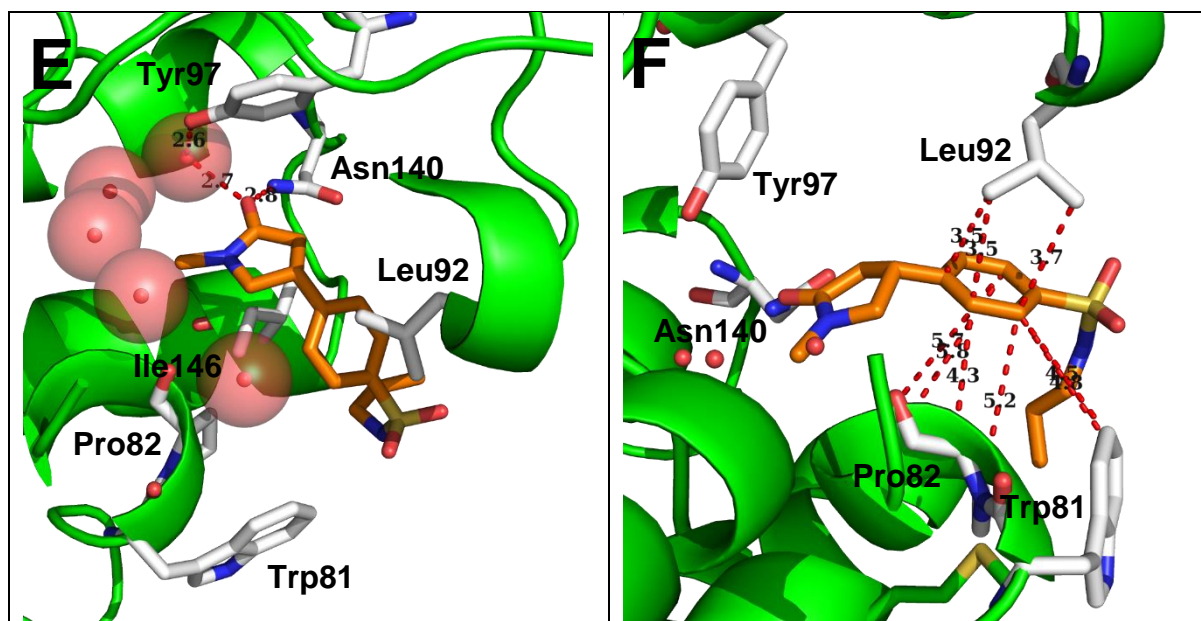


Figure 2. Comparison of X-ray crystal structures of NMP derivatives. [A, C, E] Binding site.

Pro86, Val87 and Asp88 were hidden for better visualisation. [B, D, F] Emphasis on phenyl group. [A, B] **5** (purple, resolution: 1.5 Å). [C, D] (*R*)-**7b** (raspberry, resolution: 1.55 Å). [E, F] (*R*)-**7h** (orange, resolution: 1.59 Å). Water molecules shown as red spheres. Distances in Å, highlighted by red dashes. X-ray crystal structures developed by Dr. Ian Jennings and Dr. Olga Ilyichova.

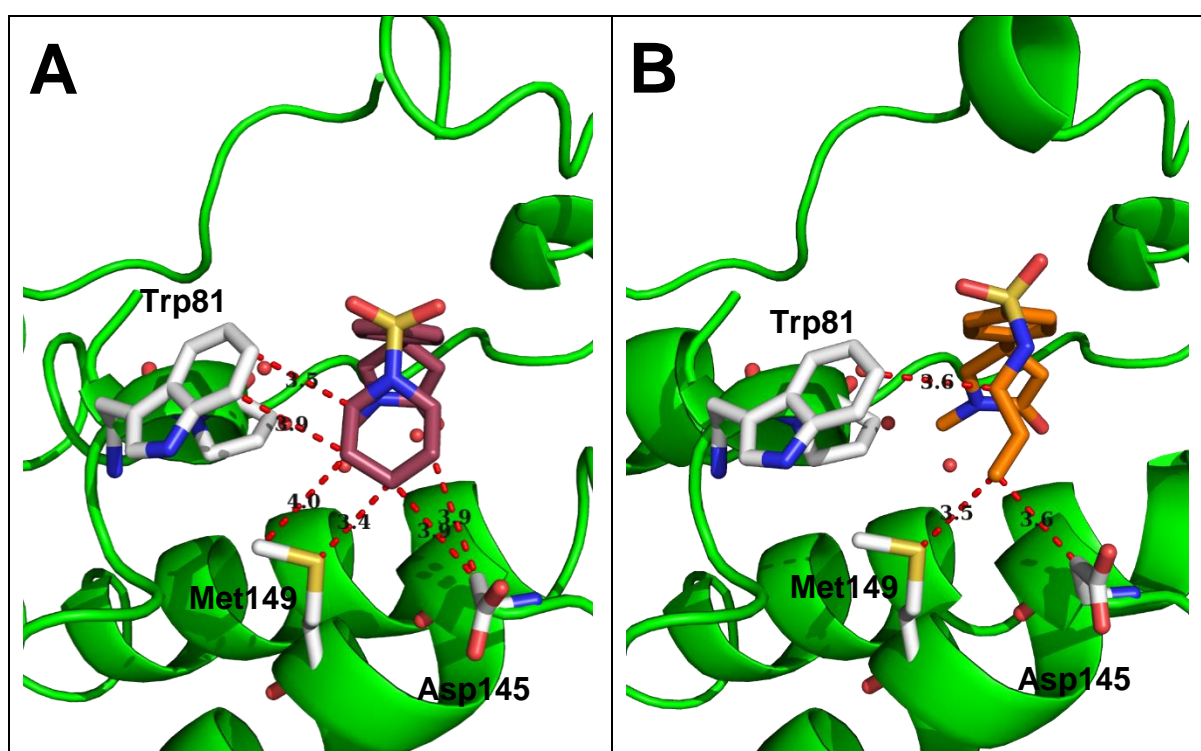


Figure 3. X-ray crystal structures illustrating the interactions between sulfonamide alkyl moieties and BRD4 BD1. [A] (*R*)-**7b** (raspberry, resolution: 1.55 Å). [B] (*R*)-**7h** (orange, resolution: 1.59 Å). Water molecules shown as red spheres. Distances in Å, highlighted by red dashes. X-ray crystal structures developed by Dr. Ian Jennings and Dr. Olga Ilyichova.

Finally, we were able to obtain a co-crystal structure of our highest affinity compound, **15c**. To our surprise, the inclusion of the dimethoxyphenyl moiety had completely changed the orientation of the molecule. As shown in Figure 4, the dimethoxyphenyl group fills the acetamide binding pocket, using the two oxygen atoms to form a pair of hydrogen bonds to Asn140. The sulfonamide was re-oriented into the ZA channel, with the sulfonyl forming a hydrogen bond with the backbone nitrogen of Asp88 and the diethyl group lining up against Gln85. One of the ethyl moieties is situated in a small pocket that is in close proximity to three backbone carbonyls: Pro82, Gln85 and Pro86. Finally, the NMP segment rested in the pocket adjacent to Trp81. Not only is the carbonyl of NMP close to the sulfur atom of Met149, the active isomer is flipped to the (*S*)-isomer compared to previous crystal structures (Figure 5). Overall, this potentially rationalises the improved affinity in comparison to the other compounds in this series, as the addition of any substituent – alkyl or aryl – would clash with the ZA channel. However, the observed NMP isomer in our co-crystal structure of **15c** contrasts our assay data as (*S*)-**15c** was found to have lower affinity than (*R*)-**15c**. This is potentially due to the difference in crystallisation conditions between the two enantiomers, particularly those with similar affinities.

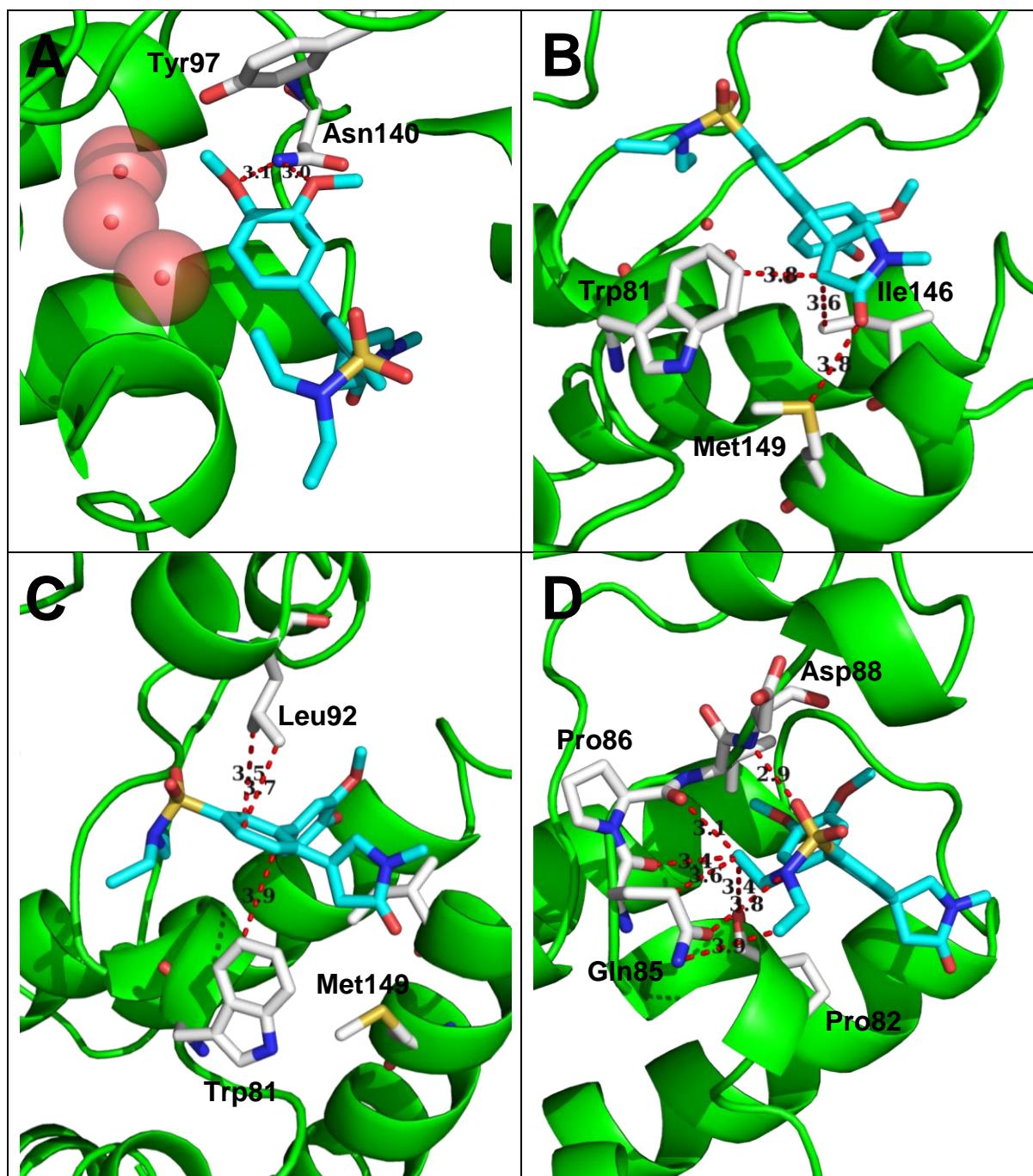


Figure 4. X-ray crystal structure of (*S*)-15c (cyan, resolution: 1.48 Å) bound to BRD4 BD1, illustrating interactions with the bromodomain. [A] Binding site. Pro86, Val87 and Asp88 were hidden for better visualisation. [B] NMP. [C] Phenyl 'hub'. [D] Sulfonamide. Water molecules shown as red spheres. Distances in Å, highlighted by red dashes. X-ray crystal structure developed by Dr. Ian Jennings and Dr. Olga Ilyichova.

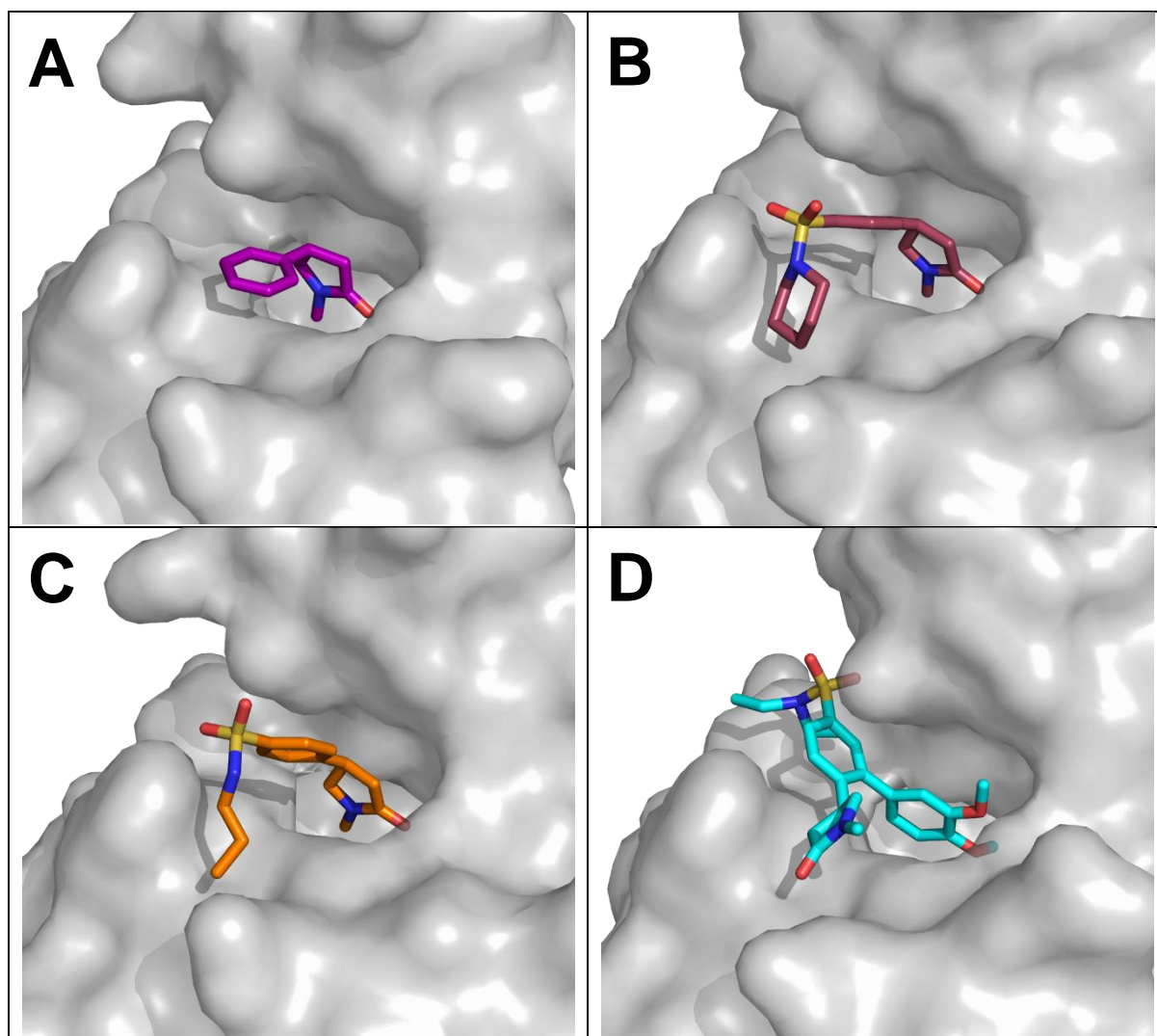
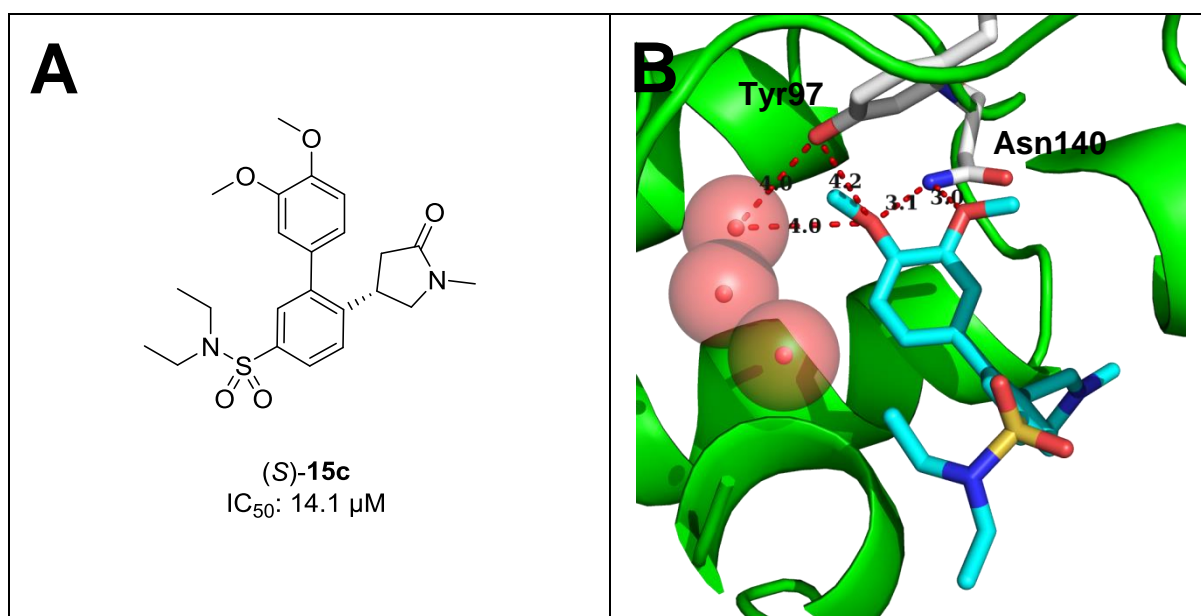


Figure 5. Comparison of X-ray crystal structures of bound NMP isomers in BRD4 BD1. [A] (*R*)-**5** (purple, resolution: 1.5 Å). [B] (*R*)-**7b** (raspberry, resolution: 1.55 Å). [C] (*R*)-**7h** (orange, resolution: 1.59 Å). [D] (*S*)-**15c** (cyan, resolution: 1.48 Å). X-ray crystal structures developed by Dr. Ian Jennings and Dr. Olga Ilyichova.

To our knowledge, only two groups have assessed compounds with mimetics that bear a close resemblance to **15c**. While the catechol ether of each compound fits in the binding pocket of BRD4 BD1, they all have subtle differences with how they interact with the conserved tyrosine and asparagine residues (Figure 6). The kinase inhibitor **GW612286X** was assessed among other inhibitors by Ember et al.³⁴ for BET inhibition. In their crystallographic studies, the trimethoxy group of **GW612286X** served as the K-ac mimetic in the binding pocket of BRD4

BD1, but it was noted that the only interaction to the main binding site was to the carbonyl of Asn140 through a water-mediated hydrogen bond instead of a direct interaction. The lack of this direct interaction, presumably due to the length between the 4-methoxy oxygen and the nitrogen of Asn140, was their rationale for a reduction in affinity. Chen et al.³⁵ evaluated the trimethoxy group as a mimetic for novel BRD4 inhibitors. In one of their compounds, **DC-BD-29**, the 3- and 4-methoxy groups also formed the dual interaction to Asn140 seen in **15c**, but the 4- and 5-methoxy groups were also paired to the water molecule that is linked to Tyr97, an interaction that is lacking in **15c** due to the displacement of the water molecule responsible for the bonds between Tyr97 and the bound substrate. Ultimately, the absence of the bonds to Tyr97 contributes to weakened interactions with the binding site.



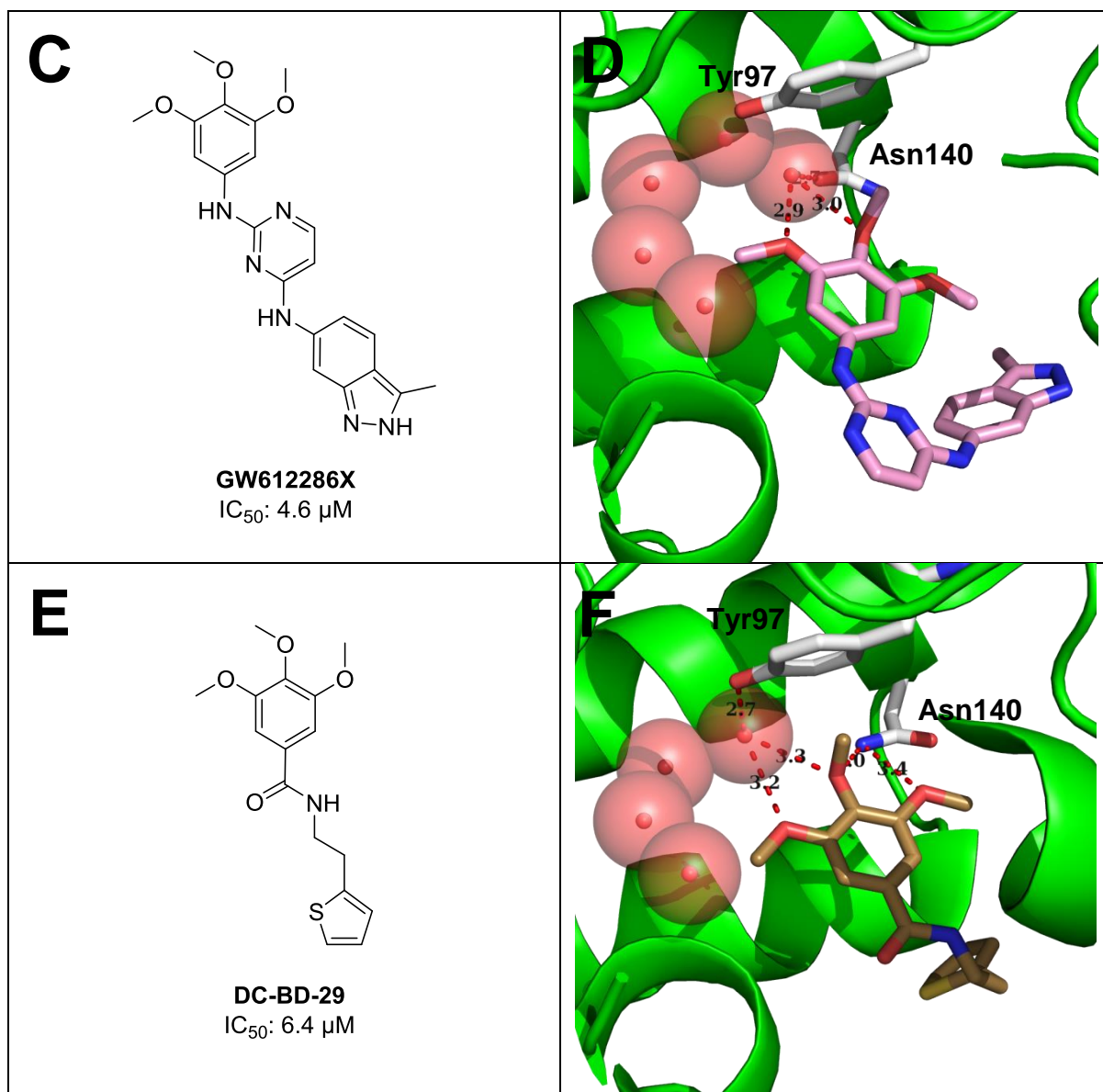


Figure 6. Comparison of catechol ether groups bound to BRD4 BD1. [A, B] (*S*)-**15c** (cyan, resolution: 1.48 Å). [C, D] **GW612286X** (pink) (PDB: 4O78). [E, F] **DC-BD-29** (sand) (PDB: 5H21). [A, C, E] Chemical structure. [B, D, F] Binding site. Water molecules shown as red spheres. Pro86, Val87 and Asp88 were hidden for better visualisation. Distances in Å, highlighted by red dashes. X-ray crystal structure of **15c** developed by Dr. Ian Jennings and Dr. Olga Ilyichova.

3.3 Conclusion and Future Directions

BRD4 is a well-characterized target for FBDD approaches and provides a useful exemplar of bromodomain inhibitor discovery in general.^{14, 36, 37} NMP itself has been co-crystallised with several bromodomains and could be a starting point for campaigns against each one. Here, we have tested these principles with a 4-phenyl derivative of NMP.

We devised a synthetic scheme for the formation of the phenyl core scaffold (**5**) which has been reliably reproduced on multigram scales. A crystal structure of **5** bound to BRD4 was generated, which has helped validate our use of the phenyl scaffold. In addition, we developed a route for the preparation of both enantiomers.

A series of electrophilic aromatic substitution reactions on this core led to three potential intermediates (**6**, **8**, **9**) to use for SAR studies. Of the compounds generated from these intermediates, a group of alkyl sulfonamides (**7a**, **7b**, **7h**, **7i**, **7n**) gave the best inhibition of this series.

We then used one such compound (**7a**) to generate another intermediate (**12**) for halide coupling, which afforded six additional compounds (**14a-14b**, **15a-15d**). While this derivatisation probably disfavors enhanced binding of the NMP motif in the binding site, in an unexpected turn, a crystal structure of the lead compound **15c** adopted a new binding orientation in the BRD4 bromodomain pocket.

Taken together, these results should be able to provide guidance for the rational design of inhibitors that possess the NMP fragment, along with the synthesis of other functionalised derivatives of NMP. Additionally, these compounds should be tested on other bromodomains, particularly those outside of the BET family to further confirm the usefulness of NMP as a mimetic fragment.

Experimental

^1H and ^{13}C Nuclear Magnetic Resonance spectra were conducted on a Bruker Advance III Nanobay 400 MHz spectrometer coupled to the BACS 60 automatic sample changer and obtained at 400.1 MHz and 100.6 MHz. All spectra were processed using MestReNova 6.0 software. The chemical shifts of all ^1H were measured relative to the expected solvent peaks of the respective NMR solvents; CDCl_3 , 7.26; MeOD, 3.31; DMSO, 2.50. The chemical shifts of all ^{13}C were measured relative to the expected solvent peaks of the respective NMR solvents; CDCl_3 , 77.2; MeOD, 49.0; DMSO, 39.5. The data for all spectra are reported in the following format: chemical shift (integration, multiplicity, coupling constant, assignment). Multiplicity is defined as; s = singlet, d = doublet, t = triplet, q = quartet, quint = quintet, dd = doublet of doublets, dt = doublet of triplets, td = triplet of doublets, tt = triplet of triplets, qd = quartet of doublets, ddd = doublet of doublet of doublets, m = multiplet. Coupling constants are applied as J in Hertz (Hz). For ^1H and ^{13}C spectra, refer to Appendix L.

All HRMS analyses were done on an Agilent 6224 TOF LC/MS Mass Spectrometer coupled to an Agilent 1290 Infinity (Agilent, Palo Alto, CA). All data were acquired and reference mass corrected via a dual-spray electrospray ionisation (ESI) source. Each scan or data point on the Total Ion Chromatogram (TIC) is an average of 13,700 transients, producing a spectrum every second. Mass spectra were created by averaging the scans across each peak and background subtracted against the first 10 seconds of the TIC. Acquisition was performed using the Agilent Mass Hunter Data Acquisition software version B.05.00 Build 5.0.5042.2 and analysis was performed using Mass Hunter Qualitative Analysis version B.05.00 Build 5.0.519.13.

All LCMS analyses were carried out on an Agilent 6100 Series Single Quad LC/MS coupled with an Agilent 1200 Series HPLC, 1260 Infinity G1312B Binary pump, 1260 Infinity G1367E 1260 HiP ALS autosampler and 1290 Infinity G4212A 1290 DAD detector. The liquid

chromatography conditions were: reverse phase HPLC analysis fitted with a Luna C8(2) 5 μ L 50 X 4.6 mm 100Å at a temperature of 30 °C. The sample injection volume was 5 μ L, which was run in 0.1% formic acid in acetonitrile at a gradient of 5-100% over 10 minutes. Detection methods were either 254 nm or 214 nm. The mass spectrum conditions were: Quadrupole ion source with Multimode-ES. The drying gas temperature was 300 °C and the vaporizer temperature was 200 °C. The capillary voltage in positive mode was 2000V, while in negative mode, the capillary voltage was 4000V. The scan range was 100-1000 m/z with a step size of 0.1 second over 10 minutes.

TLCs were carried on Merck TLC Silica gel 60 F₂₅₄ plates using the appropriate mobile phase. Purification by column chromatography was conducted with Davisil Chromatographic Silica LC60A (40-63 micron) using the specified mobile phases.

Purification on reverse-phase HPLC was done on a Waters Delta Prep 2000 Prep HPLC System that was fitted with a Waters Delta Prep 2000 Pump and Controller. Samples were injected into a Waters Prep Rack with Manual Injector, which were run through a Luna C8(2) 10 μ L 50 X 21.20 mm 100Å and Waters 486 Tunable Absorbance Detector. The conditions were: Solvent A (0.1% TFA in H₂O) and Solvent B (0.1% TFA in CH₃CN), with a gradient of 0-80% Solvent B over a 20-minute period.

Compound purity was determined using an Agilent 1260 Infinity Analytical HPLC (1260 Infinity G1322A Degasser, 1260 Infinity G1312B Binary pump, G1367E HiP ALS autosampler, 1260 Infinity G1316A Thermostatted Column Compartment, and 1260 Infinity G4212B DAD detector. The liquid chromatography conditions were: reverse phase HPLC analysis fitted with a Zorbax Eclipse Plus C18 Rapid Resolution 4.6 X 100 mm 3.5-Micron. The sample injection volume was 1 μ L, which was run in Solvent A (0.1% TFA in H₂O) and Solvent B (0.1% TFA in CH₃CN), with a gradient of 5-100% Solvent B over a 10-minute

period. All compounds submitted for assays and X-ray crystallography studies were assessed for purity of 95% or greater on 214 nm and 254 nm.

Separation on chiral HPLC was done on an Agilent 1260 Infinity Prep HPLC (1260 Infinity G1361A Prep Pump, 1260 Infinity G2260A Prep ALS, 1260 Infinity G1328C Man Inj, 1260 Infinity G1315D DAD VL, and 1260 Infinity G1364B FC-PS). The liquid chromatography conditions were: normal phase HPLC analysis fitted with a Phenomenex Lux 5 μ m Cellulose-1 4.6 x 150 mm. The sample injection volume was 10 μ L at a concentration of 1 mg/mL, which was run in Solvent A (40% petroleum ether) and Solvent B (60% ethanol), over a 10-minute period.

Specific rotations were measured using a Jasco P-2000 polarimeter. The light source was a sodium lamp with a wavelength of 589 nm. Compounds were loaded into a 3.5 mm x 100 mm cylindrical glass cell. Digital integration time was 5 seconds per cycle for 10 cycles.

The IC₅₀s were measured using a Fluorescence Resonance Energy Transfer (FRET) assay, which was carried out based on the protocol developed by CisBio Assay, France. The assay consists of a europium (Eu³⁺) cryptate-conjugated antibody attached to glutathione S-transferase (GST) fused to BRD4 BD1 (49-170) and Streptavidin-D2 bound to biotin which is attached to a Histone H4 peptide, SGRG-K(Ac)-GG-K(Ac)-GLG-K(Ac)-GGAK(Ac)-RHRKVGG-K (Biotin). Both Streptavidin-D2 and the Eu³⁺ cryptate-conjugated antibody were purchased from CisBio Assays. In the absence of inhibitors, the Histone H4 peptide is bound to BRD4 BD1. When both are in close proximity, a 337 nm laser light activates the Eu³⁺ donor and emits at 620 nm, which causes D2 to fluoresce at 665 nm. In the presence of a ligand, this reaction is interrupted. The assays were performed in 384-well small volume microtiter plates. The serially diluted small molecule inhibitors were added to a buffer mixture with a final concentration of 1% DMSO. The final buffer concentrations were 10 nM of GST-BRD4 BD1,

40 nM of Histone H4 peptide, 5 nM of Eu³⁺ cryptate-conjugated GST-antibody, 6.25 nM Streptavidin-D2, 50 mM Hepes, 50 mM NaCl, 0.5 mM CHAPS, 400 mM KF, 0.01% BSA, pH 7.5. After mixing and incubation at room temperature for at least 1.5 hours, the plates were measured in a PheraStar plate reader (BMG Labtech) (excitation: 337 nm with 10 flashes; emission: 620 and 665 nm).

X-ray crystal structures were obtained using a 6-His tagged bromodomain, BRD4 BD1, which was expressed in E.coli and purified using Ni-agarose chromatography. The 6-His tag was then removed by TEV protease digestion. The bromodomain was purified using gel filtration chromatography using a Superdex-75, 16/60 column (GE Healthcare) in a buffer containing 50 mM Hepes pH 7.5, 0.3 M NaCl and 5% glycerol. The concentrated BRD4 BD1 protein (17 mg/ml) was then incubated with 50 mM of the ligand at 40 °C for 16h. The final ligand concentration used in the hanging drop was 5 mM. Crystals were obtained using the hanging drop method in 24-well plates using 1 µl drops of protein and the reservoir solution containing 0.2 M NaNO₃, PEG-3350 (35%) and ethylene glycol (6% v/v) concentrations. This was then flash frozen in liquid nitrogen. All datasets were collected at the Australian Synchrotron on MX1 and MX2 beamlines.³⁸ Datasets were merged and scaled using *MOSFLM*³⁹ and *AIMLESS*⁴⁰ from the CCP4 suite.⁴¹ 5% of reflections in each dataset were flagged for calculation of R_{free}. A summary of statistics is provided in Appendix M. Molecular replacement was performed with *Phaser*⁴² using a previously solved structure of BRD4 as a search model (PDB: 5DW2). The final structures were obtained after several rounds of manual refinement using *Coot*⁴³ and refinement with *phenix.refine*.⁴⁴

Methyl 4-nitro-3-phenylbutanoate (**2**) – *Methyl trans-cinnamate* **1** (5.01 g, 30.9 mmol) was weighed into a 250 mL round-bottom flask with a magnetic stir-bar and dissolved in nitromethane (17 mL, 0.308 mol), to which stirring commenced. 1,1,3,3-tetramethylguanidine

(775 μ L, 6.18 mmol) was added, and the mixture was left to stir for 42 hours at room temperature, checking for completion with TLC. After completion, the mixture was quenched with 5% HCl (75 mL) and washed with diethyl ether (3 x 75 mL). The organic layers were combined, dried with MgSO₄, filtered and concentrated under reduced pressure to afford an orange-coloured oil. The oil was then purified using column chromatography (Mobile phase: 10% EtOAc in petroleum benzine, TLCs were checked in 20% EtOAc in petroleum benzine) to afford **2** (5.62 g, 82%) as a clear oil. ¹H NMR (400 MHz, CDCl₃) δ 7.37 – 7.21 (m, 5H), 4.70 (ddd, J = 20.5, 12.6, 7.5 Hz, 2H), 3.99 (quint, J = 7.4 Hz, 1H), 3.64 (s, 3H), 2.83 – 2.74 (m, 2H) ppm. ¹³C NMR (101 MHz, CDCl₃) δ 171.2, 138.4, 129.2, 128.2, 127.4, 79.5, 52.1, 40.3, 37.6 ppm.

4-phenylpyrrolidin-2-one (4) – A two-neck 250 mL round-bottom flask with a stir-bar was purged with N₂, to which palladium on carbon (10%, 453 mg) was added and submerged in a minimum amount of dichloromethane. Methyl 4-nitro-3-phenylbutanoate **2** (4.53 g, 20.3 mmol) was dissolved in acetic acid (150 mL) and pipetted into the flask while keeping it under N₂. The flask was purged three more times with N₂ and then purged with H₂ three times, to which the contents were left to stir at room temperature. The progress of the reaction was monitored by NMR. After completion, the flask was purged with N₂ three times and the contents filtered carefully through a glass microfiber filter paper under very gentle vacuum. The filtered palladium catalyst was washed with dichloromethane then separately quenched with H₂O while the filtrate was concentrated under reduced pressure to give methyl 4-amino-3-phenylbutanoate (**3**) as a caramel-coloured oil. In a 250 mL round-bottom flask, the oil was then taken up in EtOH (75 mL) and Et₃N (1 mL) and then heated under reflux overnight. Upon assessing completion via LCMS, the mixture was concentrated under reduced pressure, then purified with a silica column (Mobile phase: neat EtOAc) to afford the lactam **4** (2.73 g, 83%) as an orange crystalline solid. ¹H NMR (400 MHz, CDCl₃) δ 7.54 (br s, 1H), 7.36 – 7.29 (m,

2H), 7.28 – 7.21 (m, 3H), 3.82 – 3.74 (m, 1H), 3.66 (dt, $J = 16.9, 8.6$ Hz, 1H), 3.41 (dd, $J = 9.5, 7.3$ Hz, 1H), 2.73 (dd, $J = 16.9, 8.9$ Hz, 1H), 2.50 (dd, $J = 16.9, 8.8$ Hz, 1H) ppm. ^{13}C NMR (101 MHz, CDCl_3) δ 178.3, 142.2, 128.8, 127.0, 126.8, 49.7, 40.2, 38.2 ppm. ESI-MS: m/z 162.1 $[\text{M}+\text{H}]^+$.

Lactam Methylation - In a round-bottom flask with a magnetic stir-bar, 4-phenylpyrrolidin-2-one **4** was weighed out and dissolved in THF. The flask was partially sealed with a rubber septum, purged with N_2 and placed on an ice-bath. Sodium hydride (2 mol. eq., 60% dispersed in mineral oil) was added to the mixture under N_2 and the contents were stirred for 30 minutes. Iodomethane (5 mol. eq.) was then added via syringe, and the contents were stirred at room temperature overnight. After completion, the THF was removed under reduced pressure. The resulting residue was quenched with 50% saturated aqueous NaCl and washed with EtOAc three times. The combined organic layers were dried with MgSO_4 , filtered and concentrated under reduced pressure to obtain the crude product, which was then purified with silica column chromatography (Mobile phase: 20% petroleum benzene in EtOAc) to afford the respective products.

1-methyl-4-phenylpyrrolidin-2-one (5) – Acquired 1.44 g (88%) as a clear oil from 1.51 g of **4**. ^1H NMR (400 MHz, CDCl_3) δ 7.37 – 7.31 (m, 2H), 7.29 – 7.20 (m, 3H), 3.75 (dd, $J = 9.6, 8.3$ Hz, 1H), 3.58 (dt, $J = 16.9, 8.4$ Hz, 1H), 3.41 (dd, $J = 9.6, 7.0$ Hz, 1H), 2.91 (s, 3H), 2.82 (dd, $J = 16.9, 9.1$ Hz, 1H), 2.55 (dd, $J = 16.9, 8.3$ Hz, 1H) ppm. ^{13}C NMR (101 MHz, CDCl_3) δ 174.1, 142.6, 129.0, 127.21, 126.85, 56.9, 38.9, 37.3, 29.7 ppm. ESI-MS: m/z 176.2 $[\text{M}+\text{H}]^+$; HR-MS: m/z calcd. for $\text{C}_{11}\text{H}_{13}\text{NO}$ $[\text{M}+\text{H}]^+$: 175.0997; found 175.0992. HPLC (PP gradient, MeOH): 4.87 min.

(R)-1-methyl-4-phenylpyrrolidin-2-one ((R)-5) – Acquired 40.9 mg (85%) as a clear oil from 44.3 mg of (R)-**4**. $[\alpha]_{\text{D}}^{25}$ - 38.4 (c 1, CHCl_3). ^1H NMR (400 MHz, CDCl_3) δ 7.37 – 7.30 (m,

2H), 7.29 – 7.20 (m, 3H), 3.74 (dd, $J = 9.6, 8.3$ Hz, 1H), 3.57 (dt, $J = 16.9, 8.4$ Hz, 1H), 3.40 (dd, $J = 9.6, 7.0$ Hz, 1H), 2.90 (s, 3H), 2.81 (dd, $J = 16.9, 9.1$ Hz, 1H), 2.54 (dd, $J = 16.8, 8.3$ Hz, 1H) ppm. ^{13}C NMR (101 MHz, CDCl_3) δ 174.0, 142.7, 129.0, 127.18, 126.83, 56.8, 38.9, 37.3, 29.7 ppm. **ESI-MS**: m/z 176.0 $[\text{M}+\text{H}]^+$; **HR-MS**: m/z calcd. for $\text{C}_{11}\text{H}_{13}\text{NO}$ $[\text{M}+\text{H}]^+$: 175.0997; found 175.0996. **HPLC** (PP gradient, MeOH): 4.67 min.

(S)-1-methyl-4-phenylpyrrolidin-2-one (*(S)*-**5**) – Acquired 23.5 mg (85%) as a clear oil from 25.3 mg of *(S)*-**4**. $[\alpha]_{\text{D}}^{24} + 43.2$ (c 0.5, CHCl_3). ^1H NMR (400 MHz, CDCl_3) δ 7.37 – 7.29 (m, 2H), 7.29 – 7.19 (m, 3H), 3.74 (dd, $J = 9.6, 8.3$ Hz, 1H), 3.57 (dt, $J = 16.9, 8.4$ Hz, 1H), 3.40 (dd, $J = 9.6, 7.0$ Hz, 1H), 2.90 (s, 3H), 2.81 (dd, $J = 16.9, 9.1$ Hz, 1H), 2.54 (dd, $J = 16.8, 8.3$ Hz, 1H) ppm. ^{13}C NMR (101 MHz, CDCl_3) δ 174.0, 142.7, 129.0, 127.17, 126.82, 56.8, 38.9, 37.3, 29.7 ppm. **ESI-MS**: m/z 176.0 $[\text{M}+\text{H}]^+$; **HR-MS**: m/z calcd. for $\text{C}_{11}\text{H}_{13}\text{NO}$ $[\text{M}+\text{H}]^+$: 175.0997; found 175.0994. **HPLC** (PP gradient, MeOH): 4.71 min.

Sulfonamides (**7**) – 1-methyl-4-phenylpyrrolidin-2-one **5** was weighed in a 25 mL round-bottom flask and dissolved in CH_2Cl_2 (5 mL). Chlorosulfonic acid (8 mol. eq.) was then slowly pipetted into the mixture at room temperature and left to stir overnight. After this time, the mixture was slowly quenched with water (25 mL) at 0 °C and washed with CH_2Cl_2 (3 x 25 mL). The combined organic layers were dried with MgSO_4 , filtered and concentrated under reduced pressure to acquire the sulfonyl chloride **6** as an oil. This was then re-taken up in CH_2Cl_2 (15mL) and the appropriate amine (10 mol. eq.) was added, followed by Et_3N (5 mol. eq.). The mixture was left to stir overnight, quenched in water (20 mL)^a and then washed with CH_2Cl_2 (3 x 20 mL). The organic layers were combined, dried with MgSO_4 , filtered and concentrated under reduced pressure to afford each sulfonamide as an oil or a solid. These were purified using the specified methods to afford the sulfonamides **7a-7n**.

N,N-diethyl-4-(1-methyl-5-oxopyrrolidin-3-yl)benzenesulfonamide (**7a**) – Acquired 42.8 mg (30%) as a brown oil from 80.0 mg of **5** using diethylamine as the amine (Mobile phase: 1% MeOH in CH₂Cl₂). ¹H NMR (400 MHz, CDCl₃) δ 7.75 (d, *J* = 8.4 Hz, 2H), 7.33 (d, *J* = 8.2 Hz, 2H), 3.77 (dd, *J* = 9.7, 8.3 Hz, 1H), 3.67 – 3.57 (m, 1H), 3.39 (dd, *J* = 9.8, 6.5 Hz, 1H), 3.21 (q, *J* = 7.2 Hz, 4H), 2.90 (s, 3H), 2.83 (dd, *J* = 16.9, 9.2 Hz, 1H), 2.50 (dd, *J* = 16.9, 7.7 Hz, 1H), 1.11 (t, *J* = 7.1 Hz, 6H) ppm. ¹³C NMR (101 MHz, CDCl₃) δ 173.3, 147.4, 139.3, 127.74, 127.48, 56.3, 42.2, 38.6, 37.0, 29.7, 14.3 ppm. ESI-MS: *m/z* 311.0 [M+H]⁺. HR-MS: *m/z* calc. for C₁₅H₂₂N₂O₃S [M+H]⁺: 310.1351; found 310.1359. HPLC (PP gradient, MeOH): 5.44 min.

Upscaled Formation of 7a - 1-methyl-4-phenylpyrrolidin-2-one **5** (578 mg, 3.30 mmol) was weighed in a 100 mL round-bottom flask and dissolved in CH₂Cl₂ (20 mL). Chlorosulfonic acid (3.07 g, 1.76 mL, 8 mol. eq.) was then slowly pipetted into the mixture at room temperature and left to stir overnight. After this time, the mixture was slowly quenched with water (50 mL) at 0 °C and washed with CH₂Cl₂ (3 x 50 mL). The combined organic layers were dried with MgSO₄, filtered and concentrated under reduced pressure to acquire the sulfonyl chloride **6** as an oil. This was then re-taken up in CH₂Cl₂ (40 mL) and diethylamine (2.41 g, 3.41 mL, 10 mol. eq.) was added, followed by Et₃N (1.67 g, 2.30 mL, 5 mol. eq.). The mixture was left to stir overnight, then quenched in water (50 mL) and washed with CH₂Cl₂ (3 x 50 mL). The organic layers were combined, dried with MgSO₄, filtered and concentrated under reduced pressure to afford the crude product as an oil. This were purified using the same conditions as previously described to afford **7a** (630 mg, 62%) as a clear oil.

1-methyl-4-(4-(piperidin-1-ylsulfonyl)phenyl)pyrrolidin-2-one (7b) – Acquired 94.6 mg (64%) as a yellow solid from 80.5 mg of **5** using piperidine as the amine (Mobile phase: EtOAc). ¹H NMR (400 MHz, CDCl₃) δ 7.68 (d, *J* = 8.4 Hz, 2H), 7.35 (d, *J* = 8.2 Hz, 2H), 3.77 (dd, *J* =

9.7, 8.3 Hz, 1H), 3.63 (dt, $J = 16.0, 8.2$ Hz, 1H), 3.39 (dd, $J = 9.8, 6.5$ Hz, 1H), 2.98 – 2.91 (m, 4H), 2.88 (s, 3H), 2.82 (dd, $J = 16.9, 9.2$ Hz, 1H), 2.49 (dd, $J = 16.8, 7.8$ Hz, 1H), 1.66 – 1.55 (m, 4H), 1.44 – 1.34 (m, 2H) ppm. $^{13}\text{C NMR}$ (101 MHz, CDCl_3) δ 173.2, 147.7, 135.2, 128.33, 127.40, 56.1, 46.9, 38.6, 37.0, 29.7, 25.2, 23.5 ppm. **ESI-MS**: m/z 323.0 $[\text{M}+\text{H}]^+$. **HR-MS**: m/z calc. for $\text{C}_{16}\text{H}_{22}\text{N}_2\text{O}_3\text{S}$ $[\text{M}+\text{H}]^+$: 322.1351; found 322.1356. **HPLC** (PP gradient, MeOH): 5.63 min.

1-methyl-4-(4-(morpholin sulfonyl)phenyl)pyrrolidin-2-one (7c) – Acquired 69.9 mg (52%) as a yellow solid from 72.3 mg of **5** using morpholine as the amine (Mobile phase: 2% MeOH in CH_2Cl_2). $^1\text{H NMR}$ (400 MHz, CDCl_3) δ 7.68 (d, $J = 8.4$ Hz, 2H), 7.38 (d, $J = 8.2$ Hz, 2H), 3.77 (dd, $J = 9.7, 8.3$ Hz, 1H), 3.74 – 3.57 (m, 5H), 3.38 (dd, $J = 9.8, 6.5$ Hz, 1H), 3.01 – 2.91 (m, 4H), 2.88 (s, 3H), 2.83 (dd, $J = 16.9, 9.2$ Hz, 1H), 2.49 (dd, $J = 16.8, 7.6$ Hz, 1H) ppm. $^{13}\text{C NMR}$ (101 MHz, CDCl_3) δ 173.2, 148.3, 133.9, 128.56, 127.61, 66.1, 56.1, 46.0, 38.5, 37.0, 29.7 ppm. **ESI-MS**: m/z 324.9 $[\text{M}+\text{H}]^+$. **HR-MS**: m/z calc. for $\text{C}_{15}\text{H}_{20}\text{N}_2\text{O}_4\text{S}$ $[\text{M}+\text{H}]^+$: 324.1144; found 324.1154. **HPLC** (PP gradient, MeOH): 4.62 min.

1-methyl-4-(4-((4-phenylpiperidin-1-yl)sulfonyl)phenyl)pyrrolidin-2-one (7d) – Acquired 73.8 mg (63%) as a white solid from 51.0 mg of **5** using 4-phenylpiperidine as the amine (Mobile phase: EtOAc). $^1\text{H NMR}$ (400 MHz, CDCl_3) δ 7.76 (d, $J = 8.4$ Hz, 2H), 7.40 (d, $J = 8.2$ Hz, 2H), 7.33 – 7.25 (m, 2H), 7.23 – 7.17 (m, 1H), 7.17 – 7.11 (m, 2H), 3.93 (d, $J = 11.6$ Hz, 2H), 3.81 (dd, $J = 9.7, 8.3$ Hz, 1H), 3.73 – 3.60 (m, 1H), 3.43 (dd, $J = 9.7, 6.5$ Hz, 1H), 2.93 (s, 3H), 2.87 (dd, $J = 16.9, 9.2$ Hz, 1H), 2.54 (dd, $J = 16.9, 7.7$ Hz, 1H), 2.49 – 2.32 (m, 3H), 1.93 – 1.76 (m, 4H) ppm. $^{13}\text{C NMR}$ (101 MHz, CDCl_3) δ 173.2, 147.8, 144.8, 135.2, 128.63, 128.42, 127.46, 126.67, 56.1, 46.9, 41.8, 38.6, 37.0, 32.5 (d, $J = 2.1$ Hz), 29.7 ppm. **ESI-MS**: m/z 398.9 $[\text{M}+\text{H}]^+$. **HR-MS**: m/z calc. for $\text{C}_{22}\text{H}_{26}\text{N}_2\text{O}_3\text{S}$ $[\text{M}+\text{H}]^+$: 398.1670; found 398.1664. **HPLC** (PP gradient, 1:1 $\text{CH}_3\text{CN}:\text{H}_2\text{O}$ with 0.1% formic acid): 6.75 min.

4-(4-((3,4-dihydroquinolin-1(2H)-yl)sulfonyl)phenyl)-1-methylpyrrolidin-2-one (**7e**) –

Acquired 51.1 mg (48%) as a yellow gum from 50.1 mg of **5** using 1,2,3,4-tetrahydroquinoline as the amine (Mobile phase: EtOAc). **¹H NMR** (400 MHz, CDCl₃) δ 7.77 (dd, *J* = 8.3, 0.8 Hz, 1H), 7.57 (d, *J* = 8.5 Hz, 2H), 7.26 – 7.22 (m, 2H), 7.22 – 7.16 (m, 1H), 7.08 (td, *J* = 7.4, 1.2 Hz, 1H), 7.04 – 6.99 (m, 1H), 3.83 – 3.79 (m, 2H), 3.76 (dd, *J* = 9.8, 8.3 Hz, 1H), 3.64 – 3.55 (m, 1H), 3.39 – 3.32 (m, 1H), 2.90 (s, 3H), 2.83 (dd, *J* = 16.9, 9.3 Hz, 1H), 2.52 – 2.42 (m, 3H), 1.68 – 1.64 (m, 2H) ppm. **¹³C NMR** (101 MHz, CDCl₃) δ 173.3, 148.0, 138.7, 136.8, 130.7, 129.3, 127.81, 127.41, 126.66, 125.16, 124.79, 56.2, 46.7, 38.6, 36.9, 29.7, 26.7, 21.8 ppm. **ESI-MS**: *m/z* 370.8 [M+H]⁺. **HR-MS**: *m/z* calc. for C₁₅H₂₂N₂O₃S [M+H]⁺: 370.1351; found 370.1357. **HPLC** (PP gradient, MeOH): 6.26 min.

N-benzyl-4-(1-methyl-5-oxopyrrolidin-3-yl)benzenesulfonamide (**7f**) – Acquired 68.9 mg

(69%) as a white solid from 51.0 mg of **5** using benzylamine as the amine (Mobile phase: 2% MeOH in CH₂Cl₂). **¹H NMR** (400 MHz, CDCl₃) δ 7.80 (d, *J* = 8.4 Hz, 2H), 7.31 (d, *J* = 8.3 Hz, 2H), 7.27 – 7.12 (m, 5H), 5.38 (br t, *J* = 5.5 Hz, 1H), 4.12 (d, *J* = 5.4 Hz, 2H), 3.77 (dd, *J* = 9.7, 8.3 Hz, 1H), 3.61 (dt, *J* = 15.9, 8.1 Hz, 1H), 3.38 (dd, *J* = 9.8, 6.5 Hz, 1H), 2.95 – 2.78 (m, 4H), 2.48 (dd, *J* = 16.9, 7.7 Hz, 1H) ppm. **¹³C NMR** (101 MHz, CDCl₃) δ 173.5, 147.8, 139.0, 136.4, 128.71, 127.97, 127.93, 127.87, 127.56, 56.2, 47.3, 38.6, 37.0, 29.8 ppm. **ESI-MS**: *m/z* 344.9 [M+H]⁺. **HR-MS**: *m/z* calc. for C₁₈H₂₀N₂O₃S [M+H]⁺: 344.1195; found 344.1198. **HPLC** (PP gradient, MeOH): 5.22 min.

N-ethyl-4-(1-methyl-5-oxopyrrolidin-3-yl)benzenesulfonamide (**7g**) – Acquired 46.4 mg (58%)

as a white solid from 50.3 mg of **5** using ethylamine as the amine (Mobile phase: 2% MeOH in CH₂Cl₂). **¹H NMR** (400 MHz, CDCl₃) δ 7.82 (d, *J* = 8.4 Hz, 2H), 7.35 (d, *J* = 8.3 Hz, 2H), 5.01 (t, *J* = 6.0 Hz, 1H), 3.78 (dd, *J* = 9.7, 8.3 Hz, 1H), 3.64 (dt, *J* = 16.1, 8.2 Hz, 1H), 3.40 (dd, *J* = 9.8, 6.5 Hz, 1H), 2.98 (qd, *J* = 7.2, 6.1 Hz, 2H), 2.91 (s, 3H), 2.85 (dd, *J* = 17.0, 8.7

Hz, 1H), 2.52 (dd, $J = 16.8, 7.7$ Hz, 1H), 1.09 (t, $J = 7.2$ Hz, 3H) ppm. ^{13}C NMR (101 MHz, CDCl_3) δ 173.4, 147.7, 138.9, 127.74, 127.50, 56.2, 38.6, 38.2, 36.9, 29.7, 15.1 ppm. **ESI-MS**: m/z 282.9 $[\text{M}+\text{H}]^+$. **HR-MS**: m/z calc. for $\text{C}_{13}\text{H}_{18}\text{N}_2\text{O}_3\text{S}$ $[\text{M}+\text{H}]^+$: 282.1038; found 282.1042. **HPLC** (PP gradient, MeOH): 4.17 min.

4-(1-methyl-5-oxopyrrolidin-3-yl)-N-propylbenzenesulfonamide (7h) – Acquired 40.5 mg (59%) as a white solid from 40.3 mg of **5** using *n*-propylamine as the amine (Mobile phase: 2% MeOH in CH_2Cl_2). ^1H NMR (400 MHz, CDCl_3) δ 7.83 (d, $J = 8.5$ Hz, 2H), 7.36 (d, $J = 8.2$ Hz, 2H), 4.82 (t, $J = 6.1$ Hz, 1H), 3.79 (dd, $J = 9.8, 8.3$ Hz, 1H), 3.65 (dt, $J = 16.1, 8.2$ Hz, 1H), 3.41 (dd, $J = 9.8, 6.5$ Hz, 1H), 2.95 – 2.82 (m, 6H), 2.52 (dd, $J = 16.9, 7.7$ Hz, 1H), 1.55 – 1.43 (m, 2H), 0.86 (t, $J = 7.4$ Hz, 3H) ppm. ^{13}C NMR (101 MHz, CDCl_3) δ 173.3, 147.7, 139.0, 127.72, 127.49, 56.2, 45.0, 38.6, 36.9, 29.7, 23.0, 11.1 ppm. **ESI-MS**: m/z 297.2 $[\text{M}+\text{H}]^+$. **HR-MS**: m/z calc. for $\text{C}_{14}\text{H}_{20}\text{N}_2\text{O}_3\text{S}$ $[\text{M}+\text{H}]^+$: 296.1195; found 296.1198. **HPLC** (PP gradient, MeOH): 4.64 min.

N-isopropyl-4-(1-methyl-5-oxopyrrolidin-3-yl)benzenesulfonamide (7i) – Acquired 46.6 mg (68%) as a white solid from 40.5 mg of **5** using 2-propylamine as the amine (Mobile phase: 2% MeOH in CH_2Cl_2). ^1H NMR (400 MHz, CDCl_3) δ 7.84 (d, $J = 8.5$ Hz, 2H), 7.35 (d, $J = 8.2$ Hz, 2H), 4.62 (d, $J = 7.5$ Hz, 1H), 3.79 (dd, $J = 9.7, 8.3$ Hz, 1H), 3.65 (dt, $J = 16.7, 8.2$ Hz, 1H), 3.52 – 3.37 (m, 2H), 2.92 (s, 3H), 2.86 (dd, $J = 17.0, 9.2$ Hz, 1H), 2.53 (dd, $J = 16.9, 7.8$ Hz, 1H), 1.08 (d, $J = 6.5$ Hz, 6H) ppm. ^{13}C NMR (101 MHz, CDCl_3) δ 173.3, 147.6, 140.1, 127.66, 127.44, 56.2, 46.2, 38.5, 36.9, 29.7, 23.8 ppm. **ESI-MS**: m/z 297.2 $[\text{M}+\text{H}]^+$. **HR-MS**: m/z calc. for $\text{C}_{14}\text{H}_{20}\text{N}_2\text{O}_3\text{S}$ $[\text{M}+\text{H}]^+$: 296.1195; found 296.1198. **HPLC** (PP gradient, MeOH): 4.54 min.

8-((4-(1-methyl-5-oxopyrrolidin-3-yl)phenyl)sulfonyl)-8-azabicyclo[3.2.1]octan-3-one (7j) – Acquired 28.2 mg (34%) as a white solid from 40.5 mg of **5** using 8-azabicyclo[3.2.1]octan-3-

one as the amine (Mobile phase: 2% MeOH in CH₂Cl₂). **¹H NMR** (400 MHz, CDCl₃) δ 7.87 (d, *J* = 8.5 Hz, 2H), 7.37 (d, *J* = 8.3 Hz, 2H), 4.53 – 4.44 (m, 2H), 3.79 (dd, *J* = 9.7, 8.3 Hz, 1H), 3.65 (dt, *J* = 15.9, 8.1 Hz, 1H), 3.39 (dd, *J* = 9.8, 6.5 Hz, 1H), 2.91 (s, 3H), 2.86 (dd, *J* = 16.9, 9.2 Hz, 1H), 2.78 (dd, *J* = 16.0, 4.4 Hz, 2H), 2.50 (dd, *J* = 16.8, 7.7 Hz, 1H), 2.36 (dd, *J* = 16.4, 1.3 Hz, 2H), 1.75 (dd, *J* = 9.2, 4.4 Hz, 2H), 1.64 – 1.57 (m, 2H) ppm. **¹³C NMR** (101 MHz, CDCl₃) δ 206.7, 173.1, 148.5, 138.7, 127.98, 127.67, 56.12, 56.04, 50.1, 38.5, 36.9, 29.67, 29.42 ppm. **ESI-MS**: *m/z* 362.9 [M+H]⁺. **HR-MS**: *m/z* calc. for C₁₈H₂₂N₂O₄S [M+H]⁺: 362.1300; found 362.1306. **HPLC** (PP gradient, MeOH): 4.55 min.

(3R)-1-((4-(1-methyl-5-oxopyrrolidin-3-yl)phenyl)sulfonyl)piperidine-3-carboxylic acid (7k) – Acquired 21.4 mg (25%) as a white solid from 40.5 mg of **5** using (*R*)-nipecotic acid as the amine (Reverse-phase HPLC). **¹H NMR** (400 MHz, DMSO) δ 7.70 (d, *J* = 8.4 Hz, 2H), 7.57 (d, *J* = 8.4 Hz, 2H), 3.78 – 3.65 (m, 2H), 3.52 (d, *J* = 7.0 Hz, 1H), 3.37 (ddd, *J* = 8.8, 6.5, 2.3 Hz, 2H), 2.77 (s, 3H), 2.69 (dd, *J* = 16.5, 8.6 Hz, 1H), 2.54 – 2.49 (m, 2H), 2.44 – 2.35 (m, 2H), 1.83 – 1.75 (m, 1H), 1.75 – 1.64 (m, 1H), 1.56 – 1.42 (m, 1H), 1.42 – 1.27 (m, 1H) ppm. **¹³C NMR** (101 MHz, DMSO) δ 173.8, 172.5, 148.5 (d, *J* = 3.7 Hz), 133.8, 128.10, 127.83, 55.0 (d, *J* = 2.0 Hz), 47.5, 46.0, 40.1, 38.0 (d, *J* = 3.8 Hz), 36.5 (d, *J* = 1.8 Hz), 29.1, 25.6, 23.4 ppm. **ESI-MS**: *m/z* 366.8 [M+H]⁺. **HR-MS**: *m/z* calc. for C₁₇H₂₂N₂O₅S [M+H]⁺: 366.1249; found 366.1250. **HPLC** (PP gradient, 1:1 CH₃CN:H₂O): 4.63 min.

^aCompound was extracted from 5% HCl (pH 0).

(3S)-1-((4-(1-methyl-5-oxopyrrolidin-3-yl)phenyl)sulfonyl)piperidine-3-carboxylic acid (7l) – Acquired 17.8 mg (21%) as a white solid from 40.8 mg of **5** using (*S*)-nipecotic acid as the amine (Reverse-phase HPLC). **¹H NMR** (400 MHz, DMSO) δ 7.70 (d, *J* = 8.4 Hz, 2H), 7.58 (d, *J* = 8.4 Hz, 2H), 3.80 – 3.65 (m, 2H), 3.53 (d, *J* = 7.0 Hz, 1H), 3.40 – 3.35 (m, 2H), 2.78 (s, 3H), 2.70 (dd, *J* = 16.5, 8.6 Hz, 1H), 2.55 – 2.50 (m, 2H), 2.46 – 2.36 (m, 2H), 1.85 – 1.76 (m,

1H), 1.71 (dd, $J = 9.0, 4.4$ Hz, 1H), 1.57 – 1.43 (m, 1H), 1.43 – 1.29 (m, 1H) ppm. **^{13}C NMR** (101 MHz, DMSO) δ 173.8, 172.4, 148.5 (d, $J = 3.7$ Hz), 133.7, 128.08, 127.81, 55.0 (d, $J = 2.1$ Hz), 47.5, 46.0, 40.1, 38.0 (d, $J = 3.9$ Hz), 36.5 (d, $J = 1.9$ Hz), 29.1, 25.6, 23.4 ppm. **ESI-MS**: m/z 366.9 [M+H]⁺. **HR-MS**: m/z calc. for C₁₇H₂₂N₂O₅S [M+H]⁺: 366.1249; found 366.1250. **HPLC** (PP gradient, 1:1 CH₃CN:H₂O): 4.63 min.

^aCompound was extracted from 5% HCl (pH 0).

N-(3-(1*H*-imidazol-1-yl)propyl)-4-(1-methyl-5-oxopyrrolidin-3-yl)benzenesulfonamide (**7m**) – Acquired 13.2 mg (21%) as a white solid from 30.9 mg of **5** using 3-(1*H*-imidazol-1-yl)propan-1-amine as the amine (Reverse-phase HPLC). **^1H NMR** (400 MHz, MeOD) δ 8.84 (s, 1H), 7.80 (d, $J = 8.5$ Hz, 2H), 7.61 (s, 1H), 7.54 (s, 1H), 7.50 (d, $J = 8.3$ Hz, 2H), 4.36 (t, $J = 6.8$ Hz, 2H), 3.86 (dd, $J = 9.8, 8.3$ Hz, 1H), 3.75 (dt, $J = 16.2, 8.2$ Hz, 1H), 3.49 (dd, $J = 9.8, 6.6$ Hz, 1H), 2.90 (s, 3H), 2.89 – 2.80 (m, 3H), 2.51 (dd, $J = 16.8, 7.9$ Hz, 1H), 2.11 – 2.02 (m, 2H) ppm. **^{13}C NMR** (101 MHz, MeOD) δ 174.6, 148.0, 138.6, 135.5, 127.51, 127.17, 121.7, 120.5, 55.9, 46.0, 39.1, 38.3, 36.8, 29.6, 28.4 ppm. **ESI-MS**: m/z 362.9 [M+H]⁺. **HR-MS**: m/z calc. for C₁₇H₂₂N₄O₃S [M+H]⁺: 362.1413; found 362.1425. **HPLC** (PP gradient, 1:1 CH₃CN:H₂O): 3.49 min.

N-(adamantan-1-yl)-4-(1-methyl-5-oxopyrrolidin-3-yl)benzenesulfonamide (**7n**) – Acquired 26.4 mg (38%) as a white solid from 31.4 mg of **5** using adamantan-1-amine as the amine (Mobile phase: 1% MeOH in CH₂Cl₂). **^1H NMR** (400 MHz, CDCl₃) δ 7.86 (d, $J = 8.5$ Hz, 2H), 7.32 (d, $J = 8.3$ Hz, 2H), 4.82 (s, 1H), 3.79 (dd, $J = 9.7, 8.3$ Hz, 1H), 3.70 – 3.59 (m, 1H), 3.41 (dd, $J = 9.7, 6.6$ Hz, 1H), 2.91 (s, 3H), 2.86 (dd, $J = 17.1, 9.3$ Hz, 1H), 2.54 (dd, $J = 16.8, 7.8$ Hz, 1H), 2.00 (br s, 3H), 1.78 (br d, $J = 2.8$ Hz, 6H), 1.57 (br q, $J = 12.4$ Hz, 6H) ppm. **^{13}C NMR** (101 MHz, CDCl₃) δ 173.5, 147.2, 143.0, 127.60, 127.34, 56.3, 43.2, 38.6, 37.0, 35.9,

29.78, 29.57 ppm. **ESI-MS**: m/z 389.0 $[M+H]^+$. **HR-MS**: m/z calc. for $C_{21}H_{28}N_2O_3S$ $[M+H]^+$: 388.1821; found 388.1828. **HPLC** (PP gradient, MeOH): 6.34 min.

Bromination (NaBr) – 1-methyl-4-phenylpyrrolidin-2-one **5** (560 mg, 3.23 mmol) was weighed into a 25 mL round-bottom flask with a stir-bar. NaBr (864 mg, 8.40 mmol) and H_2SO_4 (824 mg, 8.40 mmol) were added and the mixture was heated to 80 °C. It was then stirred for 2 hours or until the dark brown colour disappeared from the walls of the flask. The mixture was cooled to room temperature before being diluted in water (40 mL) and washed with EtOAc (3 x 40 mL). The combined organic layers were dried, filtered and concentrated under reduced pressure to obtain a brown oil. The crude material was checked in analytical HPLC for completion, and was repeated until the starting material was completely consumed. The oil was then purified using column chromatography (Mobile phase: 20% petroleum benzene in EtOAc) to afford bromides **8** and **9**.

4-(2-bromophenyl)-1-methylpyrrolidin-2-one (8) – Acquire 112 mg (14%) as a yellow oil. **1H NMR** (400 MHz, $CDCl_3$) δ 7.57 (dd, $J = 8.0, 1.2$ Hz, 1H), 7.34 – 7.28 (m, 1H), 7.27 – 7.24 (m, 1H), 7.12 (ddd, $J = 8.0, 7.2, 1.9$ Hz, 1H), 4.07 – 3.96 (m, 1H), 3.82 (dd, $J = 9.9, 8.2$ Hz, 1H), 3.33 (dd, $J = 9.9, 5.5$ Hz, 1H), 2.91 – 2.78 (m, 4H), 2.54 (dd, $J = 17.0, 6.5$ Hz, 1H) ppm. **^{13}C NMR** (101 MHz, $CDCl_3$) δ 173.7, 141.7, 133.3, 128.66, 128.16, 127.1, 124.5, 55.6, 37.6, 36.1, 29.7 ppm. **ESI-MS**: m/z 253.9 $[(^{79}Br)M+H]^+$ and 255.9 $[(^{81}Br)M+H]^+$. **HR-MS**: m/z calc. for $C_{11}H_{12}BrNO$ $[M+H]^+$: 253.0102; found 253.0100. **HPLC** (PP gradient, MeOH): 5.70 min.

4-(4-bromophenyl)-1-methylpyrrolidin-2-one (9) – Acquired 184 mg (23%) as a clear oil. **1H NMR** (400 MHz, $CDCl_3$) δ 7.45 (d, $J = 8.5$ Hz, 2H), 7.09 (d, $J = 8.3$ Hz, 2H), 3.74 (dd, $J = 9.7, 8.3$ Hz, 1H), 3.53 (dt, $J = 16.6, 8.3$ Hz, 1H), 3.35 (dd, $J = 9.7, 6.8$ Hz, 1H), 2.90 (s, 3H), 2.81 (dd, $J = 16.9, 9.1$ Hz, 1H), 2.48 (dd, $J = 16.9, 8.0$ Hz, 1H) ppm. **^{13}C NMR** (101 MHz, $CDCl_3$) δ 173.7, 141.7, 132.1, 128.6, 121.0, 56.6, 38.8, 36.8, 29.7 ppm. **ESI-MS**: m/z 253.9

$[(^{79}\text{Br})\text{M}+\text{H}]^+$ and 255.9 $[(^{81}\text{Br})\text{M}+\text{H}]^+$. **HR-MS:** m/z calc. for $\text{C}_{11}\text{H}_{12}\text{BrNO}$ $[\text{M}+\text{H}]^+$: 253.0102; found 253.0099. **HPLC** (PP gradient, MeOH): 5.90 min.

Bromination (NBS) – *N,N*-diethyl-4-(1-methyl-5-oxopyrrolidin-3-yl)benzenesulfonamide **9a** (630 mg, 2.03 mmol) was weighed in a round-bottom flask, to which *N*-bromosuccinimide (434 mg, 2.44 mmol) was added, as well as a magnetic stir-bar. Concentrated sulfuric acid (4 mL) was then added, the mixture was heated to 60 °C and the contents were left to stir overnight. After this time, the mixture was quenched with water (50 mL) and washed with EtOAc (3 x 50 mL). The organic layers were combined, dried with MgSO_4 , filtered and concentrated under reduced pressure to give **12** as an oil. This was then purified with column chromatography (Mobile phase: neat EtOAc) to give the bromide **12**.

3-bromo-N,N-diethyl-4-(1-methyl-5-oxopyrrolidin-3-yl)benzenesulfonamide (**12**) – Acquired 550 mg (69%) as a purple oil. **^1H NMR** (400 MHz, CDCl_3) δ 8.01 (d, $J = 1.9$ Hz, 1H), 7.72 (dd, $J = 8.2, 1.9$ Hz, 1H), 7.36 (d, $J = 8.2$ Hz, 1H), 4.06 (tt, $J = 8.7, 5.7$ Hz, 1H), 3.86 (dd, $J = 10.2, 8.2$ Hz, 1H), 3.34 (dd, $J = 10.2, 5.2$ Hz, 1H), 3.24 (q, $J = 7.2$ Hz, 4H), 2.95 – 2.85 (m, 4H), 2.54 (dd, $J = 17.3, 5.9$ Hz, 1H), 1.15 (t, $J = 7.1$ Hz, 6H) ppm. **^{13}C NMR** (101 MHz, CDCl_3) δ 173.5, 146.1, 140.9, 131.7, 127.7, 126.6, 124.9, 55.3, 42.4, 37.4, 36.2, 29.9, 14.40 ppm. **ESI-MS:** m/z 388.7 $[(^{79}\text{Br})\text{M}+\text{H}]^+$ and 390.8 $[(^{81}\text{Br})\text{M}+\text{H}]^+$. **HR-MS:** m/z calc. for $\text{C}_{15}\text{H}_{21}\text{BrN}_2\text{O}_3\text{S}$ $[\text{M}+\text{H}]^+$: 388.0456; found 388.0459. **HPLC** (PP gradient, 1:1 $\text{CH}_3\text{CN}:\text{H}_2\text{O}$): 5.85 min.

Suzuki Coupling – The appropriate bromide was weighed and dissolved in 1,2-dimethoxyethane (5 mL). Upon addition of each reagent, N_2 was bubbled through the mixture for 5 minutes. The appropriate boronic acid (1.2 mol. eq.) was added, followed by 2 M Na_2CO_3 (5 mL) and then $\text{Pd}(\text{PPh}_3)_4$ (3 mol%). After addition of $\text{Pd}(\text{PPh}_3)_4$, the mixture was bubbled with N_2 for 10 minutes before being sealed under a nitrogen atmosphere. The mixture was heated under reflux and left to stir overnight. After this time, the mixture was quenched with

saturated aqueous NaCl (25 mL) and washed with EtOAc (3 x 25 mL). The organic layers were combined, dried with MgSO₄, filtered and concentrated under reduced pressure. The crude products was then purified accordingly to afford the respective products.

4-([1,1'-biphenyl]-2-yl)-1-methylpyrrolidin-2-one (10) – Acquired 53.7 mg (70%) as a white solid from 76.5 mg of **8** using phenylboronic acid as the boronic acid (Mobile phase: 40% petroleum benzine in EtOAc). ¹H NMR (400 MHz, CDCl₃) δ 7.47 – 7.35 (m, 5H), 7.32 – 7.22 (m, 4H), 3.72 – 3.60 (m, 1H), 3.52 (dd, *J* = 9.7, 8.5 Hz, 1H), 3.40 (dd, *J* = 9.7, 6.8 Hz, 1H), 2.86 (s, 3H), 2.68 (dd, *J* = 16.9, 9.5 Hz, 1H), 2.54 (dd, *J* = 17.0, 7.9 Hz, 1H) ppm. ¹³C NMR (101 MHz, CDCl₃) δ 173.9, 142.11, 141.29, 140.58, 130.3, 129.22, 128.42, 128.39, 127.34, 126.67, 125.82, 57.3, 39.9, 33.0, 29.7 ppm. **ESI-MS**: *m/z* 252.0 [M+H]⁺. **HR-MS**: *m/z* calc. for C₁₇H₁₇NO [M+H]⁺: 251.1310; found 251.1309. **HPLC** (PP gradient, MeOH): 6.46 min.

4-([1,1'-biphenyl]-4-yl)-1-methylpyrrolidin-2-one (11) – Acquired 44.7 mg (75%) as a white solid from 60.0 mg of **9** using phenylboronic acid as the boronic acid (Mobile phase: 35% petroleum benzine in EtOAc and reverse-phase HPLC). ¹H NMR (400 MHz, CDCl₃) δ 7.62 – 7.55 (m, 4H), 7.49 – 7.42 (m, 2H), 7.39 – 7.33 (m, 1H), 7.30 (d, *J* = 8.2 Hz, 2H), 3.84 (dd, *J* = 9.8, 8.5 Hz, 1H), 3.74 – 3.63 (m, 1H), 3.52 (dd, *J* = 9.8, 7.0 Hz, 1H), 3.04 – 2.93 (m, 4H), 2.71 (dd, *J* = 17.4, 8.1 Hz, 1H) ppm. ¹³C NMR (101 MHz, CDCl₃) δ 175.6, 140.89, 140.60, 140.47, 129.0, 127.82, 127.57, 127.26, 127.15, 57.3, 38.7, 37.0, 30.2 ppm. **ESI-MS**: *m/z* 252.0. [M+H]⁺. **HR-MS**: *m/z* calc. for C₁₇H₁₇NO [M+H]⁺: 251.1310; found 251.1310. **HPLC** (PP gradient, 1:1 CH₃CN:H₂O): 6.61 min.

N,N-diethyl-6-(1-methyl-5-oxopyrrolidin-3-yl)-[1,1'-biphenyl]-3-sulfonamide (15a) – Acquired 10.6 mg (27%) as a clear oil from 40.0 mg of **12** using phenylboronic acid as the boronic acid (Mobile phase: 3% EtOH in Et₂O and reverse-phase HPLC). ¹H NMR (400 MHz, CDCl₃) δ 7.81 (dd, *J* = 8.3, 2.1 Hz, 1H), 7.69 (d, *J* = 2.0 Hz, 1H), 7.51 – 7.40 (m, 4H), 7.22

(dd, $J = 7.7, 1.7$ Hz, 2H), 3.80 – 3.68 (m, 1H), 3.58 (dd, $J = 10.1, 8.6$ Hz, 1H), 3.42 (dd, $J = 10.1, 6.5$ Hz, 1H), 3.26 (q, $J = 7.2$ Hz, 4H), 2.90 (s, 3H), 2.79 (dd, $J = 17.3, 9.5$ Hz, 1H), 2.61 (dd, $J = 17.3, 7.5$ Hz, 1H), 1.16 (t, $J = 7.1$ Hz, 6H) ppm. ^{13}C NMR (101 MHz, CDCl_3) δ 174.5, 144.8, 143.1, 139.50, 139.08, 129.07, 128.85, 128.83, 128.25, 126.91, 126.70, 57.3, 42.4, 39.5, 33.1, 30.0, 14.5 ppm. **ESI-MS**: m/z 386.8 $[\text{M}+\text{H}]^+$. **HR-MS**: m/z calc. for $\text{C}_{21}\text{H}_{26}\text{N}_2\text{O}_3\text{S}$ $[\text{M}+\text{H}]^+$: 386.1664; found 386.1662. **HPLC** (PP gradient, 1:1 $\text{CH}_3\text{CN}:\text{H}_2\text{O}$): 6.33 min.

4'-(dimethylamino)-N,N-diethyl-6-(1-methyl-5-oxopyrrolidin-3-yl)-[1,1'-biphenyl]-3-sulfonamide (15b) – Acquired 13.1 mg (30%) as a clear oil from 39.6 mg of **12** using (4-(dimethylamino)phenyl)boronic acid as the boronic acid (Mobile phase: 4% EtOH in Et_2O and reverse-phase HPLC). ^1H NMR (400 MHz, CDCl_3) δ 7.81 (dd, $J = 8.3, 2.0$ Hz, 1H), 7.65 (d, $J = 2.0$ Hz, 1H), 7.50 (d, $J = 8.3$ Hz, 1H), 7.37 (d, $J = 8.8$ Hz, 2H), 7.29 (d, $J = 8.8$ Hz, 2H), 3.74 – 3.64 (m, 1H), 3.60 (t, $J = 9.2$ Hz, 1H), 3.44 (dd, $J = 9.9, 6.3$ Hz, 1H), 3.25 (q, $J = 7.1$ Hz, 4H), 3.18 (s, 6H), 2.90 (s, 3H), 2.77 (dd, $J = 17.2, 9.4$ Hz, 1H), 2.58 (dd, $J = 17.2, 7.5$ Hz, 1H), 1.16 (t, $J = 7.1$ Hz, 6H) ppm. ^{13}C NMR (101 MHz, CDCl_3) δ 174.2, 145.65, 144.90, 141.7, 139.3, 136.5, 130.8, 128.8, 127.17, 126.97, 118.3, 57.2, 44.5, 42.4, 39.6, 33.1, 30.0, 14.5 ppm. **ESI-MS**: m/z 429.9 $[\text{M}+\text{H}]^+$. **HR-MS**: m/z calc. for $\text{C}_{23}\text{H}_{31}\text{N}_3\text{O}_3\text{S}$ $[\text{M}+\text{H}]^+$: 429.2086; found 429.2087. **HPLC** (PP gradient, 1:1 $\text{CH}_3\text{CN}:\text{H}_2\text{O}$): 4.94 min.

N,N-diethyl-3',4'-dimethoxy-6-(1-methyl-5-oxopyrrolidin-3-yl)-[1,1'-biphenyl]-3-sulfonamide (15c) – Acquired 22.6 mg (50%) as a clear oil from 39.7 mg of **12** using (3,4-dimethoxyphenyl)boronic acid as the boronic acid (Mobile phase: 5% EtOH in Et_2O and reverse-phase HPLC). ^1H NMR (400 MHz, CDCl_3) δ 7.78 (dd, $J = 8.3, 2.1$ Hz, 1H), 7.69 (d, $J = 2.0$ Hz, 1H), 7.46 (d, $J = 8.3$ Hz, 1H), 6.94 (d, $J = 8.2$ Hz, 1H), 6.76 (dd, $J = 8.1, 2.0$ Hz, 1H), 6.72 (d, $J = 2.0$ Hz, 1H), 3.93 (s, 3H), 3.89 (s, 3H), 3.81 – 3.72 (m, 1H), 3.57 (dd, $J = 10.0, 8.6$ Hz, 1H), 3.40 (dd, $J = 10.0, 6.4$ Hz, 1H), 3.25 (q, $J = 7.1$ Hz, 4H), 2.89 (s, 3H), 2.77 (dd, $J =$

17.2, 9.6 Hz, 1H), 2.57 (dd, $J = 17.2, 7.5$ Hz, 1H), 1.16 (t, $J = 7.1$ Hz, 6H) ppm. ^{13}C NMR (101 MHz, CDCl_3) δ 174.0, 149.09, 149.06, 145.3, 142.8, 138.9, 132.1, 128.8, 126.68, 126.62, 121.5, 112.33, 111.32, 57.17, 56.18, 56.14, 42.4, 39.6, 33.1, 30.0, 14.5 ppm. **ESI-MS**: m/z 446.8 $[\text{M}+\text{H}]^+$. **HR-MS**: m/z calc. for $\text{C}_{23}\text{H}_{30}\text{N}_2\text{O}_5\text{S}$ $[\text{M}+\text{H}]^+$: 446.1875; found 446.1880. **HPLC** (PP gradient, 1:1 $\text{CH}_3\text{CN}:\text{H}_2\text{O}$): 5.98 min.

3-(benzo[b]thiophen-3-yl)-N,N-diethyl-4-(1-methyl-5-oxopyrrolidin-3-yl)benzenesulfonamide (15d) – Acquired 24.0 mg (54%) as a clear oil from 39.3 mg of **12** using benzo[b]thiophen-3-ylboronic acid as the boronic acid (Mobile phase: 3% EtOH in Et_2O and reverse-phase HPLC). ^1H NMR (400 MHz, CDCl_3) (mixture of atropisomers) δ 7.95 (d, $J = 8.0$ Hz, 1H), 7.89 (dd, $J = 8.3, 2.1$ Hz, 1H), 7.75 (d, $J = 2.0$ Hz, 1H), 7.56 (d, $J = 8.3$ Hz, 1H), 7.46 – 7.39 (m, 1H), 7.39 – 7.32 (m, 2H), 7.30 – 7.24 (m, 1H), 3.65 – 3.30 (m, 3H), 3.27 (q, $J = 7.2$ Hz, 4H), 2.83 (br d, $J = 8.7$ Hz, 3H), 2.77 – 2.44 (m, 2H), 1.15 (t, $J = 7.1$ Hz, 6H) ppm. ^{13}C NMR (101 MHz, CDCl_3) (mixture of atropisomers) δ 129.6, 127.64, 126.85, 125.1 (d, $J = 17.4$ Hz), 123.20, 122.24, 57.0 (d, $J = 67.2$ Hz), 42.3, 39.84, 38.75, 33.3 (d, $J = 19.8$ Hz), 29.9, 14.4 ppm. **ESI-MS**: m/z 442.8 $[\text{M}+\text{H}]^+$. **HR-MS**: m/z calc. for $\text{C}_{23}\text{H}_{26}\text{N}_2\text{O}_3\text{S}_2$ $[\text{M}+\text{H}]^+$: 442.1385; found 442.1391. **HPLC** (PP gradient, 1:1 $\text{CH}_3\text{CN}:\text{H}_2\text{O}$): 6.79 min.

Heck Coupling and Alkene Reduction – The appropriate bromide was weighed and dissolved in distilled DMF (1 mL). Upon addition of each reagent, N_2 was bubbled through the mixture for 5 minutes. The appropriate alkene (1.6 mol. eq.) was added, followed by DIPEA (300 μL), $\text{P}(o\text{-tol})_3$ (10 mol%) and $\text{Pd}(\text{OAc})_2$ (10 mol%). After addition of $\text{Pd}(\text{OAc})_2$, N_2 was bubbled through the mixture for 5 minutes before being sealed, and then vacuumed and backfilled with N_2 three times. The mixture was heated to 90 $^\circ\text{C}$ and left to stir overnight. After this time, the mixture was quenched with saturated aqueous NaCl (25 mL) and washed with EtOAc (3 x 25 mL). The organic layers were combined, dried with MgSO_4 , filtered and concentrated under

reduced pressure to afford the crude alkenes. These were then purified with column chromatography to afford the respective alkenes (**15**) as intermediates. A three-neck 25 mL round-bottom flask with a stir-bar was purged with N₂, to which palladium on carbon (10% w/w) was added, and submerged in a minimum amount of dichloromethane. The appropriate alkene was dissolved in ethyl acetate and pipetted into the flask while keeping it under N₂. The flask was purged three more times with N₂, and then purged with H₂ three times, to which the contents were left to stir at room temperature. The progress of the reaction was monitored by NMR. After completion, the flask was purged with N₂ three times and the contents filtered carefully through a glass microfiber filter paper under very gentle vacuum. The filtered palladium catalyst was washed with dichloromethane then quenched separately with H₂O while the filtrate was concentrated under reduced pressure to give each reduced product, which were then purified with reverse-phase HPLC.

N,N-diethyl-4-(1-methyl-5-oxopyrrolidin-3-yl)-3-phenethylbenzenesulfonamide (**14a**) –

Acquired 27.7 mg (43%) as a clear oil from 59.7 mg of **12** using styrene as the alkene. ¹H NMR (400 MHz, CDCl₃) δ 7.63 (dd, *J* = 8.2, 2.0 Hz, 1H), 7.59 (d, *J* = 2.0 Hz, 1H), 7.30 (d, *J* = 8.2 Hz, 1H), 7.28 – 7.23 (m, 2H), 7.22 – 7.17 (m, 1H), 7.08 – 7.02 (m, 2H), 3.76 – 3.66 (m, 1H), 3.54 (dd, *J* = 10.2, 8.5 Hz, 1H), 3.26 (dd, *J* = 10.2, 6.0 Hz, 1H), 3.16 (q, *J* = 7.1 Hz, 4H), 3.05 – 2.99 (m, 2H), 2.97 – 2.85 (m, 5H), 2.75 (dd, *J* = 17.3, 9.4 Hz, 1H), 2.45 (dd, *J* = 17.4, 7.0 Hz, 1H), 1.12 (t, *J* = 7.1 Hz, 6H) ppm. ¹³C NMR (101 MHz, CDCl₃) δ 174.5, 145.5, 140.31, 140.27, 139.0, 128.72, 128.65, 128.58, 126.56, 126.44, 125.76, 56.9, 42.3, 39.0, 37.7, 34.7, 32.1, 30.0, 14.4 ppm. ESI-MS: *m/z* 414.9 [M+H]⁺. HR-MS: *m/z* calc. for C₂₃H₃₀N₂O₃S [M+H]⁺: 414.1977; found 414.1981. HPLC (PP gradient, 1:1 CH₃CN:H₂O): 6.62 min.

N,N-diethyl-4-(1-methyl-5-oxopyrrolidin-3-yl)-3-(3-phenylpropyl)benzenesulfonamide (**14b**)

– Acquired 27.3 mg (41%) as a clear oil from 59.9 mg of **12** using allylbenzene as the alkene.

¹H NMR (400 MHz, CDCl₃) δ 7.64 – 7.60 (m, 2H), 7.34 – 7.28 (m, 3H), 7.24 – 7.20 (m, 1H), 7.20 – 7.16 (m, 2H), 3.69 – 3.59 (m, 2H), 3.36 – 3.31 (m, 1H), 3.22 (q, *J* = 7.2 Hz, 4H), 2.92 (s, 3H), 2.84 – 2.76 (m, 1H), 2.73 – 2.65 (m, 4H), 2.49 (dd, *J* = 17.0, 6.4 Hz, 1H), 1.93 – 1.84 (m, 2H), 1.13 (t, *J* = 7.1 Hz, 6H) ppm. **¹³C NMR** (101 MHz, CDCl₃) δ 174.2, 145.2, 141.44, 141.26, 139.1, 128.65, 128.55, 128.30, 126.49, 126.33, 125.60, 56.8, 42.2, 39.0, 35.7, 33.14, 32.43, 31.98, 30.0, 14.37 ppm. **ESI-MS**: *m/z* 428.9 [M+H]⁺. **HR-MS**: *m/z* calc. for C₂₄H₃₂N₂O₃S [M+H]⁺: 428.2134; found 428.2140. **HPLC** (PP gradient, 1:1 CH₃CN:H₂O): 6.92 min.

Diastereomer Resolution – A 100 mL oven-dried round-bottom flask with a magnetic stir-bar was purged with N₂. Diisopropylamine (138 mg, 193 μL, 1.37 mmol) was added via syringe and dissolved in distilled THF (5 mL). The contents were stirred, then placed on a dry ice-bath. While kept at –78 °C, *n*-butyllithium (850 μL, 1.37 mmol, 1.6 M in hexane) was then added via syringe and the contents were stirred for 20 minutes. A solution of 4-phenylpyrrolidin-2-one **4** (200 mg, 1.24 mmol) dissolved in distilled THF (10 mL) was added to the mixture via syringe and left to stir for 45 minutes. After this time, (*S*)-Naproxen chloride **16** (617 mg, 2.48 mmol) was dissolved in distilled THF (10 mL) and added via syringe. The contents were lifted off the dry ice-bath and allowed to stir at room temperature for 2.5 hours. Saturated aqueous NaHCO₃ (30 mL) was used to quench the mixture, which was then washed with dichloromethane (3 x 30 mL). The organic layers were combined, dried with MgSO₄, filtered and concentrated under reduced pressure to afford the crude diastereomers as a solid. The diastereomers were separated using column chromatography (Mobile phase: 10% EtOAc in petroleum benzine, TLCs were checked in 20% EtOAc in petroleum benzine) to afford both (*R,S*)-**17** and (*S,S*)-**17**.

(R)-1-((*S*)-2-(6-methoxynaphthalen-2-yl)propanoyl)-4-phenylpyrrolidin-2-one (*(R,S)*-**17**)³³ – Acquired 136 mg (29%) as a clear oil. ¹H NMR (400 MHz, CDCl₃) δ 7.73 – 7.70 (m, 3H), 7.49 (dd, *J* = 8.5, 1.8 Hz, 1H), 7.38 – 7.32 (m, 2H), 7.31 – 7.27 (m, 1H), 7.23 – 7.17 (m, 2H), 7.15 – 7.11 (m, 2H), 5.24 (q, *J* = 7.0 Hz, 1H), 4.20 (dd, *J* = 11.7, 8.2 Hz, 1H), 3.80 (dd, *J* = 11.7, 8.9 Hz, 1H), 3.45 – 3.35 (m, 1H), 2.81 (qd, *J* = 17.4, 9.3 Hz, 2H), 1.56 (d, *J* = 7.0 Hz, 3H) ppm. HPLC (PP gradient, MeOH): 7.74 min.

(S)-1-((*S*)-2-(6-methoxynaphthalen-2-yl)propanoyl)-4-phenylpyrrolidin-2-one (*(S,S)*-**17**)³³ – Acquired 136 mg (29%) as a clear oil. ¹H NMR (400 MHz, CDCl₃) δ 7.74 – 7.68 (m, 3H), 7.48 (dd, *J* = 8.6, 1.7 Hz, 1H), 7.20 – 7.12 (m, 4H), 7.12 – 7.06 (m, 2H), 6.98 – 6.92 (m, 2H), 5.24 (q, *J* = 7.0 Hz, 1H), 4.33 (dd, *J* = 11.7, 7.9 Hz, 1H), 3.93 (s, 3H), 3.70 (dd, *J* = 11.7, 6.8 Hz, 1H), 3.56 – 3.43 (m, 1H), 2.94 (dd, *J* = 17.5, 8.4 Hz, 1H), 2.60 (dd, *J* = 17.5, 8.0 Hz, 1H), 1.58 (d, *J* = 7.0 Hz, 3H) ppm. HPLC (PP gradient, MeOH): 7.64 min.

Chiral Auxiliary Uncoupling – The appropriate imide **17** was weighed in a round-bottom flask, to which a magnetic stir-bar was added. The compound was dissolved in THF and then 1 M KOH was added. The mixture was left to stir overnight. After this time, the organic solvent was evaporated off under reduced pressure, then washed with CH₂Cl₂ (3 x 20 mL). The organic layers were combined, dried with MgSO₄, filtered and concentrated under reduced pressure to afford the crude lactams. These were purified with column chromatography (Mobile phase: neat EtOAc) to afford each lactam.

(R)-4-phenylpyrrolidin-2-one (*(R)*-**4**) – Acquired 47.1 mg (84%) as a white solid from 134 mg of *(R,S)*-**17**. [α]_D²⁶ - 39.4 (*c* 0.9, CHCl₃). ¹H NMR (400 MHz, CDCl₃) δ 7.39 – 7.30 (m, 2H), 7.30 – 7.19 (m, 3H), 7.07 (br s, 1H), 3.83 – 3.74 (m, 1H), 3.68 (dt, *J* = 16.9, 8.6 Hz, 1H), 3.42 (dd, *J* = 9.4, 7.2 Hz, 1H), 2.73 (dd, *J* = 16.9, 8.9 Hz, 1H), 2.51 (dd, *J* = 16.9, 8.8 Hz, 1H) ppm.

¹³C NMR (101 MHz, CDCl₃) δ 178.1, 142.3, 128.9, 127.17, 126.86, 49.7, 40.4, 38.2 ppm. **ESI-MS**: *m/z* 162.0 [M+H]⁺.

(S)-4-phenylpyrrolidin-2-one (*(S)*-**4**) – Acquired 28.4 mg (80%) as a white solid from 81.8 mg of (*S,S*)-**7**. [α]_D²⁴ + 44.8 (*c* 1, CHCl₃). **¹H NMR** (400 MHz, CDCl₃) δ 7.39 – 7.30 (m, 2H), 7.30 – 7.21 (m, 3H), 7.08 (br s, 1H), 3.80 (dd, *J* = 13.2, 4.6 Hz, 1H), 3.69 (dt, *J* = 16.9, 8.6 Hz, 1H), 3.43 (dd, *J* = 9.4, 7.3 Hz, 1H), 2.75 (dd, *J* = 17.0, 8.9 Hz, 1H), 2.53 (dd, *J* = 17.0, 8.8 Hz, 1H) ppm. **¹³C NMR** (101 MHz, CDCl₃) δ 178.5, 142.2, 129.0, 127.24, 126.87, 49.8, 40.3, 38.2 ppm. **ESI-MS**: *m/z* 162.0 [M+H]⁺.

Formation of (R)-**17c** and *(S)*-**17c** – The phenyl NMP isomers (*R*)-**5** and (*S*)-**5** were weighed in separate 10 mL round-bottom flasks and dissolved in CH₂Cl₂ (4 mL). Chlorosulfonic acid (8 mol. eq.) was then slowly pipetted into the mixture at room temperature and left to stir overnight. After this time, the mixture was quenched with water (10 mL) at 0 °C and washed with CH₂Cl₂ (3 x 15 mL). The combined organic layers were dried with MgSO₄, filtered and concentrated under reduced pressure to acquire each sulfonyl chloride as an oil. These were then re-taken up in CH₂Cl₂ (10 mL) and diethylamine (10 mol. eq.) was added, followed by Et₃N (3 mol. eq.) The mixture was left to stir overnight, then the excess amine was evaporated off with rotary evaporation. The residue was quenched in water (10 mL) and washed with CH₂Cl₂ (3 x 15 mL). The organic layers were combined, dried with MgSO₄, filtered and concentrated under reduced pressure to afford each sulfonamide. These were then weighed in separate round-bottom flasks, to which *N*-bromosuccinimide (1.2 mol. eq.) was added, as well as a magnetic stir-bar. Concentrated sulfuric acid (3 mL) was then added, the mixtures were heated to 60 °C and the contents were left to stir overnight. After this time, each mixture was quenched with water (15 mL) and washed with EtOAc (3 x 15 mL). The organic layers were combined, dried with MgSO₄, filtered and concentrated under reduced pressure to give each

isomer as an oil. These were then purified with column chromatography (Mobile phase: neat EtOAc) to give the bromides. Lastly, the bromides were weighed and dissolved in 1,2-dimethoxyethane (5 mL). Upon addition of each reagent, N₂ was bubbled through the mixture for 5 minutes. 3,4-dimethoxyphenylboronic acid (1.2 mol. eq.) was added, followed by 2 M Na₂CO₃ (5 mL) and then Pd(PPh₃)₄ (3 mol%). After addition of Pd(PPh₃)₄, the mixture was bubbled with N₂ for 10 minutes before being sealed under a nitrogen atmosphere. The mixture was heated under reflux and left to stir overnight. After this time, the mixture was quenched with saturated aqueous NaCl (15 mL) and washed with EtOAc (3 x 15 mL). The organic layers were combined, dried with MgSO₄, filtered and concentrated under reduced pressure. The crude products was then purified with column chromatography (Mobile phase: 8% EtOH in Et₂O) to afford the respective isomers.

(R)-*N,N*-diethyl-3',4'-dimethoxy-6-(1-methyl-5-oxopyrrolidin-3-yl)-[1,1'-biphenyl]-3-sulfonamide (*(R)*-**15c**) – Acquired 5.60 mg (10%) as a clear oil from 22.3 mg of *(R)*-**5**. **¹H NMR** (400 MHz, CDCl₃) δ 7.78 (dd, *J* = 8.3, 2.0 Hz, 1H), 7.70 (d, *J* = 2.0 Hz, 1H), 7.47 (d, *J* = 8.3 Hz, 1H), 6.94 (d, *J* = 8.2 Hz, 1H), 6.77 (dd, *J* = 8.1, 2.0 Hz, 1H), 6.73 (d, *J* = 2.0 Hz, 1H), 3.94 (s, 3H), 3.89 (s, 3H), 3.79 – 3.69 (m, 1H), 3.55 (dd, *J* = 9.9, 8.5 Hz, 1H), 3.38 (dd, *J* = 9.9, 6.2 Hz, 1H), 3.26 (q, *J* = 7.1 Hz, 4H), 2.88 (s, 3H), 2.72 (dd, *J* = 17.1, 9.5 Hz, 1H), 2.51 (dd, *J* = 16.9, 7.2 Hz, 1H), 1.16 (t, *J* = 7.1 Hz, 6H) ppm. **¹³C NMR** (101 MHz, CDCl₃) δ 173.3, 149.1, 145.7, 142.8, 140.8, 138.9, 132.2, 128.8, 126.67, 126.64, 121.5, 112.4, 111.3, 56.96, 56.20, 56.17, 42.4, 39.8, 33.0, 29.8, 14.5 ppm. **ESI-MS**: *m/z* 447.2 [M+H]⁺. **HR-MS**: *m/z* calc. for C₂₃H₃₀N₂O₅S [M+H]⁺: 446.1875; found 446.1883. **HPLC** (PP gradient, CH₃CN): 5.91 min. **Chiral HPLC**: 5.88 min.

(S)-*N,N*-diethyl-3',4'-dimethoxy-6-(1-methyl-5-oxopyrrolidin-3-yl)-[1,1'-biphenyl]-3-sulfonamide (*(S)*-**15c**) – Acquired 2.40 mg (8.4%) as a clear oil from 11.2 mg of *(S)*-**5**. **¹H**

NMR (400 MHz, CDCl₃) δ 7.78 (dd, *J* = 8.3, 2.1 Hz, 1H), 7.70 (d, *J* = 2.0 Hz, 1H), 7.47 (d, *J* = 8.3 Hz, 1H), 6.94 (d, *J* = 8.2 Hz, 1H), 6.77 (dd, *J* = 8.1, 2.0 Hz, 1H), 6.73 (d, *J* = 2.0 Hz, 1H), 3.94 (s, 3H), 3.89 (s, 3H), 3.78 – 3.68 (m, 1H), 3.55 (dd, *J* = 9.9, 8.5 Hz, 1H), 3.38 (dd, *J* = 9.9, 6.3 Hz, 1H), 3.26 (q, *J* = 7.1 Hz, 4H), 2.88 (s, 3H), 2.72 (dd, *J* = 16.9, 9.7 Hz, 1H), 2.51 (dd, *J* = 17.0, 7.4 Hz, 1H), 1.16 (t, *J* = 7.1 Hz, 6H) ppm. **¹³C NMR** (101 MHz, CDCl₃) δ 128.8, 126.68, 126.65, 121.5, 112.4, 111.3, 56.97, 56.21, 56.17, 42.4, 39.8, 33.1, 29.8, 14.5 ppm. **ESI-MS:** *m/z* 447.2 [M+H]⁺. **HR-MS:** *m/z* calc. for C₂₃H₃₀N₂O₅S [M+H]⁺: 446.1875; found 446.1886. **HPLC** (PP gradient, CH₃CN): 5.91 min. **Chiral HPLC:** 4.75 min.

References

1. Murray CW, Rees DC. The rise of fragment-based drug discovery. *Nat Chem.* 2009;1(3):187-92.
2. Erlanson DA, Fesik SW, Hubbard RE, Jahnke W, Jhoti H. Twenty years on: the impact of fragments on drug discovery. *Nat Rev Drug Discov.* 2016;15(9):605-19.
3. Raheem IT, Schreier JD, Fuerst J, Gantert L, Hostetler ED, Huszar S, et al. Discovery of pyrazolopyrimidine phosphodiesterase 10A inhibitors for the treatment of schizophrenia. *Bioorg Med Chem Lett.* 2016;26(1):126-32.
4. Hay DA, Fedorov O, Martin S, Singleton DC, Tallant C, Wells C, et al. Discovery and optimization of small-molecule ligands for the CBP/p300 bromodomains. *J Am Chem Soc.* 2014;136(26):9308-19.
5. Casale E, Amboldi N, Brasca MG, Caronni D, Colombo N, Dalvit C, et al. Fragment-based hit discovery and structure-based optimization of aminotriazoloquinazolines as novel Hsp90 inhibitors. *Bioorg Med Chem.* 2014;22(15):4135-50.
6. Simpson MG, Pittelkow M, Watson SP, Sanders JK. Dynamic combinatorial chemistry with hydrazones: libraries incorporating heterocyclic and steroidal motifs. *Org Biomol Chem.* 2010;8(5):1181-7.
7. Wlochaj J, Davies RD, Burton J. Cubanes in medicinal chemistry: synthesis of functionalized building blocks. *Org Lett.* 2014;16(16):4094-7.
8. Naderi M, Alvin C, Ding Y, Mukhopadhyay S, Brylinski M. A graph-based approach to construct target-focused libraries for virtual screening. *J Cheminform.* 2016;8:14.
9. Hewings DS, Wang M, Philpott M, Fedorov O, Uttarkar S, Filippakopoulos P, et al. 3,5-dimethylisoxazoles act as acetyl-lysine-mimetic bromodomain ligands. *J Med Chem.* 2011;54(19):6761-70.
10. Bennett MJ, Wu Y, Bloor A, Matuszkiewicz J, O'Connell SM, Shi L, et al. Design, synthesis and biological evaluation of novel 4-phenylisoquinolinone BET bromodomain inhibitors. *Bioorg Med Chem Lett.* 2018;28(10):1811-6.
11. Xiang Q, Wang C, Zhang Y, Xue X, Song M, Zhang C, et al. Discovery and optimization of 1-(1H-indol-1-yl)ethanone derivatives as CBP/EP300 bromodomain inhibitors for the treatment of castration-resistant prostate cancer. *Eur J Med Chem.* 2018;147:238-52.
12. Lolli G, Caflisch A. High-Throughput Fragment Docking into the BAZ2B Bromodomain: Efficient in Silico Screening for X-Ray Crystallography. *ACS Chem Biol.* 2016;11(3):800-7.
13. Zhu J, Caflisch A. Twenty Crystal Structures of Bromodomain and PHD Finger Containing Protein 1 (BRPF1)/Ligand Complexes Reveal Conserved Binding Motifs and Rare Interactions. *J Med Chem.* 2016;59(11):5555-61.

14. Fish PV, Filippakopoulos P, Bish G, Brennan PE, Bunnage ME, Cook AS, et al. Identification of a chemical probe for bromo and extra C-terminal bromodomain inhibition through optimization of a fragment-derived hit. *J Med Chem*. 2012;55(22):9831-7.
15. Taylor AM, Cote A, Hewitt MC, Pastor R, Leblanc Y, Nasveschuk CG, et al. Fragment-Based Discovery of a Selective and Cell-Active Benzodiazepinone CBP/EP300 Bromodomain Inhibitor (CPI-637). *ACS Med Chem Lett*. 2016;7(5):531-6.
16. Sanghvi R, Narazaki R, Machatha SG, Yalkowsky SH. Solubility improvement of drugs using N-methyl pyrrolidone. *AAPS PharmSciTech*. 2008;9(2):366-76.
17. Philpott M, Yang J, Tumber T, Fedorov O, Uttarkar S, Filippakopoulos P, et al. Bromodomain-peptide displacement assays for interactome mapping and inhibitor discovery. *Mol Biosyst*. 2011;7(10):2899-908.
18. Shortt J, Hsu AK, Martin BP, Doggett K, Matthews GM, Doyle MA, et al. The drug vehicle and solvent N-methylpyrrolidone is an immunomodulator and antimyeloma compound. *Cell Rep*. 2014;7(4):1009-19.
19. NMP in Relapsed Refractory Myeloma. <https://ClinicalTrials.gov/show/NCT02468687>.
20. Gjoksi B, Ruangsawasdi N, Ghayor C, Siegenthaler B, Zenobi-Wong M, Weber FE. Influence of N-methyl pyrrolidone on the activity of the pulp-dentine complex and bone integrity during osteoporosis. *Int Endod J*. 2017;50(3):271-80.
21. Ghayor C, Corroero RM, Lange K, Karfeld-Sulzer LS, Gratz KW, Weber FE. Inhibition of osteoclast differentiation and bone resorption by N-methylpyrrolidone. *J Biol Chem*. 2011;286(27):24458-66.
22. Gjoksi B, Ghayor C, Bhattacharya I, Zenobi-Wong M, Weber FE. The bromodomain inhibitor N-methyl pyrrolidone reduced fat accumulation in an ovariectomized rat model. *Clin Epigenetics*. 2016;8:42.
23. Rooney TP, Filippakopoulos P, Fedorov O, Picaud S, Cortopassi WA, Hay DA, et al. A series of potent CREBBP bromodomain ligands reveals an induced-fit pocket stabilized by a cation-pi interaction. *Angew Chem Int Ed Engl*. 2014;53(24):6126-30.
24. Ozer HG, El-Gamal D, Powell B, Hing ZA, Blachly JS, Harrington B, et al. BRD4 Profiling Identifies Critical Chronic Lymphocytic Leukemia Oncogenic Circuits and Reveals Sensitivity to PLX51107, a Novel Structurally Distinct BET Inhibitor. *Cancer Discov*. 2018;8(4):458-77.
25. Bamborough P, Chung CW, Demont EH, Furze RC, Bannister AJ, Che KH, et al. A Chemical Probe for the ATAD2 Bromodomain. *Angew Chem Int Ed Engl*. 2016;55(38):11382-6.
26. Li X, Zhang J, Zhao L, Yang Y, Zhang H, Zhou J. Design, Synthesis, and in vitro Biological Evaluation of 3,5-Dimethylisoxazole Derivatives as BRD4 Inhibitors. *ChemMedChem*. 2018;13(13):1363-8.

27. Felluga F, Gombac V, Pitacco G, Valentin E. A short and convenient chemoenzymatic synthesis of both enantiomers of 3-phenylGABA and 3-(4-chlorophenyl)GABA (Baclofen). *Tetrahedron: Asymmetry*. 2005;16(7):1341-5.
28. Day JP, Lindsay B, Riddell T, Jiang Z, Allcock RW, Abraham A, et al. Elucidation of a structural basis for the inhibitor-driven, p62 (SQSTM1)-dependent intracellular redistribution of cAMP phosphodiesterase-4A4 (PDE4A4). *J Med Chem*. 2011;54(9):3331-47.
29. Myint YY, Pasha MA. Oxidative monobromination of electron-rich arenes by conc. H₂SO₄ / alkali metal bromides. *J Chem Research*. 2004;2004(11):732-4.
30. Goodby JW, Toyne KJ, Lewis RA, Hird M, Slaney AJ, Jones JC, inventors; the Secretary of State for Defence, UK . assignee. Quinoline 2,6-derivatives as liquid crystal material for display devices patent GB2339779A. 2000.
31. Rajesh K, Somasundaram M, Saiganesh R, Balasubramanian KK. Bromination of deactivated aromatics: a simple and efficient method. *J Org Chem*. 2007;72(15):5867-9.
32. Scott IL, Kuksa VA, Kubota R, inventors; Acucela Inc, USA . assignee. Preparation of phenylpropylamine derivatives for treating ophthalmic diseases and disorders patent GB2463151A. 2010.
33. Montoya-Balbas IJ, Valentin-Guevara B, Lopez-Mendoza E, Linzaga-Elizalde I, Ordonez M, Roman-Bravo P. Efficient Synthesis of beta-Aryl-gamma-lactams and Their Resolution with (S)-Naproxen: Preparation of (R)- and (S)-Baclofen. *Molecules*. 2015;20(12):22028-43.
34. Ember SW, Zhu JY, Olesen SH, Martin MP, Becker A, Berndt N, et al. Acetyl-lysine binding site of bromodomain-containing protein 4 (BRD4) interacts with diverse kinase inhibitors. *ACS Chem Biol*. 2014;9(5):1160-71.
35. Chen Z, Zhang H, Liu S, Xie Y, Jiang H, Lu W, et al. Discovery of novel trimethoxy-ring BRD4 bromodomain inhibitors: AlphaScreen assay, crystallography and cell-based assay. *Medchemcomm*. 2017;8(6):1322-31.
36. Navratilova I, Aristotelous T, Picaud S, Chaikuad A, Knapp S, Filappakopoulos P, et al. Discovery of New Bromodomain Scaffolds by Biosensor Fragment Screening. *ACS Med Chem Lett*. 2016;7(12):1213-8.
37. Zhao H, Gartenmann L, Dong J, Spiliotopoulos D, Caflisch A. Discovery of BRD4 bromodomain inhibitors by fragment-based high-throughput docking. *Bioorg Med Chem Lett*. 2014;24(11):2493-6.
38. McPhillips TM, McPhillips SE, Chiu H-J, Cohen AE, Deacon AM, Ellis PJ, et al. Blu-Ice and the Distributed Control System: software for data acquisition and instrument control at macromolecular crystallography beamlines. *Journal of synchrotron radiation*. 2002;9(6):401-6.
39. Battye TGG, Kontogiannis L, Johnson O, Powell HR, Leslie AGW. iMOSFLM: a new graphical interface for diffraction-image processing with MOSFLM. *Acta crystallographica Section D, Biological crystallography*. 2011;67(Pt 4):271-81.

40. Evans PR, Murshudov GN. How good are my data and what is the resolution? *Acta crystallographica Section D, Biological crystallography*. 2013;69(Pt 7):1204-14.
41. Winn MD, Ballard CC, Cowtan KD, Dodson EJ, Emsley P, Evans PR, et al. Overview of the CCP4 suite and current developments. *Acta Crystallogr D Biol Crystallogr*. 2011;67(Pt 4):235-42.
42. McCoy AJ, Grosse-Kunstleve RW, Adams PD, Winn MD, Storoni LC, Read RJ. Phaser crystallographic software. *J Appl Crystallogr*. 2007;40(Pt 4):658-74.
43. Emsley P, Lohkamp B, Scott WG, Cowtan K. Features and development of Coot. *Acta Crystallogr D Biol Crystallogr*. 2010;66(Pt 4):486-501.
44. Afonine PV, Grosse-Kunstleve RW, Echols N, Headd JJ, Moriarty NW, Mustyakimov M, et al. Towards automated crystallographic structure refinement with phenix.refine. *Acta Crystallogr D Biol Crystallogr*. 2012;68(Pt 4):352-67.

Chapter 4 – 5-methyl-3-aryl-1*H*-pyrazoles as Poised, Ligand Efficient Fragments for the Development of Novel Bromodomain Inhibitors

Keywords

BRD4, Bromodomain, Epigenetics, K-ac, Fragment, Poised

Abbreviations

BET, Bromodomain and Extra-terminal Domain; BRD4, Bromodomain-containing Protein 4; BRD4 BD1, First Bromodomain of BRD4; E3 Ligase, Ubiquitin Ligase; FBDD, Fragment-Based Drug Design; FRET, Fluorescence Resonance Energy Transfer; HDAC, histone deacetylase; HTS, high-throughput screening; K-ac, Acetyl-lysine; LE, Ligand Efficiency; NF- κ B, Nuclear Factor Kappa-B; NHA, Non-hydrogen Atom; PI3K, Phosphatidylinositol-4,5-bisphosphate 3-kinase; p-TEFb, Positive Transcription Elongation Factor b; RMS, Root Mean Square; WPF, Tryptophan-proline-phenylalanine

Abstract

The development of ligand efficient fragments for bromodomains is an important part of the continued development of novel inhibitors with therapeutic potential. Here, we examine 5-methyl-3-aryl-1*H*-pyrazoles as putative acetyl-lysine mimetics of bromodomain-containing protein 4, which were pursued using the principle of “poised fragment” design, featuring a concise synthesis built on readily available precursors. The most potent of these compounds, 5-methoxy-2-(5-methyl-1*H*-pyrazol-3-yl)phenol (**3h**), had an IC₅₀ of 26.7 μ M and a high ligand efficiency of 0.42 kcal/mol per non-hydrogen atom. The X-ray structure of **3h** in complex with the first bromodomain of bromodomain-containing protein 4 showed it to bind in a flipped pose to that expected, suggesting that both the methylpyrazole and dimethylphenol scaffolds might be exploitable in bromodomain inhibitor development.

4.1 Introduction

Over the past decade, FBDD has gradually become a mainstay approach to the discovery of new therapeutics.¹ The general objective of FBDD is to screen for fragments – molecules that are normally less than 300 Da and fall within certain parameters consistent with drug-likeness.² While these fragments are expected to bind to targets with relatively low affinity, their ligand efficiency will be on par or greater than most drug-like molecules, providing a starting point for the development of new drug leads.

One target class that has been of particular interest in FBDD efforts is the bromodomain. These protein modules are best known for their ability to recognize or “read” K-ac residues, by which they are key regulators of the histone code.³ Each bromodomain spans between 90-120 amino acids in length and comprises of a consistent three-dimensional structure: a set of four α -helices connected by two interhelical loops, with a cavity created by the loops where the K-ac residues of both histone and non-histone proteins are read. So far, there have been 61 bromodomains in 46 different proteins identified in humans.

Perhaps the most distinguished examples of bromodomain-containing proteins are the BET proteins. They regulate the transcription of regulators such as NF- κ B⁴ and p-TEFb⁵ and their role in diseases has been well-documented, having been connected to carcinogenic,⁶⁻⁸ viral,^{9, 10} inflammatory^{11, 12} and cardiovascular diseases.^{13, 14} The first potent and selective bromodomain inhibitors to be published targeted the BET family^{15, 16} and were used to demonstrate the outcomes of BET inhibition in preclinical disease models.¹⁷⁻¹⁹ Since then, the amount of literature pertaining to bromodomain inhibition has grown exponentially. Currently, over a dozen BET inhibitors have been registered for clinical trials. Several of these molecules stem from FBDD programs.²⁰⁻²³ While these have been successful, there is further impetus for generating highly efficient fragment-based bromodomain inhibitors, for example, in making

dual-targeting ligands which inhibit other target proteins such as HDACs,²⁴ PI3Ks²⁵ and E3 ligases²⁶ as a pathway to potential therapeutic agents.

Recently, Cox et al.²⁷ introduced the concept of “poised fragments” – compounds synthesised from a robust and general synthetic reaction path such that rapid elaboration of the fragment hit into a library of analogues can be readily performed using parallel chemistry. Here, we describe the consideration of this approach in pursuing 5-methyl-3-aryl-1*H*-pyrazoles; previously unexamined as K-ac mimetics but bearing an obvious resemblance to other heterocyclic fragments. We describe the application of a concise synthetic route to create a series of analogues which show high ligand efficiency as inhibitors against BRD4 BD1, marking the class as potential fragments in the pursuit of bromodomain inhibitors in general.

4.2 Results and Discussion

There are numerous heterocycles that have been described with bromodomain inhibitory activity, but we noted that 3,5-disubstituted pyrazoles could be isosteric to substituted oxazole, triazole, oxadiazole and isoxazole compounds that have been identified as both fragments and inhibitors for bromodomains (Figure 1).^{15, 20, 22, 28-30} We hypothesised that by developing a parallel synthesis of 5-methyl-3-aryl-1*H*-pyrazoles, we might identify highly ligand efficient inhibitors of a bromodomain suitable for further elaboration.

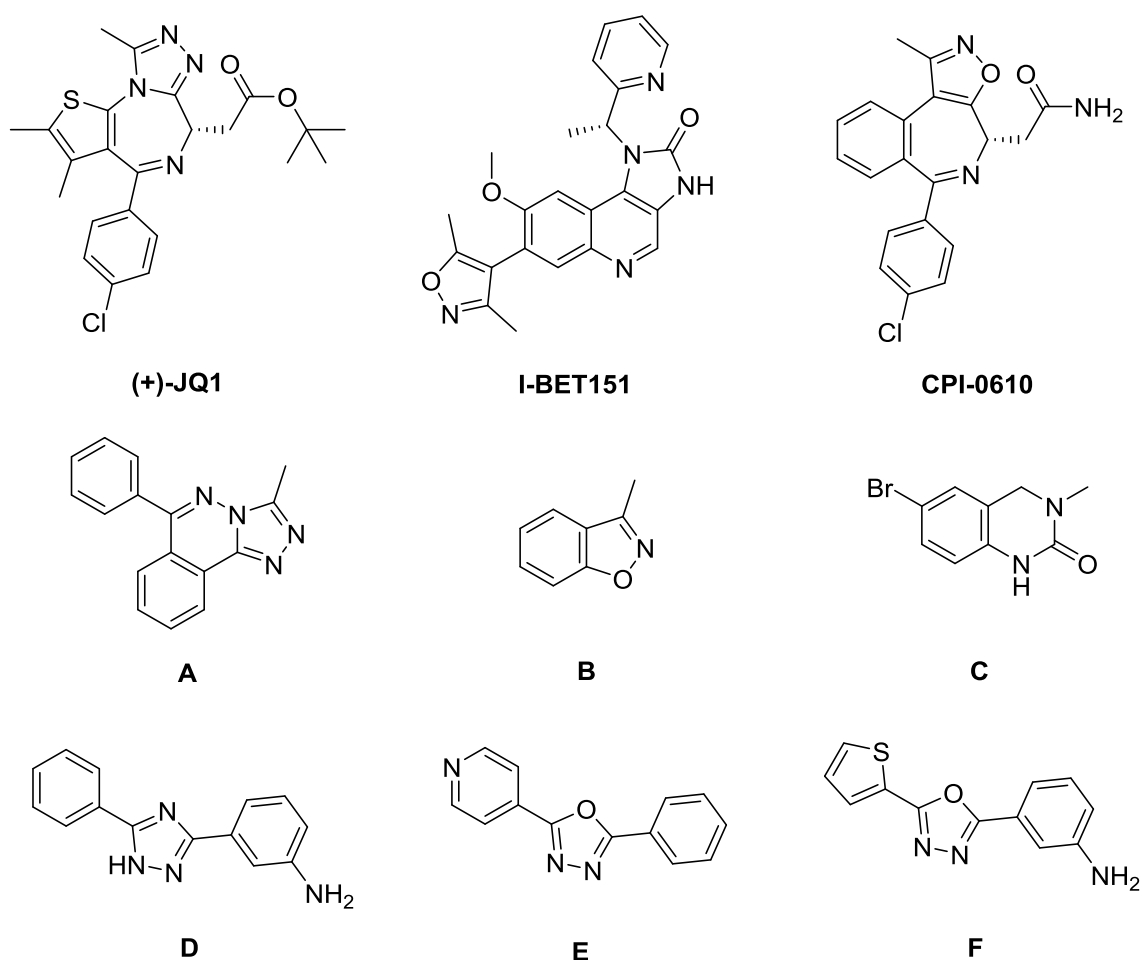
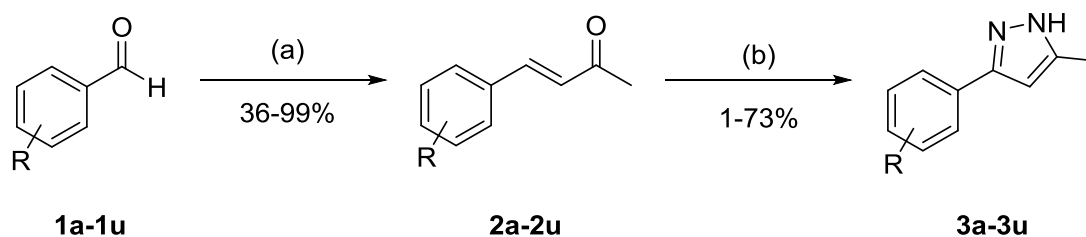


Figure 1. Previously reported heterocyclic bromodomain inhibitors and fragments.

4.2.1 Synthesis

The synthesis of the 5-methyl-3-aryl-1*H*-pyrazole scaffold has been examined by a number of groups in recent years.³¹⁻³⁴ Wen et al.³⁵ described a one-pot condensation reaction of α,β -unsaturated ketones with *p*-toluenesulfonyl hydrazide in water that was most attractive. The ketones themselves could be obtained from readily available aromatic aldehydes providing an expeditious route to a primary target set. The synthetic route is shown in Scheme 1.

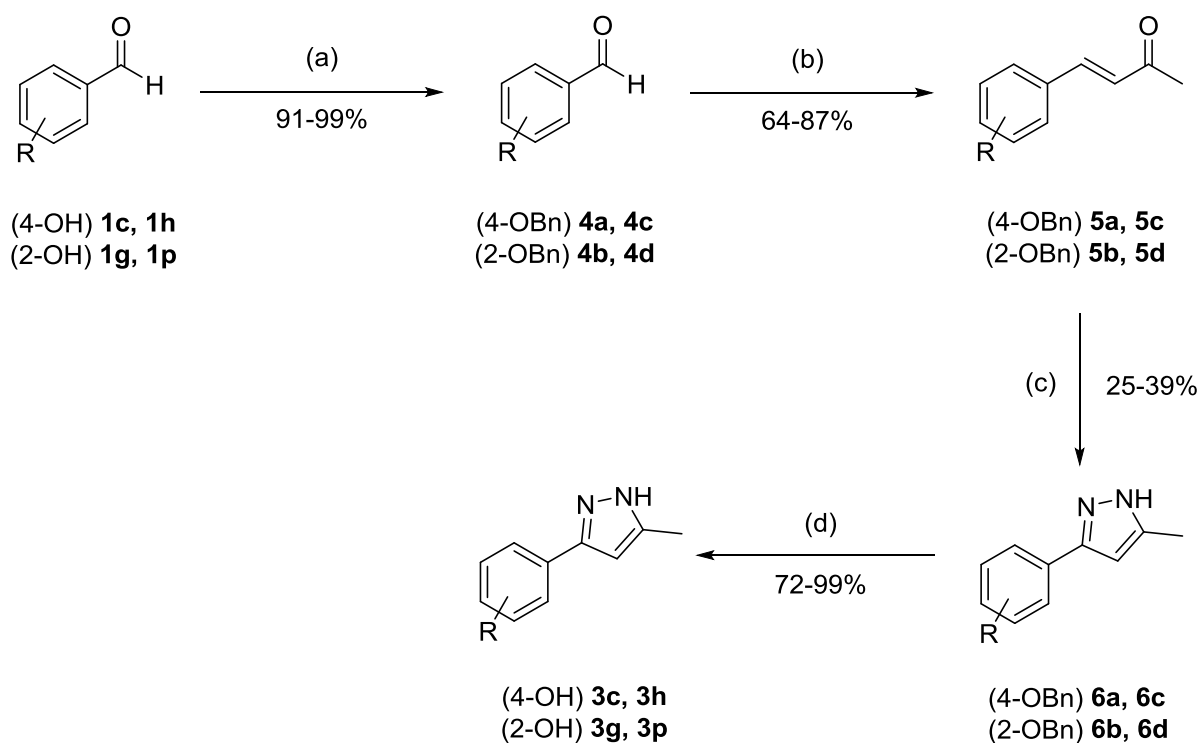


Scheme 1. Synthesis of 5-methyl-3-aryl-1*H*-pyrazoles. (a): Morpholinium trifluoroacetate, acetone, 1-5 d, 75 °C; (b) *p*-toluenesulfonyl hydrazide, TBAB, NaOH, H₂O, o/n, 80 °C.

Mono-, di- and tri-substituted benzaldehydes (**1a-1u**), which shared a small focus on methoxy-containing groups, among other different electron-donating and withdrawing groups, were first converted to α,β -unsaturated ketones through a catalysed aldol condensation reaction using acetone and morpholinium trifluoroacetate.³⁶ Reactions could be performed in parallel in a sealed tube at 75 °C. After quenching, the products were extracted with ethyl acetate. These conditions afforded the desired ketones **2a-2u** in yields ranging from moderate to near-quantitative.

The ketones were then converted to pyrazoles **3a-3u** using *p*-toluenesulfonyl hydrazide under phase-transfer catalytic conditions at 80 °C overnight,³⁵ with tetrabutylammonium bromide serving as the catalyst. Again, the product could be retrieved by extraction into ethyl acetate, and purification was achieved by chromatography to obtain the products in yields ranging from 1-73%.

There was some functional group influence on these reactions and it was found that certain phenolic and nitro compounds were not readily accessible by this route. To overcome the interference of the phenolic groups, benzyl protection was introduced for phenolic benzaldehydes as outlined in Scheme 2. The benzyl moiety was coupled to selected phenols using benzyl bromide and potassium carbonate³⁷ overnight to give the benzyloxy benzaldehydes (**4a-4d**) in yields over 90%. These protected derivatives were then subjected to the same aldol condensation and pyrazole formation conditions described above. Finally, the benzyl group was deprotected by palladium-catalysed hydrogenolysis³⁸ which afforded the originally intended phenolic pyrazoles in excellent yields.



Scheme 2. Modified scheme for the synthesis of benzyl-protected pyrazoles. (a) BnBr, K₂CO₃, DMF, o/n, rt. (b): Morpholinium trifluoroacetate, acetone, 1-3 d, 75 °C; (c) *p*-toluenesulfonyl hydrazide, TBAB, NaOH, H₂O, o/n, 80 °C. (d): H₂, Pd/C, EtOAc, o/n, rt.

Even with considering the need to protect/deprotect sensitive groups, this concise pathway to the parallel synthesis of 5-methyl-3-aryl-1*H*-pyrazoles facilitates the creation of a fragment series suited for elaboration in the event of ligand efficient inhibitors being identified.

4.2.2 BRD4 BD1 FRET Assay Results

The substituted 5-methyl-3-aryl-1*H*-pyrazoles (Figure 2) were assessed for inhibition of binding to BRD4 BD1 in a FRET-based assay (Results are shown in Figure 3). The assay method is a competitive binding assay that was developed by Cisbio Assays. It measures the fluorescence between a Eu³⁺ cryptate donor attached to a GST-tagged bromodomain (BRD4 BD1), and a Streptavidin D2 acceptor attached to a biotinylated tetra-acetylated histone peptide (H4K5K8K12K16(ac₄)). The inhibitor competes for binding with the histone peptide to the bromodomain. When it successfully displaces the peptide, it disrupts the transfer of the Eu³⁺ cryptate donor and prevents fluorescence from occurring.

The compounds were initially tested for inhibition at 1 mM to determine their effectiveness in these assays. The activity was measured as the ratio of the signal at 665 nm and 620 nm. Any interference is accounted for in the 620 nm value. The majority of compounds achieved a ratio of 0.3 (~70% inhibition) at this concentration, with five compounds (**3c**, **3h**, **3s**, **3u**, **6c**) obtaining near-complete inhibition (FRET ratio < 0.2). The *O*-benzylated variants of two of these compounds (**3c** → **6a**, **3h** → **6c**) had significantly reduced activity.

The IC₅₀ values of the five most effective compounds were then determined, as well as the unsubstituted pyrazole **3a**. As shown in Table 1, **3a** had an IC₅₀ of 1248 μM with a respectable LE of 0.33 kcal/mol per NHA. The most potent compound of this series was the dimethylphenol derivative **3h** at 26.7 μM, which enhanced inhibition by 47-fold compared to **3a** with an improved LE of 0.42. While the two phenolic compounds possessed the highest

affinity, the quinoline derivative **3s** also had promising activity ($IC_{50} = 67.4 \mu M$, $LE = 0.36$) (dose response curves of **3h** and **3s** are available in Appendix N).

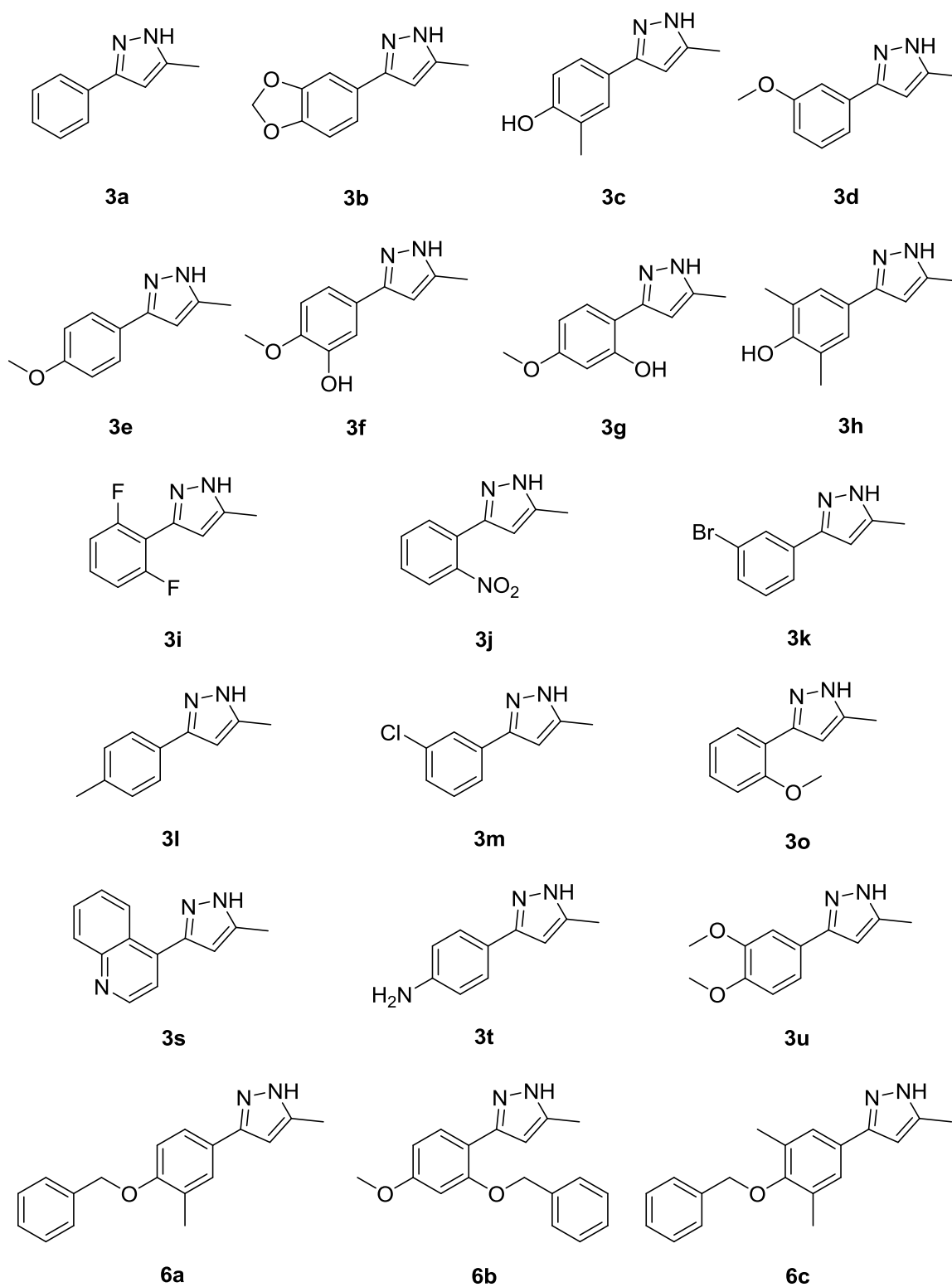


Figure 2. Synthesised 5-methyl-3-aryl-1H-pyrazoles.

**Pyrazole FRET Assay
Against BRD4 BD1 at 1 mM**

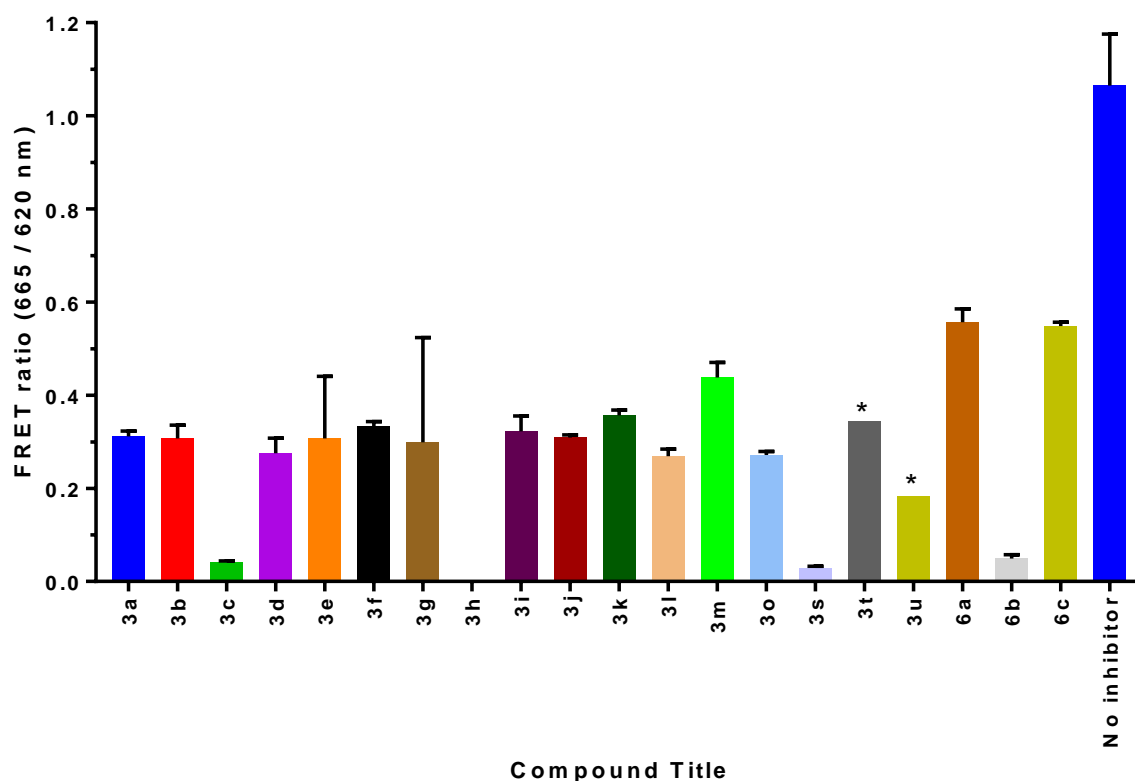


Figure 3. FRET-based assay data of substituted 5-methyl-3-aryl-1*H*-pyrazoles against BRD4 BD1. Assays carried out by Dr. Ian Jennings. Unless stated otherwise, all results of means are $n = 2$. Error bars represent the standard deviation.* $n=1$

Table 1. Inhibitory activity of selected 5-methyl-3-aryl-1*H*-pyrazoles.

Compound	IC ₅₀ ($\mu\text{M} \pm \text{SD}$) ^a	LE (kcal/mol NHA) ^b
3a	1248 \pm 156	0.33
3c	108 \pm 12	0.39
3h	26.7 \pm 6.6	0.42
3s	67.4 \pm 0.9	0.36
3u	452 \pm 39	0.29
6c	155 \pm 10	0.24

Assays carried out by Dr. Ian Jennings. ^aUnless stated otherwise, all results of means are $n =$

2. ^bLigand efficiency = $1.37(-\log(\text{IC}_{50})) / \text{NHA}$. NHA, non-hydrogen atom.

4.2.3 X-ray Crystallography

We were successful in co-crystallizing **3h** with BRD4 BD1 (For videos, refer to Appendix O. For electron density maps, refer to Appendix P). The many X-ray co-crystal structures that have been solved are typically characterized by the ligand occupying an K-ac mimetic pose with canonical hydrogen bonds between the amide of Asn140 and the water-mediated hydrogen bond to Tyr97 while the acetyl methyl group projects towards a network of water molecules lining the pocket. To our surprise, the methyl pyrazole was not bound in the expected K-ac pose but rather the dimethylphenol moiety acted as the K-ac mimetic. The hydroxyl group formed the key hydrogen bonds and one of the methyl groups approached the water pocket.

There are two considerations to take with this observation. The first is that this is not the first instance of a fragment possessing two potential binding modes. In 2011, Hewings et al.³⁹ tested a fragment possessing a quinazolinone and dimethylisoxazole. Their docking studies theorised that both components could act as K-ac mimetics and subsequent efforts by other groups have shown both can capably serve as inhibitors in their own right.^{20, 40-42}

Secondly, while this binding mode was initially a surprise, the dimethylphenol moiety has been recently exemplified as an K-ac mimetic in the BRD4 inhibitor, **FL-411** bound to BRD4 BD1 (PDB: 4ZW1).⁴³ We overlaid **FL-411** with **3h** and found two similar sets of interactions with BRD4 BD1 (Figure 4). The first set of interactions involved the dimethylphenol moieties of both compounds superimposing precisely (RMS = 0.66 Å). For the second set, there is some commonality between the pyrazole of **3h** and the pyrimidone of **FL-411**. The pyrazole interacts with the backbone of Pro82 and the sidechain of Gln85 through water-mediated hydrogen bonds. The pyrimidone nitrogen of **FL-411** interacts directly with Pro82 while the carbonyl displaces the water molecule responsible for the aforementioned interactions and forms a direct

hydrogen bond with Gln85, while creating additional water-mediated hydrogen bonds to the sidechains of Pro86 and Asp88.

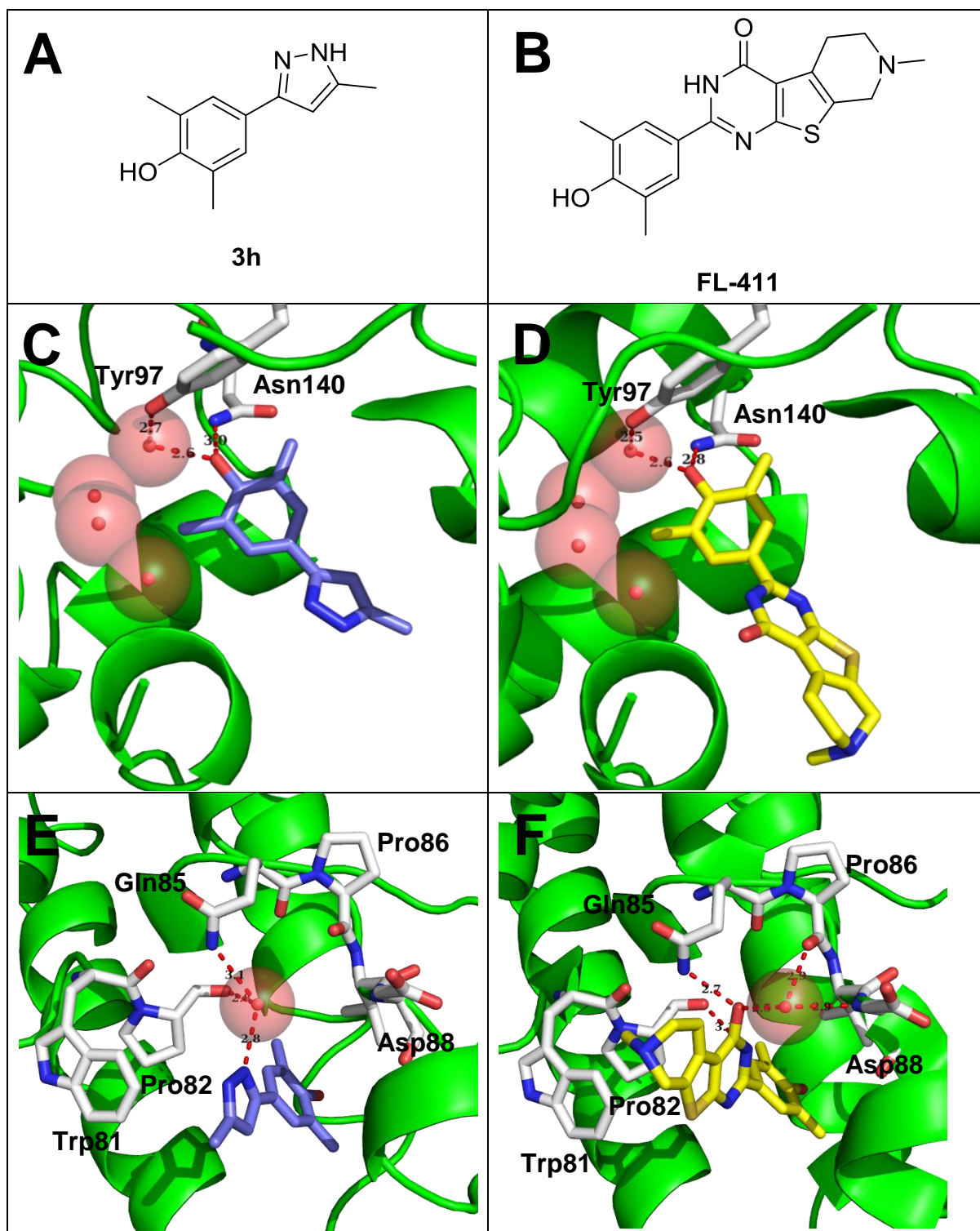


Figure 4. Comparison of X-ray crystal structures of dimethylphenols bound to BRD4 BD1. [A, C, E] **3h** (slate, resolution: 1.36 Å). [B, D, F] **FL-411** (yellow, PDB: 4ZW1). [A, B] Chemical structures. [C, D] Binding site. Pro86, Val87 and Asp88 were hidden for better visualisation. [E, F] Unique bonds formed by the heterocycles. Water molecules shown as red spheres. Distances in Å, highlighted by red dashes. Crystal structures developed by Dr. Ian Jennings and Dr. Olga Ilyichova.

4.3 Conclusion and Future Directions

In conclusion, we have applied the use of a poised fragment-based synthetic scheme for the creation of 5-methyl-3-aryl-1*H*-pyrazoles. This strategy has provided an effective route to analogues, exemplified in a focused library of 21 compounds with varying substituents. In some cases, a protecting group strategy was included which was successful and efficient. Assay work carried out on these compounds revealed two potent and ligand efficient fragments (**3h** and **3s**) for BRD4 BD1.

Our crystallographic work on **3h** revealed an unusual binding pose in that the dimethylphenol acted as another potential mimetic of K-ac instead of the pyrazole. Regardless, this work should provide further encouragement to pursue both the dimethylphenol and 5-methyl-3-aryl-1*H*-pyrazole as mimetic fragments with subsequent elaboration and optimization of these fragments into selective bromodomain inhibitors.

Experimental

^1H and ^{13}C Nuclear Magnetic Resonance spectra were conducted on a Bruker Advance III Nanobay 400 MHz spectrometer coupled to the BACS 60 automatic sample changer and obtained at 400.1 MHz and 100.6 MHz respectively. All spectra were processed using MestReNova 6.0 software. The chemical shifts of all ^1H were measured relative to the expected solvent peaks of the respective NMR solvents; CDCl_3 , 7.26; MeOD, 3.31; DMSO: 2.50. The chemical shifts of all ^{13}C were measured relative to the expected solvent peaks of the respective NMR solvents; CDCl_3 , 77.2; MeOD, 49.0; DMSO, 39.5. The data for all spectra are reported in the following format: chemical shift (integration, multiplicity, coupling constant, assignment). Multiplicity is defined as; s = singlet, d= doublet, t = triplet, dd = doublet of doublets, td = triplet of doublets, tt = triplet of triplets, ddd = doublet of doublet of doublets, m = multiplet. Coupling constants are applied as J in Hertz (Hz). For ^1H and ^{13}C spectra, refer to Appendix Q.

All HRMS analyses were done on an Agilent 6224 TOF LC/MS Mass Spectrometer coupled to an Agilent 1290 Infinity (Agilent, Palo Alto, CA). All data were acquired and reference mass corrected via a dual-spray electrospray ionisation (ESI) source. Each scan or data point on the Total Ion Chromatogram (TIC) is an average of 13,700 transients, producing a spectrum every second. Mass spectra were created by averaging the scans across each peak and background subtracted against the first 10 seconds of the TIC. Acquisition was performed using the Agilent Mass Hunter Data Acquisition software version B.05.00 Build 5.0.5042.2 and analysis was performed using Mass Hunter Qualitative Analysis version B.05.00 Build 5.0.519.13.

All LCMS analyses were carried out on an Agilent 6100 Series Single Quad LC/MS coupled with an Agilent 1200 Series HPLC, 1260 Infinity G1312B Binary pump, 1260 Infinity G1367E 1260 HiP ALS autosampler and 1290 Infinity G4212A 1290 DAD detector. The liquid

chromatography conditions were: reverse phase HPLC analysis fitted with a Luna C8(2) 5 μ L 50 X 4.6mm 100 \AA at a temperature of 30 $^{\circ}$ C. The sample injection volume was 5 μ L, which was run in 0.1% formic acid in acetonitrile at a gradient of 5-100% over 10 minutes. Detection methods were either 254 nm or 214 nm. The mass spectrum conditions were: Quadrupole ion source with Multimode-ES. The drying gas temperature was 300 $^{\circ}$ C and the vaporizer temperature was 200 $^{\circ}$ C. The capillary voltage in positive mode was 2000V, while in negative mode, the capillary voltage was 4000V. The scan range was 100-1000 m/z with a step size of 0.1 second over 10 minutes.

TLCs were carried on Merck TLC Silica gel 60 F₂₅₄ plates using the appropriate mobile phase. Purification by column chromatography was conducted with Davisil Chromatographic Silica LC60A (40-63 micron) using the specified mobile phases.

Purification on reverse-phase HPLC was done on a Waters Delta Prep 2000 Prep HPLC System that was fitted with a Waters Delta Prep 2000 Pump and Controller. Samples were injected into a Waters Prep Rack with Manual Injector, which were run through a Luna C8(2) 10 μ L 50 X 21.20mm 100 \AA and Waters 486 Tunable Absorbance Detector. The conditions were: Solvent A (0.1% TFA in H₂O) and Solvent B (0.1% TFA in CH₃CN), with a gradient of 0-80% Solvent B over a 20-minute period.

Compound purity was determined using an Agilent 1260 Infinity Analytical HPLC (1260 Infinity G1322A Degasser, 1260 Infinity G1312B Binary pump, G1367E HiP ALS autosampler, 1260 Infinity G1316A Thermostatted Column Compartment, and 1260 Infinity G4212B DAD detector. The liquid chromatography conditions were: reverse phase HPLC analysis fitted with a Zorbax Eclipse Plus C18 Rapid Resolution 4.6 X 100 mm 3.5-Micron. The sample injection volume was 1 μ L, which was run in Solvent A (0.1% TFA in H₂O) and Solvent B (0.1% TFA in CH₃CN), with a gradient of 5-100% Solvent B over a 10-minute

period. All compounds submitted for assays and X-ray crystallography studies were assessed for purity of 95% or greater on 214 nm and 254 nm.

The IC₅₀s were measured using a Fluorescence Resonance Energy Transfer (FRET) assay, which was carried out based on the protocol developed by CisBio Assay, France. The assay consists of a europium (Eu³⁺) cryptate-conjugated antibody attached to glutathione *S*-transferase (GST) fused to BRD4 BD1 (49-170) and Streptavidin-D2 bound to biotin which is attached to a Histone H4 peptide, SGRG-K(Ac)-GG-K(Ac)-GLG-K(Ac)-GGAK(Ac)-RHRKVGG-K (Biotin). Both Streptavidin-D2 and the Eu³⁺ cryptate-conjugated antibody were purchased from CisBio Assays. In the absence of inhibitors, the Histone H4 peptide is bound to BRD4 BD1. When both are in close proximity, a 337 nm laser light activates the Eu³⁺ donor and emits at 620 nm, which causes D2 to fluoresce at 665 nm. In the presence of a ligand, this reaction is interrupted. The assays were performed in 384-well small volume microtiter plates. The serially diluted small molecule inhibitors were added to a buffer mixture with a final concentration of 1% DMSO. The final buffer concentrations were 10 nM of GST-BRD4 BD1, 40 nM of Histone H4 peptide, 5 nM of Eu³⁺ cryptate-conjugated GST-antibody, 6.25 nM Streptavidin-D2, 50 mM Hepes, 50 mM NaCl, 0.5 mM CHAPS, 400 mM KF, 0.01% BSA, pH 7.5. After mixing and incubation at room temperature for at least 1.5 hours, the plates were measured in a PheraStar plate reader (BMG Labtech) (excitation: 337 nm with 10 flashes; emission: 620 and 665 nm).

X-ray crystal structures were obtained using a 6-His tagged bromodomain, BRD4 BD1, which was expressed in *E. coli* and purified using Ni-agarose chromatography. The 6-His tag was then removed by TEV protease digestion. The bromodomain was purified using gel filtration chromatography using a Superdex-75, 16/60 column (GE Healthcare) in a buffer containing 50 mM Hepes pH 7.5, 0.3 M NaCl and 5% glycerol. The concentrated BRD4 BD1 protein (17

mg/ml) was then incubated with 50 mM of the ligand at 40 °C for 16h. The final ligand concentration used in the hanging drop was 5 mM. Crystals were obtained using the hanging drop method in 24-well plates using 1 µl drops of protein and the reservoir solution containing 0.2 M NaNO₃, PEG-3350 (35%) and ethylene glycol (6% v/v) concentrations. This was then flash frozen in liquid nitrogen. All datasets were collected at the Australian Synchrotron on MX1 and MX2 beamlines.⁴⁴ Datasets were merged and scaled using *MOSFLM*⁴⁵ and *AIMLESS*⁴⁶ from the CCP4 suite.⁴⁷ 5% of reflections in each dataset were flagged for calculation of R_{free}. A summary of statistics is provided in Appendix R. Molecular replacement was performed with *Phaser*⁴⁸ using a previously solved structure of BRD4 as a search model (PDB: 5DW2). The final structures were obtained after several rounds of manual refinement using *Coot*⁴⁹ and refinement with *phenix.refine*.⁵⁰

Preparation of Morpholinium Trifluoroacetate – In a 100 mL round-bottom flask, morpholine (3.01 g, 34.4 mmol) was weighed out and dissolved in diethyl ether (60 mL). Trifluoroacetic acid (2.81 mL, 37.9 mmol) was dissolved in a 1:1 mixture of n-pentane and diethyl ether (30 mL), and then slowly added dropwise to the morpholine solution at 0 °C. This was left to stir at 0 °C for 1 hour, where a white precipitate formed. After this time, the precipitate was filtered from the solvent under vacuum and 6.35 g of a white solid was collected.

General Procedure for Aldol Condensation – The selected benzaldehydes were weighed in a carousel vessel and dissolved in acetone (5 mL). Morpholinium trifluoroacetate (25 mol %) was added and the mixture was sealed and stirred at 75 °C, with TLC used to monitor the reaction progress until completion. The mixture was quenched with saturated aqueous NaHCO₃ and washed with ethyl acetate three times. The organic layers were collected, combined and dried with MgSO₄. The solution was filtered and concentrated via rotary evaporation to afford

the α,β -unsaturated ketones. Unless stated otherwise, the ketones were taken to the next step without further purification.

(E)-4-phenylbut-3-en-2-one (**2a**) – Acquired 265 mg (36%) as a white solid from 531 mg of benzaldehyde (**1a**). $^1\text{H NMR}$ (400 MHz, CDCl_3) δ 7.54 (m, 3H), 7.45 – 7.36 (m, 3H), 6.72 (d, $J = 16.3$ Hz, 1H), 2.39 (s, 3H) ppm.

(E)-4-(benzo[*d*][1,3]dioxo-5-yl)but-3-en-2-one (**2b**) – Acquired 162 mg (85%) as a white solid from 150 mg of benzo[*d*][1,3]dioxole-5-carbaldehyde (**1b**). $^1\text{H NMR}$ (400 MHz, CDCl_3) δ 7.40 (d, $J = 16.2$ Hz, 1H), 7.02 (m, 2H), 6.80 (d, $J = 7.9$ Hz, 1H), 6.53 (d, $J = 16.2$ Hz, 1H), 6.00 (s, 2H), 2.33 (s, 3H) ppm.

(E)-4-(4-hydroxy-3-methylphenyl)but-3-en-2-one (**2c**) – Acquired 167 mg (94%) as an orange/brown solid from 136 mg of 4-hydroxy-3-methylbenzaldehyde (**1c**). $^1\text{H NMR}$ (400 MHz, CDCl_3) δ 7.45 (d, $J = 16.2$ Hz, 1H), 7.37 – 7.27 (m, 2H), 6.80 (d, $J = 8.3$ Hz, 1H), 6.60 (d, $J = 16.2$ Hz, 1H), 2.36 (s, 3H), 2.27 (s, 3H) ppm.

(E)-4-(3-methoxyphenyl)but-3-en-2-one (**2d**) – Acquired 164 mg (93%) as a yellow oil from 136 mg of 3-methoxybenzaldehyde (**1d**). $^1\text{H NMR}$ (400 MHz, CDCl_3) δ 7.47 (d, $J = 16.3$ Hz, 1H), 7.31 (t, $J = 7.9$ Hz, 1H), 7.13 (d, $J = 7.6$ Hz, 1H), 7.07 – 7.04 (m, 1H), 6.95 (m, 1H), 6.70 (d, $J = 16.3$ Hz, 1H), 3.83 (s, 3H), 2.38 (s, 3H) ppm.

(E)-4-(4-methoxyphenyl)but-3-en-2-one (**2e**) – Acquired 155 mg (88%) as a yellow solid from 136 mg of 4-methoxybenzaldehyde (**1e**). $^1\text{H NMR}$ (400 MHz, CDCl_3) δ 7.48 (m, 3H, ArH), 6.91 (d, $J = 8.8$ Hz, 2H), 6.60 (d, $J = 16.2$ Hz, 1H), 3.84 (s, 3H), 2.36 (s, 3H) ppm.

(E)-4-(3-hydroxy-4-methoxyphenyl)but-3-en-2-one (**2f**) – Acquired 181 mg (94%) as a yellow solid from 152 mg of 3-hydroxy-4-methoxybenzaldehyde (**1f**). $^1\text{H NMR}$ (400 MHz, CDCl_3) δ

7.40 (d, $J = 16.2$ Hz, 1H), 7.12 (d, $J = 2.1$ Hz, 1H), 7.01 (m, 1H), 6.81 (d, $J = 8.3$ Hz, 1H), 6.54 (d, $J = 16.2$ Hz, 1H), 3.87 (s, 3H), 2.32 (s, 3H) ppm.

(E)-4-(4-hydroxy-3,5-dimethylphenyl)but-3-en-2-one (**2h**) – Acquired 179 mg (94%) as an orange solid from 166 mg of 4-hydroxy-3,5-dimethylbenzaldehyde (**1h**). $^1\text{H NMR}$ (400 MHz, CDCl_3) δ 7.43 (d, $J = 16.2$ Hz, 1H), 7.18 (s, 2H), 6.59 (d, $J = 16.2$ Hz, 1H), 2.35 (s, 3H), 2.27 (s, 6H) ppm.

(E)-4-(2,6-difluorophenyl)but-3-en-2-one (**2i**) – Acquired 151mg (83%) as a colourless oil from 142 mg of 2,6-difluorobenzaldehyde (**1i**). $^1\text{H NMR}$ (400 MHz, CDCl_3) δ 7.60 (d, $J = 16.7$ Hz, 1H), 7.36 – 7.27 (m, 1H), 7.05 – 6.89 (m, 3H), 2.39 (s, 3H) ppm.

(E)-4-(2-nitrophenyl)but-3-en-2-one (**2j**) – Acquired 98.9 mg (52%) as a brown oil by column chromatography (Mobile phase: 15% EtOAc in petroleum benzene) from 151 mg of 2-nitrobenzaldehyde (**1j**). $^1\text{H NMR}$ (400 MHz, CDCl_3) δ 8.02 (dd, $J = 8.4, 0.7$ Hz, 1H), 7.93 (d, $J = 16.2$ Hz, 1H), 7.69 – 7.58 (m, 2H), 7.57 – 7.48 (m, 1H), 6.54 (d, $J = 16.2$ Hz, 1H), 2.38 (s, 3H) ppm.

(E)-4-(3-bromophenyl)but-3-en-2-one (**2k**) – Acquired 129 mg (57%) as a yellow oil from 185 mg of 3-bromobenzaldehyde (**1k**). $^1\text{H NMR}$ (400 MHz, CDCl_3) δ 7.69 (m, 1H), 7.52 (m, 1H), 7.49 – 7.39 (m, 2H), 7.27 (m, 1H), 6.70 (d, $J = 16.2$ Hz, 1H), 2.38 (s, 3H) ppm.

(E)-4-(*p*-tolyl)but-3-en-2-one (**2l**) – Acquired 156 mg (97%) as a yellow oil from 120 mg of 4-methylbenzaldehyde (**1l**). $^1\text{H NMR}$ (400 MHz, CDCl_3) δ 7.49 (d, $J = 16.3$ Hz, 1H), 7.44 (d, $J = 8.2$ Hz, 2H), 7.21 (d, $J = 8.0$ Hz, 2H), 6.68 (d, $J = 16.3$ Hz, 1H), 2.38 (s, 6H) ppm.

(E)-4-(3-chlorophenyl)but-3-en-2-one (**2m**) – Acquired 172 mg (95%) as a yellow oil from 141 mg of 3-chlorobenzaldehyde (**1m**). $^1\text{H NMR}$ (400 MHz, CDCl_3) δ 7.53 (t, $J = 1.8$ Hz, 1H), 7.47 – 7.31 (m, 4H), 6.71 (d, $J = 16.3$ Hz, 1H), 2.38 (s, 3H) ppm.

(*E*)-4-(2-methoxyphenyl)but-3-en-2-one (**2o**) – Acquired 167 mg (95%) as a yellow solid from 136 mg of 2-methoxybenzaldehyde (**1o**). ¹H NMR (400 MHz, CDCl₃) δ 7.87 (d, *J* = 16.5 Hz, 1H), 7.53 (dd, *J* = 7.7, 1.6 Hz, 1H), 7.35 (m, 1H), 7.02 – 6.85 (m, 2H), 6.74 (d, *J* = 16.5 Hz, 1H), 3.88 (s, 3H), 2.37 (s, 3H) ppm.

(*E*)-4-(2-methoxy-5-nitrophenyl)but-3-en-2-one (**2q**) – Acquired 62.3 mg (28%) as a white solid by column chromatography (Mobile phase: 15% EtOAc in petroleum benzine) from 181 mg of 2-methoxy-5-nitrobenzaldehyde (**1q**). ¹H NMR (400 MHz, CDCl₃) δ 8.44 (d, *J* = 2.8 Hz, 1H), 8.26 (dd, *J* = 9.1, 2.8 Hz, 1H), 7.80 (d, *J* = 16.4 Hz, 1H), 7.01 (d, *J* = 9.2 Hz, 1H), 6.85 (d, *J* = 16.4 Hz, 1H), 4.02 (s, 3H), 2.40 (s, 3H) ppm.

(*E*)-4-(quinolin-4-yl)but-3-en-2-one (**2s**) – Acquired 125 mg (63%) as a white solid by column chromatography (Mobile phase: 15% EtOAc in petroleum benzine) from 157 mg of quinolone-4-carbaldehyde (**1s**). ¹H NMR (400 MHz, CDCl₃) δ 8.90 (d, *J* = 4.5 Hz, 1H), 8.20 (d, *J* = 16.1 Hz, 1H), 8.11 (m, 2H), 7.74 (m, 1H), 7.60 (m, 1H), 7.50 (d, *J* = 4.5 Hz, 1H), 6.86 (d, *J* = 16.0 Hz, 1H), 2.45 (s, 3H) ppm.

(*E*)-4-(4-aminophenyl)but-3-en-2-one (**2t**) – Acquired 145 mg (90%) as a yellow solid from 121 mg of 4-aminobenzaldehyde (**1t**). ¹H NMR (400 MHz, CDCl₃) δ 7.42 (d, *J* = 16.2 Hz, 1H), 7.35 (d, *J* = 8.4 Hz, 2H), 6.65 (d, *J* = 8.6 Hz, 2H), 6.54 (d, *J* = 16.1 Hz, 1H), 4.03 (s, 2H), 2.33 (s, 3H) ppm.

(*E*)-4-(3,4-dimethoxyphenyl)but-3-en-2-one (**2u**) – Acquired 207 mg (99%) as a white solid by column chromatography (Mobile phase: 15% EtOAc in petroleum benzine) from 166 mg of 3,4-dimethoxybenzaldehyde (**1u**). ¹H NMR (400 MHz, CDCl₃) δ 7.44 (d, *J* = 16.2 Hz, 1H), 7.11 (dd, *J* = 8.4, 2.0 Hz, 1H), 7.05 (d, *J* = 2.0 Hz, 1H), 6.86 (d, *J* = 8.3 Hz, 1H), 6.58 (d, *J* = 16.2 Hz, 1H), 3.90 (s, 6H), 2.35 (s, 3H) ppm.

(E)-4-(4-(benzyloxy)-3-methylphenyl)but-3-en-2-one (**5a**) – Acquired 398 mg (87%) by column chromatography (Mobile phase: 15% EtOAc in petroleum benzine) as a yellow solid from 387 mg of **4a**. ¹H NMR (400 MHz, CDCl₃) δ 7.50 – 7.31 (m, 9H), 6.88 (d, *J* = 8.4 Hz, 1H), 6.61 (d, *J* = 16.2 Hz, 1H), 5.12 (s, 2H), 2.36 (s, 3H), 2.31 (s, 3H) ppm. ¹³C NMR (101 MHz, CDCl₃) δ 198.5, 159.1, 143.6, 136.9, 130.6, 128.72, 128.10, 128.09, 127.92, 127.18, 126.95, 125.0, 111.6, 70.0, 27.5, 16.6 ppm.

(E)-4-(2-(benzyloxy)-4-methoxyphenyl)but-3-en-2-one (**5b**) – Acquired 338 mg (64%) by column chromatography (Mobile phase: 20% EtOAc in petroleum benzine) as a yellow solid from 455 mg of **4b**. ¹H NMR (400 MHz, CDCl₃) δ 7.87 (d, *J* = 16.4 Hz, 1H), 7.50 (d, *J* = 8.3 Hz, 1H), 7.46 – 7.31 (m, 5H), 6.69 (d, *J* = 16.4 Hz, 1H), 6.57 – 6.48 (m, 2H), 5.13 (s, 2H), 3.80 (s, 3H), 2.31 (s, 3H) ppm. ¹³C NMR (101 MHz, CDCl₃) δ 199.1, 163.0, 158.9, 138.7, 136.5, 129.9, 128.77, 128.23, 127.3, 125.6, 116.9, 106.1, 100.0, 70.6, 55.5, 27.2 ppm.

(E)-4-(4-(benzyloxy)-3,5-dimethylphenyl)but-3-en-2-one (**5c**) – Acquired 411 mg (82%) by column chromatography (Mobile phase: 15% EtOAc in petroleum benzine) as a custard yellow solid from 428 mg of **4c**. ¹H NMR (400 MHz, CDCl₃) δ 7.47 (m, 6H), 7.24 (d, *J* = 0.4 Hz, 2H), 6.63 (d, *J* = 16.2 Hz, 1H), 4.84 (s, 2H), 2.36 (s, 3H), 2.31 (s, 6H) ppm. ¹³C NMR (101 MHz, CDCl₃) δ 198.5, 158.1, 143.4, 137.3, 132.0, 130.21, 129.19, 128.68, 128.26, 127.94, 126.3, 74.3, 27.6, 16.6 ppm.

(E)-4-(2-(benzyloxy)-5-nitrophenyl)but-3-en-2-one (**5d**) – Acquired 402 mg (72%) by column chromatography (Mobile phase: 25% EtOAc in petroleum benzine) as a cream solid from 484 mg of **4d**. ¹H NMR (400 MHz, CDCl₃) δ 8.45 (d, *J* = 2.8 Hz, 1H), 8.21 (dd, *J* = 9.1, 2.8 Hz, 1H), 7.86 (d, *J* = 16.4 Hz, 1H), 7.49 – 7.31 (m, 5H), 7.05 (d, *J* = 9.2 Hz, 1H), 6.87 (d, *J* = 16.4 Hz, 1H), 5.29 (s, 2H), 2.37 (s, 3H) ppm. ¹³C NMR (101 MHz, CDCl₃) δ 198.0, 161.6, 141.6, 135.71, 135.04, 129.71, 128.97, 128.71, 127.26, 126.83, 124.65, 123.94, 112.5, 71.3, 28.0 ppm.

General Procedure for Pyrazole Formation – In a 10 mL round-bottom flask, the α,β -unsaturated ketones were weighed out. Tetrabutylammonium bromide (2 mol. eq.), sodium hydroxide (2 mol. eq.) and *p*-toluenesulfonyl hydrazide (1.5 mol. eq.) were weighed and added to the flask, and dissolved in water (4 mL). The mixture was stirred at 80 °C overnight. After stirring, the mixture was cooled to room temperature before quenching with brine (15 mL) and washing with ethyl acetate (3 x 25 mL). The organic layers were collected, combined, dried with MgSO₄, filtered and concentrated under reduced pressure. The crudes were run through silica gel chromatography to remove the TBAB, then reverse-phase HPLC to afford the respective 5-methyl-3-phenyl-1*H*-pyrazoles.

5-methyl-3-phenyl-1H-pyrazole (3a) – Acquired 209 mg (73%) as a white solid from 265 mg of **2a**. ¹H NMR (400 MHz, CDCl₃) δ 9.67 (br s, 1H), 7.74 – 7.68 (m, 2H), 7.40 – 7.34 (m, 2H), 7.34 – 7.27 (m, 1H), 6.34 (s, 1H), 2.28 (s, 3H) ppm. ¹³C NMR (101 MHz, CDCl₃) δ 150.1, 143.3, 132.6, 128.80, 127.94, 125.8, 102.2, 11.8 ppm. **ESI-MS**: *m/z* 159.1 [M+H]⁺; **HR-MS**: *m/z* calcd. for C₁₀H₁₀N₂ [M+H]⁺: 158.0044; found 158.0049. **HPLC** (PP gradient, MeOH): 4.74 min.

3-(benzo[d][1,3]dioxo-5-yl)-5-methyl-1H-pyrazole (3b) – Acquired 28.4 mg (27%) as a white solid from 98.2 mg of **2b**. ¹H NMR (400 MHz, CDCl₃) δ 9.29 (br s, 1H), 7.20 – 7.14 (m, 2H), 6.79 (d, *J* = 8.6 Hz, 1H), 6.23 (s, 1H), 5.96 (s, 2H), 2.28 (s, 3H) ppm. ¹³C NMR (101 MHz, CDCl₃) δ 149.9, 148.1, 147.5, 143.0, 127.0, 119.5, 108.6, 106.5, 101.89, 101.20, 11.8 ppm. **ESI-MS**: *m/z* 203.0 [M+H]⁺; **HR-MS**: *m/z* calcd. for C₁₁H₁₀N₂O₂ [M+H]⁺: 202.0740; found 202.0745. **HPLC** (PP gradient, MeOH): 4.76 min.

3-(3-methoxyphenyl)-5-methyl-1H-pyrazole (3d) – Acquired 14.5 mg (18%) as a clear oil from 77.4 mg of **2d**. ¹H NMR (400 MHz, CDCl₃) δ 10.53 (br s, 1H), 7.37 – 7.30 (m, 1H), 7.27 – 7.24 (m, 2H), 6.96 (ddd, *J* = 8.3, 2.4, 1.1 Hz, 1H), 6.47 (s, 1H), 3.83 (s, 3H), 2.41 (s, 3H) ppm.

¹³C NMR (101 MHz, CDCl₃) δ 160.3, 147.9, 144.5, 130.4, 129.3, 118.9, 116.2, 111.6, 103.8, 55.5, 11.5. **ESI-MS**: *m/z* 189.1 [M+H]⁺. **HR-MS**: *m/z* calcd. for C₁₁H₁₂N₂O [M+H]⁺: 188.0950; found 188.0949. **HPLC** (PP gradient, MeOH): 5.04 min.

3-(4-methoxyphenyl)-5-methyl-1H-pyrazole (3e) – Acquired 19.9 mg (23%) as a clear oil 81.4 mg of **2e**. **¹H NMR** (400 MHz, CDCl₃) δ 7.62 (d, *J* = 8.9 Hz, 2H), 6.94 (d, *J* = 8.9 Hz, 2H), 6.41 (s, 1H), 3.84 (s, 3H), 2.41 (s, 3H). **¹³C NMR** (101 MHz, CDCl₃) δ 161.4, 147.5, 144.5, 128.1, 120.0, 114.8, 103.1, 55.5, 11.5 ppm. **ESI-MS**: *m/z* 189.1 [M+H]⁺. **HR-MS**: *m/z* calcd. for C₁₁H₁₂N₂O [M+H]⁺: 188.0950; found 188.0951. **HPLC** (PP gradient, MeOH): 4.78 min.

2-methoxy-5-(5-methyl-1H-pyrazol-3-yl)phenol (3f) – Acquired 13.2 mg (11%) of an orange solid from 109 mg of **2f**. **¹H NMR** (400 MHz, MeOD) δ 7.21 (dd, *J* = 8.2, 2.2 Hz, 1H), 7.19 (d, *J* = 2.1 Hz, 1H), 7.01 (d, *J* = 8.3 Hz, 1H), 6.58 (s, 1H), 3.90 (s, 3H), 2.40 (s, 3H) ppm. **¹³C NMR** (101 MHz, MeOD) δ 150.6, 149.9, 148.3, 146.8, 119.2, 114.2, 113.0, 103.8, 56.5, 11.2 ppm. **ESI-MS**: *m/z* 205.1 [M+H]⁺. **HR-MS**: *m/z* calcd. for C₁₁H₁₂N₂O₂ [M+H]⁺: 204.0899; found 204.0902. **HPLC** (PP gradient, MeOH): 3.77 min.

3-(2,6-difluorophenyl)-5-methyl-1H-pyrazole (3i) – Acquired 21.4 mg (28%) as a white solid from 71.0mg of **2i**. **¹H NMR** (400 MHz, MeOD) δ 7.61 (tt, *J* = 8.4, 6.4 Hz, 1H), 7.26 – 7.19 (m, 2H), 6.85 (s, 1H), 2.52 (s, 3H) ppm. **¹³C NMR** (101 MHz, MeOD) δ 161.4 (dd, *J* = 252.6, 6.0 Hz), 147.0, 137.7, 134.1 (t, *J* = 10.9 Hz), 113.66 – 113.34 (m), 109.6 (t, *J* = 4.3 Hz), 11.0 ppm. **ESI-MS**: *m/z* 195.1 [M+H]⁺; **HR-MS**: *m/z* calcd. for C₁₀H₈F₂N₂ [M+H]⁺: 194.0656; found 194.0659. **HPLC** (PP gradient, MeOH): 5.40 min.

3-(2-nitrophenyl)-5-methyl-1H-pyrazole (3j) – Acquired 4.28 mg (8.3%) as a yellow oil from 48.4mg of **2j**. **¹H NMR** (400 MHz, CDCl₃) δ 7.77 (dd, *J* = 8.0, 1.0 Hz, 1H), 7.62 (dd, *J* = 7.7, 1.7 Hz, 1H), 7.59 (td, *J* = 7.5, 1.2 Hz, 1H), 7.52 – 7.46 (m, 1H), 6.78 (br s, 1H), 6.24 (s, 1H), 2.38 (s, 3H) ppm. **¹³C NMR** (101 MHz, CDCl₃) δ 149.1, 145.7, 142.3, 132.4, 131.2, 129.56,

125.78, 124.1, 105.3, 11.3 ppm. **ESI-MS**: m/z 204.1 $[M+H]^+$. **HR-MS**: m/z calcd. for $C_{10}H_9N_3O_2$ $[M+H]^+$: 203.0695; found 203.0698. **HPLC** (PP gradient, MeOH): 5.51 min.

3-(3-bromophenyl)-5-methyl-1H-pyrazole (3k) – Acquired 19.3 mg (34%) as a clear oil from 53.3 mg of **2k**. **1H NMR** (400 MHz, $CDCl_3$) δ 12.09 (br s, 1H), 7.79 (t, $J = 1.7$ Hz, 1H), 7.62 (ddd, $J = 7.8, 1.6, 1.0$ Hz, 1H), 7.52 (ddd, $J = 8.0, 1.9, 1.0$ Hz, 1H), 7.28 (t, $J = 8.0$ Hz, 1H), 6.47 (s, 1H), 2.43 (s, 3H) ppm. **^{13}C NMR** (101 MHz, $CDCl_3$) δ 146.9, 144.4, 133.0, 130.88, 130.44, 129.55, 125.0, 123.3, 104.0, 11.4 ppm. **ESI-MS**: m/z 237.0 $[(^{79}Br)M+H]^+$ and 239.0 $[(^{81}Br)M+H]^+$. **HR-MS**: m/z calcd. for $C_{10}H_9BrN_2$ $[M+H]^+$: 235.9949; found 235.9953. **HPLC** (PP gradient, MeOH): 6.29 min.

5-methyl-3-(p-tolyl)-1H-pyrazole (3l) – Acquired 50.0 mg (61%) as a white solid from 75.8 mg of **2l**. **1H NMR** (400 MHz, $CDCl_3$) δ 11.23 (br s, 1H), 7.56 (d, $J = 8.1$ Hz, 2H), 7.21 (d, $J = 8.3$ Hz, 2H), 6.42 (s, 1H), 2.38 (d, $J = 7.6$ Hz, 6H) ppm. **^{13}C NMR** (101 MHz, $CDCl_3$) δ 148.0, 144.6, 140.4, 130.0, 126.4, 125.3, 103.3, 21.5, 11.5 ppm. **ESI-MS**: m/z 173.2 $[M+H]^+$. **HR-MS**: m/z calcd. for $C_{11}H_{12}N_2$ $[M+H]^+$: 172.1000; found 172.1008. **HPLC** (PP gradient, MeOH): 5.44 min.

3-(3-chlorophenyl)-5-methyl-1H-pyrazole (3m) – Acquired 15.3 mg (20%) as a white solid from 71.5 mg of **2m**. **1H NMR** (400 MHz, $CDCl_3$) δ 7.63 – 7.60 (m, 1H), 7.54 (d, $J = 6.7$ Hz, 1H), 7.33 – 7.26 (m, 2H), 6.41 (s, 1H), 2.38 (s, 3H) ppm. **^{13}C NMR** (101 MHz, $CDCl_3$) δ 148.1, 143.9, 135.1, 131.8, 130.4, 129.3, 126.5, 124.4, 103.5, 11.4 ppm. **ESI-MS**: m/z 193.0 $[(^{35}Cl)M+H]^+$ and 195.0 $[(^{37}Cl)M+H]^+$; **HR-MS**: m/z calcd. for $C_{10}H_9ClN_2$ $[M+H]^+$: 192.0454; found 192.0458. **HPLC** (PP gradient, MeOH): 6.03 min.

3-(2-methoxyphenyl)-5-methyl-1H-pyrazole (3o) – Acquired 33.9 mg (41%) as a crystalline solid from 77.2 mg of **2n**. **1H NMR** (400 MHz, $CDCl_3$) δ 9.93 (br s, 1H), 7.64 (dd, $J = 7.7, 1.5$ Hz, 1H), 7.40 (ddd, $J = 8.3, 7.6, 1.7$ Hz, 1H), 7.09 – 7.00 (m, 2H), 6.56 (s, 1H), 4.02 (s, 3H),

2.42 (s, 3H) ppm. ^{13}C NMR (101 MHz, CDCl_3) δ 156.7, 144.4, 142.8, 131.5, 128.5, 121.3, 115.7, 111.9, 104.0, 55.9, 11.9 ppm. **ESI-MS**: m/z 189.1 $[\text{M}+\text{H}]^+$. **HR-MS**: m/z calcd. for $\text{C}_{11}\text{H}_{12}\text{N}_2\text{O}$ $[\text{M}+\text{H}]^+$: 188.0950; found 188.0954. **HPLC** (PP gradient, MeOH): 4.80 min.

3-(2-methoxy-5-nitrophenyl)-5-methyl-1H-pyrazole (3q) – Acquired 0.31 mg (1%) as a brown solid from 28.1 mg of **2q**. ^1H NMR (400 MHz, CDCl_3) δ 8.61 (d, $J = 2.7$ Hz, 1H), 8.20 (dd, $J = 9.1, 2.8$ Hz, 1H), 7.08 (d, $J = 9.2$ Hz, 1H), 6.58 (s, 1H), 4.09 (s, 3H), 2.37 (s, 3H) ppm. **ESI-MS**: m/z 234.1 $[\text{M}+\text{H}]^+$; **HR-MS**: m/z calcd. for $\text{C}_{11}\text{H}_{11}\text{N}_3\text{O}_3$ $[\text{M}+\text{H}]^+$: 233.0800; found 233.0804. **HPLC** (PP gradient, MeOH): 5.46 min.

4-(5-methyl-1H-pyrazol-3-yl)quinoline (3s) – Acquired 36.9 mg (58%) as a white solid from 60.4 mg of **2s**. ^1H NMR (400 MHz, MeOD) δ 9.26 (dd, $J = 8.7, 0.6$ Hz, 1H), 9.05 (d, $J = 5.7$ Hz, 1H), 8.20 (ddd, $J = 8.6, 1.1, 0.6$ Hz, 1H), 8.16 (d, $J = 5.8$ Hz, 1H), 8.13 – 8.08 (m, 1H), 7.95 – 7.89 (m, 1H), 6.84 (s, 1H), 2.46 (s, 3H) ppm. ^{13}C NMR (101 MHz, MeOD) δ 148.7, 147.2, 144.0, 141.6, 140.1, 133.7, 129.29, 128.39, 126.0, 121.5, 120.0, 106.6, 9.2 ppm. **ESI-MS**: m/z 210.1 $[\text{M}+\text{H}]^+$. **HR-MS**: m/z calcd. for $\text{C}_{13}\text{H}_{11}\text{N}_3$ $[\text{M}+\text{H}]^+$: 209.0953; found 209.0955. **HPLC** (PP gradient, MeOH): 4.06 min.

4-(5-methyl-1H-pyrazol-3-yl)aniline (3t) – Acquired 109 mg (66%) as a yellow oil from 152 mg of **2t**. ^1H NMR (400 MHz, MeOD) δ 7.81 (d, $J = 8.8$ Hz, 2H), 7.28 (d, $J = 8.8$ Hz, 2H), 6.55 (d, $J = 0.6$ Hz, 1H), 2.37 (s, 3H) ppm. ^{13}C NMR (101 MHz, MeOD) δ 150.3, 144.8, 128.4, 122.3, 103.3, 11.0 ppm. **ESI-MS**: m/z 210.1 $[\text{M}+\text{H}]^+$. **HR-MS**: m/z calcd. for $\text{C}_{10}\text{H}_{11}\text{N}_3$ $[\text{M}+\text{H}]^+$: 173.0953; found 173.0955. **HPLC** (PP gradient, MeOH): 4.06 min.

3-(3,4-dimethoxyphenyl)-5-methyl-1H-pyrazole (3u) – Acquired 116 mg (62%) as a yellow solid from 174 mg of **2u**. ^1H NMR (400 MHz, CDCl_3) δ 8.83 (br s, 1H), 7.27 (d, $J = 1.9$ Hz, 1H), 7.21 (dd, $J = 8.3, 2.0$ Hz, 1H), 6.84 (d, $J = 8.3$ Hz, 1H), 6.27 (s, 1H), 3.88 (s, 3H), 3.84 (s, 3H), 2.28 (s, 3H) ppm. ^{13}C NMR (101 MHz, CDCl_3) δ 150.03, 149.20, 149.00, 143.1, 125.7, 118.4,

111.3, 109.0, 101.7, 56.01, 55.90, 11.8 ppm. **ESI-MS**: m/z 219.0 $[M+H]^+$. **HR-MS**: m/z calc. for $C_{12}H_{14}N_2O_2$ $[M+H]^+$: 218.1055; found 218.1055. **HPLC** (PP gradient, MeOH): 4.22 min.

3-(4-(benzyloxy)-3-methylphenyl)-5-methyl-1H-pyrazole (6a) – Acquired 143 mg (38%) as a white solid from 360 mg of **5a**. **1H NMR** (400 MHz, $CDCl_3$) δ 7.52 – 7.46 (m, 2H), 7.46 – 7.31 (m, 5H), 6.90 (d, $J = 8.5$ Hz, 1H), 6.39 (s, 1H), 5.11 (s, 2H), 2.40 (s, 3H), 2.30 (s, 3H) ppm. **^{13}C NMR** (101 MHz, $CDCl_3$) δ 158.7, 147.5, 144.5, 136.8, 128.95, 128.74, 128.32, 128.12, 127.22, 125.5, 119.5, 111.8, 103.0, 70.1, 16.5, 11.4 ppm. **ESI-MS**: m/z 278.9 $[M+H]^+$. **HR-MS**: m/z calc. for $C_{18}H_{18}N_2O$ $[M+H]^+$: 278.1419; found 278.1420. **HPLC** (PP gradient, 1:1 $CH_3CN:H_2O$): 6.18 min.

3-(2-(benzyloxy)-4-methoxyphenyl)-5-methyl-1H-pyrazole (6b) – Acquired 74.5 mg (25%) as a white solid from 289 mg of **5b**. **1H NMR** (400 MHz, $CDCl_3$) δ 12.14 (br s, 1H), 7.56 (d, $J = 8.6$ Hz, 1H), 7.47 – 7.41 (m, 2H), 7.40 – 7.28 (m, 3H), 6.60 – 6.54 (m, 2H), 6.50 (s, 1H), 5.35 (s, 2H), 3.78 (s, 3H), 2.42 (s, 3H) ppm. **^{13}C NMR** (101 MHz, $CDCl_3$) δ 162.7, 157.3, 143.47, 143.11, 136.0, 129.81, 128.91, 128.51, 127.84, 108.5, 106.4, 104.0, 100.6, 71.0, 55.6, 11.6 ppm. **ESI-MS**: m/z 294.9 $[M+H]^+$. **HR-MS**: m/z calc. for $C_{18}H_{18}N_2O_2$ $[M+H]^+$: 294.1368; found 294.1370. **HPLC** (PP gradient, 1:1 $CH_3CN:H_2O$): 5.71 min.

3-(4-(benzyloxy)-3,5-dimethylphenyl)-5-methyl-1H-pyrazole (6c) – Acquired 150 mg (39%) as a white solid from 369 mg of **5c**. **1H NMR** (400 MHz, $CDCl_3$) δ 9.58 (br s, 1H), 7.52 – 7.46 (m, 2H), 7.44 – 7.32 (m, 5H), 6.31 (s, 1H), 4.82 (s, 2H), 2.31 (s, 3H), 2.29 (s, 6H) ppm. **^{13}C NMR** (101 MHz, $CDCl_3$) δ 157.0, 148.4, 144.4, 137.4, 132.1, 128.68, 128.20, 127.89, 127.13, 124.7, 103.1, 74.2, 16.5, 11.5 ppm. **ESI-MS**: m/z 292.9 $[M+H]^+$. **HR-MS**: m/z calc. for $C_{19}H_{20}N_2O$ $[M+H]^+$: 292.1576; found 292.1577. **HPLC** (PP gradient, 1:1 $CH_3CN:H_2O$): 6.38 min.

General Procedure for Phenol Protection – In a 10 mL round-bottom flask, the selected hydroxybenzaldehydes (2 mmol) were weighed out, along with K₂CO₃ (3 mol. eq.). DMF (1 mL)* was added and the mixture stirred at room temperature for 30 minutes. Benzyl bromide (1.2 mol. eq.) was added and the mixture was allowed to stir at room temperature overnight. After this time, the mixture was quenched with water (30 mL) and washed with EtOAc (3 x 30 mL). The organic layers were combined, washed with water (30 mL) and then brine (30 mL). The organic layer was dried with MgSO₄, filtered and concentrated via rotary evaporation to afford the crude products. The crudes were purified with column chromatography to afford the pure benzyl-protected benzaldehydes.

4-(benzyloxy)-3-methylbenzaldehyde (4a) – Acquired 410 mg (91%) as a clear oil from 272 mg of 4-hydroxy-3-methylbenzaldehyde (**1c**) (Mobile phase: 10% EtOAc in petroleum benzine). **¹H NMR** (400 MHz, CDCl₃) δ 9.86 (s, 1H), 7.76 – 7.65 (m, 2H), 7.50 – 7.30 (m, 5H), 6.99 (d, *J* = 8.3 Hz, 1H), 5.18 (s, 2H), 2.33 (s, 3H) ppm. **¹³C NMR** (101 MHz, CDCl₃) δ 191.3, 162.1, 136.5, 131.8, 130.68, 129.79, 128.80, 128.26, 128.14, 127.22, 111.1, 70.2, 16.5 ppm.

2-(benzyloxy)-4-methoxybenzaldehyde (4b) – Acquired 491 mg (99%) as a crystallized solid from 304 mg of 2-hydroxy-4-methoxybenzaldehyde (**1g**) (Mobile phase: 12% EtOAc in petroleum benzine). **¹H NMR** (400 MHz, CDCl₃) δ 10.39 (s, 1H), 7.89 – 7.79 (m, 1H), 7.50 – 7.30 (m, 5H), 6.60 – 6.49 (m, 2H), 5.14 (s, 2H), 3.83 (s, 3H) ppm. **¹³C NMR** (101 MHz, CDCl₃) δ 188.4, 166.2, 162.9, 136.1, 130.6, 128.86, 128.42, 127.41, 119.5, 106.3, 99.4, 70.6, 55.8 ppm.

4-(benzyloxy)-3,5-dimethylbenzaldehyde (4c) – Acquired 450 mg (94%) as a crystallized solid from 300 mg of 4-hydroxy-3,5-dimethylbenzaldehyde (**1h**) (Mobile phase: 8% EtOAc in petroleum benzine). **¹H NMR** (400 MHz, CDCl₃) δ 9.90 (s, 1H), 7.59 (s, 2H), 7.44 (m, 5H), 4.88 (s, 2H), 2.36 (s, 6H) ppm. **¹³C NMR** (101 MHz, CDCl₃) δ 191.8, 161.3, 137.0, 132.55, 132.40, 130.9, 128.77, 128.44, 128.01, 74.3, 16.7 ppm.

2-(benzyloxy)-5-nitrobenzaldehyde (4d) – Acquired 512 mg (99%) as a white solid from 334 mg of 2-hydroxy-5-nitrobenzaldehyde (**1p**) (Mobile phase: 15% EtOAc in petroleum benzene). ¹H NMR (400 MHz, CDCl₃) δ 10.50 (s, 1H), 8.69 (d, *J* = 2.9 Hz, 1H), 8.39 (dd, *J* = 9.2, 2.9 Hz, 1H), 7.48 – 7.35 (m, 5H), 7.20 (dd, *J* = 9.1, 4.7 Hz, 1H), 5.33 (s, 2H) ppm. ¹³C NMR (101 MHz, CDCl₃) δ 187.5, 164.7, 141.8, 130.6, 129.04, 128.94, 127.5, 124.96, 124.68, 113.5, 71.6, 29.7 ppm.

*2-hydroxy-5-nitrobenzaldehyde had to be dissolved in 4 mL DMF.

General Procedure for Phenol Deprotection – A 25 mL three-neck round-bottom flask with a magnetic stir-bar was charged with N₂. Palladium on carbon (10% w/w) was weighed, submerged in a minimum amount of dichloromethane and added to the flask. The benzyl-protected pyrazole was then dissolved in ethyl acetate and pipetted into the flask while keeping it under N₂. The flask was purged three more times with N₂, and then purged three times with H₂, to which the contents were left to stir. The progress of the reaction was monitored by LCMS and HPLC. After completion, the flask was purged with N₂ and the contents were filtered carefully through a glass microfiber filter paper under gentle vacuum. The filtered palladium catalyst was washed with dichloromethane, followed by ethyl acetate, and then quenched separately with H₂O while the filtrate was concentrated under reduced pressure to give the deprotected pyrazoles. Each pyrazole was deemed sufficiently pure by analytical HPLC, thus requiring no further purification.

2-methyl-4-(5-methyl-1H-pyrazol-3-yl)phenol (3c) – Acquired 21.7 mg (92%) as a yellow oil from 34.7 mg of **6a**. ¹H NMR (400 MHz, MeOD) δ 7.31 (d, *J* = 1.6 Hz, 1H), 7.23 (dd, *J* = 8.3, 2.1 Hz, 1H), 6.66 (d, *J* = 8.3 Hz, 1H), 6.14 (s, 1H), 2.17 (s, 3H), 2.11 (s, 3H) ppm. ¹³C NMR (101 MHz, MeOD) δ 155.3, 127.8, 124.48, 123.87, 114.3, 100.5, 14.9 ppm. **ESI-MS**: *m/z* 189.0

[M+H]⁺. **HR-MS**: *m/z* calc. for C₁₁H₁₂N₂O [M+H]⁺: 188.0950; found 188.0948. **HPLC** (PP gradient, MeOH): 4.02 min.

5-methoxy-2-(5-methyl-1H-pyrazol-3-yl)phenol (3g) – Acquired 14.6 mg (72%) as a white solid from 29.2 mg of **6b**. **¹H NMR** (400 MHz, DMSO) δ 11.19 (br s, 1H), 7.52 (d, *J* = 9.0 Hz, 1H), 6.50 – 6.42 (m, 3H), 3.73 (s, 3H), 2.28 (s, 3H) ppm. **¹³C NMR** (101 MHz, DMSO) δ 159.7, 127.3, 110.3, 105.6, 101.3, 55.0 ppm. **ESI-MS**: *m/z* 205.0 [M+H]⁺. **HR-MS**: *m/z* calc. for C₁₁H₁₂N₂O₂ [M+H]⁺: 204.0899; found 204.0899. **HPLC** (PP gradient, MeOH): 4.32 min.

2,6-dimethyl-4-(5-methyl-1H-pyrazol-3-yl)phenol (3h) – Acquired 31.9 mg (99%) as a white solid from 45.3 mg of **6c**. **¹H NMR** (400 MHz, MeOD) δ 7.16 (s, 2H), 6.14 (s, 1H), 2.16 (s, 3H), 2.13 (s, 6H) ppm. **¹³C NMR** (101 MHz, MeOD) δ 153.2, 125.43, 124.46, 100.6, 15.3, 10.5 ppm. **ESI-MS**: *m/z* 203.0 [M+H]⁺. **HR-MS**: *m/z* calc. for C₁₂H₁₄N₂O [M+H]⁺: 202.1106; found 202.1105. **HPLC** (PP gradient, MeOH): 4.22 min.

References

1. Shuker SB, Hajduk PJ, Meadows RP, Fesik SW. Discovering high-affinity ligands for proteins: SAR by NMR. *Science*. 1996;274(5292):1531-4.
2. Schultes S, de Graaf C, Haaksma EEJ, de Esch IJP, Leurs R, Krämer O. Ligand efficiency as a guide in fragment hit selection and optimization. *Drug Discov Today Technol*. 2010;7(3):e147-202.
3. Strahl BD, Allis CD. The language of covalent histone modifications. *Nature*. 2000;403(6765):41-5.
4. Huang B, Yang XD, Zhou MM, Ozato K, Chen LF. Brd4 coactivates transcriptional activation of NF-kappaB via specific binding to acetylated RelA. *Mol Cell Biol*. 2009;29(5):1375-87.
5. Schroder S, Cho S, Zeng L, Zhang Q, Kaehlecke K, Mak L, et al. Two-pronged binding with bromodomain-containing protein 4 liberates positive transcription elongation factor b from inactive ribonucleoprotein complexes. *J Biol Chem*. 2012;287(2):1090-9.
6. Alekseyenko AA, Walsh EM, Wang X, Grayson AR, Hsi PT, Kharchenko PV, et al. The oncogenic BRD4-NUT chromatin regulator drives aberrant transcription within large topological domains. *Genes Dev*. 2015;29(14):1507-23.
7. Yan Y, Yang FQ, Zhang HM, Li J, Li W, Wang GC, et al. Bromodomain 4 protein is a predictor of survival for urothelial carcinoma of bladder. *Int J Clin Exp Pathol*. 2014;7(7):4231-8.
8. Zhang P, Dong Z, Cai J, Zhang C, Shen Z, Ke A, et al. BRD4 promotes tumor growth and epithelial-mesenchymal transition in hepatocellular carcinoma. *Int J Immunopathol Pharmacol*. 2015;28(1):36-44.
9. Jang MK, Kwon D, McBride AA. Papillomavirus E2 proteins and the host BRD4 protein associate with transcriptionally active cellular chromatin. *J Virol*. 2009;83(6):2592-600.
10. Zhu J, Gaiha GD, John SP, Pertel T, Chin CR, Gao G, et al. Reactivation of latent HIV-1 by inhibition of BRD4. *Cell Rep*. 2012;2(4):807-16.
11. Khan YM, Kirkham P, Barnes PJ, Adcock IM. Brd4 is essential for IL-1beta-induced inflammation in human airway epithelial cells. *PLoS One*. 2014;9(4):e95051.
12. Hajmirza A, Emadali A, Gauthier A, Casasnovas O, Gressin R, Callanan MB. BET Family Protein BRD4: An Emerging Actor in NFkappaB Signaling in Inflammation and Cancer. *Biomedicines*. 2018;6(1).
13. Anand P, Brown JD, Lin CY, Qi J, Zhang R, Artero PC, et al. BET bromodomains mediate transcriptional pause release in heart failure. *Cell*. 2013;154(3):569-82.
14. Spiltoir JI, Stratton MS, Cavaasin MA, Demos-Davies K, Reid BG, Qi J, et al. BET acetyl-lysine binding proteins control pathological cardiac hypertrophy. *J Mol Cell Cardiol*. 2013;63:175-9.

15. Filippakopoulos P, Qi J, Picaud S, Shen Y, Smith WB, Fedorov O, et al. Selective inhibition of BET bromodomains. *Nature*. 2010;468(7327):1067-73.
16. Nicodeme E, Jeffrey KL, Schaefer U, Beinke S, Dewell S, Chung CW, et al. Suppression of inflammation by a synthetic histone mimic. *Nature*. 2010;468(7327):1119-23.
17. Chaidos A, Caputo V, Gouvedenou K, Liu B, Marigo I, Chaudhry MS, et al. Potent antimyeloma activity of the novel bromodomain inhibitors I-BET151 and I-BET762. *Blood*. 2014;123(5):697-705.
18. Li Z, Guo J, Wu Y, Zhou Q. The BET bromodomain inhibitor JQ1 activates HIV latency through antagonizing Brd4 inhibition of Tat-transactivation. *Nucleic Acids Res*. 2013;41(1):277-87.
19. Yao W, Yue P, Khuri FR, Sun SY. The BET bromodomain inhibitor, JQ1, facilitates c-FLIP degradation and enhances TRAIL-induced apoptosis independent of BRD4 and c-Myc inhibition. *Oncotarget*. 2015;6(33):34669-79.
20. Fish PV, Filippakopoulos P, Bish G, Brennan PE, Bunnage ME, Cook AS, et al. Identification of a chemical probe for bromo and extra C-terminal bromodomain inhibition through optimization of a fragment-derived hit. *J Med Chem*. 2012;55(22):9831-7.
21. Law RP, Atkinson SJ, Bamborough P, Chung CW, Demont EH, Gordon LJ, et al. Discovery of Tetrahydroquinoxalines as Bromodomain and Extra-Terminal Domain (BET) Inhibitors with Selectivity for the Second Bromodomain. *J Med Chem*. 2018;61(10):4317-34.
22. Albrecht BK, Gehling VS, Hewitt MC, Vaswani RG, Cote A, Leblanc Y, et al. Identification of a Benzoisoxazoloazepine Inhibitor (CPI-0610) of the Bromodomain and Extra-Terminal (BET) Family as a Candidate for Human Clinical Trials. *J Med Chem*. 2016;59(4):1330-9.
23. Xiang Q, Wang C, Zhang Y, Xue X, Song M, Zhang C, et al. Discovery and optimization of 1-(1H-indol-1-yl)ethanone derivatives as CBP/EP300 bromodomain inhibitors for the treatment of castration-resistant prostate cancer. *Eur J Med Chem*. 2018;147:238-52.
24. Zhang Z, Hou S, Chen H, Ran T, Jiang F, Bian Y, et al. Targeting epigenetic reader and eraser: Rational design, synthesis and in vitro evaluation of dimethylisoxazoles derivatives as BRD4/HDAC dual inhibitors. *Bioorg Med Chem Lett*. 2016;26(12):2931-5.
25. Shen G, Jiang M, Pu J. Dual inhibition of BRD4 and PI3K by SF2523 suppresses human prostate cancer cell growth in vitro and in vivo. *Biochem Biophys Res Commun*. 2018;495(1):567-73.
26. Zhou B, Hu J, Xu F, Chen Z, Bai L, Fernandez-Salas E, et al. Discovery of a Small-Molecule Degradator of Bromodomain and Extra-Terminal (BET) Proteins with Picomolar Cellular Potencies and Capable of Achieving Tumor Regression. *J Med Chem*. 2018;61(2):462-81.
27. Cox OB, Krojer T, Collins P, Monteiro O, Talon R, Bradley A, et al. A poised fragment library enables rapid synthetic expansion yielding the first reported inhibitors of PHIP(2), an atypical bromodomain. *Chem Sci*. 2016;7(3):2322-30.

28. Harner MJ, Chauder BA, Phan J, Fesik SW. Fragment-based screening of the bromodomain of ATAD2. *J Med Chem.* 2014;57(22):9687-92.
29. Dawson MA, Prinjha RK, Dittmann A, Giotopoulos G, Bantscheff M, Chan WI, et al. Inhibition of BET recruitment to chromatin as an effective treatment for MLL-fusion leukaemia. *Nature.* 2011;478(7370):529-33.
30. Fedorov O, Lingard H, Wells C, Monteiro OP, Picaud S, Keates T, et al. [1,2,4]triazolo[4,3-a]phthalazines: inhibitors of diverse bromodomains. *J Med Chem.* 2014;57(2):462-76.
31. Choudhary S, Muthyala MK, Parang K, Kumar A. Ionic liquid-supported sulfonyl hydrazine: a useful reagent for traceless synthesis of pyrazoles. *Organic Chemistry Frontiers.* 2014;1(6):683-8.
32. Lee B, Kang P, Lee KH, Cho J, Nam W, Lee WK, et al. Solid-state and solvent-free synthesis of azines, pyrazoles, and pyridazinones using solid hydrazine. *Tetrahedron Letters.* 2013;54(11):1384-8.
33. Allahyari-Devin M, Abedi B, Navidpour L, Shafiee A. Synthesis of aryl-substituted or aryl-fused N-hydroxyethyl and N-hydroxymethylpyrazole derivatives as potential ligands for the estrogen receptor. *Journal of the Iranian Chemical Society.* 2013;10(1):43-53.
34. Hu X-Q, Chen J-R, Wei Q, Liu F-L, Deng Q-H, You-Quan Z, et al. Efficient Synthesis of Dihydropyrazoles by Halocyclization of β,γ -Unsaturated Hydrazones. *European Journal of Organic Chemistry.* 2014;2014(15):3082-6.
35. Wen J, Fu Y, Zhang RY, Zhang J, Chen SY, Yu XQ. A simple and efficient synthesis of pyrazoles in water. *Tetrahedron.* 2011;67(49):9618-21.
36. Zumbansen K, Dohring A, List B. Morpholinium Trifluoroacetate-Catalyzed Aldol Condensation of Acetone with both Aromatic and Aliphatic Aldehydes. *Advanced Synthesis & Catalysis.* 2010;352(7):1135-8.
37. Nadkarni DH, Murugesan S, Velu SE. Total synthesis of zyzzyanones A-D. *Tetrahedron.* 2013;69(20):4105-13.
38. Johnson CN, Jones DG, Liang X, Macpherson DT, Miller AB, Naylor A, et al., inventors; Glaxo Group Limited, UK . assignee. Indazole derivatives as estrogen receptor beta mediators and their preparation, pharmaceutical compositions and use in the treatment of diseases patent WO2008107455A1. 2008.
39. Hewings DS, Wang M, Philpott M, Fedorov O, Uttarkar S, Filippakopoulos P, et al. 3,5-dimethylisoxazoles act as acetyl-lysine-mimetic bromodomain ligands. *J Med Chem.* 2011;54(19):6761-70.
40. Ozer HG, El-Gamal D, Powell B, Hing ZA, Blachly JS, Harrington B, et al. BRD4 Profiling Identifies Critical Chronic Lymphocytic Leukemia Oncogenic Circuits and Reveals Sensitivity to PLX51107, a Novel Structurally Distinct BET Inhibitor. *Cancer Discov.* 2018;8(4):458-77.

41. Bamborough P, Chung CW, Demont EH, Furze RC, Bannister AJ, Che KH, et al. A Chemical Probe for the ATAD2 Bromodomain. *Angew Chem Int Ed Engl.* 2016;55(38):11382-6.
42. Hay DA, Fedorov O, Martin S, Singleton DC, Tallant C, Wells C, et al. Discovery and optimization of small-molecule ligands for the CBP/p300 bromodomains. *J Am Chem Soc.* 2014;136(26):9308-19.
43. Ouyang L, Zhang L, Liu J, Fu L, Yao D, Zhao Y, et al. Discovery of a Small-Molecule Bromodomain-Containing Protein 4 (BRD4) Inhibitor That Induces AMP-Activated Protein Kinase-Modulated Autophagy-Associated Cell Death in Breast Cancer. *J Med Chem.* 2017;60(24):9990-10012.
44. McPhillips TM, McPhillips SE, Chiu H-J, Cohen AE, Deacon AM, Ellis PJ, et al. Blu-Ice and the Distributed Control System: software for data acquisition and instrument control at macromolecular crystallography beamlines. *Journal of synchrotron radiation.* 2002;9(6):401-6.
45. Battye TGG, Kontogiannis L, Johnson O, Powell HR, Leslie AGW. iMOSFLM: a new graphical interface for diffraction-image processing with MOSFLM. *Acta crystallographica Section D, Biological crystallography.* 2011;67(Pt 4):271-81.
46. Evans PR, Murshudov GN. How good are my data and what is the resolution? *Acta crystallographica Section D, Biological crystallography.* 2013;69(Pt 7):1204-14.
47. Winn MD, Ballard CC, Cowtan KD, Dodson EJ, Emsley P, Evans PR, et al. Overview of the CCP4 suite and current developments. *Acta Crystallogr D Biol Crystallogr.* 2011;67(Pt 4):235-42.
48. McCoy AJ, Grosse-Kunstleve RW, Adams PD, Winn MD, Storoni LC, Read RJ. Phaser crystallographic software. *J Appl Crystallogr.* 2007;40(Pt 4):658-74.
49. Emsley P, Lohkamp B, Scott WG, Cowtan K. Features and development of Coot. *Acta Crystallogr D Biol Crystallogr.* 2010;66(Pt 4):486-501.
50. Afonine PV, Grosse-Kunstleve RW, Echols N, Headd JJ, Moriarty NW, Mustyakimov M, et al. Towards automated crystallographic structure refinement with phenix.refine. *Acta Crystallogr D Biol Crystallogr.* 2012;68(Pt 4):352-67.

Chapter 5 – Conclusion and Future Directions

Bromodomains have been the subject of investigation due to their involvement with disease states and the ambiguity surrounding their function in several proteins. The main strategy that has been employed is to mimic K-ac from binding to the bromodomain. Even though there is an abundance of both fragments and inhibitors for bromodomains, many of which have progressed into clinical trials, there are still numerous mimetics that have either yet to be discovered or been neglected in the search for novel inhibitors. In this thesis, we have examined the inhibitory potential of two such fragments: *N*-methylpyrrolidone and 5-methyl-3-aryl-1*H*-pyrazole. In our assays, both starting fragments showed millimolar IC₅₀ towards BRD4 BD1, which would have been seen as a deterrent for pursuing such fragments despite possessing sufficient ligand efficiency. However, using different strategies for FBDD, we have greatly improved their respective activity, developed several lead compounds with micromolar inhibition and solved crystal structures that have rationalised not only their activity but also their use as K-ac mimetics.

Chapters 2 and 3 involved the elaboration of the solvent molecule *N*-methylpyrrolidone. Prior to the commencement of this work, *N*-methylpyrrolidone was well-known as an K-ac mimetic. Despite the literature linking its therapeutic activity to its bromodomain inhibition, it was yet to be elaborated as a fragment. Here, we applied two strategies to prove the worth of NMP as an K-ac mimetic.

In Chapter 2, we used NMP as an acetamide substitute to replace the K-ac mimetic of the BET inhibitor Olinone. The six derivatives we created in this work – a pair of methyl ester, alcohol and mesylate homologues - are useful in their own right in FBDD and should be taken further to develop functionalised esters, amides, ethers and amines. Using the mesylate homologues, we successfully created two Olinone-based analogues. Both analogues retained the binding

interactions to BRD4 BD1, as revealed by X-ray crystallography, while **17** also retained its inhibitory activity in spite of being tested as a racemic mixture. Given the success of the strategy of acetamide substitution in Olinone, this should give us further incentive to put forward the case that NMP can reliably serve as an K-ac mimetic substitute and can be extended towards replacing K-ac with NMP in certain peptidomimetics or other known inhibitors.

The strategy of fragment growing was applied to NMP in Chapter 3 in order to gradually improve its inhibitory activity. This work saw the creation of a phenyl-derived NMP fragment which showed an initial improvement to inhibition while retaining the mimicry of NMP. Using electrophilic aromatic substitution, four intermediates were created for SAR studies, which showed a gradual enhancement to activity and culminated with the lead compound **15c**. The information generated by the new binding pose is two-fold. Firstly, the X-ray crystal structure of **15c** provides a blueprint for future optimization, despite NMP no longer acting as the mimetic. Secondly, given that certain substitutions on the phenyl ring proved detrimental to activity, there should be more careful consideration of the functional groups used to grow the NMP fragment.

Chapter 4 covered the development of potential inhibitors focusing on the 5-methyl-3-aryl-1*H*-pyrazole scaffold. While there have been plenty of heterocycles covered in literature that act as bromodomain inhibitors, especially those among the first to be reported as potent and selective, there has been no evidence of this particular scaffold being used as a mimetic. Here, we sought to elaborate on this compound through the generation of a “poised fragment” library that was realised through a simple synthetic scheme that was easily adjustable to include the attachment and removal of a protecting group for certain labile functional groups. Two compounds of this series, **3h** and **3s**, showed promising inhibitory activity against BRD4 BD1 and good ligand efficiency. An X-ray crystal structure of **3h** revealed a flipped pose in that the

dimethylphenol moiety fit in the bromodomain binding pocket, showing preference as the K-ac mimetic over the pyrazole. If the 5-methyl-3-aryl-1*H*-pyrazole scaffold is to be validated as a mimetic, more crystal structures will need to be developed. Either way, the aryl-pyrazole scaffold has shown potential to be a viable fragment in bromodomain inhibitor design, while the serendipitous discovery of the dimethylphenol scaffold has given a second exploitable scaffold.

A major limitation to this project is that there are 61 bromodomains, but every compound was tested on a single bromodomain: BRD4 BD1. While restrictive, the results should encourage the application of these mimetics and methods on other bromodomains, particularly outside the BET family. However, if efforts for optimization on these lead compounds were to take place, it would be necessary for successive compounds to be tested for selectivity in assays that cover multiple bromodomains, as well as other biological activities. One example is the downregulation of *Myc*, which has been well-connected to BRD4 inhibition in cancer models.

In summary, we have laid the groundwork for the use of two fragments for bromodomain inhibition using various techniques of fragment elaboration. The lead compounds generated in this project, together with the X-ray crystal structures, will undoubtedly go a long way in assisting with the development of inhibitors with high affinity and selectivity. Additionally, we believe that these techniques can be carried through to other bromodomains, especially those that have been predicted to be difficult to drug. Lastly, this work should encourage the pursuit of other innovative fragment-based drug design methods to identify novel fragments.

Appendices

Appendix A – Video of Bromodomain Structure

Video provided on USB.

Video to be uploaded in the near-future.

PDB code provided in video. Video edited and narrated by Joseph Hilton-Proctor.

Appendix B – Video of NMP Bound to Various Bromodomains

Video provided on USB.

Video to be uploaded in the near-future.

PDB codes provided in video. Video edited and narrated by Joseph Hilton-Proctor.

Appendix C – Dose Response Curves of Olinone Analogues

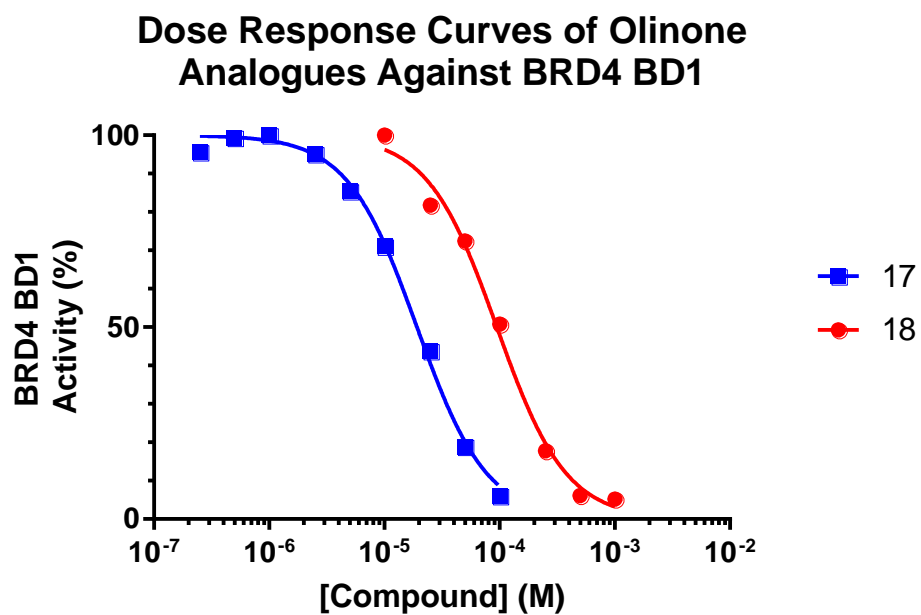


Figure S1. Dose-response curves to determine the IC₅₀ of Olinone-based analogues **17** and **18**.

Curve fits were calculated using GraphPad Prism. Experiments were performed in duplicates.

Appendix D – Video of Olinone-based Derivatives

Video provided on USB.

Video to be uploaded in the near-future.

PDB code of **Olinone** provided in video. Crystal structures of **17** and **18** developed by Dr. Ian Jennings and Dr. Olga Ilyichova. Video edited and narrated by Joseph Hilton-Proctor.

Appendix E – Electron Density Map of NMP Derivatives

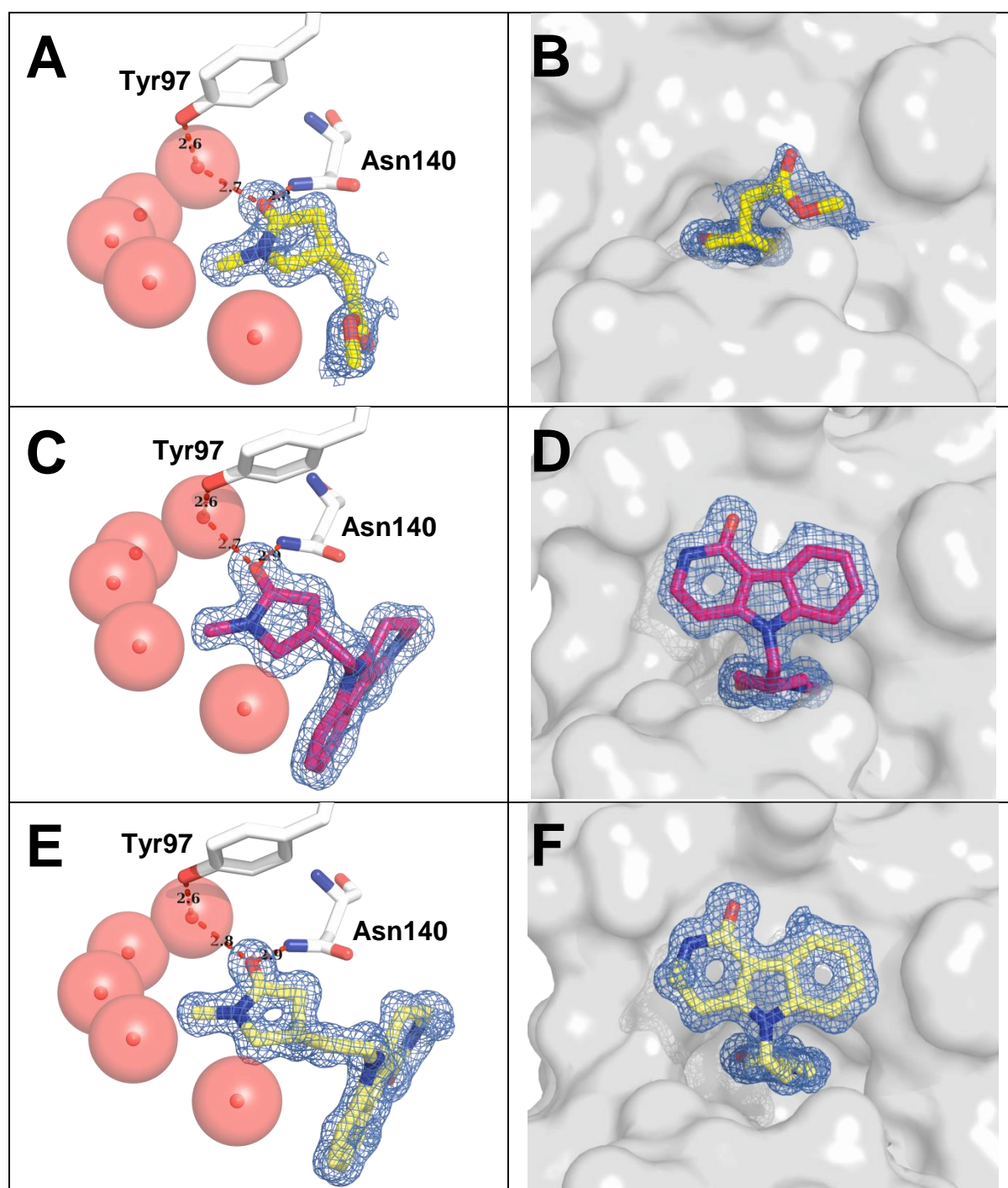
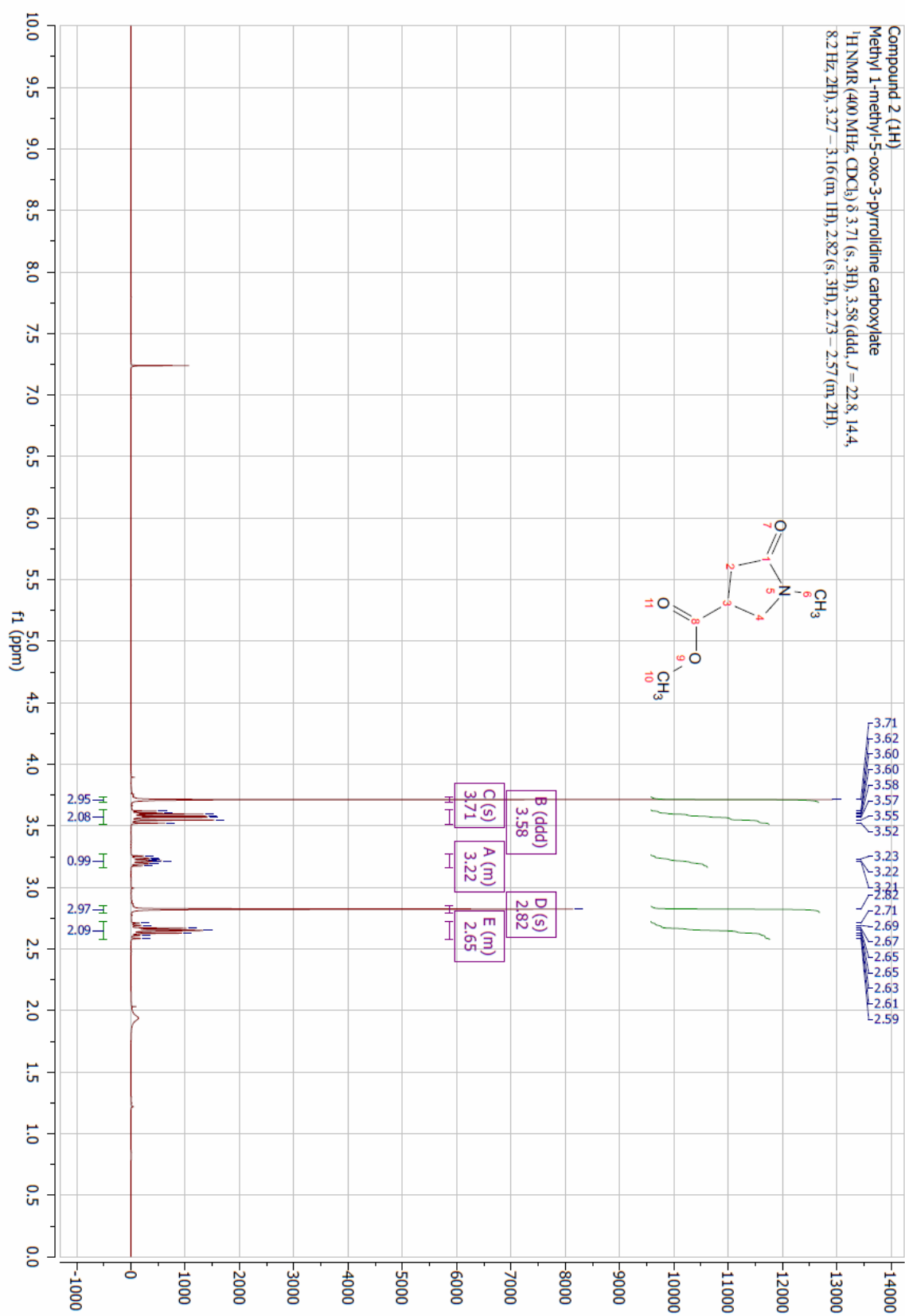
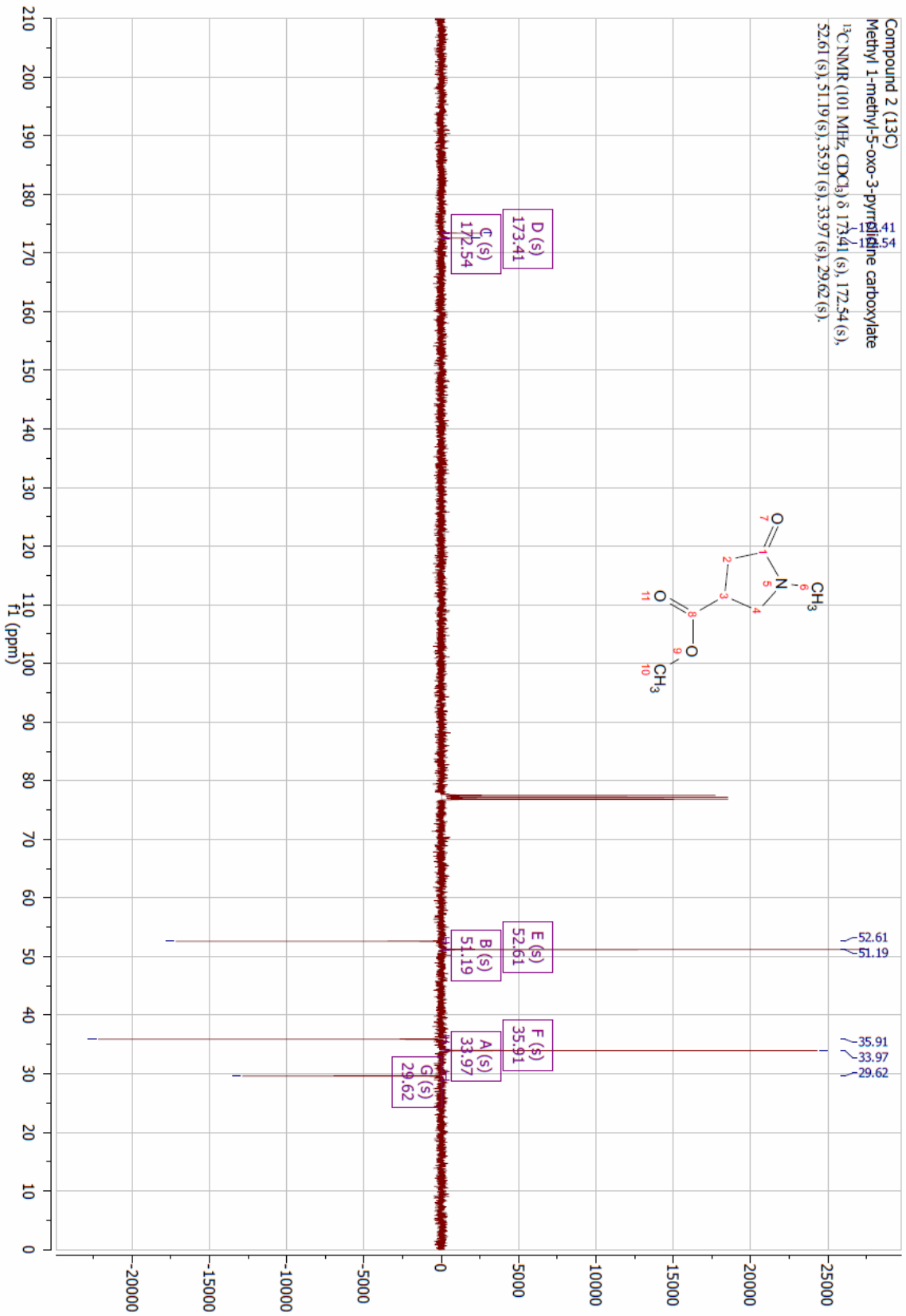
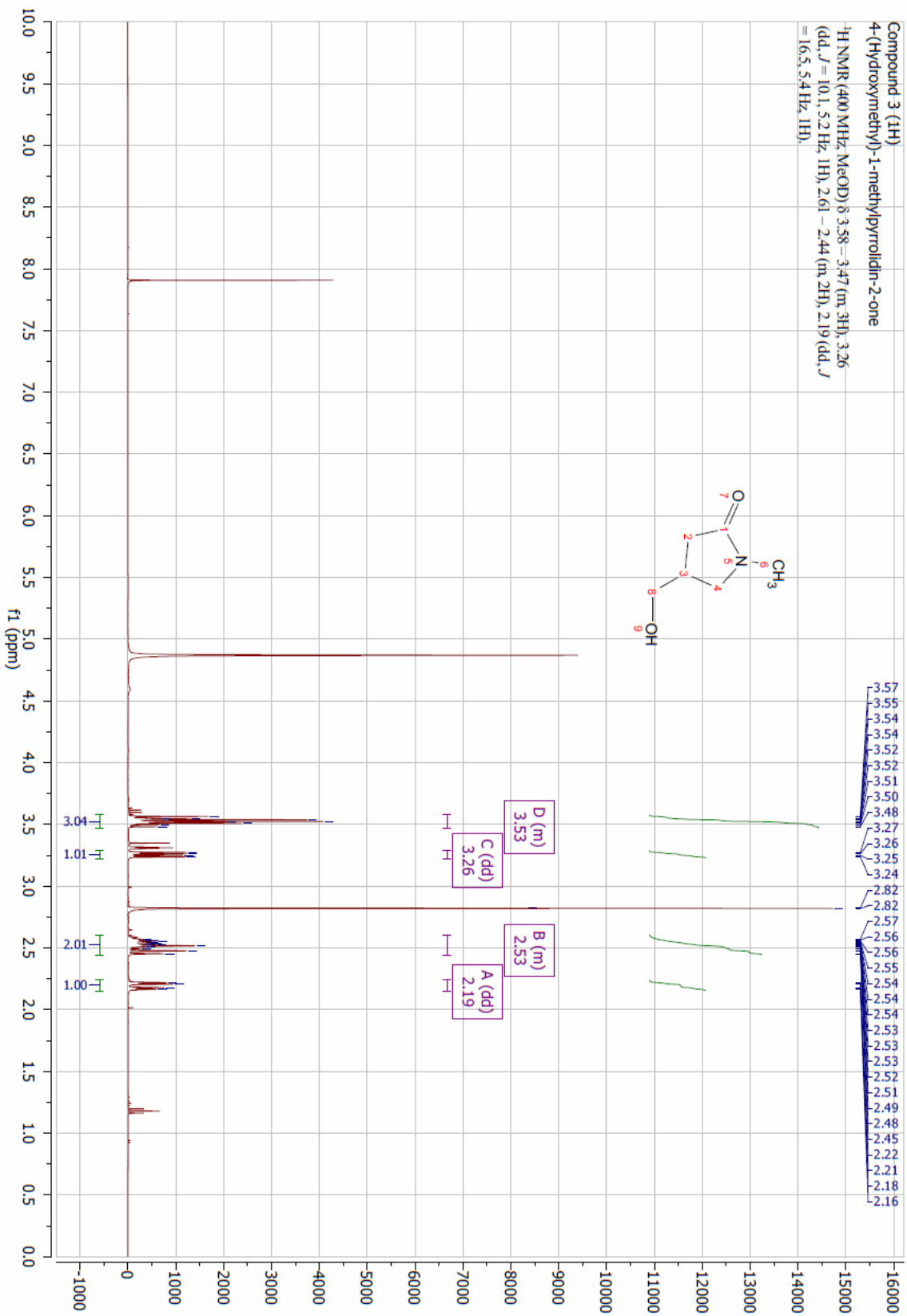


Figure S1. Electron density maps of NMP derivatives. [A, B] (*R*)-**10** (yellow, resolution: 1.3 Å). [C, D] (*R*)-**17** (warm pink, resolution: 1.59 Å). [E, F] (*R*)-**18** (pale yellow, resolution: 1.21 Å). [A, C, E] Binding site. [B, D, F] Top-down view of functional groups. The 2Fo-Fc electron density maps are shown in blue mesh at a contour level of 1.0 sigma. Electron density maps developed by Dr. Olga Ilyichova.

Appendix F – Chapter 2 NMR Data

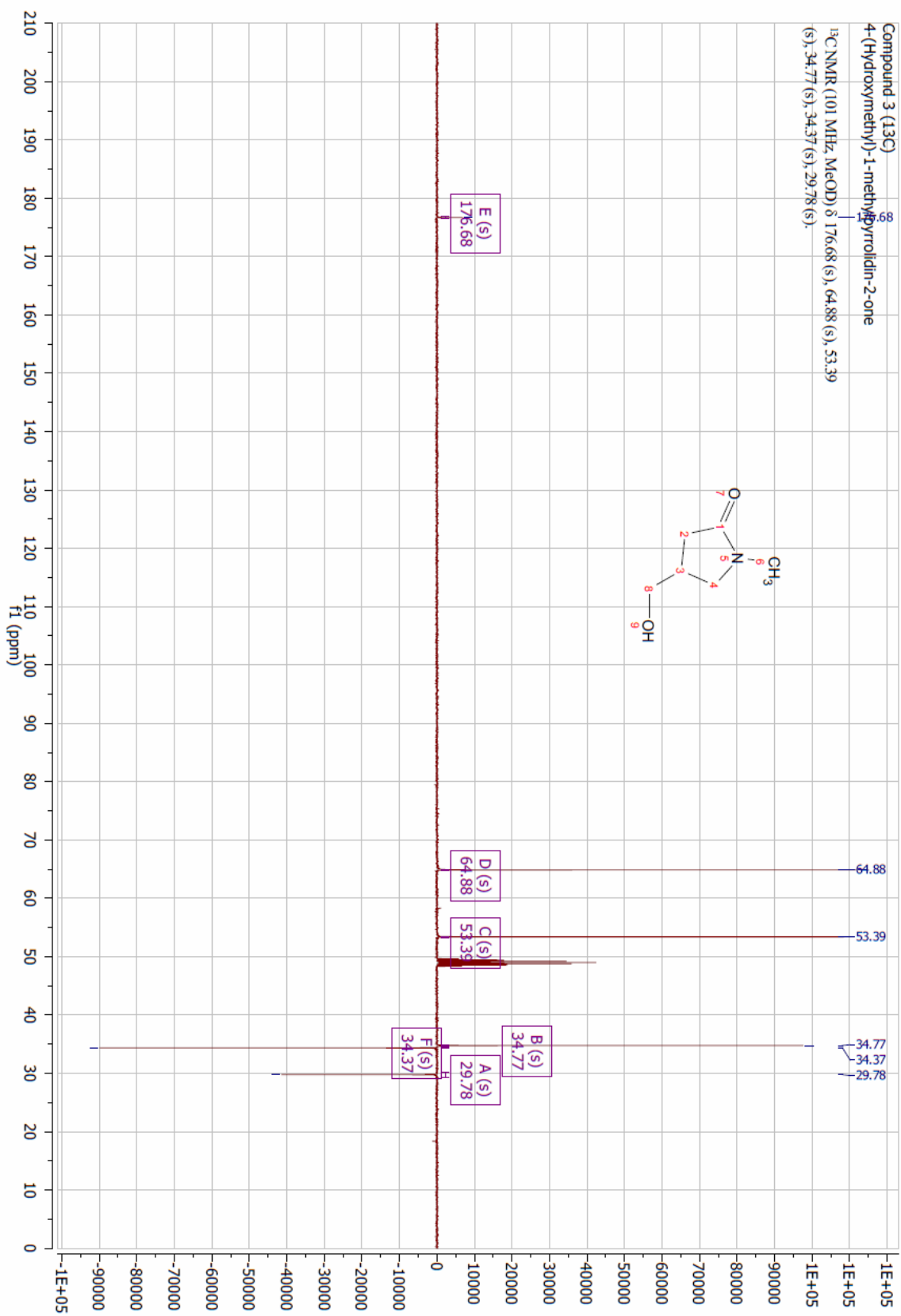
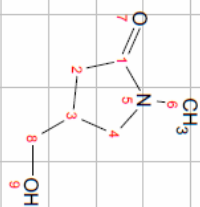


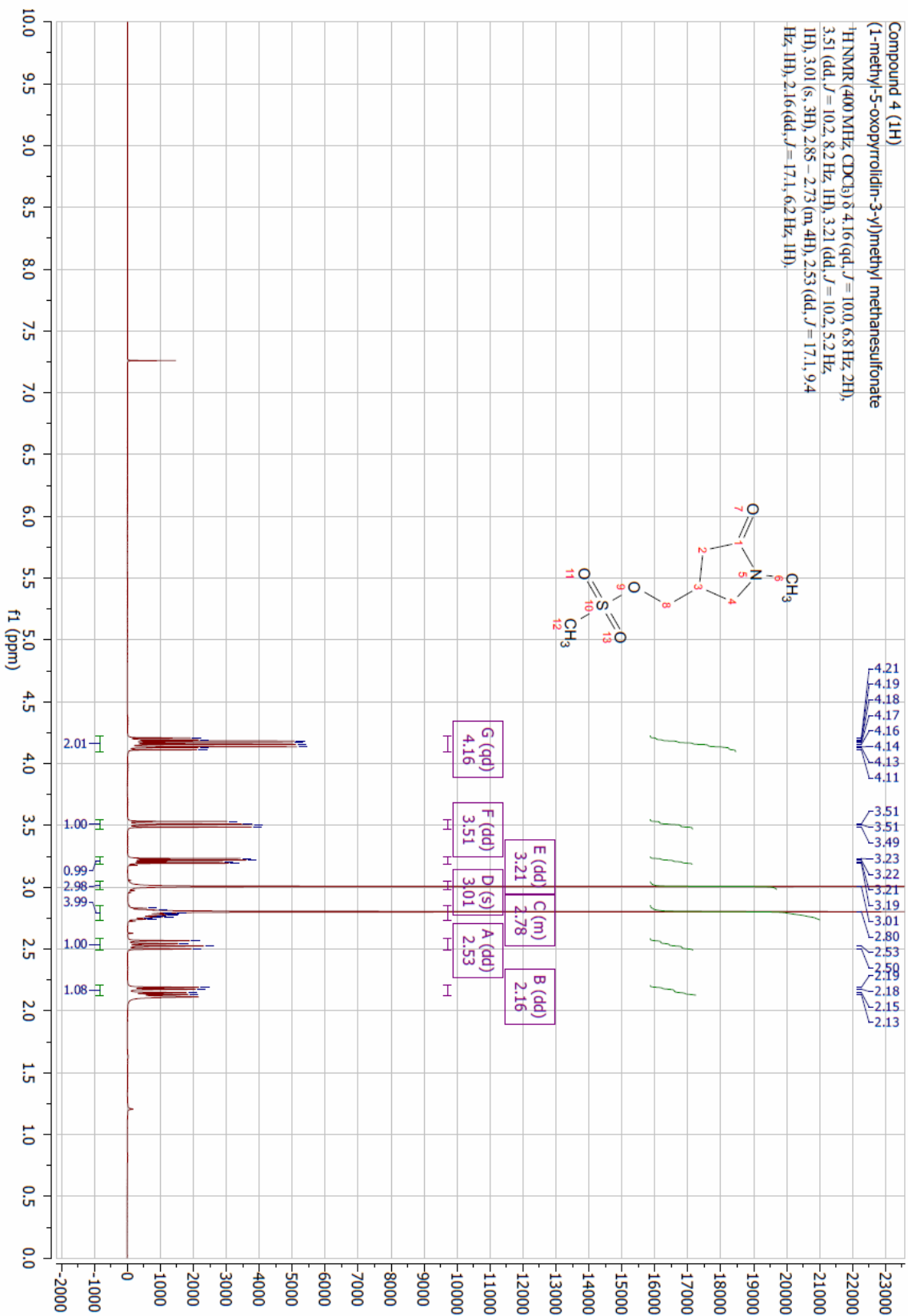




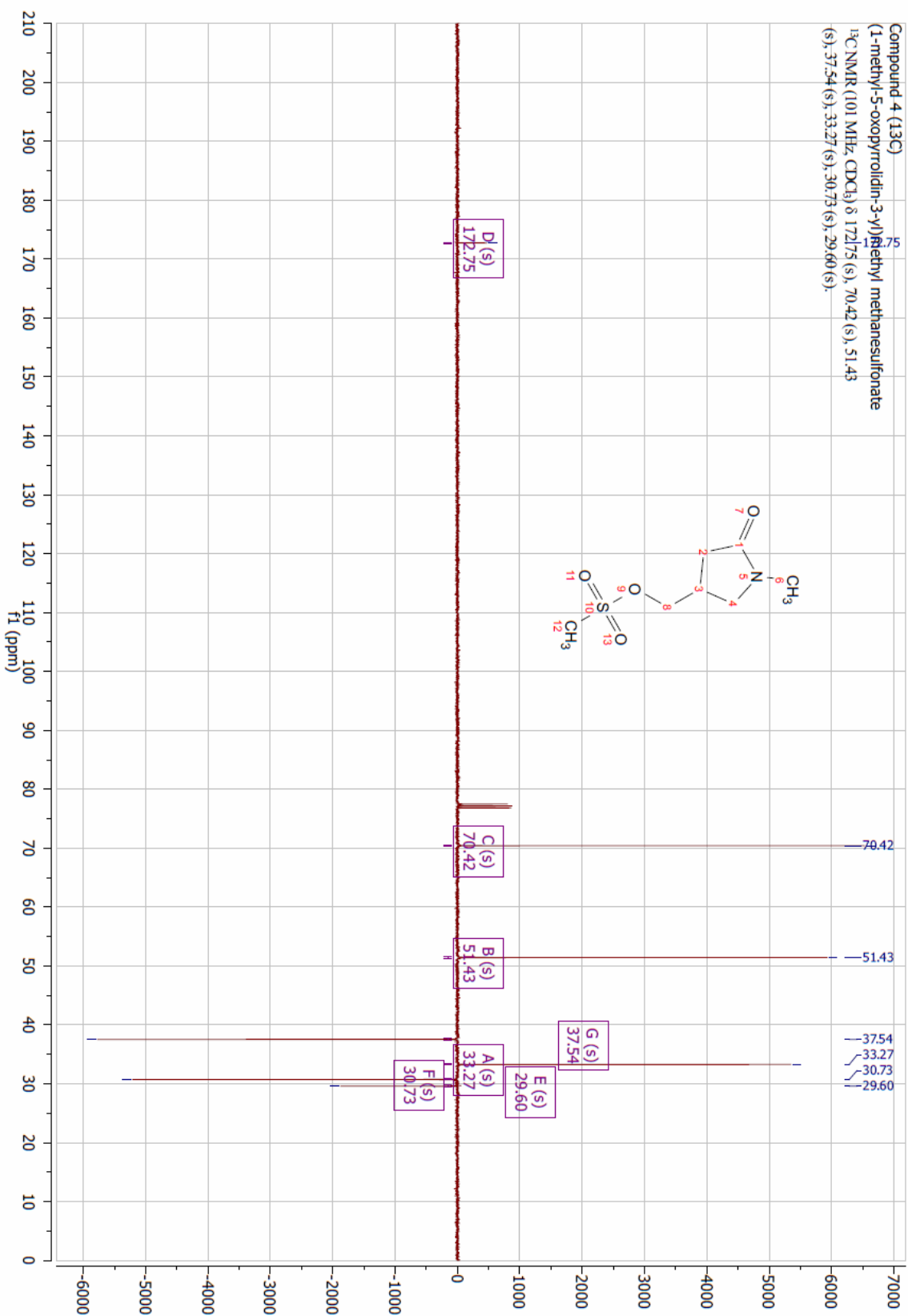
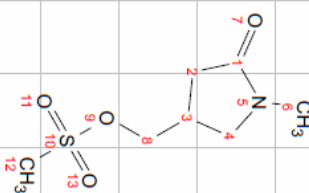
Compound 3 (13C)
4-(Hydroxymethyl)-1-methylpyrrolidin-2-one

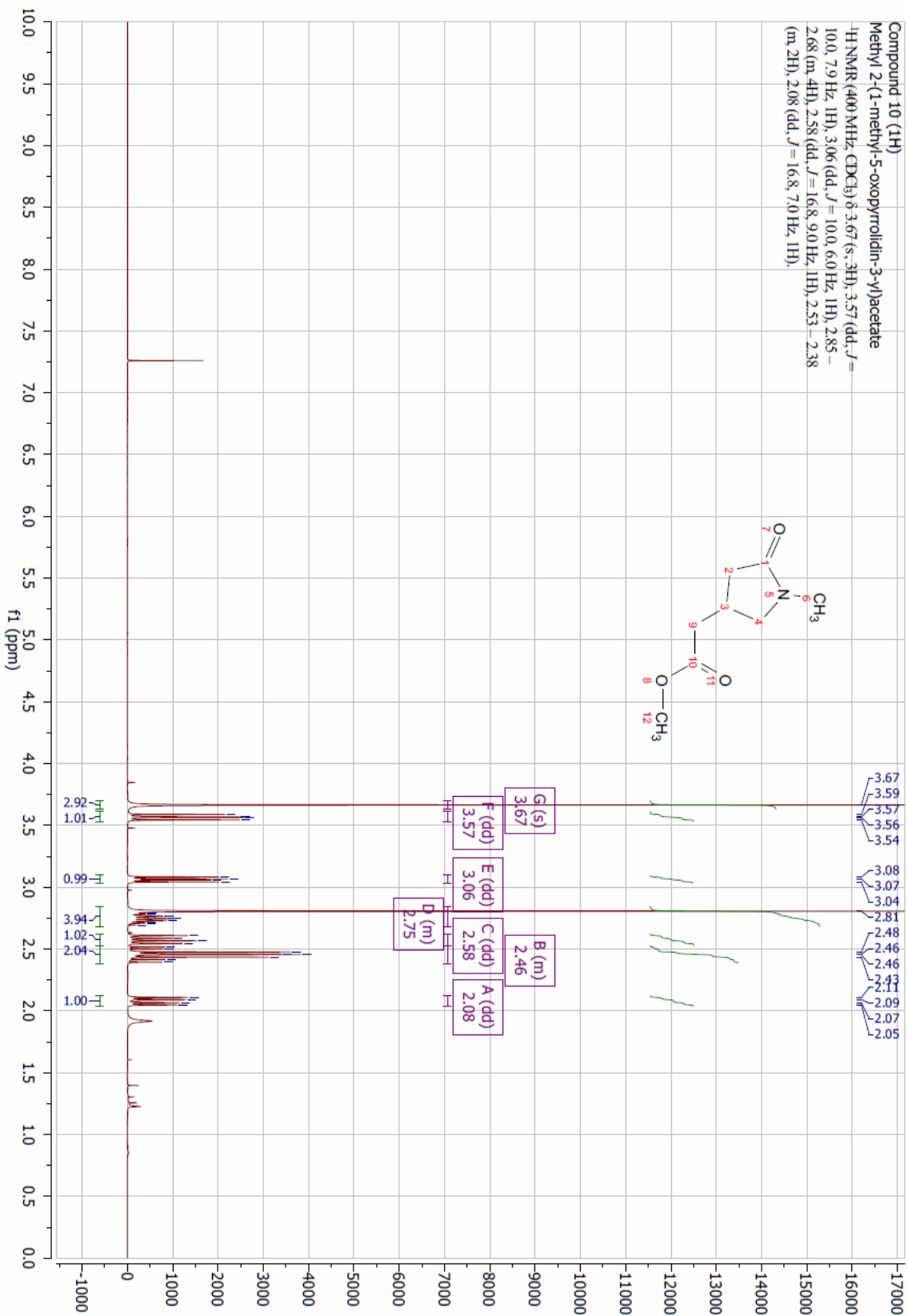
¹³C NMR (101 MHz, MeOD) δ 176.68 (s), 64.88 (s), 53.39 (s), 34.77 (s), 34.37 (s), 29.78 (s).

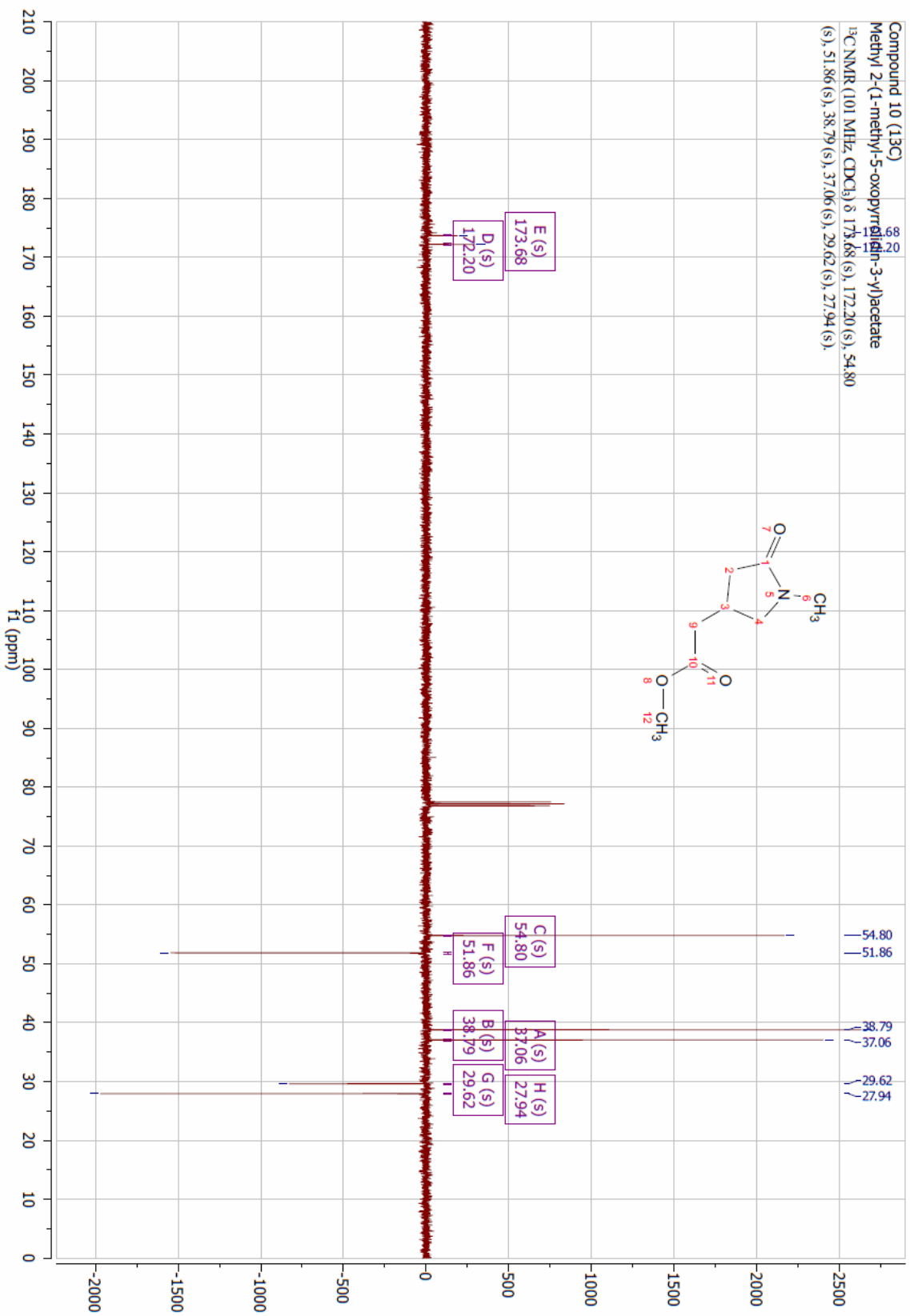


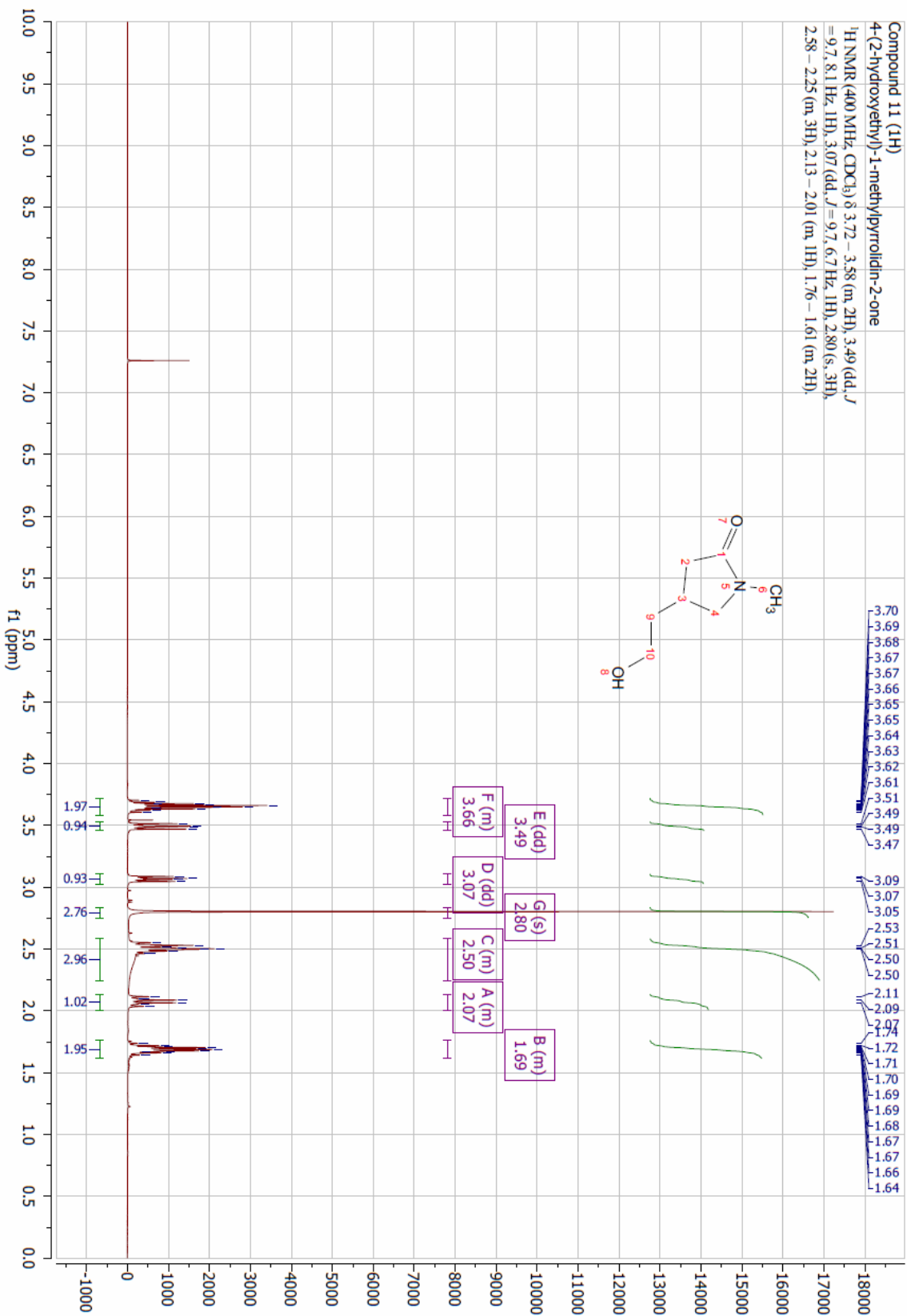


Compound 4 (13C)
(1-methyl-5-oxopyrrolidin-3-yl)methyl methanesulfonate
¹³C NMR (101 MHz, CDCl₃) δ 172.75 (s), 70.42 (s), 51.43 (s), 37.54 (s), 33.27 (s), 30.73 (s), 29.60 (s).



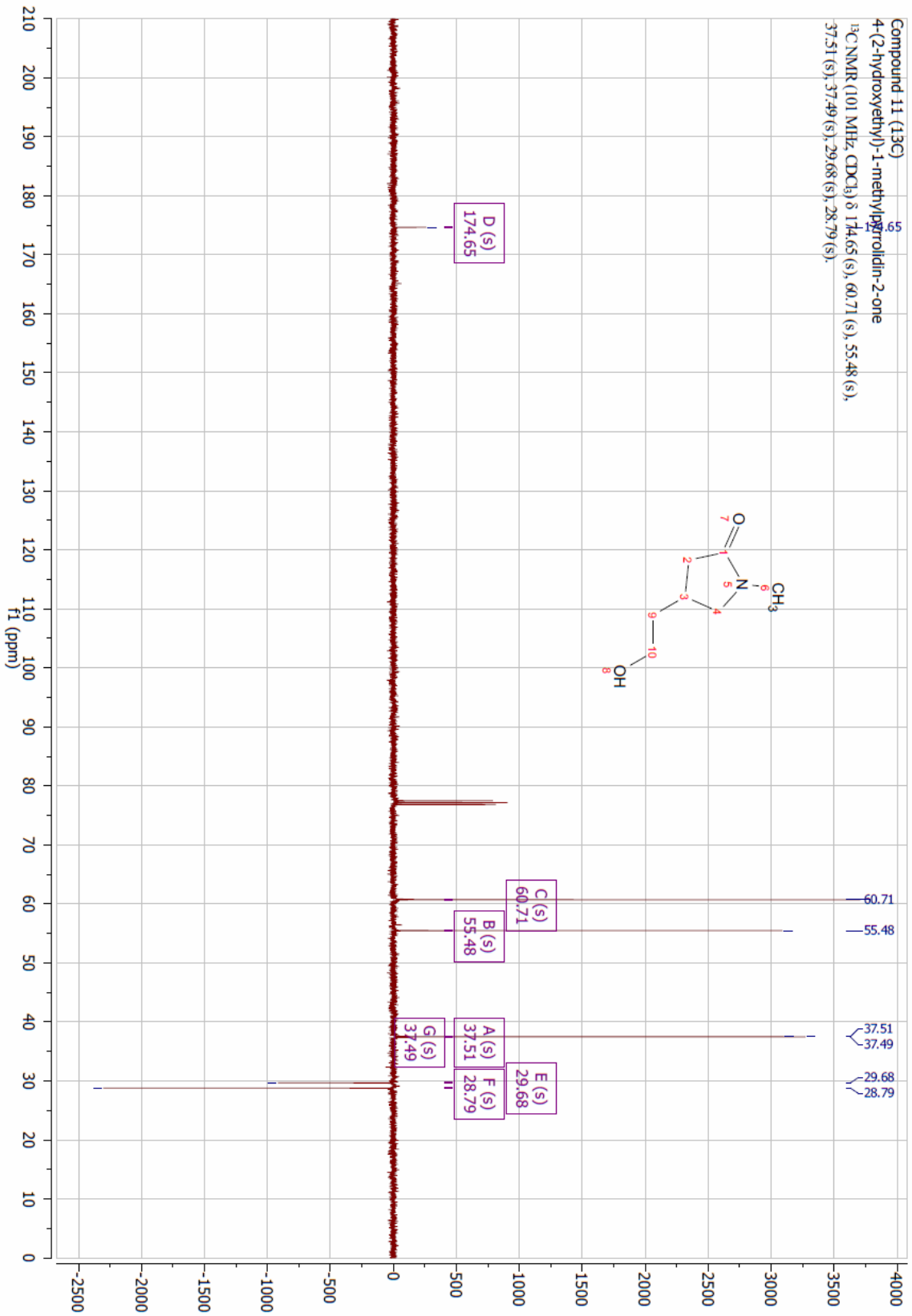
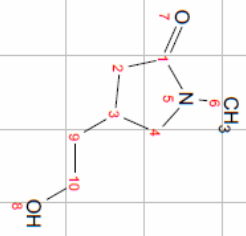


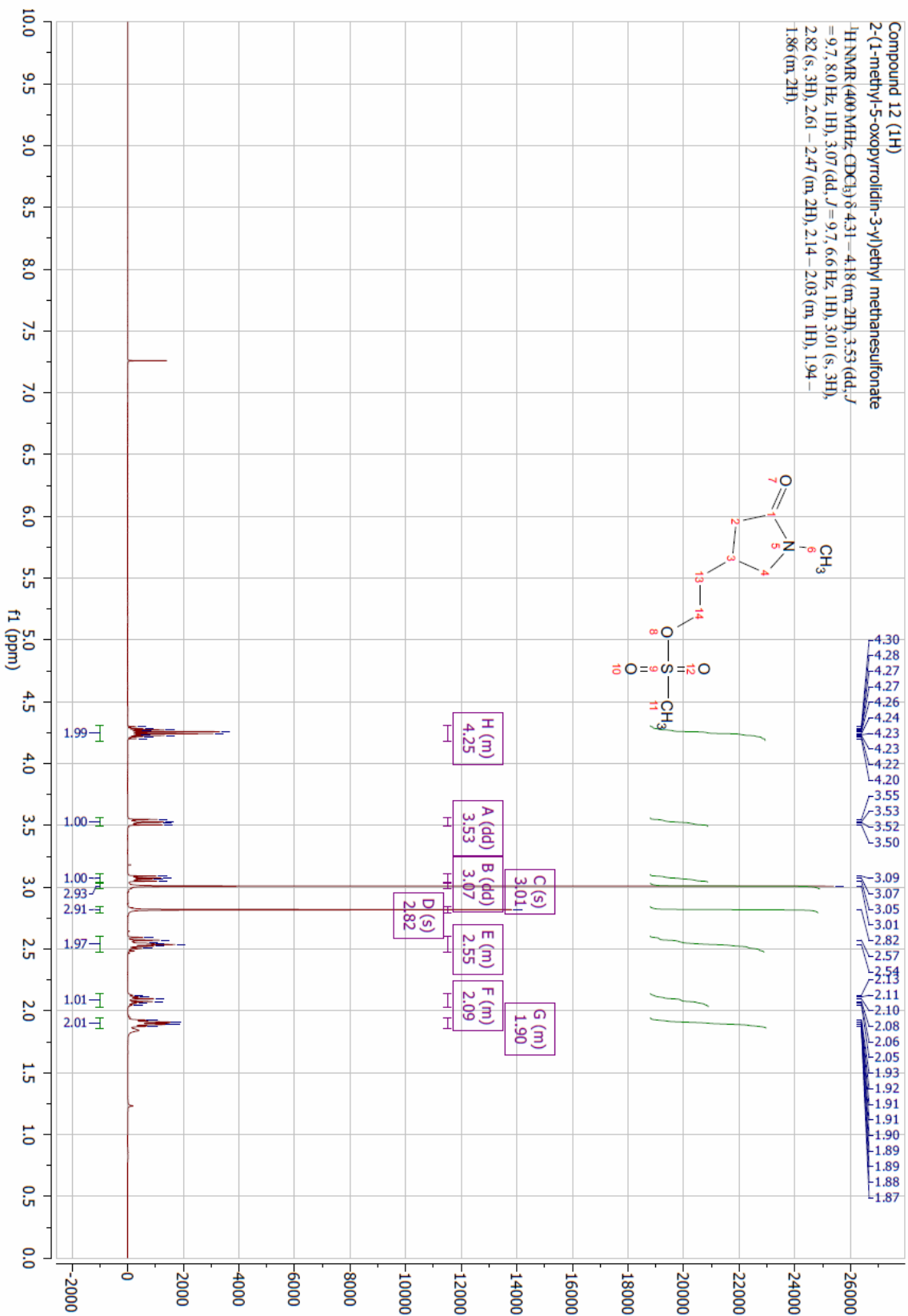


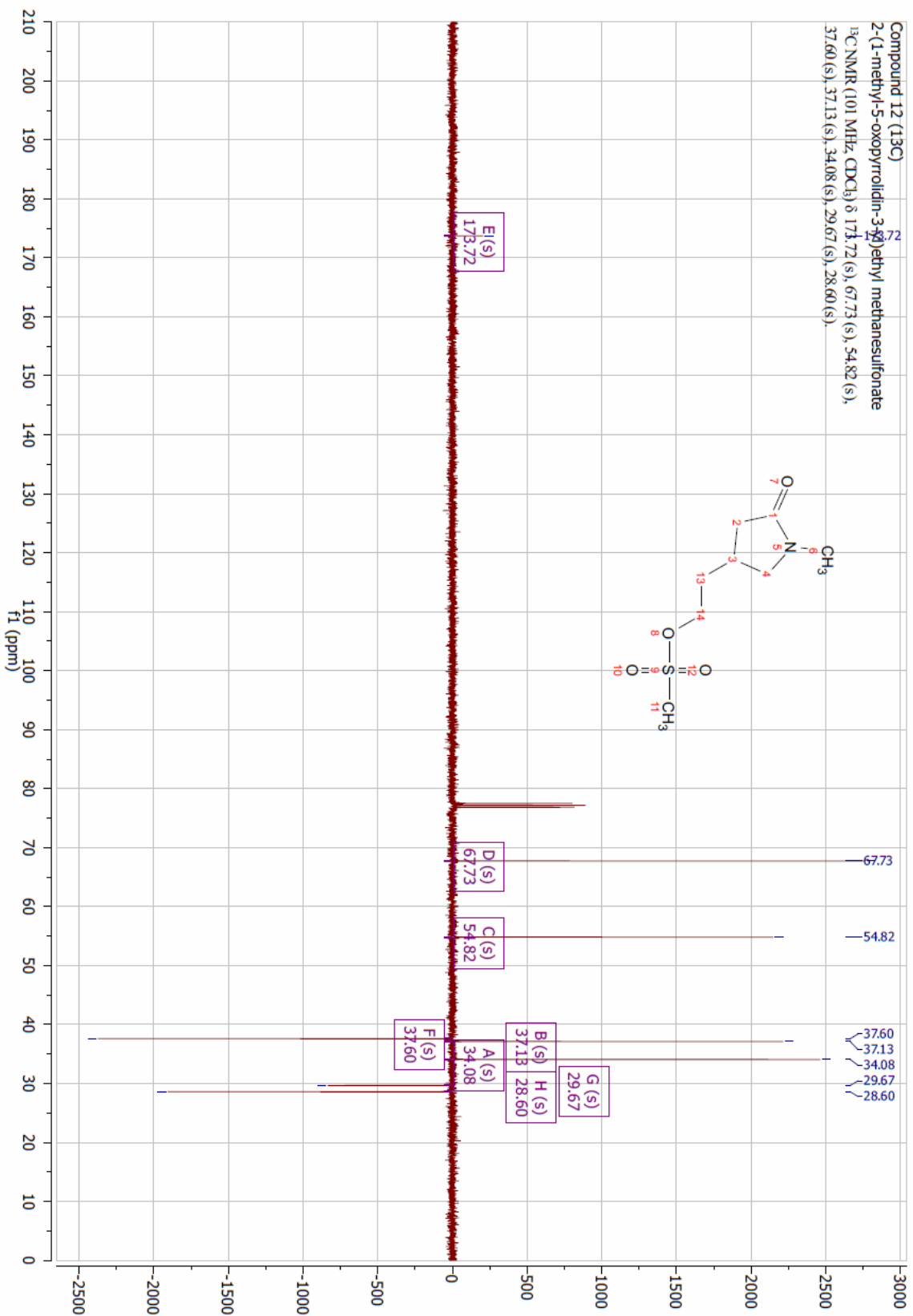


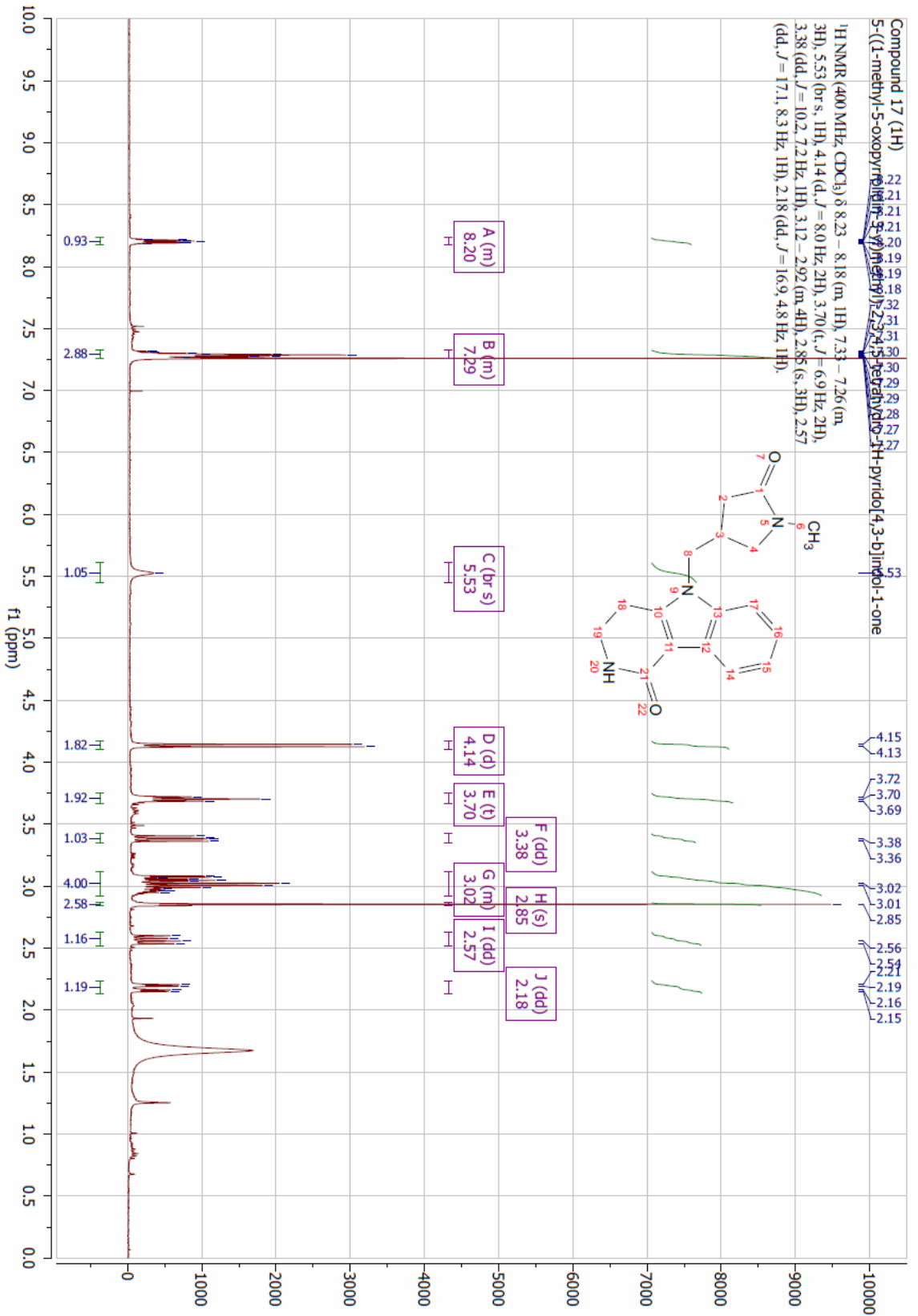
Compound 11 (13C)

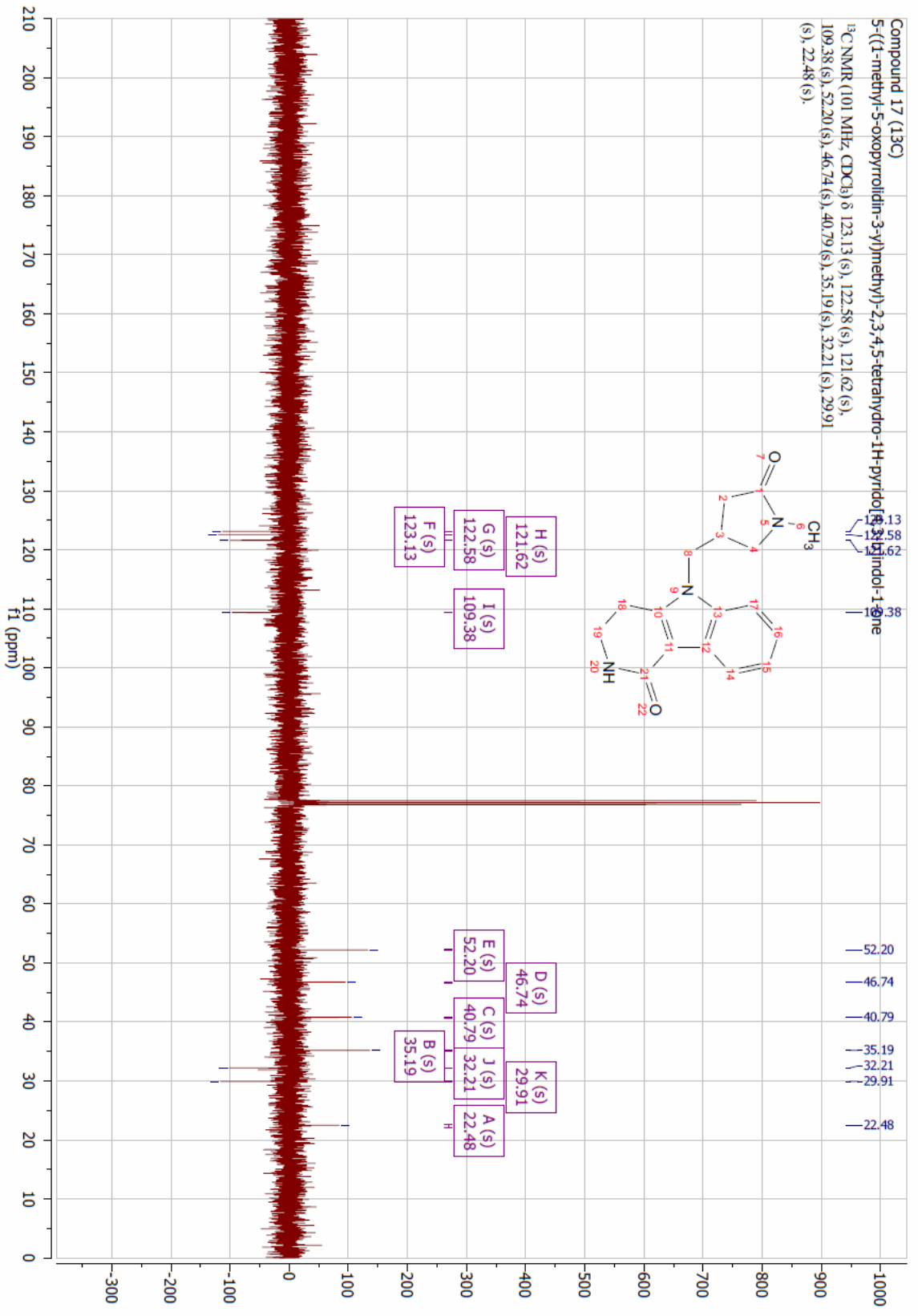
¹³C NMR (101 MHz, CDCl₃) δ 174.65 (s), 60.71 (s), 55.48 (s), 37.51 (s), 37.49 (s), 29.68 (s), 28.79 (s).

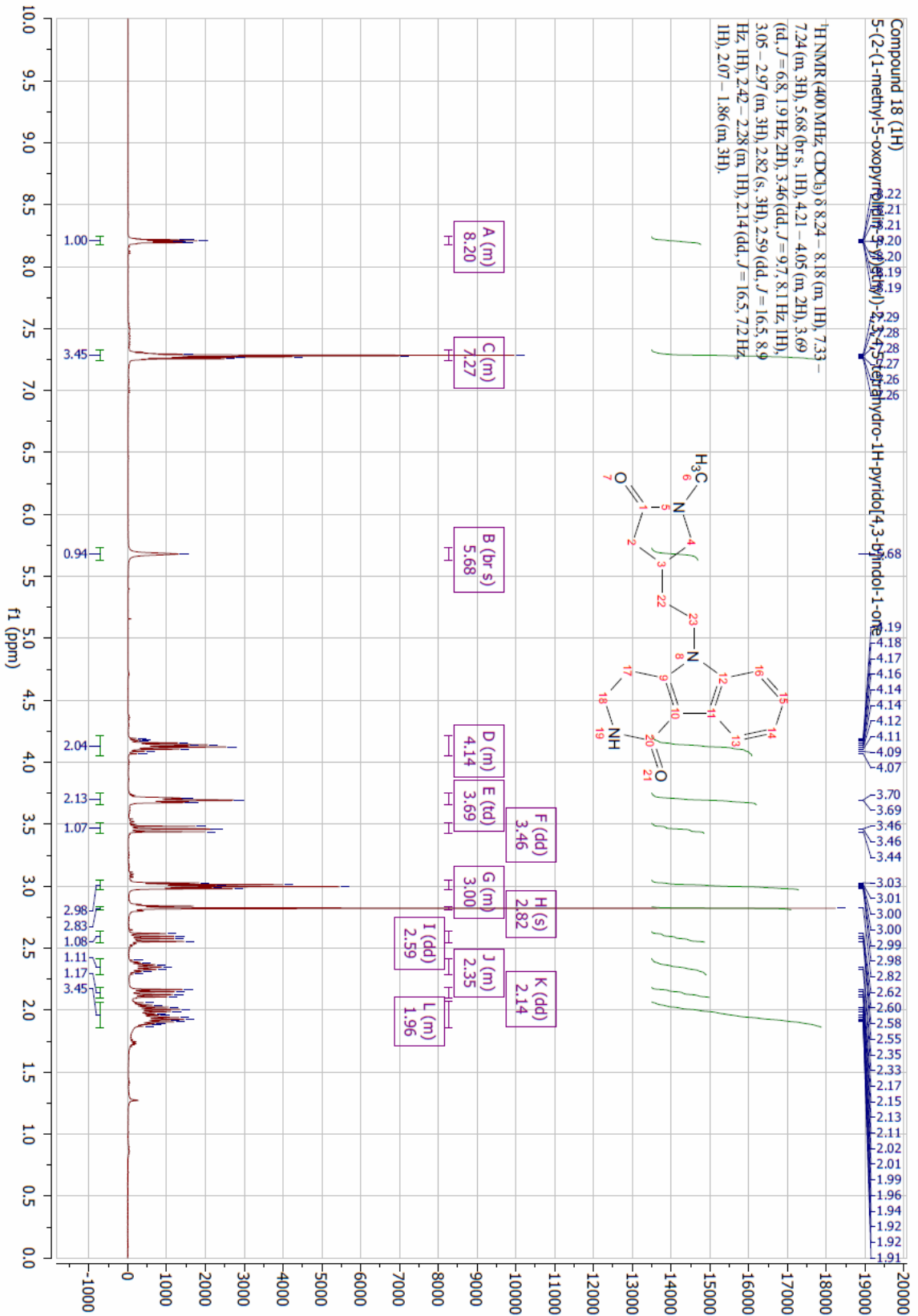


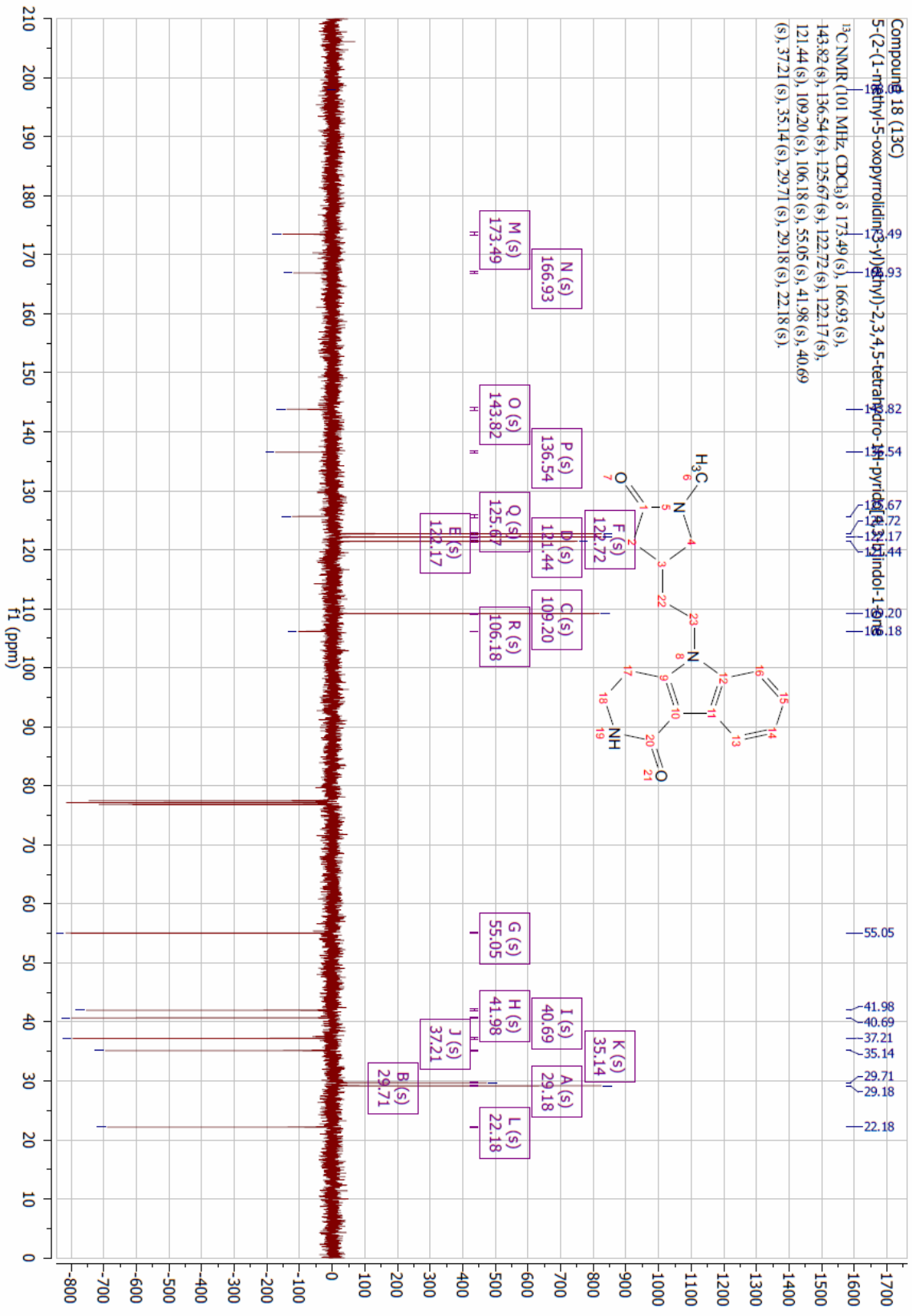












Appendix G – Chapter 2 X-ray Crystallographic Data Collection and

Refinement Statistics

Compound Title	10
Resolution range	21.24 - 1.3 (1.346 - 1.3)
Space group	P 21 21 21
Unit cell	37.6997 44.1299 78.3898 90 90 90
Total reflections	63844 (6189)
Unique reflections	31993 (3105)
Multiplicity	2.0 (2.0)
Completeness (%)	97.15 (95.89)
Mean I/sigma(I)	21.77 (5.06)
Wilson B-factor	7.74
R-merge	0.01997 (0.1354)
R-meas	0.02824 (0.1915)
R-pim	0.01997 (0.1354)
CC1/2	1 (0.949)
CC*	1 (0.987)
Reflections used in refinement	31982 (3105)
Reflections used for R-free	1590 (159)
R-work	0.1670 (0.1831)
R-free	0.1873 (0.1937)
CC(work)	0.964 (0.926)
CC(free)	0.956 (0.892)
Number of non-hydrogen atoms	1441
macromolecules	1167
ligands	12
solvent	262
Protein residues	126
RMS(bonds)	0.007
RMS(angles)	0.90
Ramachandran favoured (%)	99.19
Ramachandran allowed (%)	0.81
Ramachandran outliers (%)	0.00
Rotamer outliers (%)	2.99
Clashscore	6.73
Average B-factor	13.17
macromolecules	10.72
ligands	16.01
solvent	23.98
Number of TLS groups	10

Statistics for the highest-resolution shell are shown in parentheses.

Compound Title	17
Resolution range	38.72 - 1.59 (1.647 - 1.59)
Space group	P 21 21 21
Unit cell	42.614 52.008 58 90 90 90
Total reflections	35755 (3484)
Unique reflections	17904 (1752)
Multiplicity	2.0 (2.0)
Completeness (%)	99.85 (99.55)
Mean I/sigma(I)	41.01 (10.22)
Wilson B-factor	13.03
R-merge	0.01121 (0.06453)
R-meas	0.01586 (0.09125)
R-pim	0.01121 (0.06453)
CC1/2	1 (0.988)
CC*	1 (0.997)
Reflections used in refinement	17893 (1752)
Reflections used for R-free	912 (95)
R-work	0.1985 (0.1904)
R-free	0.2319 (0.2321)
CC(work)	0.954 (0.921)
CC(free)	0.935 (0.863)
Number of non-hydrogen atoms	1312
macromolecules	1085
ligands	22
solvent	205
Protein residues	124
RMS(bonds)	0.007
RMS(angles)	0.87
Ramachandran favoured (%)	98.35
Ramachandran allowed (%)	1.65
Ramachandran outliers (%)	0.00
Rotamer outliers (%)	0.82
Clashscore	2.72
Average B-factor	20.52
macromolecules	19.04
ligands	13.23
solvent	29.10

Statistics for the highest-resolution shell are shown in parentheses.

Compound Title	18
Resolution range	38.5 - 1.212 (1.25 - 1.212)
Space group	P 21 21 21
Unit cell	37.944 44.141 78.697 90 90 90
Total reflections	81396 (7769)
Unique reflections	40779 (3921)
Multiplicity	2.0 (2.0)
Completeness (%)	99.52 (97.20)
Mean I/sigma(I)	18.32 (3.15)
Wilson B-factor	12.06
R-merge	0.01823 (0.248)
R-meas	0.02578 (0.3507)
R-pim	0.01823 (0.248)
CC1/2	1 (0.848)
CC*	1 (0.958)
Reflections used in refinement	40709 (3920)
Reflections used for R-free	1995 (208)
R-work	0.1673 (0.2516)
R-free	0.1799 (0.2476)
CC(work)	0.973 (0.870)
CC(free)	0.965 (0.837)
Number of non-hydrogen atoms	1426
macromolecules	1141
ligands	24
solvent	261
Protein residues	127
RMS(bonds)	0.006
RMS(angles)	0.87
Ramachandran favoured (%)	99.20
Ramachandran allowed (%)	0.80
Ramachandran outliers (%)	0.00
Rotamer outliers (%)	1.55
Clashscore	1.72
Average B-factor	17.78
macromolecules	15.23
ligands	12.77
solvent	29.37
Number of TLS groups	7

Statistics for the highest-resolution shell are shown in parentheses.

Appendix H – Chapter 3 Lipophilic Ligand Efficiency Plot Graphs

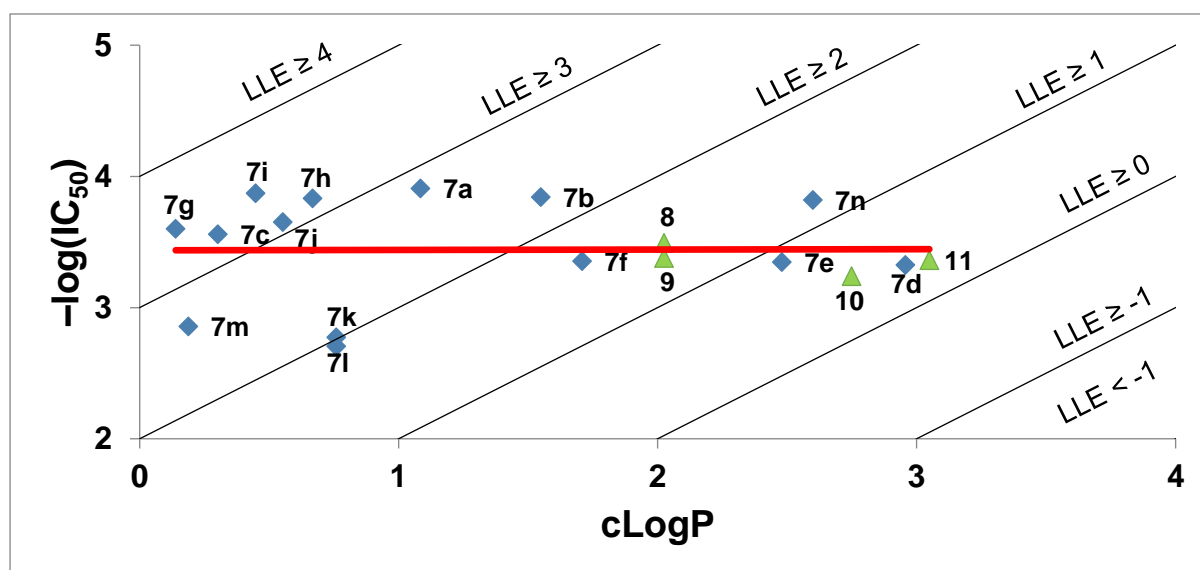


Figure S1. Plot and correlation of the affinity of sulfonamides **7a-7n**, halides **8** and **9**, and biaryl derivatives **10** and **11** vs cLogP values of the compounds. \blacklozenge Sulfonamides. \blacktriangle Halides and biaryl compounds. — Line of best fit. cLogP values were calculated with ChemDraw 17.0.

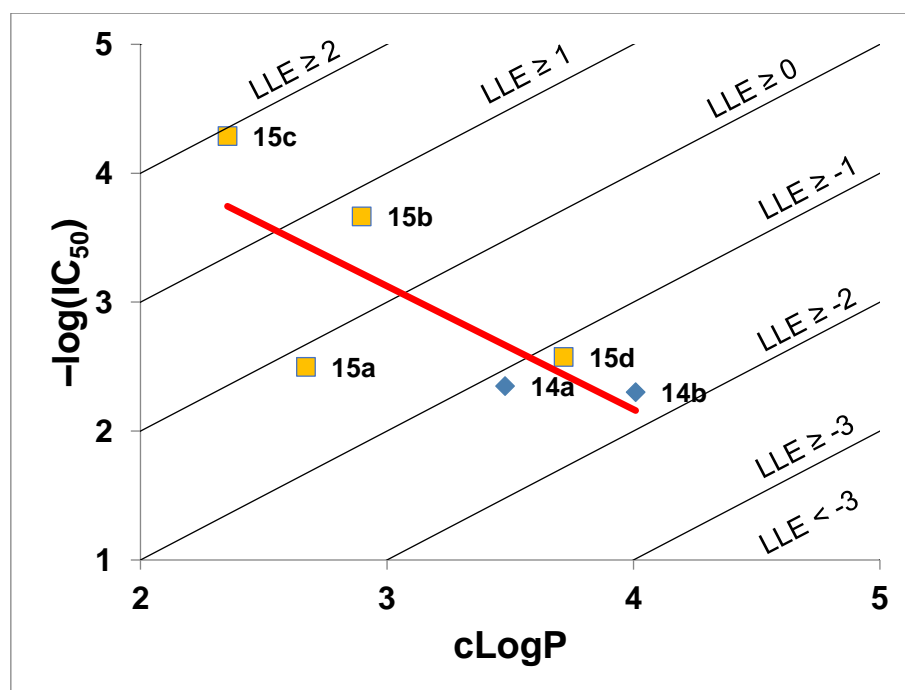


Figure S2. Plot and correlation of the affinity of cross-coupled products **14a-14b** and **15a-15d** vs cLogP values of the compounds. \blacklozenge Heck/hydrogenation compounds. \blacksquare Suzuki compounds. — Line of best fit. cLogP values were calculated with ChemDraw 17.0.

Appendix I – Dose Response Curves of Phenyl NMP Derivatives

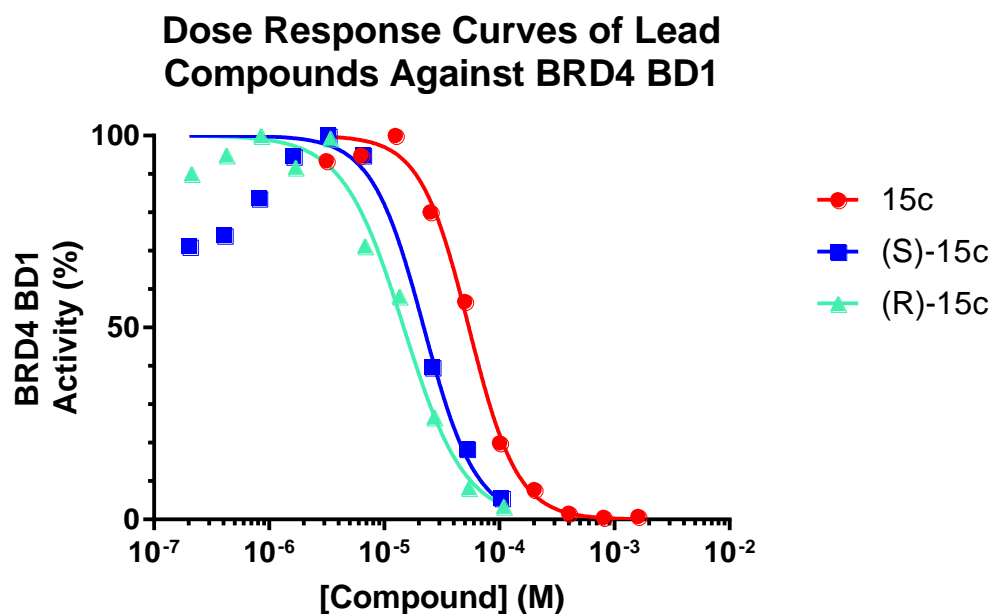


Figure S1. Dose-response curves to determine the IC₅₀ of the lead compound **15c** and the pure enantiomers. Curve fits were calculated using GraphPad Prism. Experiments were performed in duplicates.

Appendix J – Video of Phenyl NMP Derivatives

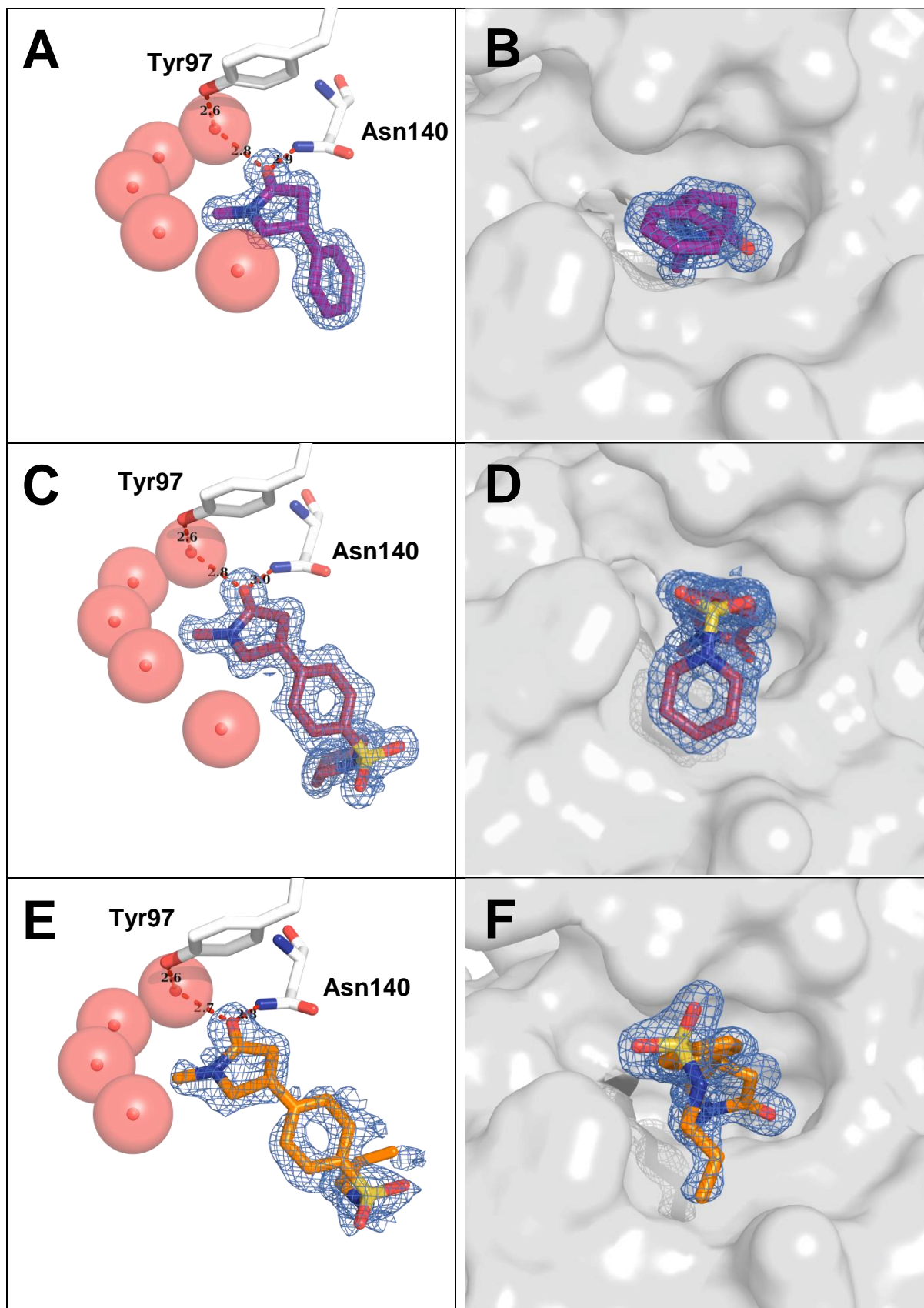
Video provided on USB.

Video to be uploaded in the near-future.

Crystal structures of **5**, **7b**, **7h** and **15c** developed by Dr. Ian Jennings and Dr. Olga Ilyichova.

Video edited and narrated by Joseph Hilton-Proctor.

Appendix K – Electron Density Map of NMP Derivatives



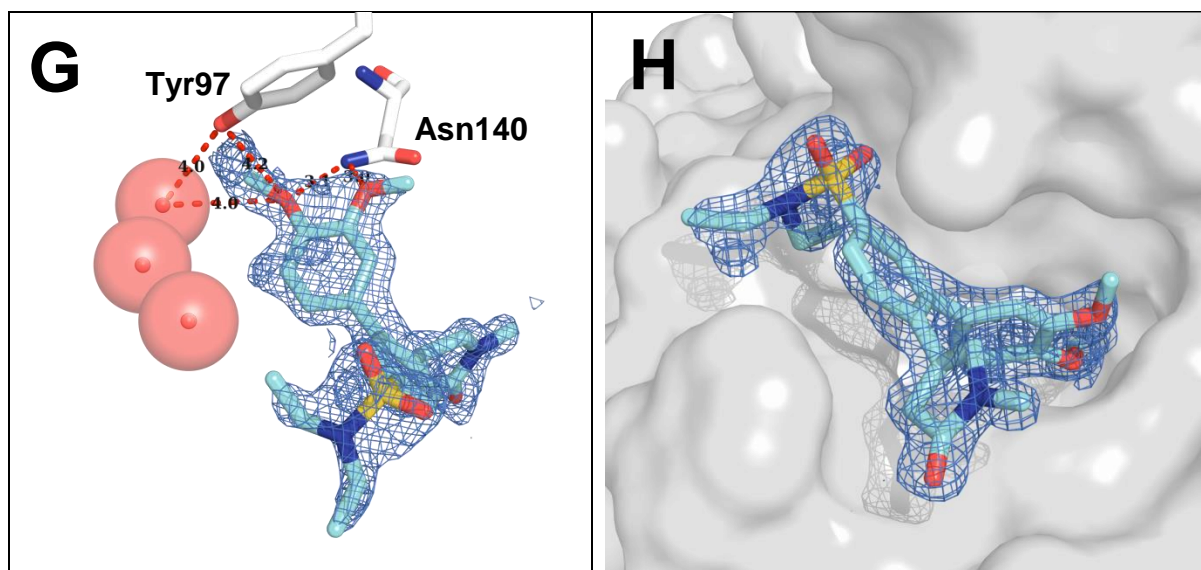
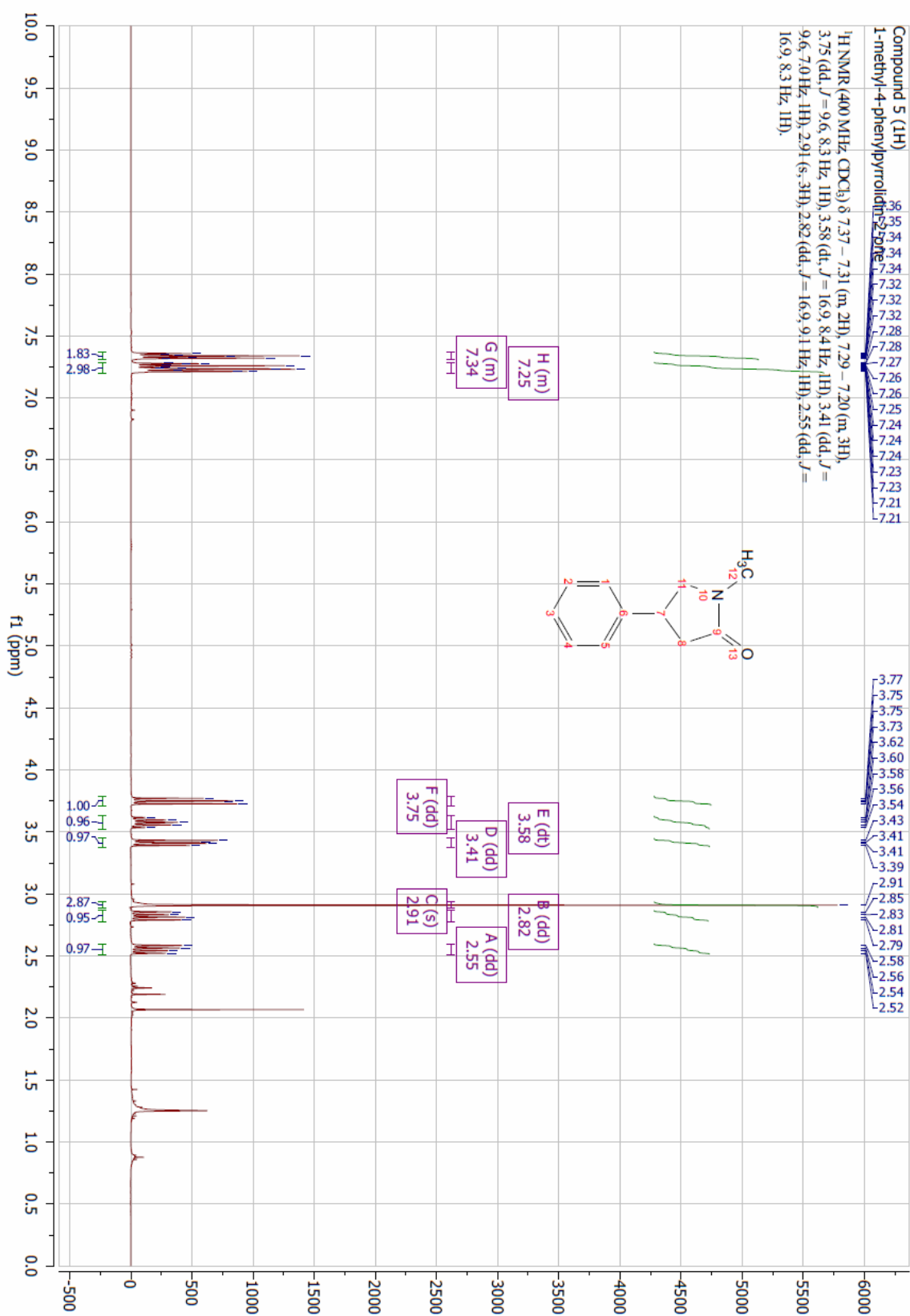
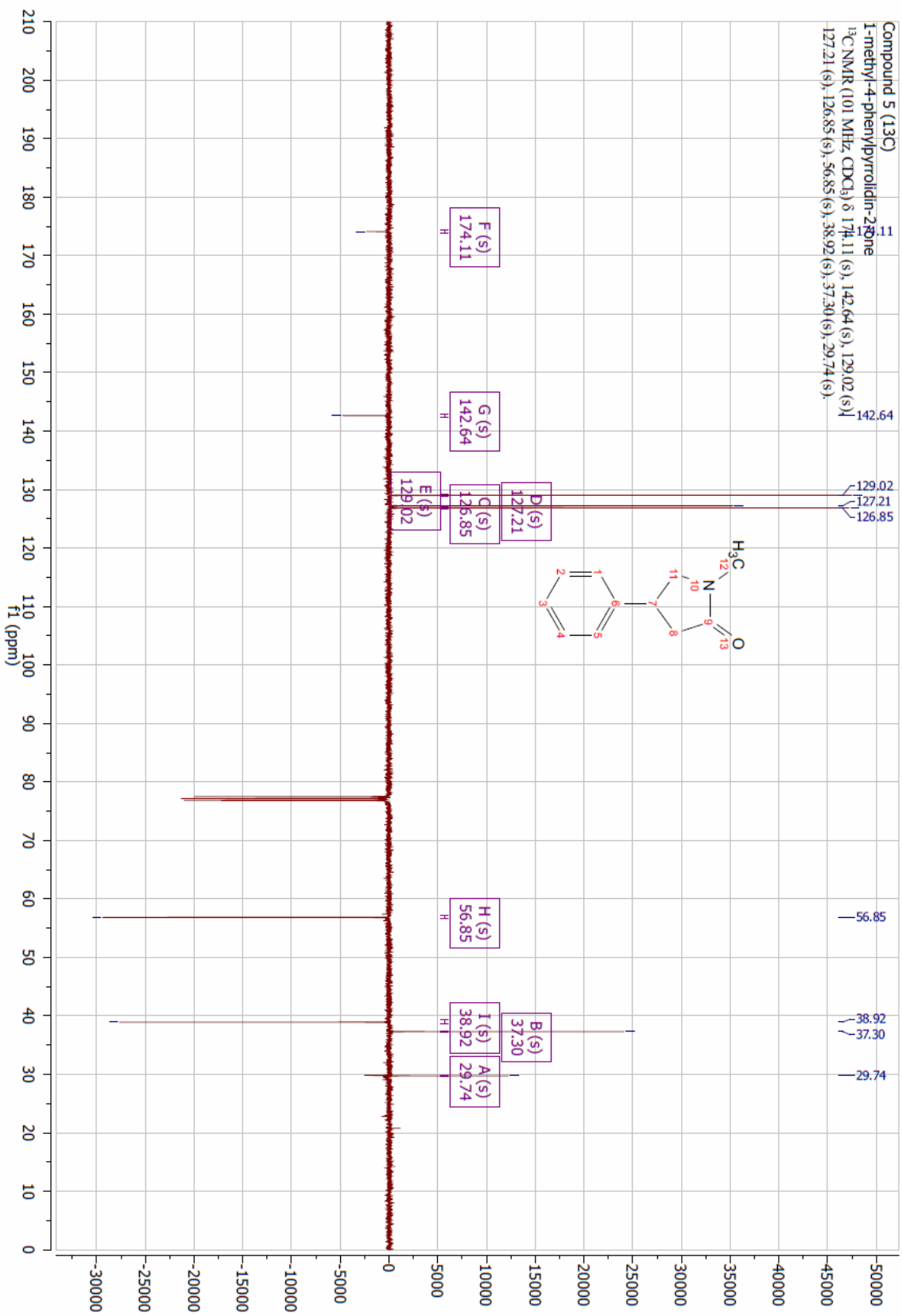
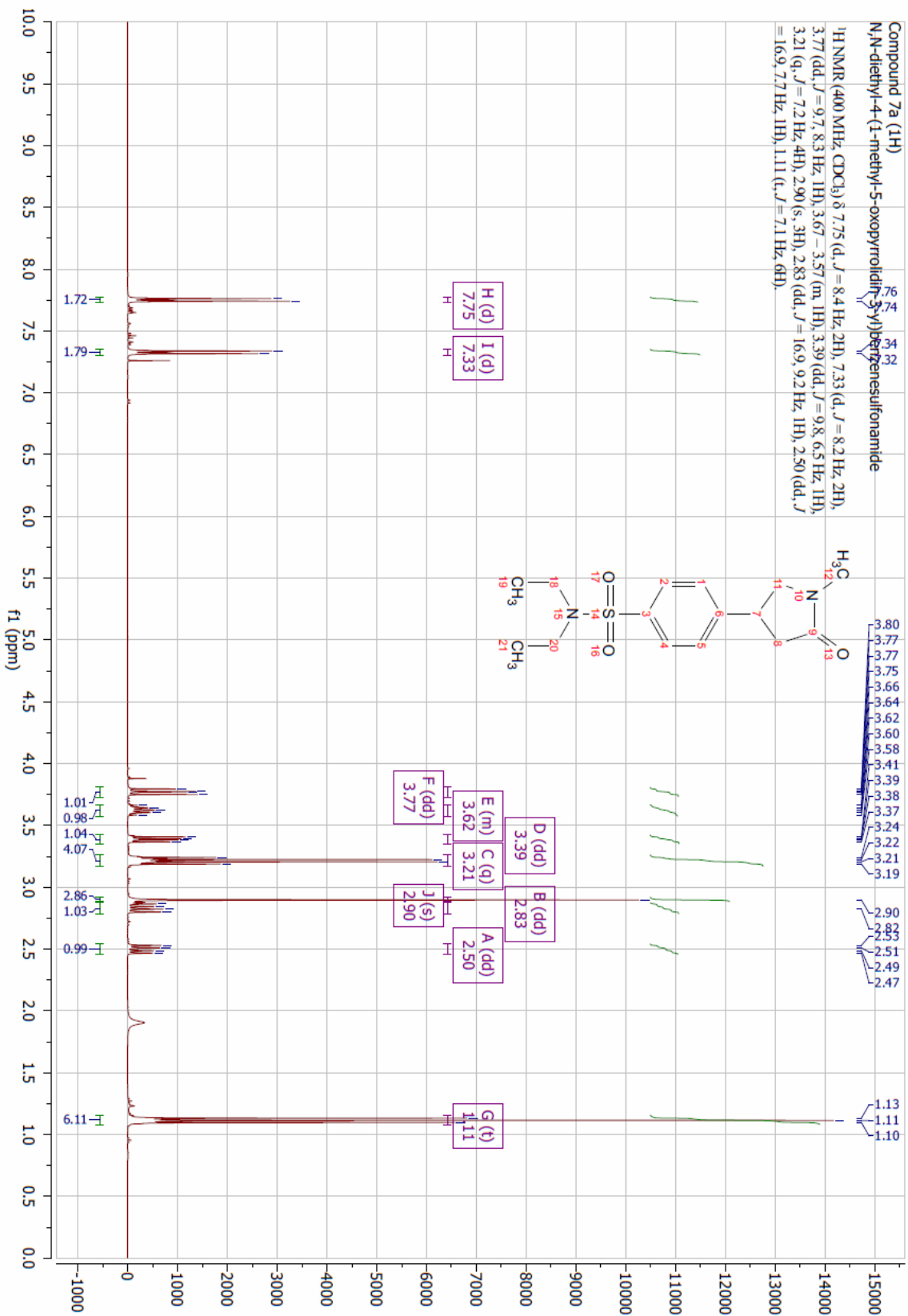


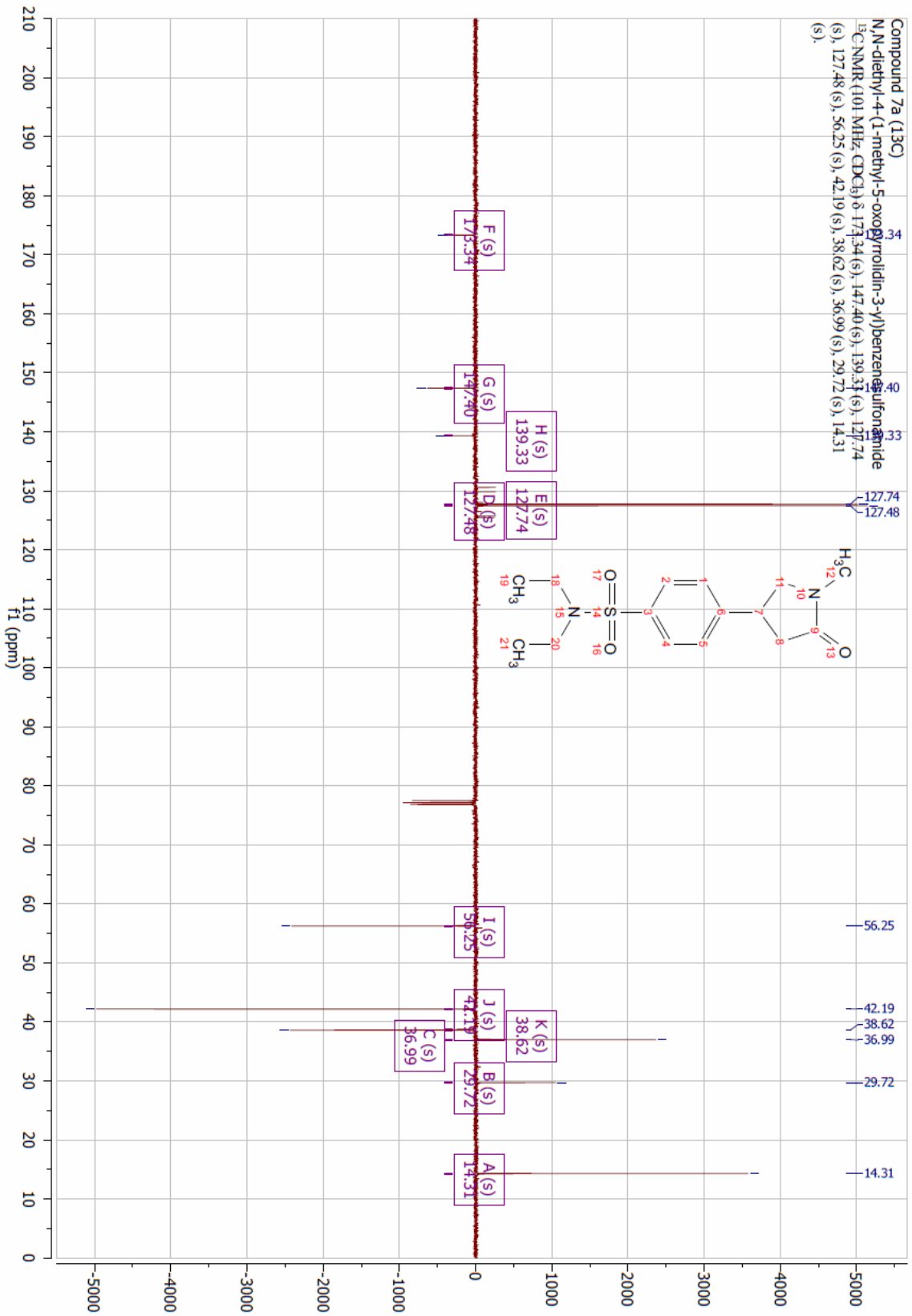
Figure S1. Electron density maps of phenyl NMP derivatives. [A, B] (*R*)-**5** (purple, resolution: 1.5 Å). [C, D] (*R*)-**7b** (raspberry, resolution: 1.55 Å). [E, F] (*R*)-**7h** (orange, resolution: 1.59 Å). [G, H] (*S*)-**15c** (cyan, resolution: 1.48 Å). [A, C, E, G] Binding site. [B, D, F, H] Outside the binding site. The 2Fo-Fc electron density maps are shown in blue mesh at a contour level of 1.0 sigma. Electron density maps developed by Dr. Olga Ilyichova.

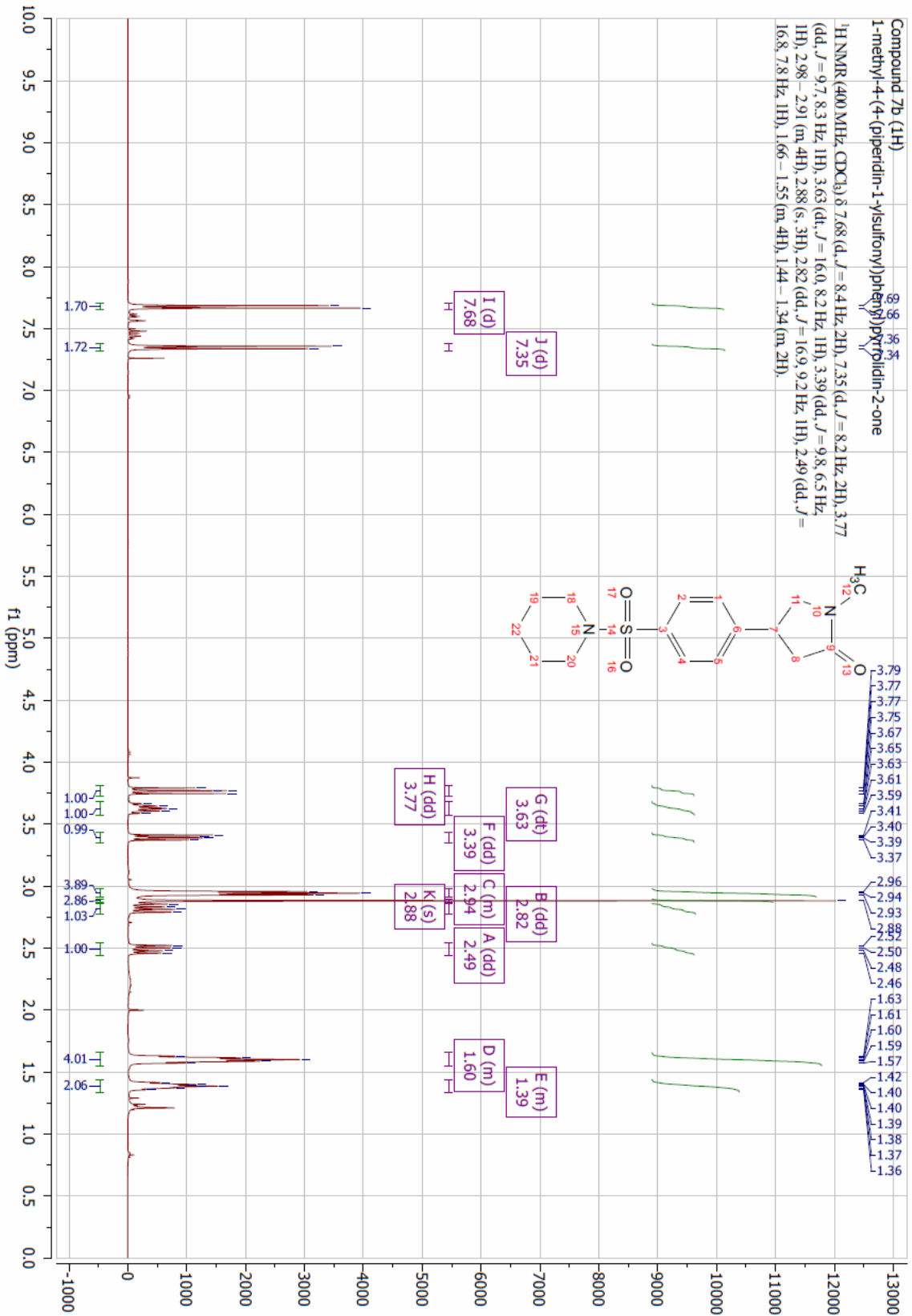
Appendix L – Chapter 3 NMR Data

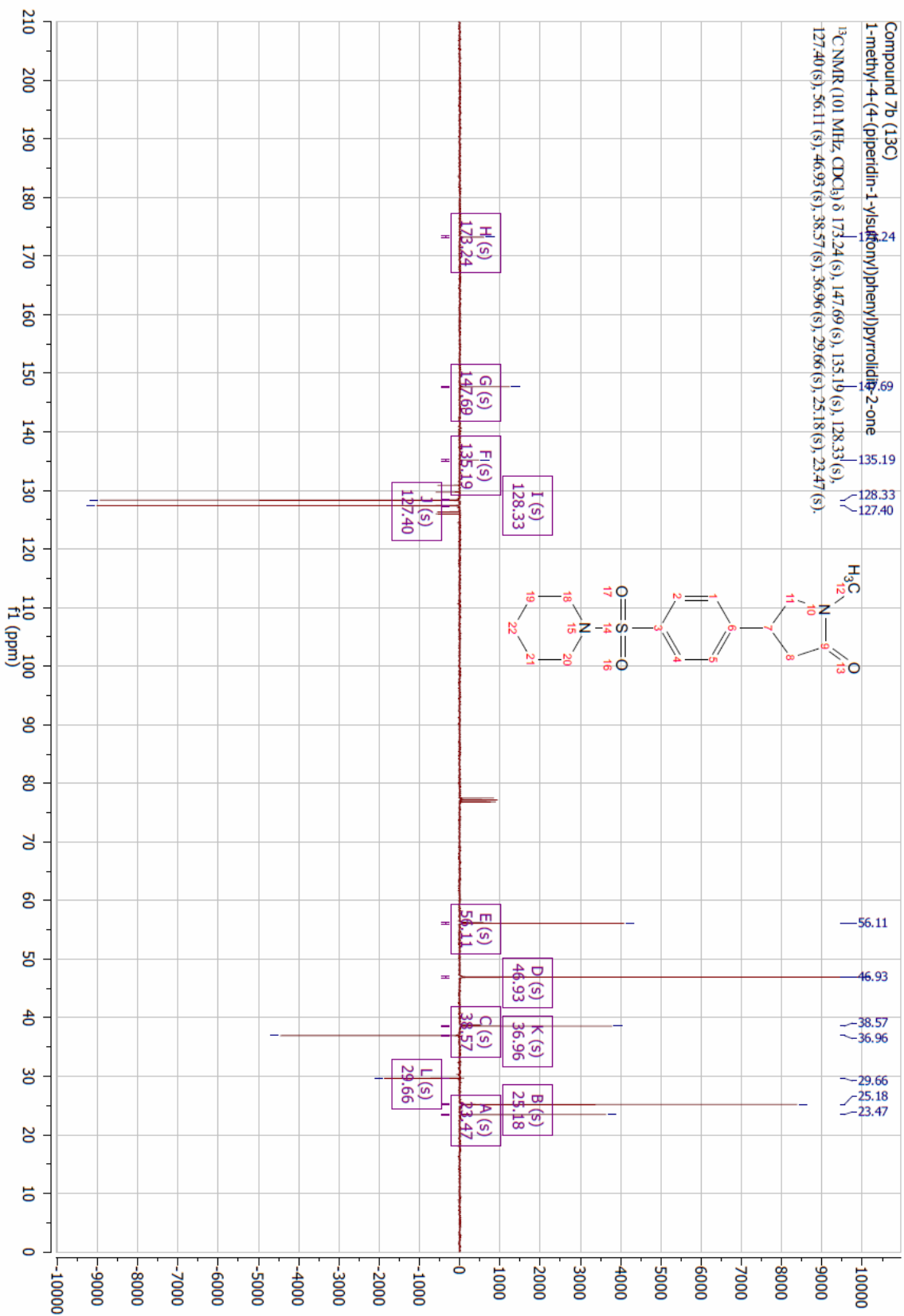


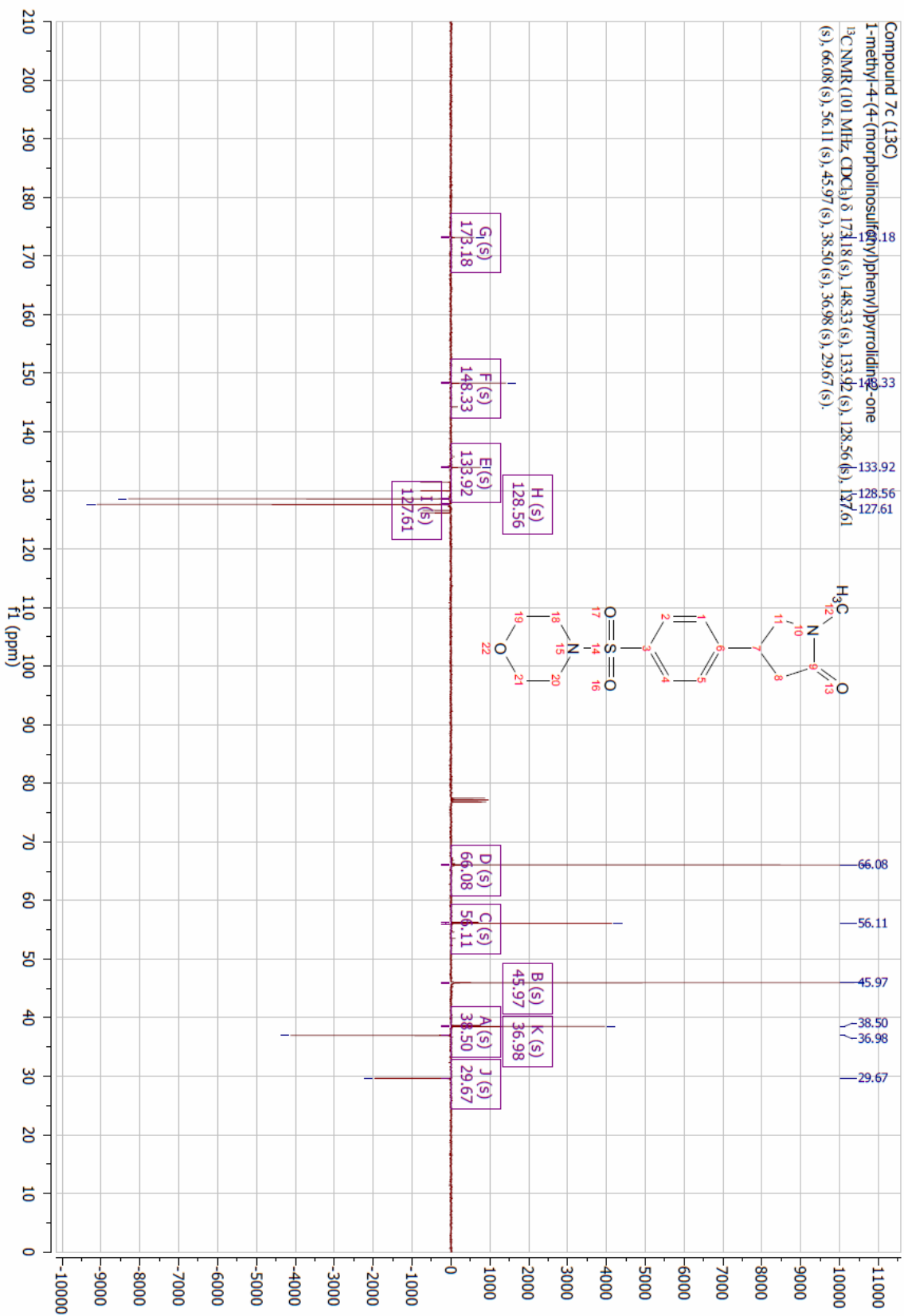


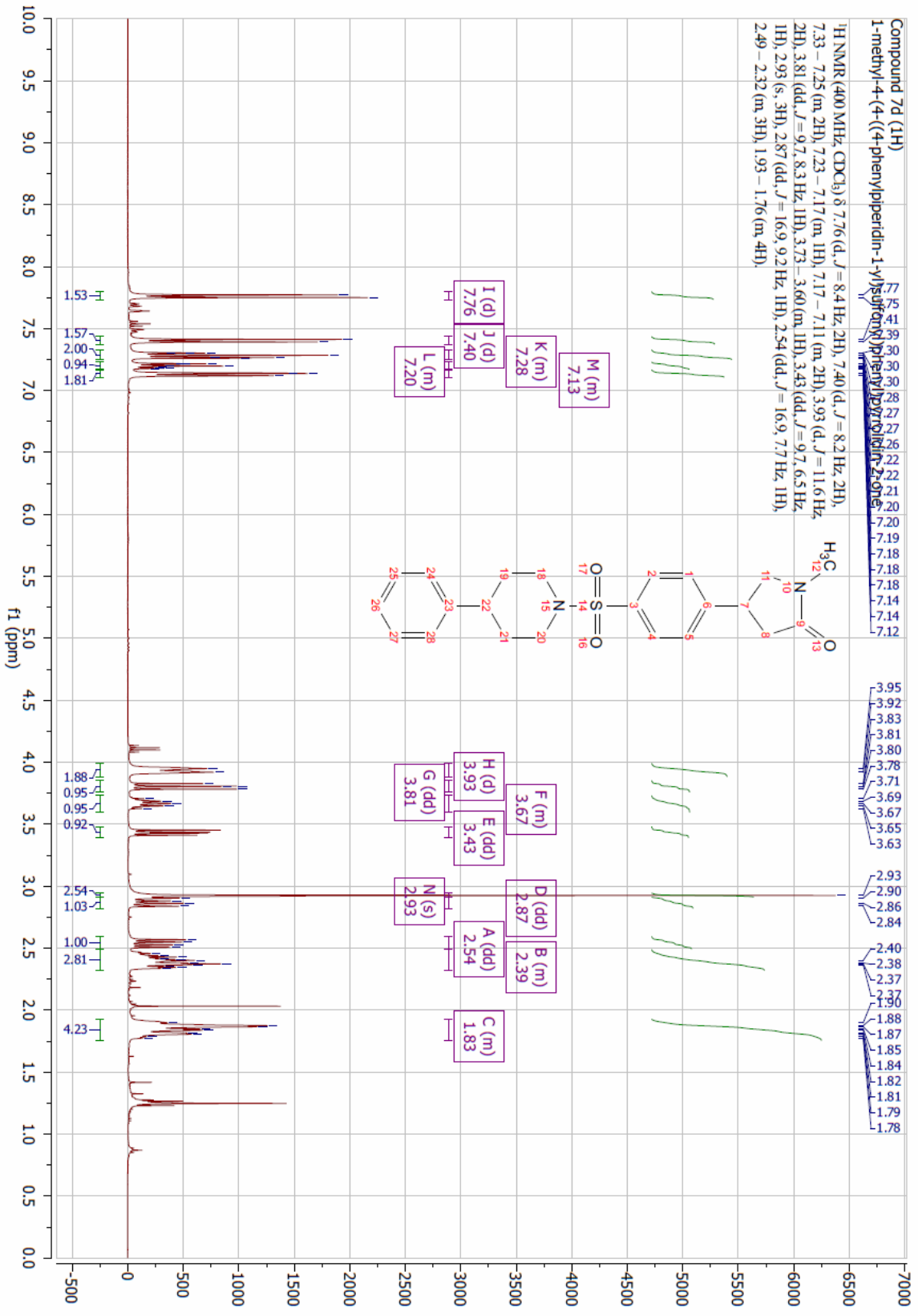


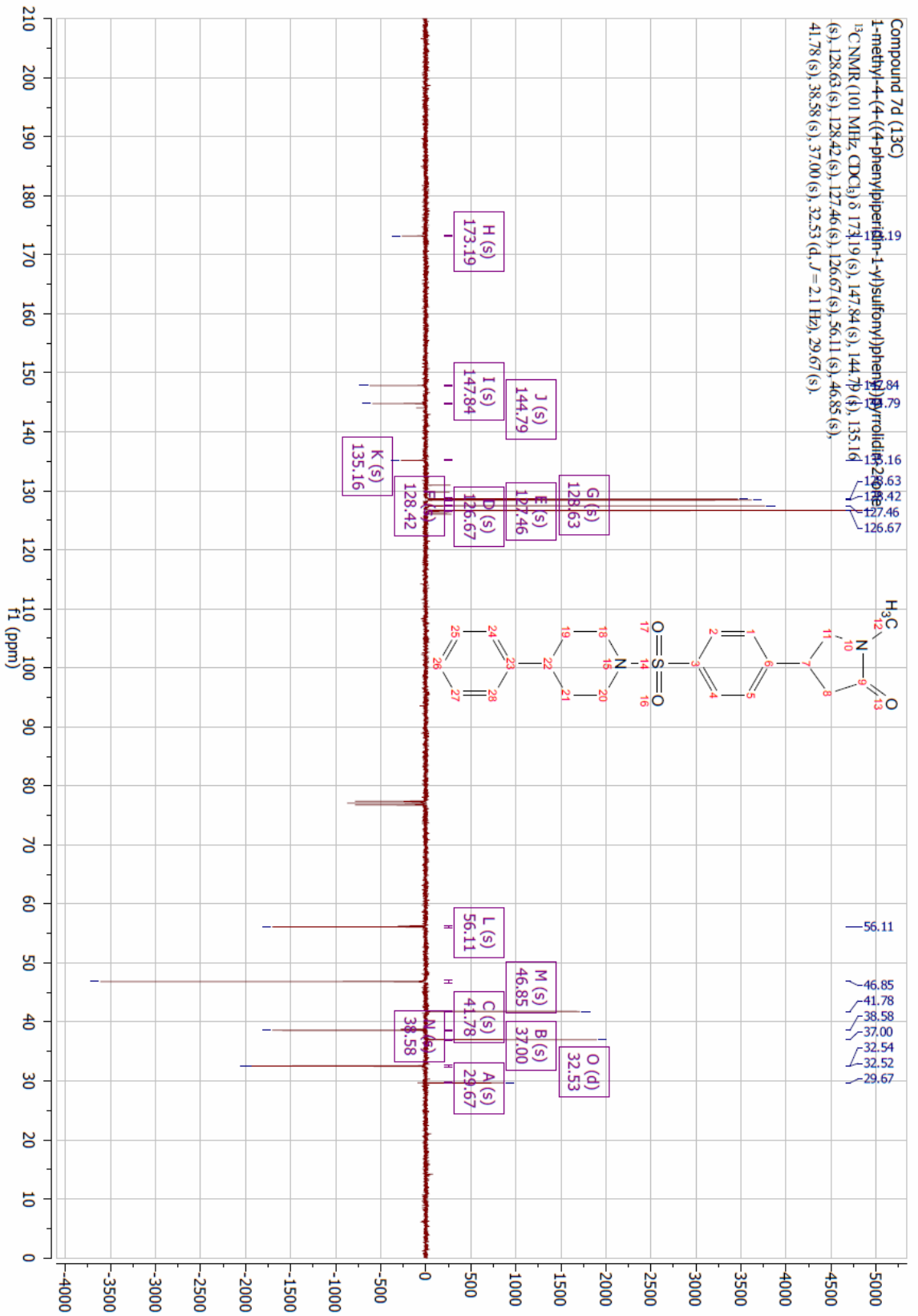


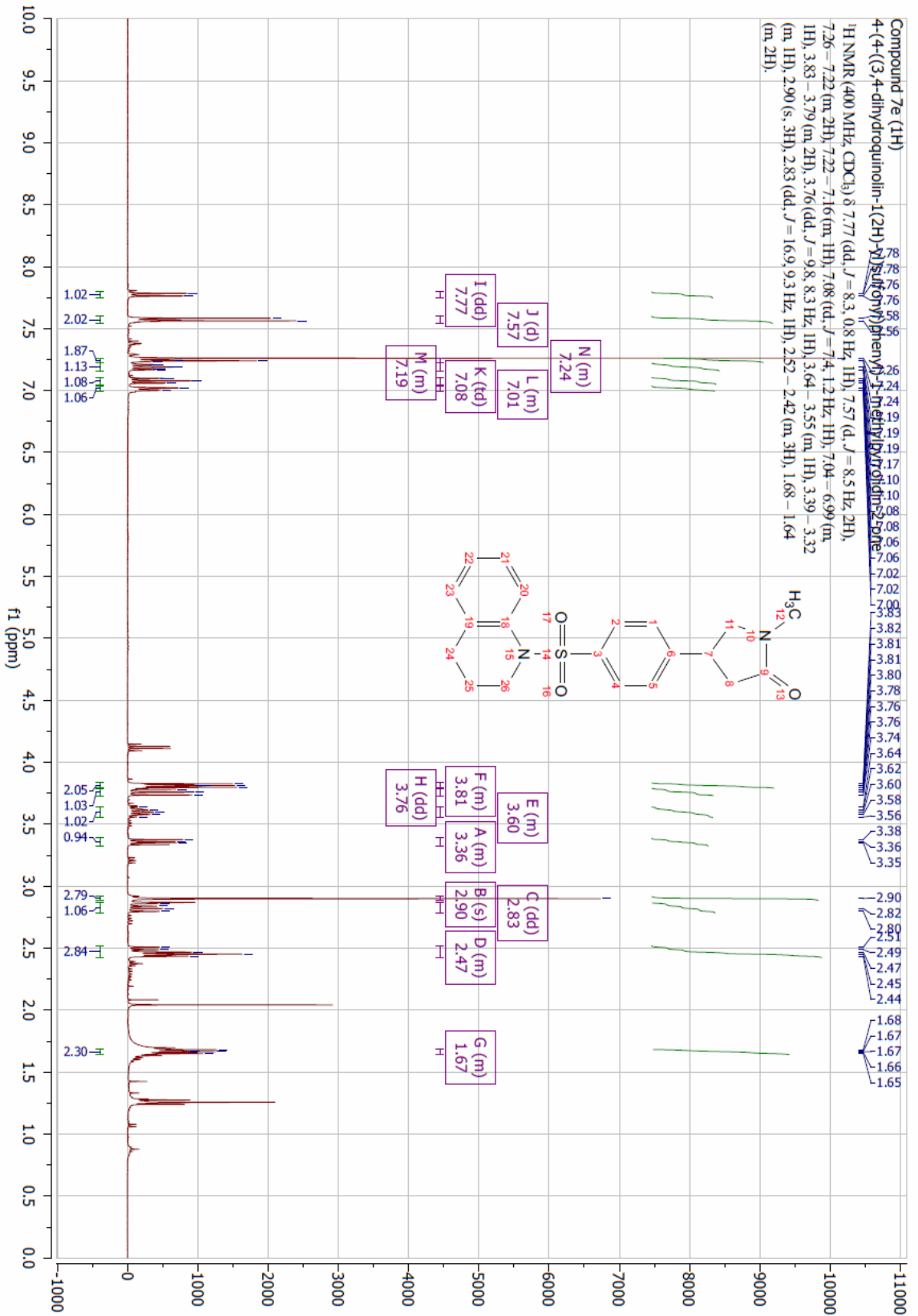


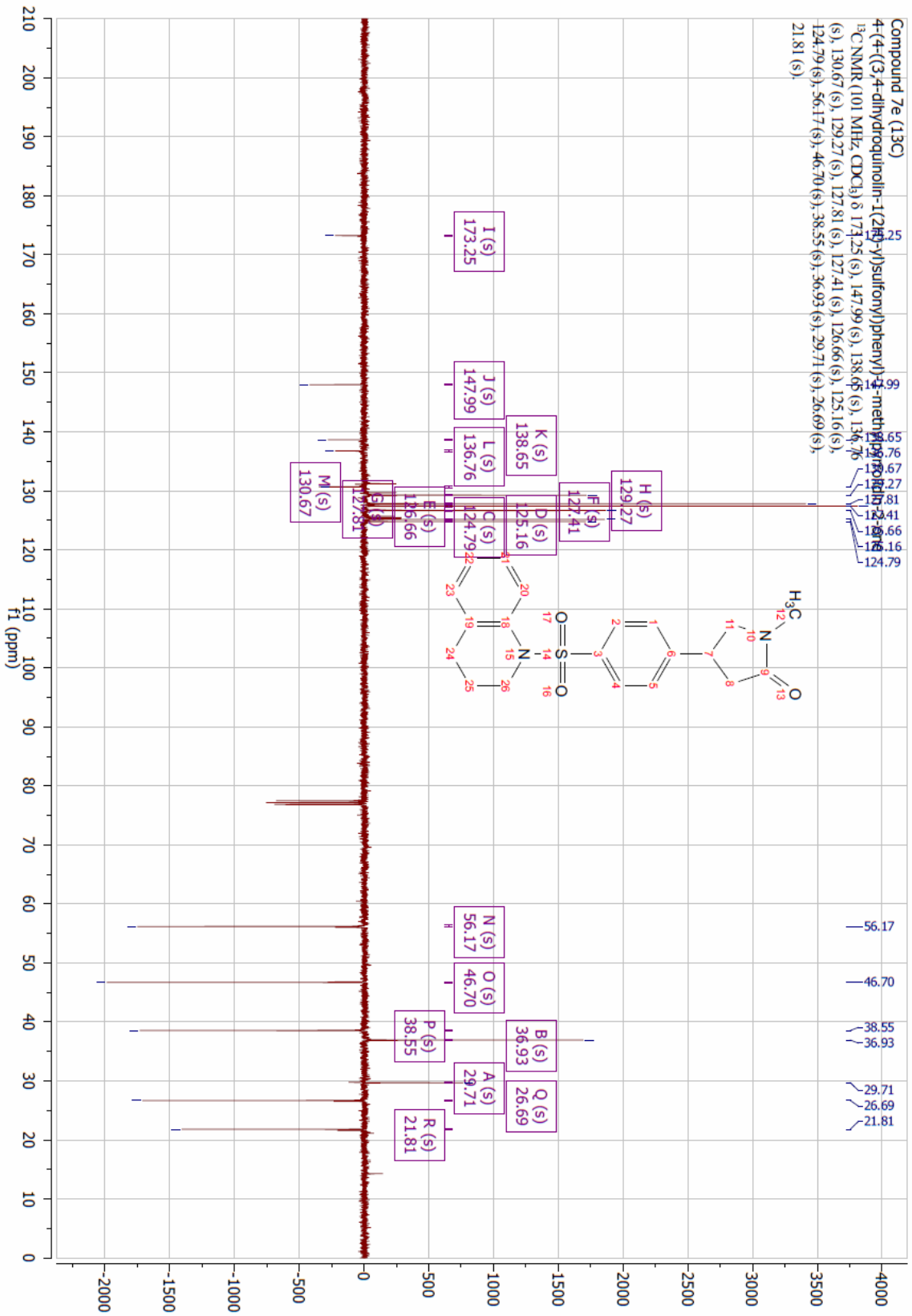


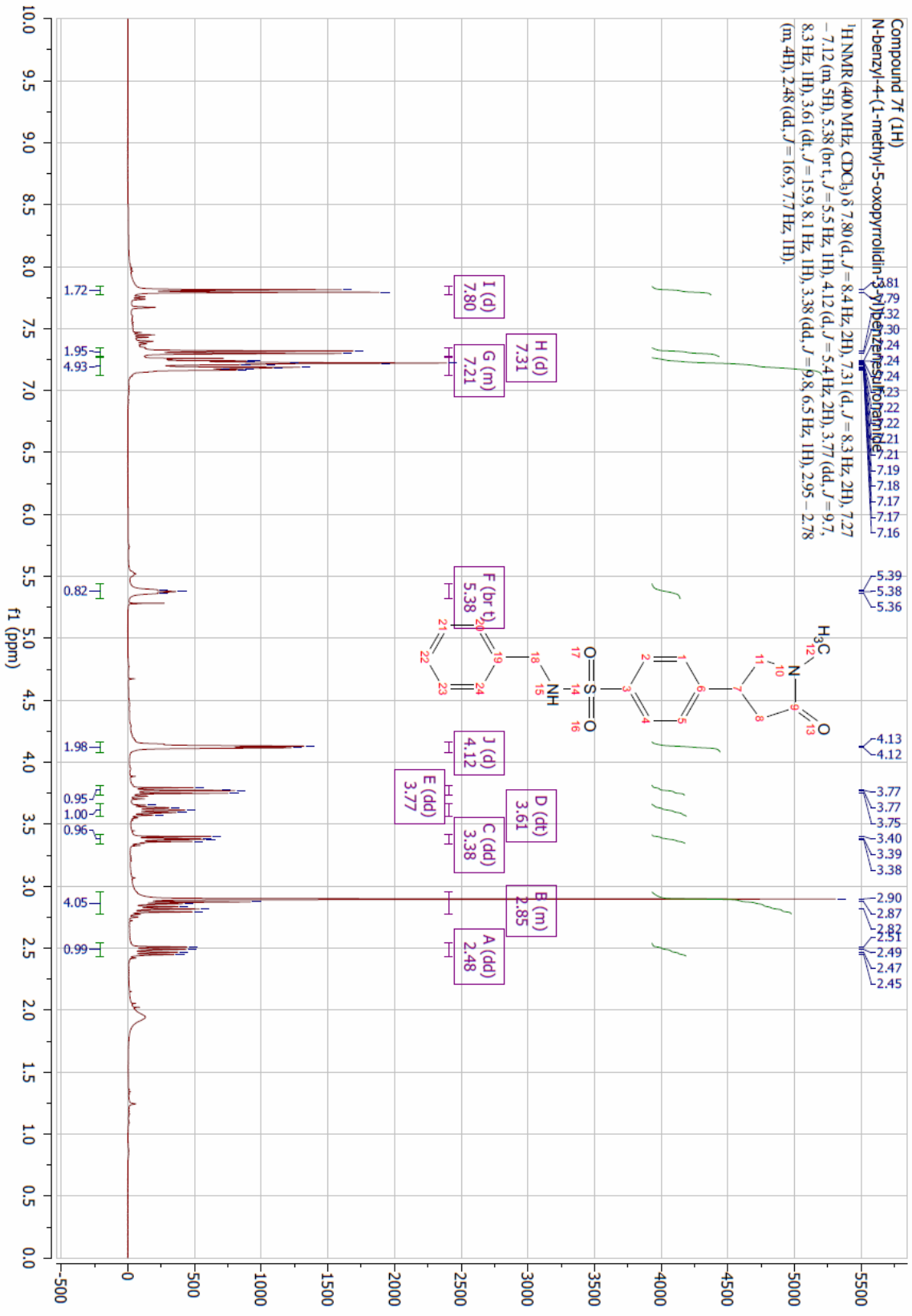


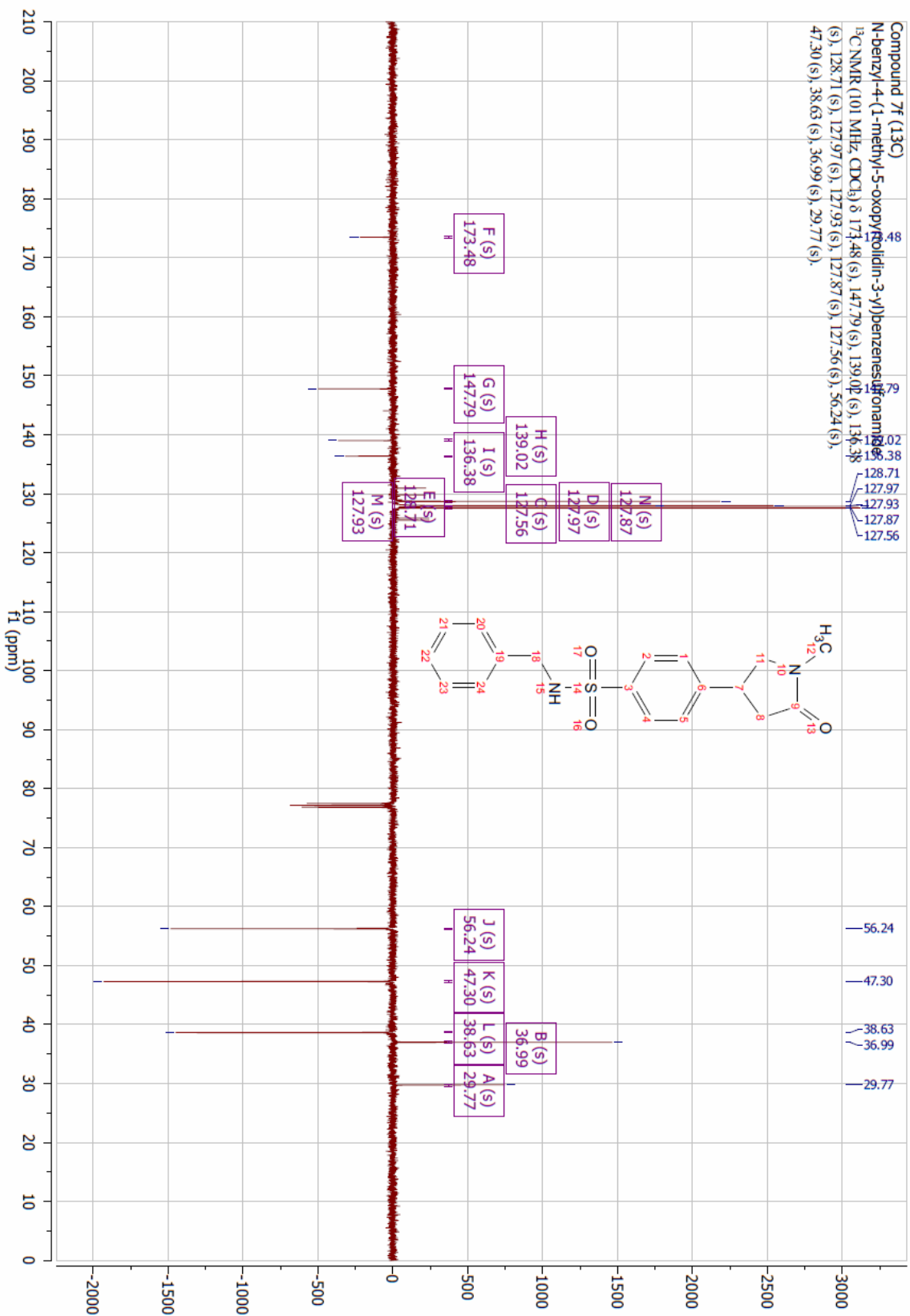


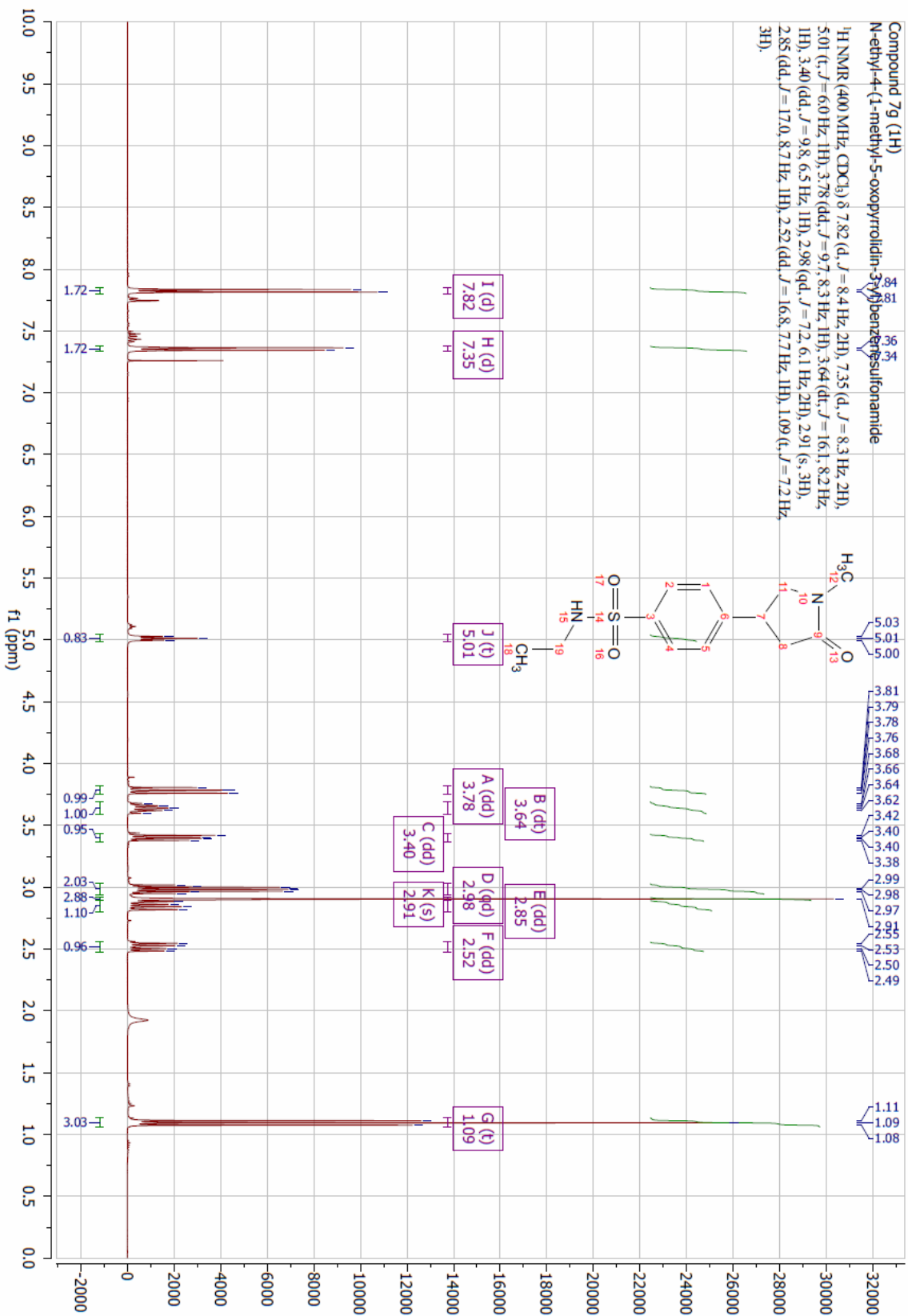


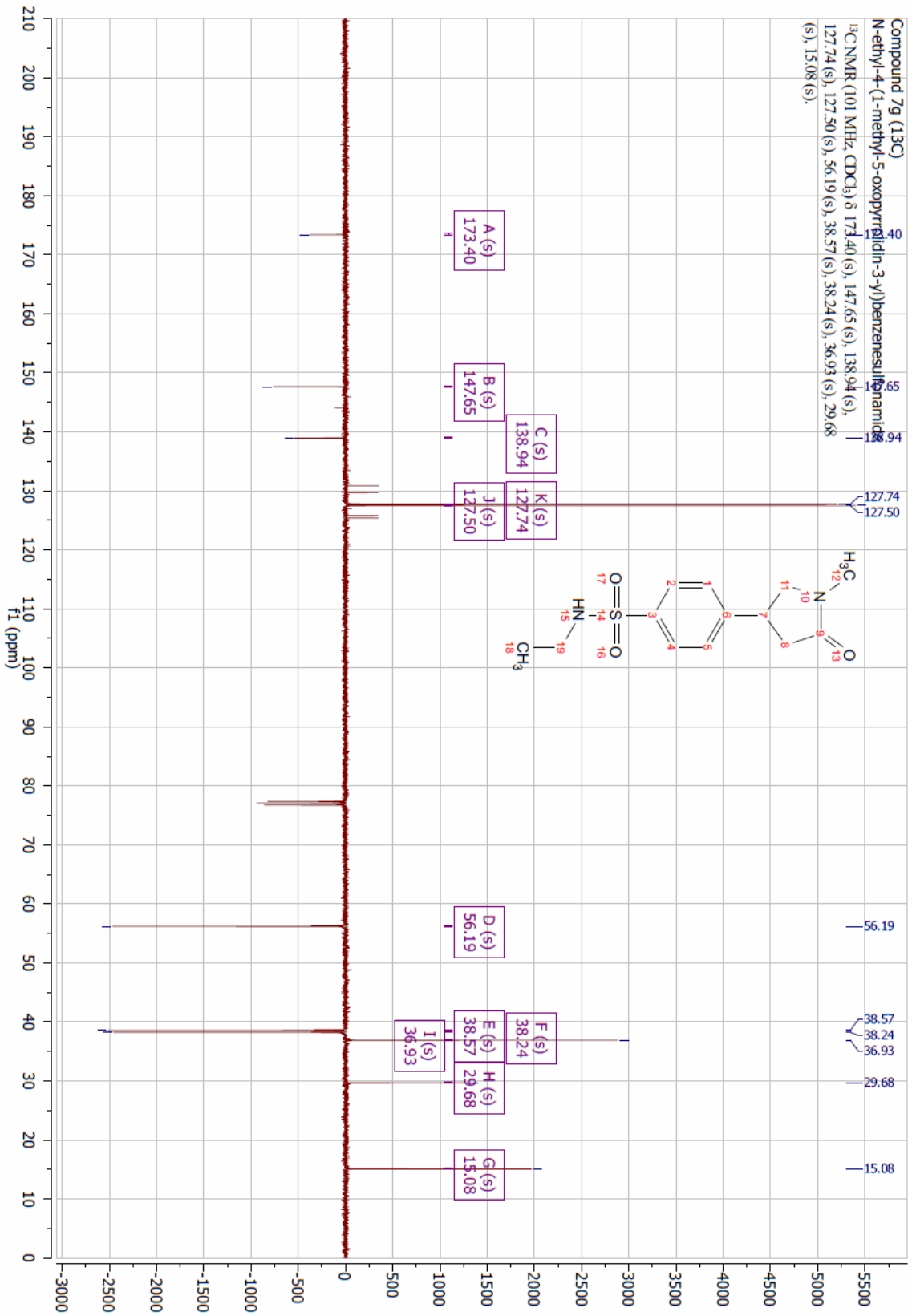


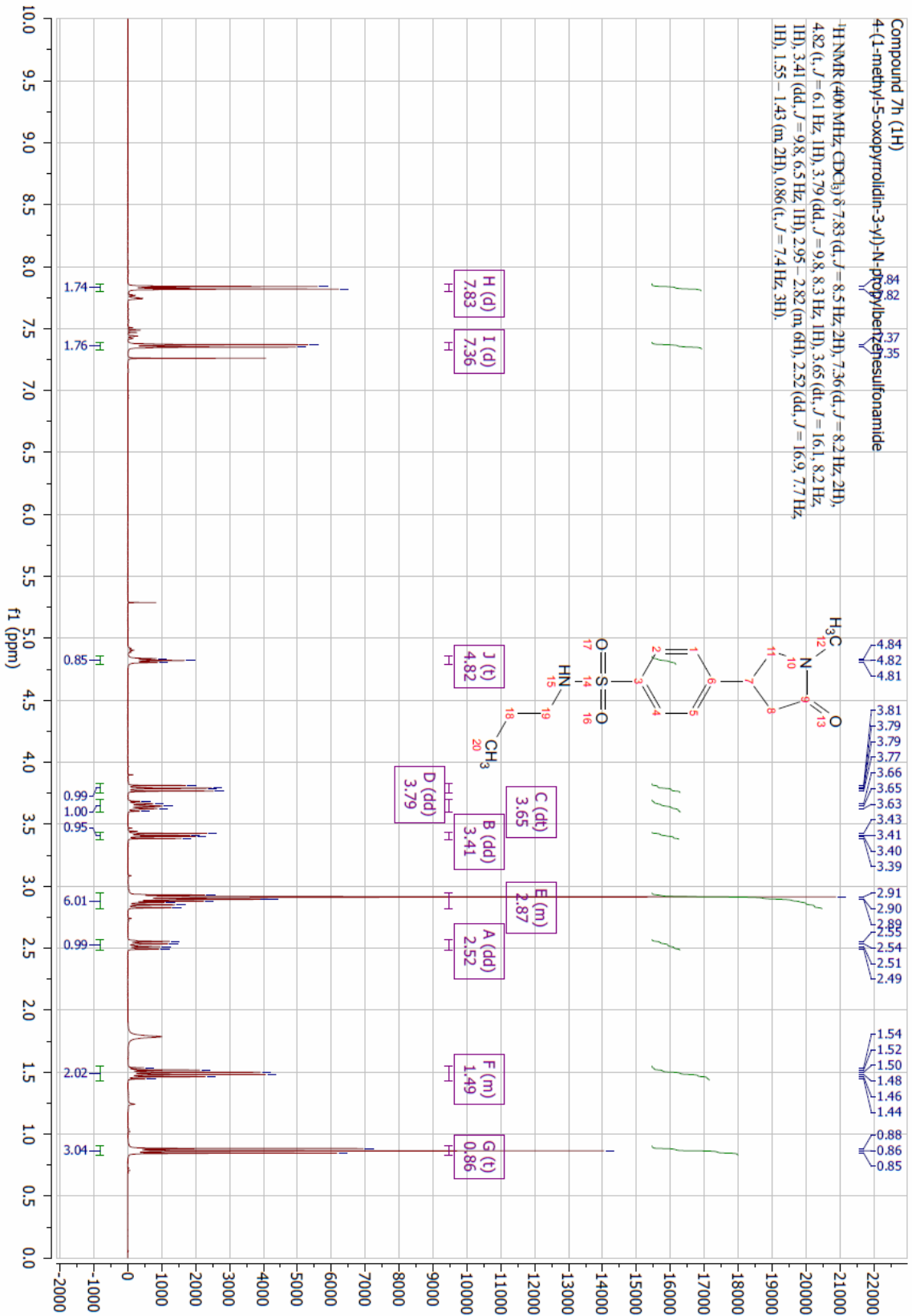


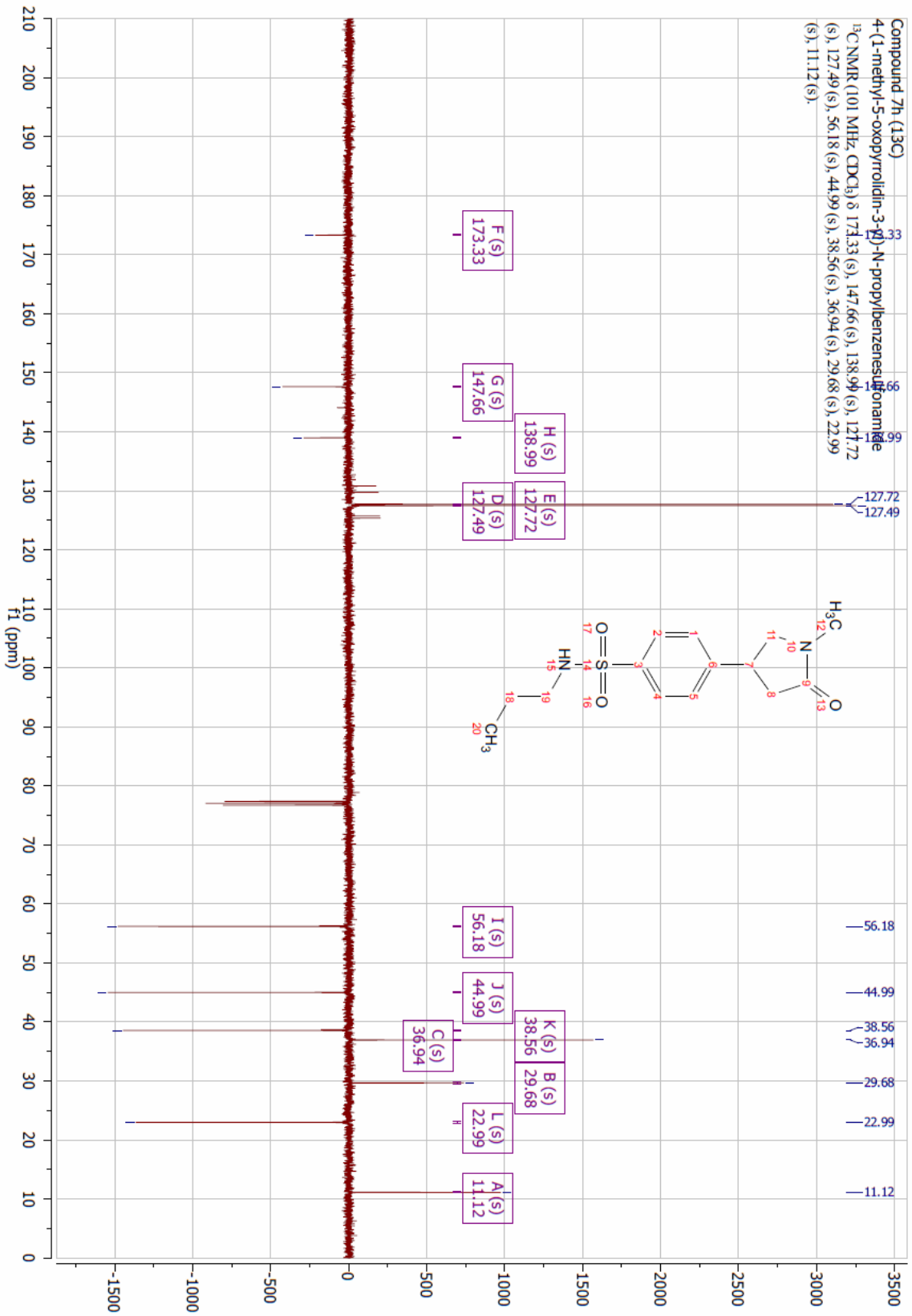


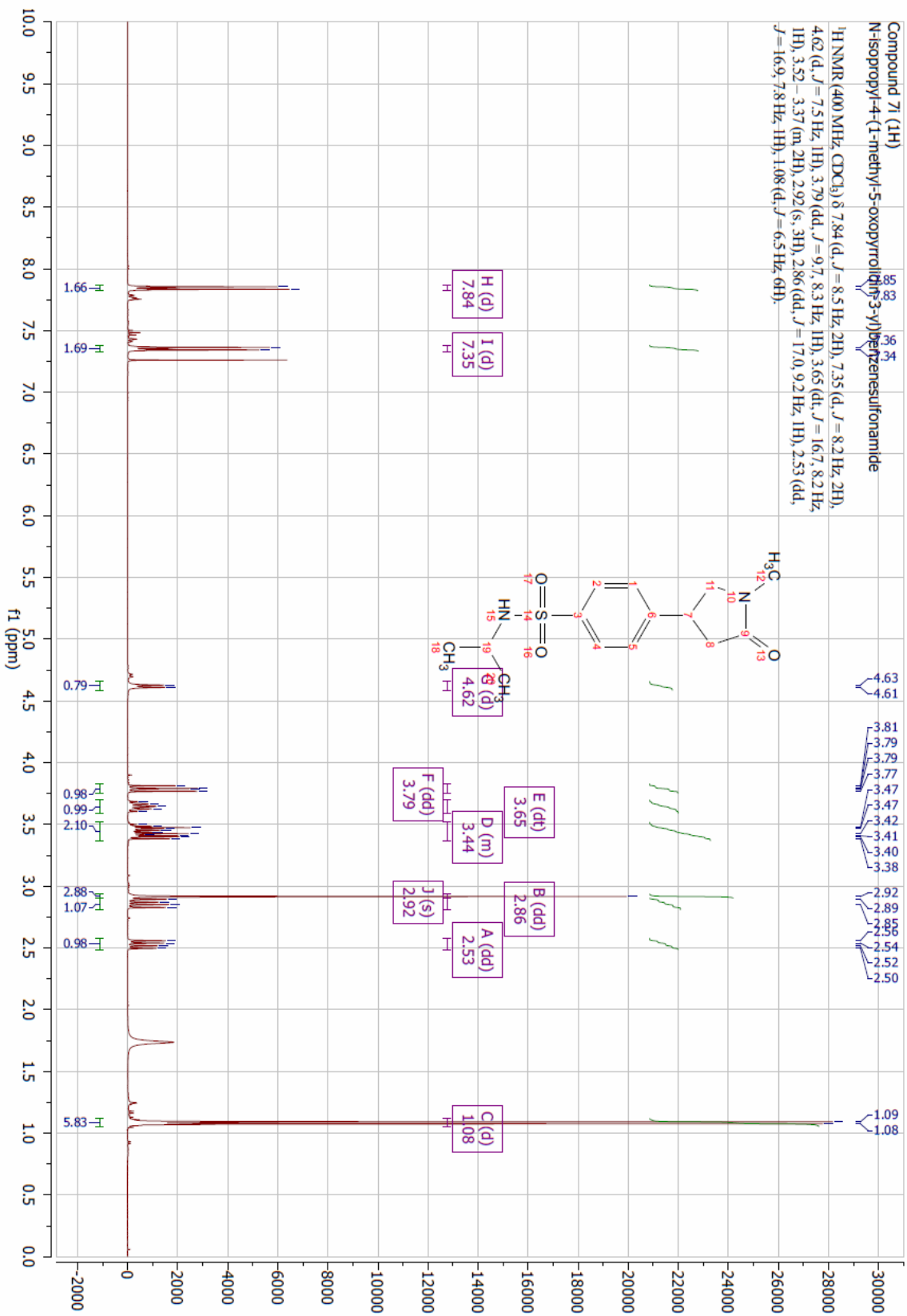


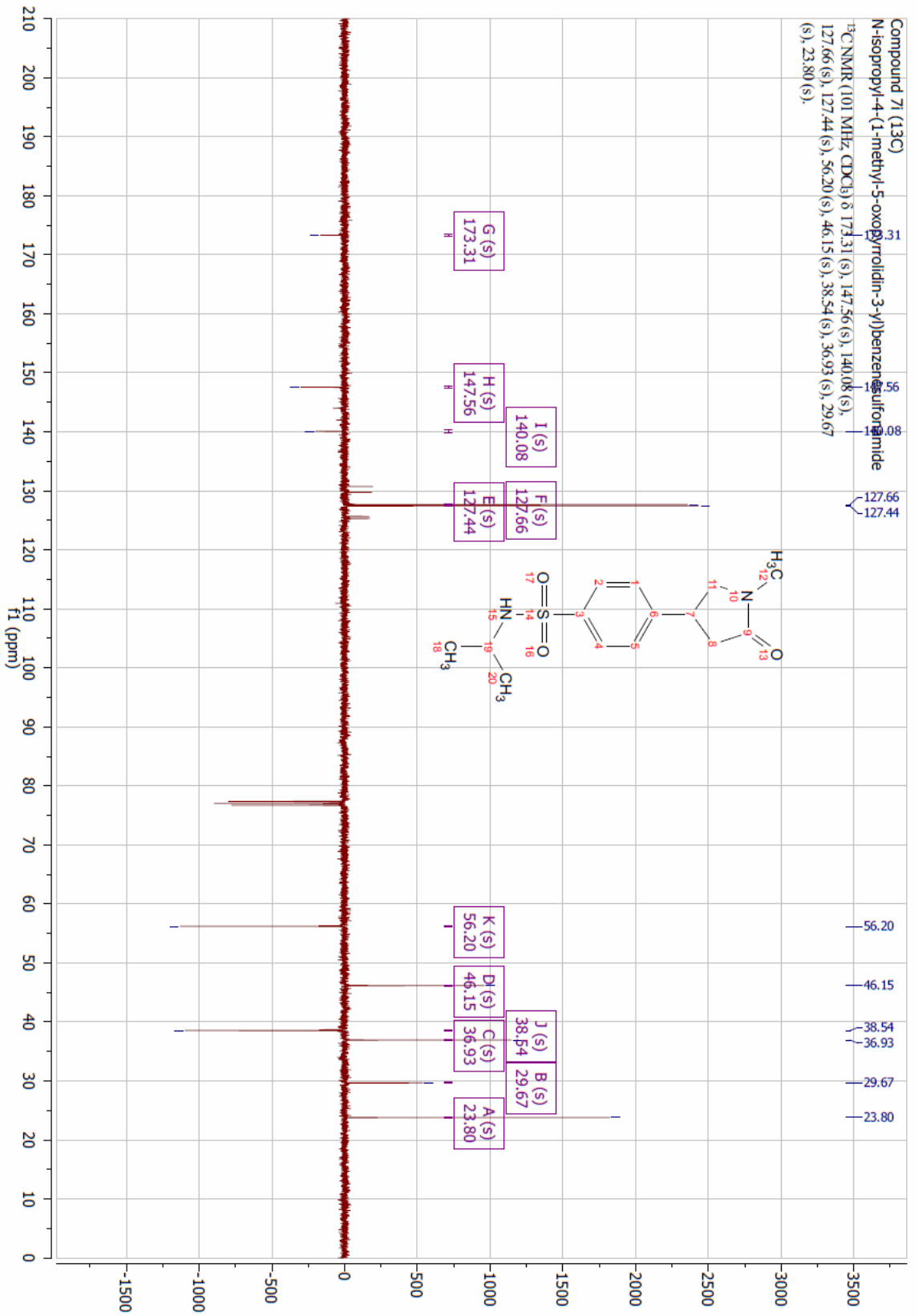


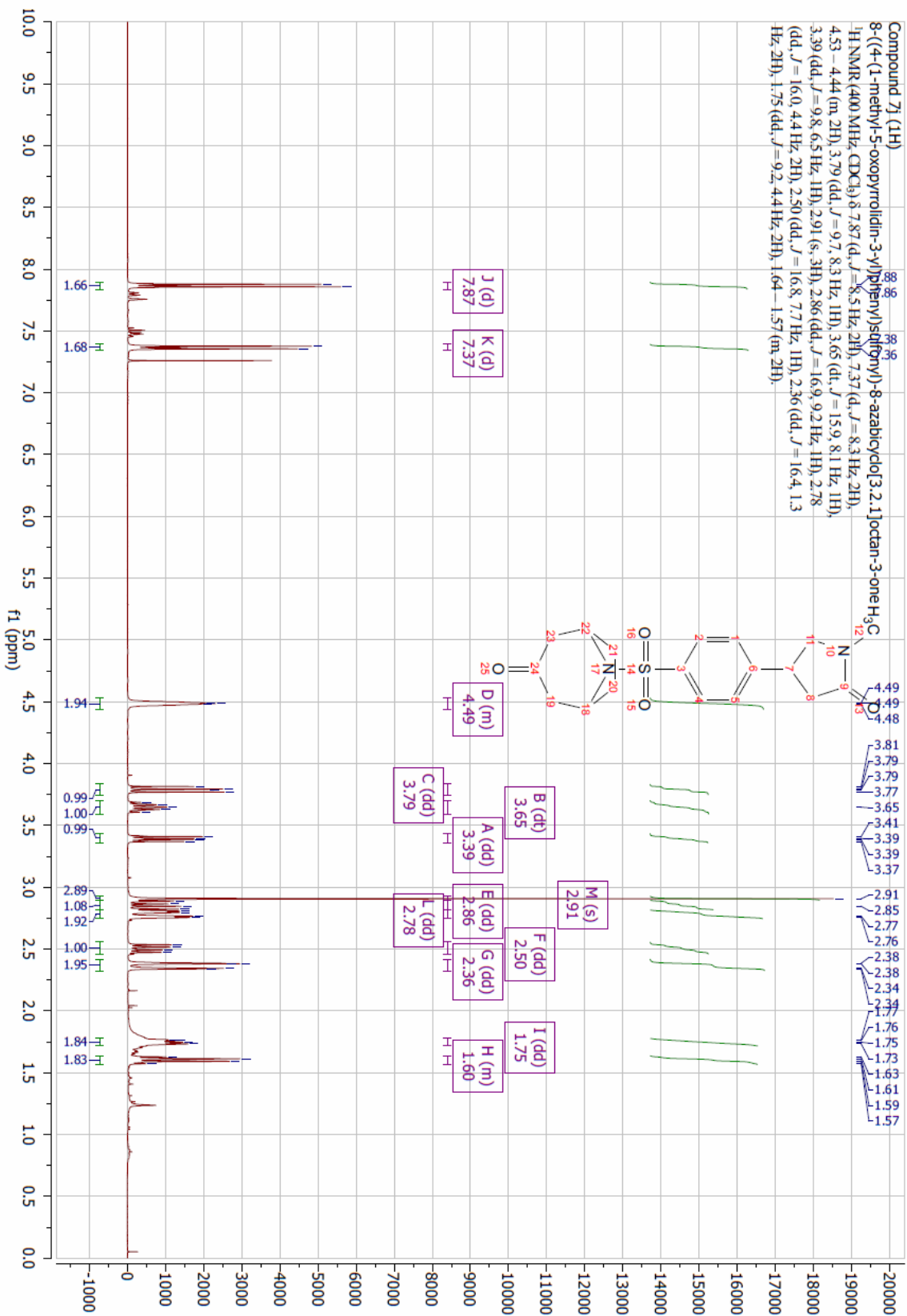


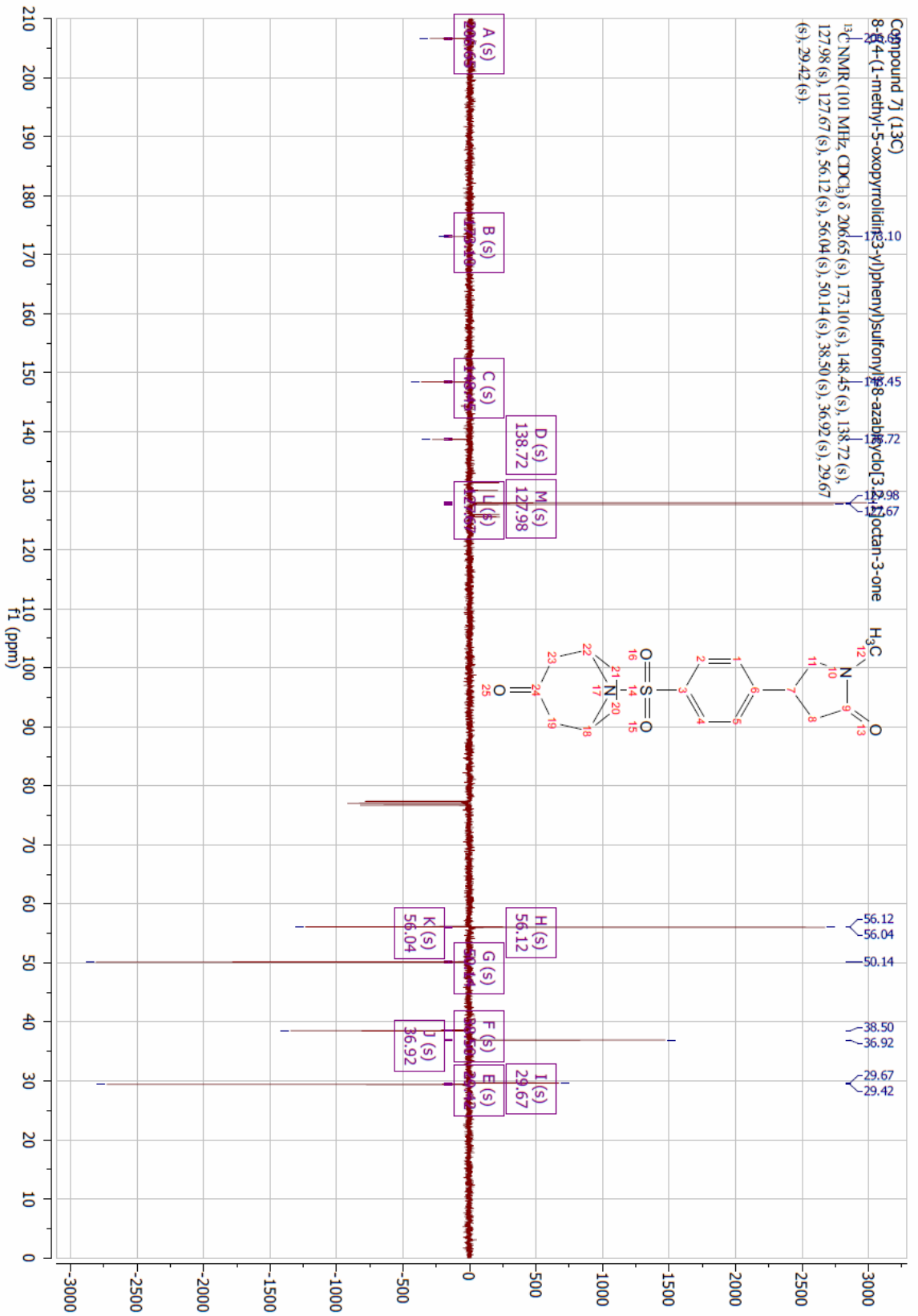


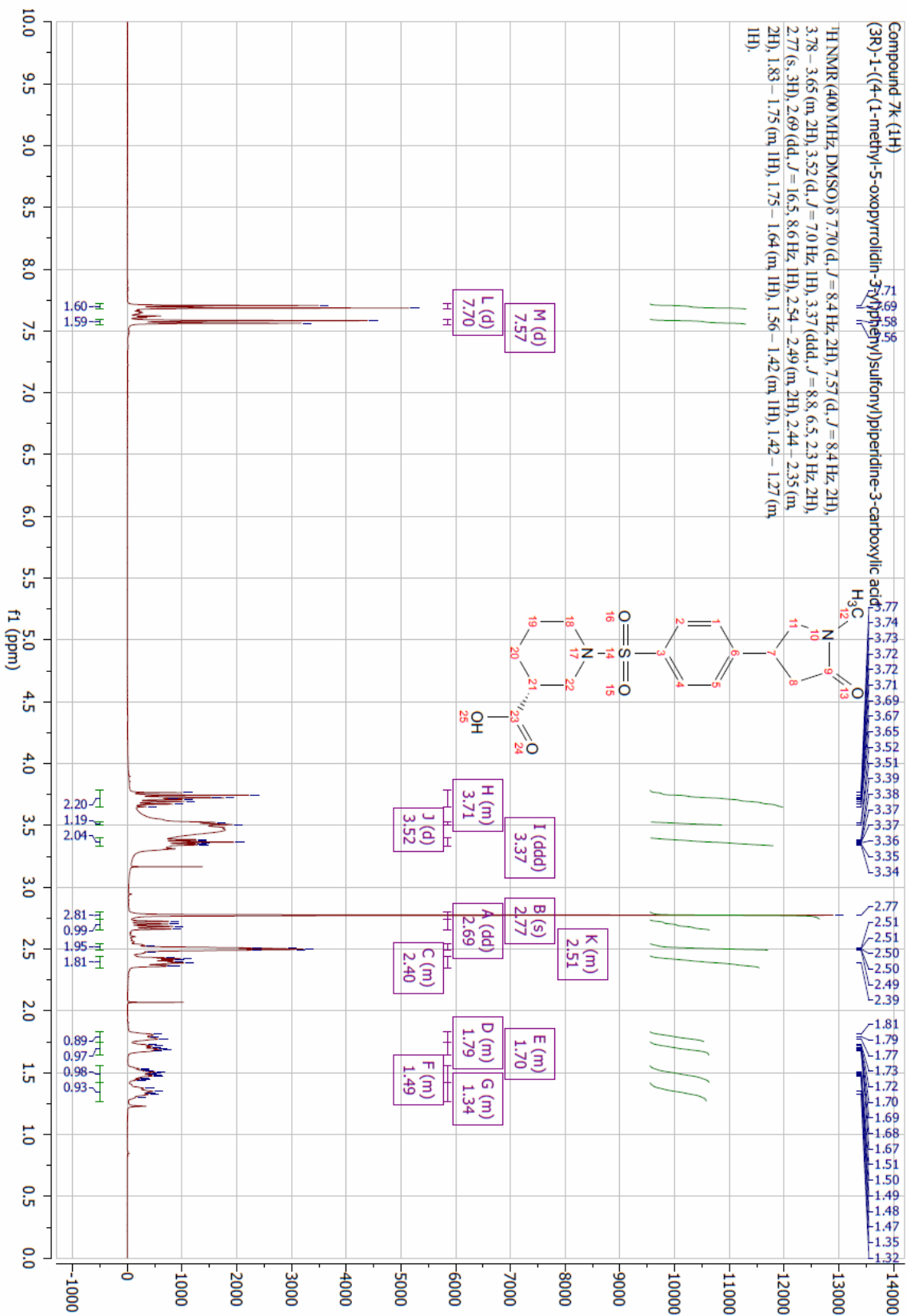


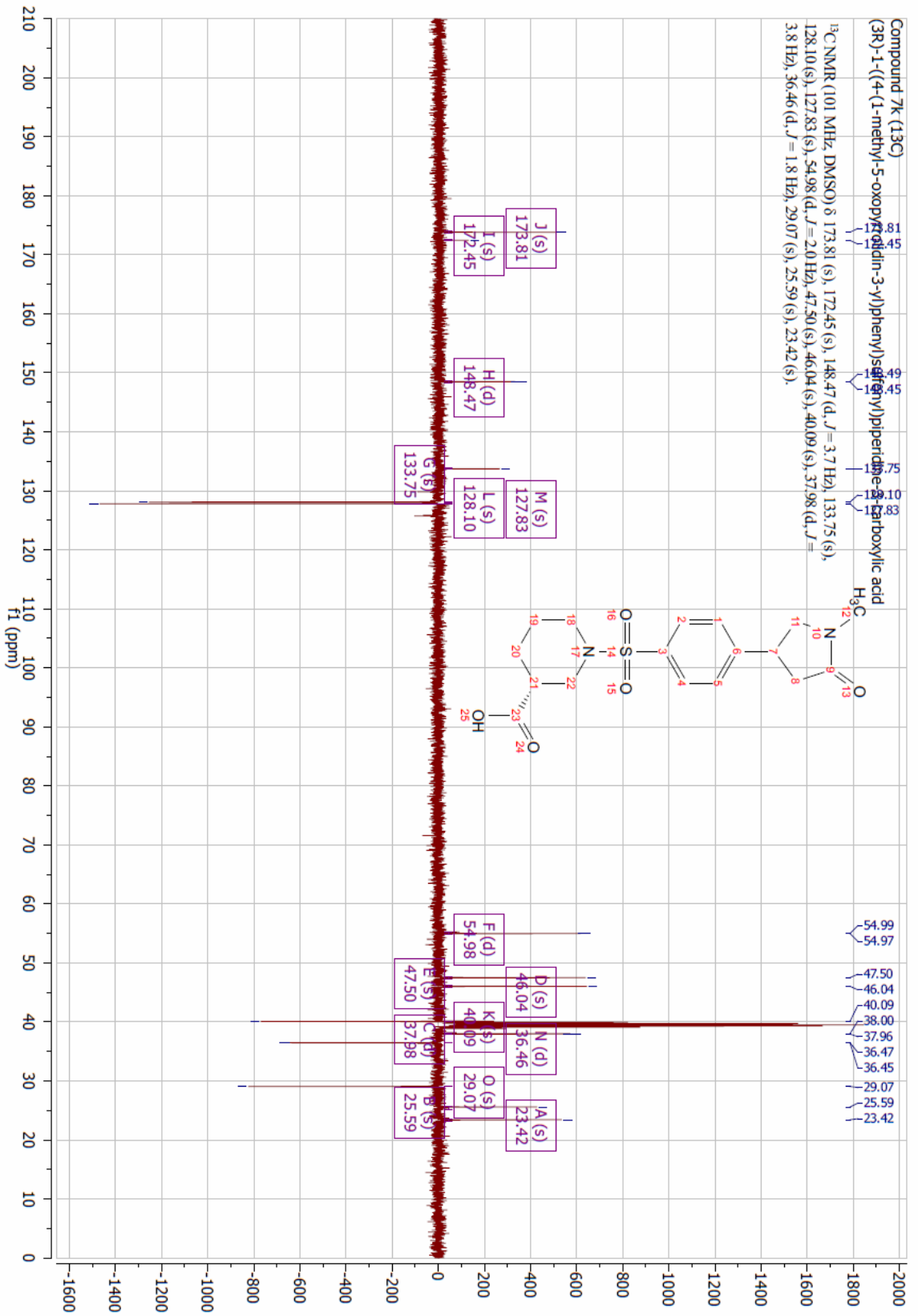


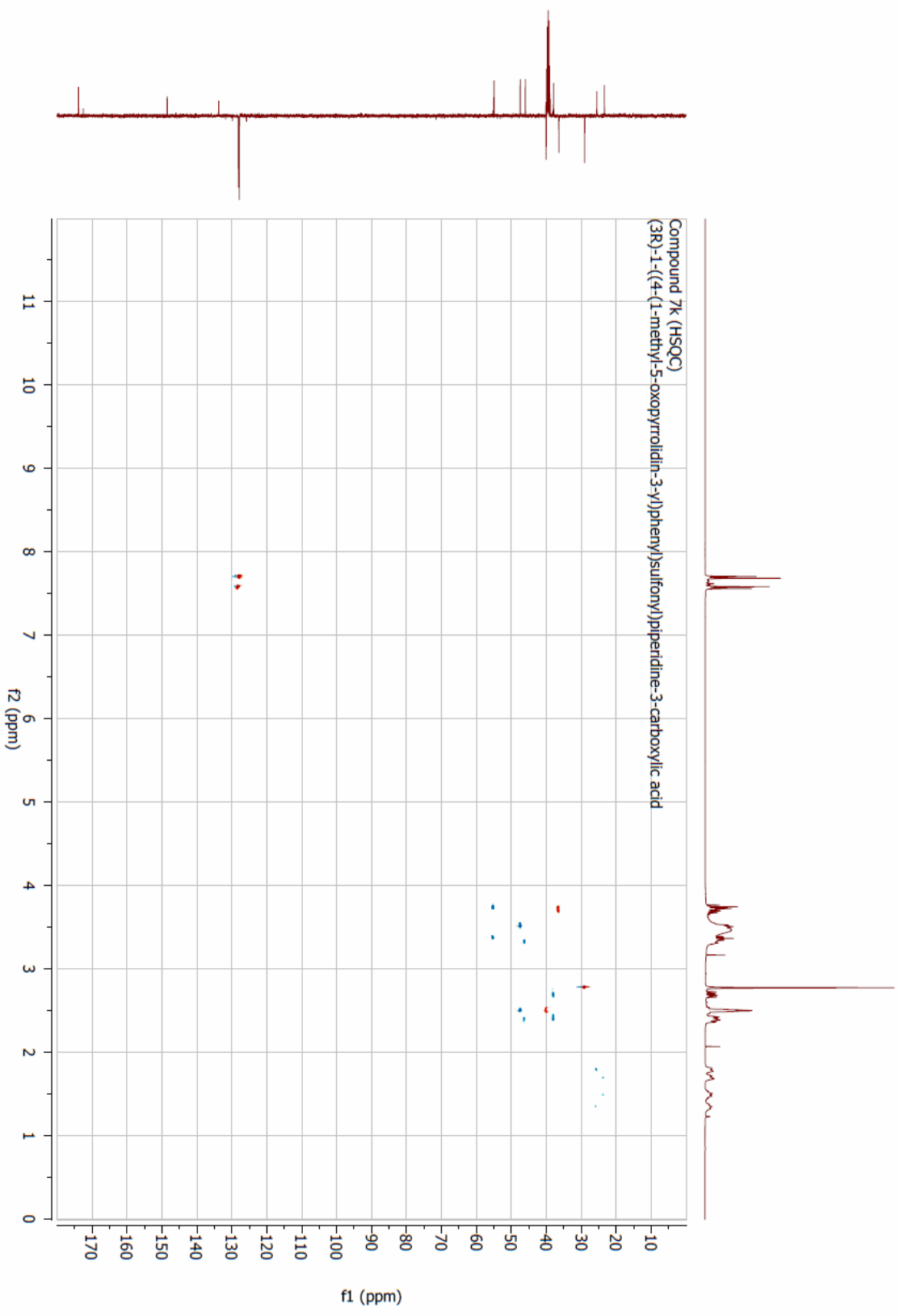


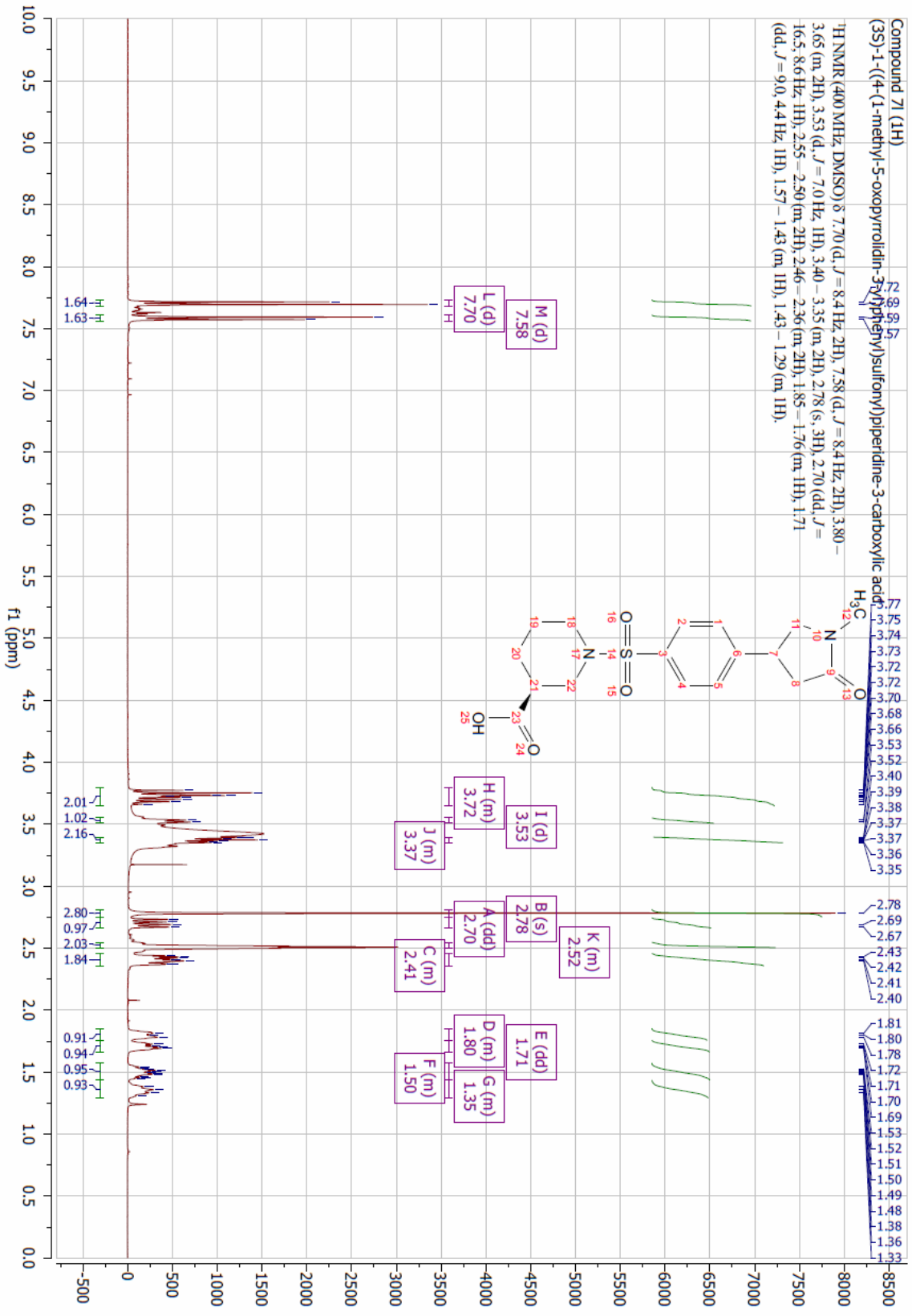


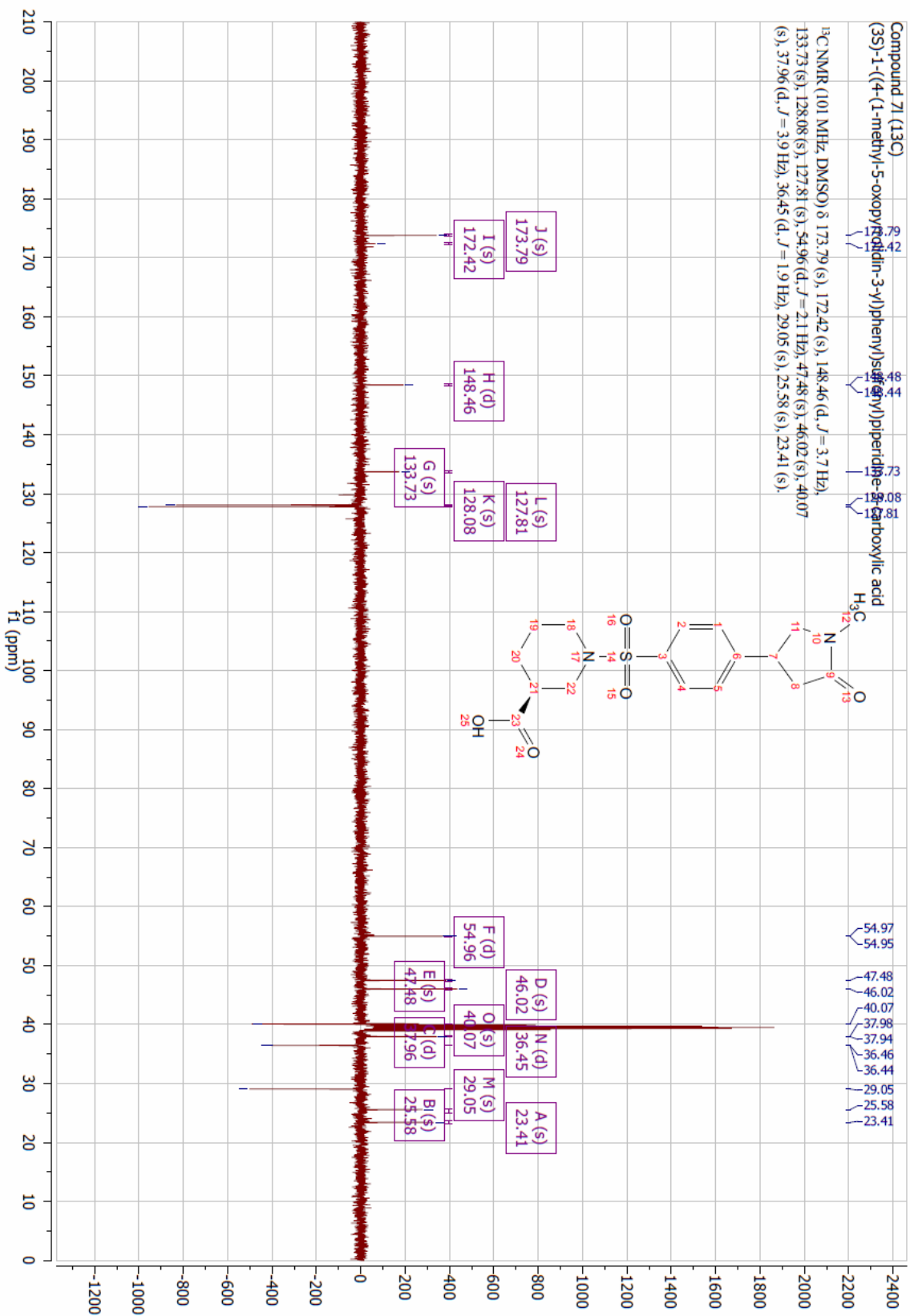


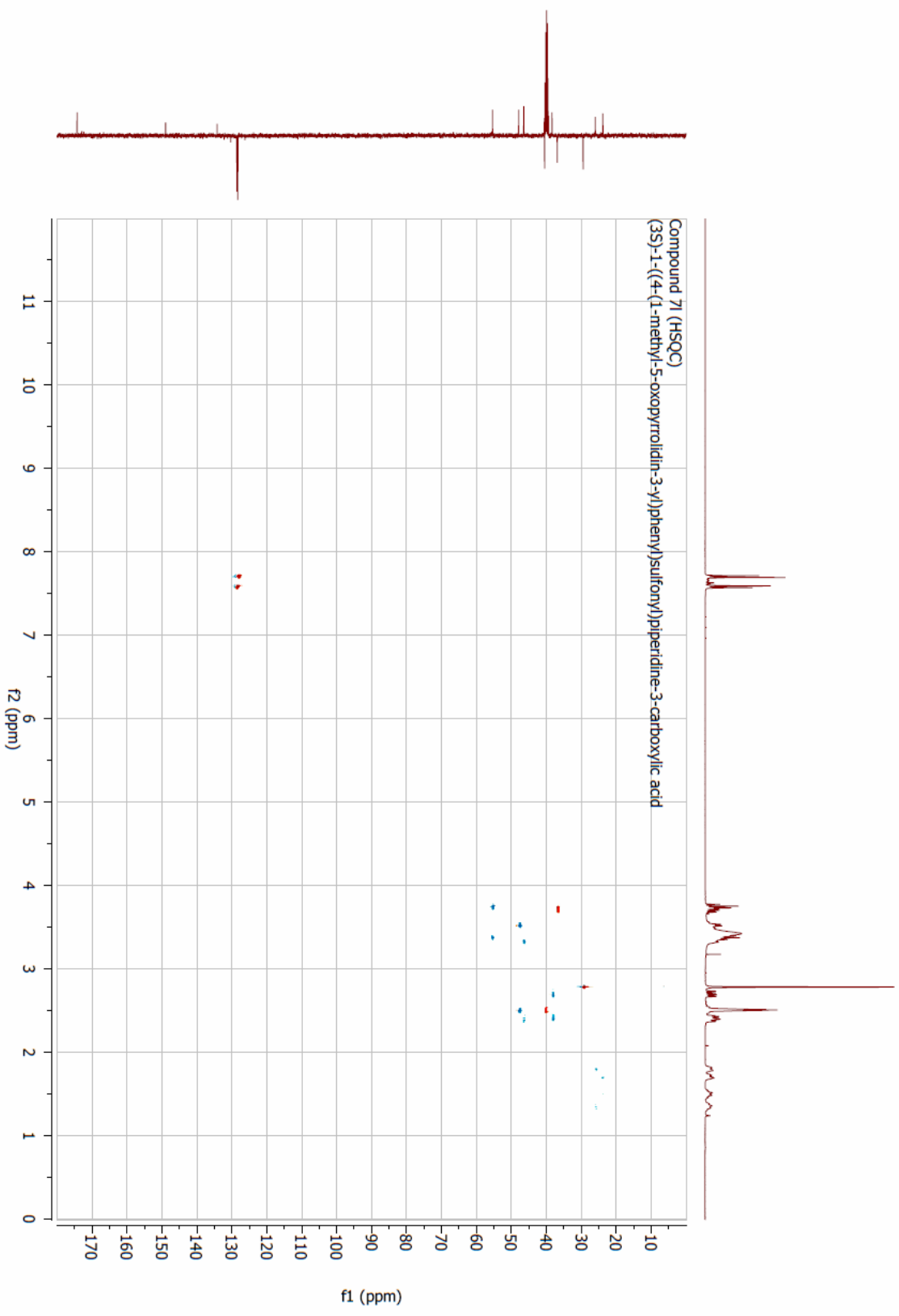


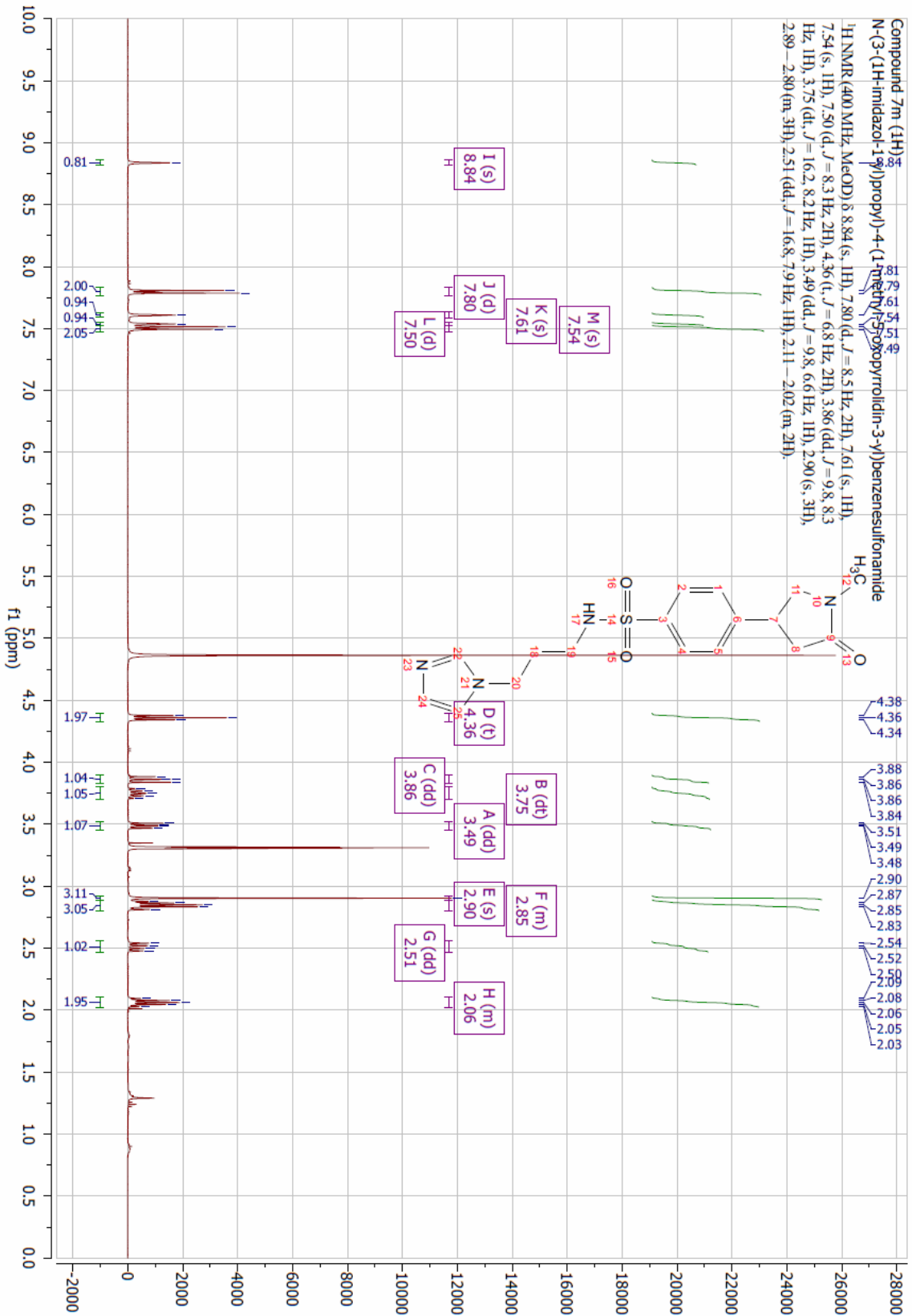


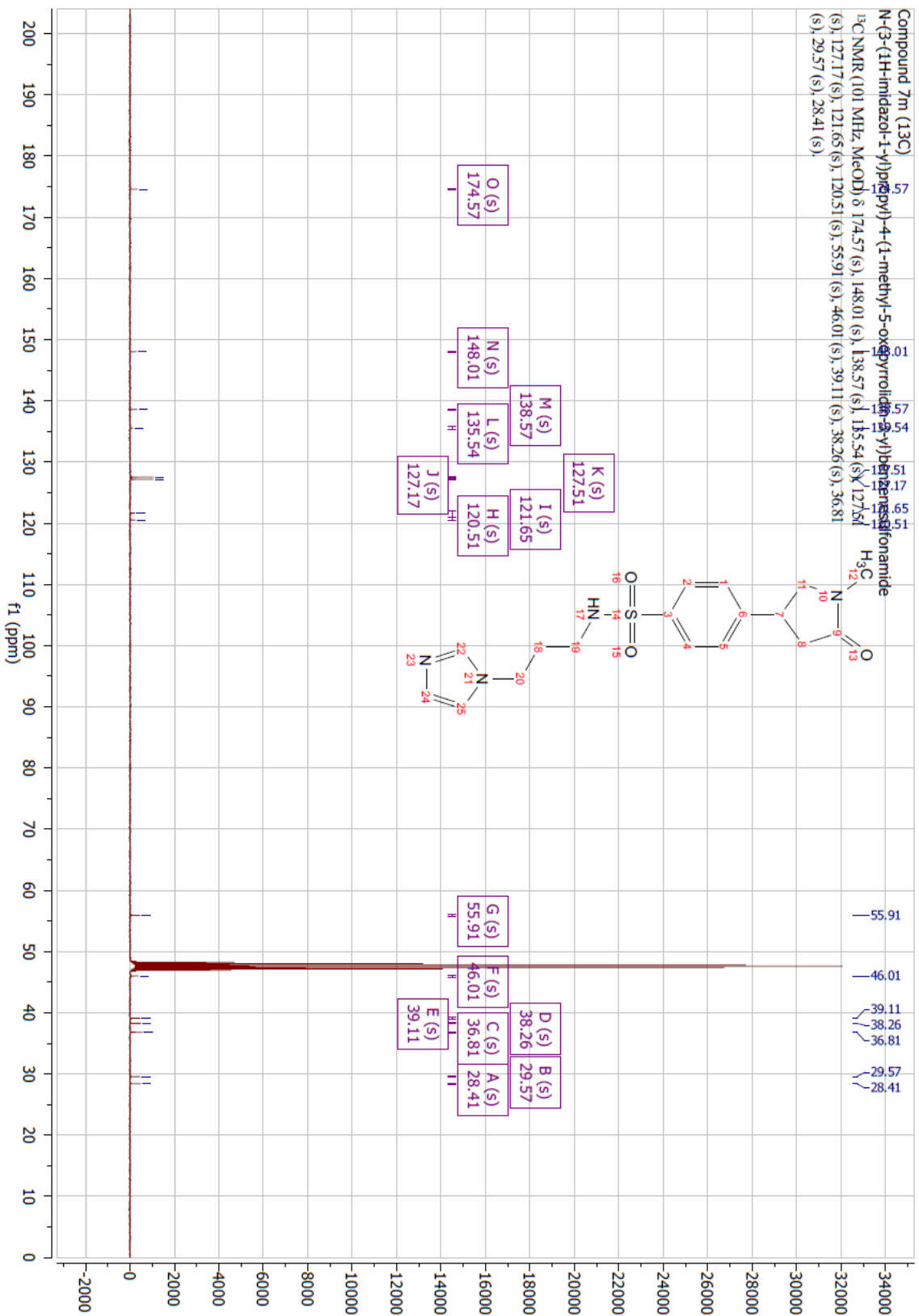


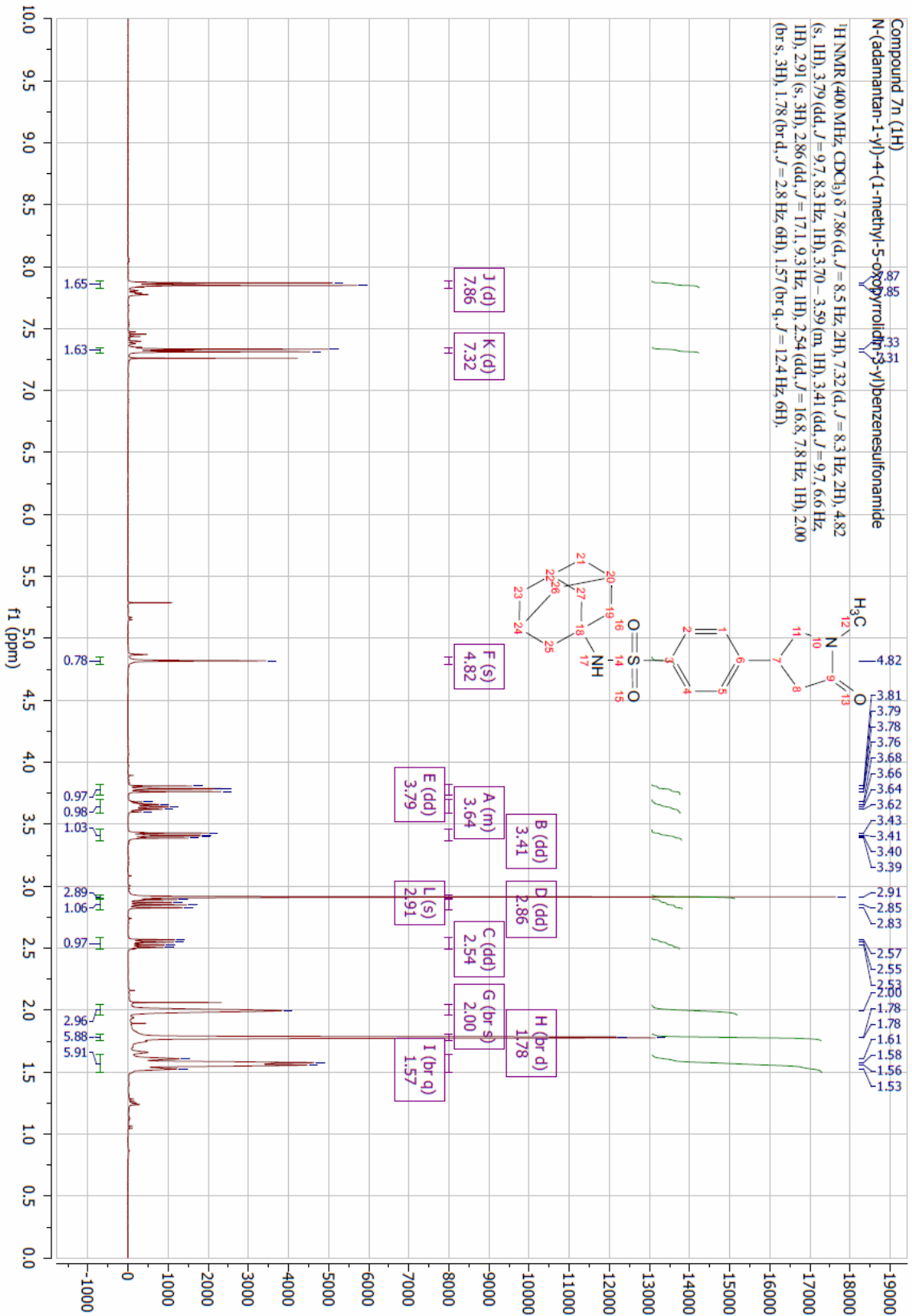


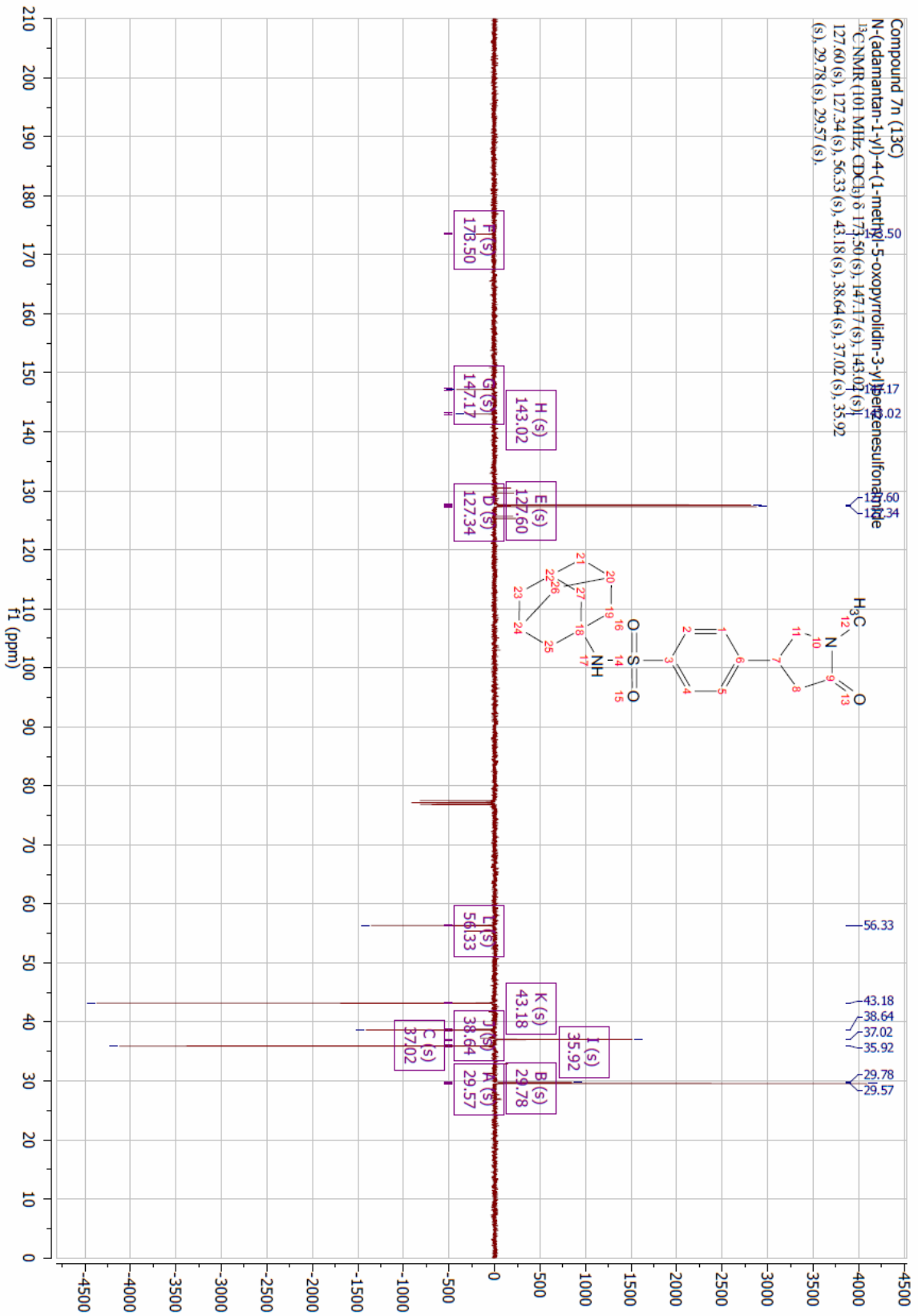


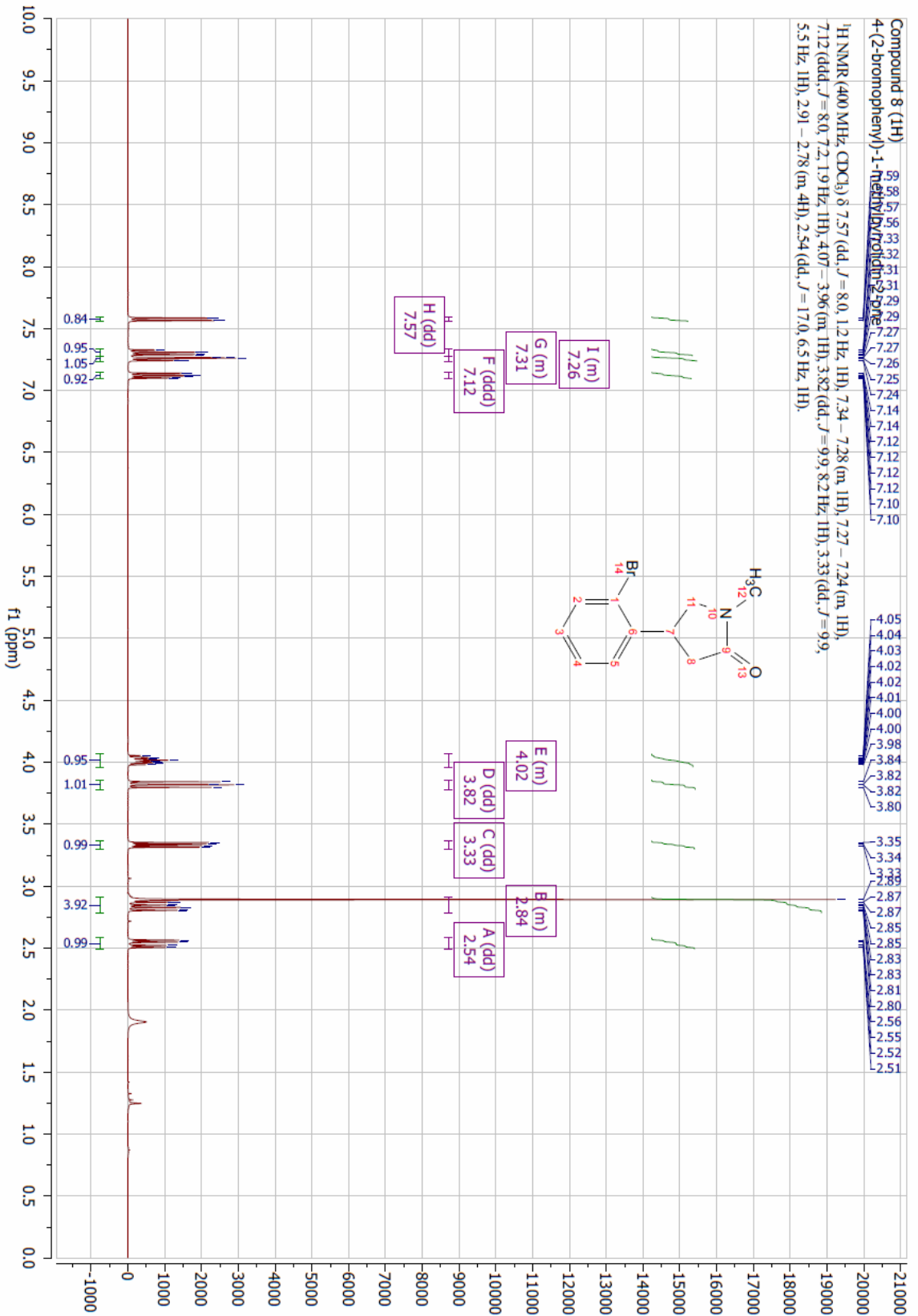


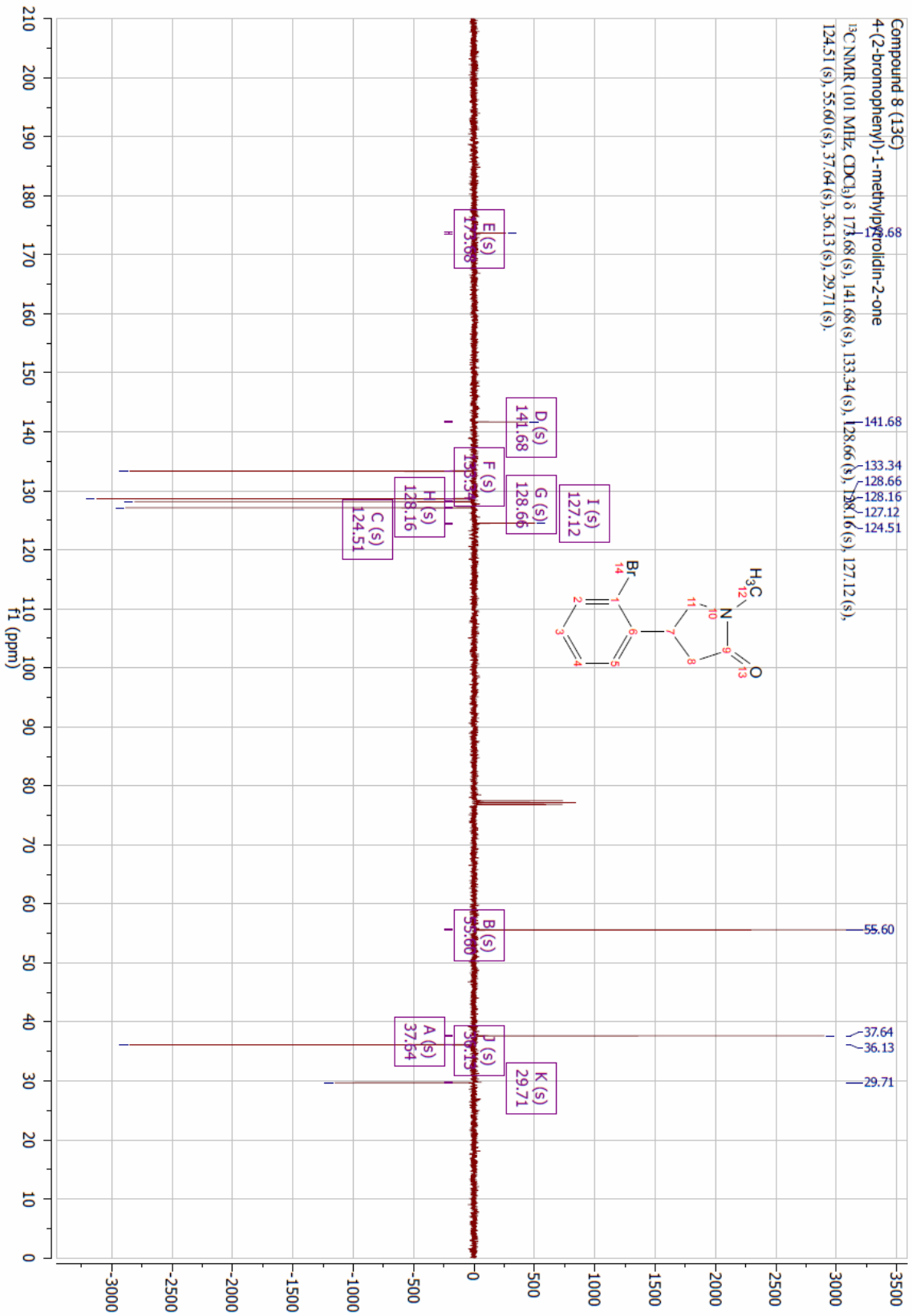


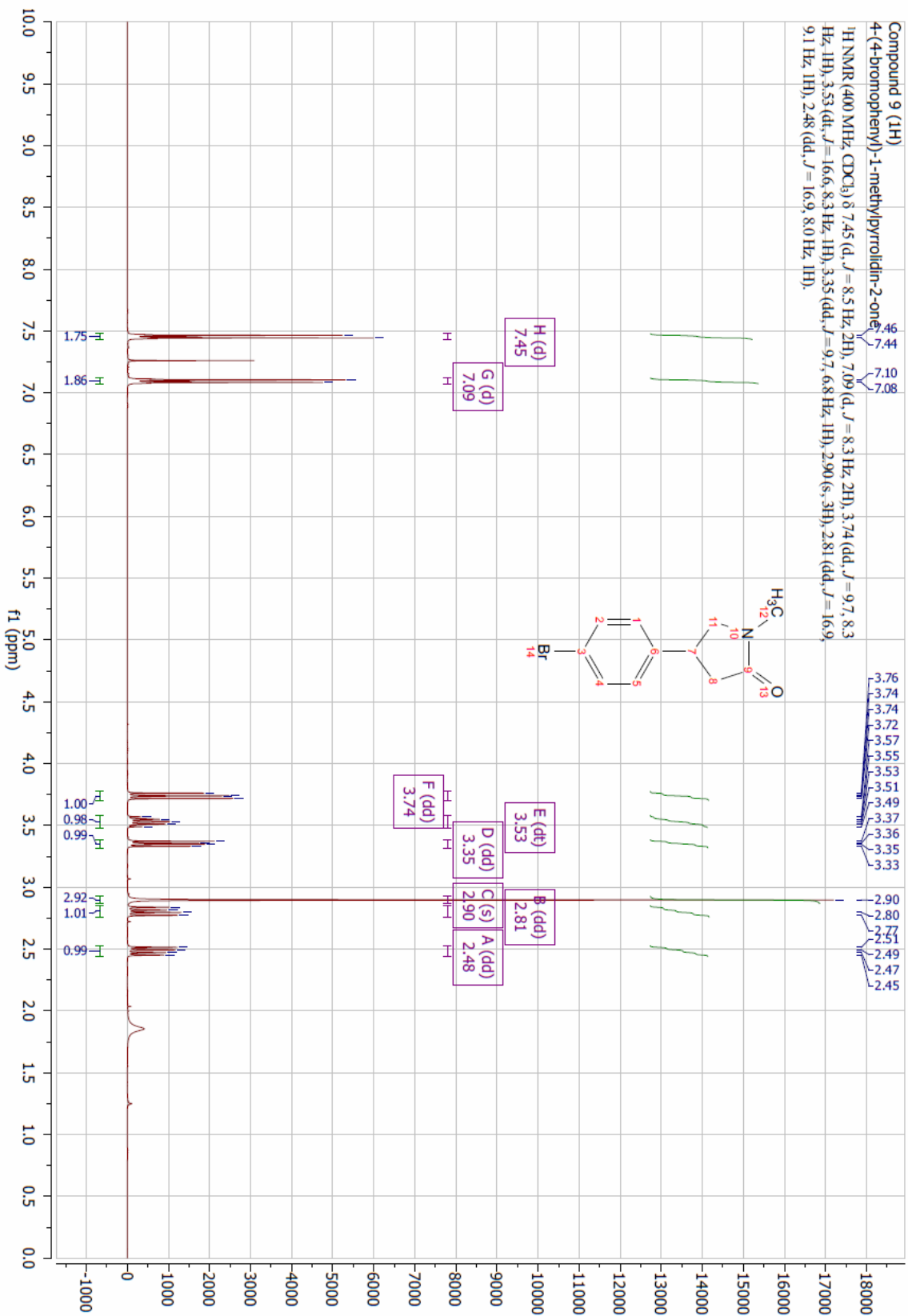


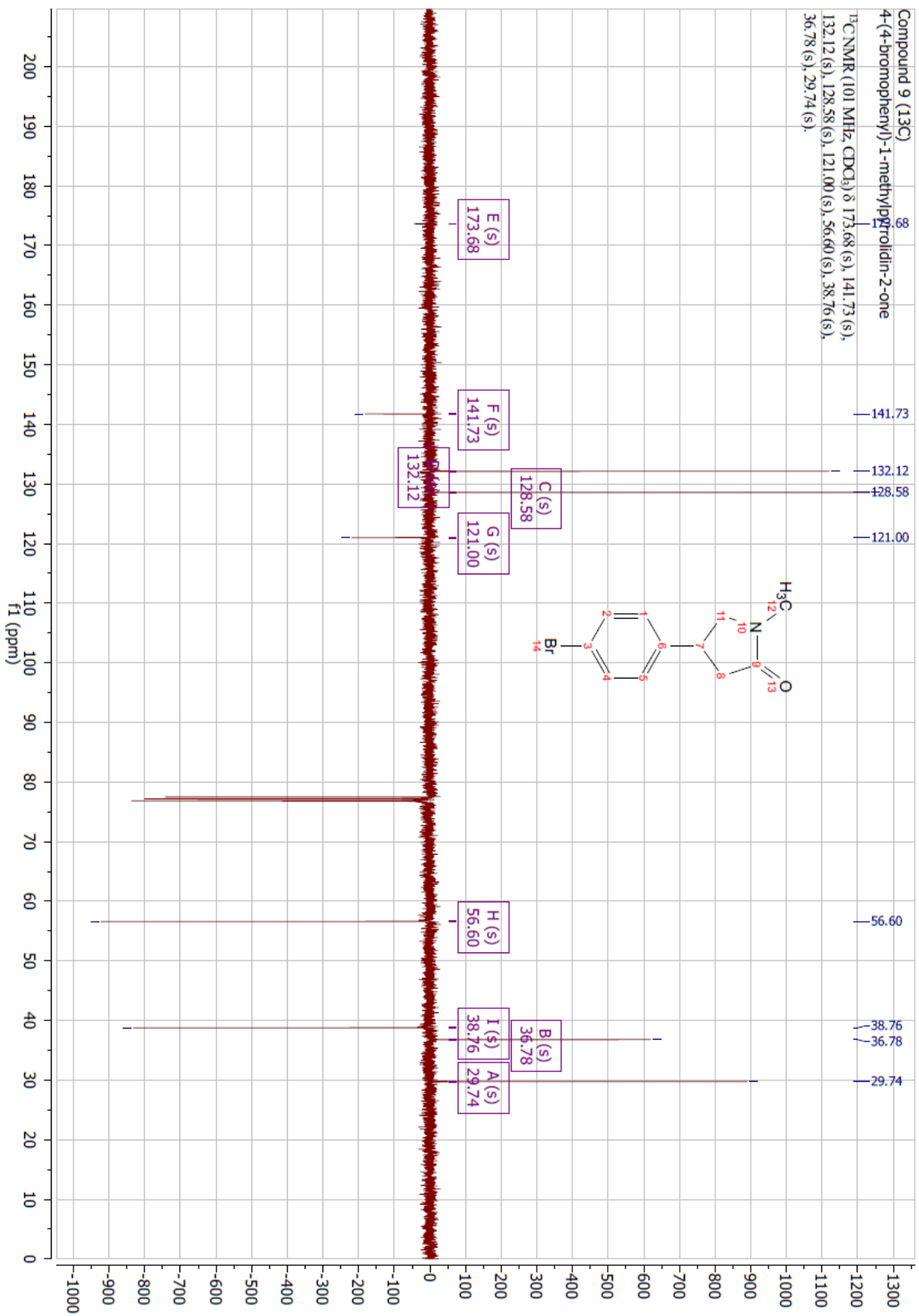


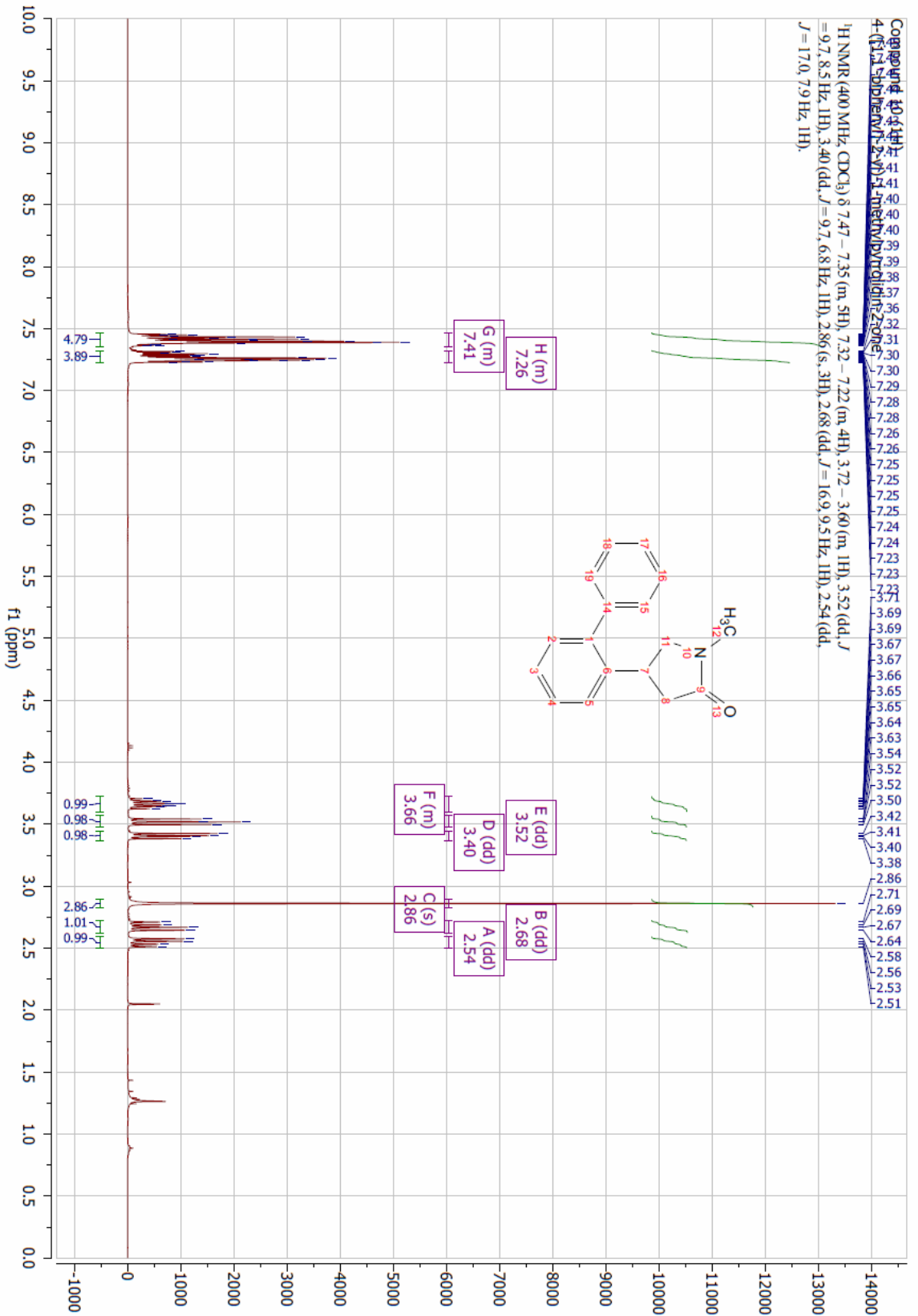


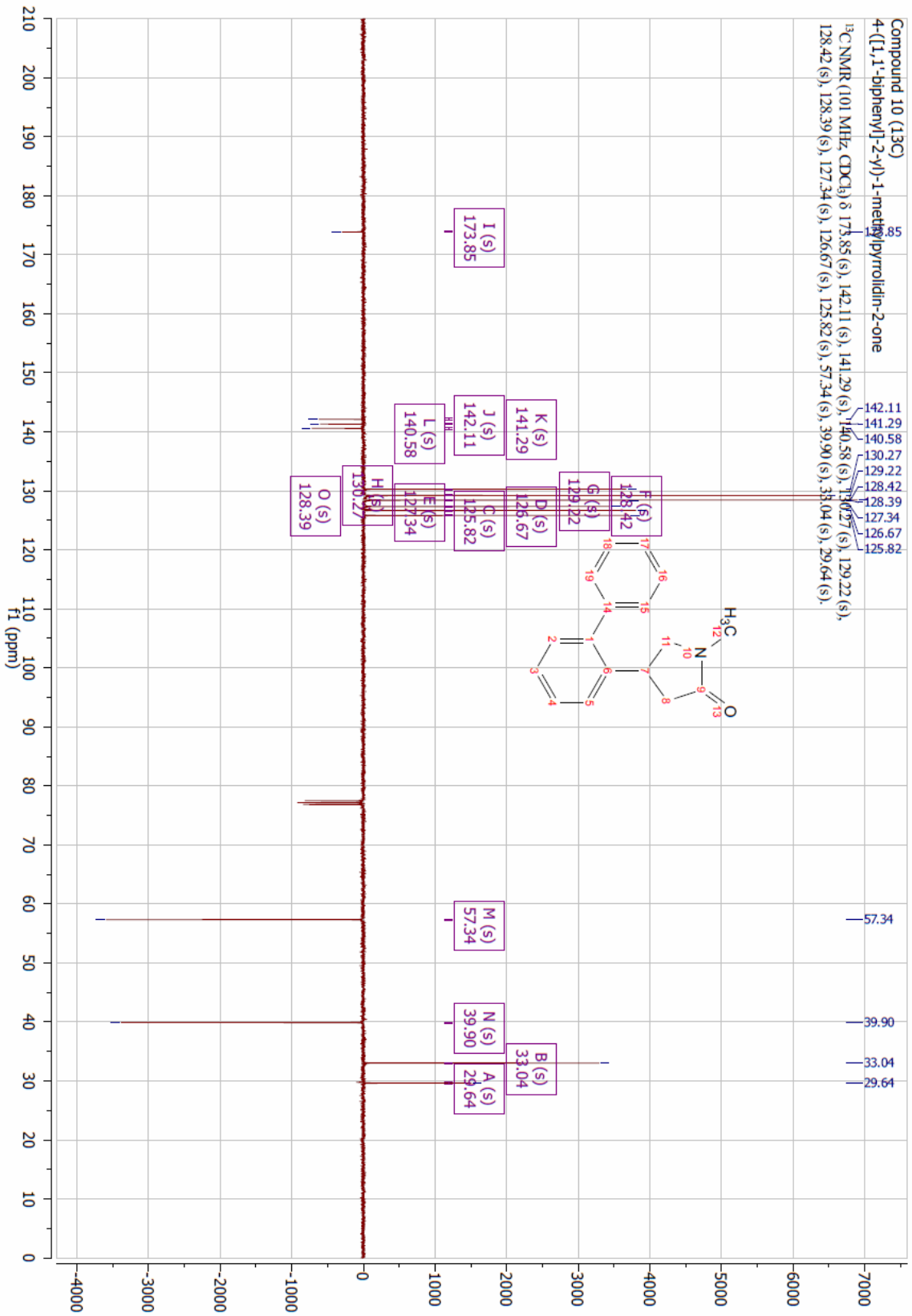


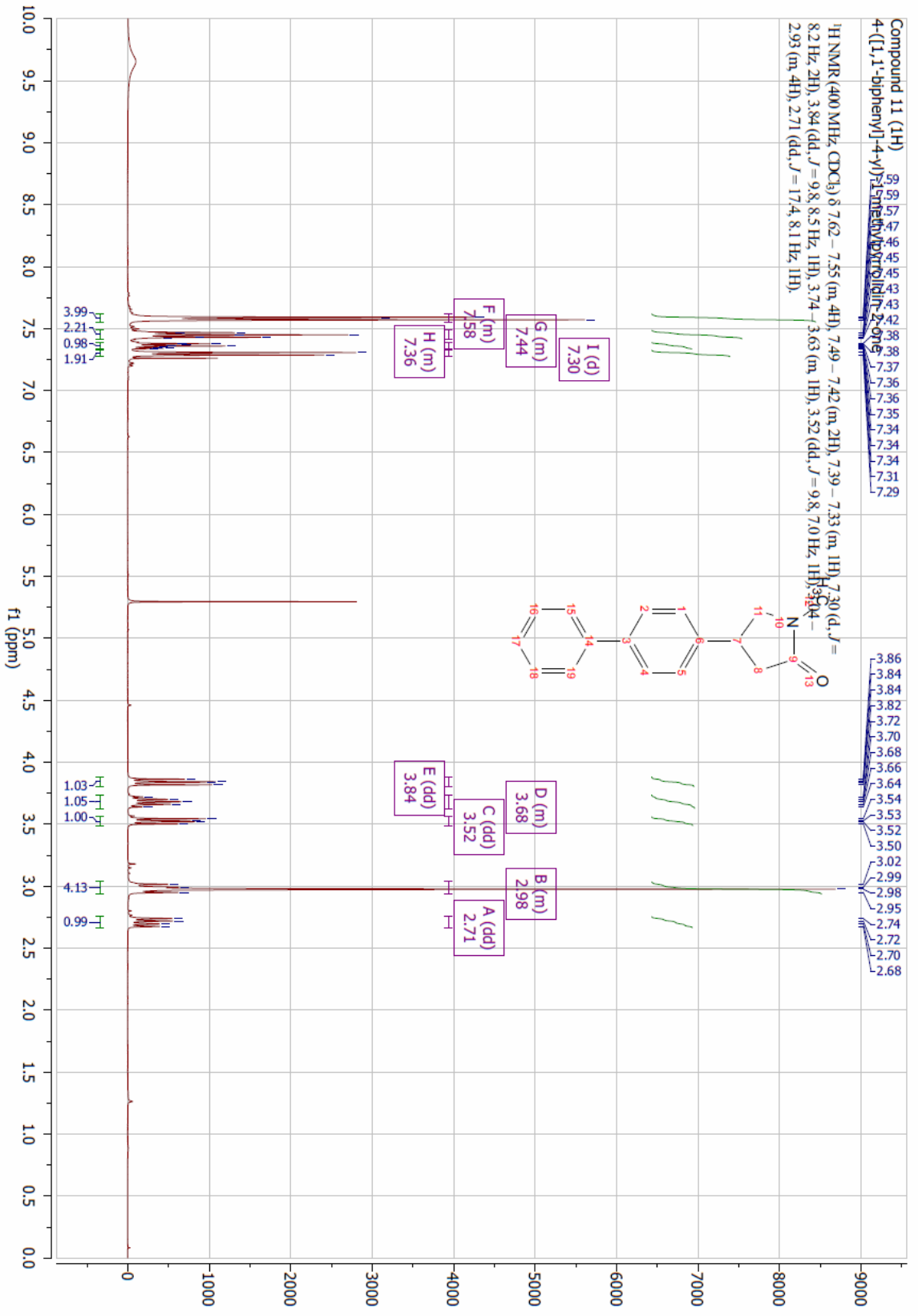


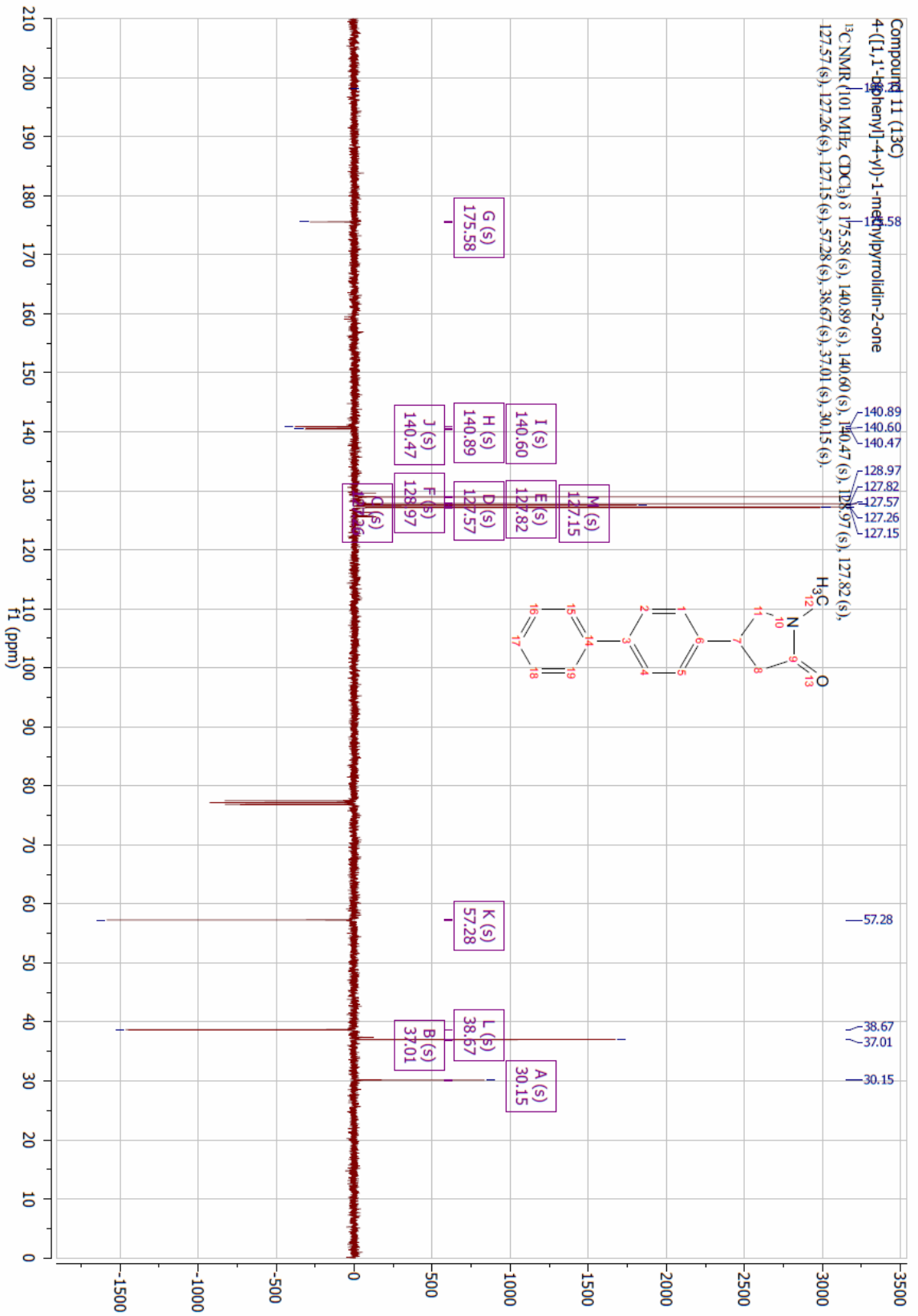


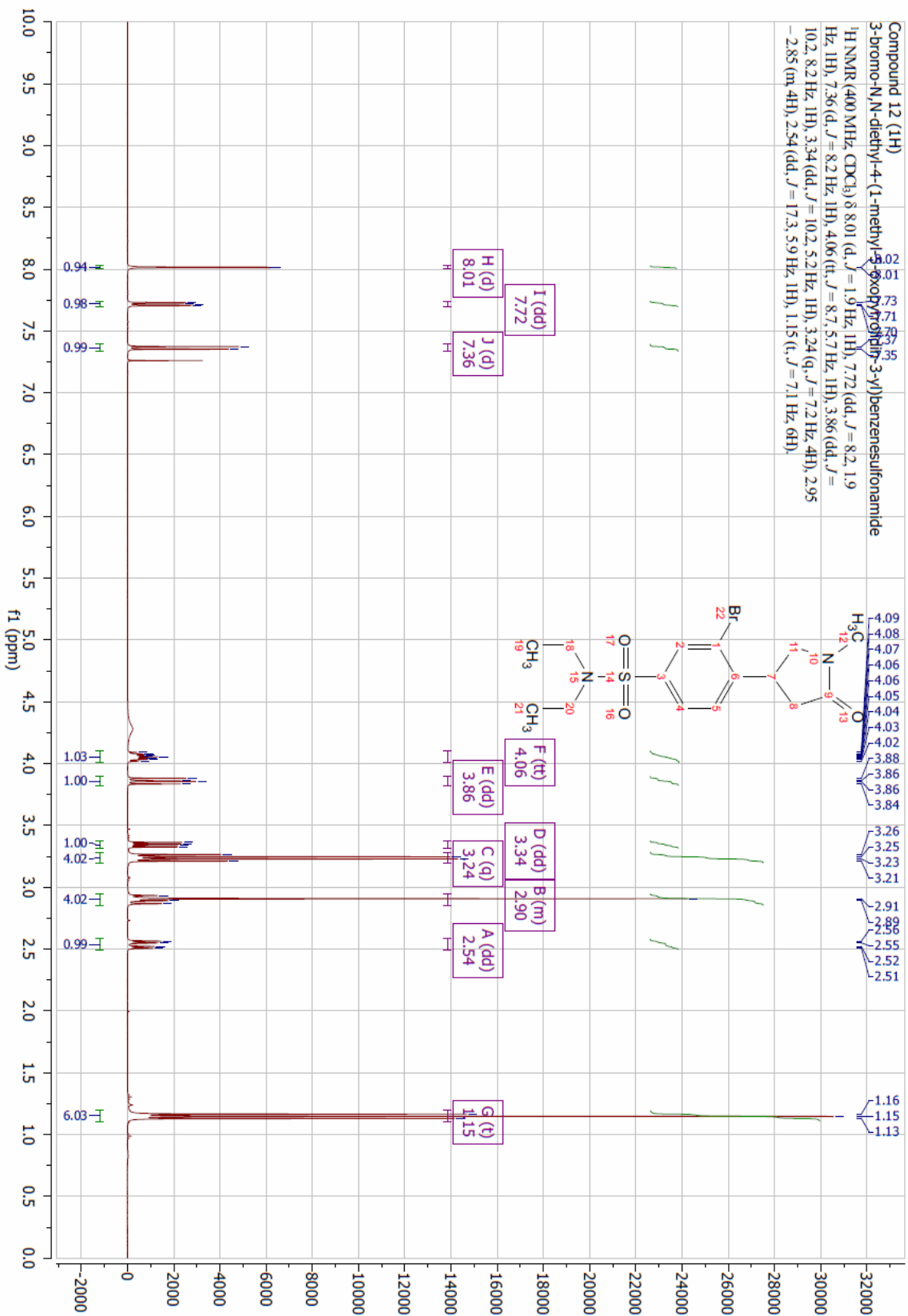


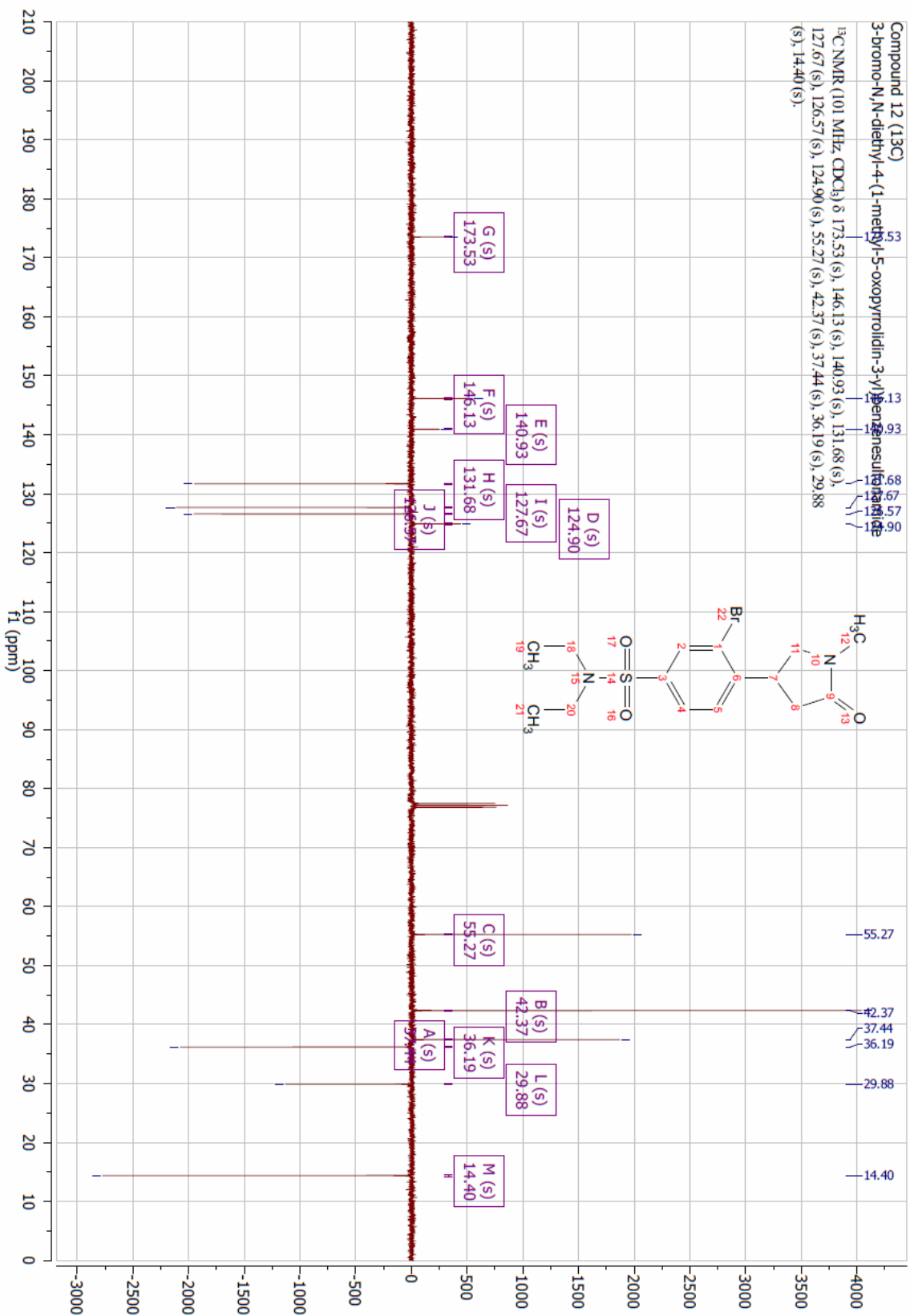


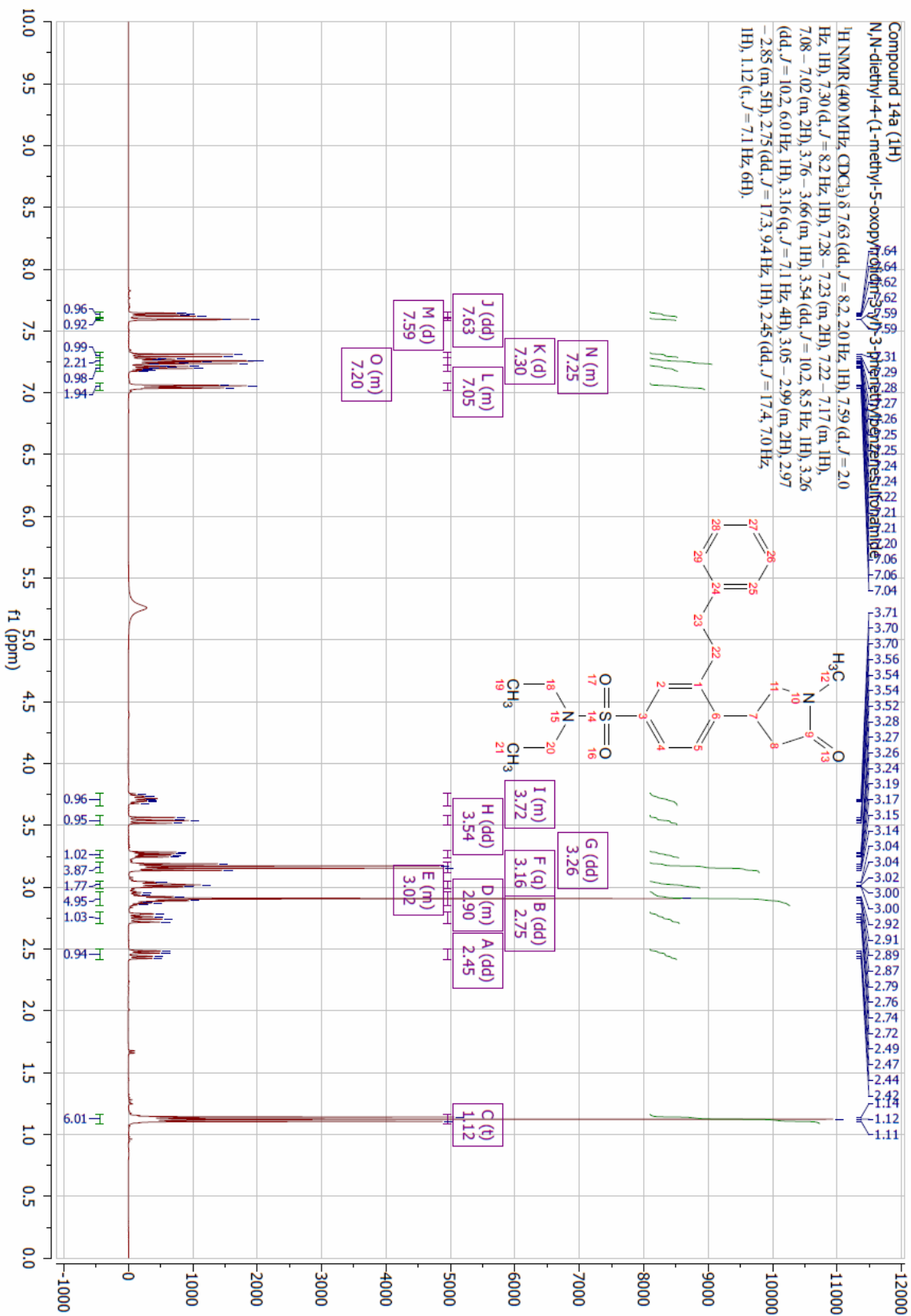


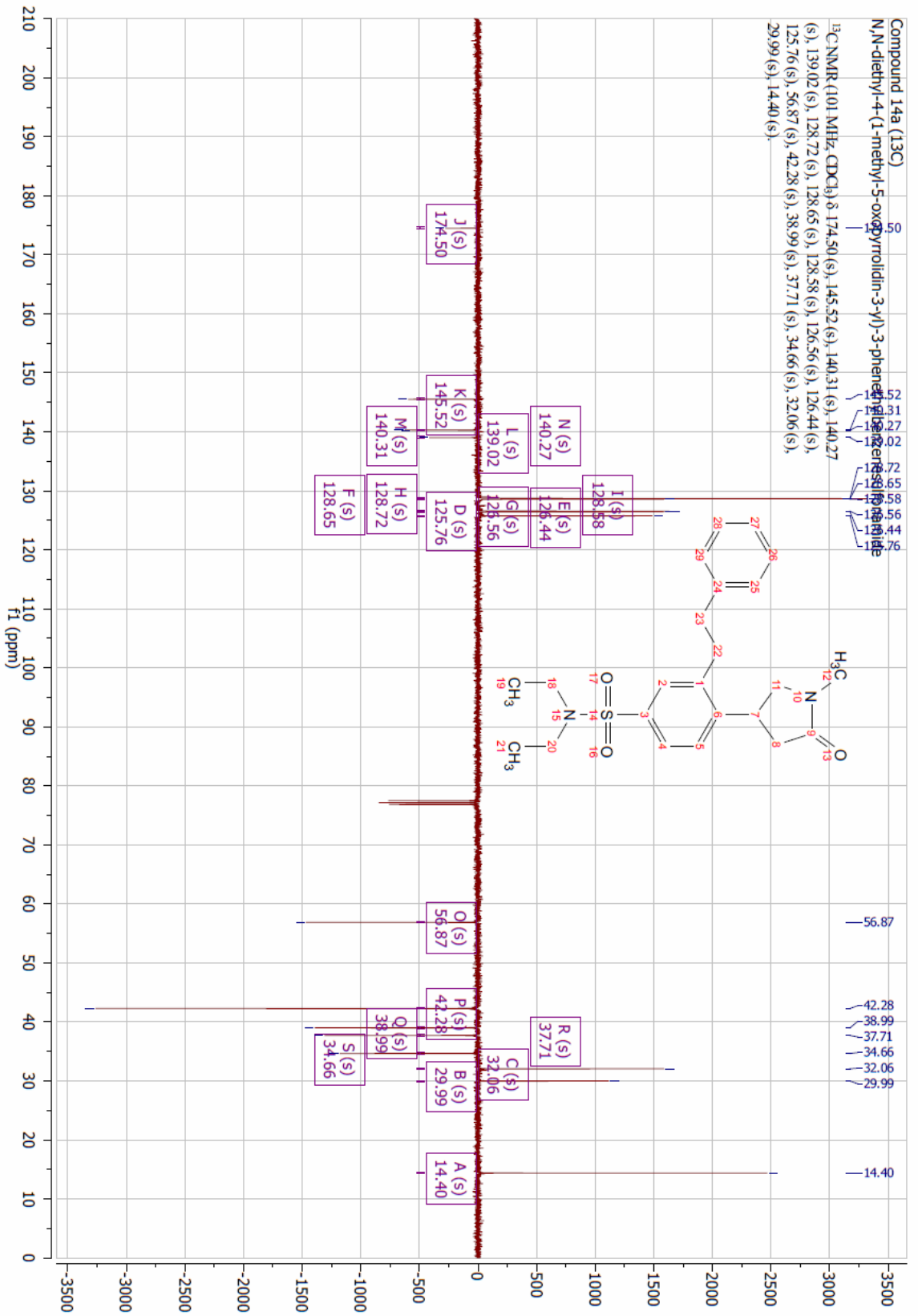


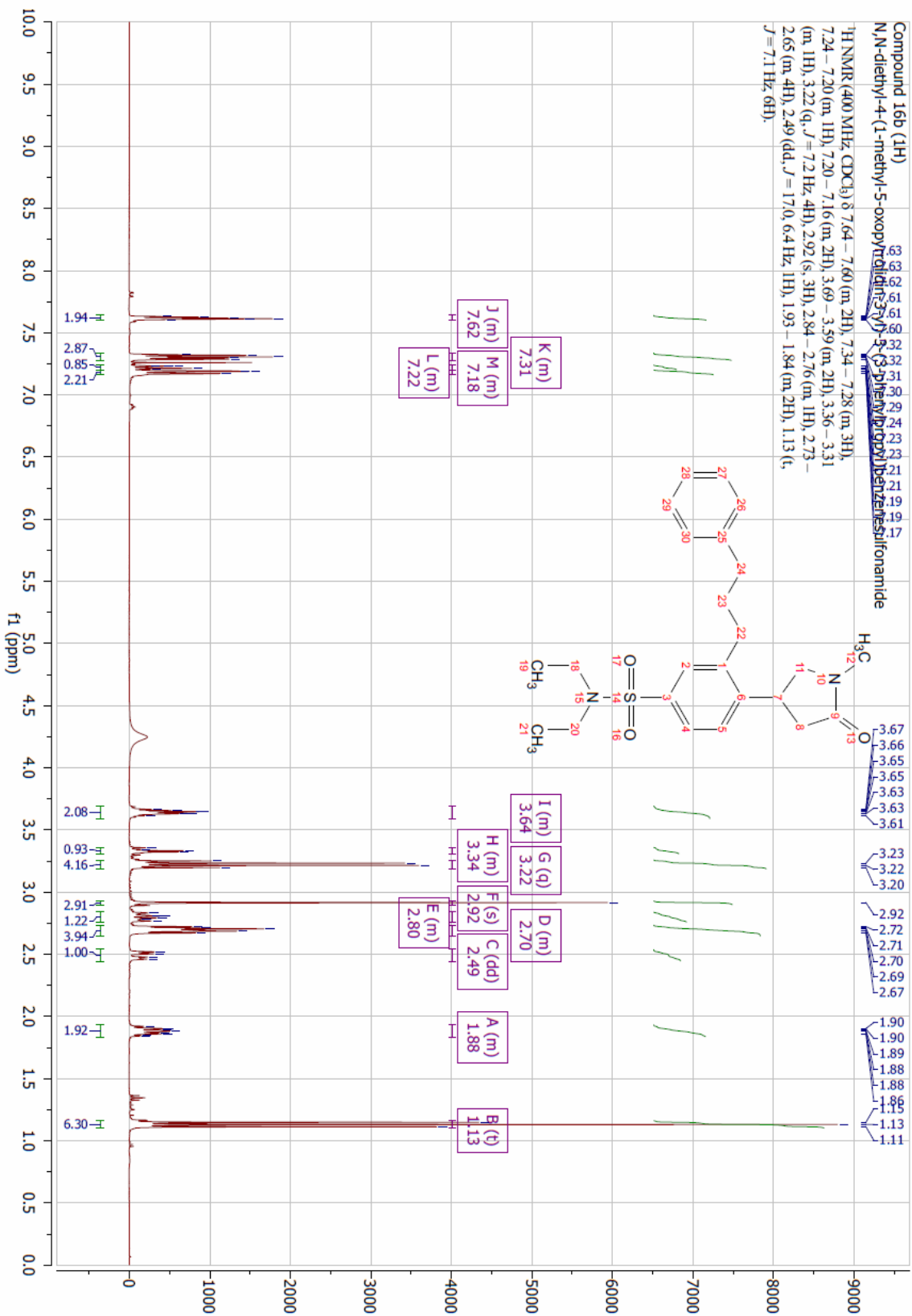


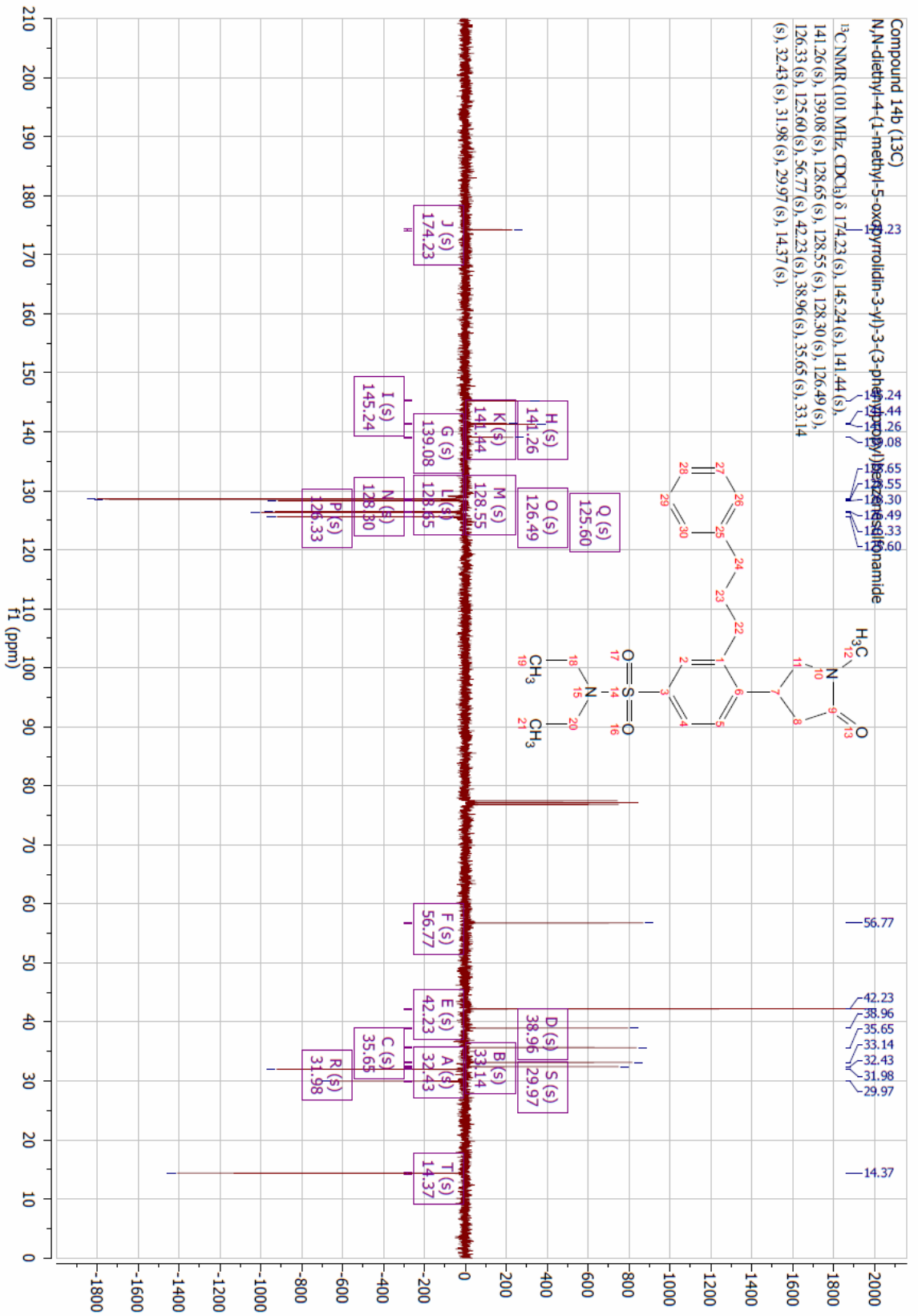


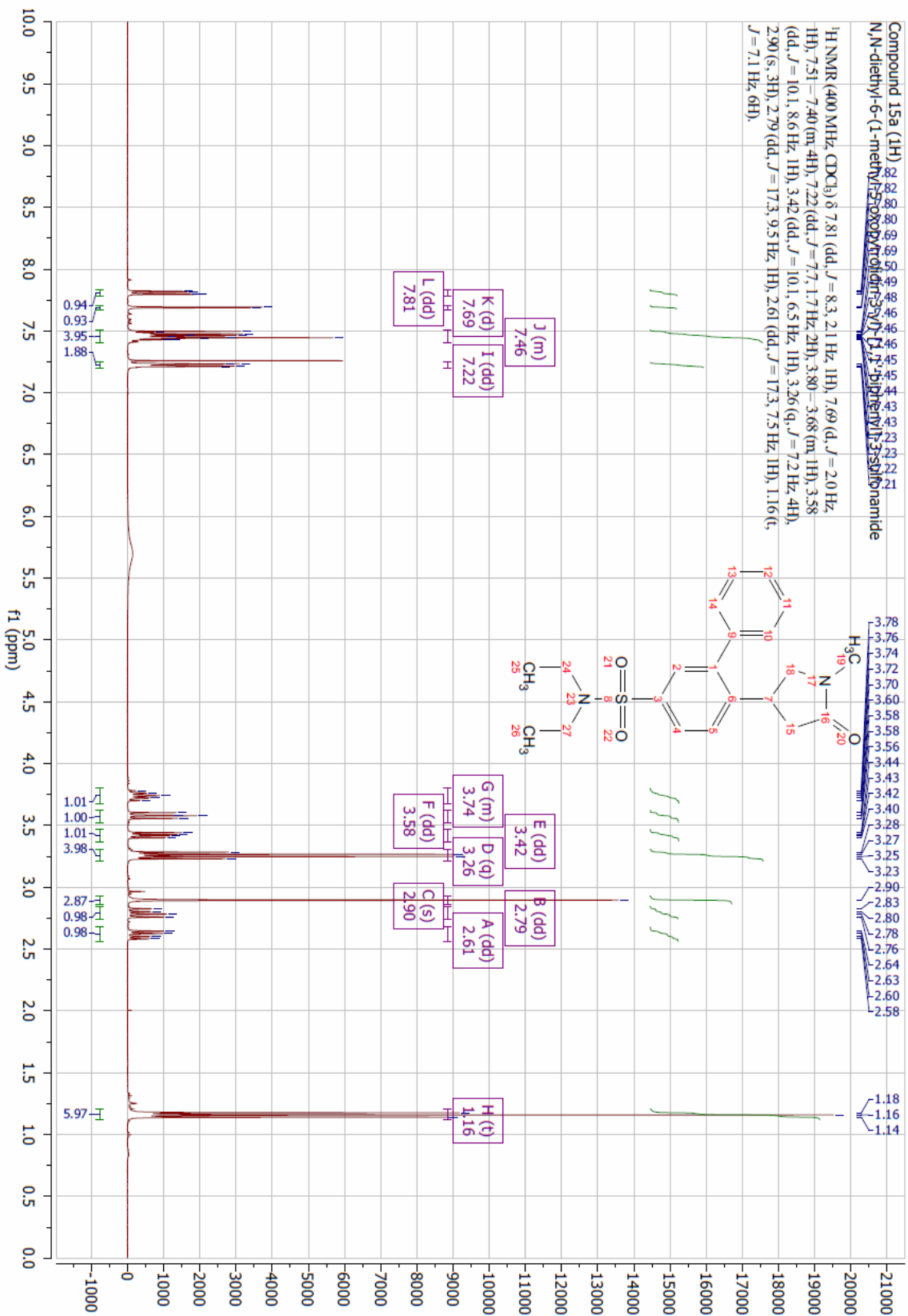


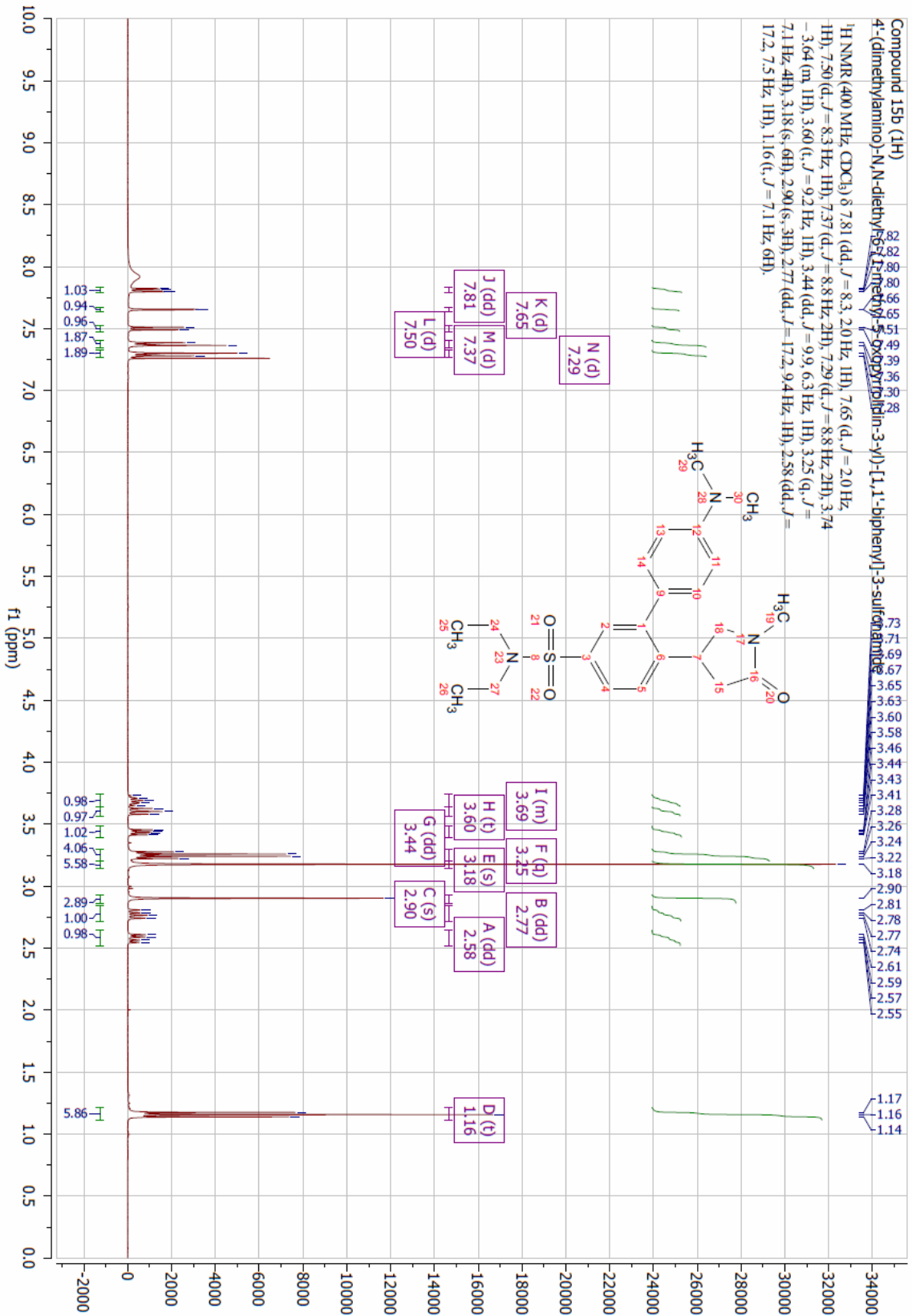


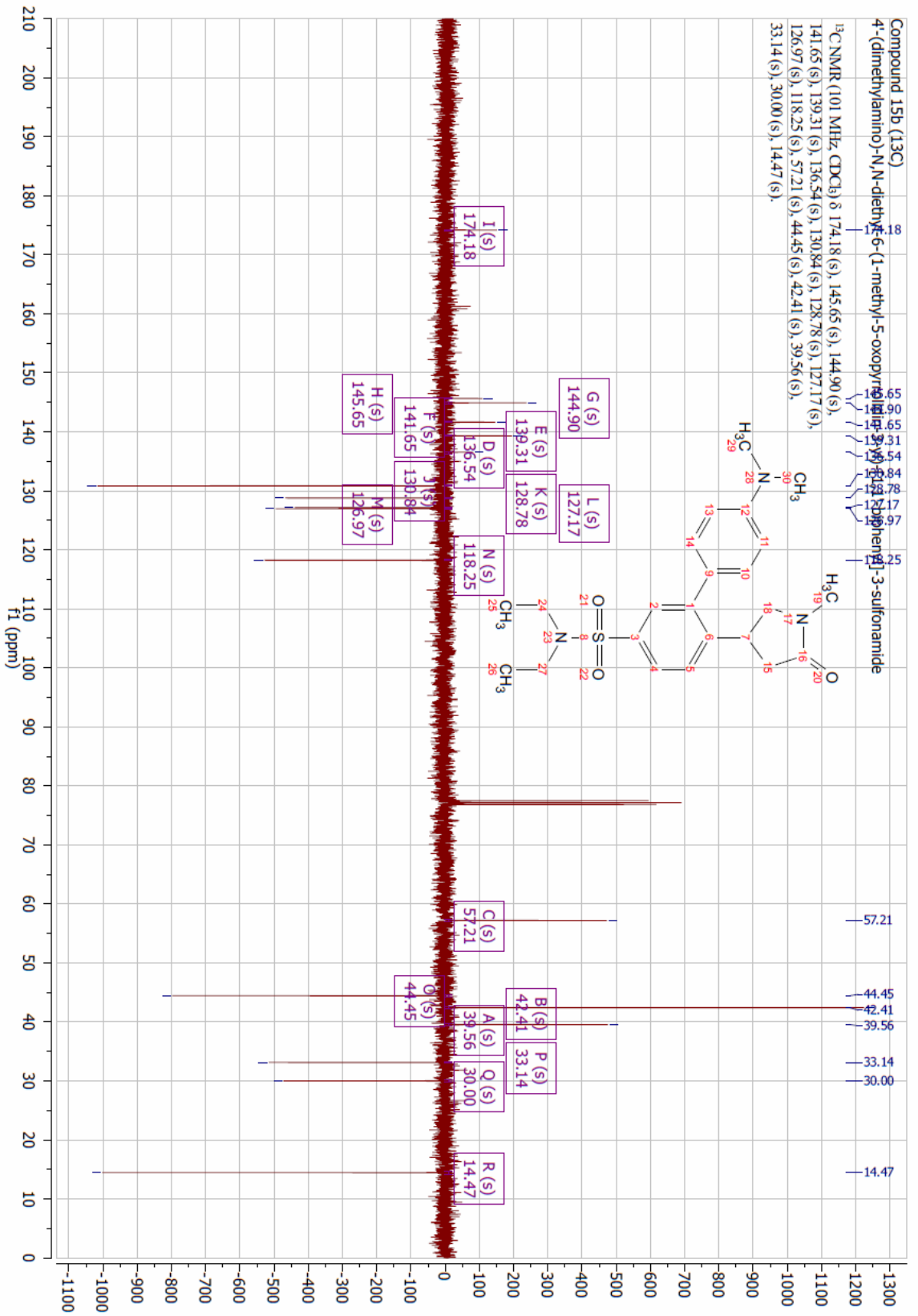


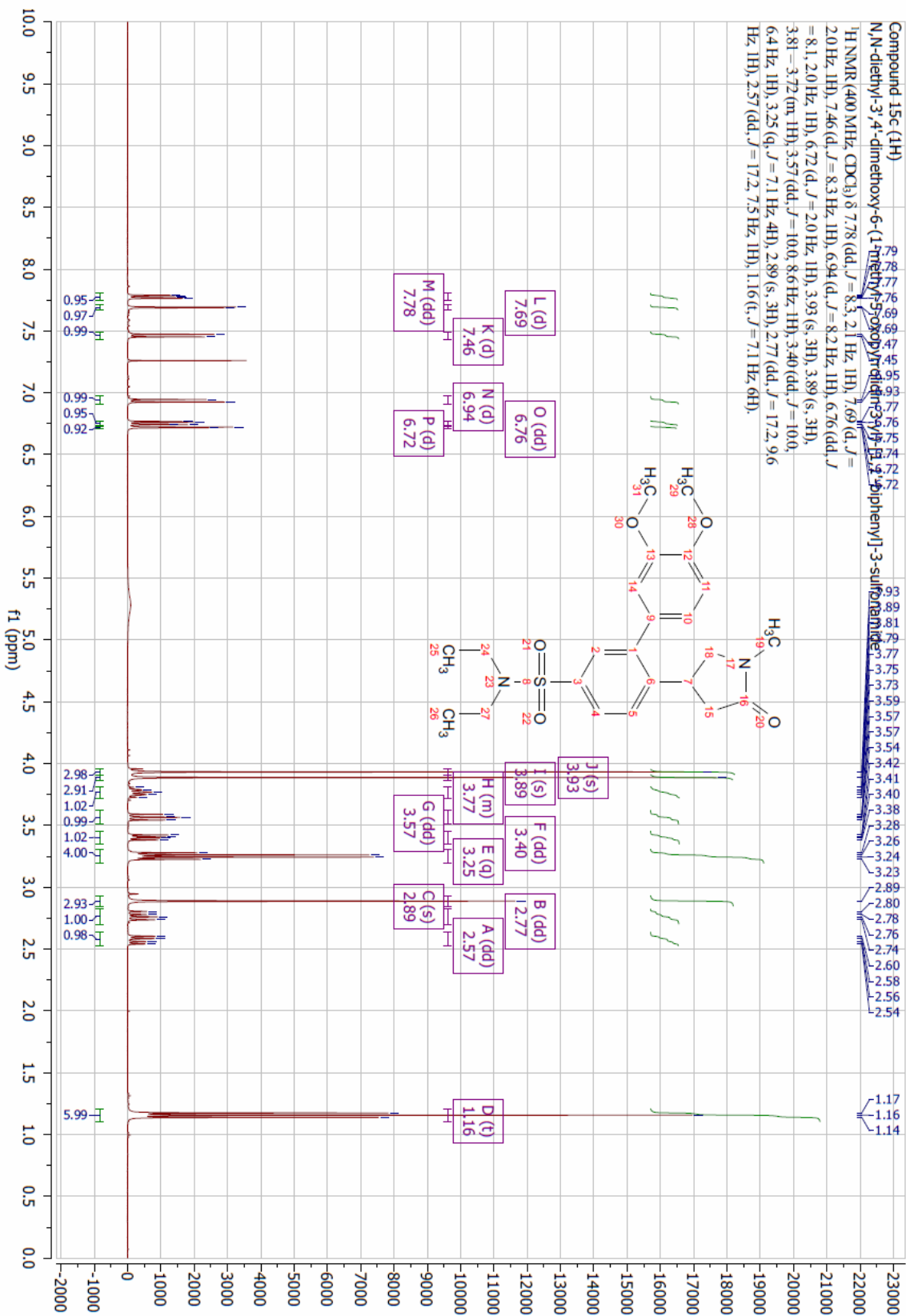


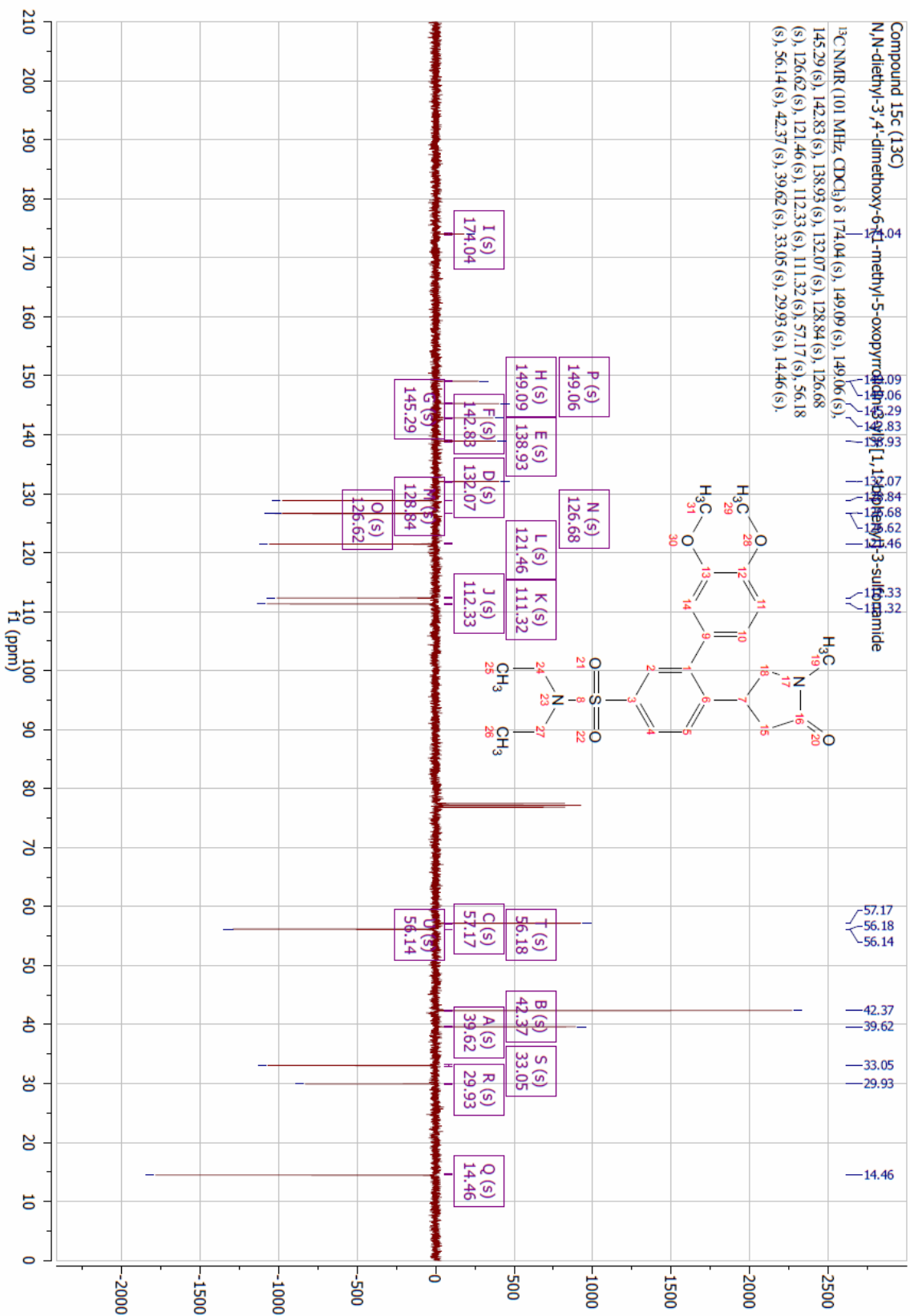


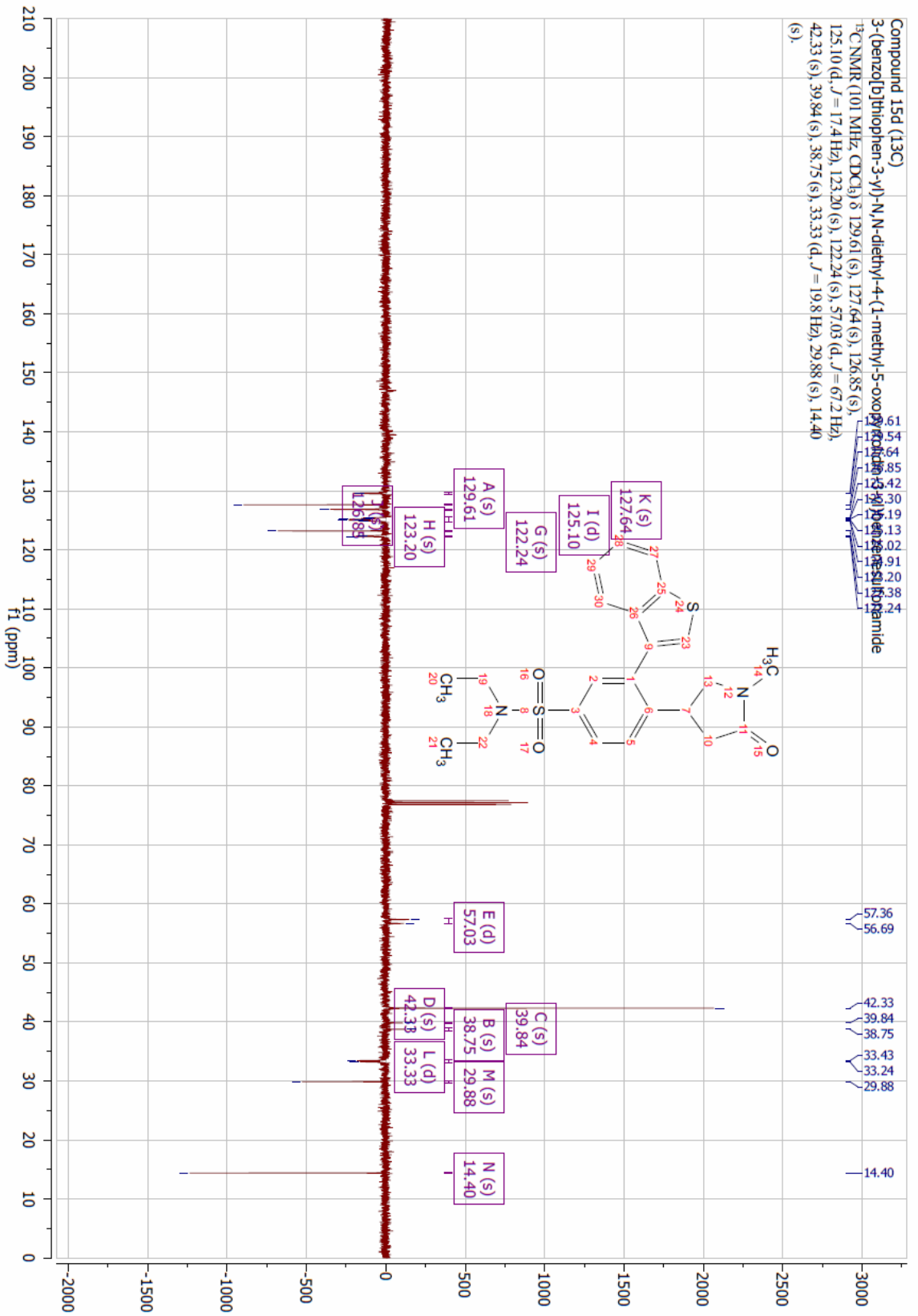


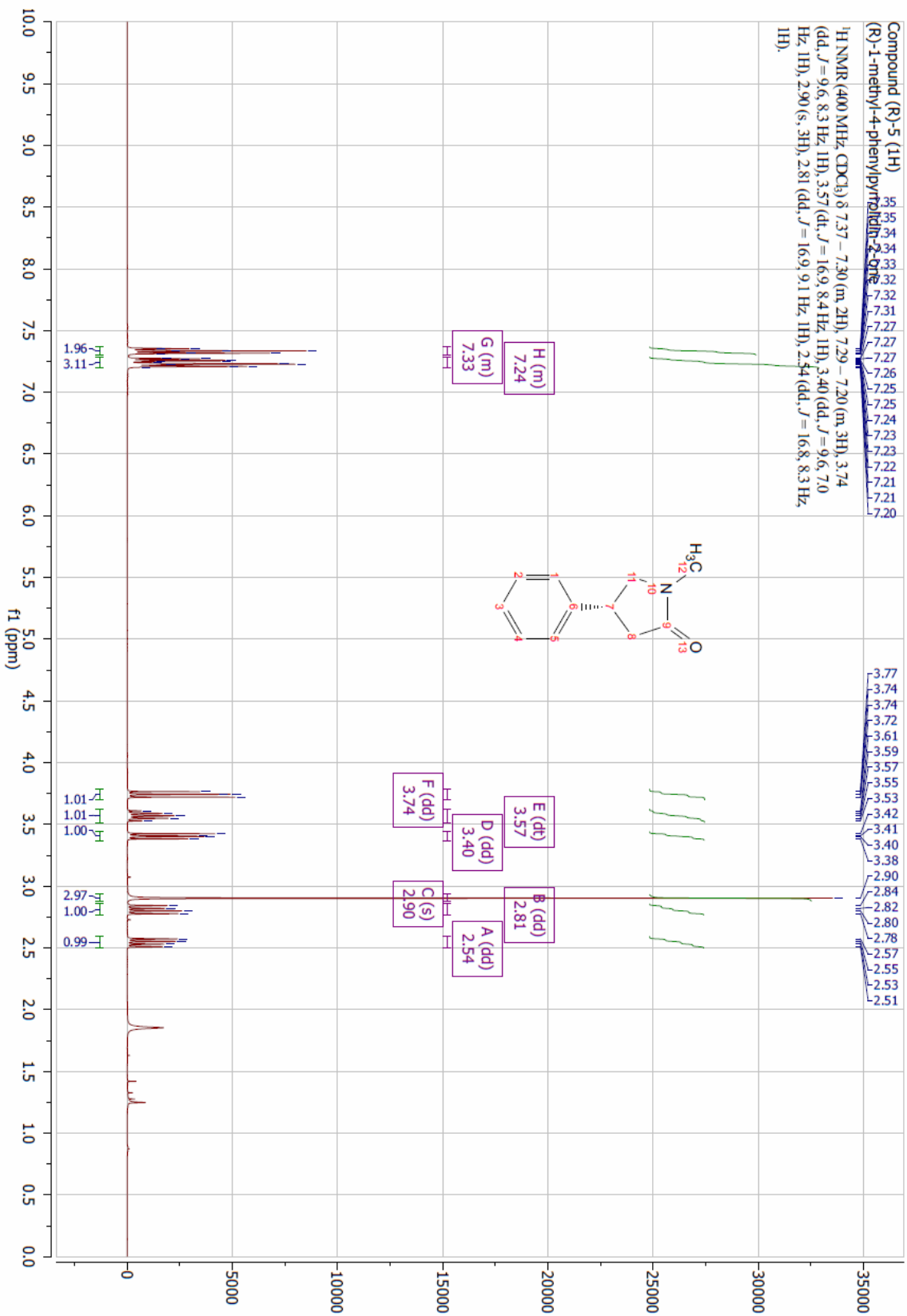


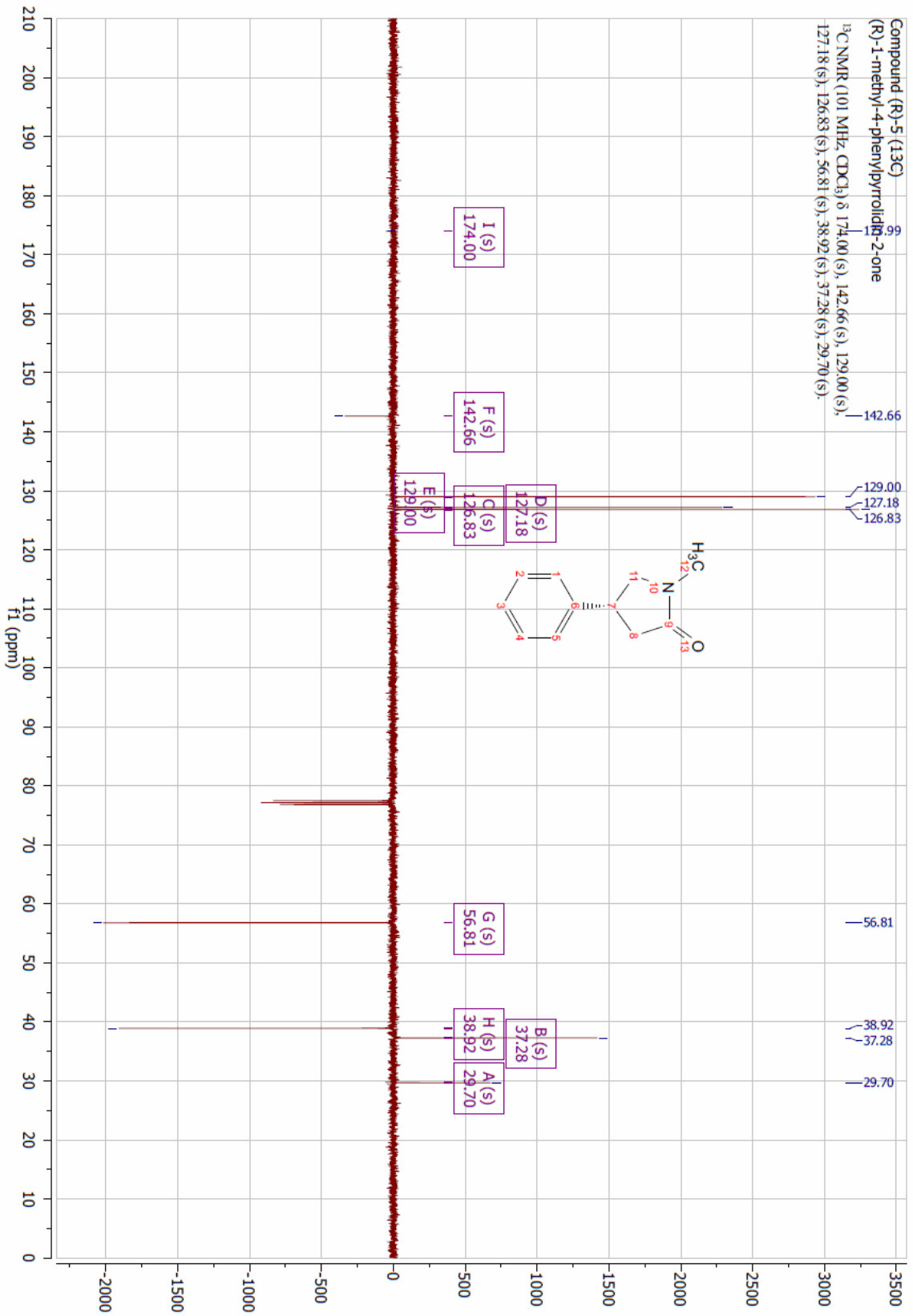


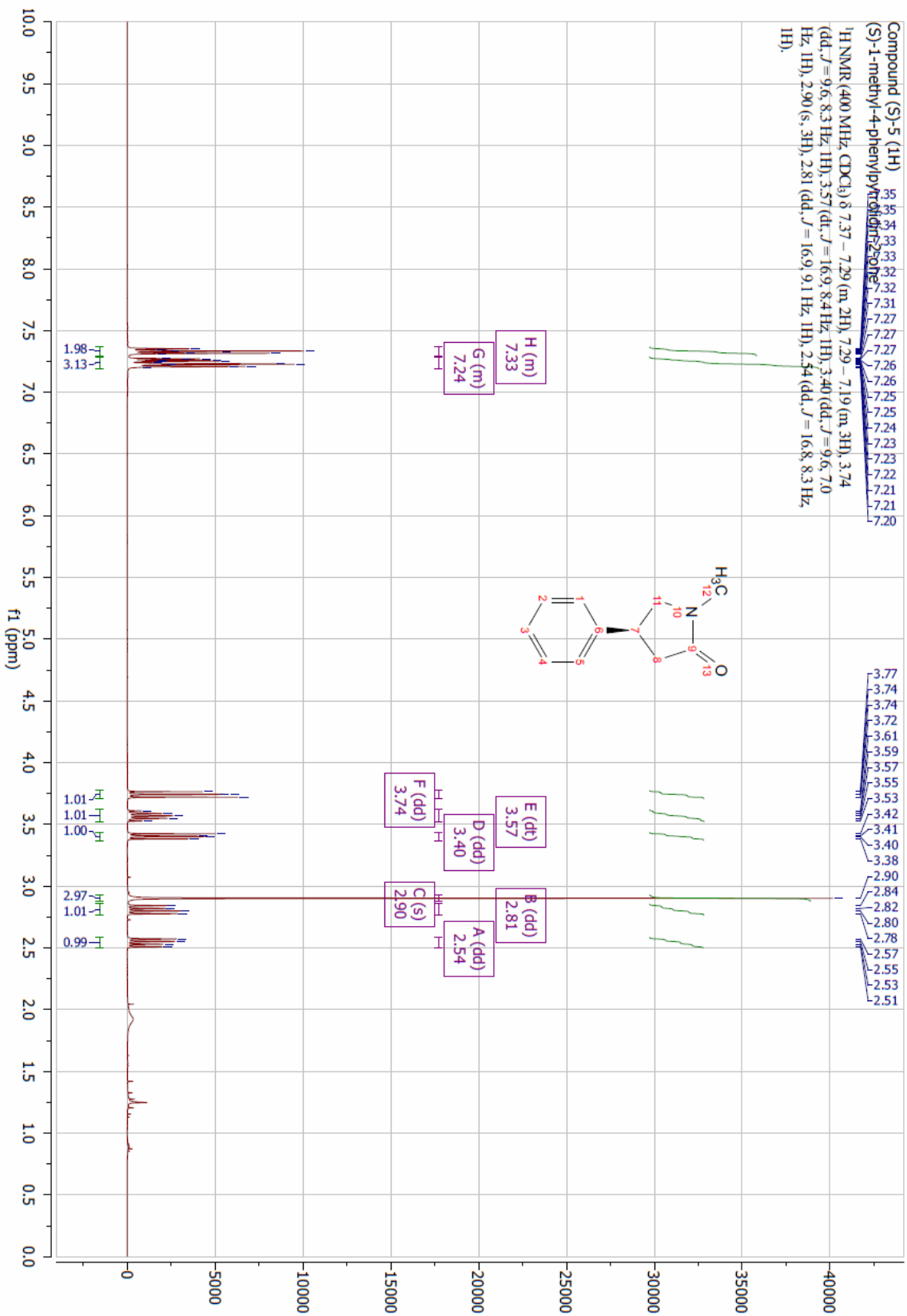


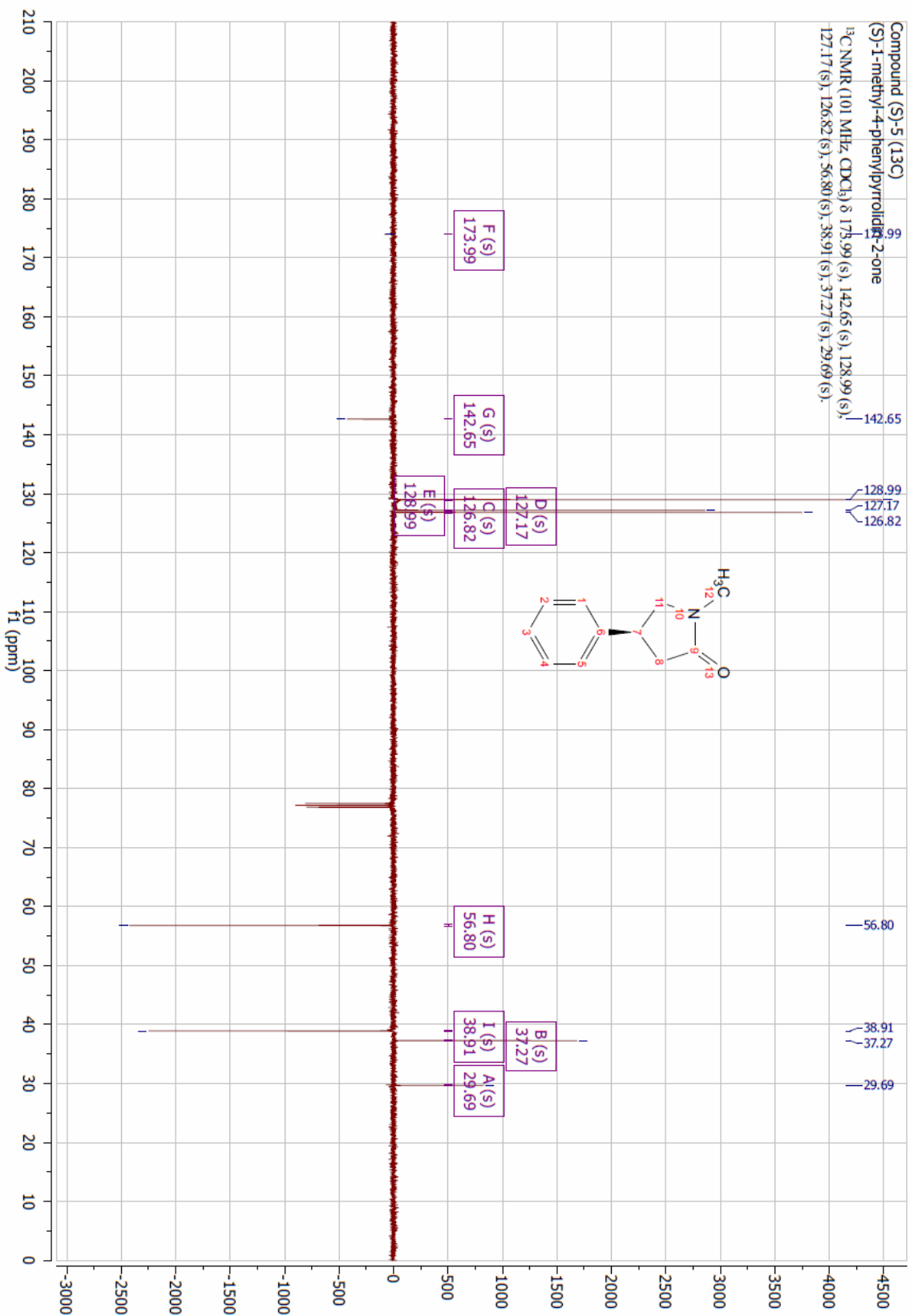


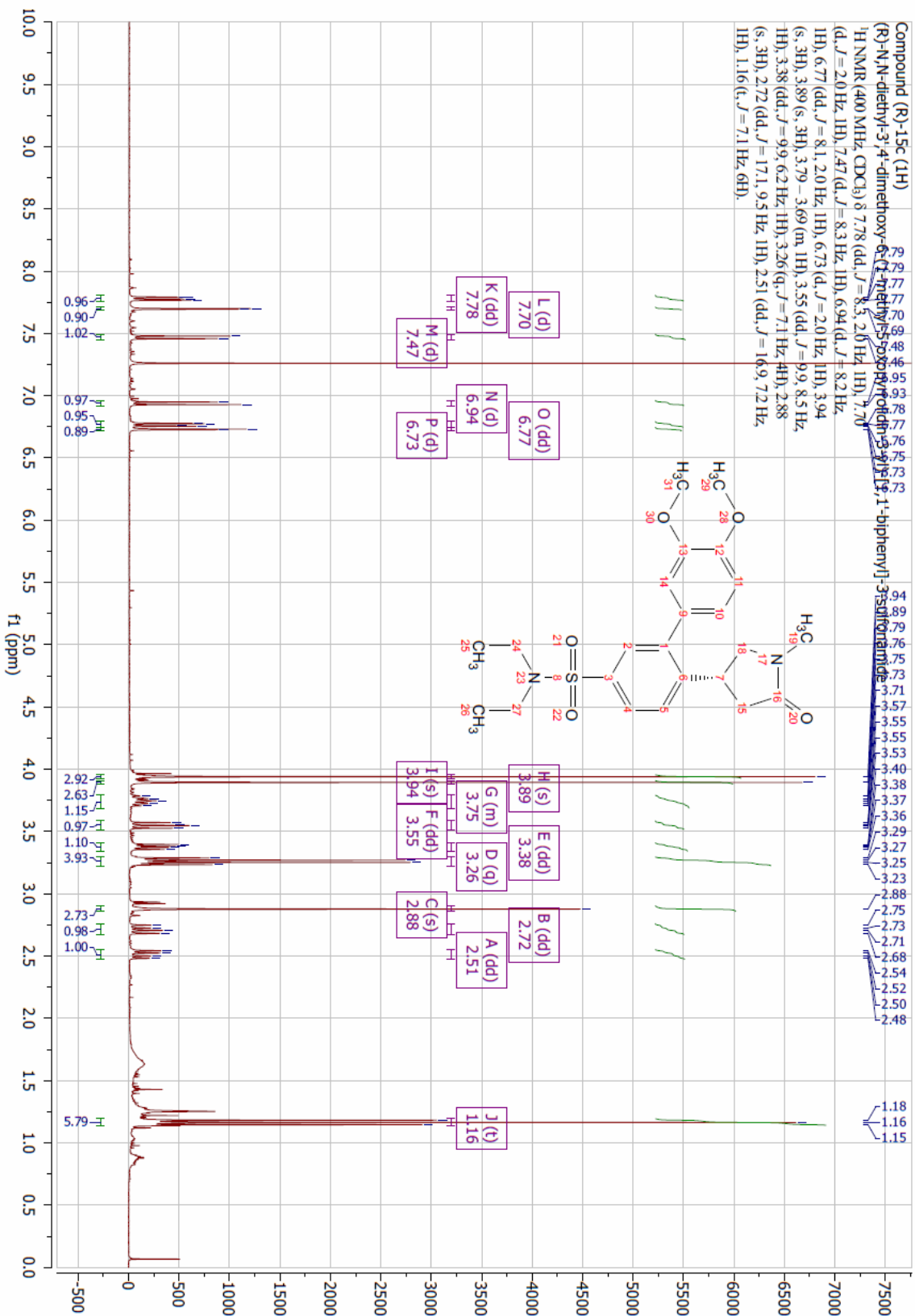


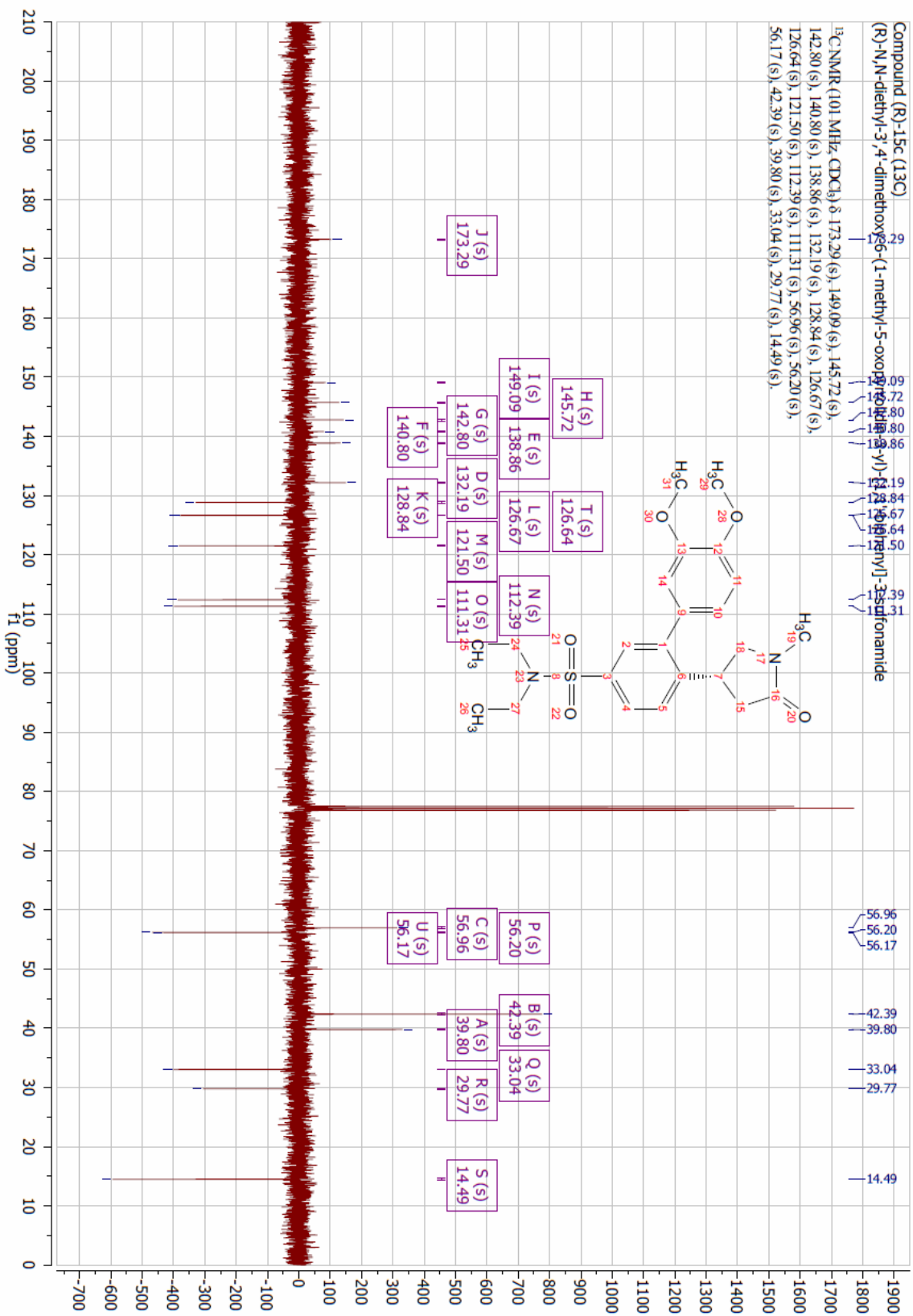


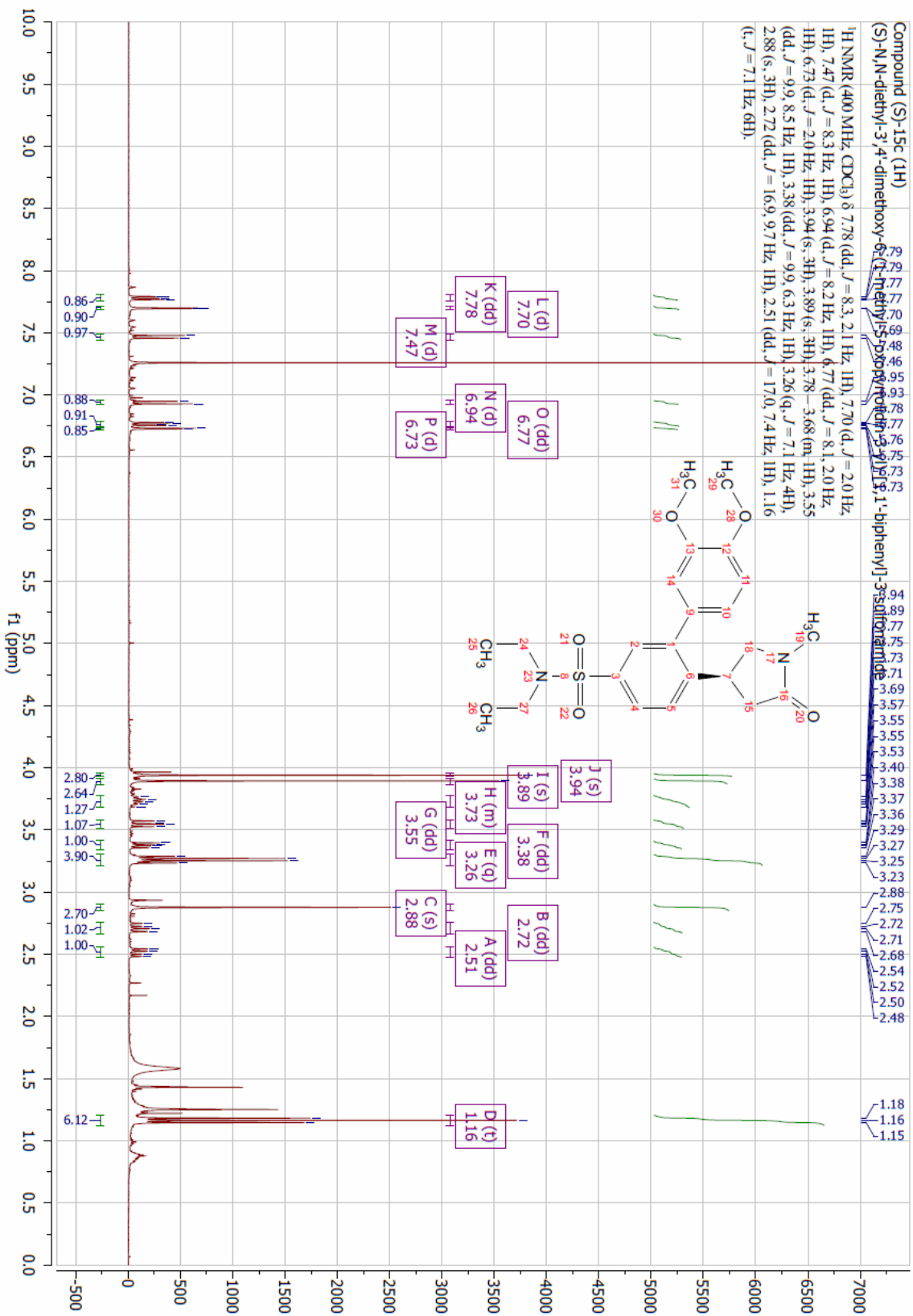


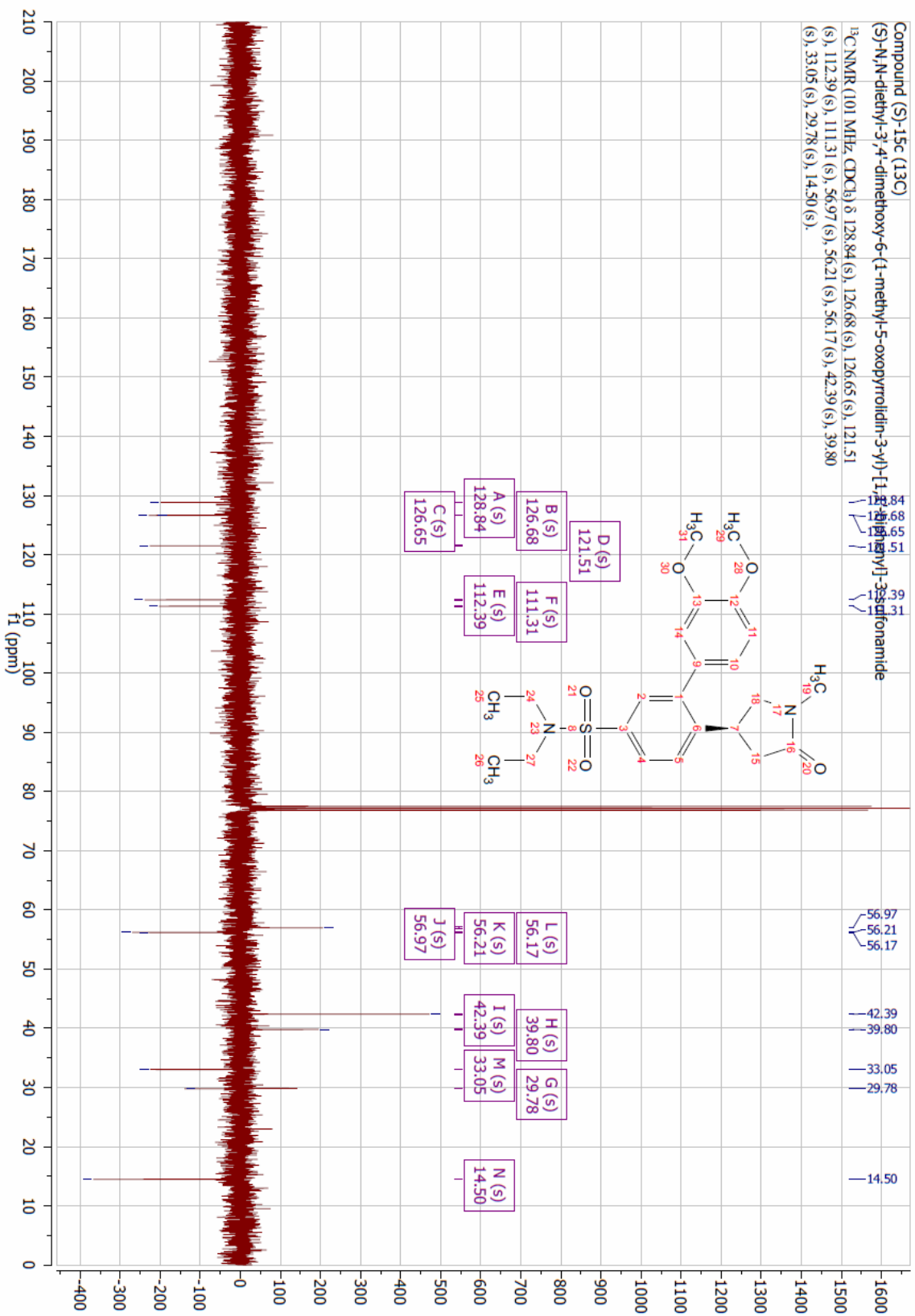












Appendix M – Chapter 3 X-ray Crystallographic Data Collection and

Refinement Statistics

Compound Title	5
Resolution range	39.24 - 1.5 (1.554 - 1.5)
Space group	P 21 21 21
Unit cell	37.619 44.022 78.478 90 90 90
Total reflections	43068 (4224)
Unique reflections	21534 (2112)
Multiplicity	2.0 (2.0)
Completeness (%)	99.97 (99.95)
Mean I/sigma(I)	9.00 (2.95)
Wilson B-factor	7.59
R-merge	0.04589 (0.2057)
R-meas	0.0649 (0.2909)
R-pim	0.04589 (0.2057)
CC1/2	0.991 (0.895)
CC*	0.998 (0.972)
Reflections used in refinement	21531 (2112)
Reflections used for R-free	1083 (115)
R-work	0.1587 (0.1861)
R-free	0.1799 (0.2349)
CC(work)	0.966 (0.932)
CC(free)	0.962 (0.831)
Number of non-hydrogen atoms	1409
macromolecules	1145
ligands	13
solvent	251
Protein residues	127
RMS(bonds)	0.007
RMS(angles)	0.88
Ramachandran favoured (%)	99.18
Ramachandran allowed (%)	0.82
Ramachandran outliers (%)	0.00
Rotamer outliers (%)	3.03
Clashscore	7.42
Average B-factor	12.86
macromolecules	10.31
ligands	10.33
solvent	24.62
Number of TLS groups	11

Statistics for the highest-resolution shell are shown in parentheses.

Compound Title	7b
Resolution range	38.22 - 1.55 (1.605 - 1.55)
Space group	P 21 21 21
Unit cell	43.744 48.942 61.184 90 90 90
Total reflections	38813 (3766)
Unique reflections	19417 (1888)
Multiplicity	2.0 (2.0)
Completeness (%)	98.64 (97.42)
Mean I/sigma(I)	10.83 (3.34)
Wilson B-factor	10.18
R-merge	0.02792 (0.1815)
R-meas	0.03949 (0.2566)
R-pim	0.02792 (0.1815)
CC1/2	0.998 (0.929)
CC*	1 (0.981)
Reflections used in refinement	19416 (1887)
Reflections used for R-free	967 (96)
R-work	0.1921 (0.2224)
R-free	0.2317 (0.2986)
CC(work)	0.954 (0.910)
CC(free)	0.907 (0.812)
Number of non-hydrogen atoms	1321
macromolecules	1088
ligands	22
solvent	211
Protein residues	125
RMS(bonds)	0.008
RMS(angles)	0.87
Ramachandran favoured (%)	97.56
Ramachandran allowed (%)	2.44
Ramachandran outliers (%)	0.00
Rotamer outliers (%)	0.00
Clashscore	5.89
Average B-factor	16.12
macromolecules	14.43
ligands	10.56
solvent	25.40

Statistics for the highest-resolution shell are shown in parentheses.

Compound Title	7h
Resolution range	40.27 - 1.59 (1.647 - 1.59)
Space group	P 1 21 1
Unit cell	36.03 79.205 46.819 90 92.82 90
Total reflections	70281 (6907)
Unique reflections	35239 (3490)
Multiplicity	2.0 (2.0)
Completeness (%)	99.01 (98.67)
Mean I/sigma(I)	10.29 (1.76)
Wilson B-factor	14.82
R-merge	0.04201 (0.4002)
R-meas	0.05941 (0.566)
R-pim	0.04201 (0.4002)
CC1/2	0.997 (0.75)
CC*	0.999 (0.926)
Reflections used in refinement	34938 (3488)
Reflections used for R-free	1769 (179)
R-work	0.2150 (0.2897)
R-free	0.2653 (0.3388)
CC(work)	0.946 (0.869)
CC(free)	0.924 (0.883)
Number of non-hydrogen atoms	2661
macromolecules	2164
ligands	40
solvent	457
Protein residues	253
RMS(bonds)	0.007
RMS(angles)	0.89
Ramachandran favoured (%)	97.99
Ramachandran allowed (%)	2.01
Ramachandran outliers (%)	0.00
Rotamer outliers (%)	0.82
Clashscore	6.89
Average B-factor	19.89
macromolecules	17.96
ligands	25.01
solvent	28.58
Number of TLS groups	22

Statistics for the highest-resolution shell are shown in parentheses.

Compound Title	15c
Resolution range	38.54 - 1.48 (1.533 - 1.48)
Space group	P 21 21 21
Unit cell	42.83 52.047 57.354 90 90 90
Total reflections	43743 (4078)
Unique reflections	21884 (2051)
Multiplicity	2.0 (2.0)
Completeness (%)	99.53 (95.35)
Mean I/sigma(I)	20.37 (3.99)
Wilson B-factor	17.41
R-merge	0.01351 (0.1648)
R-meas	0.01911 (0.2331)
R-pim	0.01351 (0.1648)
CC1/2	1 (0.894)
CC*	1 (0.971)
Reflections used in refinement	21882 (2051)
Reflections used for R-free	1097 (92)
R-work	0.1776 (0.2258)
R-free	0.2034 (0.2628)
CC(work)	0.969 (0.861)
CC(free)	0.949 (0.755)
Number of non-hydrogen atoms	1349
macromolecules	1137
ligands	31
solvent	181
Protein residues	125
RMS(bonds)	0.007
RMS(angles)	0.93
Ramachandran favoured (%)	100.00
Ramachandran allowed (%)	0.00
Ramachandran outliers (%)	0.00
Rotamer outliers (%)	2.33
Clashscore	4.74
Average B-factor	25.30
macromolecules	23.30
ligands	34.76
solvent	36.21
Number of TLS groups	9

Statistics for the highest-resolution shell are shown in parentheses.

Appendix N – Dose Response Curve of 5-methyl-3-aryl-1H-pyrazoles

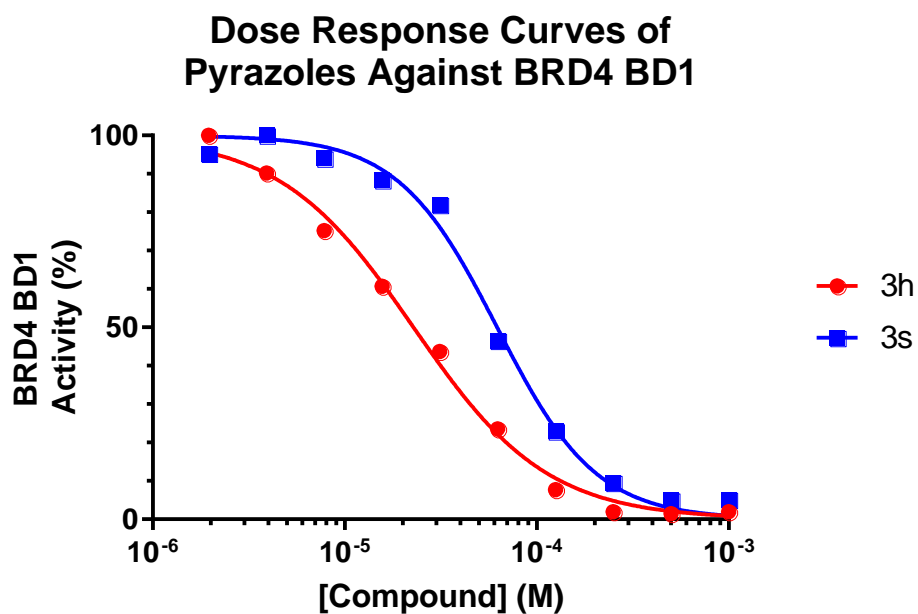


Figure S1. Dose-response curves to determine the IC₅₀ of pyrazoles **3h** and **3s**. Curve fits were calculated using GraphPad Prism. Experiments were performed in duplicates.

Appendix O – Video of Pyrazole 3h

Video provided on USB.

Video to be uploaded in the near-future.

PDB code of **FL-411** provided in video. Crystal structure of **3h** developed by Dr. Ian Jennings and Dr. Olga Ilyichova. Video edited and narrated by Joseph Hilton-Proctor.

Appendix P – Electron Density Map of 3h

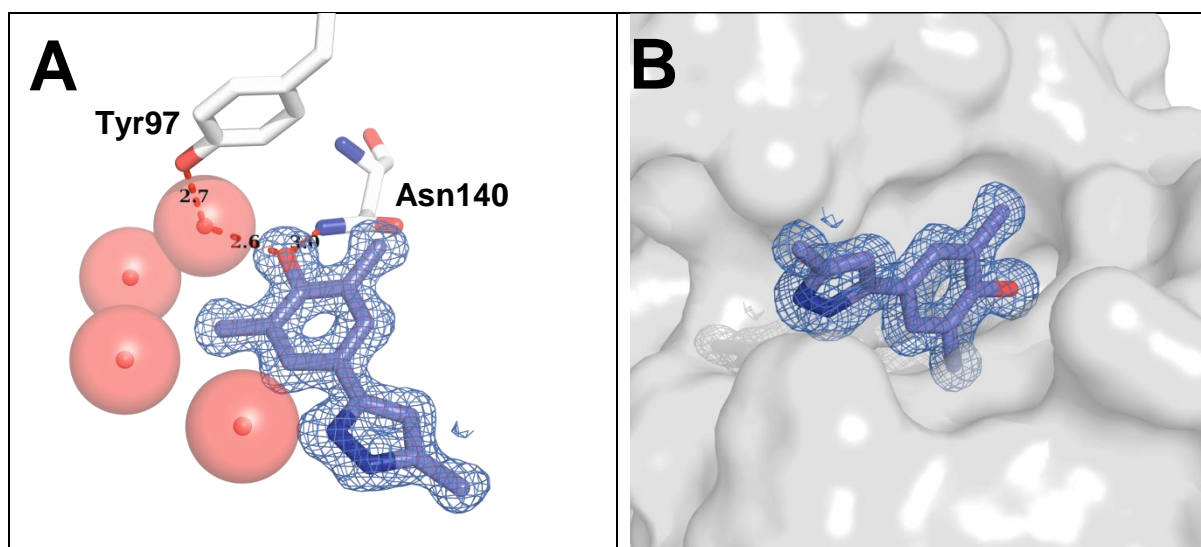
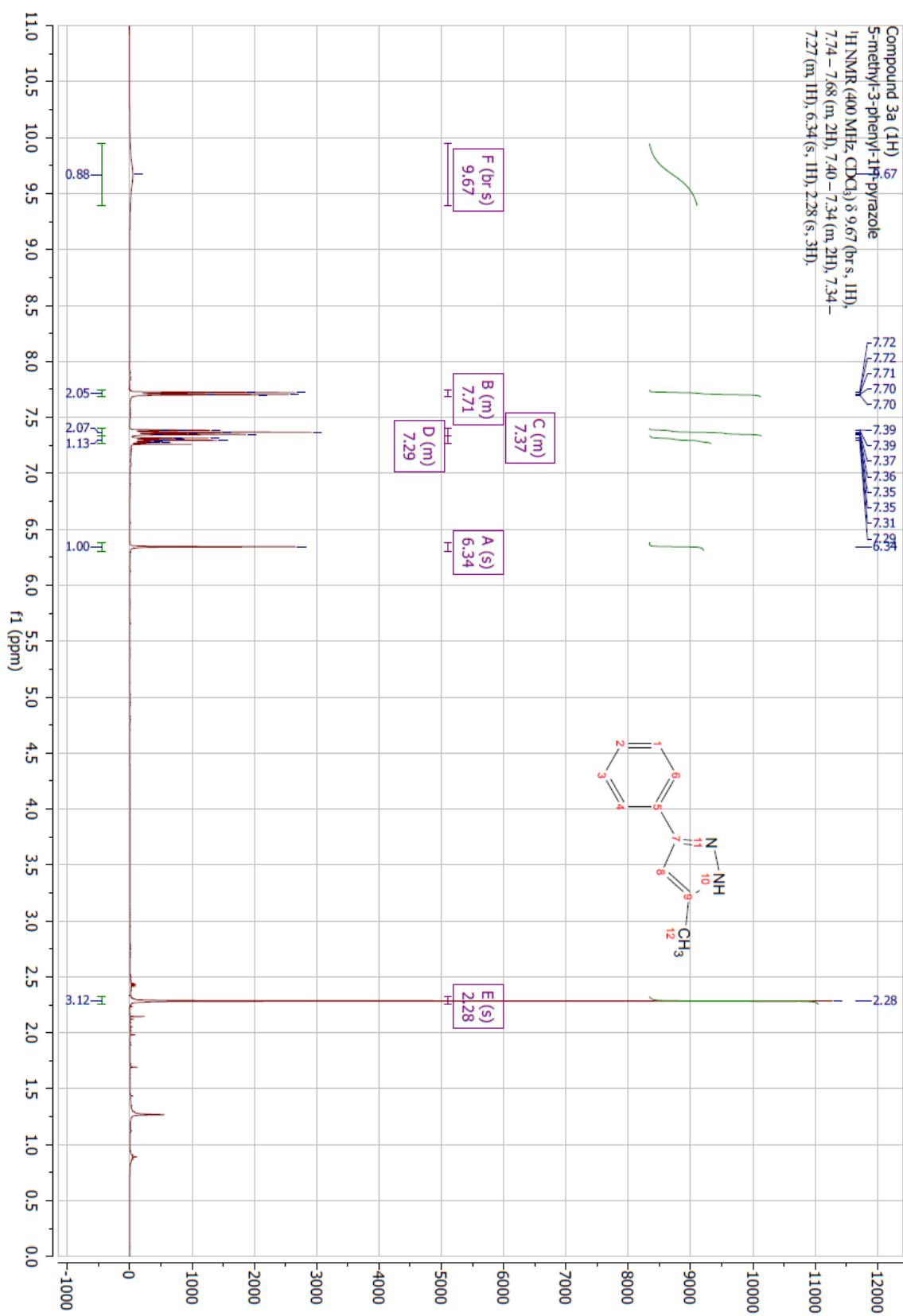
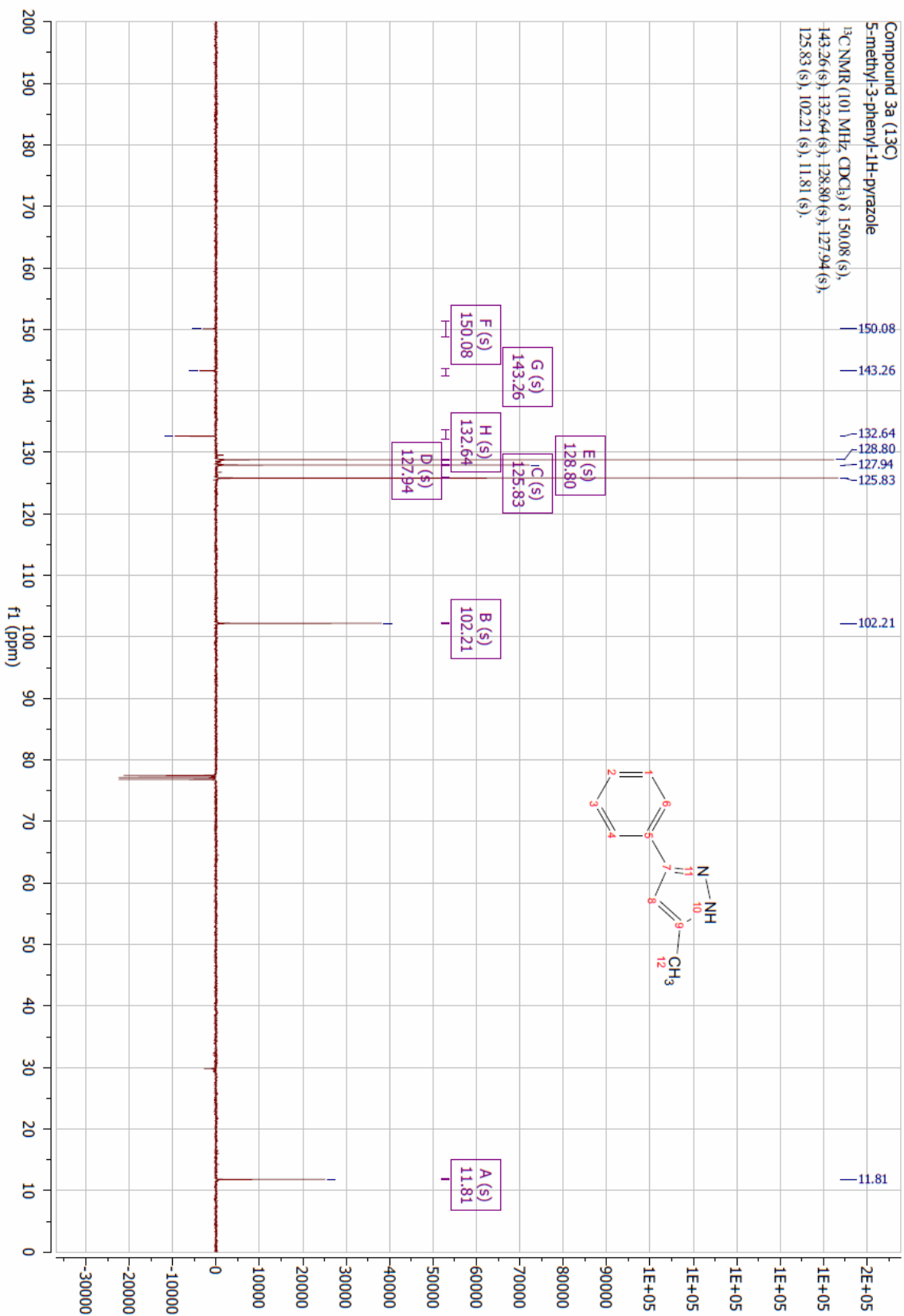
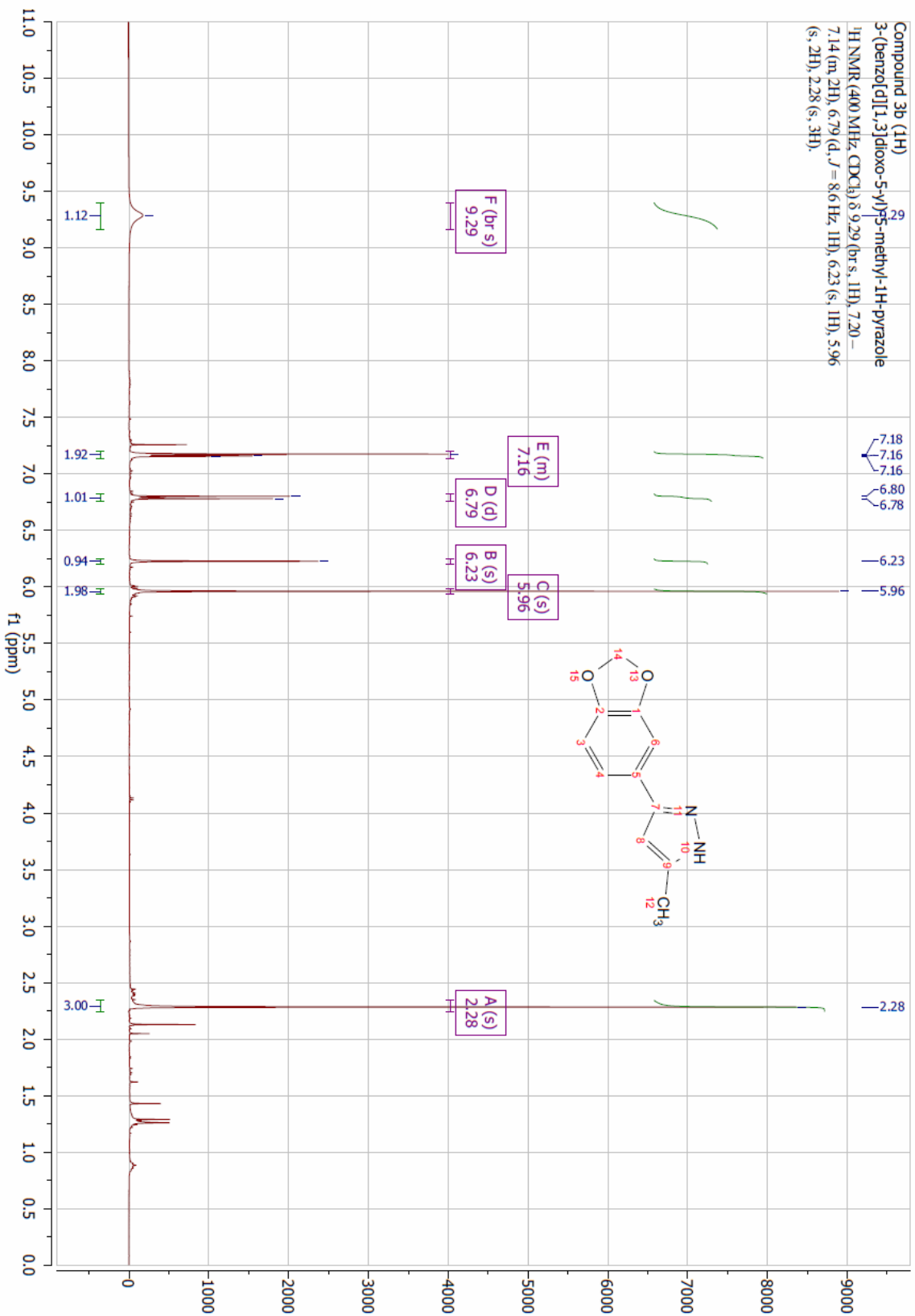


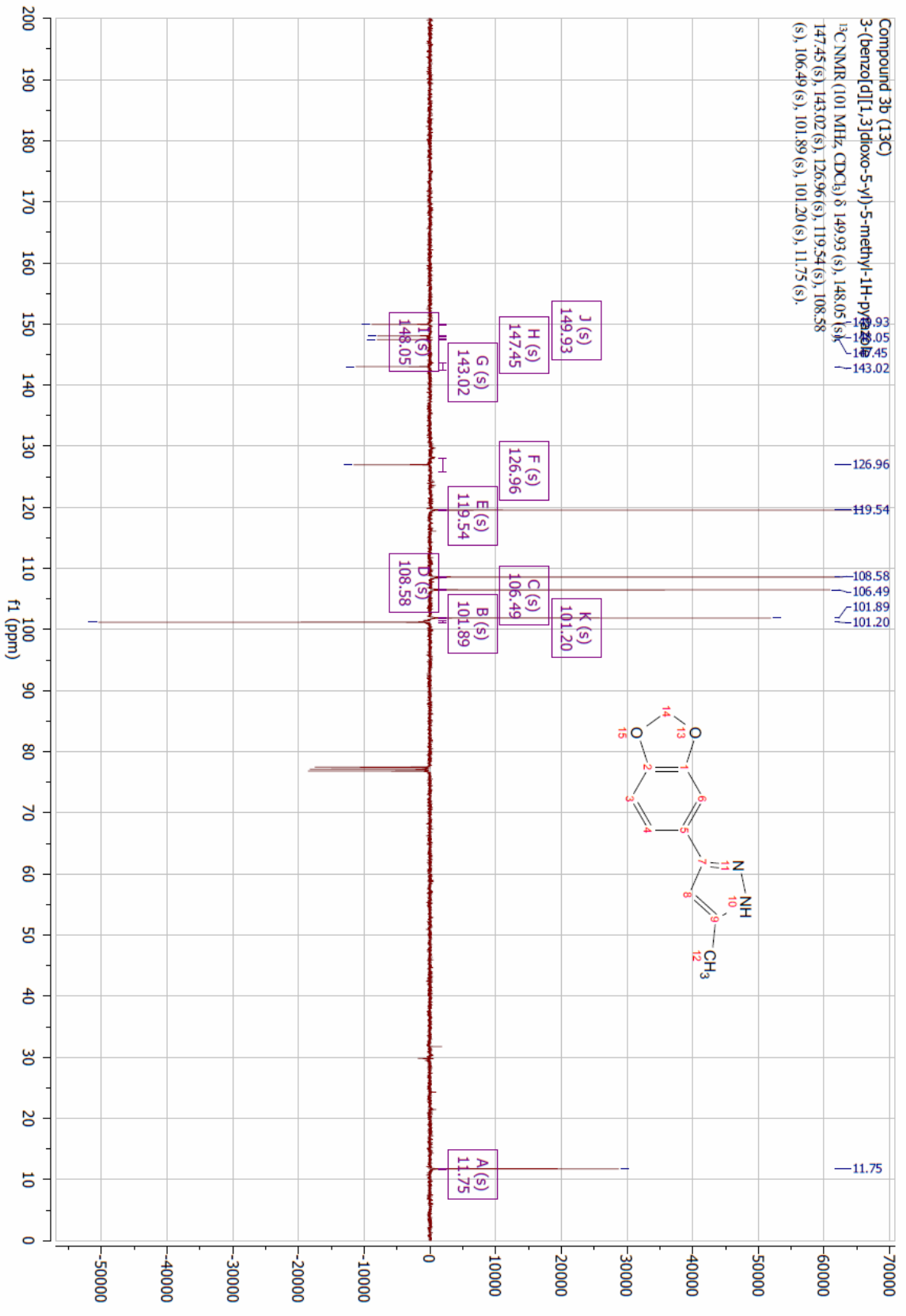
Figure S1. Electron density maps of 3h. [A] Binding site. [B] Outside the binding site. The 2Fo-Fc electron density map is shown in blue mesh at a contour level of 1.0 sigma. Electron density map developed by Dr. Olga Ilyichova.

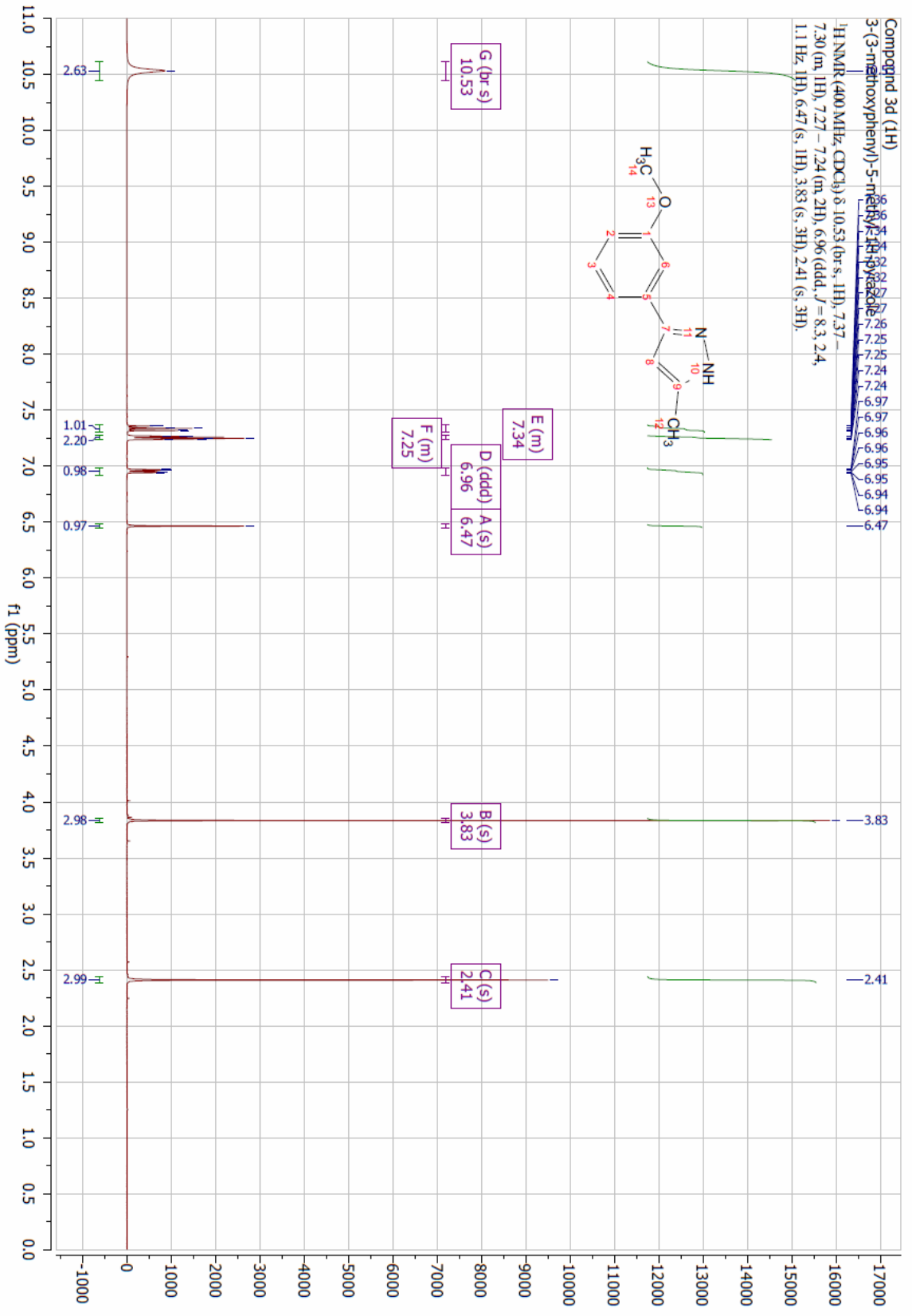
Appendix Q – Chapter 4 NMR Data

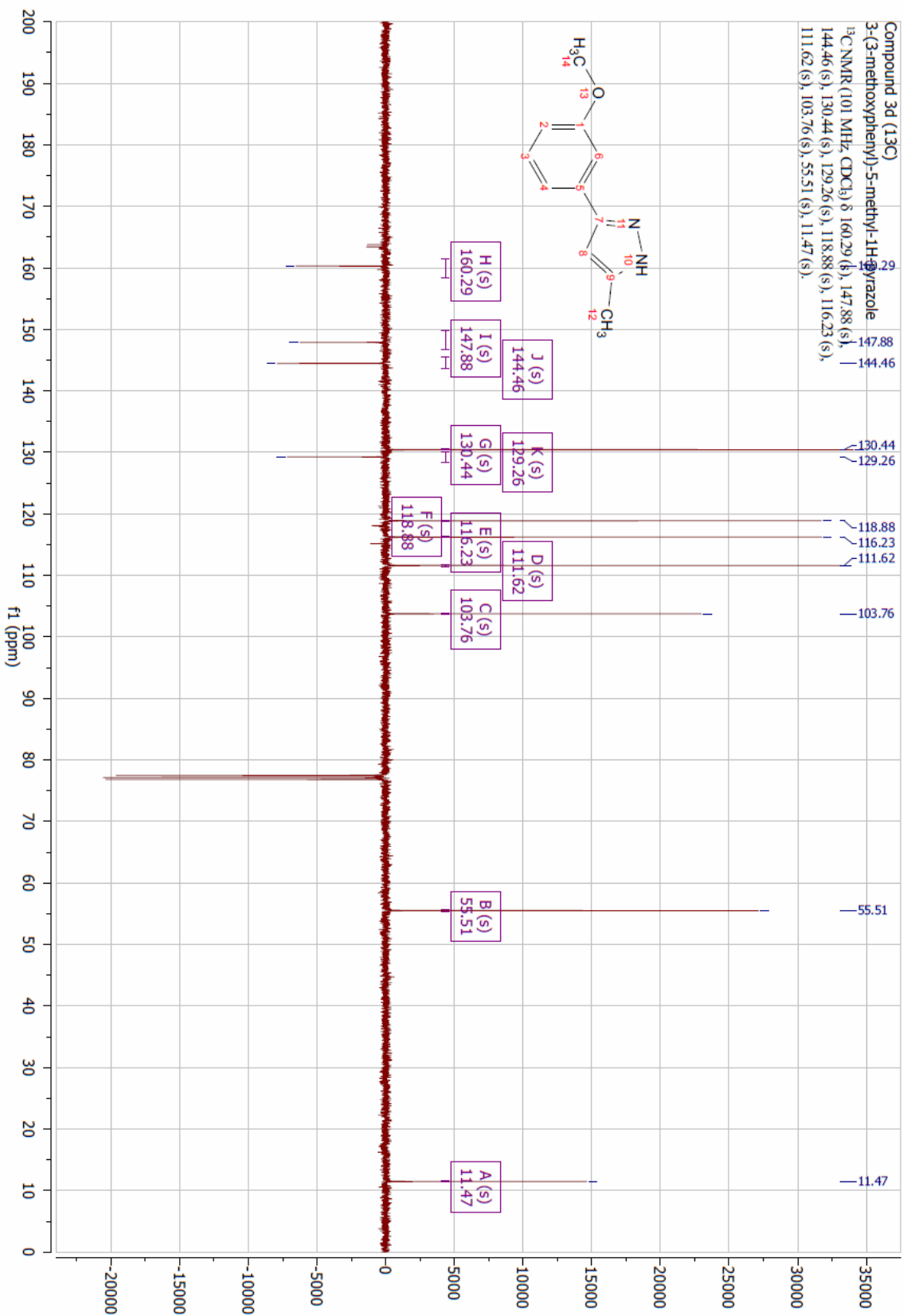


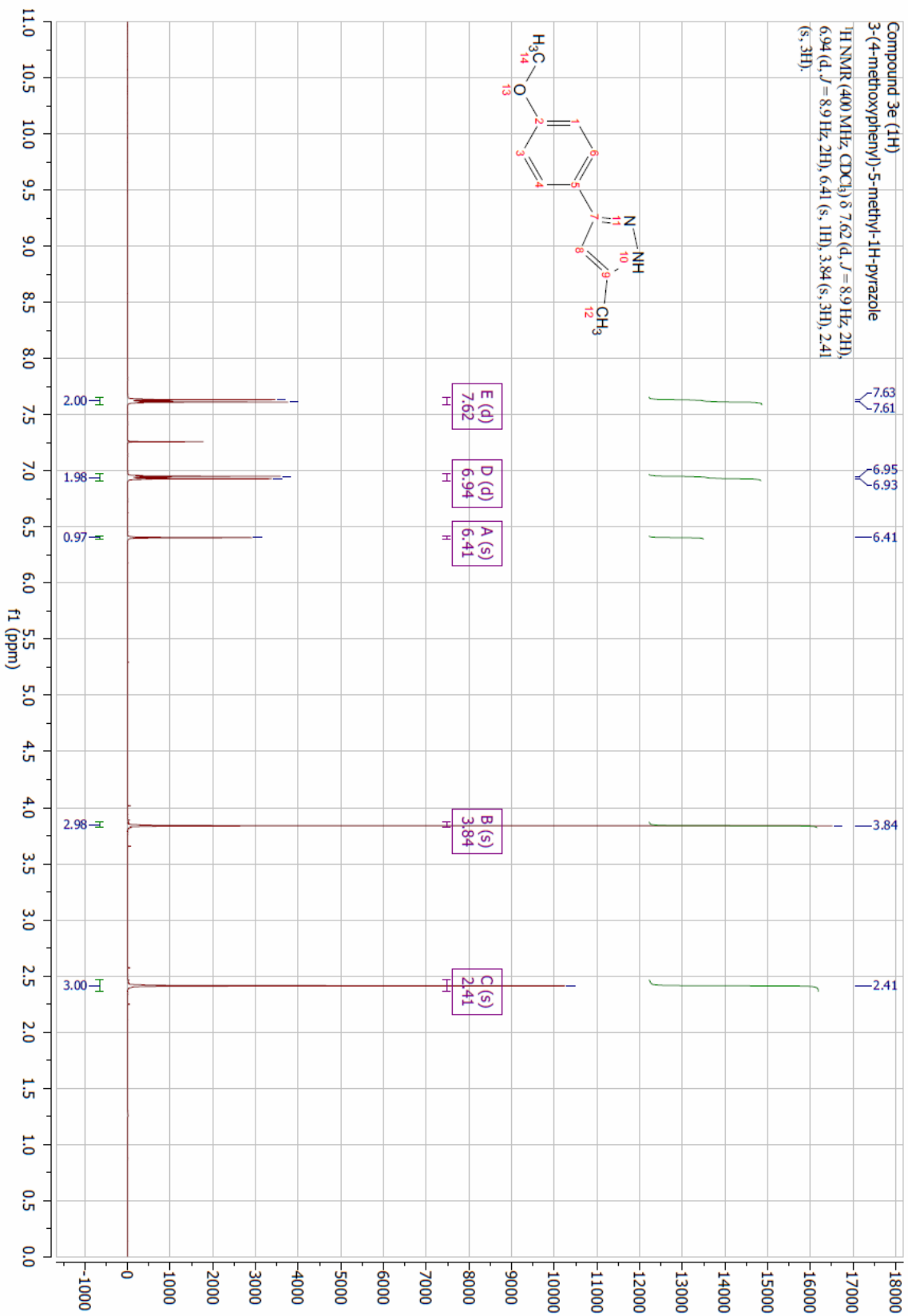


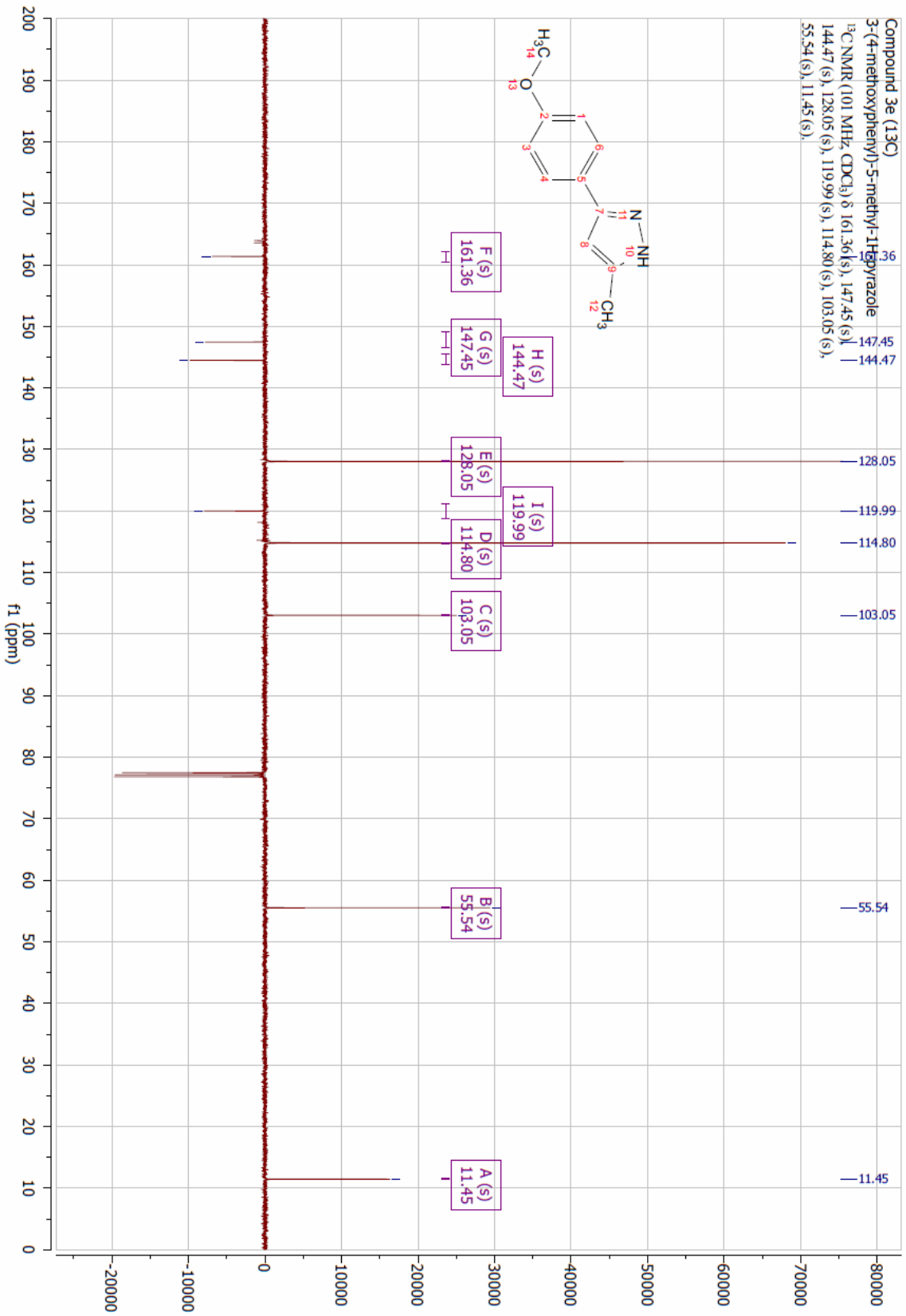


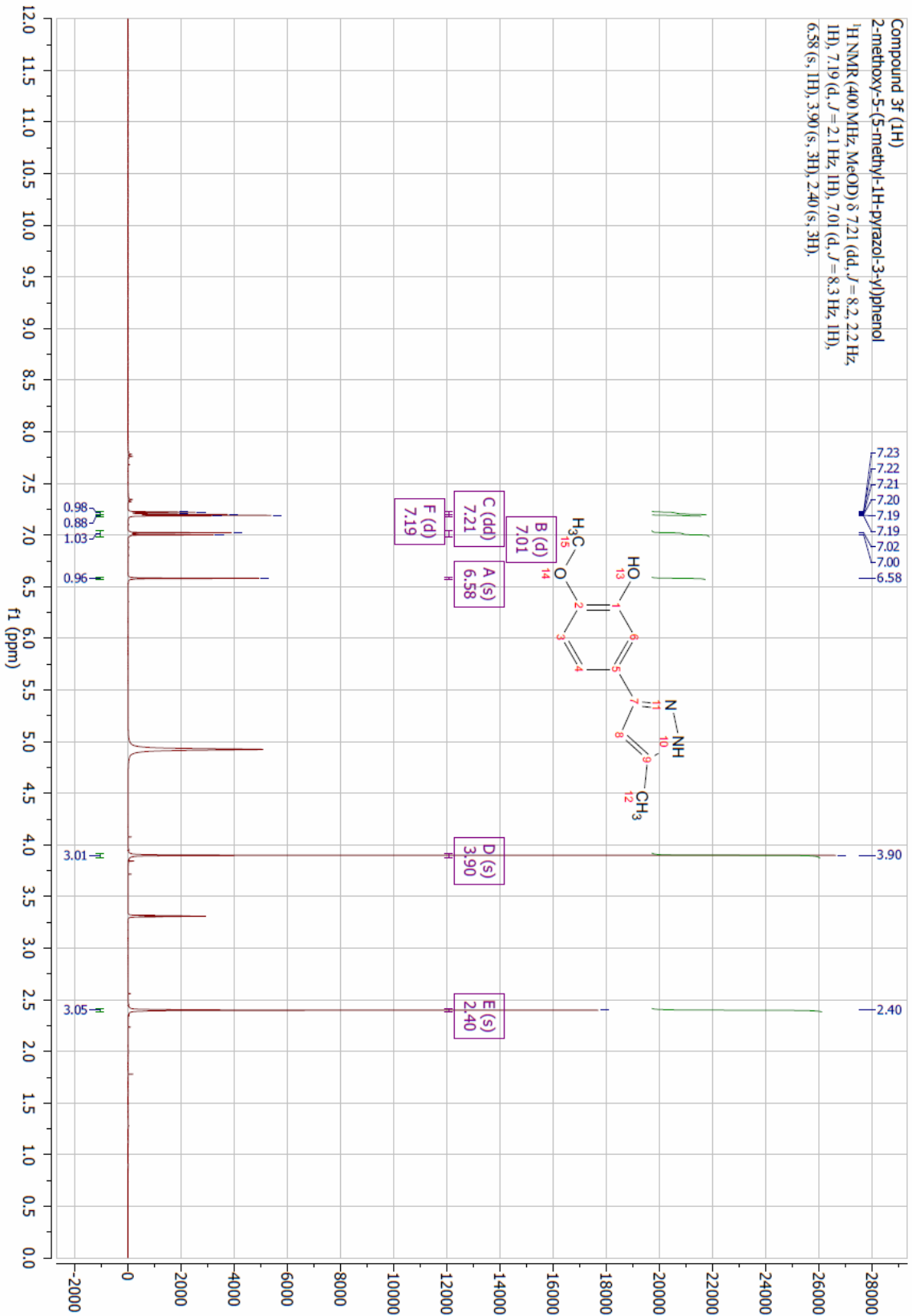


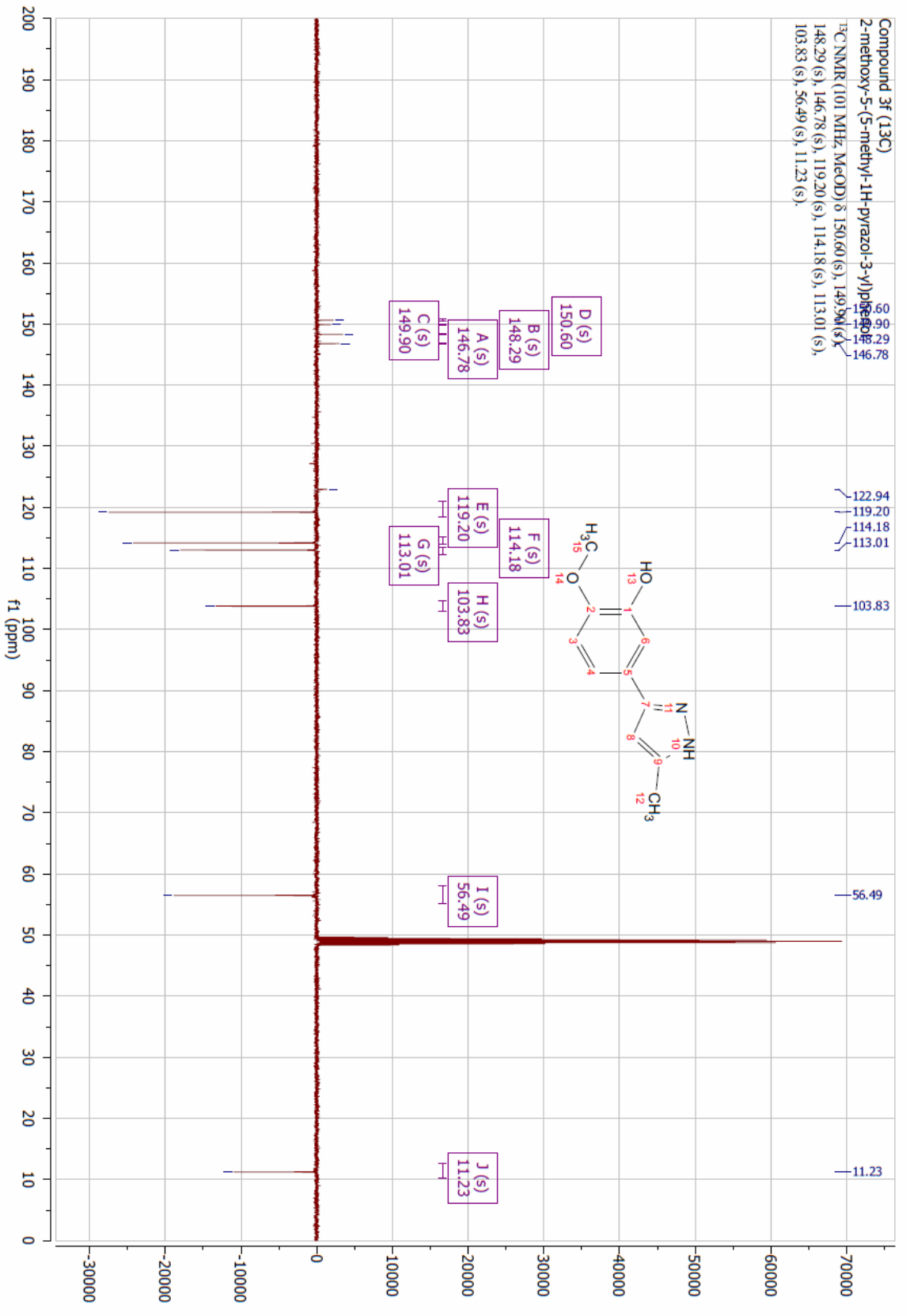


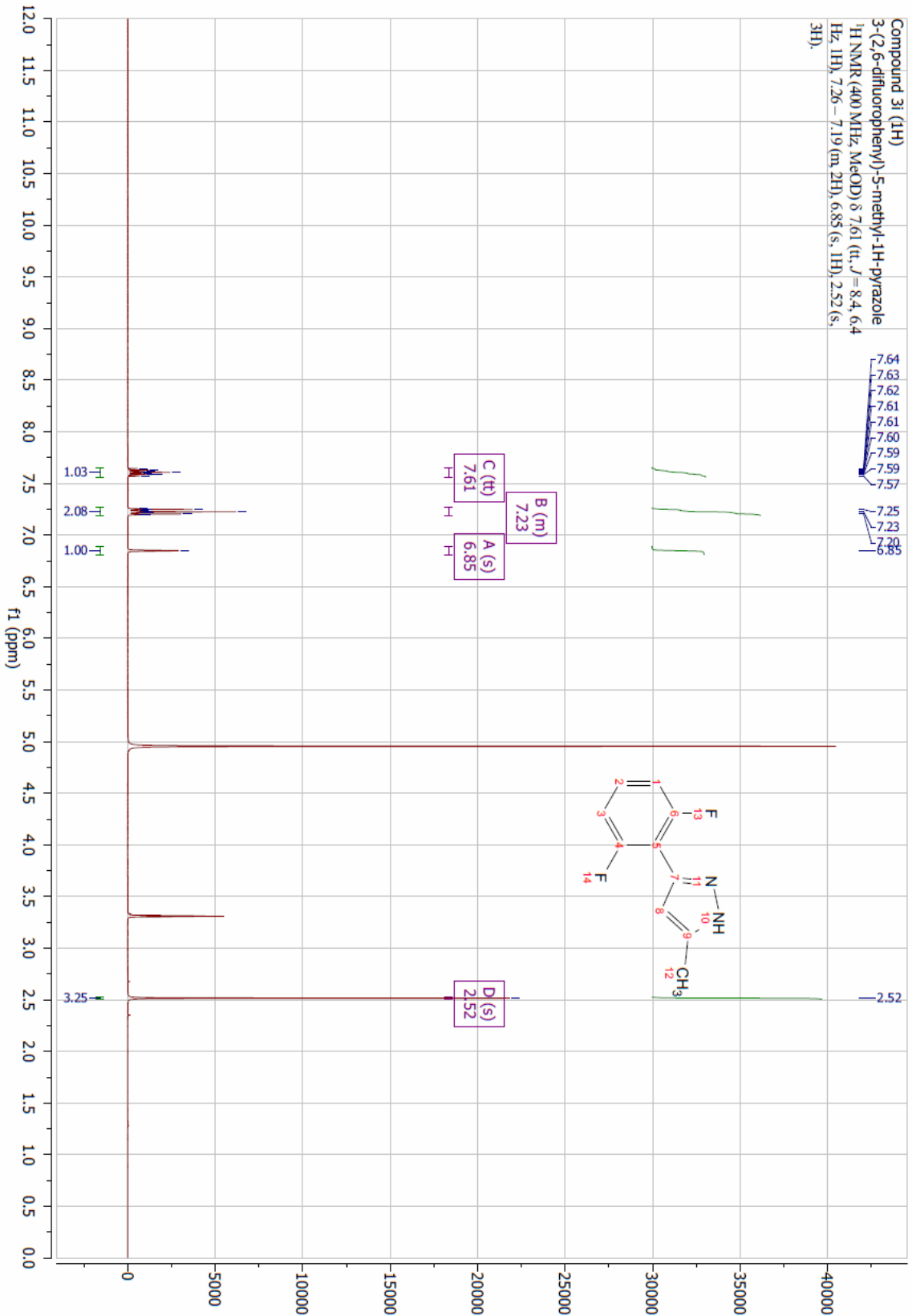


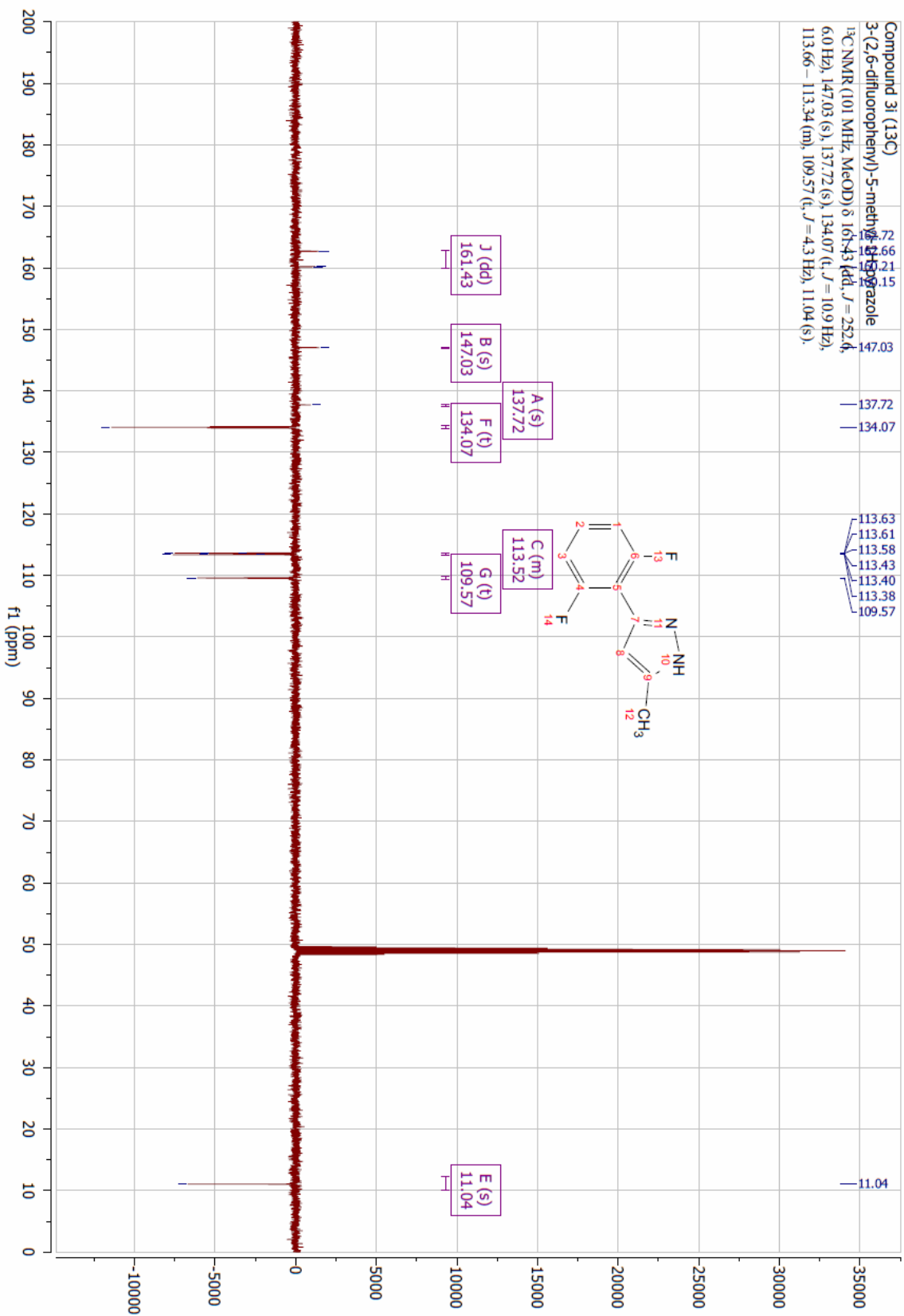


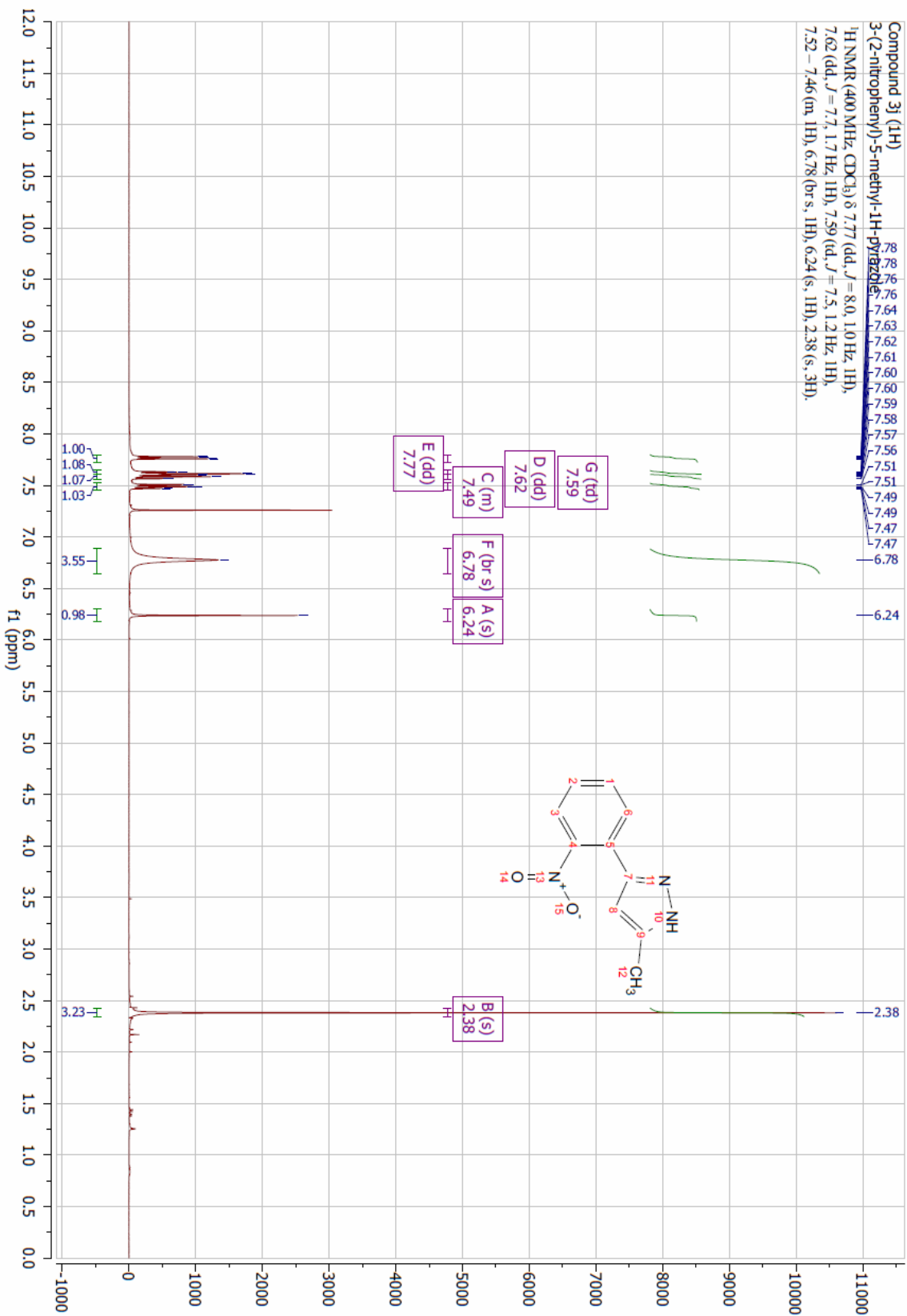


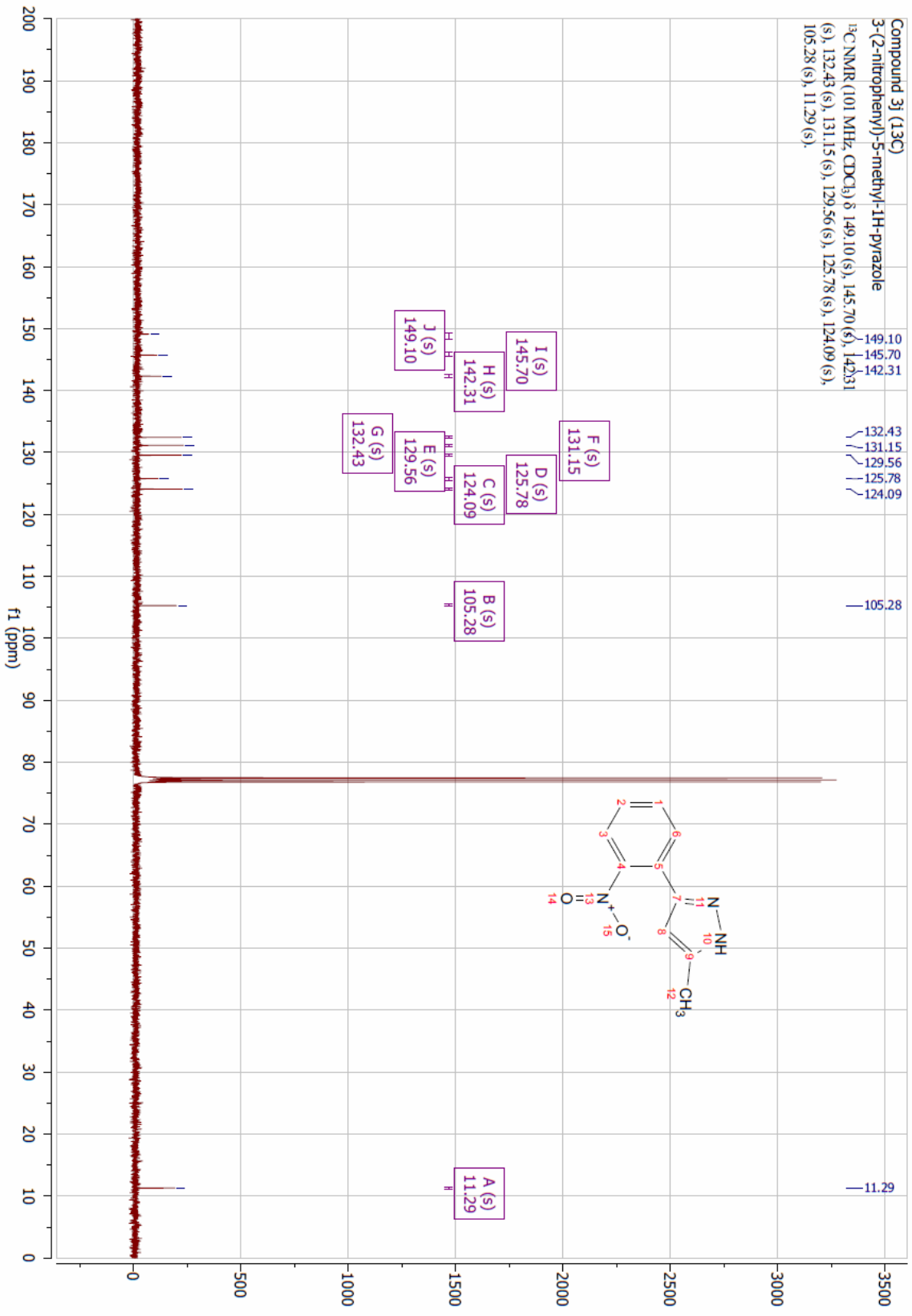


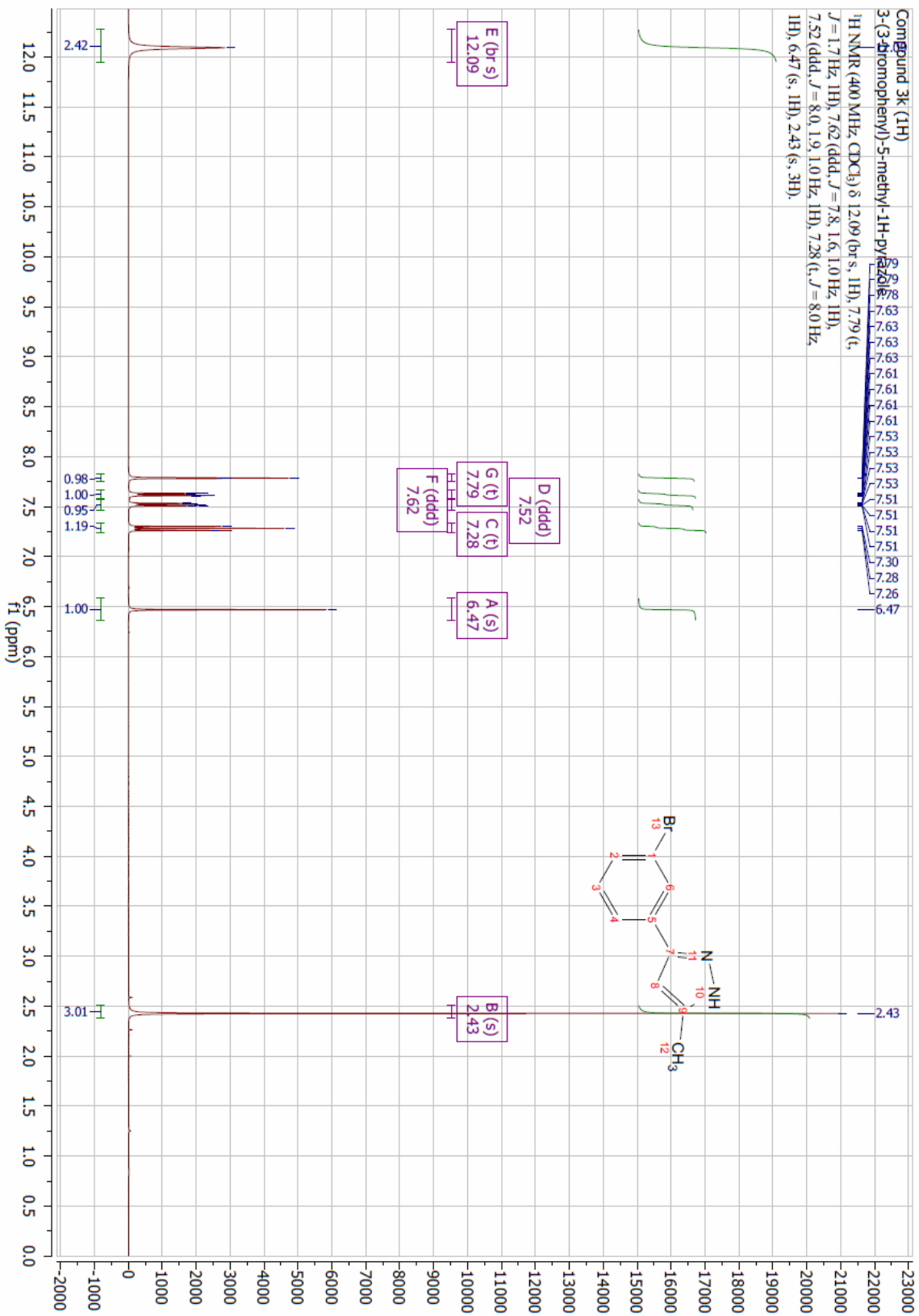


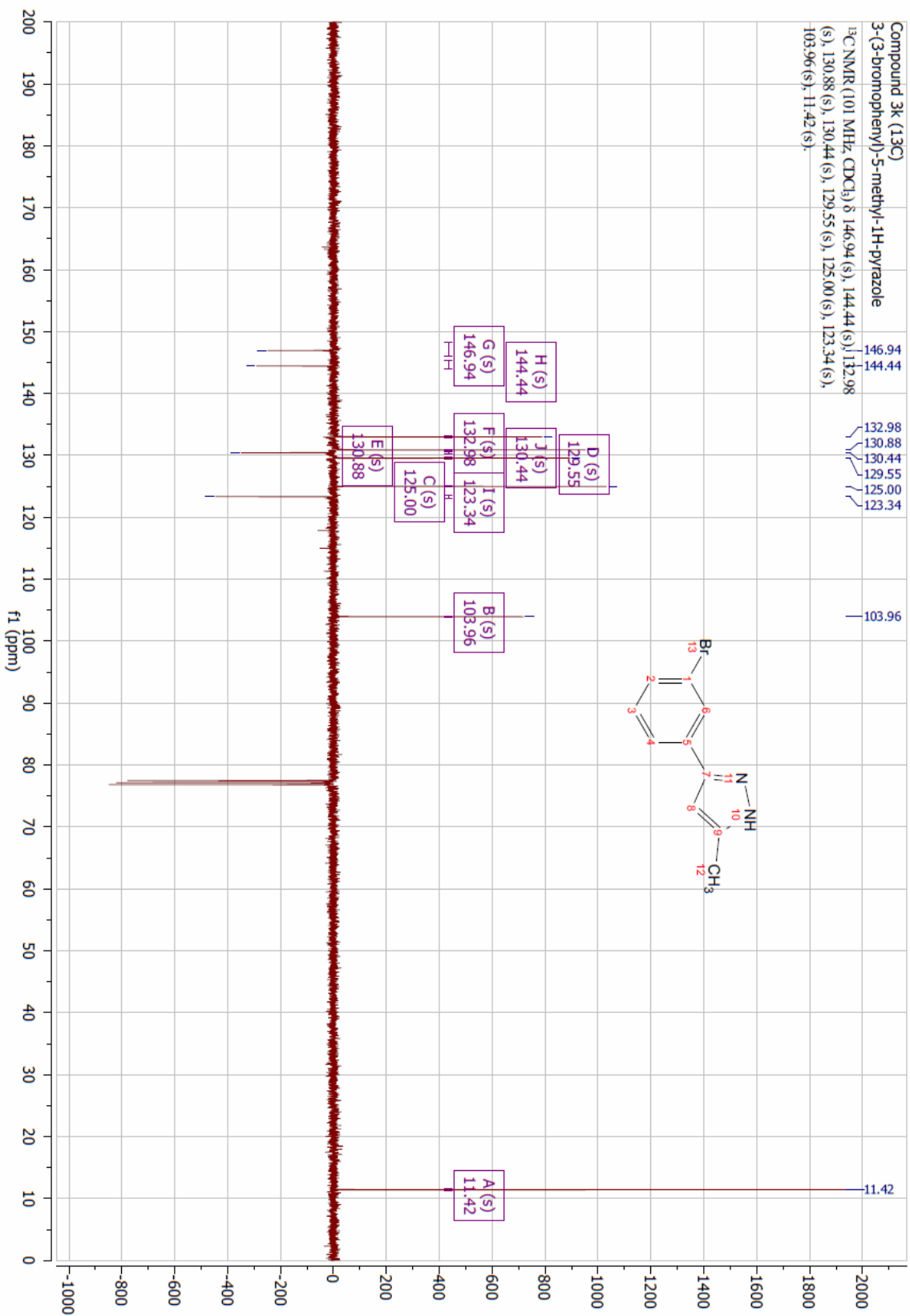


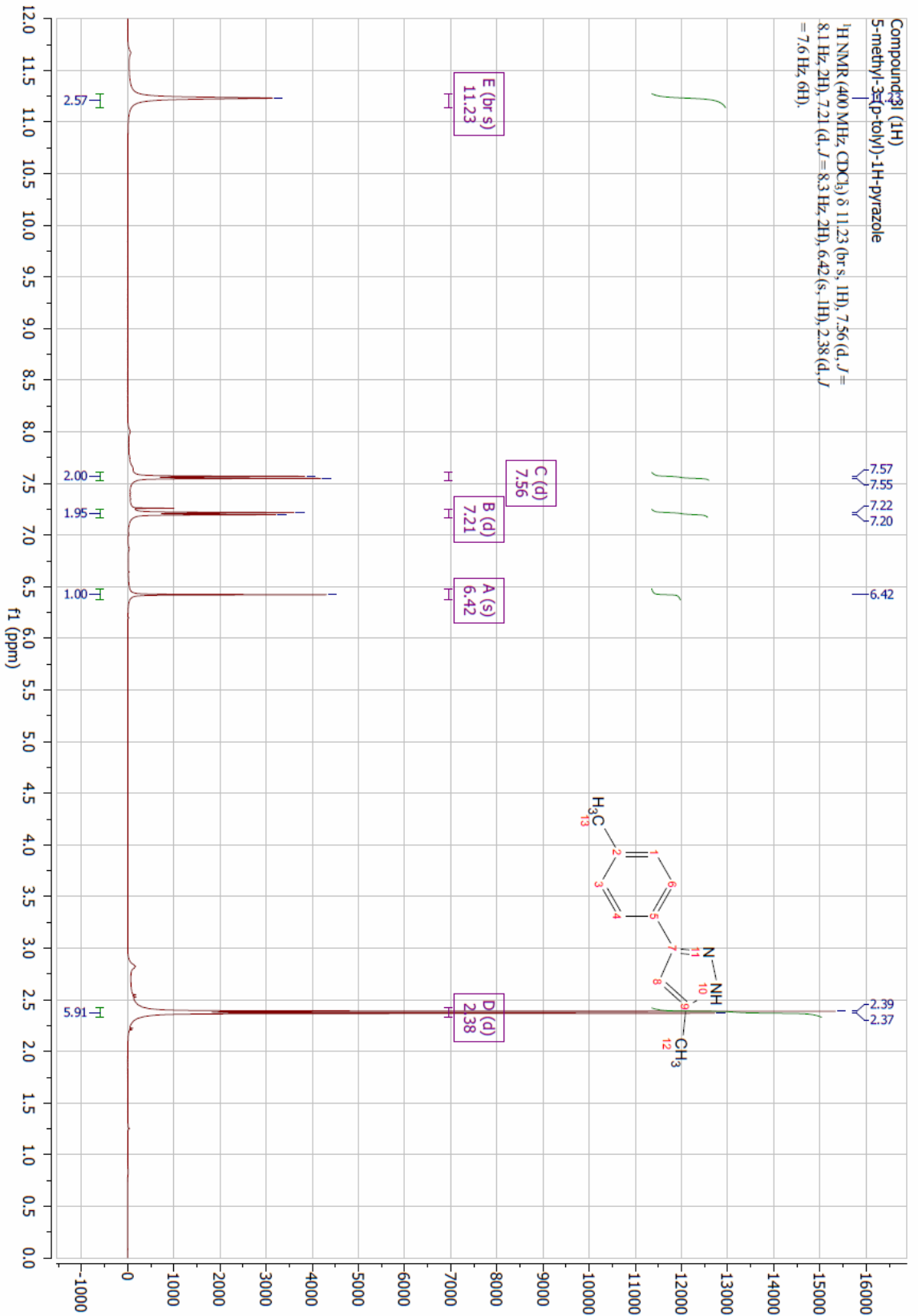


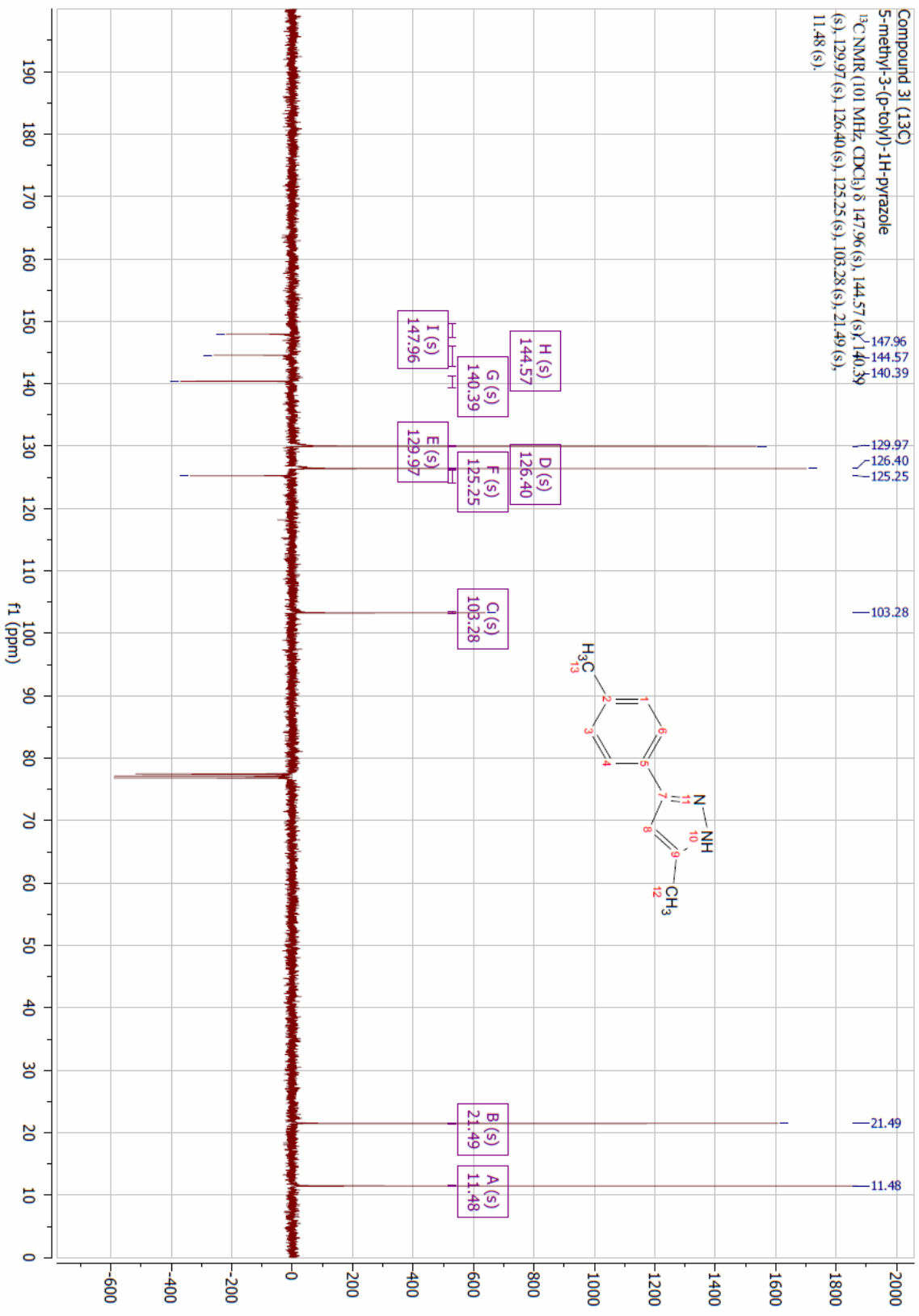


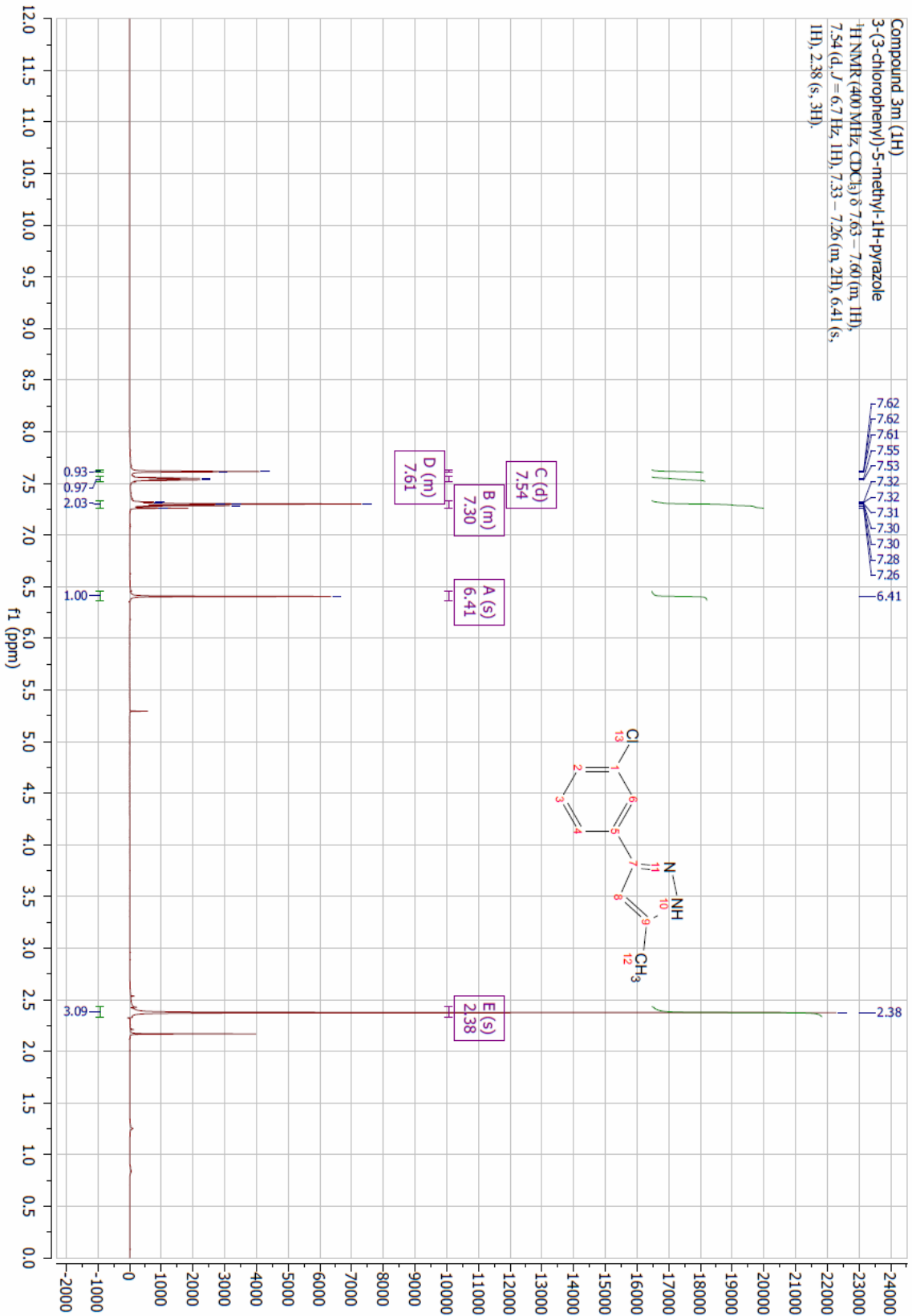


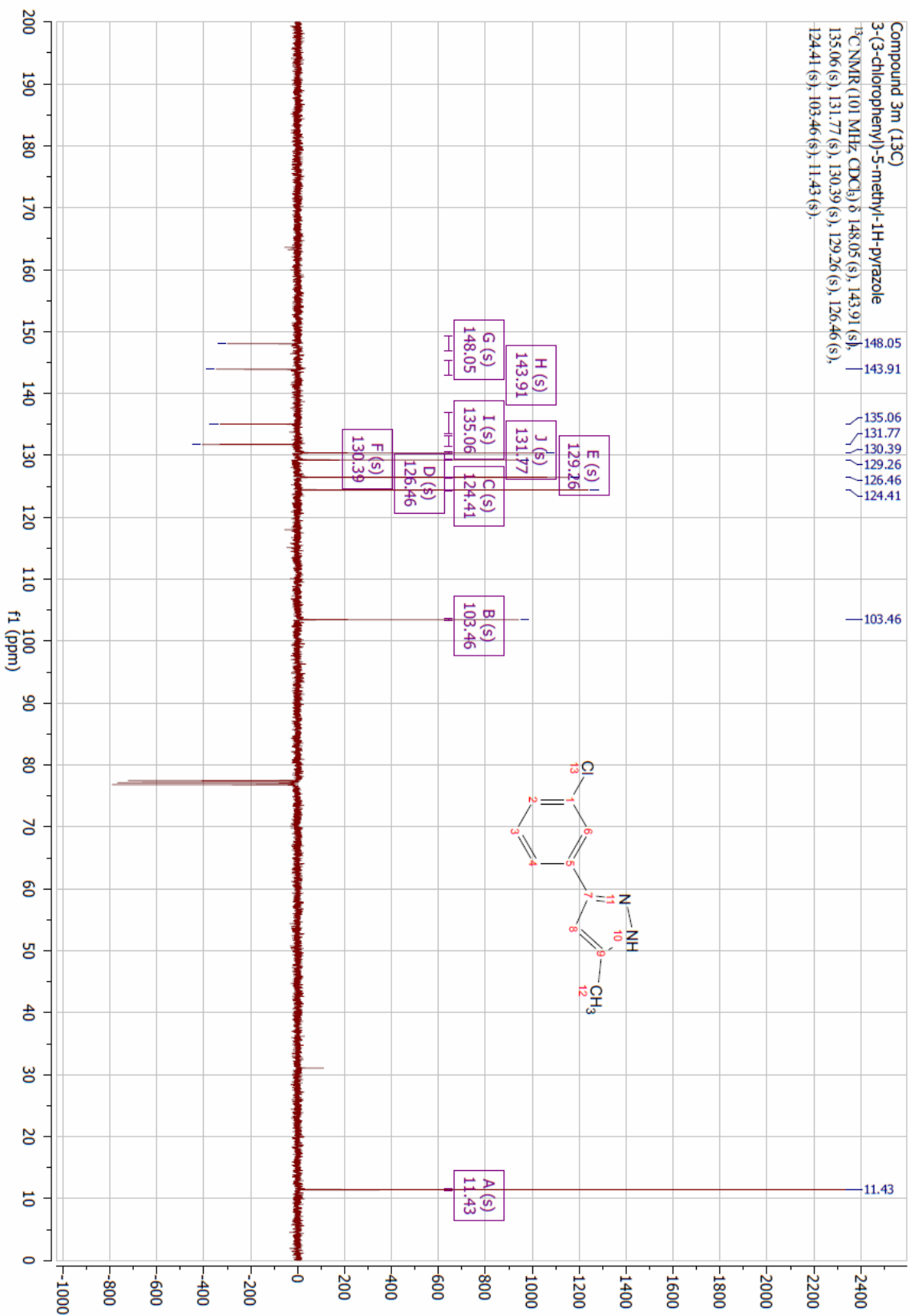


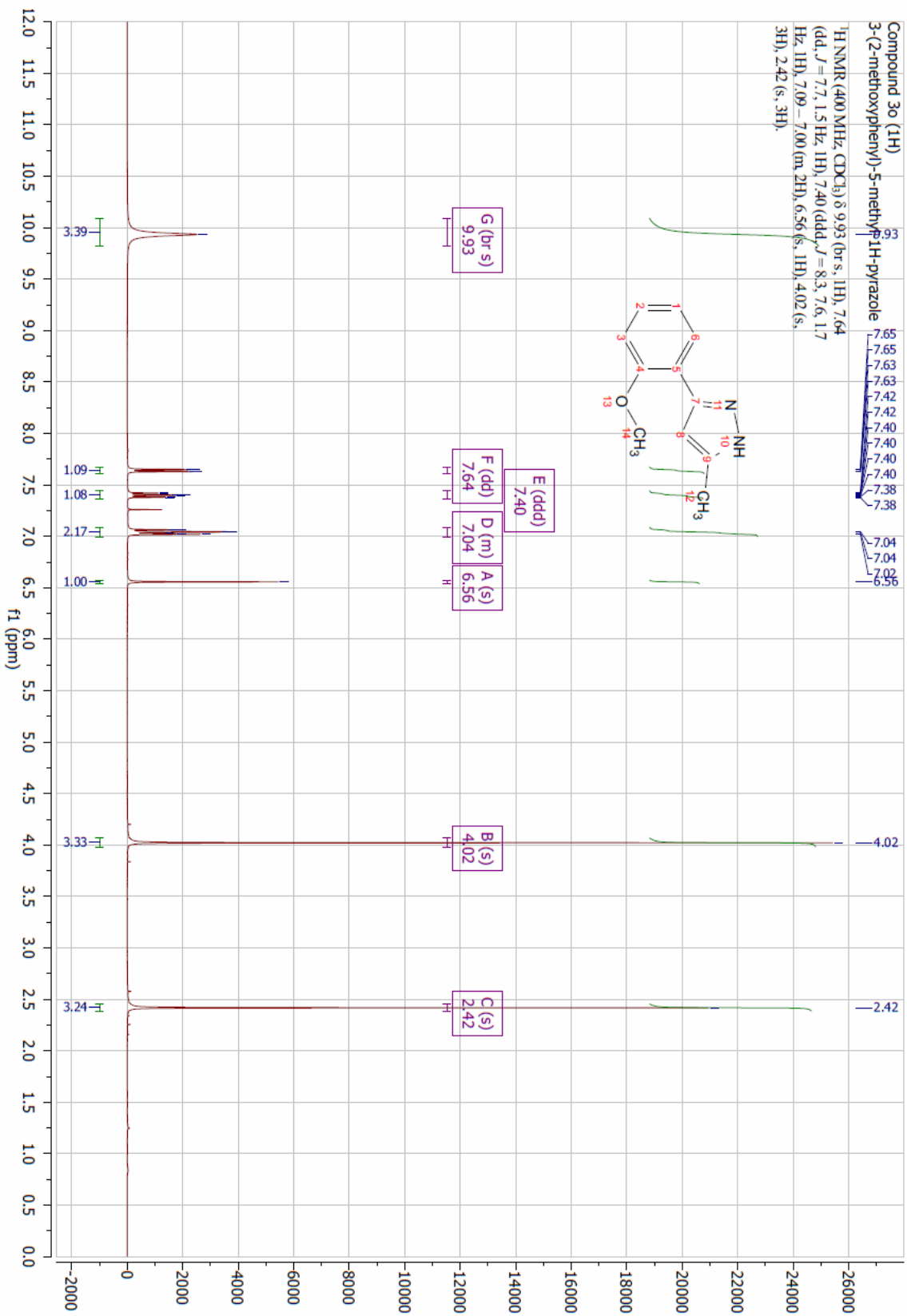


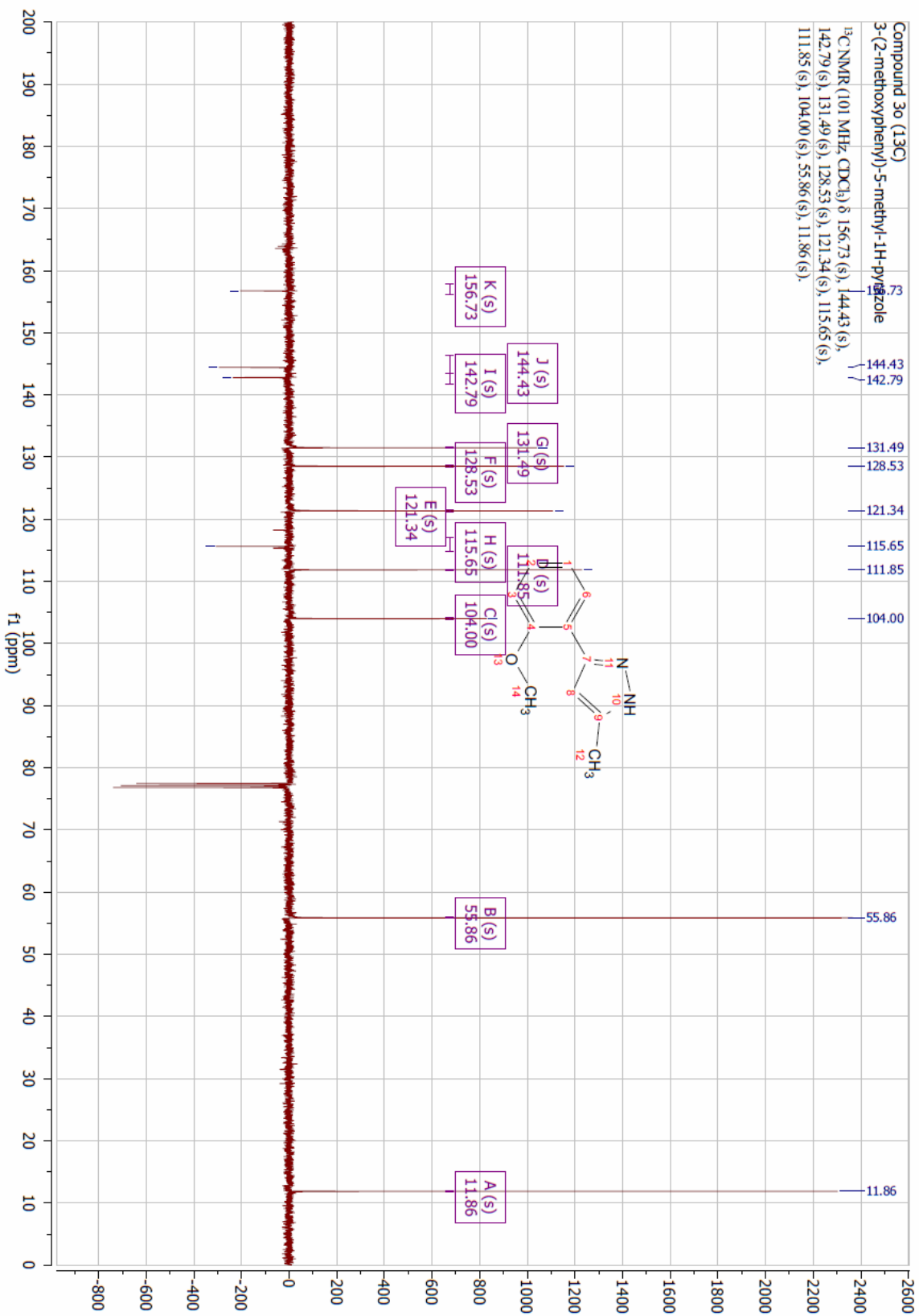


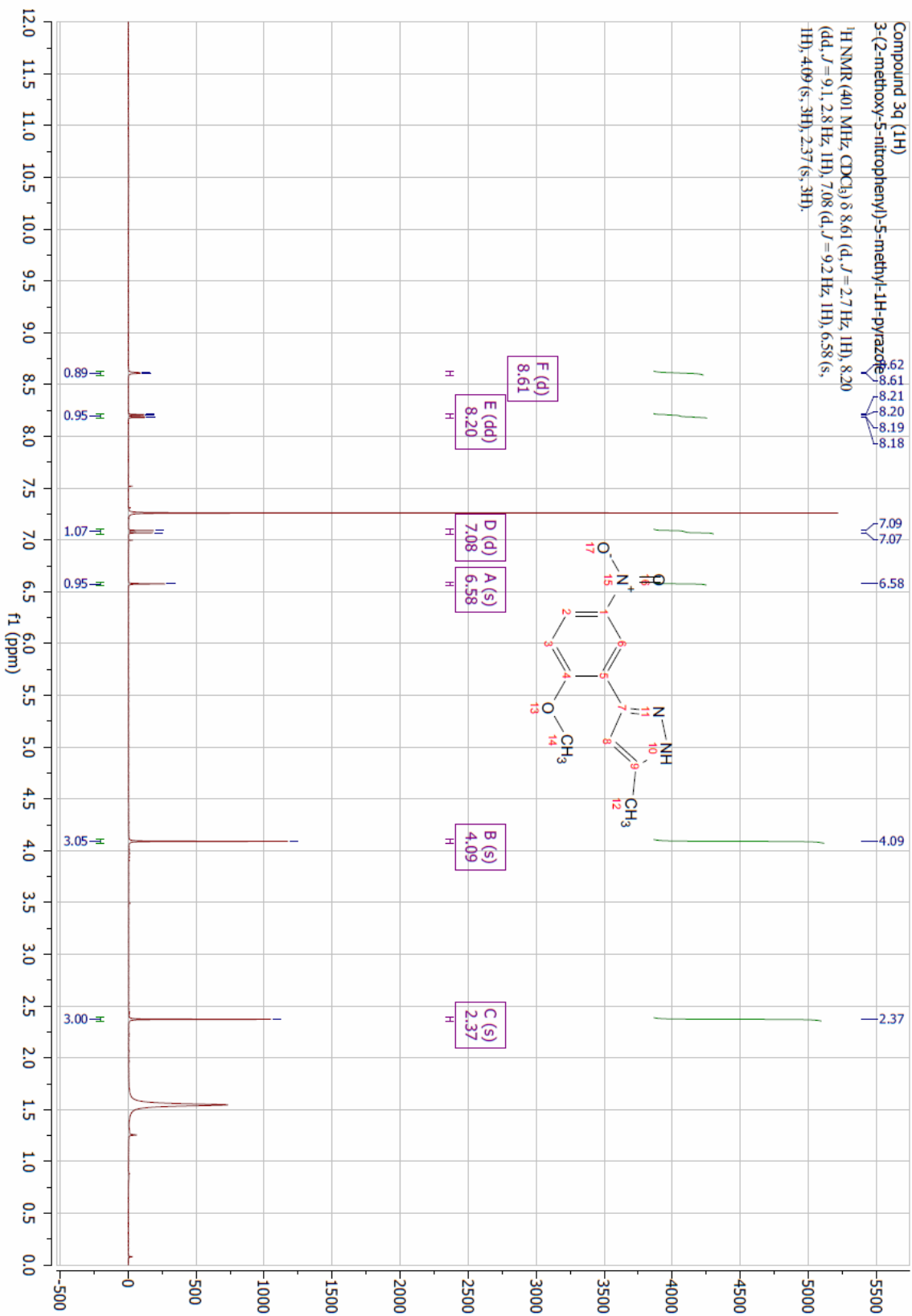


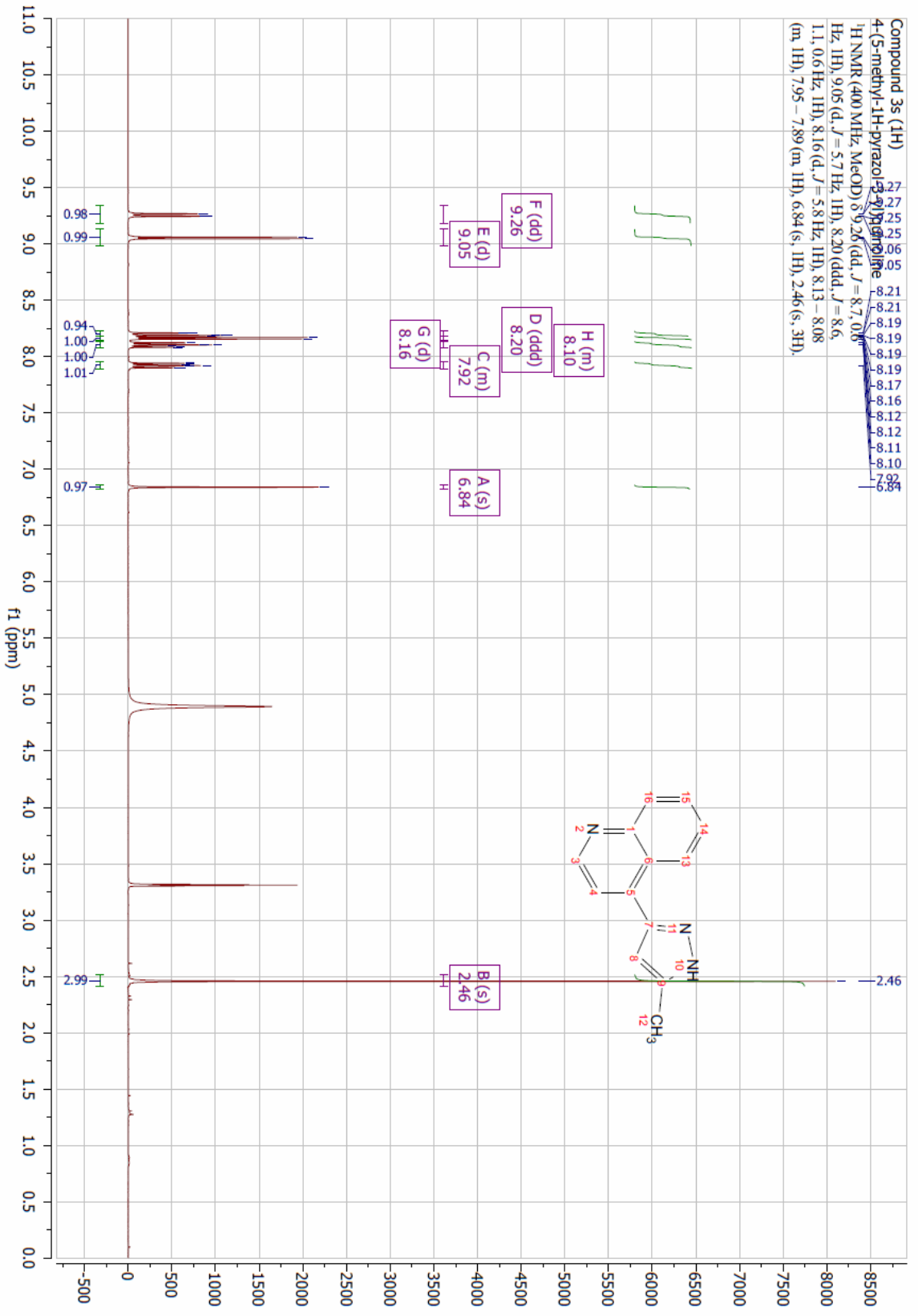


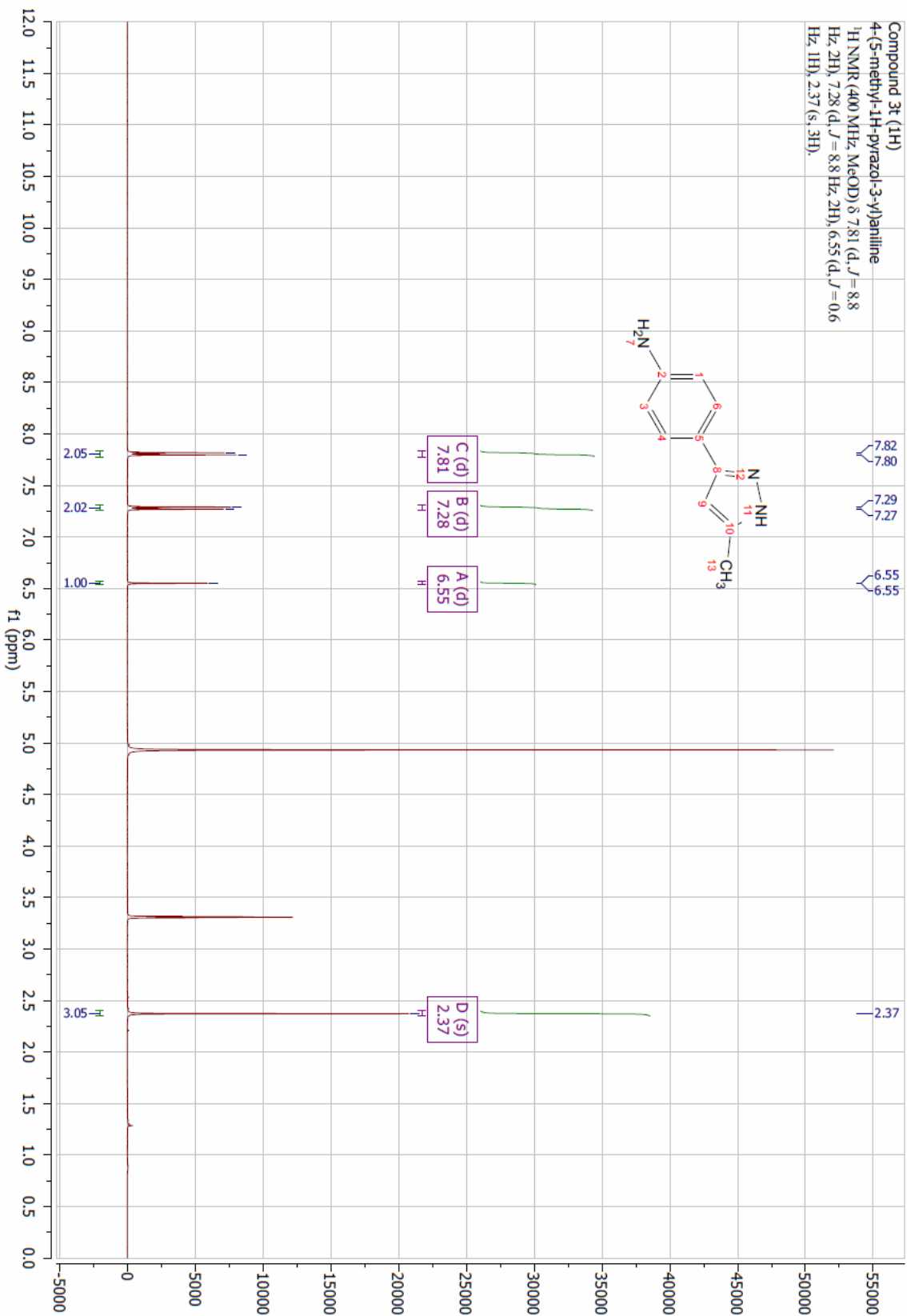


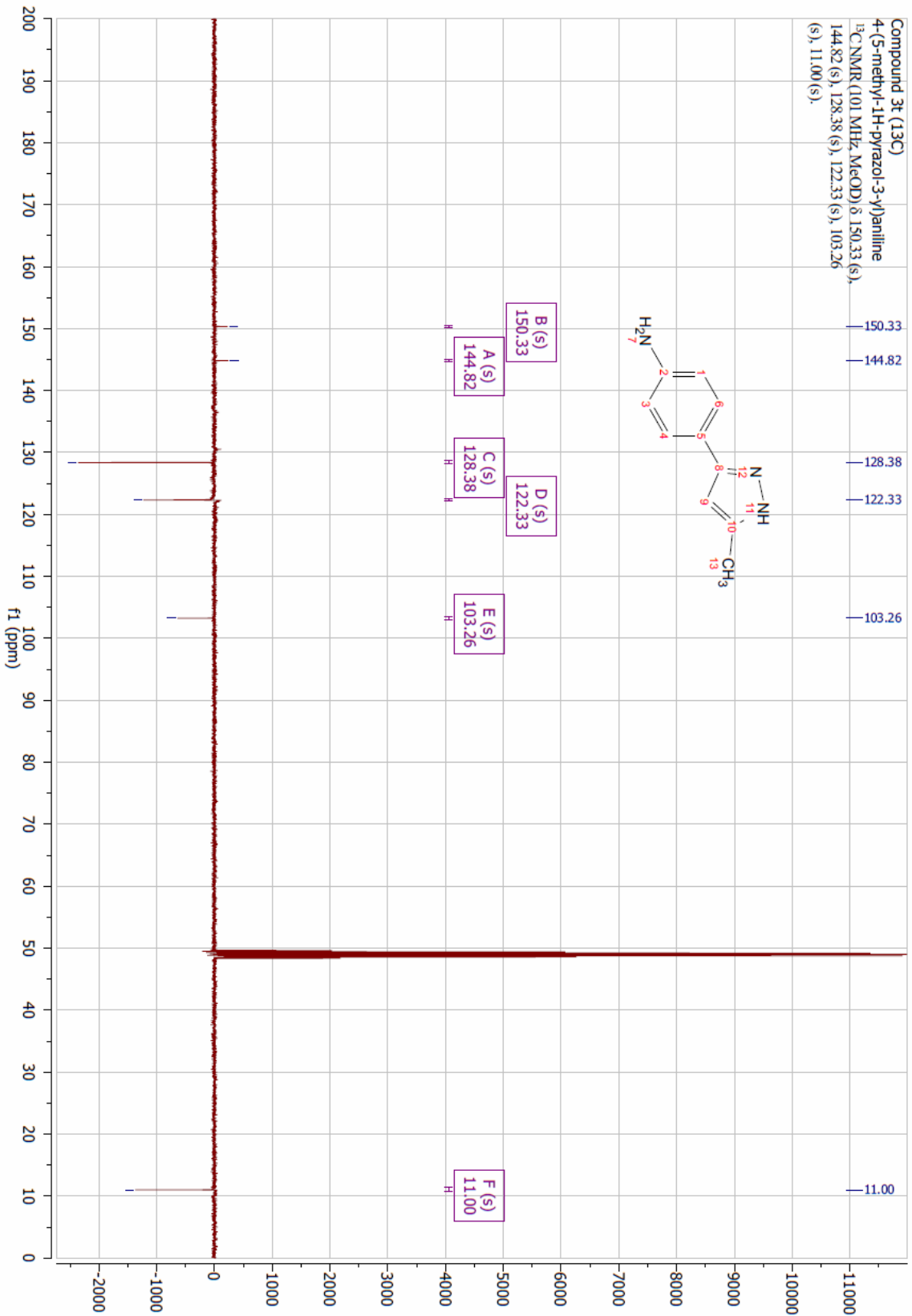


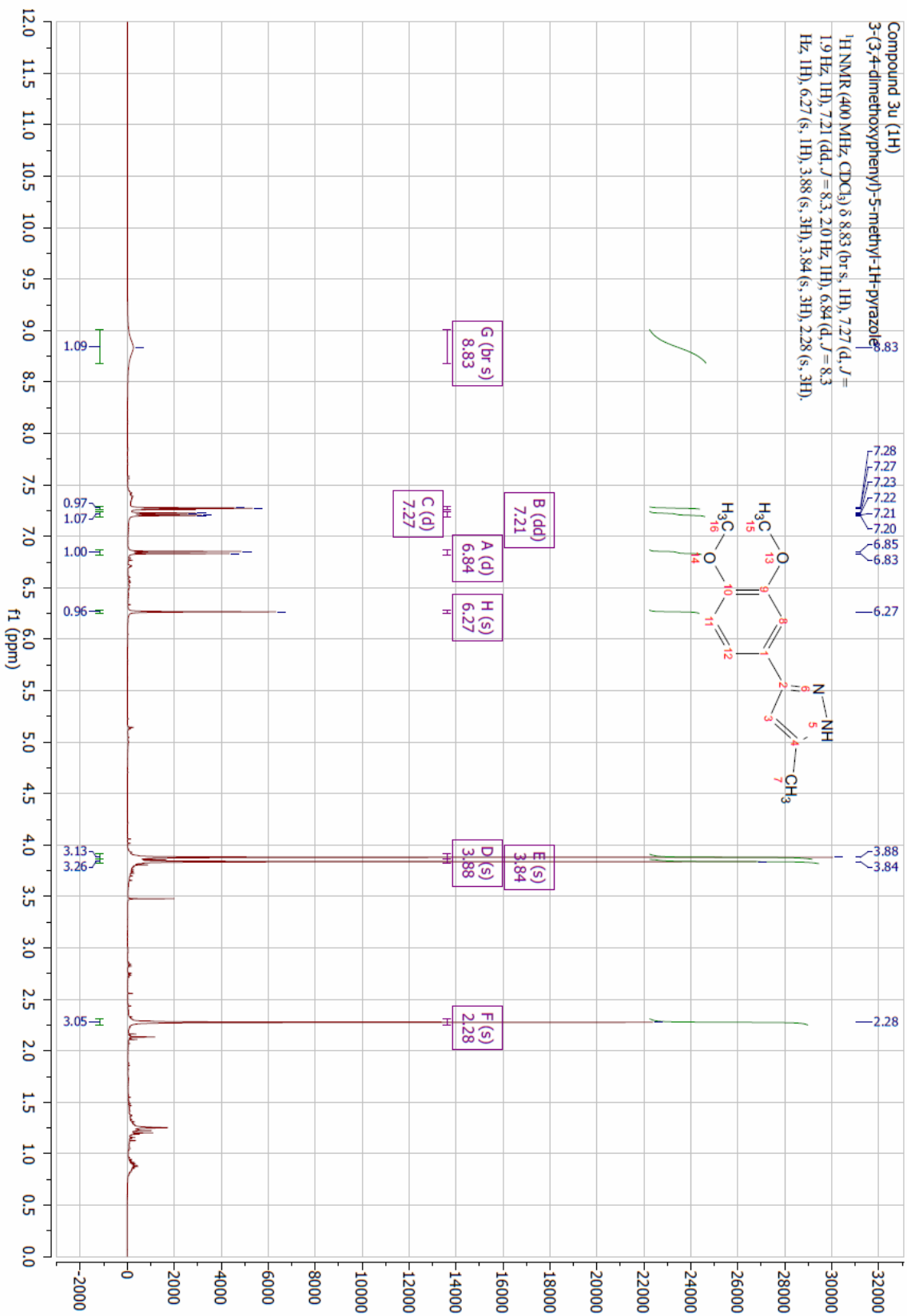


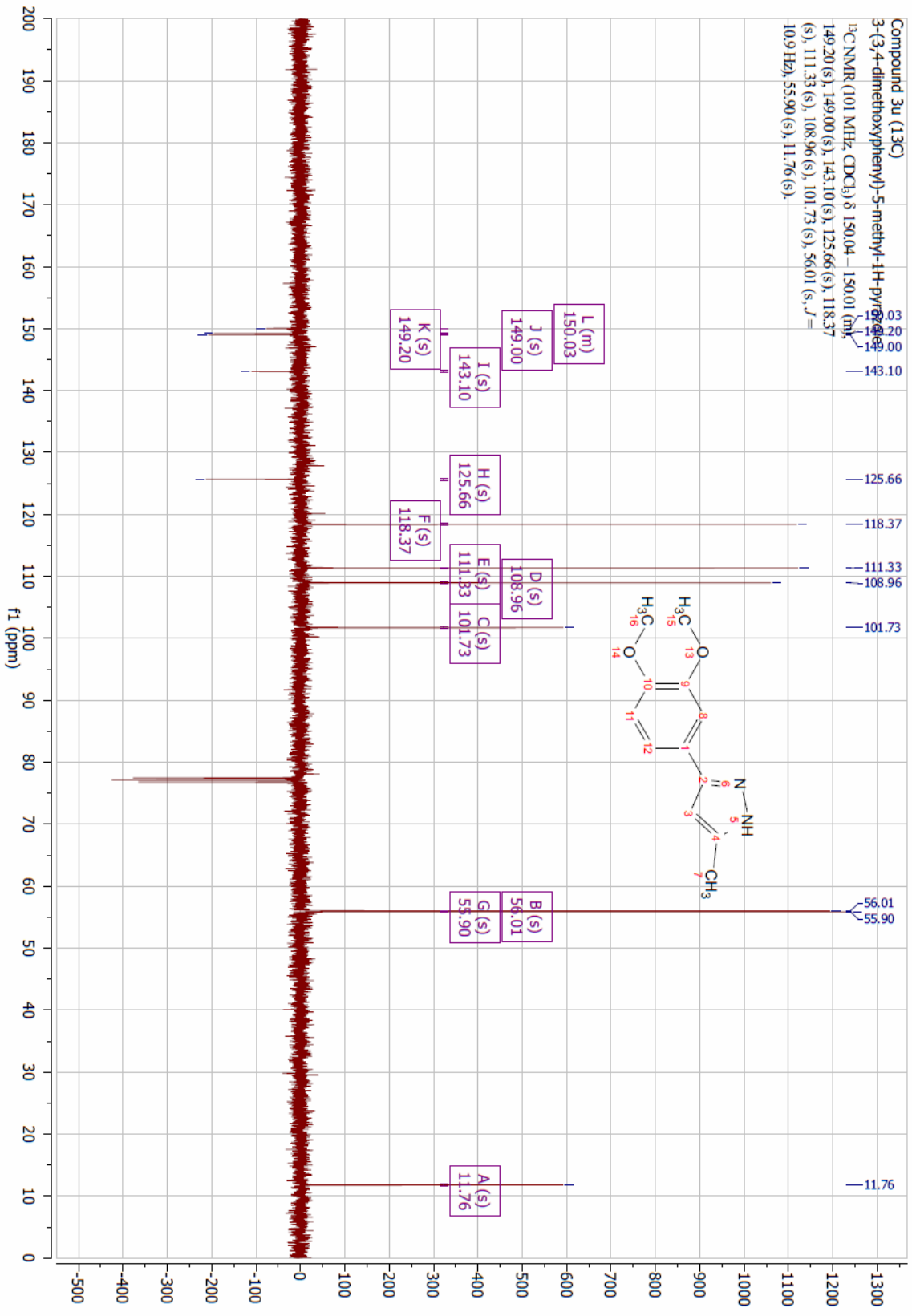


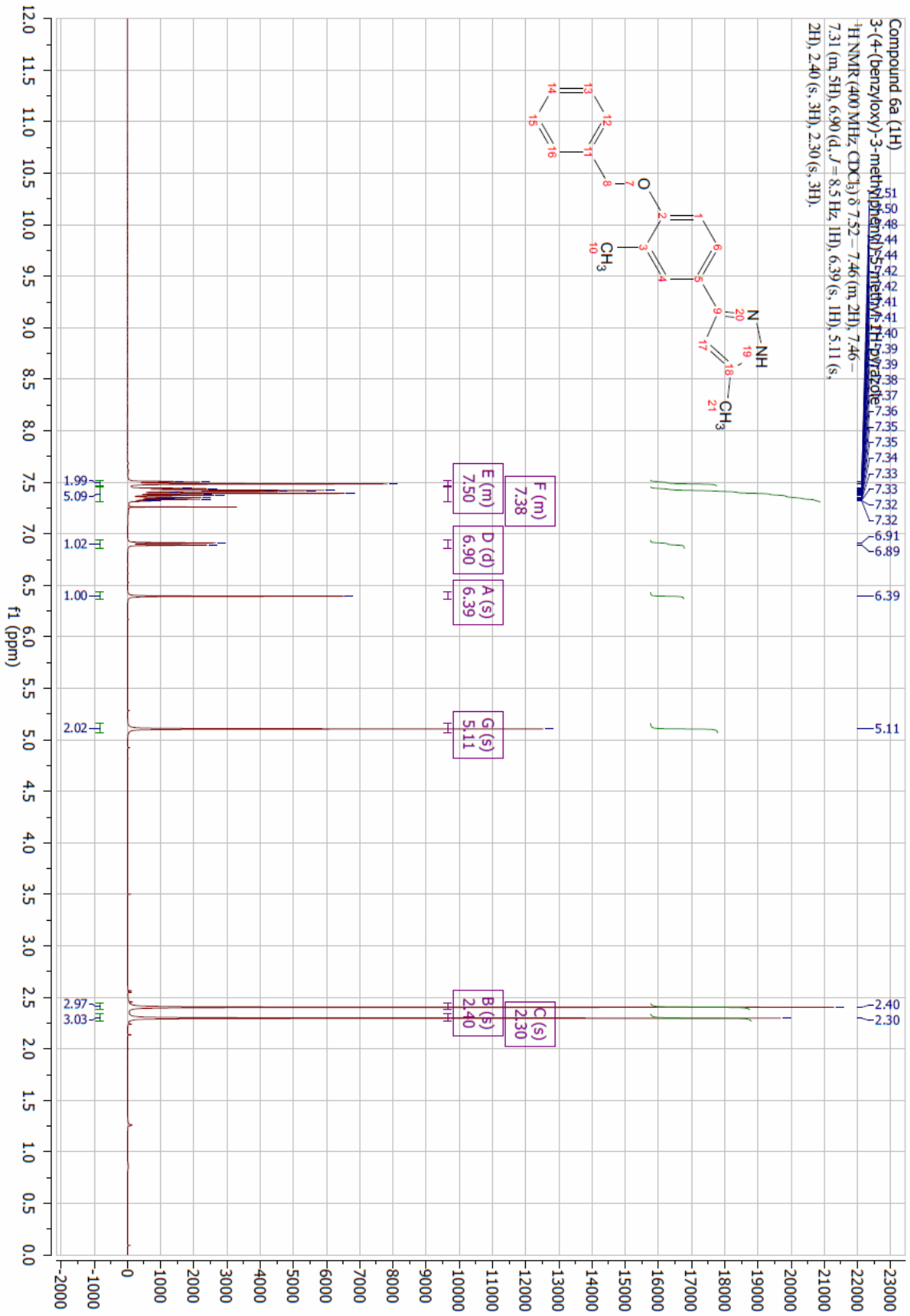


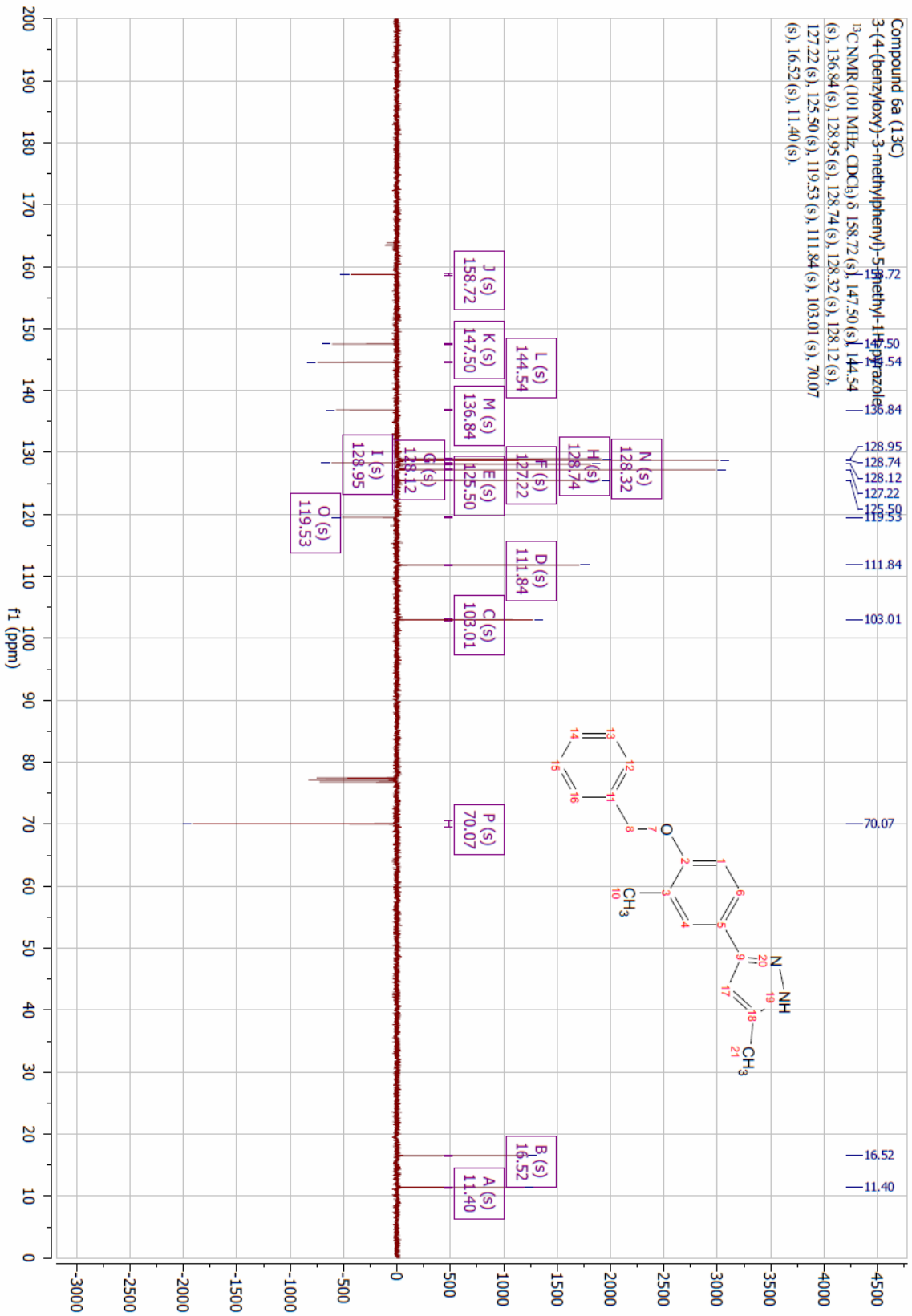


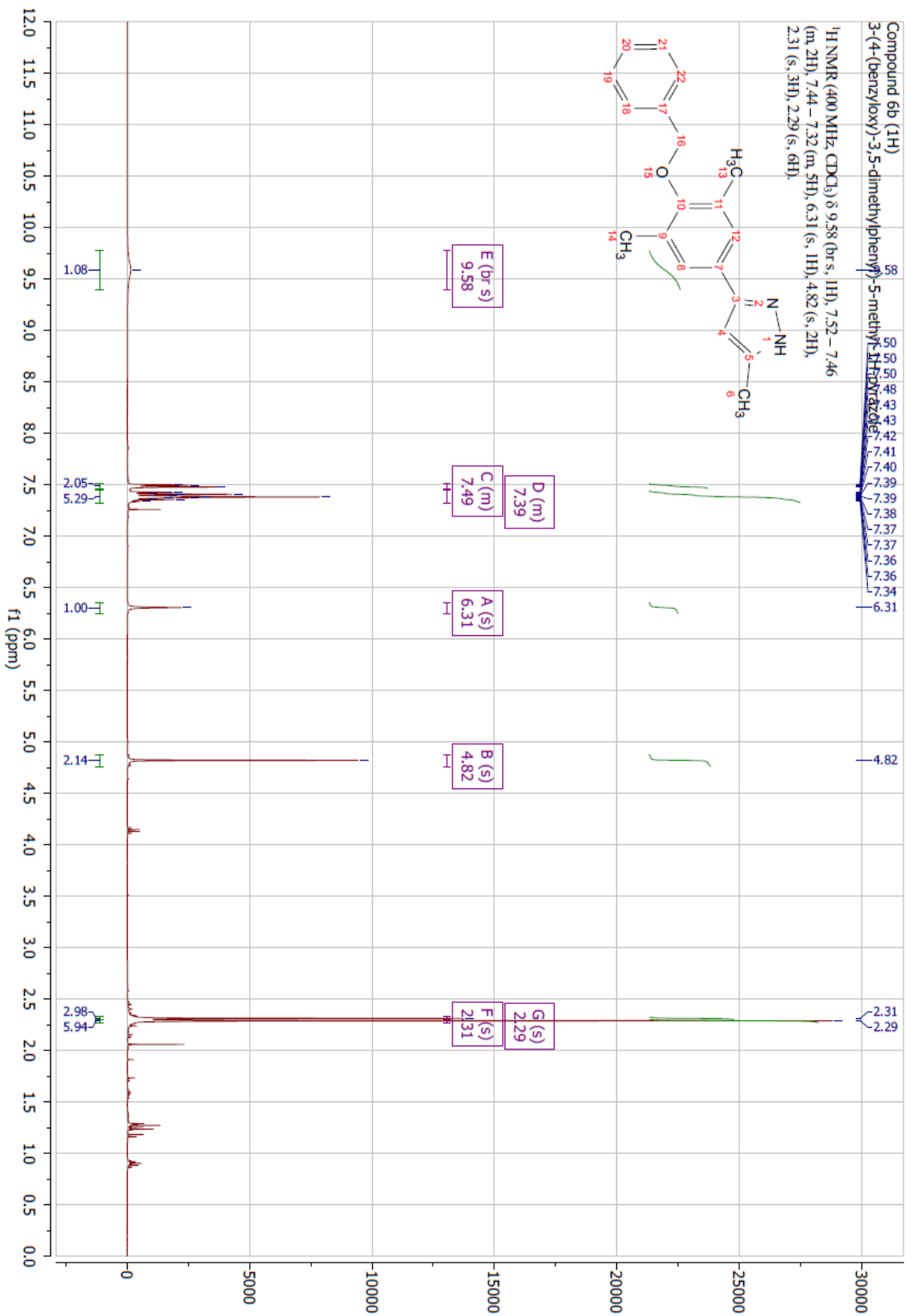


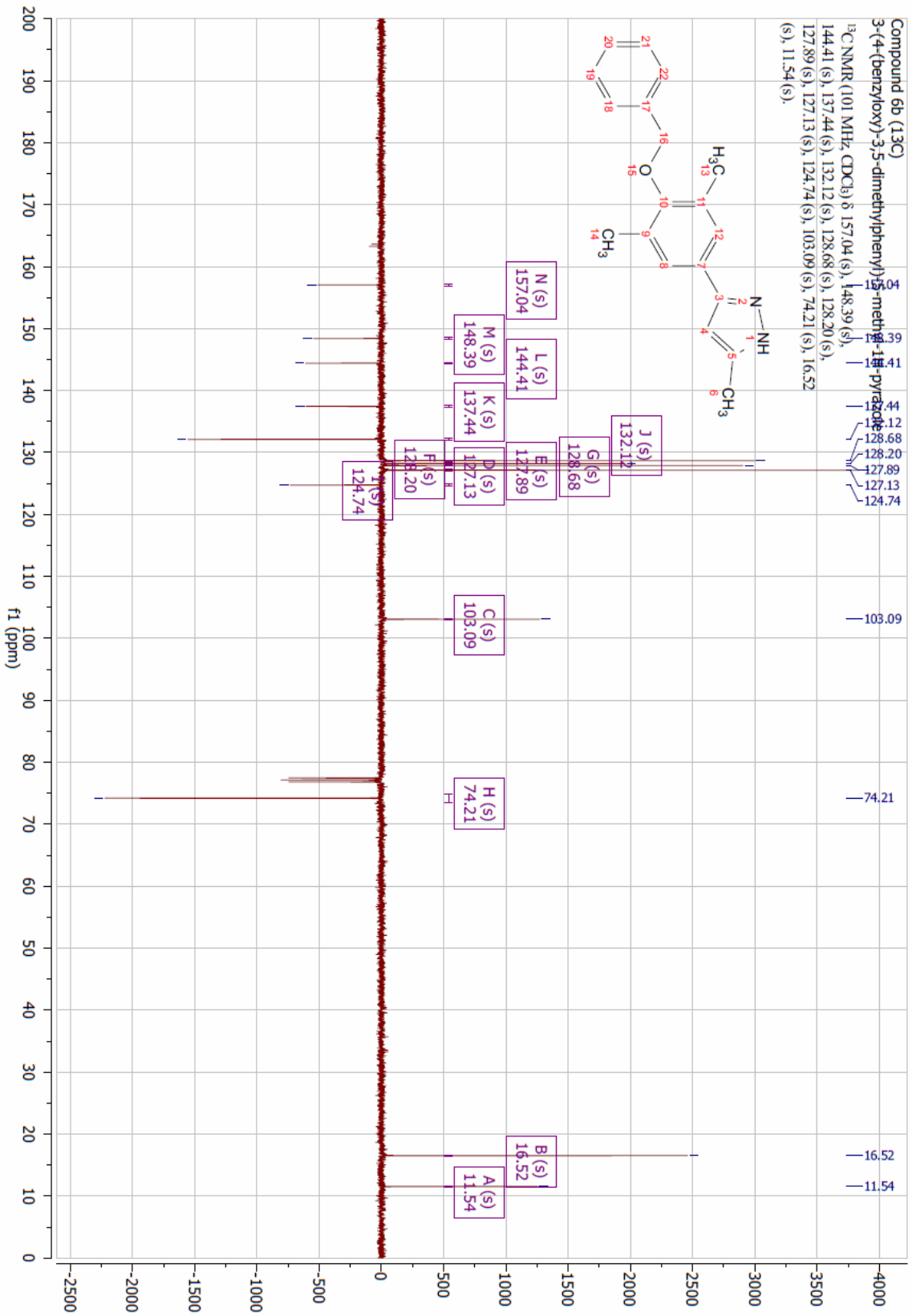


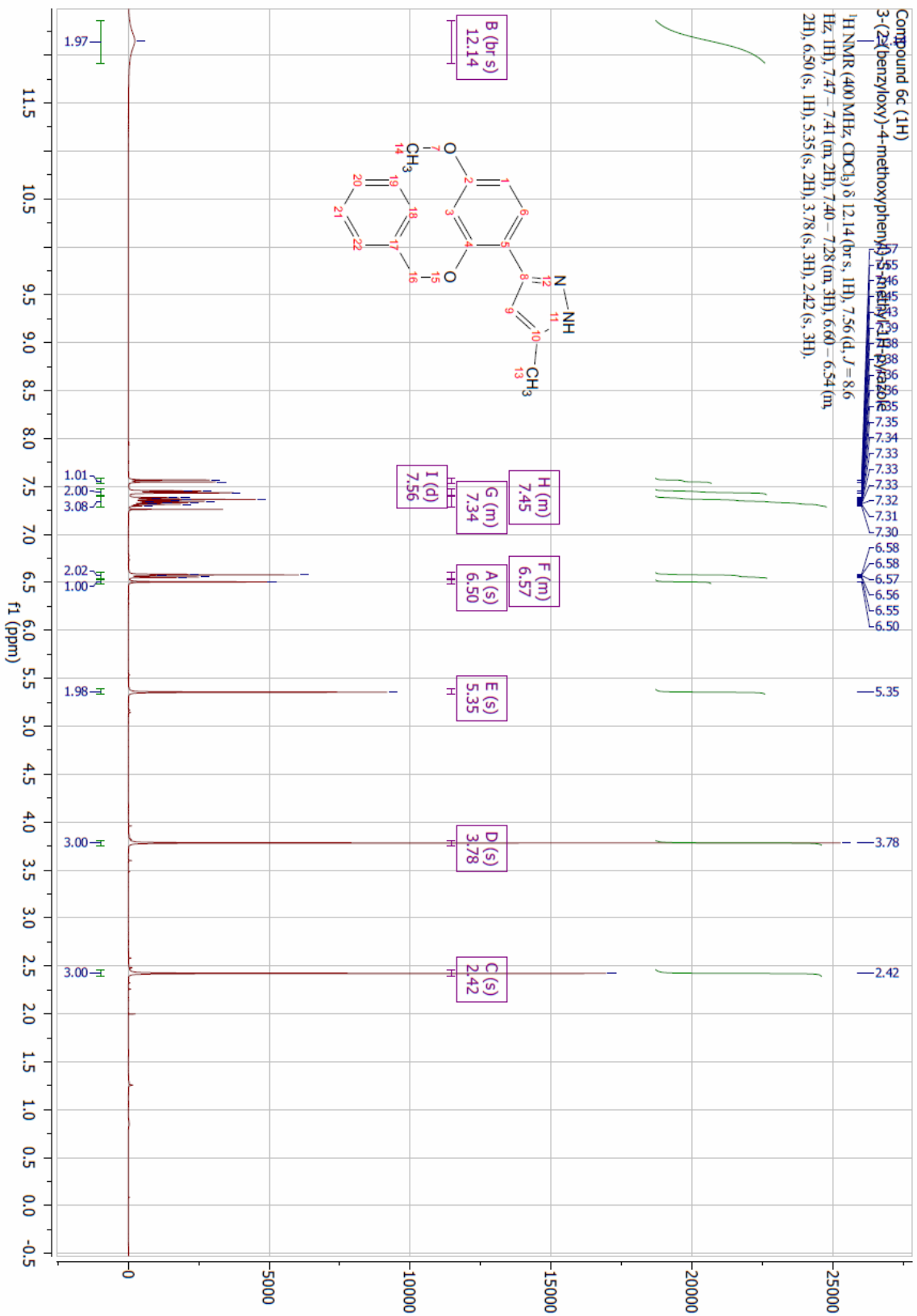


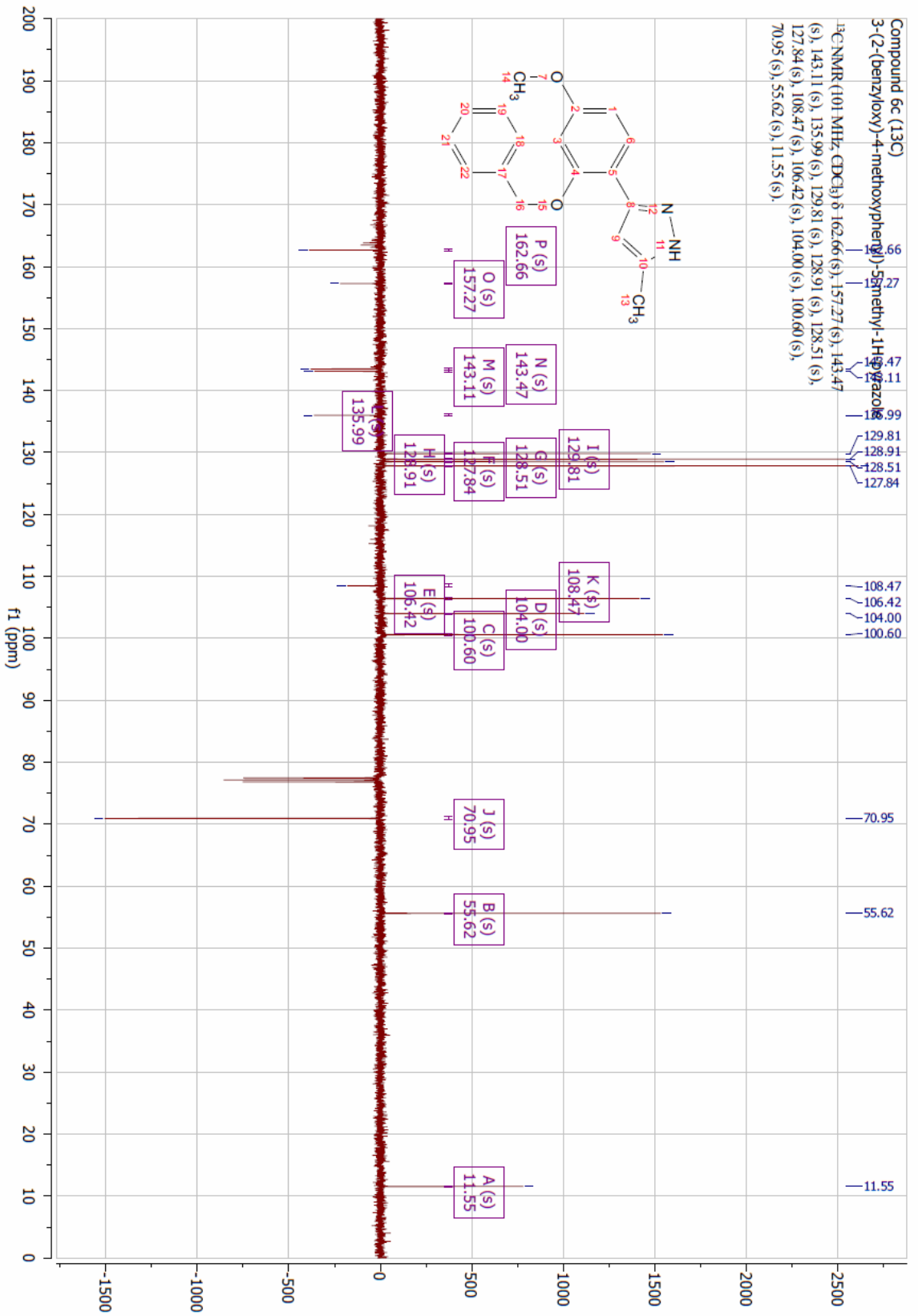


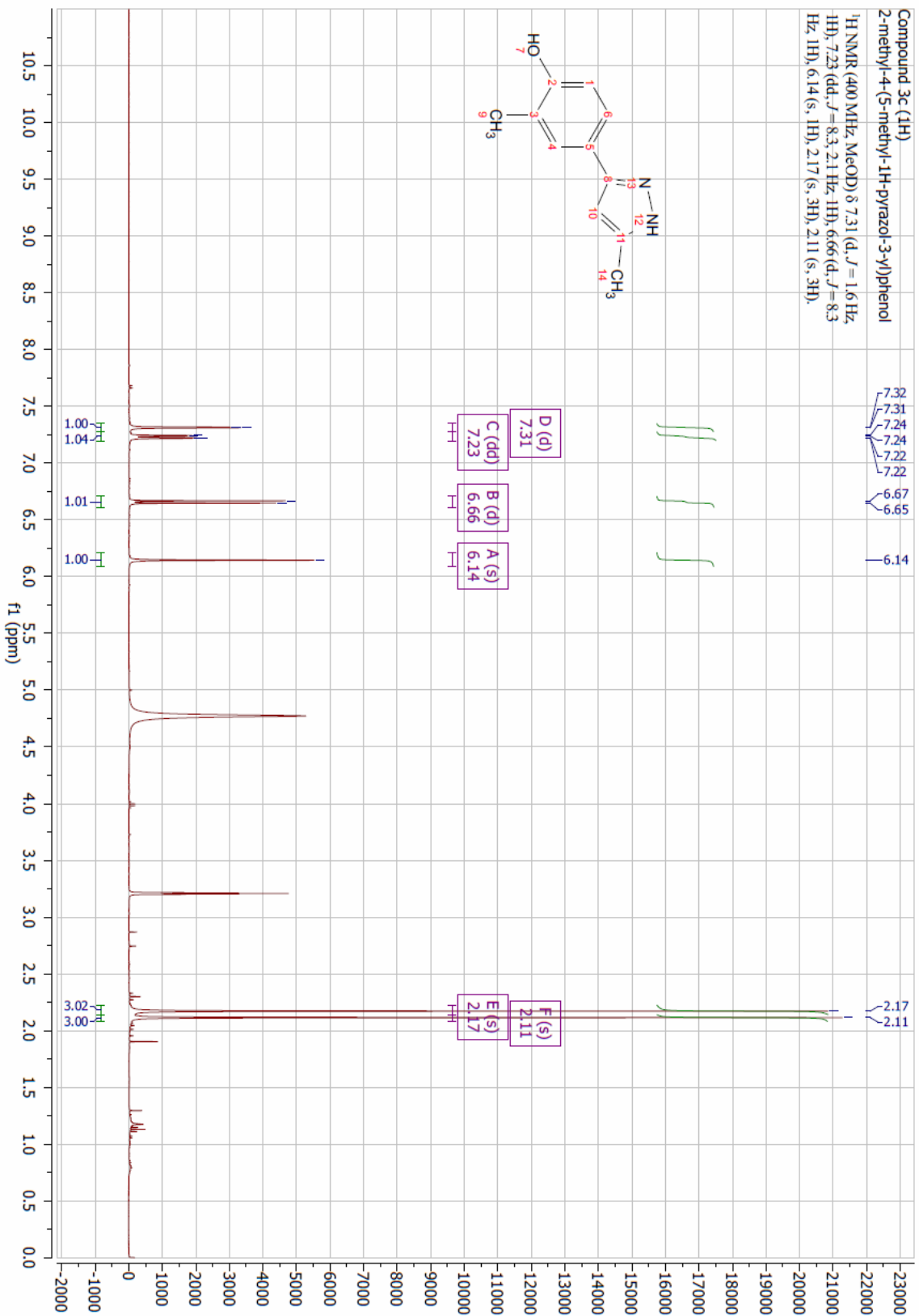


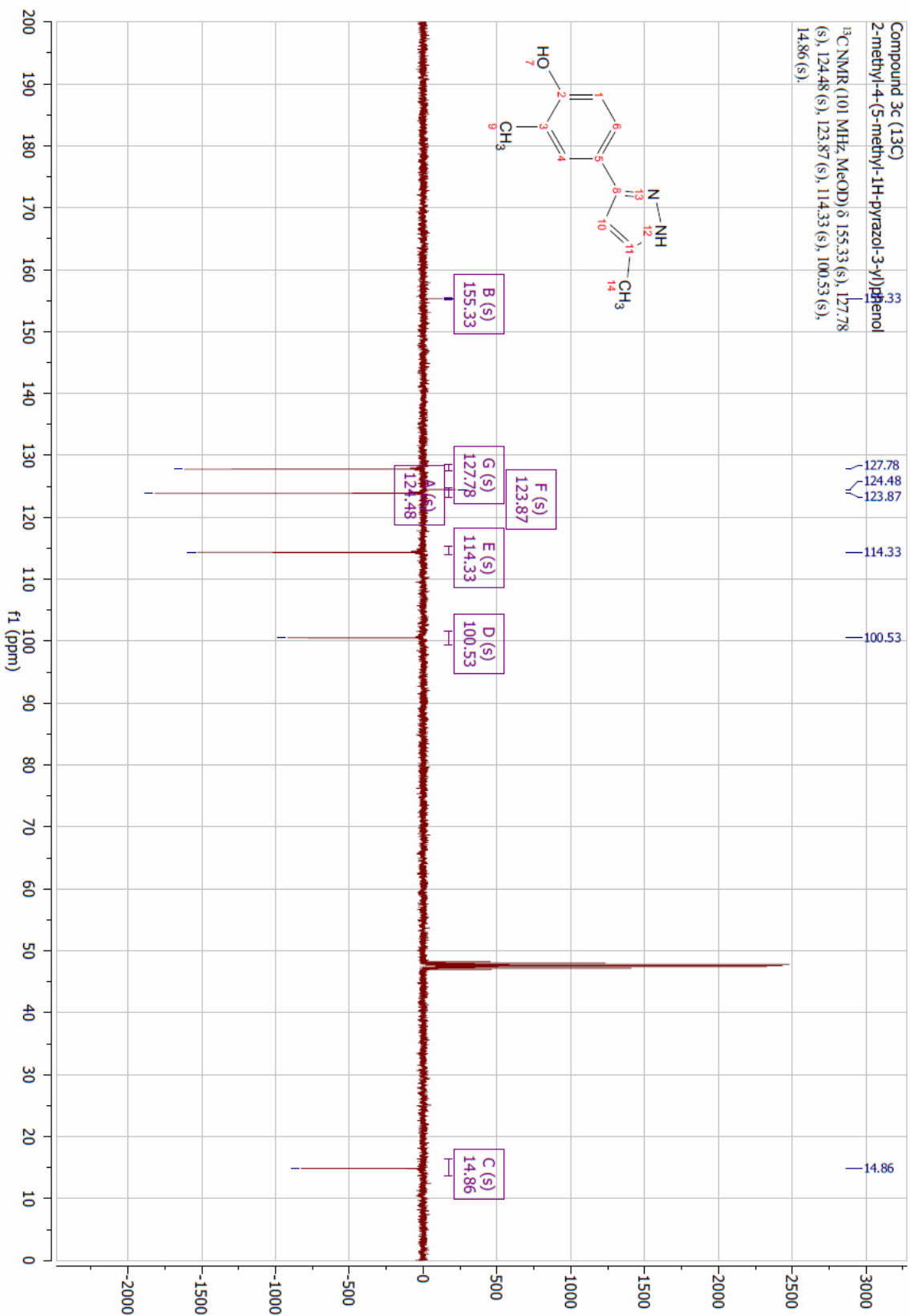


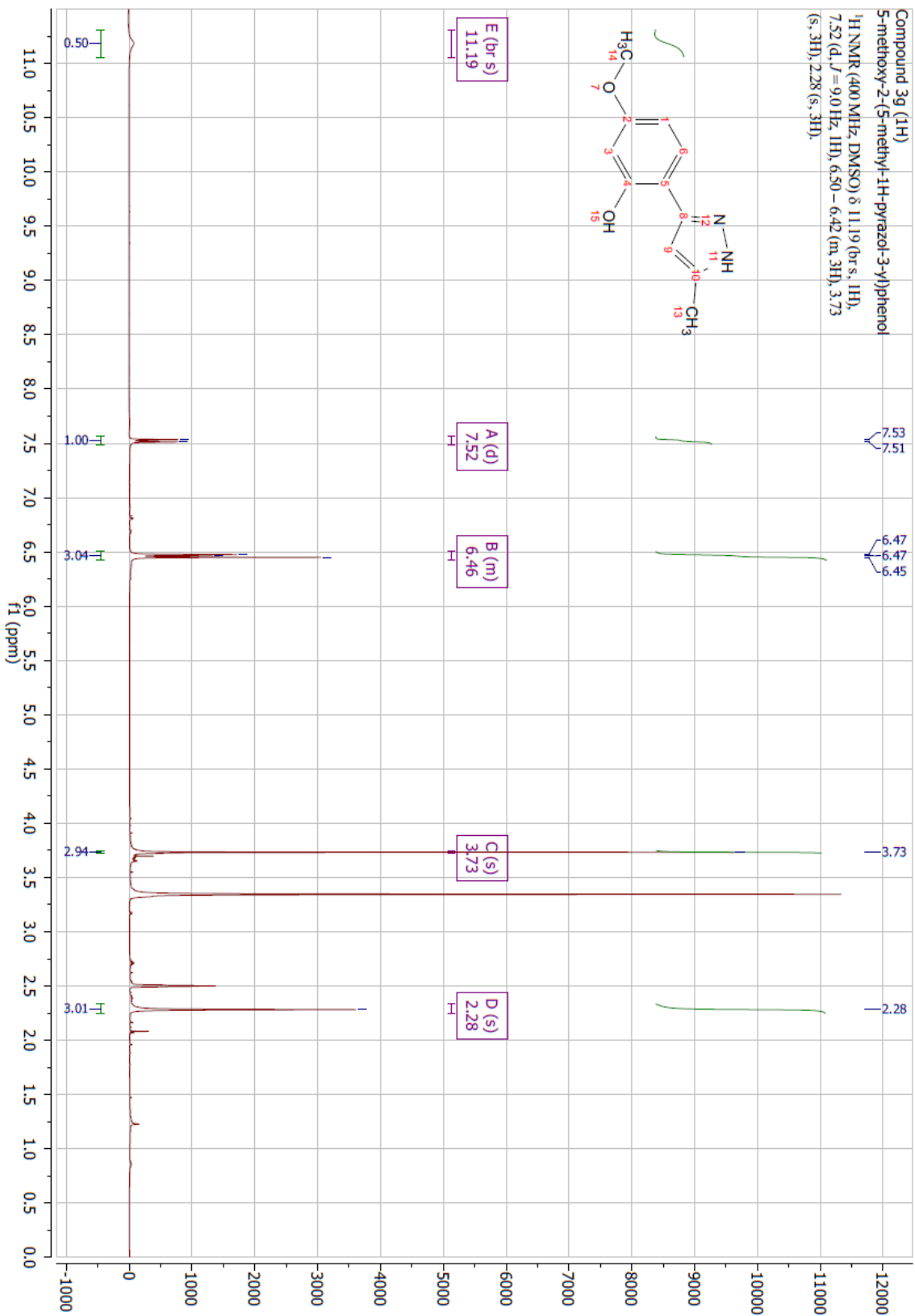


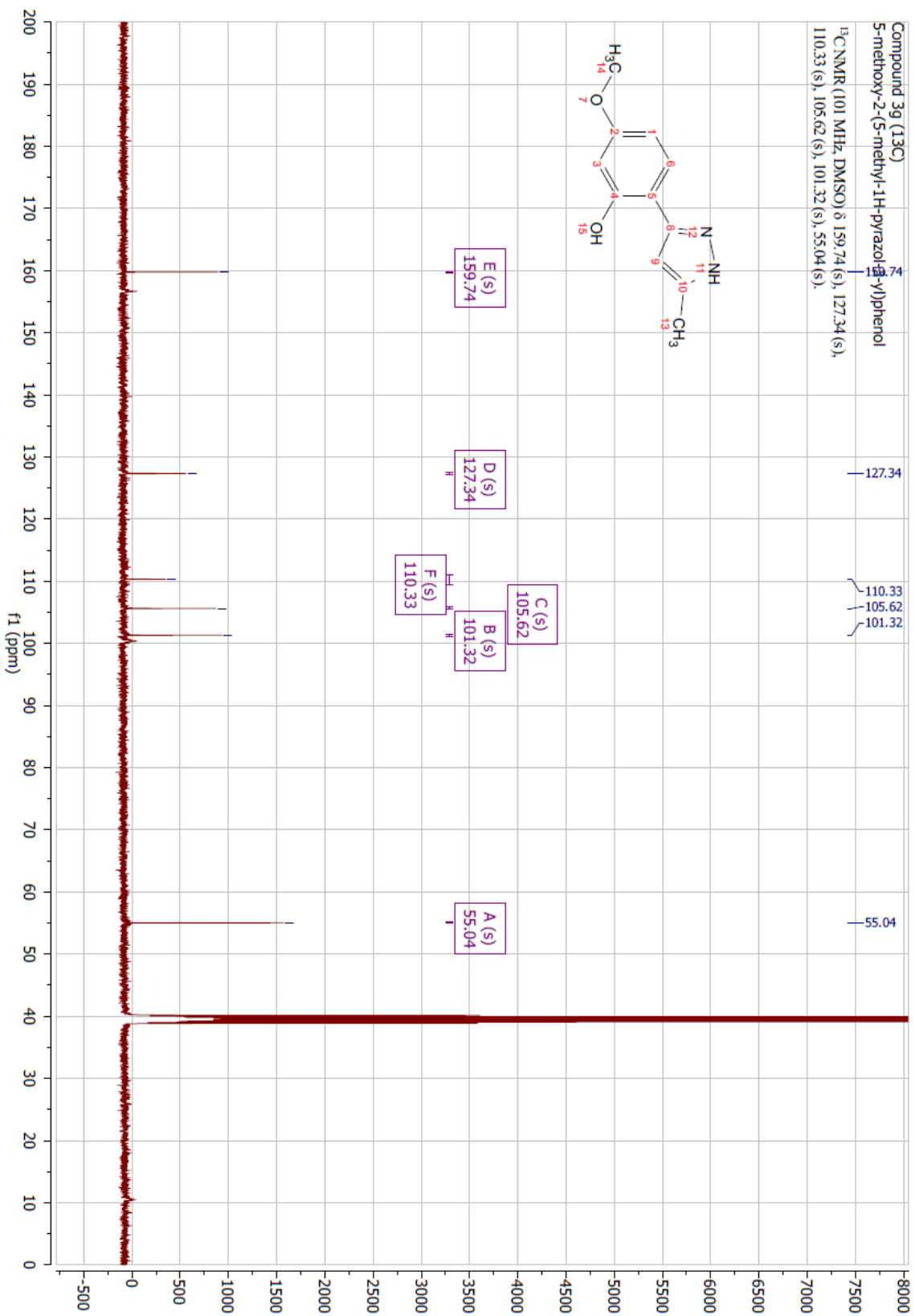




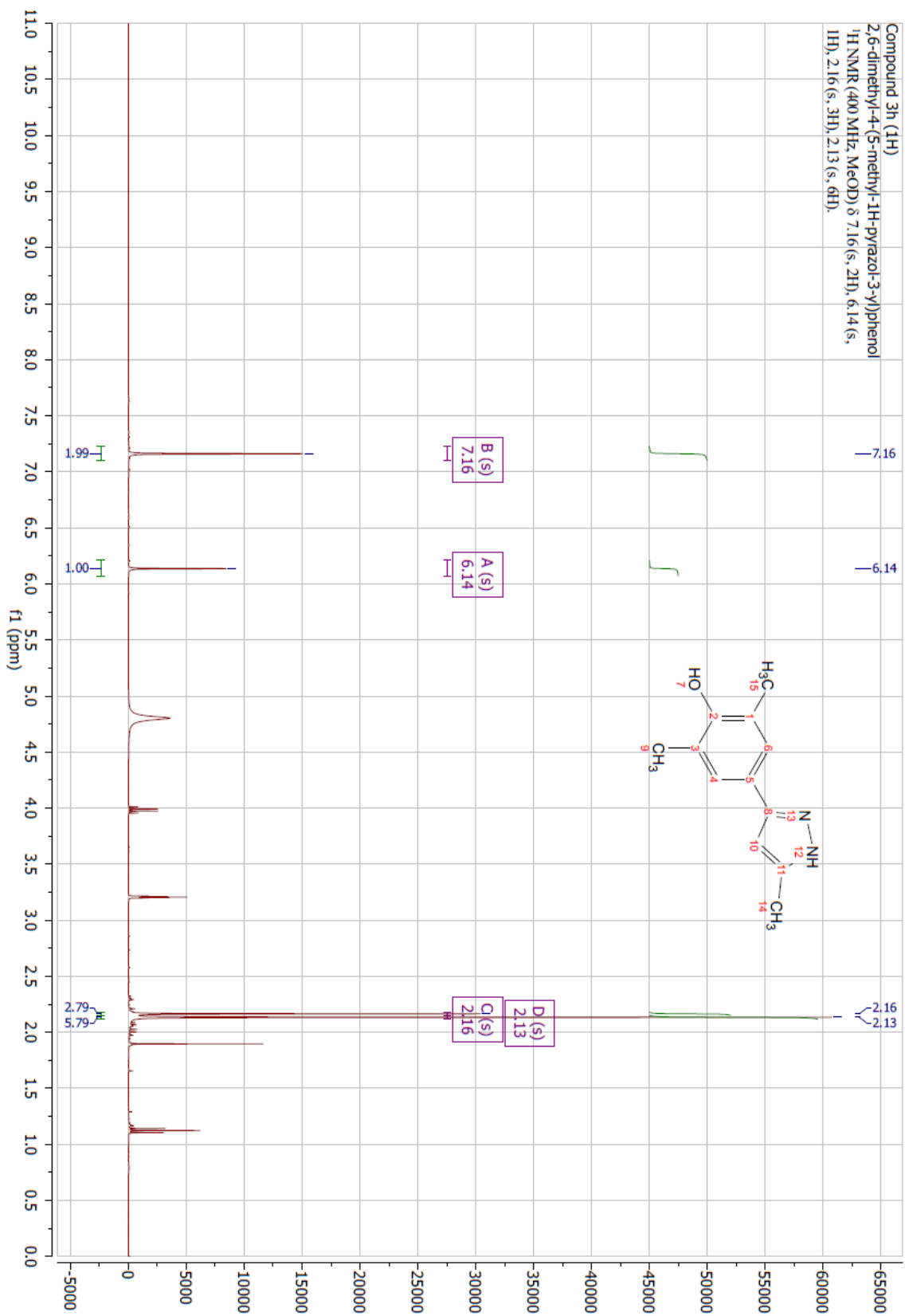




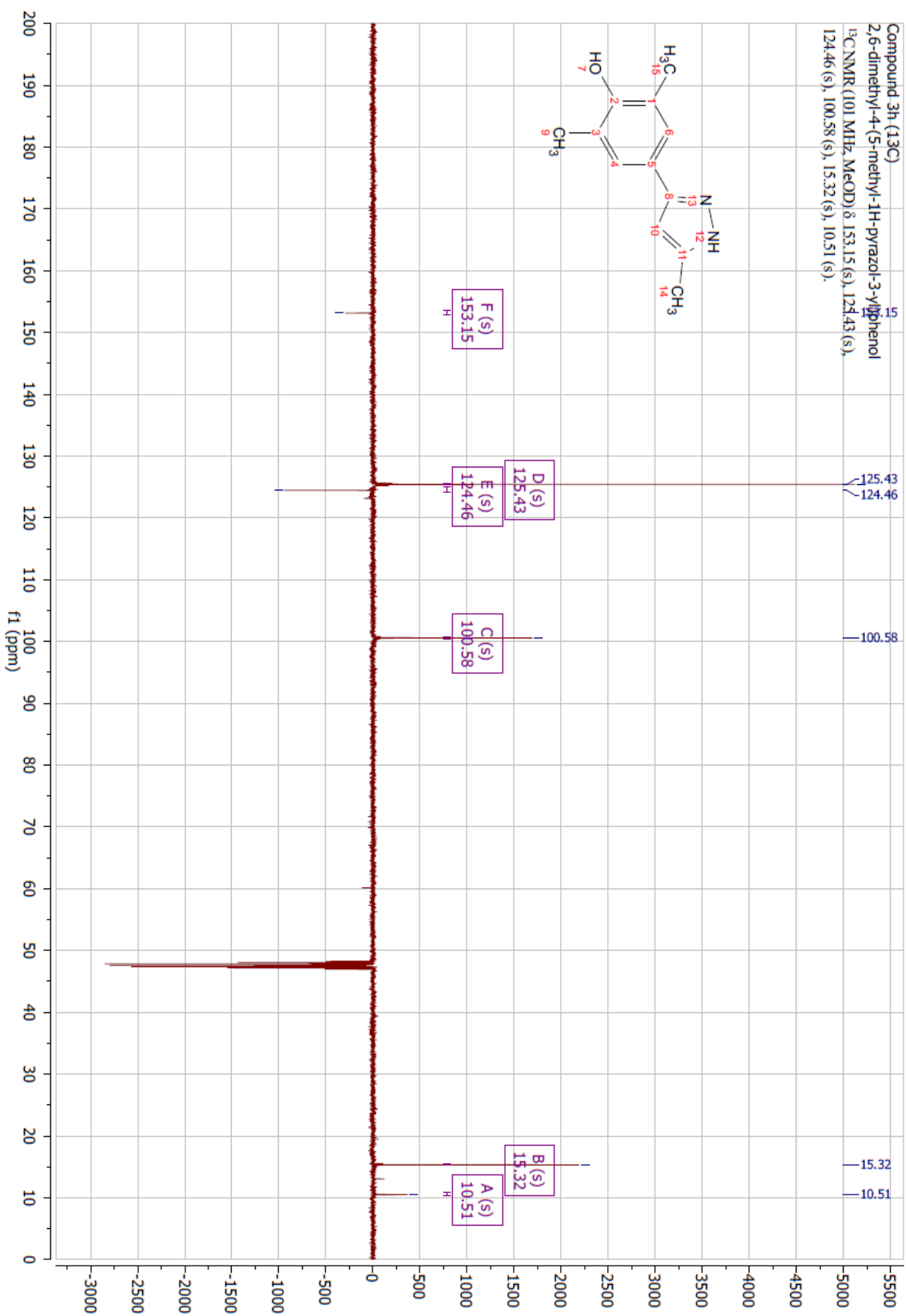
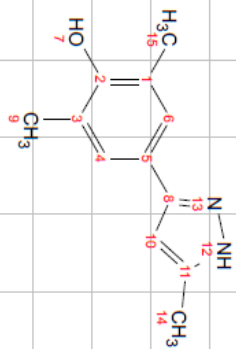




Compound 3h (1H)
2,6-dimethyl-4-(5-methyl-1H-pyrazol-3-yl)phenol
1H NMR (400 MHz, MeOD) δ 7.16 (s, 2H), 6.14 (s,
1H), 2.16 (s, 3H), 2.13 (s, 6H).



Compound 3h (13C)
2,6-dimethyl-4-(5-methyl-1H-pyrazol-3-yl)phenol
¹³C NMR (101 MHz, MeOD) δ 153.15 (s), 124.43 (s),
124.46 (s), 100.58 (s), 15.32 (s), 10.51 (s).



Appendix R – Chapter 4 X-ray Crystallographic Data Collection and

Refinement Statistics

Compound Title	3h
Resolution range	29.38 - 1.359 (1.408 - 1.359)
Space group	P 21 21 21
Unit cell	37.91 44.139 78.715 90 90 90
Total reflections	57792 (5563)
Unique reflections	28911 (2793)
Multiplicity	2.0 (2.0)
Completeness (%)	99.12 (97.15)
Mean I/sigma(I)	43.02 (7.83)
Wilson B-factor	10.64
R-merge	0.01017 (0.08816)
R-meas	0.01439 (0.1247)
R-pim	0.01017 (0.08816)
CC1/2	1 (0.98)
CC*	1 (0.995)
Reflections used in refinement	28909 (2793)
Reflections used for R-free	1420 (132)
R-work	0.1669 (0.1811)
R-free	0.1876 (0.2023)
CC(work)	0.964 (0.936)
CC(free)	0.944 (0.924)
Number of non-hydrogen atoms	1398
macromolecules	1152
ligands	15
solvent	231
Protein residues	128
RMS(bonds)	0.062
RMS(angles)	2.39
Ramachandran favoured (%)	99.18
Ramachandran allowed (%)	0.82
Ramachandran outliers (%)	0.00
Rotamer outliers (%)	0.00
Clashscore	3.00
Average B-factor	16.35
macromolecules	13.97
ligands	11.96
solvent	28.50
Number of TLS groups	3

Statistics for the highest-resolution shell are shown in parentheses.